JAERI-M
87-043

BWR 2% MAIN RECIRCULATION LINE BREAK LOCA TESTS RUNS 915 AND 920 WITHOUT HPCS IN ROSA-III PROGRAM
—EFFECTS OF PRESSURE CONTROL SYSTEM—

March 1987

Mitsuhiro SUZUKI, Hideo NAKAMURA, Yoshinari ANODA,
Hiroshige KUMAMARU, Taisuke YONOMOTO
Yasuo KOIZUMI and Kanji TASAKA

日本原子力研究所
Japan Atomic Energy Research Institute

JAERI-Mレポートは，日本原子力研究所が不定期に公刊している研究報告書です。
入手の問合わせは，日本原子力研究所技術情報部情報資料課（〒319-11茨城県那珂郡東海村）あて，お申しこしください。なお，このほかに財団法人原子力弘済会資料センター（〒319-11 茨城県那珂郡東海村日本原子力研究所内）で複写による実費頒布をおこなっております。

JAERI-M reports are issued irregularly.
Inquiries about availability of the reports should be addressed to Information Division Department of Technical Information, Japan Atomic Energy Research Institute, Tokai-mura, Naka-gun, Ibaraki-ken 319-11, Japan.

編集兼発行　日本原子力研究所
印　　刷　㈱高野高速印刷

JAERI-M 87-043

BWR 2% MAIN RECIRCULATION LINE BREAK LOCA TESTS RUNS 915 AND 920 WITHOUT HPCS IN ROSA-III PROGRAM — EFFECTS OF PRESSURE CONTROL SYSTEM —

Mitsuhiro SUZUKI, Hideo NAKAMURA, Yoshinari ANODA,
Hiroshige KUMAMARU, Taisuke YONOMOTO, Yasuo KOIZUMI
and Kanji TASAKA

Department of Reactor Safety Research,
Tokai Research Establishment
Japan Atomic Energy Research Institute
Tokai-mura, Naka-gun, Ibaraki-ken

(Received February 17, 1987)

This report presents the experimental results of BWR LOCA integral tests, RUNs 915 and 920, which are performed in the ROSA-III program simulating 2% main recirculation line break LOCA tests with and without pressure control system operation. The ROSA-III test facility simulates a BWR system with volume scale of 1/424 and has four half-length electrically heated fuel bundles, two active recirculation loops, four types of ECCS's, and steam and feedwater systems.

The report presents (1) the experimental results of 2% small break LOCA phanomena in the ROSA-III system and (2) the effects of the pressure control system on the LOCA phenomena. The pressure control system contributed to (A) prevent bulk flashing in the early blowdown phase, (B) early closure of MSIV by L2 level trip, (C) early actuation of ADS by L1 level trip. However, the core thermal responses of the two tests were similar because of the similar mass inventory in PV after the ADS actuation in both tests.

Keywords: BWR, LOCA, ECCS, Integral Test, ROSA-III Program, Small Break, Recirculation Line, ADS, Pressure Control System, Data Report

ROSA－Ⅲにおける高圧炉心スプレイ系不作動を仮定したＢＷＲ再循環系配管２％破断ＬＯＣＡ実験，RUN９１５，９２０

－圧力制御系作動のＬＯＣＡに及ぼす影響－

日本原子力研究所東海研究所原子炉安全工学部
鈴木光弘・中村秀夫・安濃田良成・熊丸博滋
与能本泰介・小泉安郎・田坂完二

（１９８７年２月１７日受理）

本報はROSA－Ⅲ計画において実施した，ＢＷＲの再循環ループ配管２％破断ＬＯＣＡ総合実験，RUN９１５及び９２０の実験結果をまとめたものであり，これらは圧力制御系作動の有無のみが異なる実験である。ROSA－Ⅲ試験装置はＢＷＲを容積比1／４２４で模擬するシステムであり，中に1／2実長の電気加熱燃料集合体４体，２つの再循環ループ，ECCS４系統，蒸気系及び給水系を有する。

本報は，(1)ROSA－Ⅲにおける２％小破断ＬＯＣＡの実験結果をまとめ，(2)圧力制御系がＬＯＣＡ事象に及ぼす影響を明らかにした。圧力制御系は，(A)破断初期の系全体のフラッシングを抑制し，(B)Ｌ２水位トリップ信号による主蒸気隔離弁および(C)Ｌ１水位トリップ信号による自動減圧系の早期作動をもたらした。しかし，自動減圧系作動後においては，両実験とも圧力容器内保有水量が同程度の値になり，この結果炉心内熱的挙動も同じ変化を示した。

東海研究所：〒319－11 茨城県那珂郡東海村白方字白根２－4

Contents

目　　次

List of Tables for RUNs 915 and 920

List of Figures

List of Figures of Experiment Data for RUN 915

List of Figures of Experiment Data for RUN 920

List of Figures for Section 6

1. Introduction

The rig of safety assessment (ROSA)-III program[1][2] was initiated in 1976 to study the thermal hydraulic behavior of a boiling water reactor (BWR)[3] during a postulated loss-of-coolant accident (LOCA) with the emergency core cooling system (ECCS) actuation and to provide the data base to evaluate the predictability of computer codes developed for reactor safety analysis. To meet these objectives, various kinds of ROSA-III tests have been performed.[4]-[40] Similar experimental studies on the BWR/LOCA phenomena have been performed also at TLTA,[41] FIST[42] and TBL[43] with the similar initial fluid conditions as the BWR. The ROSA-III test facility fabricated in 1978 consists of a volumetrically scaled (1/424) primary system of a 3800 MW BWR/6(251-848) with the electrically heated core, the break simulator and the scaled ECCS.

In a BWR system, a pressure control (or regulation) system is furnished to prevent bulk fluid flashing caused by depressurization below the saturation pressure of 6.4 MPa in the lower plenum. In the ROSA-III program, effects of the pressure control system have been experimentally studied [44] for small break LOCAs with break areas of 5% (RUNs 912[21] and 922[31], 1% (RUNs 918 and 921) and 0% (RUNs 919 and 923) in addition to 2% break tests (RUNs 915 and 920) shown below.

The primary objectives of this report are (A) to clarify the effects of pressure control system on a 2% main recirculation line break (MRLB) LOCA and (B) to present experimental data of 2% small break LOCA phanomena for the code assessment. In Section 5 the experimental data are presented. The pressure control system effects are clarified using the experimental data in Section 6.

2. ROSA-III Test Facility

The ROSA-III test facility is a volumetrically scaled (1/424) BWR system with an electrically heated core designed to study the response of the primary system, the core and the ECCS during the postulated LOCA. The test facility is instrumented such that various thermal-hydraulic parameters are measured and recorded during the test. Details of the test facility can be refered to the reference (2).

The test facility consists of four subsystems. These subsystems are : (a) the pressure vessel, (b) the steam line and the feedwater line, (c) the recirculation loops and (d) the ECCS. Figures 2.1, 2.2 and 2.3 illustrate configuration of the test facility, the pressure vessel internals and the piping schematics, respectively. Table 2.1 compares the major dimensions of the ROSA-III test facility to the corresponding dimensions of the reference BWR system.

The ROSA-III pressure vessel includes various components in it simulating the internal structures of the reactor vessel in the BWR system as shown in Fig. 2.4. The interior of the vessel is divided into the core, the lower plenum, the upper plenum, the downcomer annulus, the steam separator, the steam dome and the steam dryer.

The core consists of four simulated fuel assemblies of half length and a control rod simulator. Each fuel assembly contains 62 heater rods (Fig. 2.5) and 2 water rods spaced in a 8 x 8 square array and supported by spacers and upper and lower tie plates. The heater rod is heated electrically with chopped cosine power distribution along the axis as shown in Fig. 2.6. The effective heated length is 1880 mm, one half of the active length of a BWR fuel rod. The high power with radial peaking factor of 1.4 was supplied to the fuel assembly "A" and average power was supplied to the other three bundles "B", "C" and "D" with radial peaking factor of 1.0. The heater rods in each assembly are divided into three groups with respect to heat generation rate as shown in Fig. 2.7. The total electric power is limitted as 4.24 MW by limitation of the power supply system. The relative power generation rate of a heater rod in each group is 1.1, 1.0 and 0.875 respectively. The orifice plate with 44 mm I.D. in one assembly is inserted at each core inlet to control the core inlet flow.

The steam line is connected to the steam dome of the pressure vessel. A control valve (CV-130) is installed in the steam line to control the steam dome pressure in steady state before the initiation of the tests and tran-

sient state to simulate both the pressure control system and the safety/relief valve (SRV) operation. The steam line has a branch in which the automatic depressurization system (ADS) is installed. The operation of valves in the steam line is described in Section 4. The feedwater is supplied from the feedwater tank (FWT) through the feedwater line (Fig. 2.8) and the feedwater sparger (Fig.2.9) below the steam separator.

Figure 2.10 shows the recirculation lines consisted of two loops. Each line is furnished with a pump and two jet pumps. The jet pumps are installed outside the pressure vessel to simulate the relative volume and the relative height to the core in addition to simulate the performance. Two break simulators and a quick shut-off valve (QSV) are installed in one of these loops to simulate the various break conditions. Each break simulator consists of nozzle or orifice to determine the break size and a quick opening blowdown valve (QOBV) to initiate the test. The break mode (double-ended or split), the break size and the break location can be changed as the test parameters. The diameter of the largest nozzle and orifice available is 26.2 mm. Figure 2.10 shows two QOBVs, a QSV and flow nozzles installed upstream of the QOBVs. Several flow nozzles and orifices of different size are prepared to vary the break size.

The ROSA-III test facility is furnished with all kinds of the ECCS's available in the BWR system, i.e., the high pressure core spray (HPCS), the low pressure core spray (LPCS), the low pressure coolant injection (LPCI), and the ADS. The HPCS and the LPCS spray the cooling water on the top of the core. The LPCI injects the cooling water into the core bypass. Each ECCS consists of a pump, a tank, piping, and a control system.

The water level in the upper downcomer was measured by a differential pressure transducer and used for the actuations of MSIV and ECCS's. The LPCS and LPCI in the BWR/6 system are designed to actuate by either the high containment pressure signal or the low downcomer level signal (L1) and to inject the water at their design pressure, P=2.16 MPa and 1.57 MPa, respectively. The actuation signal for the LPCS and LPCI for the present tests is represented by the low downcomer level (L1). The ADS and the MSIV were actuated as follows.

LPCS Actuation = (L1 + 40 s) + (P less than 2.16 MPa)
LPCI Actuation = (L1 + 40 s) + (P less than 1.57 MPa)
ADS Actuation = L1 + 120 s
MSIV Closure = L2 + 3 s

3. Instrumentation

The instrumentation of the ROSA-III is designed to obtain thermal-hydraulic data during the simulated BWR LOCA. The data obtained from the experiments will contribute to assess the analytical computer codes for LOCA analyses and to investigate the transient fluid and fuel responses during the simulated LOCA. Table 3.1 summarizes the No.4 instrumentation list used in the present tests. Tables 3.2 and 3.3 show the measurement list and the core instrumentation list, respectively. The signatures of NM, NU and FL in the figure number column of Table 3.2 mean "not measured", "not used" and "failure", respectively. Instrumentation locations are shown in Fig. 3.1 through Fig. 3.6. Typical measured parameters in the ROSA-III are pressure, differential pressure, flow rate, electric power, pump speed, fluid and metal temperatures, collapsed liquid level, two-phase mixture level, fluid density, trip signals and so on.

Pressure and differential pressure transducers are two-wire, direct-current type which convert diaphragm displacement to electric capacitance. The pressure lead pipes are either the standard single, cylindrical pipes used in conjunction with condensate pots, or dual concentric cylinders capable of the circulation of cooling water to prevent flashing of the fluid.

The flow rate is measured by four types of instrumentations, i.e., turbine flow meter, orifice type flow meter, Venturi type flow meter and momentum flux measurement equipment depending on the fluid condition and measuring location. The turbine flow meter is used for subcooled water flow such as ECCS injection flow and feedwater flow. The orifice type flow meter is used for both flows, one is steam line flow including ADS flow and another one is jet pump discharge flow in the broken loop. The Venturi flow meters used for recirculation flows in both loops and jet pump discharge flow in the intact loop. The momentum flux measurement using drag-disk is shown later.

The temperatures of the fluid, structural material and fuel rod cladding are measured with chromel-alumel thermocouples (CA T/C) of 1.6 or 1.0 mmϕ. The thermocouples for fuel rod cladding temperatures are imbedded at the surface of the cladding as shown in Fig. 2.5. There are seven (maximum) thermocouples for one fuel rod along the axial direction.

Liquid levels are measured by either differential pressure transducers,

described above or needle type electrical conductivity probes (CP) developed in the ROSA-III program. The probes are distributed along the vessel height to detect the existence of water or vapor at different levels.

The electric power supplied to the simulated fuel rods is controlled to follow the predetermined power curve with function of time and measured by a fast response electric power meter.

Pump speed is measured by a pulse generator integral of the pump. Trip signals such as selected valve positions and pump coastdown simulation initiations and so on, are detected in order to record the exact actuation times of trip signals.

Fluid density in the pipe is measured by means of gamma densitometers. Preliminary studies indicate that two-beam and three-beam densitometers should be used to determine the flow regime. Figures 3.7 and 3.8 show the beam directions of the three-beam and two-beam gamma densitometers. The gamma-ray source is ^{137}Cs and the detector is a water cooled NaI(Tl) scintillation counter.

Momentum flux is measured by a drag disk as shown in Fig. 3.9. The combination of signals from a drag disk and a gamma densitometer is used to determine the two-phase flow rate as shown in Fig. 3.10.

The data acquisition system (DATAC 2000B, Iwasaki Tsushinki Co.) scans all of signals with the frequency up to 30 Hz. The data recorded on magnetic tape are processed by the FACOM M200 system computer at JAERI by off-line control. After evaluation, for example by comparing the initial and final pressure values with standard values, the data is reprocessed using the correct conversion factors as determined from the consistency examination.

More detailed information on the data processing procedure are available in reference (45).

4. Test Conditions and Procedure

The tests described in the present report simulated the 2% recirculation line split breaks with and without pressure control system (PCS) assuming the HPCS failure. The break orifice with inner diameter of 3.7 mm was installed in the break simulator. The test conditions of RUNs 915 and 920 are the same except for the PCS operation as shown in Table 4.1. The test procedures in each test are summarized in Table 4.2 or Table 4.3. The valve characteristics and control sequences for the steam line valves are shown in Tables 4.4 and 4.5, respectively.

4.1 RUN 915, A 2% Break without Pressure Control System

The measured initial test conditions were; steam dome pressure of 7.30 MPa, total core power of 3.98 MW, core inlet mass flow of 16.5 kg/s, core inlet subcooling of 10.8 K, main steam flow of 2.04 kg/s, feedwater flow of 2.04 kg/s, and pressure vessel water level of 5.0 m. The initial average fluid quality in the upper plenum was estimated as 12.7%. The initial core power corresponds to 44% of the 1/424 scaled BWR/6 rated power. The initial core flow was lowered to establish the same enthalpy distribution in the system as in the BWR rated condition.

RUN 915 was performed by the following procedures as shown in Table 4.2. Break was initiated by quickly opening the QOBV in the break unit B. At the same time, the power supply to both recirculation pumps was terminated and the pump speed coasted down rapidly. After the break, the steady state core power was maintained for 9.0 seconds and then decreased along the power curve shown in Fig. 4.2, which simulated the heat transfer rate to coolant during a hypothetical BWR/LOCA.[46] The steam flow to heat up the feedwater from the third steam line was manually stopped immerdiately after the break by closing the valves CV-1 and CV-2. The feedwater line was closed at the same time of the break.

The MSIV was tripped at 87 s after the break to close by L2 trip level with time delay of 3 s. ADS was actuatedat 235 s after the break by L1 level trip with time delay of 120 s. The LPCS was actuated at 419 s after the break (at 2.3 MPa of the system pressure) and LPCI was actuated at 514 s

after the break (at 1.7 MPa of the system pressure).

The test was performed on June 10, 1981. The experiment data acquisition system started 128 seconds prior to the break initiation and continued up to 897 seconds after the break. Most of the instruments functioned successfully.

4.2 RUN 920, A 2% Break with Pressure Control System

The measured initial test conditions were 7.35 MPa of steam dome pressure, 3.962 MW of total core power, 16.5 kg/s of core inlet mass flow, 10.3 K of core inlet subcooling, 2.08 kg/s of main steam flow, 2.06 kg/s of feedwater flow, and 5.0 m of water level. The initial average fluid quality in the upper plenum was estimated as 12.5%. The initial enthalpy distribution in the system in RUN 920 was similar as that of RUN 915.

RUN 920 was performed by the procedures as shown in Table 4.3. The pressure control system was initiated to operate at the system pressure of 6.6 MPa (24 s after break) and the MSIV was tripped at 29 s after the break. The ADS was tripped at 188 s after the break by the L1 level signal with a time delay of 120 s. The LPCS was actuated at 435 s after break (at 2.3 MPa of the system pressure) and the LPCI was actuated at 531 s after the break (at 1.7 MPa of the system pressure).

The test was performed on August 29, 1981. The experimental data acquisition system was started 121 seconds prior to the break initiation and continued up to 890 seconds after the break. Most of the instrumentation functioned successfully.

5. Data Processing for RUNs 915 and 920

The data acquisition frequency was 10 Hz and 5 Hz in RUNs 915 and 920, respectively. The test data was processed and reduced to 1000 data points in each data channel for computer plotting.

The test data of RUN 915 are shown in Figs. 5.1 through 5.120. In these figures, the measured quantity is identified by the channel number and the alphabetic characters (ref. Table 3.2). The test data of RUN 920 are described after the description of RUN 915 data, in Figs. 5.121 through 5.240. Maximum cladding temperatures including the PCT of RUNs 915 and 920 are shown in Tables 5.1 and 5.2, respectively. Following test data are selected among the all test data for simple but important understandings of the test results.

First the test data of RUN 915 are described below.

Figure 5.1 shows the representative pressure data in the pressur vessel (PV). Figures 5.2 through 5.25 show differential pressure data between various positions in the pressure vessel and the recirculation loops. Figures 5.26 and 5.27 show the liquid levels in the ECCS tanks and downcomer. Figures 5.28 through 5.33 show the flow rates. Figure 5.34 shows the power supplied to the core with the maximum capacities of 2100 and 3150 kW. The pump speed of the recirculation pump is shown in Fig. 5.35. The trip signals such as the break initiation signal and the valve positioning signals are shown in Figs. 5.36 through 5.38. Figures 5.39 through 5.48 show the fluid densities measured by the gamma densitometer. Figures 5.49 and 5.50 show momentum fluxes measured by drag disks. Figures 5.51 through 5.57 show the fluid temperatures at various positions in the system. The fuel rod cladding temperature and the surface temperatures of the water rods and the channel boxes measured at positions 1 through 7 are given in Figs. 5.58 through 5.66. Figures 5.67 through 5.80 show the fuel rod cladding temperatures in a different manner. Figures 5.81 through 5.86 show the fluid temperatures at the outlet of the channel boxes. The liquid level signals in the core, the upper and lower plena, the guide tube and the downcomer are shown in Figs. 5.87 through 5.99.

Quantities obtained from reduction of the test data are shown in Figs.

5.100 through 5.120. Figures 5.100 through 5.103 show the average fluid density calculated from the data shown in Fig. 5.39 through Fig. 5.48. The average density is calculated as an arithmetic mean of the densities in multi-directions with the weight of each cord length.

For the three-beam densitometer at the jet pump outlet spool,

$$\rho_{av} = 0.3221\rho_A + 0.43\rho_B + 0.2479\rho_C \tag{5.1}$$

where,

ρ_{av}: average density obtained from the three-beam gamma densitometer,
ρ_A : density measured by beam A (bottom),
ρ_B : density measured by beam B (middle).
ρ_C : density measured by beam C (top).

For the two-beam densitometer at the break spool piece,

$$\rho_{av} = 0.5863\rho_A + 0.4137\rho_B \tag{5.2}$$

where,

ρ_{av}: average density obtained from the two-beam gamma densitometer,
ρ_A : density measured by beam A (bottom),
ρ_B : density measured by beam B (top).

Figure 5.104 shows total break flow rate measured by low-range drag-disk flow meters and is described after the following paragraphs.

Figures 5.105 through 5.111 show the fluid flow rates at the main steam line, channel inlet orifices and the bypass hole. The fluid flow rates are calculated from the test data which are the pressure drop across the orifices or venturi flow meters and the liquid density obtained from the temperature and the pressure condition. The equation used for the calculation is as follows :

$$G = C_D \cdot A \cdot \sqrt{2g \cdot \rho_l \cdot \Delta P} \tag{5.3}$$

where,

G : flow rate,
ΔP : pressure drop across the orifice,

C_D : discharge coefficient,
= 0.6552 (the orifice to measure the steam discharge flow rate)
= 0.4761 (the channel inlet orifice)
= 0.8032 (the bypass hole)
= 0.7383 (the orifice to measure the jet pump outlet flow rate)
= 1.1260 (the venturi tube to measure the jet pump outlet flow rate)

A : flow area (m^2)
= 2.875×10^{-3} (the orifice to measure the steam discharge flow rate)
= 1.521×10^{-3} (the channel inlet orifice)
= 1.758×10^{-4} (the bypass hole)
= 1.133×10^{-3} (the orifice to measure the jet pump outlet flow rate)
= 9.095×10^{-4} (the venturi tube to measure the jet pump outlet flow rate)

g : gravitational acceleration (= 9.807 m/s^2),

ρ_l : density of the single-phase liquid (kg/m^3),

This calculation method is not applicable for two-phase flow condition after the LPF initiation at the channel inlet orifice, the bypass hole and the jet pump outlet. The calculated value shows only a trend in two-phase flow condition. Total channel inlet flow rate presents the sum of four channel inlet flow rates.

The total break flow (Fig.5.104) is derived from the flow rates in the recirculation loop as follows,

$$G_B = G_P + G_V \tag{5.4}$$

where,

G_B: break flow,

G_P: flow rate at the pump side of the break,

G_V: flow rate st the vessel side of the break,

Figures 5.112 and 5.113 show the collapsed water levels in downcomer and inside the core-shroud, respectively. Each level is obtained from the

corresponding differential pressure. The differential pressure may include the flow resistance effect, however, the flow resistance becomes negligible after slowdown of the recirculation pump coastdown and lower plenum flashing.

Figure 5.114 shows the fluid mass inventory in downcomer. The fluid mass inventory is determined from the density and configurational data outside the core shroud,

$$M = \rho_l \cdot Q \tag{5.5}$$

where,

M : fluid inventory,

ρ_l : liquid density estimated from the satulation temperature and/or pressure,

Q : liquid volume calculated from the liquid level.

The volume Q (m^3) inside the shroud is also given as a function of collapsed water level in downcomer (L),

$$\begin{aligned}
Q &= 0.0 && (\quad L \leqq 0.494) \\
Q &= 0.0225L - 0.0111 && (0.494 < L \leqq 1.384) \\
Q &= 0.0697L - 0.0769 && (1.384 < L \leqq 1.519) \\
Q &= 0.0225L - 0.0048 && (1.519 < L \leqq 3.355) \\
Q &= 0.0801L - 0.1980 && (3.355 < L \leqq 4.250) \\
Q &= 0.2443L - 0.8959 && (4.250 < L \leqq 4.413) \\
Q &= 0.2611L - 0.9700 && (4.413 < L \leqq 4.578) \\
Q &= 0.2504L - 0.9211 && (4.578 < L \leqq 4.654) \\
Q &= 0.2375L - 0.8610 && (4.654 < L \leqq 4.815) \\
Q &= 0.2866L - 1.0974 && (4.815 < L \leqq 4.915) \\
Q &= 0.3396L - 1.3580 && (4.915 < L \leqq 5.143) \\
Q &= 0.3607L - 1.4665 && (5.143 < L \leqq 5.365) \\
Q &= 0.3848L - 1.5960 && (5.365 < L \leqq 5.995) \\
Q &= 0.7111 && (5.995 < L \quad)
\end{aligned} \tag{5.6}$$

Figure 5.115 shows the fluid mass inventory inside core shroud. The fluid mass inventory is determined from the density and configurational data inside the core-shroud,

$$M = \rho_l \cdot Q \tag{5.7}$$

where,

M : fluid inventory,

ρ_l : liquid density estimated from the saturation temperature and/or pressure,

Q : liquid volume calculated from the liquid level.

The volume Q (m^3) inside the shroud is also given as a function of collapsed water level inside core-shroud (L),

$$\begin{aligned}
Q &= 0.0 && (\quad L \leqq 0.0) \\
Q &= 0.2350L && (0.0 < L \leqq 0.497) \\
Q &= 0.1245L + 0.0549 && (0.497 < L \leqq 1.354) \\
Q &= 0.0698L + 0.1290 && (1.354 < L \leqq 3.589) \\
Q &= 0.1648L - 0.2120 && (3.589 < L \leqq 3.744) \\
Q &= 0.1963L - 0.3299 && (3.744 < L \leqq 4.243) \\
Q &= 0.0196L + 0.4199 && (4.243 < L \leqq 4.578) \\
Q &= 0.0186L + 0.4244 && (4.578 < L \leqq 4.654) \\
Q &= 0.0410L + 0.3201 && (4.654 < L \leqq 5.099) \\
Q &= 0.0196L + 0.4292 && (5.099 < L \leqq 5.365) \\
Q &= 0.5344 && (5.365 < L \quad)
\end{aligned} \tag{5.8}$$

Figure 5.116 shows a total fluid inventory in PV, which is a sun of fluid mass in downcomer (see Fig. 5.114) and inside core-shroud (see Fig. 5.115).

Figure 5.117 compares the collapsed water levels measured by by the corresponding differential pressure data in PV (see Figs. 5.27, 5.112 and 5.113). Figure 5.118 shows the mixture responses in PV obtained from the conductivity probe signals (see Figs. 5.87 through 5.99). Figures 5.119 and 120 show the dryout and quenching times of the fuel rods in the high-power bundle (A) and four bundles, respectively.

The test data of RUN 920 are presented in Figs. 5.121 through 5.240 in the similar order as RUN 915.

Figures 5.121 shows the pressure data in PV. Figures 5.122 through 5.145 show differential pressure data between various positions in the pressure vessel and recirculation loops. Figures 5.146 and 5.147 show the liquid levels in the ECCS tanks and downcomer. Figures 5.148 through 5.153 show the flow rates. Figure 5.154 shows the power supplied to the core with the maximum capacities of 2100 and 3150 kW. The pump speed of the recirculation pump is shown in Fig. 5.155. The trip signals such as the break initiation signal and the valve positioning signals are shown in Figs. 5.156 through 5.158. Figures 5.159 through 5.168 show the fluid densities measured by the gamma densitometers. Figures 5.169 through 5.172 show momentum fluxes measured by the drag-disks. Figures 5.173 through 5.177 show the fluid temperatures at various positions in the system. The fuel rod cladding temperatures and the surface temperatures of the water rods and the channel boxes are given in the Figs. 5.178 through 5.186. Figures 5.187 through 5.200 show the fuel rod cladding temperatures in a different manner. Figures 5.201 through 5.206 show the fluid temperatures at the inlet and outlet of the channel boxes. The liquid level signals in the core, the upper and lower plena, the guide tube and the downcomer are shown in Figs. 5.207 through 5.219.

Quantities obtained from reduction of the test data in RUN 920 are shown in Figs. 5.220 through 5.240.

Figures 5.220 through 5.223 show the average fluid density calculated from the data shown in Figs. 5.159 through 5.168. Figure 5.224 shows the break flow rate measured by the low range drag-disk flow meters in the main recirculation loop. Figures 5.225 through 5.231 show the fluid flow rates at the main steam line, channel inlet orifices and the bypass hole. The fluid flow rates are calculated like as the calculation of RUN 915. Total channel inlet flow rate presents the sum of four channel inlet flow rates.

Figures 5.232 and 5.233 show the collapsed water levels in downcomer and inside the core shroud, respectively. Each level is obtained from the corresponding differential pressure data. The differential pressure may include the flow resistance effect, however, the flow resistance becomes negligible after slowdown of the recirculation flow and lower plenum flash-

ing.

Figures 5.234 and 5.235 show the fluid mass inventories in the pressure vessel. The fluid mass inventory was determined from the fluid density and configurational data inside and outside the core-shroud, like as the data of RUN 915. Total fluid inventory (Fig. 5.236) is a sun of these two mass inventories.

Figure 5.237 compares the collapsed water levels measured by the corresponding differential pressure data in PV (see Figs. 5.147, 5.232 and 5.233). Figure 5.238 shows mixture levles shown in Figs. 5.207 through 5.219. Figures 5.239 and 5.240 show the dryout and quenching times of the fuel rods in the high-power bundle (A) and four bundles, respectively.

6. Test Results of RUNs 915 and 920

6.1 Major Events of RUN 915

Characteristic features of the 2% break test, RUN 915, are presented. There were four characteristic phases in RUN 915, i.e., first depressurization after the break, pressurization after the MSIV closure, second depressurization after the ADS opening, and mass recovery phase after the LPCS actuation. Some characteristic phenomena were observed in these four phases as shown later. The pressure response related with the major events, water level, mass inventory and core thermal responses are presented below.

(1) Pressure Response and Major Events

The system pressure responses (see Fig. 5.1) began to decrease at 9 s after the break due to the core power decrease and reached the saturation pressure of the lower plenum fluid (6.4 MPa) at 25 s after the break. Thereafter bulk flashing continued in the all system until the MSIV closure at 87 s after the break. The MSIV closure was tripped by the low downcomer level (L2) with time delay of 3 s at the system pressure of 4.4 MPa. The pressurization after the MSIV closure rapidly collapsed steam void in the system and changed the differential pressures (Figs. 5.3, 5.10 through 5.19), water levels (Fig. 5.27) and fluid density (Figs. 5.39 through 5.48).

The downcomer water levels of L2 and L1 were tripped at 84 s and 115 s, respectively. The ADS was actuated at 235 s after the break due to the L1 trip level with time delay of 120 s. The bulk flashing in the all system began to initiate again at 254 s after the break (at system pressure of 4.7 MPa) and caused slower depressurization as shown in the pressure response. Void formation was observed again in the differential pressure data and fluid density data.

The LPCS and LPCI were actuated at 419 s and 514 s after the break respectively as shown in Fig. 5.28. Thereafter the system mass inventory (see Figs. 5.114 through 5.116) recovered rapidly.

(2) Water Levels and Mass Inventory

Water levels in PV are shown in Figs. 5.27, 5.112 and 5.113. These are

compared in Fig. 6.1. In the first depressurizing phase from break initiation to MSIV closure time, the whole downcomer collapsed level and of course, the upper downcomer water level were higher than the colalpsed water level inside core-shroud. This relation between the collapsed water levels across the core-shroud was reversed during 40 s in the pressurization phase after the MSIV closure. This reverse accompanied water mass transfer from the downcomer to the core. And the whole downcomer collapsed level became higher again than the collapsed water level inside core-shroud in the second depressurization phase after the ADS actuation. These changes were caused by the change of pressure balance in PV, i.e., changes of the void distribution in each region and pressure loss of uprising two-phase flow inside the core-shroud.

The total fluid mass in RUN 915 (see Fig. 5.116) shows a very low value before the MSIV closure time and therefore it seems as if the total fluid mass increased after the MSIV closure. However, there was no mass increase after the MSIV closure but a continuing mass discharge through the break unit in the main recirculation line. The under-estimation of total fluid mass was caused by an under-estimation of upper downcomer fluid mass as shown below. There is an abrupt change of downcomer flow area at the elevation of 4.25 m. The whole downcomer collapsed level was lower than 4.25 m before the MSIV trip time at 87 s. The upper downcomer water level, however, was higher enough than 4.25 m as shwon in Fig. 6.1. An under-estimated fluid mass in the downcomer region was calculated roughly from the level difference between the two water levels in Fig. 6.1. At the time of MSIV trip, the upper downcomer and whole eowncomer water levels were 4.77 m and 3.85 m, respectively. The fluid volume between these two levels is approximately 0.175 $m^{(3)}$. By using the saturation water density at 4.4 MPa (790 $kg/m^{(3)}$, the under-estimated mass is obtained as 138 kg. This value is sufficient to recover the under-estimated mass in the total fluid mass before the MSIV closure time (see Fig. 6.1). Therefore, the total fluid mass in Fig. 6.1 can be corrected by the upper downcomer water mass in the first depressurization phase. In the second depressurization phase, there was no such under-estimation.

The pressurization due to MSIV closure collapsed the void completely in the system except for the core region as shown in the conduction probe signals (see Figs. 5.95 through 5.99). The upper downcomer level and the whole downcomer collapsed level agreed at 100 s after the break as shown in Fig. 6.1 (4.6 m). On the other hand, the collapsed water level inside

core-shroud was 2.6 m at 100 s after the break. Thus, a water level difference across the core-shroud became 2.0 m at 100 s after the break. This difference of water head was a motive force of water mass transfer from the downcomer region to core region. Therefore, the collapsed level inside core-shroud increased and the downcomer water level decreased simultaneously in the pressurization phase.

The initial PV fluid mass was calculated by RELAP5/MOD1 code as 579 kg as shown in the reference (37). An error is included in the initial state and also in the flashing state. The lowest PV mass was 35% of the initial value.

(3) Core Thermal Responses

The fuel rod surface temperature responses are strongly related with the mixture level responses in the core as shown in Figs. 5.117 through 5.120.

In the pressurization phase after the MSIV closure, a temporary fuel rod temperature increase was observed in the upper core region (Figs. 5.58 through 5.80). This temperature increase was caused by the core mixture level decrease or mixture level collapse due to void diminishing. The PV total fluid inventory at this first dryout was 420 kg (72% of the initial value). The void diminishing behaviors are shown clearly in the liquid level signals in the core (see Figs. 5.88 through 5.90). Namely, the conduction proves in the upper core region detected steam condition for 20 or 30 seconds after the MSIV closure, whereas those in the lower core region detected constant water signals or small void fraction signals in the pressurization phase. The core mixture level recovery, which was caused by a mass transfer from the downcomer region diminished the temporary fuel rod dryout in the upper core region.

The second fuel rod dryout was observed at the end of pressurization phase in the top core region (positions 1, 2) due to decrease of fluid inventory. However, these dryout were diminished again by the mixture level small caused by the ADS actuation at 235 s.

The third fuel rod dryout initiated at 270 s after the break due to the mixture level decrease from top to bottom of the core. The PV total mass was 285 kg at this time (49% of the initial PV mass).

After the LPCS actuation, the fuel rod were rapidly quenched. In the quenching process, two quench patterns were observed. One was the top down quench due to the fall back water (see Figs. 5.58 and 5.65). Another one

was the bottom up quench observed in the lower core region (see Figs. 5.59, 5.61, 5.62). Thus the quenching times of fuel rods had large distribution in the core.

It is shown from these data that these core thermal responses the dryout and quenching phenomena are observed above the core mixture level and also above the collapsed water level inside core-shroud.

The PCT was observed at 518 s (in the third dryout phase) as 811 K at position 4 of A 68 rod in the high-power bundle.

6.2 Major Events of RUN 920

Characteristic features of the 2% main recirculation line break test, RUN 920, with the pressrue control system (PCS) operation are presented below as in the previous section.

(1) Pressure Response and Major Events

Figure 5.121 shows representative pressure response of RUN 920. The system pressure began to decrease at 9 s after the break due to the core power decrease. The PCS operation was initiated at 24 s after the break at the system pressure of 6.6 MPa and kept constantly the system pressure.

The MSIV closure was tripped at 29 s by the L2 level with time delay of 3 s. Thus the L2 level was tripped 2 s after PCS operation in RUN 920. Thereafter the system was pressurized. The safety/relief valve (SRV) was actuated at 71 s after the break in order to prevent the overpressure of system above 8.16 MPa. The SRV operation was continued until the ADS actuation at 188 s after the break, which was tripped by L1 level signal with time delay of 120 s. Thus the L1 level trip was sent at 68 s after the break.

The system pressure began to decrease rapidly after the ADS actuation. The bulk flashing was initiated at 197 s after the break. The fluid in the lower plenum and recirculation loops initiated flashing with some time delay as shown in the differential pressure data (Figs. 5.130 through 5.139) and fluid density (Figs. 5.159 through 5.168). The delayed flahsing in the lower plenum and loops was due to existence of lower temperature fluid (see Figs. 5.173 through 5.177). The main reason of the fluid temperature

distribution below the initial lower plenum temperature is a large heat loss (150 KW in the initial state [38]) through the pressre boundary.

The LPCS and LPCI were actuated at 435 s, 531 s after the break, respectively.

(2) Water Levels and Mass Inventory

Figure 6.2 compares the upper downcomer water level (Fig. 5.147), the whole downcomer collapsed level (Fig. 5.232) and the collapsed water level inside core-shroud (Fig. 5.233). It is shown that the downcomer water level was kept lower than the collapsed water level inside core-shroud before the ADS actuation. However, the ADS actuation reversed this level relation as in RUN 915. The main reasons of this level reversal are (1) the change of void distribution both in the dowcomer and recirculation loops, and inside core shroud and (2) increased pressure loss of uprising two phase flow across the steam separator.

The PV total mass inventory in RUN 920 is shown in Fig. 5.236. The lowest mass was 38% of the initial value[37] at the time of LPCS actuationl.

(3) Core Thermal Response

All of the fuel rods showed the similar temperature increase in the mixture level decreasing phase after the ADS actuation (see Figs. 5.238 through 5.240). The top part of the fuel rod showed dryout at the PV fluid mass of 305 kg (53% of the initial mass). The dryout times of the top and bottom of the core were 280 s and 420 s after the break, respectively.

After the LPCS actuation, two types of quenching were observed, i.e., top-down quenching and bottom-up quenching. All the fuel rods were quenched within 119 s from the LPCS actuation (23 s from the LPCI actutation). These dryout and quench responses are strongly related with the core mixture level responses and also with the collapsed water level inside core-shroud.

The peak cladding temperature (PCT) was observed at 530 s after the break as 801 K at position 4 of the A 68 rod in the high-power bundle.

6.3 Effects of Pressure Control System

The effects of pressure control system (PCS) on the 2% small MRLB LCOA

are shown below. Figures 6.3 through 6.19 compare the test results of system pressure, downcomer water level, steam flow, ECCS flow, collapsed water levels in PV, total mass inventory in PV and fuel rod surface temperatures between the two tests of RUNs 915 and 920.

The PCS operation directly affected the system pressure response as shown in Fig. 6.3. Namely, the system pressure did not decrease lower than the saturation pressure of the lower plenum fluid (6.4 MPa) by actuation of PCS operation at 24 s after the break in RUN 920. And the L2 level signal for the MSIV closure was actuated 2 s after the PCS operation. On the other hand, the system pressure of RUN 915 decreased continuously after the break and caused bulk flashing at 25 s after the break. This flashing in the downcomer immediately increased the mixture level and resulted in increase of the upper downcomer collapsed water level, which was measured by a differential pressure transducer between EL 3.90 m to EL 6.04 m (top of PV). Therefore, the L2 level signal in RUN 915 was not sent at 26 s after the break (like as RUN 920) but sent at 84 s after the break (see Fig. 6.4). It is concluded that the bulk flashing initiation just before the L2 level trip is the main reason of continuous depressurization in RUN 915. The PCS directly affected this bulk flashing in RUN 920 and caused early L2 level trip for MSIV closure.

The bulk flashing in the first depressurization phase and the pressurization after the MSIV closure in RUN 915 caused large changes in void distribution and pressure balance in the system and resulting mass transfer between the downcomer and core as shown in Section 6.1. However, the PCS actuation in RUN 920 did not cause this change from void formation to void diminishing. Difference of fuel rod surface temperature responses (Figs. 6.12 through 6.19) before the ADS actuation time between the two tests was caused by the condition with or without PCS operation.

The pressure responses of both tests became close after the ADS actuation as shown in Fig. 6.3. Especially, the pressure responses after the bulk flashing initiation in both tests (254 s after the break) became quite the same within 10 s difference. This resulted in similar actuations of LPCS and LPCI between the two tests (see Figs. 6.7 and 6.8).

The main reason of the similar pressure resonses after the ADS actuation in both tests is the similar total mass inventory in the system. The collapsed levels in PV (Figs. 6.9 and 6.10) and PV total fluid mass (Fig. 6.11) of RUN 920 were close to those of RUN 915. The difference of PV fluid mass at 254 s after the break between the two tests was approximately 23 kg

(only 7% of the remaining PV mass in RUN 920). The similar responses of PV total fluid mass and the similar actuations of LPCS and LPCI in both tests resulted in similar core thermal responses after the bulk flashing as shown in Figs. 6.12 through 6.19. The PCTs of both tests were observed at the same region (position 4 of A 68 rod), and were 811 K in RUN 915 and 801 K in RUN 920. Slightly earlier dryout initiation and slightly higher PCT in RUN 915 were the result of the slightly lower mass inventory than in RUN 920.

The main reason of similar PV fluid mass at the ADS actuation time in both tests is that the excess discharged steam mass in RUN 915 before the MSIV closure was approximately compensated by the steam mass discharged through the SRV and earlier ADS actuation in RUN 920 (see Figs. 6.5 and 6.6). Also the difference in the break flow rates between the two tests contributed to the similar responses of PV mass inventory. PV total mass inventory estimated from the collapsed water levels in PV showed consistent responses with the pressure transient and core thermal responses in both tests.

7. Conclusions

Two 2% main recirculation line break (MRLB) LOCA tests, RUNs 915 and 920, were performed in the ROSA-III program to clarify the effects of pressure control system (PCS) on the small LOCA phenomena. The two tests were performed successfully. Major conclusions obtained are as follows.

(1) The PCS operation at 6.7 MPa suppresses bulk flashing of coolant in the early blowdown phase and contributes to early closure of the MSIV. Therefore, the flashing does not initiate until the ADS opening. It contributes to improve the core cooling condition in the early blowdown phase, when the linear heat generation rate is high.

(2) In the case of PCS operation failure, the bulk flashing initiates at 6.4 MPa and causes the consequent upper downcomer water level rise, which delays the level trip signals of L2 for the MSIV closure, and L1 for the ADS actuation. The delayed MSIV closure diminishes steam void in the core and causes a temporary fuel rod dryout in the upper half core. The pressurization also collapses the downcomer void and causes larger water head in downcomer than inside core-shroud, which transfers the downcomer water into the core region.

(3) The ADS actuation has a controlling influence on the transient system responses in a small break LOCA and the peak cladding temperature (PCT) occurrs after the ADS actuation. As the ADS actuates earlier in the PCS operation case, the system fluid mass decreases earlier than the PCS failure case. The similar system fluid mass inventory after the ADS actuation time results in the similar core thermal response in both tests. The PCT in the PCS operation case is 10 K lower than the PCS failure case.

(4) Following relations are commonly observed in both tests.

(A) The downcomer water level is kept higher than the collapsed water level inside core-shroud in the depressurization phase. The pressurization due to the MSIV closure changes the pressure balance in PV and establishes a new balanced state, which shows a reverese level

relation of lower downcomer level than core-shroud level.

(B) The core dryout and quench phenomena are strongly related with the core mixture level responses, and also with the collapsed water level inside core-shroud in the two tests. The dryout and quench fronts are observed above the core mixture level after the ADS actuation. However, a wide distribution of dryout and quench times is observed in each fuel bundle.

Acknowledgment

The authors are grateful to H. MURATA of Reactor Safety Laboratory I of JAERI for his large contribution to conduct the test, H. ASAHI, T. ODAIRA, T. TAKAYASU, Y. KITANO and T. NUMATA of Nuclear Engineering Corporation for their assistance in conducting the experiment, K. HAKUTA of Information System Laboratory Corporation for preparing the data plots and M. KIKUCHI of Nihon Computer Bureau for type writing the manuscript.

References

(1) K.TASAKA, et al., "Study on the Similarity between ROSA-III Experiment and BWR LOCA", JAERI-M 6703 (1976) (in Japanese).

(2) Y.ANODA, et al.,"ROSA-III System Description for Fuel Assembly No. 4", JAERI-M 9363 (1981) (in Japanese).

(3) General Electric Company, "General Electric Standard Safety Analysis Report, BWR/6", DOCKET-STN-50477 (1978).

(4) K.TASAKA, et al.,"ROSA-III Base Test Series for a Large Break Loss of Coolant Accident in a Boiling Water Reactor", Nucl. Technol. 57, 179-191 (1982).

(5) K.SODA, et al.,"Boiling Water Reactor Loss of Coolant Test (Single Failure Test with ROSA-III)", J. Nucl. Sci. Technol. 20, 89-104 (1983).

(6) K.TASAKA, et al.,"Simulation Experiment of Five Percent Small Break

relation of lower downcomer level than core-shroud level.

(B) The core dryout and quench phenomena are strongly related with the core mixture level responses, and also with the collapsed water level inside core-shroud in the two tests. The dryout and quench fronts are observed above the core mixture level after the ADS actuation. However, a wide distribution of dryout and quench times is observed in each fuel bundle.

Acknowledgment

The authors are grateful to H. MURATA of Reactor Safety Laboratory I of JAERI for his large contribution to conduct the test, H. ASAHI, T. ODAIRA, T. TAKAYASU, Y. KITANO and T. NUMATA of Nuclear Engineering Corporation for their assistance in conducting the experiment, K. HAKUTA of Information System Laboratory Corporation for preparing the data plots and M. KIKUCHI of Nihon Computer Bureau for type writing the manuscript.

References

(1) K.TASAKA, et al., "Study on the Similarity between ROSA-III Experiment and BWR LOCA", JAERI-M 6703 (1976) (in Japanese).

(2) Y.ANODA, et al.,"ROSA-III System Description for Fuel Assembly No. 4", JAERI-M 9363 (1981) (in Japanese).

(3) General Electric Company, "General Electric Standard Safety Analysis Report, BWR/6", DOCKET-STN-50477 (1978).

(4) K.TASAKA, et al.,"ROSA-III Base Test Series for a Large Break Loss of Coolant Accident in a Boiling Water Reactor", Nucl. Technol. 57, 179-191 (1982).

(5) K.SODA, et al.,"Boiling Water Reactor Loss of Coolant Test (Single Failure Test with ROSA-III)", J. Nucl. Sci. Technol. 20, 89-104 (1983).

(6) K.TASAKA, et al.,"Simulation Experiment of Five Percent Small Break

relation of lower downcomer level than core-shroud level.

(B) The core dryout and quench phenomena are strongly related with the core mixture level responses, and also with the collapsed water level inside core-shroud in the two tests. The dryout and quench fronts are observed above the core mixture level after the ADS actuation. However, a wide distribution of dryout and quench times is observed in each fuel bundle.

Acknowledgment

The authors are grateful to H. MURATA of Reactor Safety Laboratory I of JAERI for his large contribution to conduct the test, H. ASAHI, T. ODAIRA, T. TAKAYASU, Y. KITANO and T. NUMATA of Nuclear Engineering Corporation for their assistance in conducting the experiment, K. HAKUTA of Information System Laboratory Corporation for preparing the data plots and M. KIKUCHI of Nihon Computer Bureau for type writing the manuscript.

References

(1) K.TASAKA, et al., "Study on the Similarity between ROSA-III Experiment and BWR LOCA", JAERI-M 6703 (1976) (in Japanese).

(2) Y.ANODA, et al.,"ROSA-III System Description for Fuel Assembly No. 4", JAERI-M 9363 (1981) (in Japanese).

(3) General Electric Company, "General Electric Standard Safety Analysis Report, BWR/6", DOCKET-STN-50477 (1978).

(4) K.TASAKA, et al.,"ROSA-III Base Test Series for a Large Break Loss of Coolant Accident in a Boiling Water Reactor", Nucl. Technol. 57, 179-191 (1982).

(5) K.SODA, et al.,"Boiling Water Reactor Loss of Coolant Test (Single Failure Test with ROSA-III)", J. Nucl. Sci. Technol. 20, 89-104 (1983).

(6) K.TASAKA, et al.,"Simulation Experiment of Five Percent Small Break

LOCA of BWR", J. Nucl. Sci. Technol. 20, 89-104 (1983).

(7) K.TASAKA, et al.,"ROSA-III Double-Ended Break Test Series for a Loss-of-Coolant Accident in a Boiling Water Reactor", Nucl. Technol. 68, 77-93 (1985).

(8) M.SUZUKI, et al.,"Recirculation Pump Discharge Line Break Tests at ROSA-III for a Boiling Water Reactor", Nucl. Technol., 70, 189-203 (1985).

(9) Y.KOIZUMI, et al., "Experimental Analysis of Power Curve Sensitivity Test Series at ROSA-III", Nucl. Eng. and Design 86 267-287, (1985).

(10) H.KUMAMARU, et al.,"Five Percent Break BWR LOCA/ECC Test at ROSA-III without HPCS Actuation---Two Dimensional Core Thermal Hydraulic Phenomena", Nucl. Eng. and Design 86, 219-239 (1985).

(11) K.TASAKA, et al.,"Analysis of ROSA-III Break Area Spectrum Experiments on BWR Loss-of-Coolant Accident", Nucl. Technol. 71, 3, 628-643 (1985).

(12) T.YONOMOTO, et al.,"Investigation of BWR/LOCA at ROSA-III---Effect of Break Configuration on System Transient---", Nucl. Eng. and Design 92, 198-205 (1986).

(13) M.SUZUKI, et al., "Similarity Study of Large Steam Line Break LOCAs in ROSA-III, FIST and BWR/6", Nucl. Eng. and Design 98, 1, 39-56 (1987).

(14) M.SOBAJIMA, et al.,"Experiment Test Data of ROSA-III Test RUN 701 (Decay Heat Simulation Test with ECCS Actuation)", JAERI-M 8604 (1979).

(15) Y.ANODA et al.,"Experiment Data of ROSA-III Test RUN 703 (Split Break Simulation Test with ECCS Actuation)", JAERI-M 8967 (1980).

(16) Y.ANODA et al.,"Experiment Data of ROSA-III Test RUN 704 (Standard Test with ECCS Actuation)", JAERI-M 8968 (1980).

(17) M.OKAZAKI et al.,"Experimet Test Data of ROSA-III Integral Test RUN 705 (Isothermal Blowdown Test without ECCS Actuation)", JAERI-M 8723 (1980).

(18) M.SUZUKI et al.,"Experiment Data of ROSA-III Integral Test, RUN 706", JAERI-M 8737 (1980).

(19) M.OKAZAKI et al.,"Experiment Data of ROSA-III Integral Test RUN 708 (Standard Test without ECCS Actuation)", JAERI-M 8738 (1980).

(20) Y.KOIZUMI et al.,"Experiment Data of ROSA-III Integral Test, RUN 710", JAERI-M 9249 (1981).

(21) Y.ANODA et al.,"Experimet Data of ROSA-III Integral Test RUN912 (5% Split Break Test without HPCS Actuation)", JAERI-M 82-010.

(22) H.NAKAMURA et al.,"Experiment Data of ROSA-III Integral Test RUN 901 (200% Double-Ended Break with Full ECCS Actuation)", JAERI-M 84-007.

(23) H.NAKAMURA et al.,"Experiment Data of ROSA-III Integral Test RUN 926 (200% Double-Ended Break with HPCS Failure)", JAERI-M 84-008.

(24) M.SUZUKI et al.,"Experiment Data of 200% Recirculation Pump Discharge Line Break Integral Test RUN 961 with HPCS Failure at ROSA-III and Comparison with Results of Suction Line Break Tests", JAERI-M 84-045, (1984).

(25) M.SUZUKI, et al.,"Recirculation Pump Suction Line 2.8% Break Integral Test at ROSA-III with HPCS Failure, RUN 984", JAERI-M 84-100, (1984).

(26) M.SUZUKI, et al.,"Recirculation Pump Suction Line 200% Break Integral Test at ROSA-III with Two LPCI Failures, RUN 983", JAERI-M 84-135, (1984).

(27) M.KAWAJI, et al.,"A Main Steam Line Break Experiment at ROSA-III RUN 952 (Standard Run with Full ECCS)", JAERI-M 84-229, (1984).

(28) M.KAWAJI, et al.,"A Main Steam Line Break Experiment at ROSA-III, RUN 953 (100% Break with an HPCS Failure)", JAERI-M 85-029 (1985).

(29) M.SUZUKI, et al.,"BWR Recirculation Loop Discharge Line Break LOCA Tests with Break Areas of 50 and 100% Assuming HPCS Failure at ROSA-III Facility", JAERI-M 85-037, (1985).

(30) T.YONOMOTO, et al.,"ROSA-III 50% Break Integral Test RUN 916 (Break Area Parameter Test)", JAERI-M 85-109, (1985).

(31) H.NAKAMURA, et al.,"Recirculation Pump Suction Line 5% Split Break Test of ROSA-III (RUNs 922 and 923 with HPCS Failure)", JAERI-M 85-128, (1985).

(32) T. YONOMOTO, et al.,"ROSA-III 50% Break Integral Test RUN 928 (Break Configuration Sensivity Test)", JAERI-M 85-151, (1985).

(33) M. SUZUKI, et al.,"BWR Main Steam Line Break LOCA Tests RUNs 951, 954 and 956 at ROSA-III (Break Area Effects with HPCS Failure)", JEARI-M 85-202, (1985).

(34) H. NAKAMURA, et al.,"Recircualtion Pump Suction Line 1% Spilit Break LOCA Test of ROSA-III (RUNs 921 and 931 with HPCS Failure)", JAERI-M 85-209, (1986).

(35) K.TASAKA, et al.,"Comparison of ROSA-III and FIST BWR Loss of Coolant Accident Simulation Tests", JAERI-M 85-158 (1985).

(36) M.SUZUKI, et al., "BWR 200% Recirculation Pump Suction Line Break LOCA Tests, RUNs 942 and 943 at ROSA-III without HPCS (Effects of Initial Fluid Conditions on LOCA)", JAERI-M 86-038 (1986).

(37) M.SUZUKI, et al., "BWR LOCA Integral Test Simulating a 100% Main Steam Line Break outside Reactor Containment Vessel in ROSA-III Program, RUN

955 (Analogy of Steam and Recirculation Line Small Break LOCAs)", JAERI-M to be published (1987).

(38) M.SUZUKI, et al.,"Heat Loss and Fluid Leakage Tests of the ROSA-III Facility", JAERI-M 9834 (1981).

(39) M.SUZUKI, et al.,"Characteristics of the ROSA-III Test Facility (Characteristics Test of the Jet Pumps in Normal and Reverse Flow)", JAERI-M 8670, (1980) (in Japanese).

(40) M.SUZUKI, et al.,"Evaluation of a Jet Pump Model for RELAP5 Code", JAERI-M 84-245, (1985) (in Japanese).

(41) W. J. Letzring, et al.,"BWR Blowdown/ECC Program Preliminary Facility Description Report for the BD/ECC1a Test Phase", GEAP-23592.

(42) GE, EPRI and NRC,"Full Integral Simulation Test (FIST) Program Test Plan", EPRI NP-2313, GEAP 22053, (1981).

(43) M.MURASE et al.,"BWR Loss-of-Coolant Integral Test -- Parallel Channel Effect", NUREG/CP-0027-Vol.3, (1982).

(44) H.KUMAMARU, et al.,"Investigation of Effect of Pressure Control System on BWR LOCA Phenomena using ROSA-III Facility", J. Nucl. Sci. and Technol., to be published.

(45) M.SOBAJIMA et al.,"Instrumentation and Data Processing Method of the ROSA-III Test", JAERI-M 8499 (1979) (in Japanese).

(46) N.ABE et al.,"Electric Power Tansient Curve for ROSA-III Tests", JAERI-M 8728 (1980).

Table 2.1 Primary chracteristics of ROSA-III and BWR/6

	BWR-6	ROSA-III	BWR/ROSA
No. of Recirc. Loops	2	2	1
No. of Jet Pumps	24	4	6
No. of Separators	251	1	251
No. of Fuel Assemblies	848	4	212
Active Fuel Length (m)	3.76	1.88	2
Total Volume (m^3)	621	1.42	437
Power (MW)	3800	4.40	864
Pressure (MPa)	7.23	7.23	1
Core Flow (kg/s)	1.54×10^4	36.4	424
Recirculation Flow (l/s)	2970	7.01	424
Feedwater Flow (kg/s)	2060	4.86	424
Feedwater Temp (K)	489	489	1

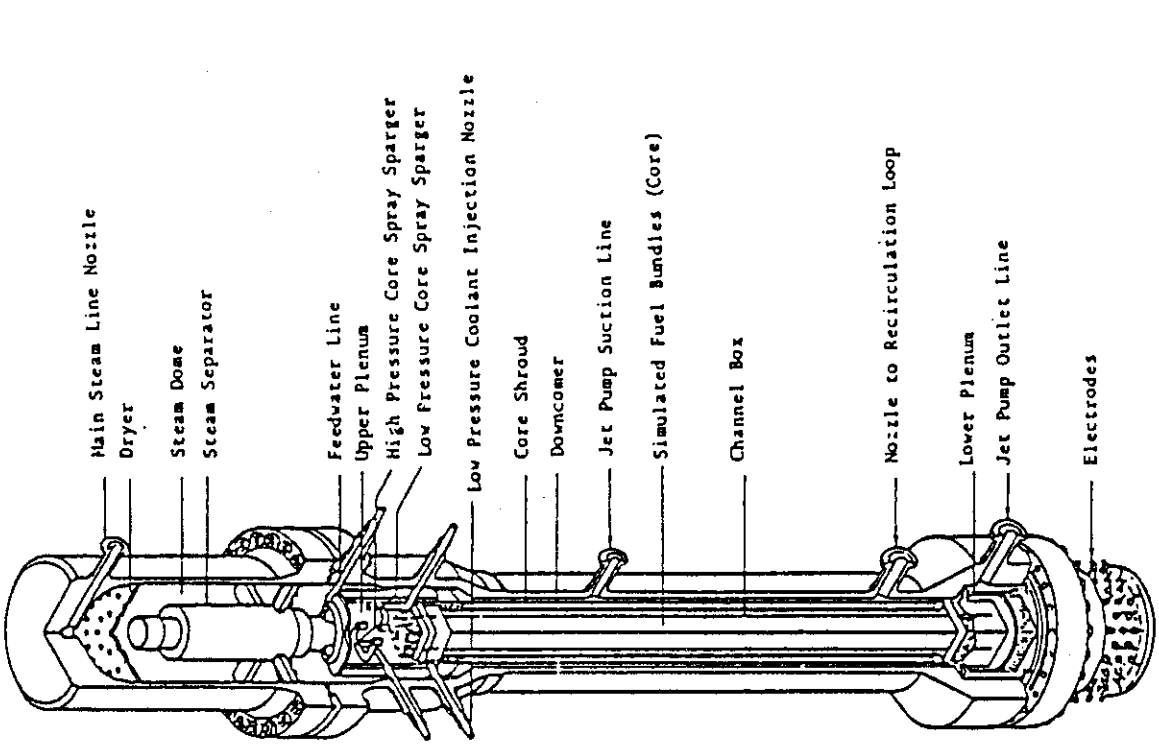

Fig.2.2 Internal structure of the pressure vessel of ROSA-III

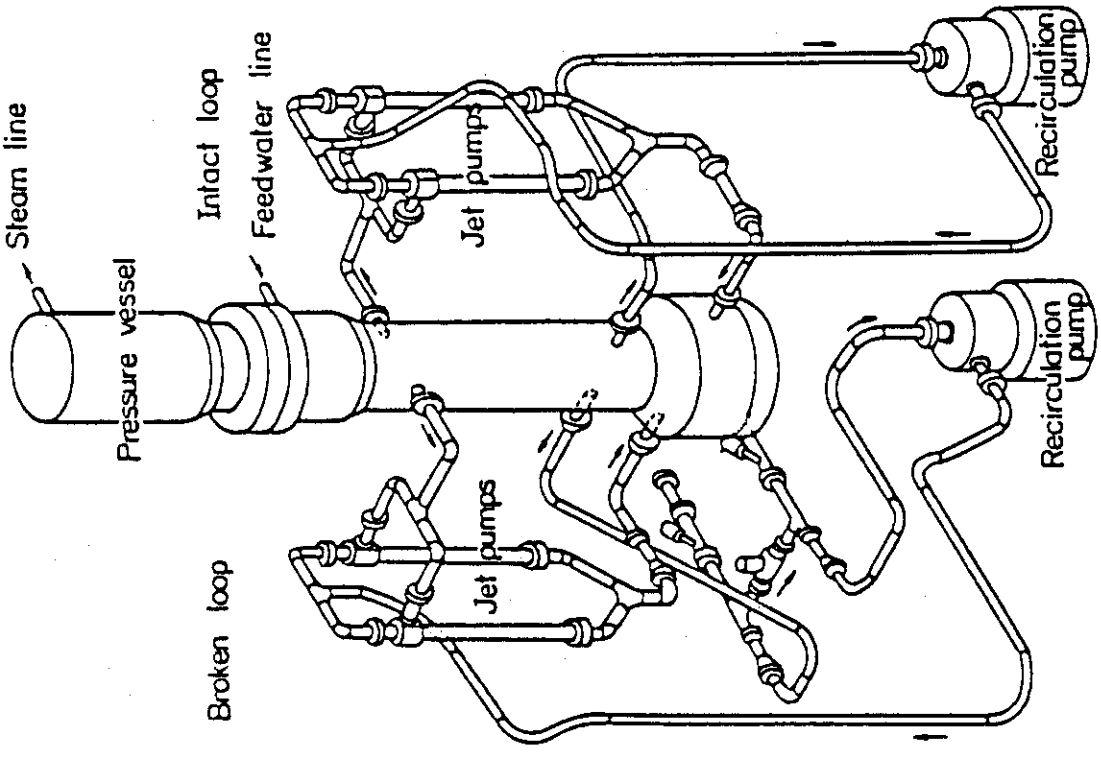

Fig.2.1 Schematic diagram of ROSA-III Test Facility

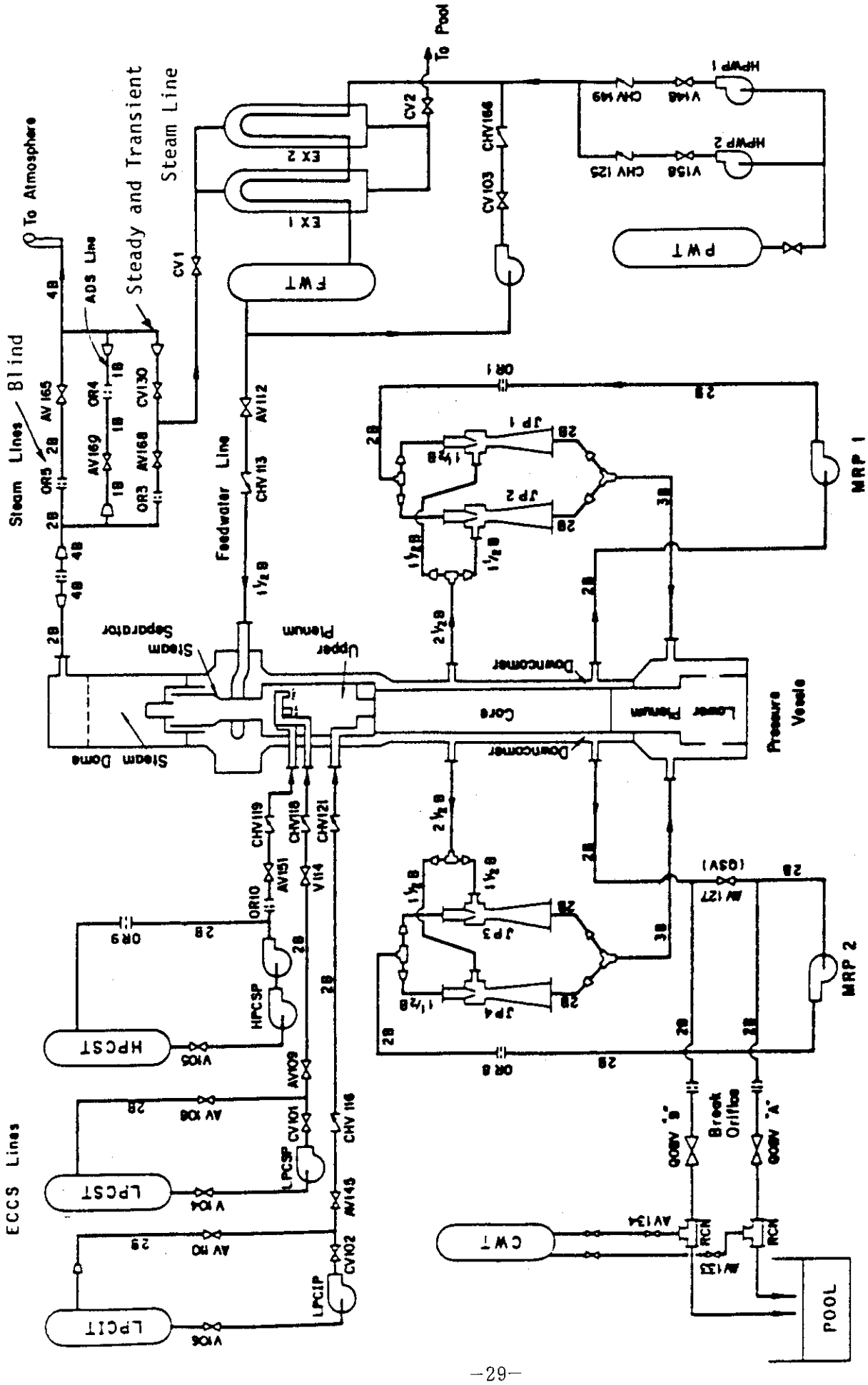

Fig. 2.3 ROSA-III piping schematic

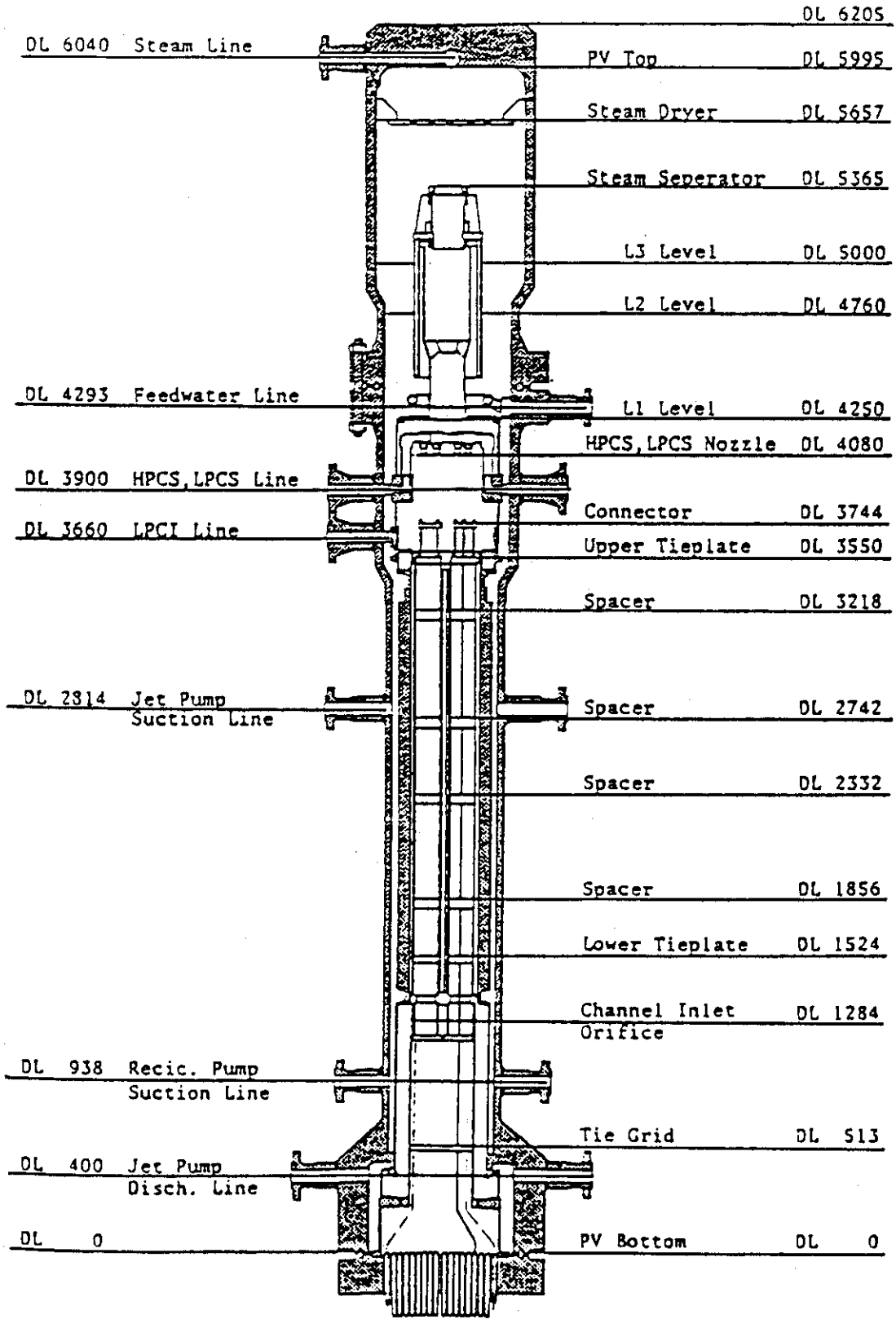

Fig. 2.4 Pressure vessel internals arrangement

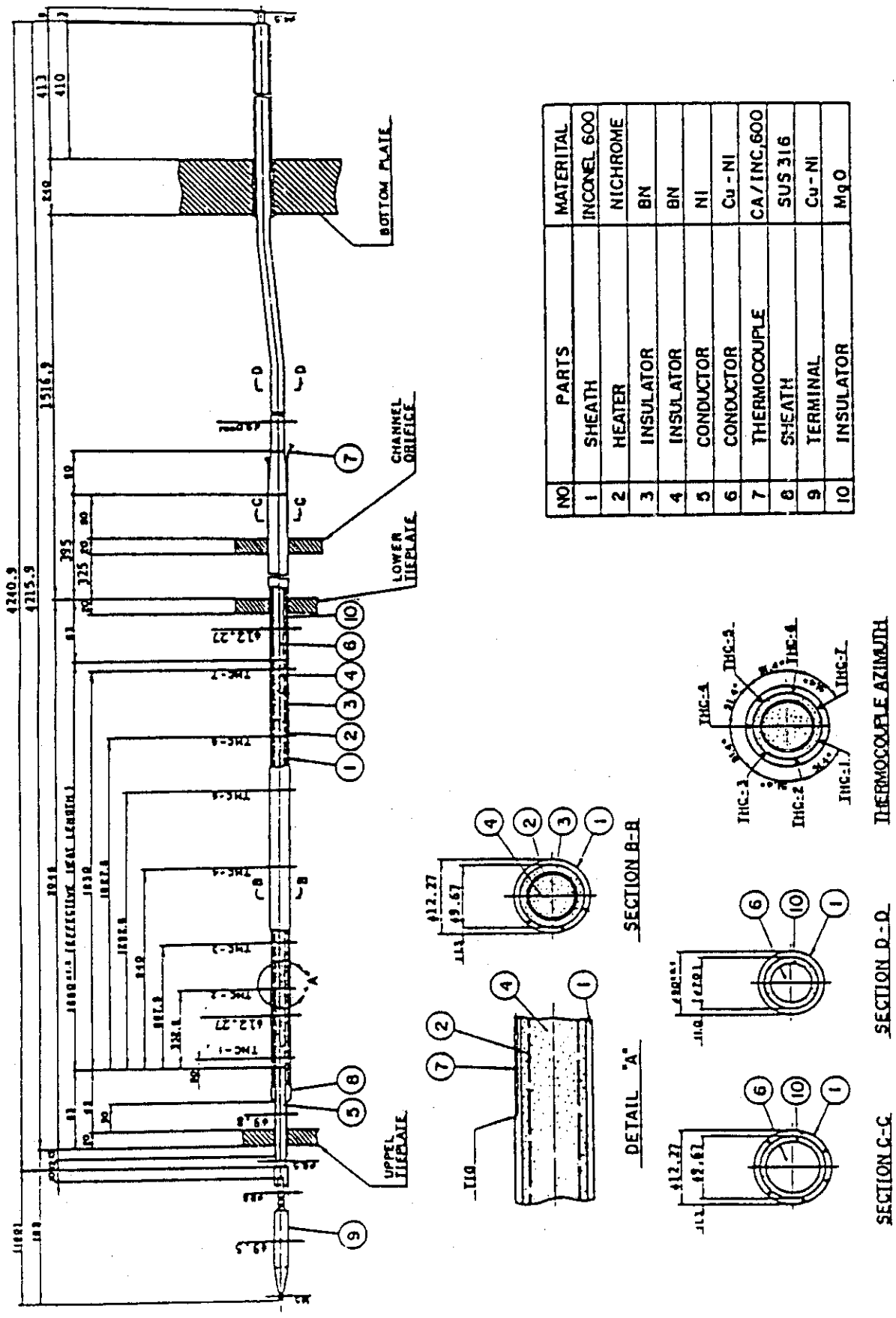

NO	PARTS	MATERITAL
1	SHEATH	INCONEL 600
2	HEATER	NICHROME
3	INSULATOR	BN
4	INSULATOR	BN
5	CONDUCTOR	NI
6	CONDUCTOR	Cu-NI
7	THERMOCOUPLE	CA/INC.600
8	SHEATH	SUS 316
9	TERMINAL	Cu-NI
10	INSULATOR	MgO

Fig. 2.5 Simulated fuel rod of ROSA-III

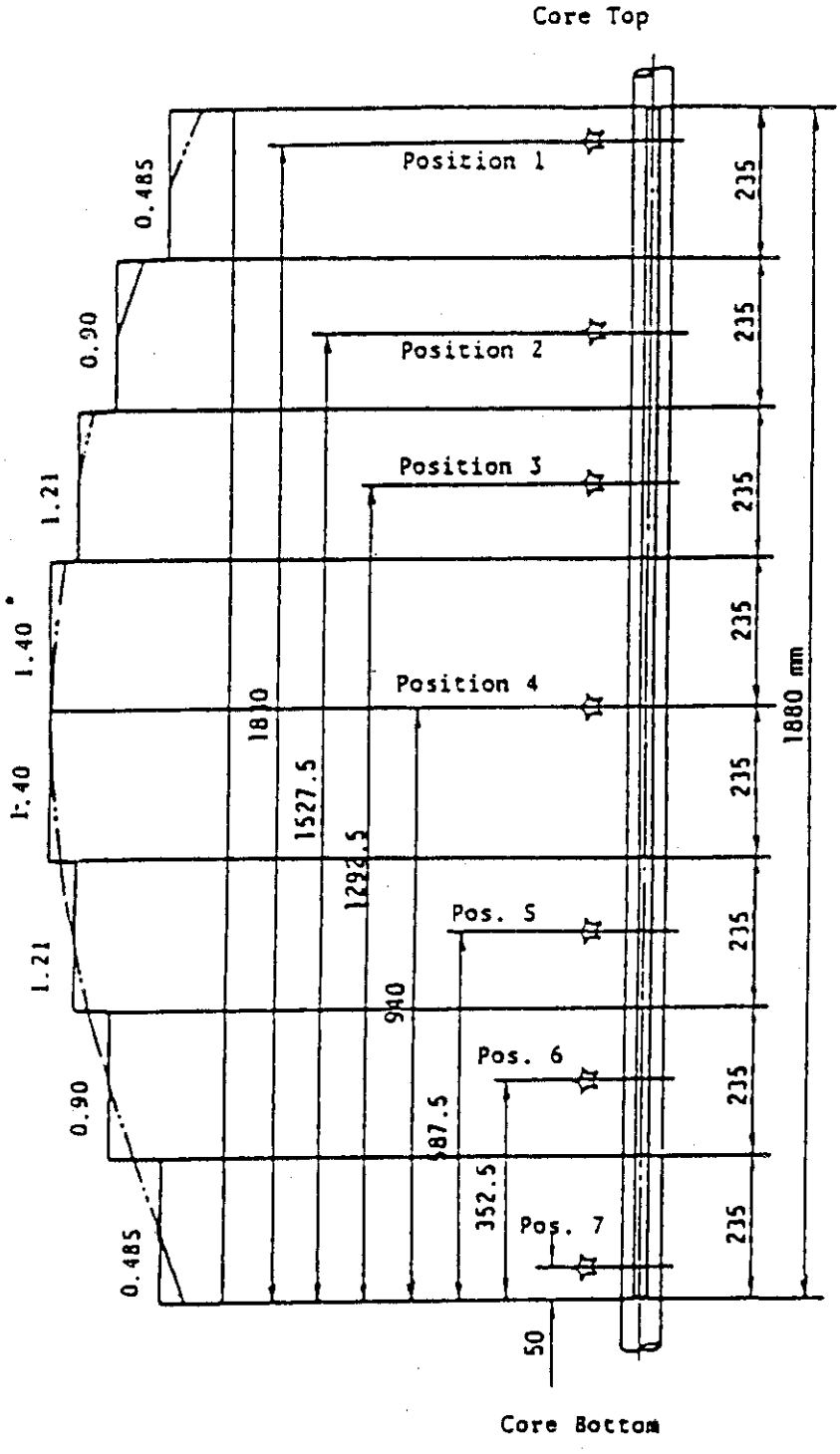

Fig. 2.6 Axial power distribution of heater rod

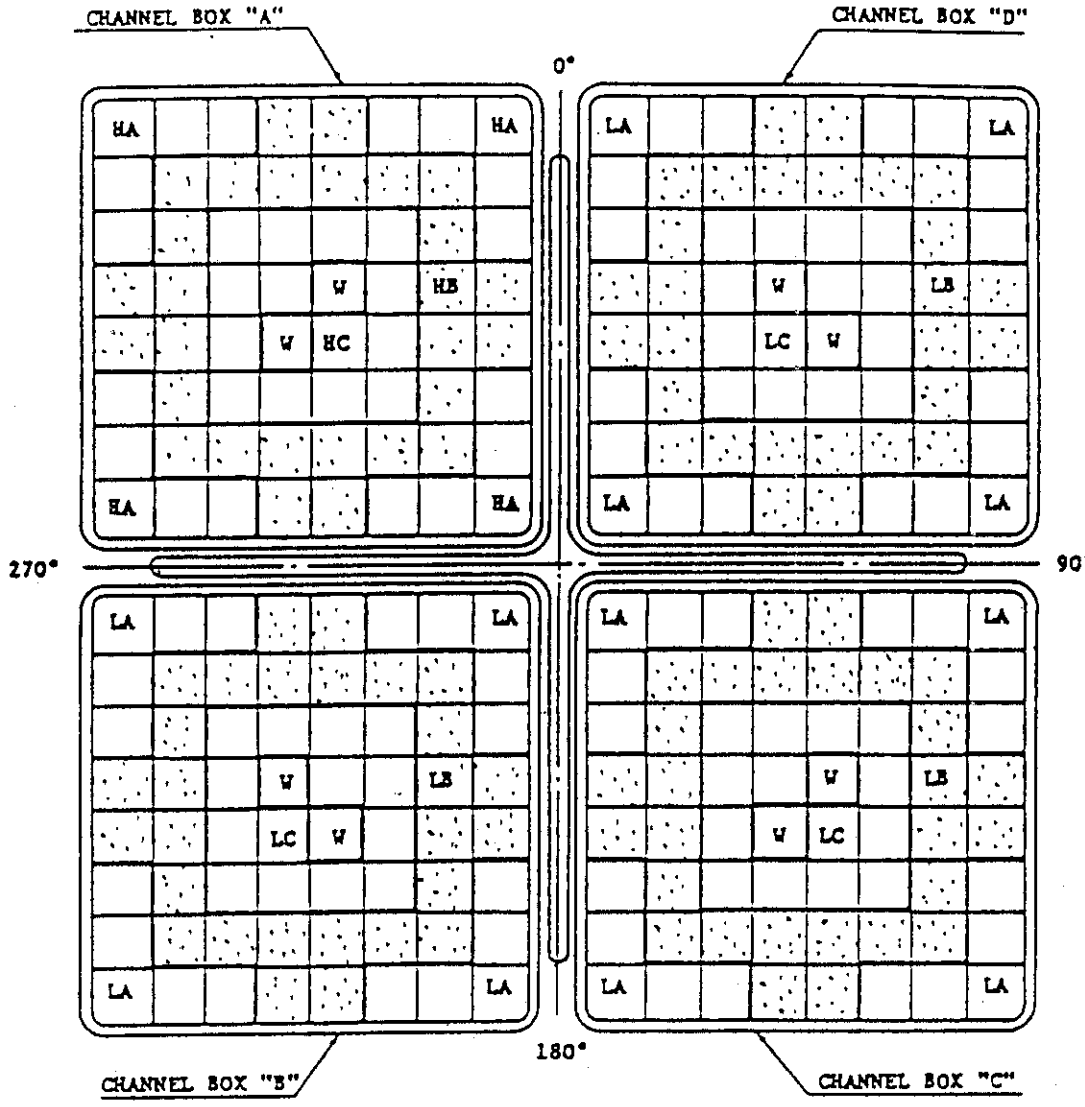

Region	HA	HB	HC	LA	LB	LC	W
Lenear Heat Rate (kW/m)	18.5	16.81	14.41	13.21	12.01	10.29	0.0
Local peaking factor	1.1	1.0	0.875	1.1	1.0	0.875	0.0
No. of Rods	20	28	14	60	84	42	8

* note : Radial peaking factor is 1.4

Fig. 2.7 Radial power distribution of core

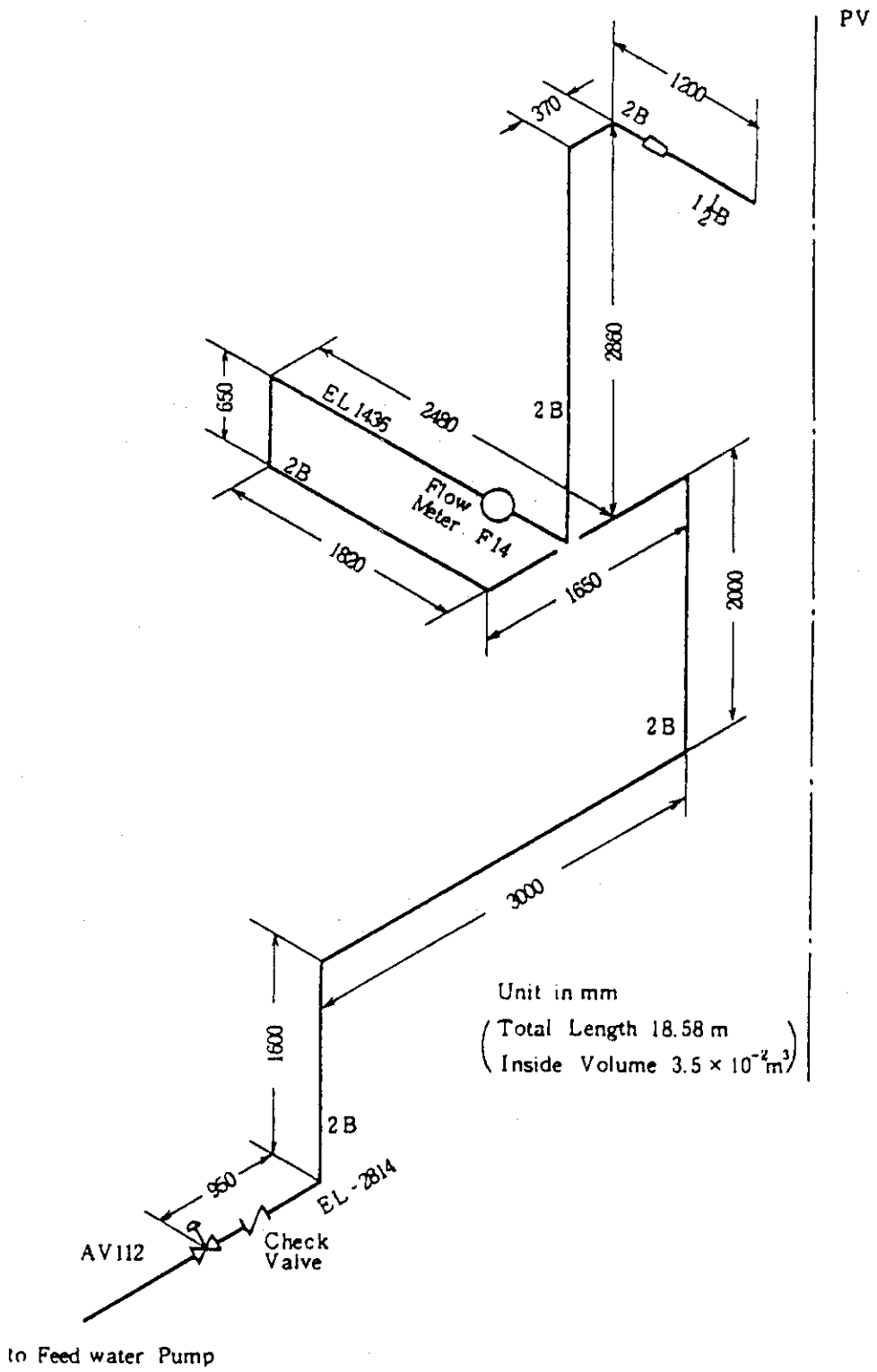

Fig. 2.8 Feedwater line between PV and AV-112

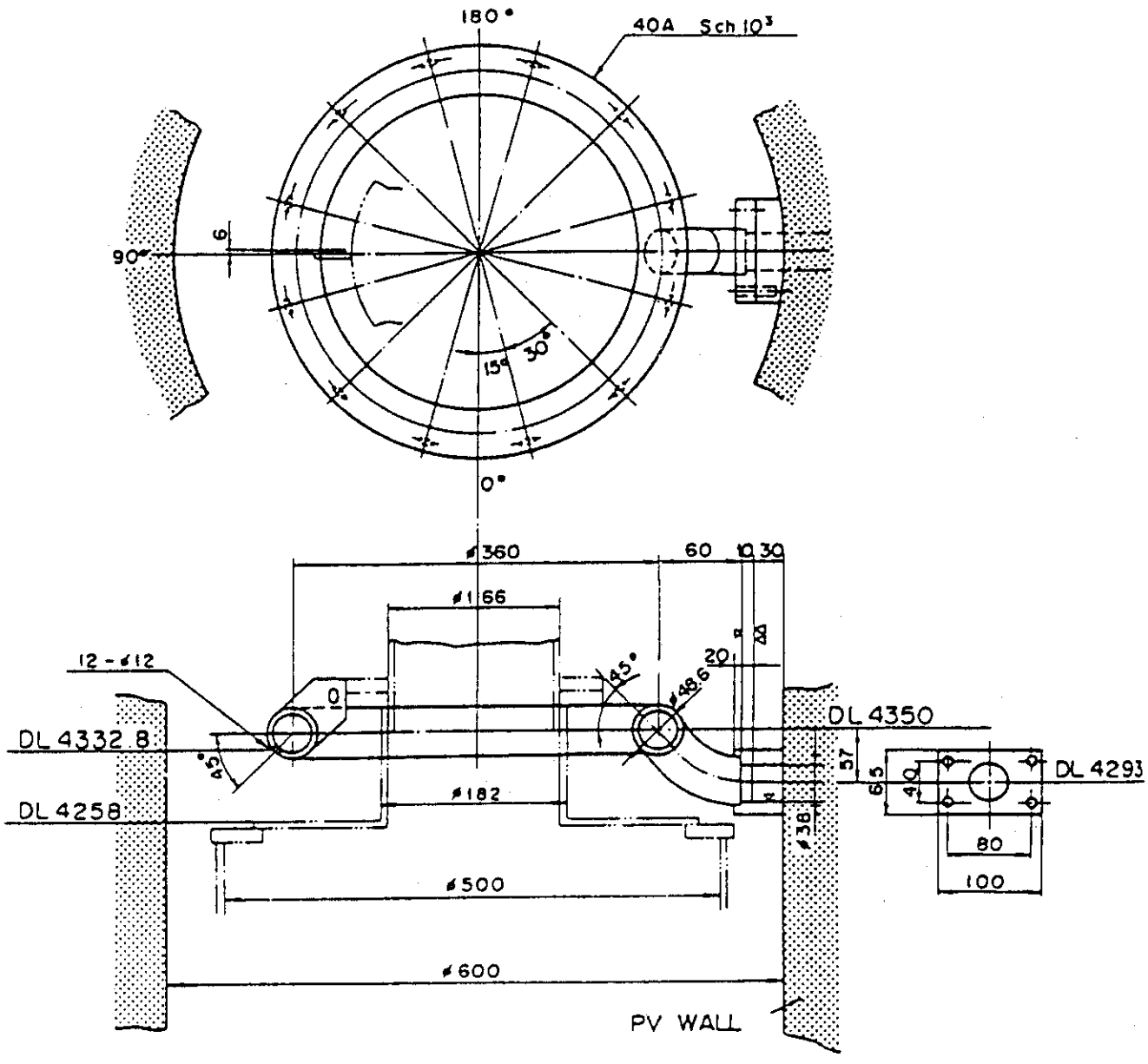

Fig. 2.9 Feedwater sparger configuration

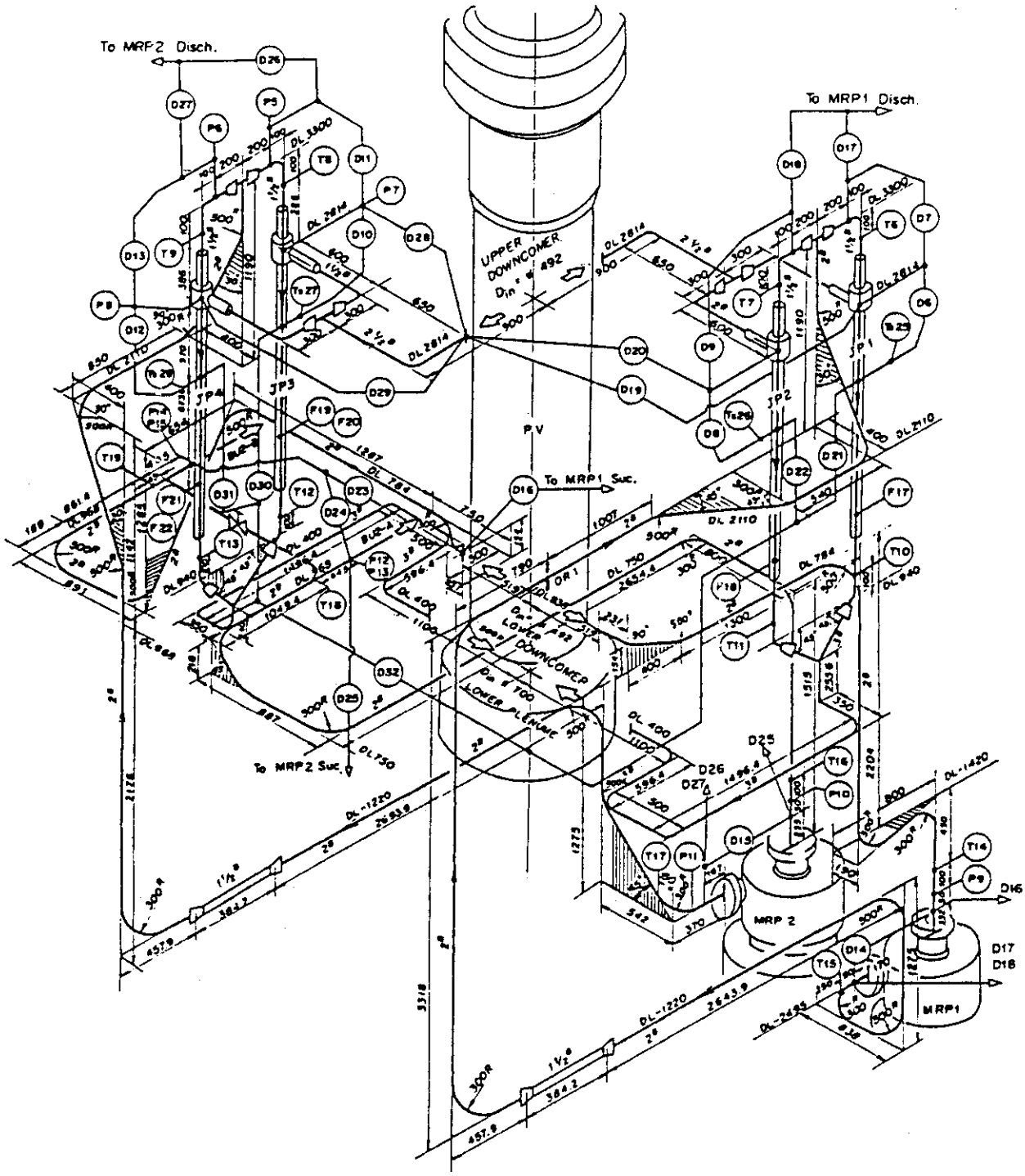

Fig. 2.10 Details of ROSA III system piping

Table 3.1 ROSA-III instrumentation summary list

TYPE	SENSOR	NUMBER	NOTE	
PRESSURE	PRESSURE TRANSDUCER	20		
DIFFERENTIAL PRESSURE	DP CELL	60	PV AND LOOP	44
			LEVEL MEASUREMENT	5
			FLOW METER	11
FLUID TEMPERATURE	CA THERMOCOUPLE	129	PRIMARY LOOP	23
			DTT	4
			TIE ROD	28
			UPPER PLENUM	10
			LOWER PLENUM	10
			TIE PLATE	40
			BY PASS	14
FUEL ROD TEMPERATURE	CA THERMOCOUPLE	213		
SLAB SURFACE TEMPERATURE	CA THERMOCOUPLE	70	CORE BARREL	24
			PRESSURE VESSEL	3
			CHANNEL BOX	35
			SHROUD SUPPORT	8
SLAB INNER TEMPERATURE	CA THERMOCOUPLE	9	JP DIFFUSER	4
			PV WALL	5
VOLUMETRIC FLOW RATE	TURBINE METER	3	ECCS LOOP	3
	VENTURI METER	4	PRIMARY LOOP	10
	ORIFICE METER	6		
MASS FLOW RATE	TURBINE METER	4	RECIC. LOOP	4
	ORIFICE METER	3	STEAM LINE	3
LIQUID LEVEL	CONDUCTIVITY PROBE	138		
	CAPACITANCE PROBE	2		
DENSITY	GAMMA DENSITOMETER	10	2 BEAM GD	2
			3 BEAM GD	2
MOMENTUMR FLUX	DRAG DISK	7		
SIGNAL	ON/OFF SWITCH	14		
PUMP SPEED	REVOLUTION COUNTER	2		
ELECTRIC POWER	VA METER	2		
TOTAL		696		

Table 3.2 Measurement List for RUN 915 and 920

1Ch.- 50Ch.

Ch.	Item	Symbol	ID.		Location	Fig.No.	Range			Unit	Accuracy
1	Press.	P- 1	PA	1	Lower Plenum	5. 1,121	0.100	-	10.0	MPa	1.08%FS
2	Press.	P- 2	PA	2	Upper Plenum	5. 1,121	0.100	-	10.0	MPa	1.08%FS
3	Press.	P- 3	PA	3	Steam Dome	5. 1,121	0.100	-	10.0	MPa	1.08%FS
4	Press.	P- 4	PA	4	Downcomer Bottom	5. 1,121	0.100	-	10.0	MPa	1.08%FS
5	Press.	P- 5	PA	5	JP-3 Drive		0.100	-	10.0	MPa	1.08%FS
6	Press.	P- 6	PA	6	JP-4 Drive		0.100	-	10.0	MPa	1.08%FS
7	Press.	P- 7	PA	7	JP-3 Suction		0.100	-	10.0	MPa	1.08%FS
8	Press.	P- 8	PA	8	JP-4 Suction		0.100	-	10.0	MPa	1.08%FS
9	Press.	P- 9	PA	9	MRP-1 Suction		0.100	-	10.0	MPa	1.08%FS
10	Press.	P-10	PA	10	MRP-2 Suction		0.100	-	10.0	MPa	1.08%FS
11	Press.	P-11	PA	11	MRP-2 Delivery		0.100	-	10.0	MPa	1.08%FS
12	Press.	P-12	PA	12	Break A Upstream		0.100	-	10.0	MPa	1.08%FS
13	Press.	P-13	PA	13	Break A Downstream		0.100	-	10.0	MPa	1.08%FS
14	Press.	P-14	PA	14	Break B Upstream		0.100	-	10.0	MPa	1.08%FS
15	Press.	P-15	PA	15	Break B Downstream		0.100	-	10.0	MPa	1.08%FS
16	Press.	P-16	PA	16	Steam Line		0.100	-	10.0	MPa	1.08%FS
17	Press.	P-17	PA	17	JP-1,2 Outlet Spool		0.100	-	10.0	MPa	1.08%FS
18	Press.	P-18	PA	18	JP-3,4 Outlet Spool		0.100	-	10.0	MPa	1.08%FS
19	Press.	P-19	PA	19	Break A Spool Piece		0.100	-	10.0	MPa	1.08%FS
20	Press.	P-30	PA	20	Break B Spool Piece		0.100	-	10.0	MPa	1.08%FS
21	Diff.P.	D- 1	PD	21	Lower Pl.-Upper Pl.	5. 2,122	-50.0	-	350.	kPa	0.63%FS
22	Diff.P.	D- 2	PD	22	Upper Pl.-Steam Dome	5. 3,123	-10.0	-	90.0	kPa	0.63%FS
23	Diff.P.	D- 3	PD	23	Lower Plenum Head	NM, NM					
24	Diff.P.	D- 4	PD	24	Downcomer Head		0.0	-	100.	kPa	0.63%FS
25	Diff.P.	D- 5	PD	25	PV Bottom-Top	5. 4,124	-100.	-	900.	kPa	0.63%FS
26	Diff.P.	D- 6	PD	26	JP-1 Disch.-Suction	5. 5,125	-100.	-	300.	kPa	0.63%FS
27	Diff.P.	D- 7	PD	27	JP-1 Drive -Suction	5. 6,126	0.0	-	2.50	MPa	0.63%FS
28	Diff.P.	D- 8	PD	28	JP-2 Disch.-Suction	5. 5,125	-100.	-	300.	kPa	0.63%FS
29	Diff.P.	D- 9	PD	29	JP-2 Drive -Suction	5. 6,126	0.0	-	2.50	MPa	0.63%FS
30	Diff.P.	D-10	PD	30	JP-3 Disch.-Suction	5. 7,127	-100.	-	300.	kPa	0.63%FS
31	Diff.P.	D-11	PD	31	JP-3 Drive -Suction	5. 8,128	-4.00	-	2.00	MPa	0.63%FS
32	Diff.P.	D-12	PD	32	JP-4 Disch.-Suction	5. 7,127	-100.	-	300.	kPa	0.63%FS
33	Diff.P.	D-13	PD	33	JP-4 Drive -Suction	5. 8,128	-4.00	-	2.00	MPa	0.63%FS
34	Diff.P.	D-14	PD	34	MRP-1 Deliv.-Suction	5. 9,129	-0.100	-	2.50	MPa	0.63%FS
35	Diff.P.	D-15	PD	35	MRP-2 Deliv.-Suction	5. 9,129	-0.100	-	2.50	MPa	0.63%FS
36	Diff.P.	D-16	PD	36	DC Bottom- MRP-1 Suc.	5. 10,130	-50.0	-	50.0	kPa	0.63%FS
37	Diff.P.	D-17	PD	37	MRP1 Deliv.-JP1 Drive	5. 11,131	0.0	-	250.	kPa	0.63%FS
38	Diff.P.	D-18	PD	38	MRP1 Deliv.-JP2 Drive	5. 11,131	0.0	-	250.	kPa	0.63%FS
39	Diff.P.	D-19	PD	39	DC Middle-JP1 Suction	5. 12,132	0.0	-	250.	kPa	0.63%FS
40	Diff.P.	D-20	PD	40	DC Middle-JP2 Suction	5. 12,132	0.0	-	250.	kPa	0.63%FS
41	Diff.P.	D-21	PD	41	JP1 Disch.-Lower Pl.	5. 13,133	-100.	-	100.	kPa	0.63%FS
42	Diff.P.	D-22	PD	42	JP2 Disch.-Lower Pl.	5. 13,133	-100.	-	100.	kPa	0.63%FS
43	Diff.P.	D-23	PD	43	DC Bottom- Break B		-60.0	-	540.	kPa	0.63%FS
44	Diff.P.	D-24	PD	44	Break B- Break A		0.0	-	100.	kPa	0.63%FS
45	Diff.P.	D-25	PD	45	Break A- MRP2 Suction		-500.	-	100.	kPa	0.63%FS
46	Diff.P.	D-26	PD	46	MRP2 Deliv.-JP3 Drive	5. 14,134	-500.	-	500.	kPa	0.63%FS
47	Diff.P.	D-27	PD	47	MRP2 Deliv.-JP4 Drive	5. 14,134	-500.	-	500.	kPa	0.63%FS
48	Diff.P.	D-28	PD	48	DC Middle-JP3 Suction	5. 15,135	-250.	-	250.	kPa	0.63%FS
49	Diff.P.	D-29	PD	49	DC Middle-JP4 Suction	5. 15,135	-250.	-	250.	kPa	0.63%FS
50	Diff.P.	D-30	PD	50	JP3 Disch.-Confluence	5. 16,136	-100.	-	100.	kPa	0.63%FS

Table 3.2 Measurement List (Continued)

Ch.	Item	Symbol	ID.		Location	Fig.No.	51Ch.- 100Ch. Range			Unit	Accuracy
51	Diff.P.	D-31	PD	51	JP4 Disch.-Confluence	5. 16,136	-100.	-	100.	kPa	0.63%FS
52	Diff.P.	D-32	PD	52	Confluence -Lower Pl.	5. 17,137	-50.0	-	50.0	kPa	0.63%FS
53	Diff.P.	D-33	PD	53	Lower Pl.-DC Middle		-250.	-	250.	kPa	0.63%FS
54	Diff.P.	D-34	PD	54	Lower Pl.-DC Bottom		-250.	-	250.	kPa	0.63%FS
55	Diff.P.	D-35	PD	55	DC Bottom-DC Middle	5. 18,138	-50.0	-	50.0	kPa	0.63%FS
56	Diff.P.	D-36	PD	56	DC Middle-Steam Dome	5. 19,139	-50.0	-	50.0	kPa	0.63%FS
57	Diff.P.	D-37	PD	57	Lower Pl.Mid-Upper PL						
58	Diff.P.	D-38	PD	58	Lower Pl.Bottom-Mid.	5. 20,140	0.0	-	50.0	kPa	0.63%FS
59	Diff.P.	D-39	PD	59	Upper Pl.-DC High	NU, NM	-20.0	-	100.	kPa	0.63%FS
60	Diff.P.	D-40	PD	60	Channel Orifice A	5. 21,141	-50.0	-	50.0	kPa	0.63%FS
61	Diff.P.	D-41	PD	61	Channel Orifice B	5. 22,142	-50.0	-	50.0	kPa	0.63%FS
62	Diff.P.	D-42	PD	62	Channel Orifice C	5. 23,143	-25.0	-	75.0	kPa	0.63%FS
63	Diff.P.	D-43	PD	63	Channel Orifice D	5. 24,144	-50.0	-	50.0	kPa	0.63%FS
64	Diff.P.	D-44	PD	64	Bypass Hole	5. 25,145	-100.	-	100.	KPA	0.63%FS
65	Level	WL- 1	LM	65	HPCS Tank	NU NU	0.0	-	2.30	m	1.00%FS
66	Level	WL- 2	LM	66	LPCS Tank	5. 26,146	0.0	-	2.30	m	1.00%FS
67	Level	WL- 3	LM	67	LPCI Tank	5. 26,146	0.0	-	4.25	m	1.00%FS
68	Level	WL- 4	LM	68	Upper Downcomer	5. 27,147	3.90	-	6.04	m	1.00%FS
69	Level	WL- 5	LM	69	Lower Downcomer	5. 27,147	0.938	-	3.90	m	1.00%FS
70	Mass.F.	F- 1	FM	70	Steam Line (Low Range)		0.0	-	1.13	kg/s	0.92%FS
71	Mass.F.	F- 2	FM	71	Steam Line(High Range)		0.0	-	3.00	kg/s	0.92%FS
72	Mass.F.	F- 3	FM	72	Steam Line (Mid Range)		0.0	-	1.94	kg/s	1.40%FS
73	Vol.F.	F- 7	FV	73	HPCS (Upper Plenum)	NU, NU	0.0	-	0.250E-02	m3/s	0.79%FS
74	Vol.F.	F- 9	FV	74	LPCS (Upper Plenum)	5. 28,148	0.0	-	0.250E-02	m3/s	0.79%FS
75	Vol.F.	F-11	FV	75	LPCI (Core Bypass)	5. 28,148	0.0	-	0.830E-02	m3/s	0.79%FS
76	Vol.F.	F-15	FV	76	Feedwater	5. 29,149	0.0	-	0.100E-01	m3/s	0.79%FS
77	Vol.F.	F-16	FV	77	PWT Flow	NU, NU	0.0	-	0.420E-02	m3/s	0.79%FS
78	Vol.F.	F-17	FV	78	JP1 Discharge	5. 30,150	0.0	-	0.170E-01	m3/s	0.88%FS
79	Vol.F.	F-18	FV	79	JP2 Discharge	5. 30,150	0.0	-	0.170E-01	m3/s	0.88%FS
80	Vol.F.	F-19	FV	80	JP3 Disch. Positive	5. 31,151	0.0	-	0.170E-01	m3/s	0.92%FS
81	Vol.F.	F-20	FV	81	JP3 Disch. Negative	5. 32,152	0.0	-	0.500E-02	m3/s	0.92%FS
82	Vol.F.	F-21	FV	82	JP4 Disch. Positive	5. 31,151	0.0	-	0.170E-01	m3/s	0.92%FS
83	Vol.F.	F-22	FV	83	JP4 Disch. Negative	5. 32,152	0.0	-	0.500E-02	m3/s	0.92%FS
84	Mass.F.	F-23	FM	84	JP1,2 Outlet Spool	NM, NM	0.0	-	30.0	kg/s	1.40%FS
85	Mass.F.	F-24	FM	85	JP3,4 Outlet Spool	NM, NM	0.0	-	30.0	kg/s	1.40%FS
86	Mass.F.	F-25	FM	86	Break A Spool Piece	NM, NM	0.0	-	30.0	kg/s	1.40%FS
87	Mass.F.	F-26	FM	87	Break B Spool Piece	NM, NM	0.0	-	30.0	kg/s	1.40%FS
88	Vol.F.	F-27	FV	88	MRP-1	5. 33,153	0.0	-	0.120E-01	m3/s	0.88%FS
89	Vol.F.	F-28	FV	89	MRP-2	5. 33,153	0.0	-	0.120E-01	m3/s	0.63%FS
90	Diff.P.	D-F1	PD	90	F1 Orifice		0.0	-	4.90	kPa	0.63%FS
91	Diff.P.	D-F2	PD	91	F2 Orifice		0.0	-	34.9	kPa	0.63%FS
92	Diff.P.	D-F3	PD	92	F3 Orifice		0.0	-	14.6	kPa	0.63%FS
93	Diff.P.	D-F17	PD	93	F17 Venturi		0.0	-	98.1	kPa	0.63%FS
94	Diff.P.	D-F18	PD	94	F18 Venturi		0.0	-	98.1	kPa	0.63%FS
95	Diff.P.	D-F19	PD	95	F19 Orifice		0.0	-	147.	kPa	0.63%FS
96	Diff.P.	D-F20	PD	96	F20 Orifice		0.0	-	13.2	kPa	0.63%FS
97	Diff.P.	D-F21	PD	97	F21 Orifice		0.0	-	147.	kPa	0.63%FS
98	Diff.P.	D-F22	PD	98	F22 Orifice		0.0	-	13.2	kPa	0.63%FS
99	Diff.P.	D-F27	PD	99	F27 Venturi		0.0	-	200.	kPa	0.63%FS
100	Diff.P.	D-F28	PD	100	F28 Venturi		0.0	-	200.	kPa	0.63%FS

Table 3.2 Measurement List (Continued)

101Ch.- 150Ch.

Ch.	Item	Symbol	ID.		Location	Fig.No.	Range			Unit	Accuracy
101	Power	W- 1	WE	101	2100 kW Power Supplier	5. 34,154	0.0	-	0.210E+04	kW	1.00%FS
102	Power	W- 2	WE	102	3150 kW Power Supplier	5. 34,154	0.0	-	0.315E+04	kW	1.00%FS
103						NU, NU					
104	Rev.	N- 1	SR	104	MRP-1 Revolution		0.0	-	0.500E+04	RPM	1.08%FS
105	Rev.	N- 2	SR	105	MRP-2 Revolution	5. 35,155	0.0	-	0.500E+04	RPM	1.08%FS
106	Signal	S- 1	EV	106	Break Signal A	5. 36,156					
107	Signal	S- 2	EV	107	Break Signal B	5. 36,156					
108	Signal	S- 3	EV	108	QSV Signal	5. 36,156					
109	Signal	S- 6	EV	109	HPCS Valve	5. 37,157					
110	Signal	S- 7	EV	110	LPCS Valve	5. 37,157					
111	Signal	S- 8	EV	111	LPCI Valve	5. 37,157					
112	Signal	S- 9	EV	112	Feedwater Control	5. 36,156					
113	Signal	S-10	EV	113	MSIV Signal	5. 36,156					
114	Signal	S-11	EV	114	Steam Line Valve	5. 36,156					
115	Signal	S-12	EV	115	ADS Valve	5. 37,157					
116	Signal	S-13	EV	116	MRP-1 Power OFF	5. 38,158					
117	Signal	S-14	EV	117	MRP-2 Power OFF	5. 38,158					
118	Signal	RD- 1	EV	118	MRP-1 Rev. Direction	NU, NU					
119	Signal	RD- 2	EV	119	MRP-2 Rev. Direction	NU, NU					
120	Density	DF- 1	DE	120	JP1,2 Outlet Beam A	5. 39,159	0.0	-	0.100E+04	kg/m3	1.00%FS
121	Density	DF- 2	DE	121	JP1,2 Outlet Beam B	5. 40,160	0.0	-	0.100E+04	kg/m3	1.00%FS
122	Density	DF- 3	DE	122	JP1,2 Outlet Beam C	5. 41,161	0.0	-	0.100E+04	kg/m3	1.00%FS
123	Density	DF- 4	DE	123	JP3,4 Outlet Beam A	5. 42,162	0.0	-	0.100E+04	kg/m3	1.00%FS
124	Density	DF- 5	DE	124	JP3,4 Outlet Beam B	5. 43,163	0.0	-	0.100E+04	kg/m3	1.00%FS
125	Density	DF- 6	DE	125	JP3,4 Outlet Beam C	5. 44,164	0.0	-	0.100E+04	kg/m3	1.00%FS
126	Density	DF- 7	DE	126	Break A Beam A	5. 45,165	0.0	-	0.100E+04	kg/m3	1.00%FS
127	Density	DF- 8	DE	127	Break A Beam B	5. 46,166	0.0	-	0.100E+04	kg/m3	1.00%FS
128	Density	DF- 9	DE	128	Break B Beam A	5. 47,167	0.0	-	0.100E+04	kg/m3	1.00%FS
129	Density	DF-10	DE	129	Break B Beam B	5. 48,168	0.0	-	0.100E+04	kg/m3	1.00%FS
130	Mo.Flux	M- 1	MF	130	JP1,2 Outlet Spool	5. 49,169	0.0	-	0.220E+05	kg/ms2	1.00%FS
131	Mo.Flux	M- 2	MF	131	JP3,4 Outlet Spool	5. 50,170	0.0	-	0.220E+05	kg/ms2	1.00%FS
132	Mo.Flux	M- 3	MF	132	Break A (Low Range)	5. 51,171	0.0	-	0.220E+05	kg/ms2	1.00%FS
133	Mo.Flux	M- 4	MF	133	Break B (Low Range)	5. 52,172	0.0	-	0.220E+05	kg/ms2	1.00%FS
134	Mo.Flux	M- 5	MF	134	Break A (High Range)		0.0	-	0.220E+06	kg/ms2	1.00%FS
135	Mo.Flux	M- 6	MF	135	Break B (High Range)		0.0	-	0.220E+06	kg/ms2	1.00%FS
136	Mo.Flux	M- 7	MF	136	Break Orifice	NM, NM	0.0	-	0.220E+05	kg/ms2	1.00%FS
137											
138	Fluid T.	T- 1	TE	138	Lower Plenum	5. 53,173	273.	-	673.	K	0.64%FS
139	Fluid T.	T- 2	TE	139	Upper Plenum	5. 53,173	273.	-	673.	K	0.64%FS
140	Fluid T.	T- 3	TE	140	Steam Dome	5. 53,173	273.	-	673.	K	0.64%FS
141	Fluid T.	T- 4	TE	141	Upper Downcomer	5. 54,174	273.	-	673.	K	0.64%FS
142	Fluid T.	T- 5	TE	142	Lower Downcomer	5. 54,174	273.	-	673.	K	0.64%FS
143	Fluid T.	T- 6	TE	143	JP-1 Drive	5. 55,175	273.	-	673.	K	0.64%FS
144	Fluid T.	T- 7	TE	144	JP-2 Drive	5. 55,175	273.	-	673.	K	0.64%FS
145	Fluid T.	T- 8	TE	145	JP-3 Drive	5. 56,176	273.	-	673.	K	0.64%FS
146	Fluid T.	T- 9	TE	146	JP-4 Drive	5. 56,176	273.	-	673.	K	0.64%FS
147	Fluid T.	T-10	TE	147	JP-1 Discharge		273.	-	673.	K	0.64%FS
148	Fluid T.	T-11	TE	148	JP-2 Discharge		273.	-	673.	K	0.64%FS
149	Fluid T.	T-12	TE	149	JP-3 Discharge		273.	-	673.	K	0.64%FS
150	Fluid T.	T-13	TE	150	JP-4 Discharge		273.	-	673.	K	0.64%FS

Table 3.2 Measurement List (Continued)

151Ch.- 200Ch.

Ch.	Item	Symbol	ID.		Location	Fig.No.	Range			Unit	Accuracy
151	Fluid T.	T-14	TE	151	MRP-1 Suction	5. 55,175	273.	-	673.	K	0.64%FS
152	Fluid T.	T-15	TE	152	MRP-1 Delivery	5. 55,175	273.	-	673.	K	0.64%FS
153	Fluid T.	T-16	TE	153	MRP-2 Suction	5. 56,176	273.	-	673.	K	0.64%FS
154	Fluid T.	T-17	TE	154	MRP-2 Delivery	5. 56,176	273.	-	673.	K	0.64%FS
155	Fluid T.	T-18	TE	155	Break A Upstream	5. 57,177	273.	-	673.	K	0.64%FS
156	Fluid T.	T-19	TE	156	Break B Upstream	5. 57,177	273.	-	673.	K	0.64%FS
157	Fluid T.	T-20	TE	157	RCN A Condenced Water	NU, NU	273.	-	698.	K	0.64%FS
158	Fluid T.	T-21	TE	158	RCN B Condenced Water	NU, NU	273.	-	698.	K	0.64%FS
159	Fluid T.	T-22	TE	159	Discharged Steam	5. 53,173	273.	-	673.	K	0.64%FS
160	Fluid T.	T-24	TE	160	JP-1,2 Outlet Spool		273.	-	763.	K	0.64%FS
161	Fluid T.	T-25	TE	161	JP-3,4 Outlet Spool		273.	-	763.	K	0.64%FS
162	Fluid T.	T-26	TE	162	Break A Spool Piece	5. 57,177	273.	-	763.	K	0.64%FS
163	Fluid T.	T-27	TE	163	Break B Spool Piece		273.	-	763.	K	0.64%FS
164	Fluid T.	T-28	TE	164	Feedwater	5. 57,177	273.	-	673.	K	0.64%FS
165	Fluid T.	T-29	TE	165	Break Orifice 1	NM, NM	273.	-	673.	K	0.64%FS
166	Fluid T.	T-30	TE	166	Break Orifice 2	NM, NM	273.	-	673.	K	0.64%FS
167	Fluid T.	T-31	TE	167	Break A Down DD(Low)	NM, NM	273.	-	673.	K	0.64%FS
168	Fluid T.	T-32	TE	168	Break B Down DD(Low)	NM, NM	273.	-	673.	K	0.64%FS
169	Fluid T.	T-33	TE	169	Break A Up. DD(High)	NM, NM	273.	-	673.	K	0.64%FS
170	Fluid T.	T-34	TE	170	Break B Up. DD(High)	NM, NM	273.	-	673.	K	0.64%FS
171	Fluid T.	T-F17	TE	171	JP1 Fluid D. Correc.	NM, NM	273.	-	673.	K	0.64%FS
172	Fluid T.	T-F18	TE	172	JP2 Fluid D. Correc.	NM, NM	273.	-	673.	K	0.64%FS
173	Fluid T.	T-F19	TE	173	JP3 Fluid D. Correc.	NM, NM	273.	-	673.	K	0.64%FS
174	Fluid T.	T-F21	TE	174	JP4 Fluid D. Correc.	NM, NM	273.	-	673.	K	0.64%FS
175	Slab T.	TS-11	TE	175	Core Barrel A Pos.5	NM, NM	273.	-	673.	K	0.64%FS
176	Slab T.	TS-12	TE	176	Core Barrel A Pos.6	NM, NM	273.	-	673.	K	0.64%FS
177	Slab T.	TS-13	TE	177	Filler Block C Pos.1	NM, NM	273.	-	673.	K	0.64%FS
178	Slab T.	TS-14	TE	178	Filler Block C Pos.2	NM, NM	273.	-	673.	K	0.64%FS
179	Slab T.	TS-15	TE	179	Filler Block C Pos.3	NM, NM	273.	-	673.	K	0.64%FS
180	Slab T.	TS-16	TE	180	Filler Block C Pos.4	NM, NM	273.	-	673.	K	0.64%FS
181	Slab T.	TS-17	TE	181	Filler Block C Pos.5	NM, NM	273.	-	673.	K	0.64%FS
182	Slab T.	TS-18	TE	182	Filler Block C Pos.6	NM, NM	273.	-	673.	K	0.64%FS
183	Slab T.	TS-19	TE	183	Filler Block A Pos.1	NM, NM	273.	-	673.	K	0.64%FS
184	Slab T.	TS-20	TE	184	Filler Block A Pos.2	NM, NM	273.	-	673.	K	0.64%FS
185	Slab T.	TS-21	TE	185	Filler Block A Pos.3	NM, NM	273.	-	673.	K	0.64%FS
186	Slab T.	TS-22	TE	186	Filler Block A Pos.4	NM, NM	273.	-	673.	K	0.64%FS
187	Slab T.	TS-23	TE	187	Filler Block A Pos.5	NM, NM	273.	-	673.	K	0.64%FS
188	Slab T.	TS-24	TE	188	Filler Block A Pos.6	NM, NM	273.	-	673.	K	0.64%FS
189	Slab T.	TS-25	TE	189	JP-1 Diffuser Wall	NM, NM	273.	-	673.	K	0.64%FS
190	Slab T.	TS-26	TE	190	JP-2 Diffuser Wall	NM, NM	273.	-	673.	K	0.64%FS
191	Slab T.	TS-27	TE	191	JP-3 Diffuser Wall	NM, NM	273.	-	673.	K	0.64%FS
192	Slab T.	TS-28	TE	192	JP-4 Diffuser Wall	NM, NM	273.	-	673.	K	0.64%FS
193	Slab T.	TS-29	TE	193	PV Wall Inside 1-1	NM, NM	273.	-	673.	K	0.64%FS
194	Slab T.	TS-30	TE	194	PV Inner Surface 1-2	NM, NM	273.	-	673.	K	0.64%FS
195	Slab T.	TS-31	TE	195	PV Inner Surface 1-3	NM, NM	273.	-	673.	K	0.64%FS
196	Slab T.	TS-32	TE	196	PV Wall Inside 2	NM, NM	273.	-	673.	K	0.64%FS
197	Slab T.	TS-33	TE	197	PV Wall Inside 3	NM, NM	273.	-	673.	K	0.64%FS
198	Slab T.	TS-34	TE	198	PV Wall Inside 4	NM, NM	273.	-	673.	K	0.64%FS
199	Slab T.	TS-35	TE	199	L.P. Inner Surface	NM, NM	273.	-	673.	K	0.64%FS
200	Slab T.	TS-36	TE	200	L.P. Wall Inside		273.	-	673.	K	0.64%FS

Table 3.2 Measurement List (Continued)

201Ch.- 250Ch.

Ch.	Item	Symbol	ID.	Location	Fig.No.	Range	Unit	Accuracy
201	Temp.	TF- 1	TE 201	A11 Fuel Rod Pos.1	5. 58,178	273. - 0.147E+04	K	0.64%FS
202	Temp.	TF- 2	TE 202	A11 Fuel Rod Pos.2	5. 58,178	273. - 0.147E+04	K	0.64%FS
203	Temp.	TF- 3	TE 203	A11 Fuel Rod Pos.3	5. 58,178	273. - 0.147E+04	K	0.64%FS
204	Temp.	TF- 4	TE 204	A11 Fuel Rod Pos.4	5. 58,178	273. - 0.147E+04	K	0.64%FS
205	Temp.	TF- 5	TE 205	A11 Fuel Rod Pos.5	5. 58,178	273. - 0.147E+04	K	0.64%FS
206	Temp.	TF- 6	TE 206	A11 Fuel Rod Pos.6	5. 58,178	273. - 0.147E+04	K	0.64%FS
207	Temp.	TF- 7	TE 207	A11 Fuel Rod Pos.7	5. 58,178	273. - 0.147E+04	K	0.64%FS
208	Temp.	TF- 8	TE 208	A12 Fuel Rod Pos.1		273. - 0.147E+04	K	0.64%FS
209	Temp.	TF- 9	TE 209	A12 Fuel Rod Pos.2		273. - 0.147E+04	K	0.64%FS
210	Temp.	TF- 10	TE 210	A12 Fuel Rod Pos.3		273. - 0.147E+04	K	0.64%FS
211	Temp.	TF- 11	TE 211	A12 Fuel Rod Pos.4		273. - 0.147E+04	K	0.64%FS
212	Temp.	TF- 12	TE 212	A12 Fuel Rod Pos.5		273. - 0.147E+04	K	0.64%FS
213	Temp.	TF- 13	TE 213	A12 Fuel Rod Pos.6		273. - 0.147E+04	K	0.64%FS
214	Temp.	TF- 14	TE 214	A12 Fuel Rod Pos.7		273. - 0.147E+04	K	0.64%FS
215	Temp.	TF- 15	TE 215	A13 Fuel Rod Pos.1		273. - 0.147E+04	K	0.64%FS
216	Temp.	TF- 16	TE 216	A13 Fuel Rod Pos.2		273. - 0.147E+04	K	0.64%FS
217	Temp.	TF- 17	TE 217	A13 Fuel Rod Pos.3		273. - 0.147E+04	K	0.64%FS
218	Temp.	TF- 18	TE 218	A13 Fuel Rod Pos.4		273. - 0.147E+04	K	0.64%FS
219	Temp.	TF- 19	TE 219	A13 Fuel Rod Pos.5		273. - 0.147E+04	K	0.64%FS
220	Temp.	TF- 20	TE 220	A13 Fuel Rod Pos.6	5. 67,224	273. - 0.147E+04	K	0.64%FS
221	Temp.	TF- 21	TE 221	A13 Fuel Rod Pos.7	5. 67,224	273. - 0.147E+04	K	0.64%FS
222	Temp.	TF- 22	TE 222	A14 Fuel Rod Pos.1	5. 68,225	273. - 0.147E+04	K	0.64%FS
223	Temp.	TF- 23	TE 223	A14 Fuel Rod Pos.2	5. 68,225	273. - 0.147E+04	K	0.64%FS
224	Temp.	TF- 24	TE 224	A14 Fuel Rod Pos.3	5. 68,225	273. - 0.147E+04	K	0.64%FS
225	Temp.	TF- 25	TE 225	A14 Fuel Rod Pos.4	5. 68,225	273. - 0.147E+04	K	0.64%FS
226	Temp.	TF- 26	TE 226	A14 Fuel Rod Pos.5	5. 68,225	273. - 0.147E+04	K	0.64%FS
227	Temp.	TF- 27	TE 227	A14 Fuel Rod Pos.6	5. 68,225	273. - 0.147E+04	K	0.64%FS
228	Temp.	TF- 28	TE 228	A14 Fuel Rod Pos.7	FL, FL	273. - 0.147E+04	K	0.64%FS
229	Temp.	TF- 29	TE 229	A15 Fuel Rod Pos.1		273. - 0.147E+04	K	0.64%FS
230	Temp.	TF- 30	TE 230	A15 Fuel Rod Pos.4		273. - 0.147E+04	K	0.64%FS
231	Temp.	TF- 31	TE 231	A17 Fuel Rod Pos.1		273. - 0.147E+04	K	0.64%FS
232	Temp.	TF- 32	TE 232	A17 Fuel Rod Pos.4		273. - 0.147E+04	K	0.64%FS
233	Temp.	TF- 33	TE 233	A22 Fuel Rod Pos.1	5. 59,179	273. - 0.147E+04	K	0.64%FS
234	Temp.	TF- 34	TE 234	A22 Fuel Rod Pos.2	5. 59,179	273. - 0.147E+04	K	0.64%FS
235	Temp.	TF- 35	TE 235	A22 Fuel Rod Pos.3	5. 59,179	273. - 0.147E+04	K	0.64%FS
236	Temp.	TF- 36	TE 236	A22 Fuel Rod Pos.4	5. 59,179	273. - 0.125E+04	K	0.64%FS
237	Temp.	TF- 37	TE 237	A22 Fuel Rod Pos.5	5. 59,179	273. - 0.125E+04	K	0.64%FS
238	Temp.	TF- 38	TE 238	A22 Fuel Rod Pos.6	5. 59,179	273. - 0.125E+04	K	0.64%FS
239	Temp.	TF- 39	TE 239	A22 Fuel Rod Pos.7	5. 59,179	273. - 0.125E+04	K	0.64%FS
240	Temp.	TF- 40	TE 240	A24 Fuel Rod Pos.1		273. - 0.125E+04	K	0.64%FS
241	Temp.	TF- 41	TE 241	A24 Fuel Rod Pos.2		273. - 0.125E+04	K	0.64%FS
242	Temp.	TF- 42	TE 242	A24 Fuel Rod Pos.3		273. - 0.125E+04	K	0.64%FS
243	Temp.	TF- 43	TE 243	A24 Fuel Rod Pos.4		273. - 0.125E+04	K	0.64%FS
244	Temp.	TF- 44	TE 244	A24 Fuel Rod Pos.5		273. - 0.125E+04	K	0.64%FS
245	Temp.	TF- 45	TE 245	A24 Fuel Rod Pos.6		273. - 0.125E+04	K	0.64%FS
246	Temp.	TF- 46	TE 246	A24 Fuel Rod Pos.7		273. - 0.125E+04	K	0.64%FS
247	Temp.	TF- 47	TE 247	A26 Fuel Rod Pos.1		273. - 0.125E+04	K	0.64%FS
248	Temp.	TF- 48	TE 248	A26 Fuel Rod Pos.2		273. - 0.125E+04	K	0.64%FS
249	Temp.	TF- 49	TE 249	A28 Fuel Rod Pos.1		273. - 0.125E+04	K	0.64%FS
250	Temp.	TF- 50	TE 250	A28 Fuel Rod Pos.4		273. - 0.125E+04	K	0.64%FS

Table 3.2 Measurement List (Continued)

251Ch.- 300Ch.

Ch.	Item	Symbol	ID.	Location	Fig.No.	Range	Unit	Accuracy
251	Temp.	TF- 51	TE 251	A31 Fuel Rod Pos.1		273. - 0.125E+04	K	0.64%FS
252	Temp.	TF- 52	TE 252	A31 Fuel Rod Pos.4		273. - 0.125E+04	K	0.64%FS
253	Temp.	TF- 53	TE 253	A33 Fuel Rod Pos.1	5. 60,180	273. - 0.125E+04	K	0.64%FS
254	Temp.	TF- 54	TE 254	A33 Fuel Rod Pos.2	5. 60,180	273. - 0.125E+04	K	0.64%FS
255	Temp.	TF- 55	TE 255	A33 Fuel Rod Pos.3	5. 60,180	273. - 0.125E+04	K	0.64%FS
256	Temp.	TF- 56	TE 256	A33 Fuel Rod Pos.4	5. 60,180	273. - 0.125E+04	K	0.64%FS
257	Temp.	TF- 57	TE 257	A33 Fuel Rod Pos.5	5. 60,180	273. - 0.125E+04	K	0.64%FS
258	Temp.	TF- 58	TE 258	A33 Fuel Rod Pos.6	5. 60,180	273. - 0.125E+04	K	0.64%FS
259	Temp.	TF- 59	TE 259	A33 Fuel Rod Pos.7	5. 60,180	273. - 0.125E+04	K	0.64%FS
260	Temp.	TF- 60	TE 260	A34 Fuel Rod Pos.1	NN, NM	273. - 0.125E+04	K	0.64%FS
261	Temp.	TF- 61	TE 261	A34 Fuel Rod Pos.2		273. - 0.125E+04	K	0.64%FS
262	Temp.	TF- 62	TE 262	A34 Fuel Rod Pos.3		273. - 0.125E+04	K	0.64%FS
263	Temp.	TF- 63	TE 263	A34 Fuel Rod Pos.4		273. - 0.125E+04	K	0.64%FS
264	Temp.	TF- 64	TE 264	A34 Fuel Rod Pos.5		273. - 0.125E+04	K	0.64%FS
265	Temp.	TF- 65	TE 265	A34 Fuel Rod Pos.6		273. - 0.125E+04	K	0.64%FS
266	Temp.	TF- 66	TE 266	A34 Fuel Rod Pos.7		273. - 0.125E+04	K	0.64%FS
267	Temp.	TF- 67	TE 267	A37 Fuel Rod Pos.1		273. - 0.125E+04	K	0.64%FS
268	Temp.	TF- 68	TE 268	A37 Fuel Rod Pos.4		273. - 0.125E+04	K	0.64%FS
269	Temp.	TF- 69	TE 269	A42 Fuel Rod Pos.1		273. - 0.125E+04	K	0.64%FS
270	Temp.	TF- 70	TE 270	A42 Fuel Rod Pos.4		273. - 0.125E+04	K	0.64%FS
271	Temp.	TF- 71	TE 271	A44 Fuel Rod Pos.1		273. - 0.125E+04	K	0.64%FS
272	Temp.	TF- 72	TE 272	A44 Fuel Rod Pos.2		273. - 0.125E+04	K	0.64%FS
273	Temp.	TF- 73	TE 273	A44 Fuel Rod Pos.3		273. - 0.125E+04	K	0.64%FS
274	Temp.	TF- 74	TE 274	A44 Fuel Rod Pos.4		273. - 0.125E+04	K	0.64%FS
275	Temp.	TF- 75	TE 275	A44 Fuel Rod Pos.5		273. - 0.125E+04	K	0.64%FS
276	Temp.	TF- 76	TE 276	A44 Fuel Rod Pos.6		273. - 0.125E+04	K	0.64%FS
277	Temp.	TF- 77	TE 277	A44 Fuel Rod Pos.7		273. - 0.125E+04	K	0.64%FS
278	Temp.	TF- 78	TE 278	A48 Fuel Rod Pos.1		273. - 0.125E+04	K	0.64%FS
279	Temp.	TF- 79	TE 279	A48 Fuel Rod Pos.4		273. - 0.125E+04	K	0.64%FS
280	Temp.	TF- 80	TE 280	A51 Fuel Rod Pos.1		273. - 0.125E+04	K	0.64%FS
281	Temp.	TF- 81	TE 281	A51 Fuel Rod Pos.4		273. - 0.125E+04	K	0.64%FS
282	Temp.	TF- 82	TE 282	A53 Fuel Rod Pos.1		273. - 0.125E+04	K	0.64%FS
283	Temp.	TF- 83	TE 283	A53 Fuel Rod Pos.4		273. - 0.125E+04	K	0.64%FS
284	Temp.	TF- 84	TE 284	A57 Fuel Rod Pos.1		273. - 0.125E+04	K	0.64%FS
285	Temp.	TF- 85	TE 285	A57 Fuel Rod Pos.4		273. - 0.125E+04	K	0.64%FS
286	Temp.	TF- 86	TE 286	A62 Fuel Rod Pos.1		273. - 0.125E+04	K	0.64%FS
287	Temp.	TF- 87	TE 287	A62 Fuel Rod Pos.4		273. - 0.125E+04	K	0.64%FS
288	Temp.	TF- 88	TE 288	A66 Fuel Rod Pos.1		273. - 0.125E+04	K	0.64%FS
289	Temp.	TF- 89	TE 289	A66 Fuel Rod Pos.4		273. - 0.125E+04	K	0.64%FS
290	Temp.	TF- 90	TE 290	A68 Fuel Rod Pos.1		273. - 0.125E+04	K	0.64%FS
291	Temp.	TF- 91	TE 291	A68 Fuel Rod Pos.4		273. - 0.125E+04	K	0.64%FS
292	Temp.	TF- 92	TE 292	A71 Fuel Rod Pos.1		273. - 0.125E+04	K	0.64%FS
293	Temp.	TF- 93	TE 293	A71 Fuel Rod Pos.4		273. - 0.125E+04	K	0.64%FS
294	Temp.	TF- 94	TE 294	A73 Fuel Rod Pos.1		273. - 0.125E+04	K	0.64%FS
295	Temp.	TF- 95	TE 295	A73 Fuel Rod Pos.4		273. - 0.125E+04	K	0.64%FS
296	Temp.	TF- 96	TE 296	A75 Fuel Rod Pos.1		273. - 0.125E+04	K	0.64%FS
297	Temp.	TF- 97	TE 297	A75 Fuel Rod Pos.4		273. - 0.125E+04	K	0.64%FS
298	Temp.	TF- 98	TE 298	A77 Fuel Rod Pos.1	5. 61,181	273. - 0.125E+04	K	0.64%FS
299	Temp.	TF- 99	TE 299	A77 Fuel Rod Pos.2	5. 61,181	273. - 0.125E+04	K	0.64%FS
300	Temp.	TF-100	TE 300	A77 Fuel Rod Pos.3	5. 61,181	273. - 0.125E+04	K	0.64%FS

Table 3.2 Measurement List (Continued)

301Ch.- 350Ch.

Ch.	Item	Symbol	ID.		Location	Fig.No.	Range			Unit	Accuracy
301	Temp.	TF-101	TE	301	A77 Fuel Rod Pos.4	5. 61,181	273.	-	0.125E+04	K	0.64%FS
302	Temp.	TF-102	TE	302	A77 Fuel Rod Pos.5	5. 61,181	273.	-	0.125E+04	K	0.64%FS
303	Temp.	TF-103	TE	303	A77 Fuel Rod Pos.6	5. 61,181	273.	-	0.125E+04	K	0.64%FS
304	Temp.	TF-104	TE	304	A77 Fuel Rod Pos.7		273.	-	0.125E+04	K	0.64%FS
305	Temp.	TF-105	TE	305	A82 Fuel Rod Pos.1		273.	-	0.125E+04	K	0.64%FS
306	Temp.	TF-106	TE	306	A82 Fuel Rod Pos.4	FL, FL	273.	-	0.125E+04	K	0.64%FS
307	Temp.	TF-107	TE	307	A84 Fuel Rod Pos.1		273.	-	0.125E+04	K	0.64%FS
308	Temp.	TF-108	TE	308	A84 Fuel Rod Pos.4		273.	-	0.125E+04	K	0.64%FS
309	Temp.	TF-109	TE	309	A85 Fuel Rod Pos.1		273.	-	0.125E+04	K	0.64%FS
310	Temp.	TF-110	TE	310	A85 Fuel Rod Pos.2		273.	-	0.125E+04	K	0.64%FS
311	Temp.	TF-111	TE	311	A85 Fuel Rod Pos.3		273.	-	0.125E+04	K	0.64%FS
312	Temp.	TF-112	TE	312	A85 Fuel Rod Pos.4		273.	-	0.125E+04	K	0.64%FS
313	Temp.	TF-113	TE	313	A85 Fuel Rod Pos.5		273.	-	0.125E+04	K	0.64%FS
314	Temp.	TF-114	TE	314	A85 Fuel Rod Pos.6		273.	-	0.125E+04	K	0.64%FS
315	Temp.	TF-115	TE	315	A85 Fuel Rod Pos.7		273.	-	0.125E+04	K	0.64%FS
316	Temp.	TF-116	TE	316	A87 Fuel Rod Pos.1		273.	-	0.125E+04	K	0.64%FS
317	Temp.	TF-117	TE	317	A87 Fuel Rod Pos.2		273.	-	0.125E+04	K	0.64%FS
318	Temp.	TF-118	TE	318	A87 Fuel Rod Pos.3		273.	-	0.125E+04	K	0.64%FS
319	Temp.	TF-119	TE	319	A87 Fuel Rod Pos.4		273.	-	0.125E+04	K	0.64%FS
320	Temp.	TF-120	TE	320	A87 Fuel Rod Pos.5		273.	-	0.125E+04	K	0.64%FS
321	Temp.	TF-121	TE	321	A87 Fuel Rod Pos.6		273.	-	0.125E+04	K	0.64%FS
322	Temp.	TF-122	TE	322	A87 Fuel Rod Pos.7		273.	-	0.125E+04	K	0.64%FS
323	Temp.	TF-123	TE	323	A88 Fuel Rod Pos.1	5. 62,182	273.	-	0.125E+04	K	0.64%FS
324	Temp.	TF-124	TE	324	A88 Fuel Rod Pos.2	5. 62,182	273.	-	0.125E+04	K	0.64%FS
325	Temp.	TF-125	TE	325	A88 Fuel Rod Pos.3	5. 62,182	273.	-	0.125E+04	K	0.64%FS
326	Temp.	TF-126	TE	326	A88 Fuel Rod Pos.4	5. 62,182	273.	-	0.125E+04	K	0.64%FS
327	Temp.	TF-127	TE	327	A88 Fuel Rod Pos.5	5. 62,182	273.	-	0.125E+04	K	0.64%FS
328	Temp.	TF-128	TE	328	A88 Fuel Rod Pos.6	5. 62,182	273.	-	0.125E+04	K	0.64%FS
329	Temp.	TF-129	TE	329	A88 Fuel Rod Pos.7	5. 62,182	273.	-	0.125E+04	K	0.64%FS
330	Temp.	TF-130	TE	330	B11 Fuel Rod Pos.1		273.	-	0.125E+04	K	0.64%FS
331	Temp.	TF-131	TE	331	B11 Fuel Rod Pos.2		273.	-	0.125E+04	K	0.64%FS
332	Temp.	TF-132	TE	332	B11 Fuel Rod Pos.3		273.	-	0.125E+04	K	0.64%FS
333	Temp.	TF-133	TE	333	B11 Fuel Rod Pos.4		273.	-	0.125E+04	K	0.64%FS
334	Temp.	TF-134	TE	334	B11 Fuel Rod Pos.5		273.	-	0.125E+04	K	0.64%FS
335	Temp.	TF-135	TE	335	B11 Fuel Rod Pos.6		273.	-	0.125E+04	K	0.64%FS
336	Temp.	TF-136	TE	336	B11 Fuel Rod Pos.7	FL, FL	273.	-	0.125E+04	K	0.64%FS
337	Temp.	TF-137	TE	337	B13 Fuel Rod Pos.4		273.	-	0.125E+04	K	0.64%FS
338	Temp.	TF-138	TE	338	B22 Fuel Rod Pos.1	5. 63,183	273.	-	0.125E+04	K	0.64%FS
339	Temp.	TF-139	TE	339	B22 Fuel Rod Pos.2	5. 63,183	273.	-	0.125E+04	K	0.64%FS
340	Temp.	TF-140	TE	340	B22 Fuel Rod Pos.3	5. 63,183	273.	-	0.125E+04	K	0.64%FS
341	Temp.	TF-141	TE	341	B22 Fuel Rod Pos.4	5. 63,183	273.	-	0.125E+04	K	0.64%FS
342	Temp.	TF-142	TE	342	B22 Fuel Rod Pos.5	5. 63,183	273.	-	0.125E+04	K	0.64%FS
343	Temp.	TF-143	TE	343	B22 Fuel Rod Pos.6	5. 63,183	273.	-	0.125E+04	K	0.64%FS
344	Temp.	TF-144	TE	344	B22 Fuel Rod Pos.7	5. 63,183	273.	-	0.125E+04	K	0.64%FS
345	Temp.	TF-145	TE	345	B31 Fuel Rod Pos.4		273.	-	0.125E+04	K	0.64%FS
346	Temp.	TF-146	TE	346	B33 Fuel Rod Pos.4		273.	-	0.125E+04	K	0.64%FS
347	Temp.	TF-147	TE	347	B51 Fuel Rod Pos.4		273.	-	0.125E+04	K	0.64%FS
348	Temp.	TF-148	TE	348	B53 Fuel Rod Pos.4		273.	-	0.125E+04	K	0.64%FS
349	Temp.	TF-149	TE	349	B66 Fuel Rod Pos.4		273.	-	0.125E+04	K	0.64%FS
350	Temp.	TF-150	TE	350	B77 Fuel Rod Pos.1		273.	-	0.125E+04	K	0.64%FS

Table 3.2 Measurement List (Continued)

351Ch.- 400Ch.

Ch.	Item	Symbol	ID.		Location	Fig.No.	Range	Unit	Accuracy
351	Temp.	TF-151	TE	351	B77 Fuel Rod Pos.2		273. - 0.125E+04	K	0.64%FS
352	Temp.	TF-152	TE	352	B77 Fuel Rod Pos.3		273. - 0.125E+04	K	0.64%FS
353	Temp.	TF-153	TE	353	B77 Fuel Rod Pos.4		273. - 0.125E+04	K	0.64%FS
354	Temp.	TF-154	TE	354	B77 Fuel Rod Pos.5		273. - 0.125E+04	K	0.64%FS
355	Temp.	TF-155	TE	355	B77 Fuel Rod Pos.6		273. - 0.125E+04	K	0.64%FS
356	Temp.	TF-156	TE	356	B77 Fuel Rod Pos.7		273. - 0.125E+04	K	0.64%FS
357	Temp.	TF-157	TE	357	B86 Fuel Rod Pos.4		273. - 0.125E+04	K	0.64%FS
358	Temp.	TF-158	TE	358	C11 Fuel Rod Pos.1		273. - 0.125E+04	K	0.64%FS
359	Temp.	TF-159	TE	359	C11 Fuel Rod Pos.2		273. - 0.125E+04	K	0.64%FS
360	Temp.	TF-160	TE	360	C11 Fuel Rod Pos.3		273. - 0.125E+04	K	0.64%FS
361	Temp.	TF-161	TE	361	C11 Fuel Rod Pos.4		273. - 0.125E+04	K	0.64%FS
362	Temp.	TF-162	TE	362	C11 Fuel Rod Pos.5		273. - 0.125E+04	K	0.64%FS
363	Temp.	TF-163	TE	363	C11 Fuel Rod Pos.6		273. - 0.125E+04	K	0.64%FS
364	Temp.	TF-164	TE	364	C11 Fuel Rod Pos.7		273. - 0.125E+04	K	0.64%FS
365	Temp.	TF-165	TE	365	C13 Fuel Rod Pos.1		273. - 0.125E+04	K	0.64%FS
366	Temp.	TF-166	TE	366	C13 Fuel Rod Pos.2		273. - 0.125E+04	K	0.64%FS
367	Temp.	TF-167	TE	367	C13 Fuel Rod Pos.3		273. - 0.125E+04	K	0.64%FS
368	Temp.	TF-168	TE	368	C13 Fuel Rod Pos.4		273. - 0.125E+04	K	0.64%FS
369	Temp.	TF-169	TE	369	C13 Fuel Rod Pos.5		273. - 0.125E+04	K	0.64%FS
370	Temp.	TF-170	TE	370	C13 Fuel Rod Pos.6		273. - 0.125E+04	K	0.64%FS
371	Temp.	TF-171	TE	371	C13 Fuel Rod Pos.7		273. - 0.125E+04	K	0.64%FS
372	Temp.	TF-172	TE	372	C15 Fuel Rod Pos.4		273. - 0.125E+04	K	0.64%FS
373	Temp.	TF-173	TE	373	C22 Fuel Rod Pos.1	5. 64,184	273. - 0.125E+04	K	0.64%FS
374	Temp.	TF-174	TE	374	C22 Fuel Rod Pos.2	5. 64,184	273. - 0.125E+04	K	0.64%FS
375	Temp.	TF-175	TE	375	C22 Fuel Rod Pos.3	5. 64,184	273. - 0.125E+04	K	0.64%FS
376	Temp.	TF-176	TE	376	C22 Fuel Rod Pos.4	5. 64,184	273. - 0.125E+04	K	0.64%FS
377	Temp.	TF-177	TE	377	C22 Fuel Rod Pos.5	5. 64,184	273. - 0.125E+04	K	0.64%FS
378	Temp.	TF-178	TE	378	C22 Fuel Rod Pos.6	5. 64,184	273. - 0.125E+04	K	0.64%FS
379	Temp.	TF-179	TE	379	C22 Fuel Rod Pos.7	5. 64,184	273. - 0.125E+04	K	0.64%FS
380	Temp.	TF-180	TE	380	C31 Fuel Rod Pos.4		273. - 0.125E+04	K	0.64%FS
381	Temp.	TF-181	TE	381	C33 Fuel Rod Pos.1		273. - 0.125E+04	K	0.64%FS
382	Temp.	TF-182	TE	382	C33 Fuel Rod Pos.2		273. - 0.125E+04	K	0.64%FS
383	Temp.	TF-183	TE	383	C33 Fuel Rod Pos.3		273. - 0.125E+04	K	0.64%FS
384	Temp.	TF-184	TE	384	C33 Fuel Rod Pos.4		273. - 0.125E+04	K	0.64%FS
385	Temp.	TF-185	TE	385	C33 Fuel Rod Pos.5		273. - 0.125E+04	K	0.64%FS
386	Temp.	TF-186	TE	386	C33 Fuel Rod Pos.6		273. - 0.125E+04	K	0.64%FS
387	Temp.	TF-187	TE	387	C33 Fuel Rod Pos.7		273. - 0.125E+04	K	0.64%FS
388	Temp.	TF-188	TE	388	C35 Fuel Rod Pos.4		273. - 0.125E+04	K	0.64%FS
389	Temp.	TF-189	TE	389	C66 Fuel Rod Pos.4		273. - 0.125E+04	K	0.64%FS
390	Temp.	TF-190	TE	390	C68 Fuel Rod Pos.4		273. - 0.125E+04	K	0.64%FS
391	Temp.	TF-191	TE	391	C77 Fuel Rod Pos.1	5. 74,194	273. - 0.125E+04	K	0.64%FS
392	Temp.	TF-192	TE	392	C77 Fuel Rod Pos.2	5. 75,195	273. - 0.125E+04	K	0.64%FS
393	Temp.	TF-193	TE	393	C77 Fuel Rod Pos.3	5. 76,196	273. - 0.125E+04	K	0.64%FS
394	Temp.	TF-194	TE	394	C77 Fuel Rod Pos.4	5. 77,197	273. - 0.125E+04	K	0.64%FS
395	Temp.	TF-195	TE	395	C77 Fuel Rod Pos.5	5. 78,198	273. - 0.125E+04	K	0.64%FS
396	Temp.	TF-196	TE	396	C77 Fuel Rod Pos.6	5. 79,199	273. - 0.125E+04	K	0.64%FS
397	Temp.	TF-197	TE	397	C77 Fuel Rod Pos.7	5. 80,200	273. - 0.125E+04	K	0.64%FS
398	Temp.	TF-198	TE	398	D11 Fuel Rod Pos.4		273. - 0.125E+04	K	0.64%FS
399	Temp.	TF-199	TE	399	D13 Fuel Rod Pos.4		273. - 0.125E+04	K	0.64%FS
400	Temp.	TF-200	TE	400	D22 Fuel Rod Pos.1	5. 65,185	273. - 0.125E+04	K	0.64%FS

Table 3.2 Measurement List (Continued)

401Ch.- 450Ch.

Ch.	Item	Symbol	ID.		Location	Fig.No.	Range	Unit	Accuracy
401	Temp.	TF-201	TE	401	D22 Fuel Rod Pos.2	5. 65,185	273. - 0.125E+04	K	0.64%FS
402	Temp.	TF-202	TE	402	D22 Fuel Rod Pos.3	5. 65,185	273. - 0.125E+04	K	0.64%FS
403	Temp.	TF-203	TE	403	D22 Fuel Rod Pos.4	5. 65,185	273. - 0.125E+04	K	0.64%FS
404	Temp.	TF-204	TE	404	D22 Fuel Rod Pos.5	5. 65,185	273. - 0.125E+04	K	0.64%FS
405	Temp.	TF-205	TE	405	D22 Fuel Rod Pos.6	5. 65,185	273. - 0.125E+04	K	0.64%FS
406	Temp.	TF-206	TE	406	D22 Fuel Rod Pos.7	5. 65,185	273. - 0.125E+04	K	0.64%FS
407	Temp.	TF-207	TE	407	D31 Fuel Rod Pos.4		273. - 0.125E+04	K	0.64%FS
408	Temp.	TF-208	TE	408	D33 Fuel Rod Pos.4		273. - 0.125E+04	K	0.64%FS
409	Temp.	TF-209	TE	409	D51 Fuel Rod Pos.4		273. - 0.125E+04	K	0.64%FS
410	Temp.	TF-210	TE	410	D53 Fuel Rod Pos.4		273. - 0.125E+04	K	0.64%FS
411	Temp.	TF-211	TE	411	D66 Fuel Rod Pos.4		273. - 0.125E+04	K	0.64%FS
412	Temp.	TF-212	TE	412	D77 Fuel Rod Pos.4	FL, FL	273. - 0.125E+04	K	0.64%FS
413	Temp.	TF-213	TE	413	D86 Fuel Rod Pos.4		273. - 0.125E+04	K	0.64%FS
414	Fluid T.	TW- 1	TE	414	A45 Tie Rod Pos.1		273. - 0.125E+04	K	0.64%FS
415	Fluid T.	TW- 2	TE	415	A45 Tie Rod Pos.2		273. - 0.125E+04	K	0.64%FS
416	Fluid T.	TW- 3	TE	416	A45 Tie Rod Pos.3		273. - 0.125E+04	K	0.64%FS
417	Fluid T.	TW- 4	TE	417	A45 Tie Rod Pos.4		273. - 0.125E+04	K	0.64%FS
418	Fluid T.	TW- 5	TE	418	A45 Tie Rod Pos.5		273. - 0.125E+04	K	0.64%FS
419	Fluid T.	TW- 6	TE	419	A45 Tie Rod Pos.6		273. - 0.125E+04	K	0.64%FS
420	Fluid T.	TW- 7	TE	420	A45 Tie Rod Pos.7		273. - 0.125E+04	K	0.64%FS
421	Fluid T.	TW- 8	TE	421	B45 Tie Rod Pos.1		273. - 0.125E+04	K	0.64%FS
422	Fluid T.	TW- 9	TE	422	B45 Tie Rod Pos.2		273. - 0.125E+04	K	0.64%FS
423	Fluid T.	TW-10	TE	423	B45 Tie Rod Pos.3		273. - 0.125E+04	K	0.64%FS
424	Fluid T.	TW-11	TE	424	B45 Tie Rod Pos.4		273. - 0.125E+04	K	0.64%FS
425	Fluid T.	TW-12	TE	425	B45 Tie Rod Pos.5		273. - 0.125E+04	K	0.64%FS
426	Fluid T.	TW-13	TE	426	B45 Tie Rod Pos.6		273. - 0.125E+04	K	0.64%FS
427	Fluid T.	TW-14	TE	427	B45 Tie Rod Pos.7		273. - 0.125E+04	K	0.64%FS
428	Fluid T.	TW-15	TE	428	C45 Tie Rod Pos.1		273. - 0.125E+04	K	0.64%FS
429	Fluid T.	TW-16	TE	429	C45 Tie Rod Pos.2		273. - 0.125E+04	K	0.64%FS
430	Fluid T.	TW-17	TE	430	C45 Tie Rod Pos.3		273. - 0.125E+04	K	0.64%FS
431	Fluid T.	TW-18	TE	431	C45 Tie Rod Pos.4		273. - 0.125E+04	K	0.64%FS
432	Fluid T.	TW-19	TE	432	C45 Tie Rod Pos.5		273. - 0.125E+04	K	0.64%FS
433	Fluid T.	TW-20	TE	433	C45 Tie Rod Pos.6		273. - 0.125E+04	K	0.64%FS
434	Fluid T.	TW-21	TE	434	C45 Tie Rod Pos.7		273. - 0.125E+04	K	0.64%FS
435	Fluid T.	TW-22	TE	435	D45 Tie Rod Pos.1		273. - 0.125E+04	K	0.64%FS
436	Fluid T.	TW-23	TE	436	D45 Tie Rod Pos.2		273. - 0.125E+04	K	0.64%FS
437	Fluid T.	TW-24	TE	437	D45 Tie Rod Pos.3	FL, FL	273. - 0.125E+04	K	0.64%FS
438	Fluid T.	TW-25	TE	438	D45 Tie Rod Pos.4	FL, FL	273. - 0.125E+04	K	0.64%FS
439	Fluid T.	TW-26	TE	439	D45 Tie Rod Pos.5	FL, FL	273. - 0.125E+04	K	0.64%FS
440	Fluid T.	TW-27	TE	440	D45 Tie Rod Pos.6	FL, FL	273. - 0.125E+04	K	0.64%FS
441	Fluid T.	TW-28	TE	441	D45 Tie Rod Pos.7	FL, FL	273. - 0.125E+04	K	0.64%FS
442	Fluid T.	TC- 1	TE	442	Channel Box A Inlet	5. 81,201	273. - 0.125E+04	K	0.64%FS
443	Fluid T.	TC- 2	TE	443	Channel Box B Inlet	5. 81,201	273. - 0.125E+04	K	0.64%FS
444	Fluid T.	TC- 3	TE	444	Channel Box C Inlet	5. 81,201	273. - 0.125E+04	K	0.64%FS
445	Fluid T.	TC- 4	TE	445	Channel Box D Inlet	5. 81,201	273. - 0.125E+04	K	0.64%FS
446	Fluid T.	TC- 5	TE	446	Channel Box Outlet A-1		273. - 0.125E+04	K	0.64%FS
447	Fluid T.	TC- 6	TE	447	Channel Box Outlet A-2		273. - 0.125E+04	K	0.64%FS
448	Fluid T.	TC- 7	TE	448	Channel Box Outlet A-3		273. - 0.125E+04	K	0.64%FS
449	Fluid T.	TC- 8	TE	449	Channel Box Outlet A-4		273. - 0.125E+04	K	0.64%FS
450	Fluid T.	TC- 9	TE	450	Channel Box Outlet A-6		273. - 0.125E+04	K	0.64%FS

Table 3.2 Measurement List (Continued) 451Ch.- 500Ch.

Ch.	Item	Symbol	ID.	Location	Fig.No.	Range	Unit	Accuracy
451	Fluid T.	TC-10	TE 451	Channel Box Outlet C-1		273. - 0.125E+04	K	0.64%FS
452	Fluid T.	TC-11	TE 452	Channel Box Outlet C-2		273. - 0.125E+04	K	0.64%FS
453	Fluid T.	TC-12	TE 453	Channel Box Outlet C-3		273. - 0.125E+04	K	0.64%FS
454	Fluid T.	TC-13	TE 454	Channel Box Outlet C-4		273. - 0.125E+04	K	0.64%FS
455	Fluid T.	TC-14	TE 455	Channel Box Outlet C-6		273. - 0.125E+04	K	0.64%FS
456	Fluid T.	TG- 1	TE 456	Upper Tieplate A Up.1	5. 82,202	273. - 0.125E+04	K	0.64%FS
457	Fluid T.	TG- 2	TE 457	Upper Tieplate A Up.2		273. - 0.125E+04	K	0.64%FS
458	Fluid T.	TG- 3	TE 458	Upper Tieplate A Up.3		273. - 0.125E+04	K	0.64%FS
459	Fluid T.	TG- 4	TE 459	Upper Tieplate A Up.4	5. 83,203	273. - 0.125E+04	K	0.64%FS
460	Fluid T.	TG- 5	TE 460	Upper Tieplate A Up.5	5. 84,204	273. - 0.125E+04	K	0.64%FS
461	Fluid T.	TG- 6	TE 461	Upper Tieplate A Up.6		273. - 0.125E+04	K	0.64%FS
462	Fluid T.	TG- 7	TE 462	Upper Tieplate A Up.7		273. - 0.125E+04	K	0.64%FS
463	Fluid T.	TG- 8	TE 463	Upper Tieplate A Up.8	5. 85,205	273. - 0.125E+04	K	0.64%FS
464	Fluid T.	TG- 9	TE 464	Upper Tieplate A Up.9		273. - 0.125E+04	K	0.64%FS
465	Fluid T.	TG-10	TE 465	Upper Tieplate A Up.10	5. 86,206	273. - 0.125E+04	K	0.64%FS
466	Fluid T.	TG-11	TE 466	Upper Tieplate A Lo.1	5. 82,202	273. - 0.125E+04	K	0.64%FS
467	Fluid T.	TG-12	TE 467	Upper Tieplate A Lo.2		273. - 0.125E+04	K	0.64%FS
468	Fluid T.	TG-13	TE 468	Upper Tieplate A Lo.3		273. - 0.125E+04	K	0.64%FS
469	Fluid T.	TG-14	TE 469	Upper Tieplate A Lo.4	5. 83,203	273. - 0.125E+04	K	0.64%FS
470	Fluid T.	TG-15	TE 470	Upper Tieplate A Lo.5	5. 84,204	273. - 0.125E+04	K	0.64%FS
471	Fluid T.	TG-16	TE 471	Upper Tieplate A Lo.6		273. - 0.125E+04	K	0.64%FS
472	Fluid T.	TG-17	TE 472	Upper Tieplate A Lo.7		273. - 0.125E+04	K	0.64%FS
473	Fluid T.	TG-18	TE 473	Upper Tieplate A Lo.8	5. 85,205	273. - 0.125E+04	K	0.64%FS
474	Fluid T.	TG-19	TE 474	Upper Tieplate A Lo.9		273. - 0.125E+04	K	0.64%FS
475	Fluid T.	TG-20	TE 475	Upper Tieplate A Lo.10	5. 86,206	273. - 0.125E+04	K	0.64%FS
476	Fluid T.	TG-21	TE 476	Upper Tieplate C Up.1		273. - 0.125E+04	K	0.64%FS
477	Fluid T.	TG-22	TE 477	Upper Tieplate C Up.2		273. - 0.125E+04	K	0.64%FS
478	Fluid T.	TG-23	TE 478	Upper Tieplate C Up.3		273. - 0.125E+04	K	0.64%FS
479	Fluid T.	TG-24	TE 479	Upper Tieplate C Up.4		273. - 0.125E+04	K	0.64%FS
480	Fluid T.	TG-25	TE 480	Upper Tieplate C Up.5		273. - 0.125E+04	K	0.64%FS
481	Fluid T.	TG-26	TE 481	Upper Tieplate C Up.6		273. - 0.125E+04	K	0.64%FS
482	Fluid T.	TG-27	TE 482	Upper Tieplate C Up.7		273. - 0.125E+04	K	0.64%FS
483	Fluid T.	TG-28	TE 483	Upper Tieplate C Up.8		273. - 0.125E+04	K	0.64%FS
484	Fluid T.	TG-29	TE 484	Upper Tieplate C Up.9		273. - 0.125E+04	K	0.64%FS
485	Fluid T.	TG-30	TE 485	Upper Tieplate C Up.10		273. - 0.125E+04	K	0.64%FS
486	Fluid T.	TG-31	TE 486	Upper Tieplate C Lo.1		273. - 0.125E+04	K	0.64%FS
487	Fluid T.	TG-32	TE 487	Upper Tieplate C Lo.2		273. - 0.125E+04	K	0.64%FS
488	Fluid T.	TG-33	TE 488	Upper Tieplate C Lo.3		273. - 0.125E+04	K	0.64%FS
489	Fluid T.	TG-34	TE 489	Upper Tieplate C Lo.4		273. - 0.125E+04	K	0.64%FS
490	Fluid T.	TG-35	TE 490	Upper Tieplate C Lo.5		273. - 0.125E+04	K	0.64%FS
491	Fluid T.	TG-36	TE 491	Upper Tieplate C Lo.6		273. - 0.125E+04	K	0.64%FS
492	Fluid T.	TG-37	TE 492	Upper Tieplate C Lo.7		273. - 0.125E+04	K	0.64%FS
493	Fluid T.	TG-38	TE 493	Upper Tieplate C Lo.8		273. - 0.125E+04	K	0.64%FS
494	Fluid T.	TG-39	TE 494	Upper Tieplate C Lo.9		273. - 0.125E+04	K	0.64%FS
495	Fluid T.	TG-40	TE 495	Upper Tieplate C Lo.10		273. - 0.125E+04	K	0.64%FS
496	Slab T.	TB- 1	TE 496	C.B. A1 Inner ,Pos.1		273. - 0.125E+04	K	0.64%FS
497	Slab T.	TB- 2	TE 497	C.B. A1 Inner ,Pos.2		273. - 0.125E+04	K	0.64%FS
498	Slab T.	TB- 3	TE 498	C.B. A1 Inner ,Pos.3		273. - 0.125E+04	K	0.64%FS
499	Slab T.	TB- 4	TE 499	C.B. A1 Inner ,Pos.4		273. - 0.125E+04	K	0.64%FS
500	Slab T.	TB- 5	TE 500	C.B. A1 Inner ,Pos.5		273. - 0.125E+04	K	0.64%FS

Table 3.2 Measurement List (Continued)

501Ch.- 550Ch.

Ch.	Item	Symbol	ID.		Location	Fig.No.	Range			Unit	Accuracy
501	Slab T.	TB- 6	TE	501	C.B. A1 Inner ,Pos.6		273.	-	0.125E+04	K	0.64%FS
502	Slab T.	TB- 7	TE	502	C.B. A1 Inner ,Pos.7		273.	-	0.125E+04	K	0.64%FS
503	Slab T.	TB- 8	TE	503	C.B. A2 Inner ,Pos.1	FL, FL	273.	-	0.125E+04	K	0.64%FS
504	Slab T.	TB- 9	TE	504	C.B. A2 Inner ,Pos.2		273.	-	0.125E+04	K	0.64%FS
505	Slab T.	TB-10	TE	505	C.B. A2 Inner ,Pos.3		273.	-	0.125E+04	K	0.64%FS
506	Slab T.	TB-11	TE	506	C.B. A2 Inner ,Pos.4		273.	-	0.125E+04	K	0.64%FS
507	Slab T.	TB-12	TE	507	C.B. A2 Inner ,Pos.5		273.	-	0.125E+04	K	0.64%FS
508	Slab T.	TB-13	TE	508	C.B. A2 Inner ,Pos.6		273.	-	0.125E+04	K	0.64%FS
509	Slab T.	TB-14	TE	509	C.B. A2 Inner ,Pos.7	FL, FL	273.	-	0.125E+04	K	0.64%FS
510	Slab T.	TB-15	TE	510	C.B. B Inner ,Pos.1		273.	-	0.125E+04	K	0.64%FS
511	Slab T.	TB-16	TE	511	C.B. B Inner ,Pos.2		273.	-	0.125E+04	K	0.64%FS
512	Slab T.	TB-17	TE	512	C.B. B Inner ,Pos.3		273.	-	0.125E+04	K	0.64%FS
513	Slab T.	TB-18	TE	513	C.B. B Inner ,Pos.4		273.	-	0.125E+04	K	0.64%FS
514	Slab T.	TB-19	TE	514	C.B. B Inner ,Pos.5		273.	-	0.125E+04	K	0.64%FS
515	Slab T.	TB-20	TE	515	C.B. B Inner ,Pos.6		273.	-	0.125E+04	K	0.64%FS
516	Slab T.	TB-21	TE	516	C.B. B Inner ,Pos.7		273.	-	0.125E+04	K	0.64%FS
517	Slab T.	TB-22	TE	517	C.B. C Inner ,Pos.1		273.	-	0.125E+04	K	0.64%FS
518	Slab T.	TB-23	TE	518	C.B. C Inner ,Pos.2		273.	-	0.125E+04	K	0.64%FS
519	Slab T.	TB-24	TE	519	C.B. C Inner ,Pos.3		273.	-	0.125E+04	K	0.64%FS
520	Slab T.	TB-25	TE	520	C.B. C Inner ,Pos.4		273.	-	0.125E+04	K	0.64%FS
521	Slab T.	TB-26	TE	521	C.B. C Inner ,Pos.5		273.	-	0.125E+04	K	0.64%FS
522	Slab T.	TB-27	TE	522	C.B. C Inner ,Pos.6		273.	-	0.125E+04	K	0.64%FS
523	Slab T.	TB-28	TE	523	C.B. C Inner ,Pos.7		273.	-	0.125E+04	K	0.64%FS
524	Slab T.	TB-29	TE	524	C.B. D Inner ,Pos.1		273.	-	0.125E+04	K	0.64%FS
525	Slab T.	TB-30	TE	525	C.B. D Inner ,Pos.2		273.	-	0.125E+04	K	0.64%FS
526	Slab T.	TB-31	TE	526	C.B. D Inner ,Pos.3		273.	-	0.125E+04	K	0.64%FS
527	Slab T.	TB-32	TE	527	C.B. D Inner ,Pos.4		273.	-	0.125E+04	K	0.64%FS
528	Slab T.	TB-33	TE	528	C.B. D Inner ,Pos.5		273.	-	0.125E+04	K	0.64%FS
529	Slab T.	TB-34	TE	529	C.B. D Inner ,Pos.6		273.	-	0.125E+04	K	0.64%FS
530	Slab T.	TB-35	TE	530	C.B. D Inner ,Pos.7		273.	-	0.125E+04	K	0.64%FS
531	Fluid T.	TB-36	TE	531	C.B. A Outer ,Pos.1	5. 66,186	273.	-	0.125E+04	K	0.64%FS
532	Fluid T.	TB-37	TE	532	C.B. A Outer ,Pos.2	5. 66,186	273.	-	0.125E+04	K	0.64%FS
533	Fluid T.	TB-38	TE	533	C.B. A Outer ,Pos.3	5. 66,186	273.	-	0.125E+04	K	0.64%FS
534	Fluid T.	TB-39	TE	534	C.B. A Outer ,Pos.4	5. 66,186	273.	-	0.125E+04	K	0.64%FS
535	Fluid T.	TB-40	TE	535	C.B. A Outer ,Pos.5	5. 66,186	273.	-	0.125E+04	K	0.64%FS
536	Fluid T.	TB-41	TE	536	C.B. A Outer ,Pos.6	5. 66,186	273.	-	0.125E+04	K	0.64%FS
537	Fluid T.	TB-42	TE	537	C.B. A Outer ,Pos.7	5. 66,186	273.	-	0.125E+04	K	0.64%FS
538	Fluid T.	TB-43	TE	538	C.B. C Outer ,Pos.1		273.	-	0.125E+04	K	0.64%FS
539	Fluid T.	TB-44	TE	539	C.B. C Outer ,Pos.2		273.	-	0.125E+04	K	0.64%FS
540	Fluid T.	TB-45	TE	540	C.B. C Outer ,Pos.3		273.	-	0.125E+04	K	0.64%FS
541	Fluid T.	TB-46	TE	541	C.B. C Outer ,Pos.4		273.	-	0.125E+04	K	0.64%FS
542	Fluid T.	TB-47	TE	542	C.B. C Outer ,Pos.5		273.	-	0.125E+04	K	0.64%FS
543	Fluid T.	TB-48	TE	543	C.B. C Outer ,Pos.6		273.	-	0.125E+04	K	0.64%FS
544	Fluid T.	TB-49	TE	544	C.B. C Outer ,Pos.7		273.	-	0.125E+04	K	0.64%FS
545	Fluid T.	TP- 1	TE	545	Lower Pl. Center 1		273.	-	0.125E+04	K	0.64%FS
546	Fluid T.	TP- 2	TE	546	Lower Pl. Center 2		273.	-	0.125E+04	K	0.64%FS
547	Fluid T.	TP- 3	TE	547	Lower Pl. Center 3		273.	-	0.125E+04	K	0.64%FS
548	Fluid T.	TP- 4	TE	548	Lower Pl. Center 4		273.	-	0.125E+04	K	0.64%FS
549	Fluid T.	TP- 5	TE	549	Lower Pl. Center 5		273.	-	0.125E+04	K	0.64%FS
550	Fluid T.	TP- 6	TE	550	Lower Pl. Center 7		273.	-	0.125E+04	K	0.64%FS

Table 3.2 Measurement List (Continued)

551Ch.- 600Ch.

Ch.	Item	Symbol	ID.		Location	Fig.No.	Range			Unit	Accuracy
551	Slab T.	TP- 7	TE	551	Lower Pl. North 1		273.	-	0.125E+04	K	0.64%FS
552	Slab T.	TP- 8	TE	552	Lower Pl. North 2		273.	-	673.	K	0.64%FS
553	Slab T.	TP- 9	TE	553	Lower Pl. North 4		273.	-	673.	K	0.64%FS
554	Slab T.	TP-10	TE	554	Lower Pl. North 6		273.	-	673.	K	0.64%FS
555	Slab T.	TP-11	TE	555	Lower Pl. South 1		273.	-	673.	K	0.64%FS
556	Slab T.	TP-12	TE	556	Lower Pl. South 2		273.	-	673.	K	0.64%FS
557	Slab T.	TP-13	TE	557	Lower Pl. South 4		273.	-	673.	K	0.64%FS
558	Slab T.	TP-14	TE	558	Lower Pl. South 6		273.	-	673.	K	0.64%FS
559	Level	LB- 1	LM	559	C.B.Liquid Level A1-1						
560	Level	LB- 2	LM	560	C.B.Liquid Level A1-2	FL, FL					
561	Level	LB- 3	LM	561	C.B.Liquid Level A1-3						
562	Level	LB- 4	LM	562	C.B.Liquid Level A1-4						
563	Level	LB- 5	LM	563	C.B.Liquid Level A1-5						
564	Level	LB- 6	LM	564	C.B.Liquid Level A1-6						
565	Level	LB- 7	LM	565	C.B.Liquid Level A1-7						
566	Level	LB- 8	LM	566	C.B.Liquid Level A2-1	5. 87,207					
567	Level	LB- 9	LM	567	C.B.Liquid Level A2-2	5. 87,207					
568	Level	LB-10	LM	568	C.B.Liquid Level A2-3	5. 87,207					
569	Level	LB-11	LM	569	C.B.Liquid Level A2-4	5. 87,207					
570	Level	LB-12	LM	570	C.B.Liquid Level A2-5	5. 87,207					
571	Level	LB-13	LM	571	C.B.Liquid Level A2-6	5. 87,207					
572	Level	LB-14	LM	572	C.B.Liquid Level A2-7	5. 87,207					
573	Level	LB-15	LM	573	C.B.Liquid Level B-1	5. 88,208					
574	Level	LB-16	LM	574	C.B.Liquid Level B-2	5. 88,208					
575	Level	LB-17	LM	575	C.B.Liquid Level B-3	5. 88,208					
576	Level	LB-18	LM	576	C.B.Liquid Level B-4	5. 88,208					
577	Level	LB-19	LM	577	C.B.Liquid Level B-5	5. 88,208					
578	Level	LB-20	LM	578	C.B.Liquid Level B-6	5. 88,208					
579	Level	LB-21	LM	579	C.B.Liquid Level B-7	5. 88,208					
580	Level	LB-22	LM	580	C.B.Liquid Level C-1	5. 89,209					
581	Level	LB-23	LM	581	C.B.Liquid Level C-2	5. 89,209					
582	Level	LB-24	LM	582	C.B.Liquid Level C-3	5. 89,209					
583	Level	LB-25	LM	583	C.B.Liquid Level C-4	5. 89,209					
584	Level	LB-26	LM	584	C.B.Liquid Level C-5	5. 89,209					
585	Level	LB-27	LM	585	C.B.Liquid Level C-6	5. 89,209					
586	Level	LB-28	LM	586	C.B.Liquid Level C-7	5. 89,209					
587	Level	LB-29	LM	587	C.B.Liquid Level D-1	5. 90,210					
588	Level	LB-30	LM	588	C.B.Liquid Level D-2	5. 90,210					
589	Level	LB-31	LM	589	C.B.Liquid Level D-3	5. 90,210					
590	Level	LB-32	LM	590	C.B.Liquid Level D-4	5. 90,210					
591	Level	LB-33	LM	591	C.B.Liquid Level D-5	5. 90,210					
592	Level	LB-34	LM	592	C.B.Liquid Level D-6	5. 90,210					
593	Level	LB-35	LM	593	C.B.Liquid Level D-7	5. 90,210					
594	Level	LL- 1	LM	594	Ch.Box Outlet A1-5						
595	Level	LL- 2	LM	595	Ch.Box Outlet A1-6						
596	Level	LL- 3	LM	596	Ch.Box Outlet A1-7	FL, FL					
597	Level	LL- 4	LM	597	Ch.Box Outlet A2-5	5. 91,211					
598	Level	LL- 5	LM	598	Ch.Box Outlet A2-6	5. 91,211					
599	Level	LL- 6	LM	599	Ch.Box Outlet A2-7	5. 91,211					
600	Level	LL- 7	LM	600	Ch.Box Outlet A-1	5. 92,212					

Table 3.2 Measurement List (Continued)

601Ch.- 650Ch.

Ch.	Item	Symbol	ID.		Location	Fig.No.	Range	Unit	Accuracy
601	Level	LL- 8	LM	601	Ch.Box Outlet A-2	FL, FL			
602	Level	LL- 9	LM	602	Ch.Box Outlet A-3	5. 92,212			
603	Level	LL-10	LM	603	Ch.Box Outlet A-4	5. 92,212			
604	Level	LL-11	LM	604	Ch.Box Outlet A-6	5. 92,212			
605	Level	LL-12	LM	605	Ch.Box Outlet C1-5	5. 93,213			
606	Level	LL-13	LM	606	Ch.Box Outlet C1-6	5. 93,213			
607	Level	LL-14	LM	607	Ch.Box Outlet C1-7	5. 93,213			
608	Level	LL-15	LM	608	Ch.Box Outlet C2-5				
609	Level	LL-16	LM	609	Ch.Box Outlet C2-6				
610	Level	LL-17	LM	610	Ch.Box Outlet C2-7				
611	Level	LL-18	LM	611	Ch.Box Outlet C-1	5. 94,214			
612	Level	LL-19	LM	612	Ch.Box Outlet C-2	5. 94,214			
613	Level	LL-20	LM	613	Ch.Box Outlet C-3	5. 94,214			
614	Level	LL-21	LM	614	Ch.Box Outlet C-4	5. 94,214			
615	Level	LL-22	LM	615	Ch.Box Outlet C-6	5. 94,214			
616	Level	LL-23	LM	616	Ch.Box Inlet A-1	5. 95,215			
617	Level	LL-24	LM	617	Ch.Box Inlet A-2	5. 95,215			
618	Level	LL-25	LM	618	Ch.Box Inlet B-1				
619	Level	LL-26	LM	619	Ch.Box Inlet B-2				
620	Level	LL-27	LM	620	Ch.Box Inlet C-1	5. 96,216			
621	Level	LL-28	LM	621	Ch.Box Inlet C-2	5. 96,216			
622	Level	LL-29	LM	622	Ch.Box Inlet D-1				
623	Level	LL-30	LM	623	Ch.Box Inlet D-2				
624	Level	LL-31	LM	624	Lower Pl. North 1	5. 97,217			
625	Level	LL-32	LM	625	Lower Pl. North 2	5. 97,217			
626	Level	LL-33	LM	626	Lower Pl. North 3	5. 97,217			
627	Level	LL-34	LM	627	Lower Pl. North 4	5. 97,217			
628	Level	LL-35	LM	628	Lower Pl. North 5	5. 97,217			
629	Level	LL-36	LM	629	Lower Pl. North 6	5. 97,217			
630	Level	LL-37	LM	630	Lower Pl. South 1				
631	Level	LL-38	LM	631	Lower Pl. South 2				
632	Level	LL-39	LM	632	Lower Pl. South 3				
633	Level	LL-40	LM	633	Lower Pl. South 4				
634	Level	LL-41	LM	634	Lower Pl. South 5				
635	Level	LL-42	LM	635	Lower Pl. South 6				
636	Level	LL-43	LM	636	Guide Tube North 0	5. 98,218			
637	Level	LL-44	LM	637	Guide Tube North 1	5. 98,218			
638	Level	LL-45	LM	638	Guide Tube North 3	5. 98,218			
639	Level	LL-46	LM	639	Guide Tube North 6	5. 98,218			
640	Level	LL-47	LM	640	Guide Tube South 0				
641	Level	LL-48	LM	641	Guide Tube South 1				
642	Level	LL-49	LM	642	Guide Tube South 3				
643	Level	LL-50	LM	643	Guide Tube South 6				
644	Level	L- 1	LM	644	Downcomer D-Side 1	5. 99,219			
645	Level	L- 2	LM	645	Downcomer D-Side 2	5. 99,219			
646	Level	L- 3	LM	646	Downcomer D-Side 3	5. 99,219			
647	Level	L- 4	LM	647	Downcomer D-Side 4	5. 99,219			
648	Level	L- 5	LM	648	Downcomer D-Side 5	5. 99,219			
649	Level	L- 6	LM	649	Downcomer B-Side 1				
650	Level	L- 7	LM	650	Downcomer B-Side 2				

Table 3.2 Measurement List (Continued)

651Ch.- 700Ch.

Ch.	Item	Symbol	ID.		Location	Fig.No.	Range			Unit	Accuracy
651	Level	L- 8	LM	651	Downcomer B-Side 3						
652	Level	L- 9	LM	652	Downcomer B-Side 4						
653	Level	L-10	LM	653	Downcomer B-Side 5	FL, FL					
654	Void	VF- 1	VD	654	A54 Tie Rod Pos.1	NM, NM	0.0	-	1.00		
655	Void	VF- 2	VD	655	A54 Tie Rod Pos.2	NM, NM	0.0	-	1.00		
656	Void	VF- 3	VD	656	A54 Tie Rod Pos.3	NM, NM	0.0	-	1.00		
657	Void	VF- 4	VD	657	A54 Tie Rod Pos.4	NM, NM	0.0	-	1.00		
658	Void	VF- 5	VD	658	A54 Tie Rod Pos.5	NM, NM	0.0	-	1.00		
659	Void	VF- 6	VD	659	A54 Tie Rod Pos.6	NM, NM	0.0	-	1.00		
660	Void	VF- 7	VD	660	A54 Tie Rod Pos.7	NM, NM	0.0	-	1.00		
661	Void	VF- 8	VD	661	B54 Tie Rod Pos.1	NM, NM	0.0	-	1.00		
662	Void	VF- 9	VD	662	B54 Tie Rod Pos.2	NM, NM	0.0	-	1.00		
663	Void	VF-10	VD	663	B54 Tie Rod Pos.3	NM, NM	0.0	-	1.00		
664	Void	VF-11	VD	664	B54 Tie Rod Pos.4	NM, NM	0.0	-	1.00		
665	Void	VF-12	VD	665	B54 Tie Rod Pos.5	NM, NM	0.0	-	1.00		
666	Void	VF-13	VD	666	B54 Tie Rod Pos.6	NM, NM	0.0	-	1.00		
667	Void	VF-14	VD	667	B54 Tie Rod Pos.7	NM, NM	0.0	-	1.00		
668	Void	VF-15	VD	668	C54 Tie Rod Pos.1	NM, NM	0.0	-	1.00		
669	Void	VF-16	VD	669	C54 Tie Rod Pos.2	NM, NM	0.0	-	1.00		
670	Void	VF-17	VD	670	C54 Tie Rod Pos.3	NM, NM	0.0	-	1.00		
671	Void	VF-18	VD	671	C54 Tie Rod Pos.4	NM, NM	0.0	-	1.00		
672	Void	VF-19	VD	672	C54 Tie Rod Pos.5	NM, NM	0.0	-	1.00		
673	Void	VF-20	VD	673	C54 Tie Rod Pos.6	NM, NM	0.0	-	1.00		
674	Void	VF-21	VD	674	C54 Tie Rod Pos.7	NM, NM	0.0	-	1.00		
675	Void	VF-22	VD	675	D54 Tie Rod Pos.7	NM, NM	0.0	-	1.00		
676	Void	VF-23	VD	676	D54 Tie Rod Pos.7	NM, NM	0.0	-	1.00		
677	Void	VF-24	VD	677	D54 Tie Rod Pos.7	NM, NM	0.0	-	1.00		
678	Void	VF-25	VD	678	D54 Tie Rod Pos.7	NM, NM	0.0	-	1.00		
679	Void	VF-26	VD	679	D54 Tie Rod Pos.7	NM, NM	0.0	-	1.00		
680	Void	VF-27	VD	680	D54 Tie Rod Pos.7	NM, NM	0.0	-	1.00		
681	Void	VF-28	VD	681	D54 Tie Rod Pos.7	NM, NM	0.0	-	1.00		
682	Void	VE- 1	VD	682	Channel A Outlet 1	NM, NM	0.0	-	1.00		
683	Void	VE- 2	VD	683	Channel A Outlet 2	NM, NM	0.0	-	1.00		
684	Void	VE- 3	VD	684	Channel A Outlet 3	NM, NM	0.0	-	1.00		
685	Void	VE- 4	VD	685	Channel B Outlet 1	NM, NM	0.0	-	1.00		
686	Void	VE- 5	VD	686	Channel B Outlet 2	NM, NM	0.0	-	1.00		
687	Void	VE- 6	VD	687	Channel B Outlet 3	NM, NM	0.0	-	1.00		
688	Void	VE- 7	VD	688	Channel C Outlet 1	NM, NM	0.0	-	1.00		
689	Void	VE- 8	VD	689	Channel C Outlet 2	NM, NM	0.0	-	1.00		
690	Void	VE- 9	VD	690	Channel C Outlet 3	NM, NM	0.0	-	1.00		
691	Void	VE-10	VD	691	Channel D Outlet 1	NM, NM	0.0	-	1.00		
692	Void	VE-11	VD	692	Channel D Outlet 2	NM, NM	0.0	-	1.00		
693	Void	VE-12	VD	693	Channel D Outlet 3	NM, NM	0.0	-	1.00		
694	Void	VE-13	VD	694	Lower Plenum Bottom 1	NM, NM	0.0	-	1.00		
695	Void	VE-14	VD	695	Lower Plenum Bottom 2	NM, NM	0.0	-	1.00		
696	Void	VE-15	VD	696	Lower Plenum Bottom 3	NM, NM	0.0	-	1.00		
697	Void	VP- 1	VD	697	Lower Plenum Inlet	NM, NM	0.0	-	1.00		
698	Void	VP- 2	VD	698	Lower Plenum Inlet	NM, NM	0.0	-	1.00		

Table 3.3 Core instrumentation map

Item	Pos. / DL / Rod NO.	Core Outlet	Pos.1	Pos.2	Pos.3	Pos.4	Pos.5	Pos.6	Pos.7	Core Inlet
		3660	3417	3114.5	2879.5	2527	2174.5	1939.5	1637	1454
Surface Temp.	A11		TF 1	TF 2	TF 3	TF 4	TF 5	TF 6	TF 7	
	A12		TF 8	TF 9	TF 10	TF 11	TF 12	TF 13	TF 14	
	A13		TF 15	TF 16	TF 17	TF 18	TF 19	TF 20	TF 21	
	A14		TF 22	TF 23	TF 24	TF 25	TF 26	TF 27	TF 28	
	A15		TF 29			TF 30				
	A17		TF 31			TF 32				
	A22		TF 33	TF 34	TF 35	TF 36	TF 37	TF 38	TF 39	
	A23		TF 40	TF 41	TF 42	TF 43	TF 44	TF 45	TF 46	
	A24		TF 47	TF 48	TF 49	TF 50	TF.51	TF 52	TF 53	
	A26		TF 54			TF 55				
	A28		TF 56			TF 57				
	A31		TF 58			TF 59				
	A33		TF 60	TF 61	TF 62	TF 63	TF 64	TF 65	TF 66	
	A34		TF 67	TF 68	TF 69	TF 70	TF 71	TF 72	TF 73	
	A35		TF 74			TF 75				
	A37		TF 76			TF 77				
	A42		TF 78			TF 79				
Fluid Temp.	A44	TC 1	TF180	TF181	TF182	TF183	TF184	TF185	TF186	TC 2
Surface Temp.	A45		TF 80			TF 81				
	A46		TF 82			TF 83				
	A48		TF 84			TF 85				
	A51		TF 86			TF 87				
	A53		TF 88			TF 89				
	A54		TF 90							
	A57		TF 91			TF 92				
	A62		TF 93			TF 94				
	A64		TF 95			TF 96				
	A66		TF 97			TF 98				
	A68		TF 99			TF100				
	A71		TF101			TF102				
	A73		TF103			TF104				
	A75		TF105			TF106				
	A77		TF107			TF108				

Table 3.3 Core instrumentation map (Continued)

Item	Pos. / DL / Rod NO.	Core Outlet	Pos.1	Pos.2	Pos.3	Pos.4	Pos.5	Pos.6	Pos.7	Core Inlet
		3660	3417	3114.5	2879.5	2527	2174.5	1939.5	1637	1454
Surface Temp.	A82		TF109			TF110				
	A84		TF111			TF112				
	A86		TF113			TF114				
	A88		TF115			TF116				
	B11					TF117				
	B13					TF118				
	B15		TF119	TF120	TF121	TF122	TF123	TF124	TF125	
	B31					TF126				
	B33					TF127				
	B35					TF128				
Fluid Temp.	B44	TC 3	TF187	TF188	TF189	TF190	TF191	TF192	TF193	TC 4
Surface Temp.	B51					TF129				
	B53					TF130				
	B85		TF131	TF132	TF133	TF134	TF135	TF136	TF137	
	C11					TF138				
	C13					TF139				
	C15					TF140				
	C31					TF141				
	C33		TF142	TF143	TF144	TF145	TF146	TF147	TF148	
	C35					TF149				
Fluid Temp.	C44	TC 5	TF194	TF195	TF196	TF197	TF198	TF199	TF200	TC 6
Surface Temp.	C51					TF150				
	C53					TF151				
	C77		TF152	TF153	TF154	TF155	TF156	TF157	TF158	
	D11					TF159				
	D13					TF160				
	D27		TF161	TF162	TF163	TF164	TF165	TF166	TF167	
	D31					TF168				
	D33					TF169				
	D35					TF170				
Fluid Temp.	D44	TC 7	TF201	TF202	TF203	TF204	TF205	TF206	TF207	TC 8
Surface Temp.	D51					TF171				
	D53					TF172				
	D88		TF173	TF174	TF175	TF176	TF177	TF178	TF179	

Table 3.3 Core instrumentation map (Continued)

Item	Pos. / Rod NO. / DL	Core Outlet	Pos.1	Pos.2	Pos.3	Pos.4	Pos.5	Pos.6	Pos.7	Core Inlet
		3660	3417	3114.5	2879.5	2527	2174.5	1939.5	1673	1454
Void	A55		VF 1	VF 2	VF 3	VF 4	VF 5	VF 6	VF 7	
	B55		VF 8	VF 9	VF 10	VF 11	VF 12	VF 13	VF 14	
	C55		VF 15	VF 16	VF 17	VF 18	VF 19	VF 20	VF 21	
	D55		VF 22	VF 23	VF 24	VF 25	VF 26	VF 27	VF 28	
Channel Box Surface Temp.	A1*		TB 1	TB 2	TB 3	TB 4	TB 5	TB 6	TB 7	
	A2*		TB 8	TB 9	TB 10	TB 11	TB 12	TB 13	TB 14	
	B*		TB 15	TB 16	TB 17	TB 18	TB 19	TB 20	TB 21	
	C*		TB 22	TB 23	TB 24	TB 25	TB 26	TB 27	TB 28	
	D*		TB 29	TB 30	TB 31	TB 32	TB 33	TB 34	TB 35	
Liquid Level in the Channel Box	A1*		LB 1	LB 2	LB 3	LB 4	LB 5	LB 6	LB 7	
	A2*		LB 8	LB 9	LB 10	LB 11	LB 12	LB 13	LB 14	
	B*		LB 15	LB 16	LB 17	LB 18	LB 19	LB 20	LB 21	
	C*		LB 22	LB 23	LB 24	LB 25	LB 26	LB 27	LB 28	
	D*		LB 29	LB 30	LB 31	LB 32	LB 33	LB 34	LB 35	

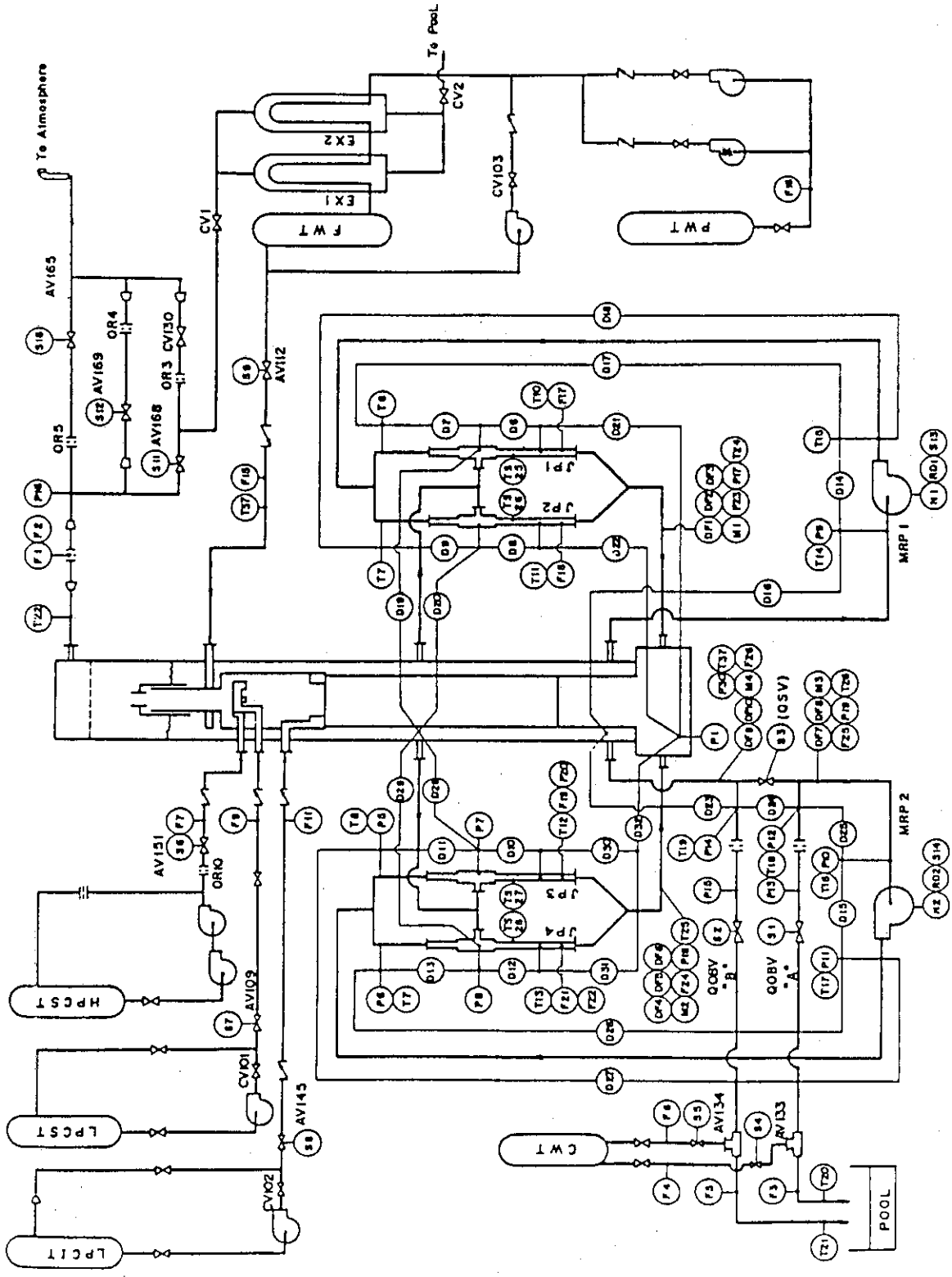

Fig. 3.1 Instrumentation location of ROSA-III test facility

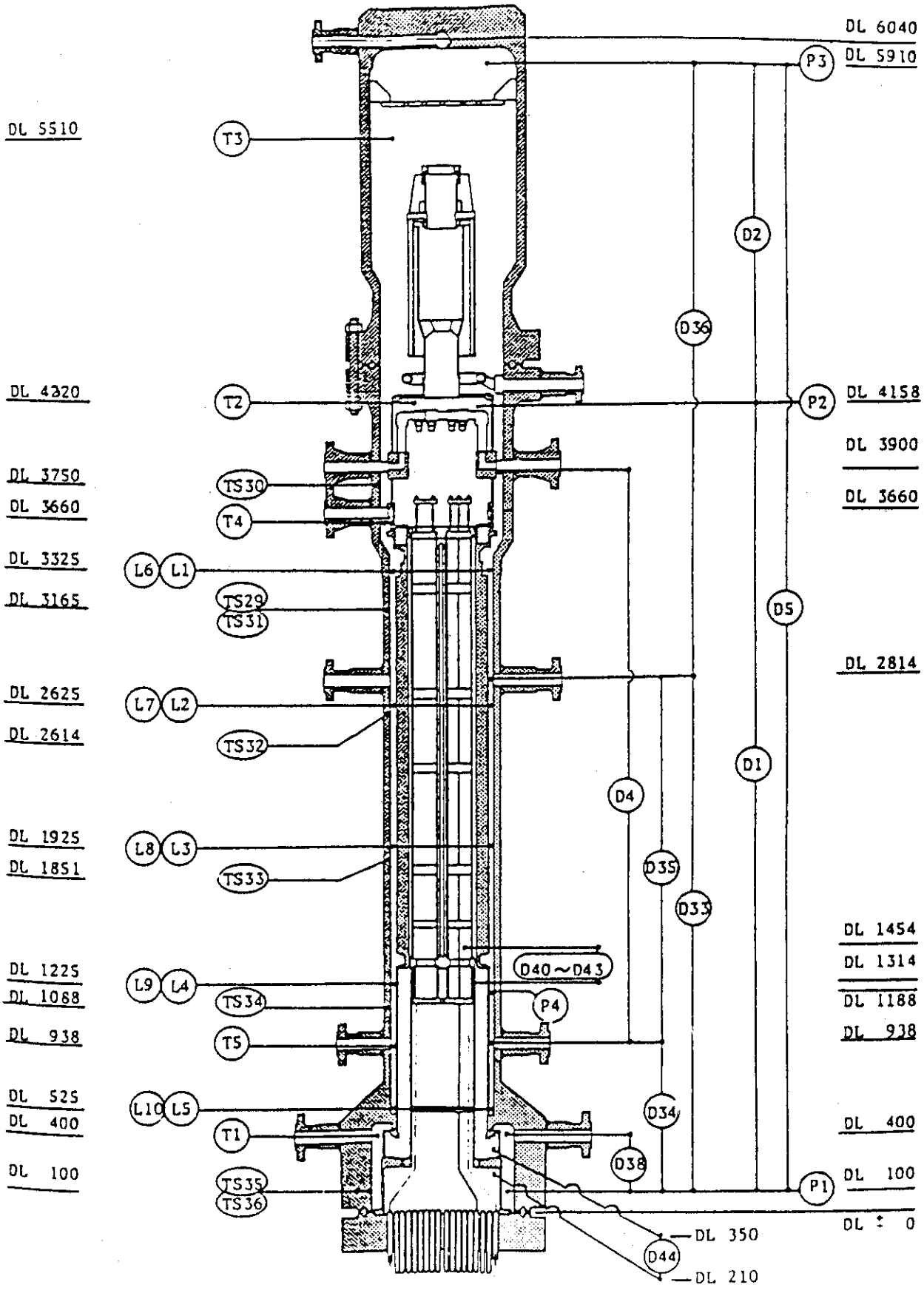

Fig. 3.2 Instrumentation location in pressure vessel

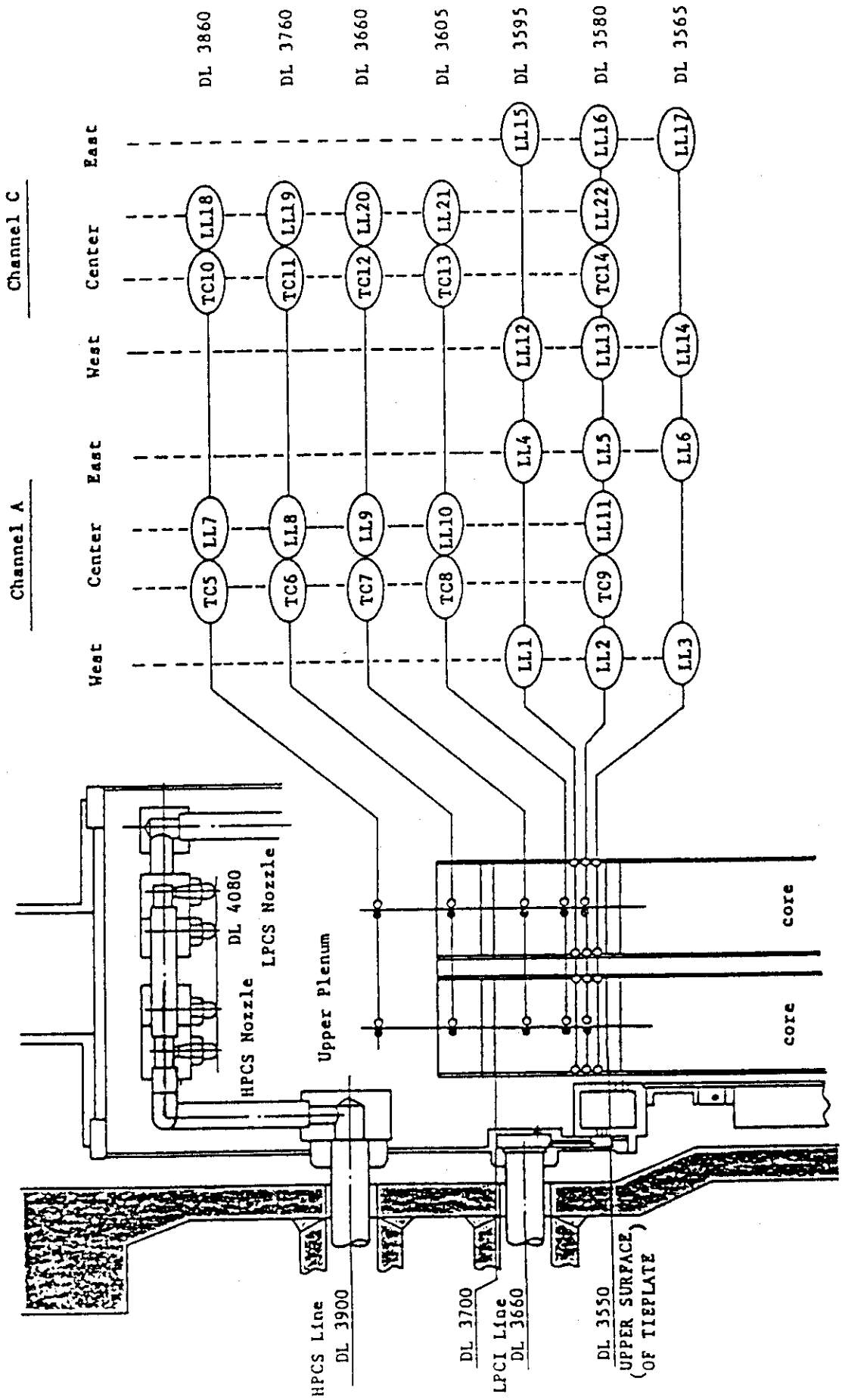

Fig. 3.3 Upper plenum instrumentation

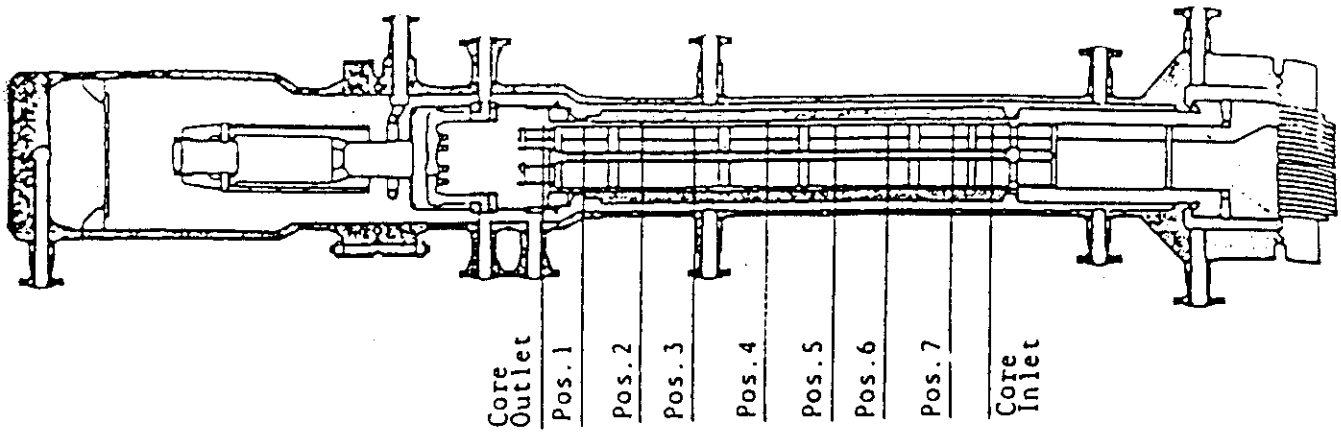

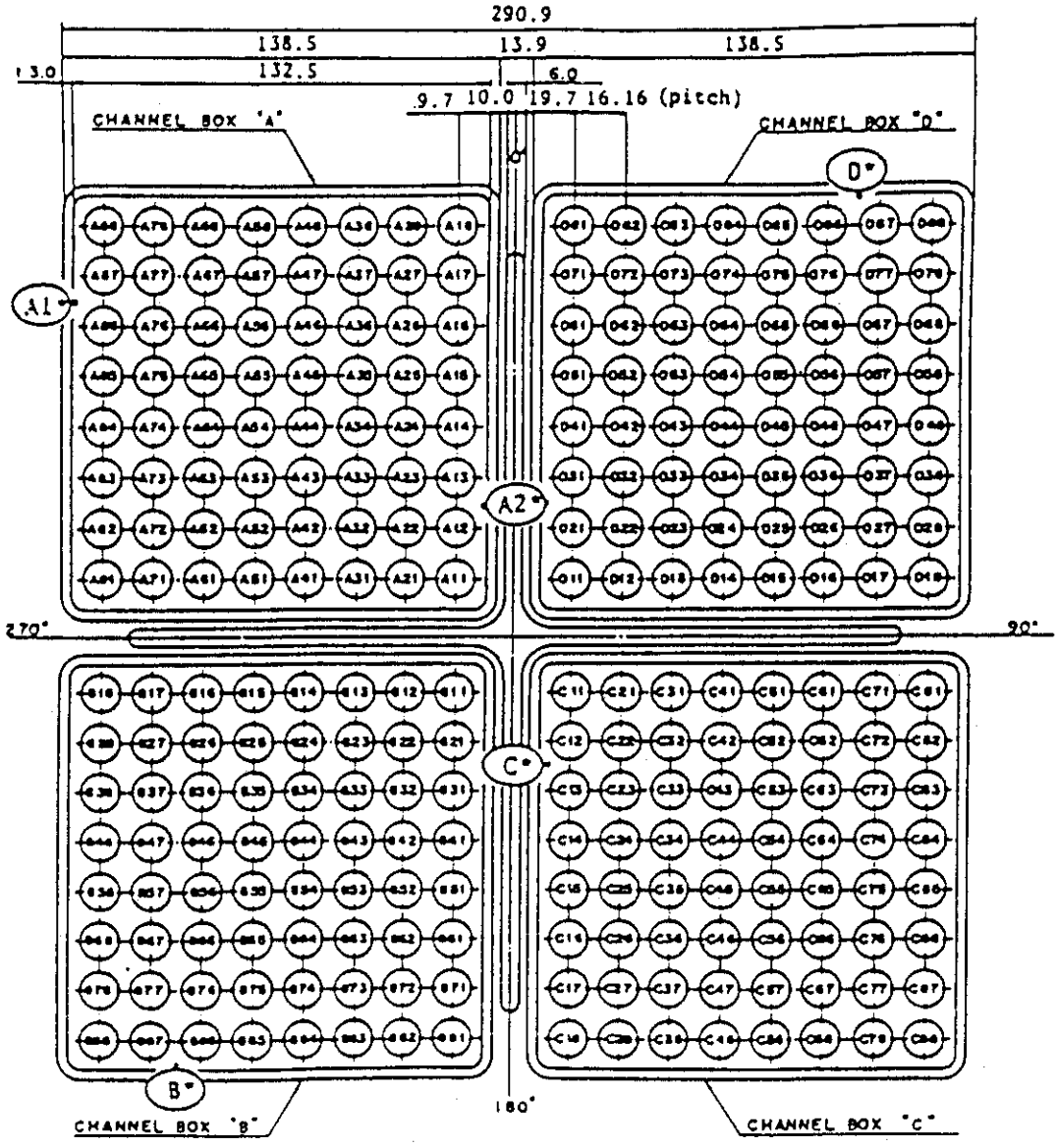

Heater rod O.D. is 12.27mm

A54,B54,C54 and D54 are water rod simulators with void probes, O.D.= 15.01mm

A4S,B4S,C4S and D4S are water rod simulators with thermocouples, O.D.= 15.01mm

Fig. 3.5 Core instrumentation (cf. Table 3.3)

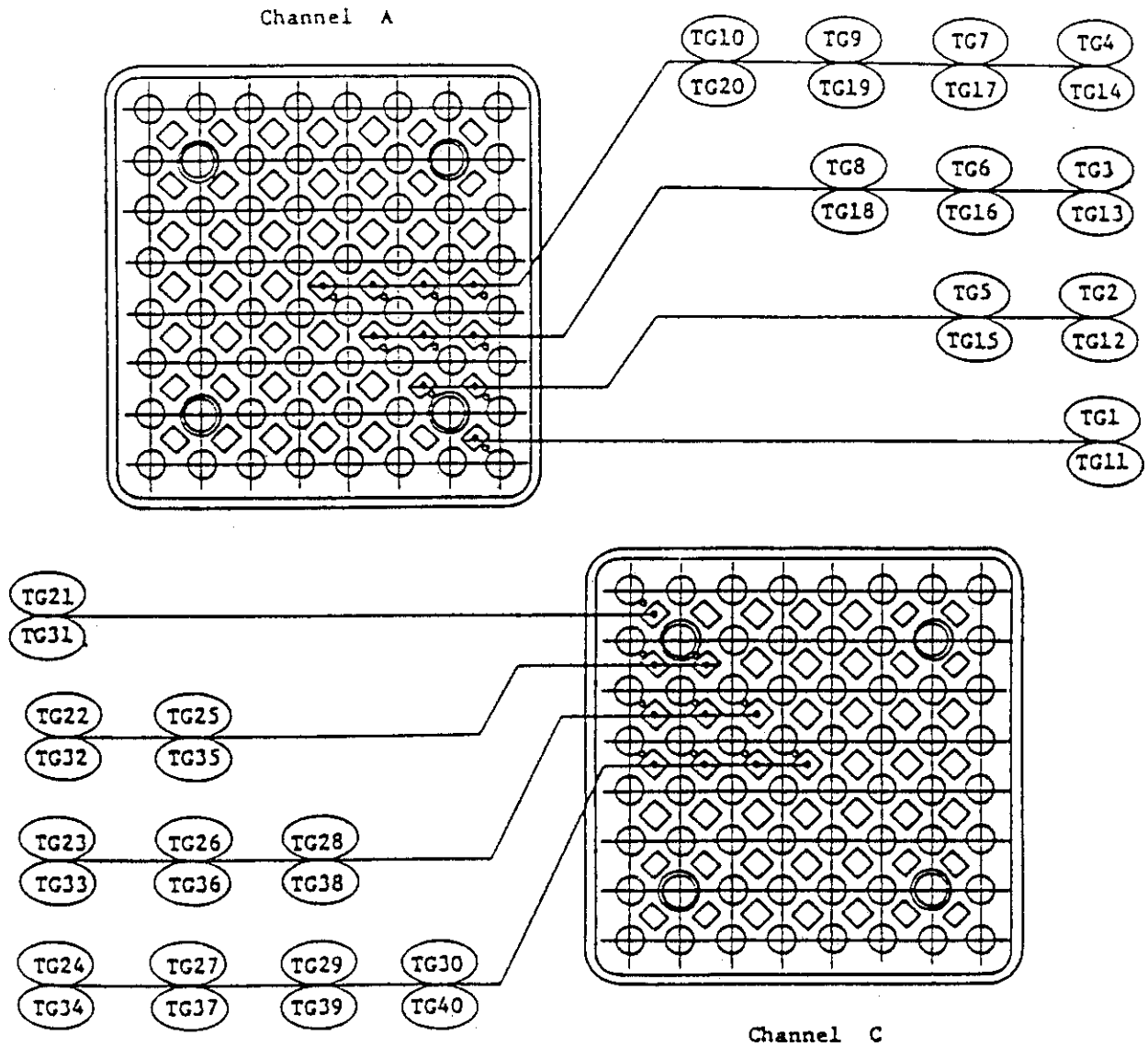

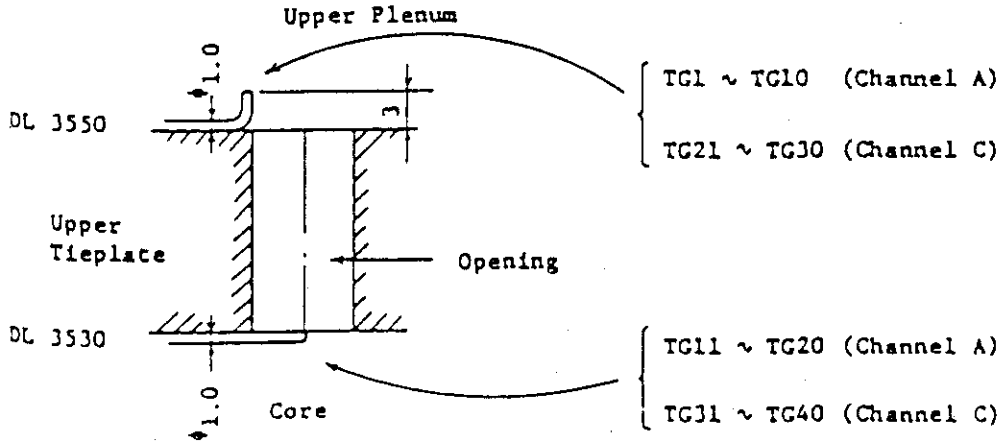

Fig. 3.6 Upper tieplate instrumentations

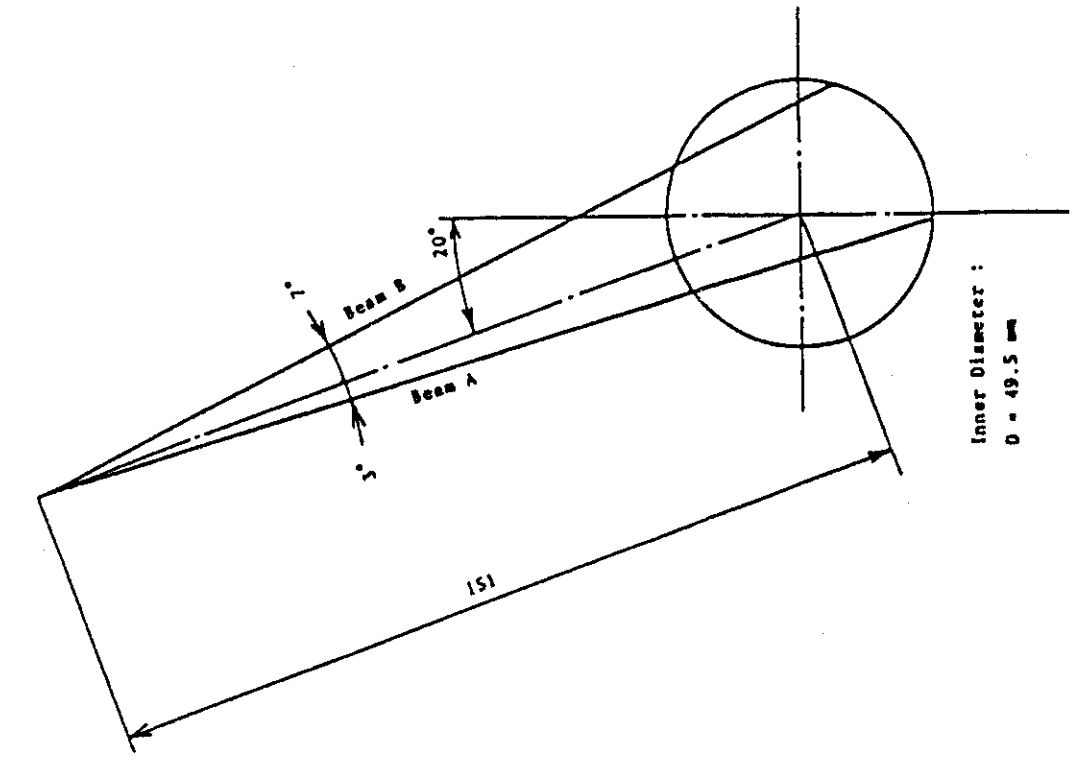

Fig. 3.8 Beam directions of two-beam gamma densitometer

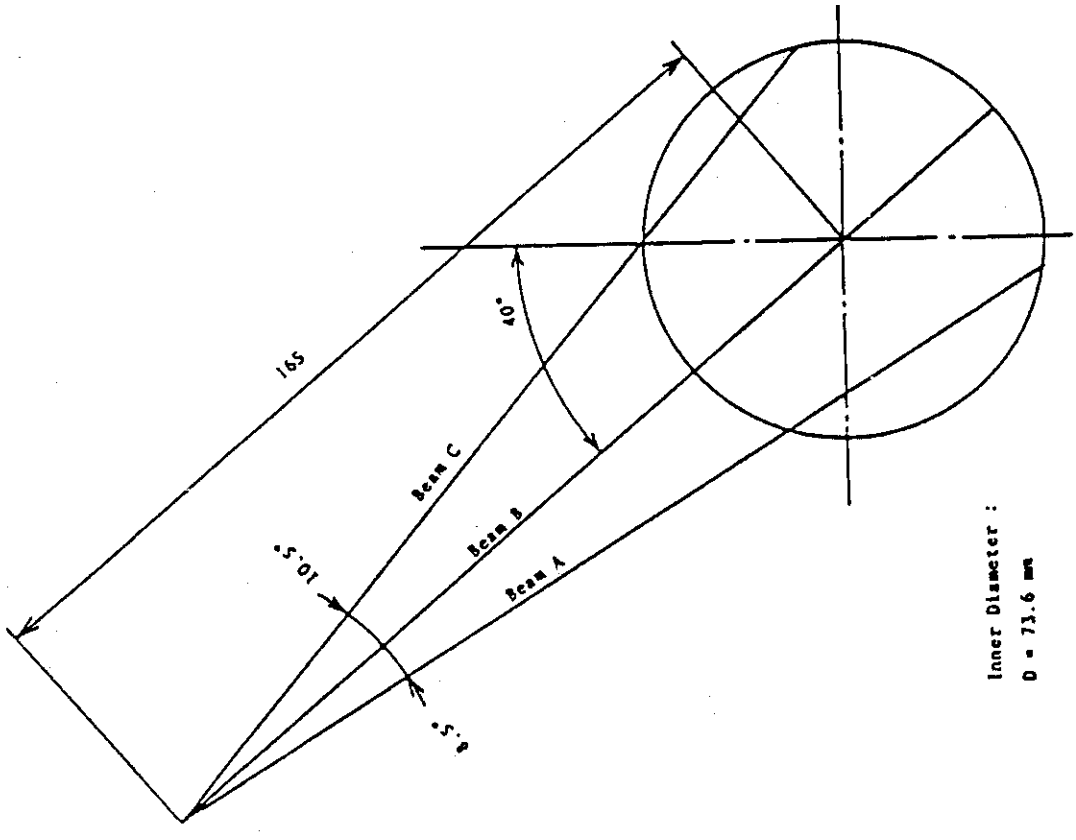

Fig. 3.7 Beam directions of three-beam gamma densitometer

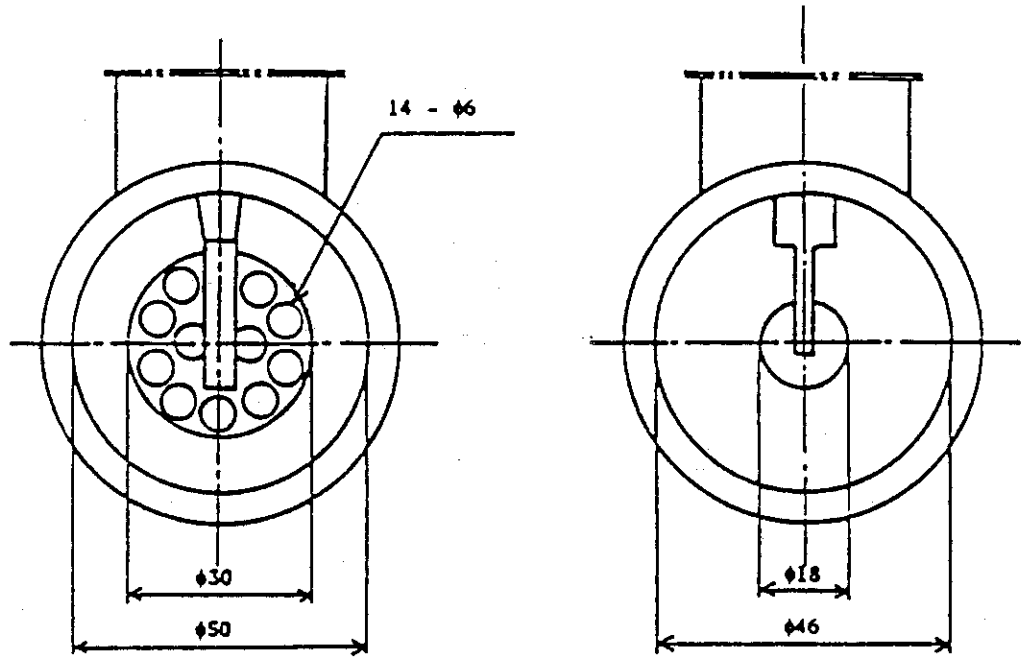

(a) High Range Drag Disc

(b) Low Range Drag Disc

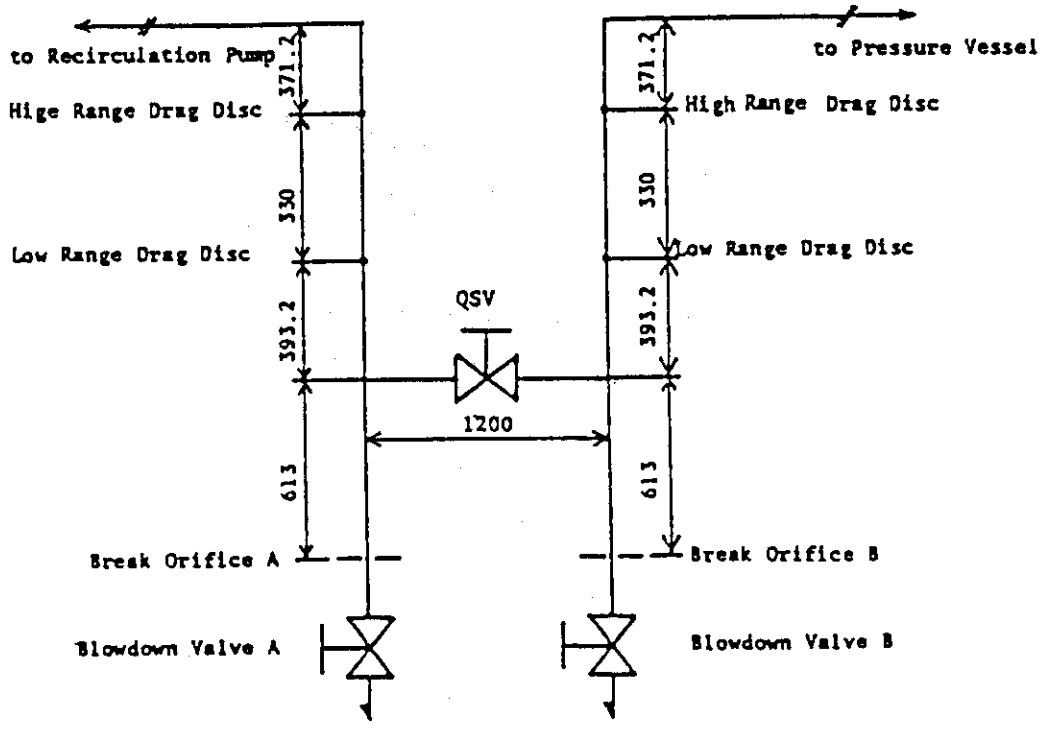

(c) Location of Drag Discs

Fig. 3.9 Arrangement and location of drag disks

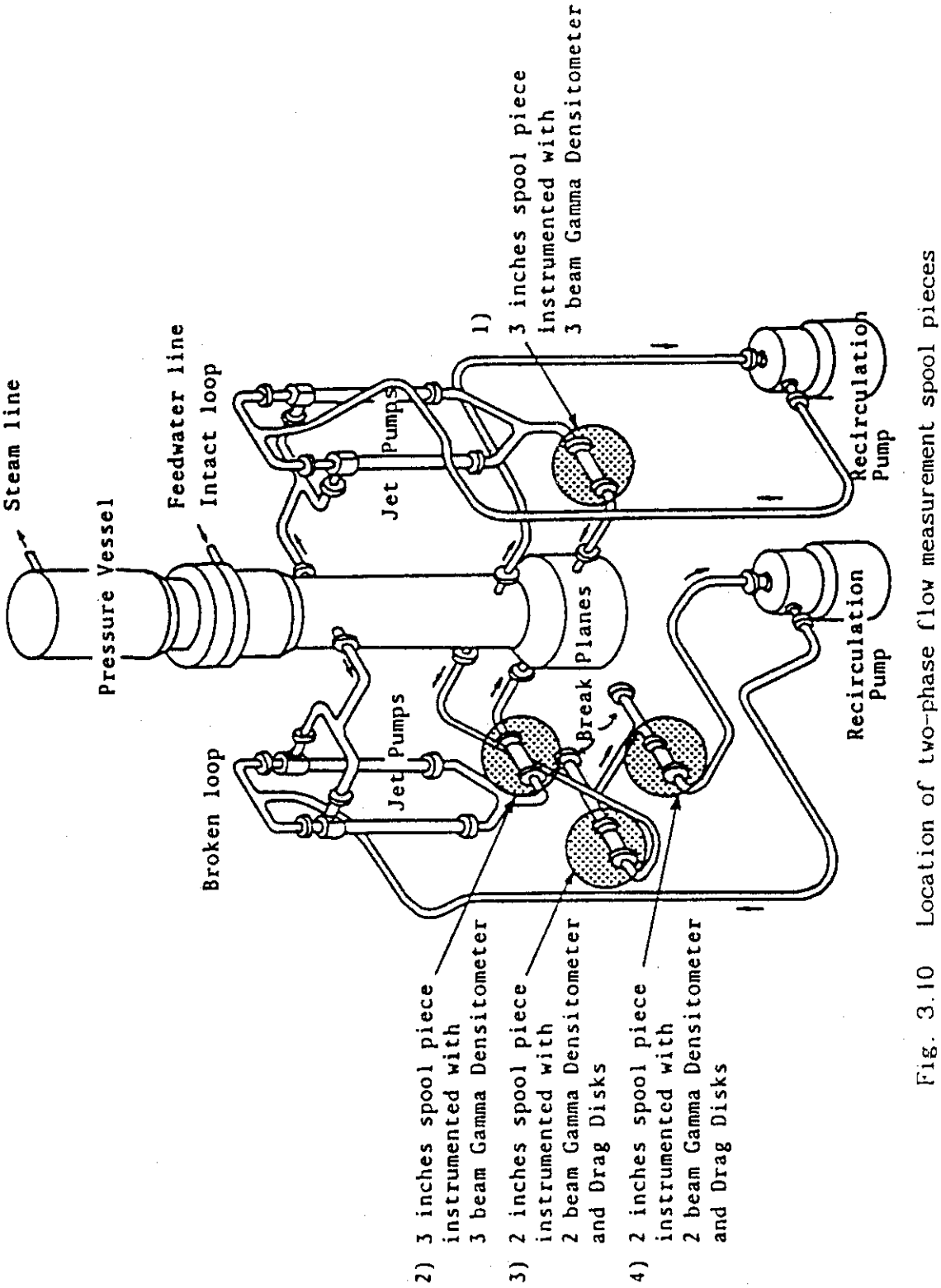

Fig. 3.10 Location of two-phase flow measurement spool pieces

Table 4.1 Test conditions of RUNs 915 and 920

Parameter	Unit	Measured Value		Parameter	Unit	Measured Value	
		RUN 915	RUN 920			RUN 915	RUN 920
Break Condition				Steam Flow Rate	kg/s	2.04	2.08
Orifice Diameter	mm	3.7	3.7	Feedwater Flow Rate	kg/s	2.04	2.06
Break Area Ratio	%	2	2	Feedwater Temperature	K	489	489
PCS Operation	MPa		6.6	Transient Conditions			
Initial Conditions				MSIV Closure	s	L2+3	L2+3
Steam Dome Pressure	MPa	7.30	7.35	SRV Operation	MPa	—	8.16
Lower Plenum Subcooling	K	10.8	10.3	ECCS Conditions			
Core Inlet Flow Rate	kg/s	16.5	16.5	HPCS Actuation		Failure	Failure
Total Core Power	MW	3.98	3.96	LPCS Actuation Time	s	419	435
Max. Linear Heat Rate				Initiation Pressure	MPa	2.3	2.3
Channel A (LPF = 1.1)	kW/m	16.75	16.67	Trip Logic	s	L1+40	L1+40
(LPF = 1.0)	kW/m	15.24	15.16	Water Temperature	K	310	310
(LPF=0.875)	kW/m	13.33	13.26	LPCI Actuation Time	s	514	531
Channels B.C.D (LPF = 1.1)	kW/m	11.95	11.89	Initiation Pressure	MPa	1.7	1.7
(LPF = 1.0)	kW/m	10.86	10.81	Trip Logic	s	L1+40	L1+40
(LPF=0.875)	kW/m	9.51	9.46	Water Temperature	K	310	310
Lower Plenum Temperature	K	552	552	ADS Actuation Time		235	188
Upper Plenum Quality	%	12.7	12.5	Trip Logic	s	L1+120	L1+120
DC Water Level	m	5.0	5.0	Orifice Diameter	mm	15.5	15.5

Table 4.2 Major events and test procedures of RUN915

Time (s)	Events
-128	• Initiation of data recording
- 12	• Initiation of data plotting
0	• Break and depressurization initiation
	• MRP pump trip
	• Feedwater stop (completed at 3.1 s)
9	• Initiation of core power decrease
25	• Lower plenum flashing
84	• L2 level trip
87	• MSIV closure and pressurization
	• First core dryout initiation
115	• L1 level trip
120	• Rewetting of dryout core
170	• Second core dryout initiation
235	• ADS actuation and depressurization
	• Second rewetting of core
260	• Initiation of second bulk flashing
270	• Third core dryout initiation
395	• Bottom of core uncovered
419	• LPCS actuation at 2.3 MPa
514	• LPCI actuation at 1.7 MPa
518	• PCT at position 4 of A68 rod
535	• Whole core quenching completion
788	• Completion of data plotting
897	• Completion of data recording

Table 4.3 Major events and test procedures of RUN950

Time (s)	Events
-121	• Initiation of data recording
- 14	• Initiation of data plotting
0	• Break and depressurization
	• MRP pump trip
1.6	• Feedwater stop (completed at 2.4 s)
9	• Initiation of core power decrease
24	• Operation of PCS at 6.6 MPa
26	• L2 level trip
29	• MSIV closure and pressurization
68	• L1 level trip
71	• Operation of SRV at 8.16 MPa
188	• ADS actuation and depressurization
197	• Initiation of lower plenum flashing
280	• Initiation of top core dryout
420	• Bottom core uncovered
435	• LPCS actuation
530	• LPCI actuation
	• PCT at position 4 of A68 rod
554	• Whole core quenching completion
786	• Completion of data plotting
890	• Completion of data recording

Table 4.4 Characteristics of steam discharge line valves

Valve	Time (Close to Open)	Time (Open to Close)
AV 165	not used	not used
AV 168	—	0.1 s
AV 169	0.3 s	2.0 s

Table 4.5 Control sequence for steam line valves in RUNs 915 and 920

(1) RUN 915

Valves	before brack (t<0s)	after Break (t≧0s)	MSIV Closure (t≧87s)	ADS Open (t≧235s)
CV-1,2	Open	Close	Close	Close
CV-130	Open	Open	Close	Close
AV-168	Open	Open	Open	Close
AV-169	Open	Close	Close	Open

(2) RUN 920

Valves	before Break (t<0s)	after Break (t≧0s)	PCS Operation (t≧24s)	MSIV Close (t≧29s)	SRV (t≧71s)	ADS (t≧188s)
CV-1,2	Open	Close	Close	Close	Close	Close
CV-130	Open	Open	Control	Close	Control	Close
AV-168	Open	Open	Open	Open	Open	Close
AV-169	Open	Close	Close	Close	Close	Open

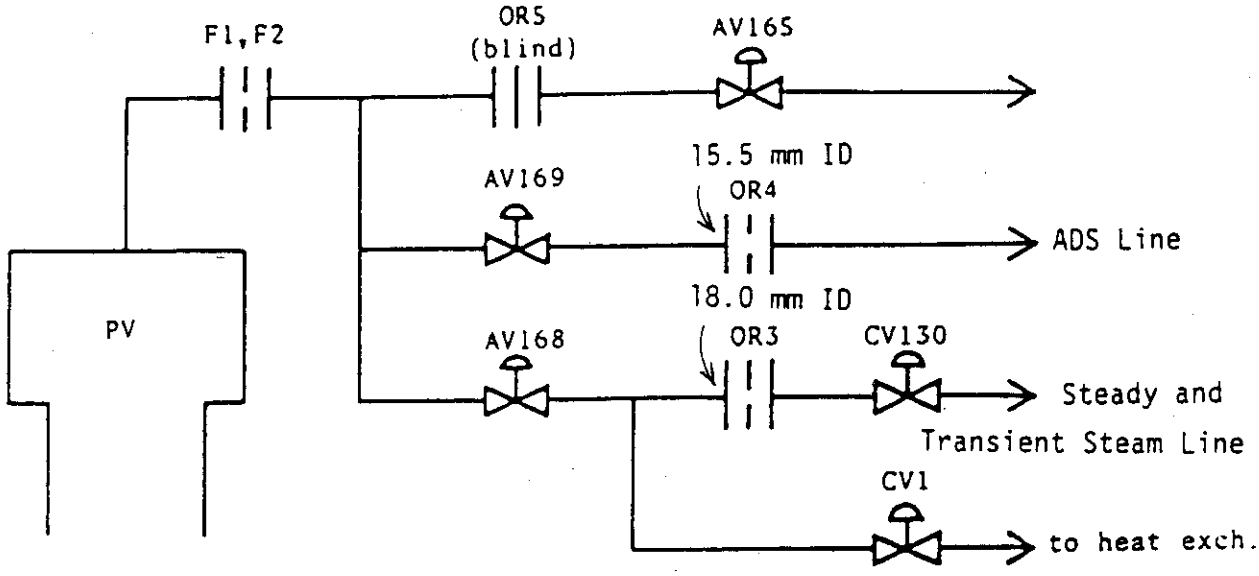

Fig. 4.1 Main steam line schematic

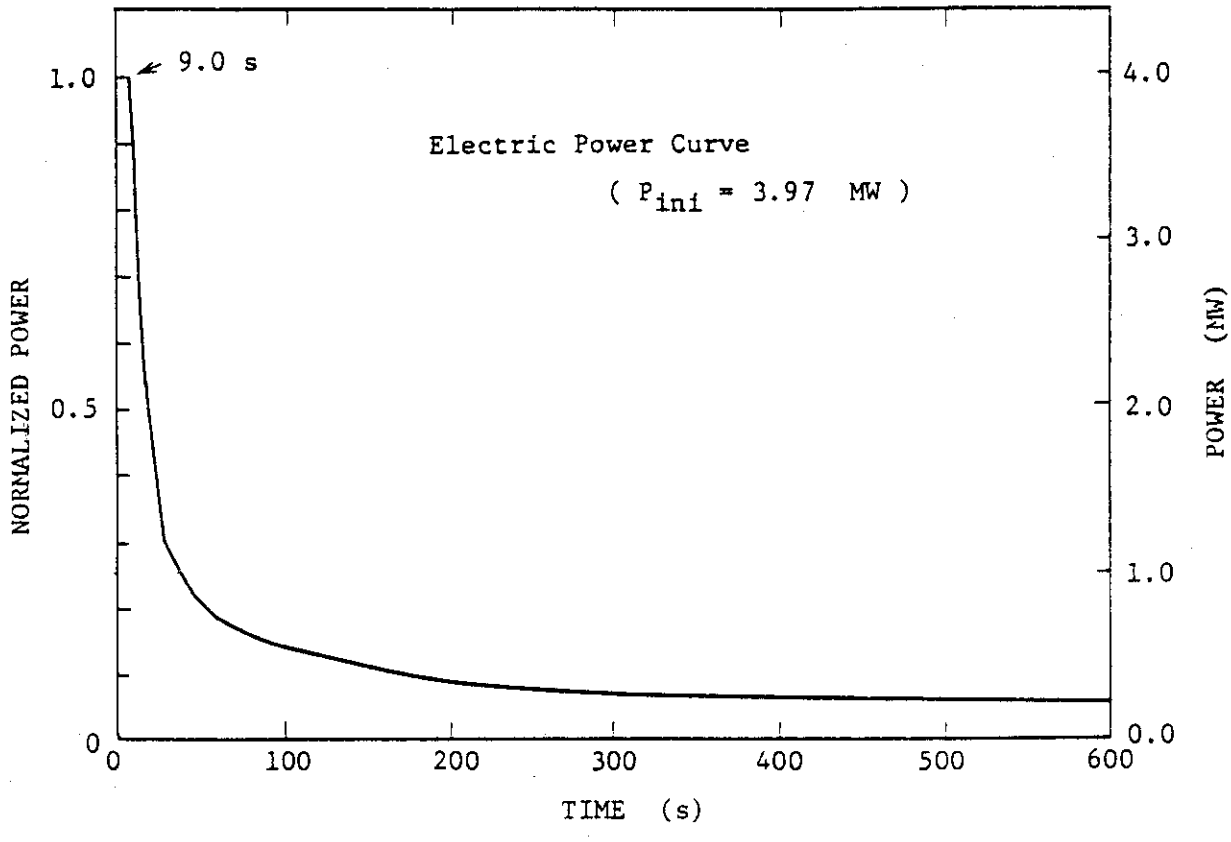

Fig. 4.2 Normalized power transient for ROSA-III test

Table 5.1 Maximum Cladding Temperature Distribution in the Core of RUN 915

	Pos.1	Pos.2	Pos.3	Pos.4	Pos.5	Pos.6	Pos.7
A-11 rod	TE 201	TE 202	TE 203	TE 204	TE 205	TE 206	TE 207
PCT (K)	611.5	727.9	767.5	778.3	721.9	630.7	568.1
Time (s)	258.4	428.8	430.4	456.8	485.6	477.6	0.0
A-12 rod	TE 208	TE 209	TE 210	TE 211	TE 212	TE 213	TE 214
PCT (K)	617.5	705.1	748.3	751.9	689.5	612.7	570.9
Time (s)	419.2	428.0	430.4	454.4	476.0	471.2	0.8
A-13 rod	TE 215	TE 216	TE 217	TE 218	TE 219	TE 220	TE 221
PCT (K)	615.1	703.9	747.1	751.9	691.9	615.1	569.2
Time (s)	417.6	429.6	428.8	460.0	473.6	472.0	0.0
A-14 rod	TE 222	TE 223	TE 224	TE 225	TE 226	TE 227	TE 228
PCT (K)	606.7	690.7	732.7	737.5	682.3	601.9	564.6
Time (s)	419.2	435.2	443.2	461.6	488.0	472.8	0.0
A-15 rod	TE 229			TE 230			
PCT (K)	610.3			736.3			
Time (s)	419.2			462.4			
A-17 rod	TE 231			TE 232			
PCT (K)	637.8			750.7			
Time (s)	421.6			460.0			
A-22 rod	TE 233	TE 234	TE 235	TE 236	TE 237	TE 238	TE 239
PCT (K)	646.4	724.3	762.7	766.6	702.6	619.0	566.5
Time (s)	420.8	428.8	441.6	459.2	472.8	476.0	0.0
A-24 rod	TE 240	TE 241	TE 242	TE 243	TE 244	TE 245	TE 246
PCT (K)	628.6	700.7	740.3	742.1	681.8	602.8	564.3
Time (s)	419.2	426.4	441.6	456.0	478.4	468.0	0.0

Table 5.1 Maximum Cladding Temperature Distribution in the Core of RUN 915 (Continued)

	Pos.1	Pos.2	Pos.3	Pos.4	Pos.5	Pos.6	Pos.7
A-26 rod	TE 247			TE 248			
PCT (K)	629.5			748.7			
Time (s)	418.4			460.8			
A-28 rod	TE 249			TE 250			
PCT (K)	639.1			770.3			
Time (s)	421.6			459.2			
A-31 rod	TE 251			TE 252			
PCT (K)	660.7			791.9			
Time (s)	424.0			471.2			
A-33 rod	TE 253	TE 254	TE 255	TE 256	TE 257	TE 258	TE 259
PCT (K)	624.8	685.6	714.8	713.0	636.2	572.0	562.3
Time (s)	424.0	427.2	433.6	440.8	431.2	434.4	0.0
A-34 rod	TE 260	TE 261	TE 262	TE 263	TE 264	TE 265	TE 266
PCT (K)	621.9	681.8	714.8	715.8	648.6	575.9	563.4
Time (s)	419.2	427.2	437.6	456.0	467.2	435.2	0.0
A-37 rod	TE 267			TE 268			
PCT (K)	641.9			651.4			
Time (s)	423.2			424.0			
A-42 rod	TE 269			TE 270			
PCT (K)	768.5			764.7			
Time (s)	472.0			451.2			
A-44 rod	TE 271	TE 272	TE 273	TE 274	TE 275	TE 276	TE 277
PCT (K)	617.1	674.2	704.5	708.9	636.2	573.0	562.7
Time (s)	423.2	427.2	430.4	451.2	442.4	437.6	0.0

Table 5.1 Maximum Cladding Temperature Distribution in the Core of RUN 915 (Continued)

	Pos.1	Pos.2	Pos.3	Pos.4	Pos.5	Pos.6	Pos.7
A-48 rod	TE 278			TE 279			
PCT (K)	632.4			766.6			
Time (s)	425.6			488.0			
A-51 rod	TE 280			TE 281			
PCT (K)	646.7			776.0			
Time (s)	424.8			484.8			
A-53 rod	TE 282			TE 283			
PCT (K)	622.9			716.7			
Time (s)	424.0			477.6			
A-57 rod	TE 284			TE 285			
PCT (K)	676.5			797.5			
Time (s)	520.8			518.4			
A-62 rod	TE 286			TE 287			
PCT (K)	657.1			785.4			
Time (s)	425.6			477.6			
A-66 rod	TE 288			TE 289			
PCT (K)	632.4			742.1			
Time (s)	432.0			511.2			
A-68 rod	TE 290			TE 291			
PCT (K)	655.2			810.7			
Time (s)	442.4			518.4			
A-71 rod	TE 292			TE 293			
PCT (K)	658.1			791.9			
Time (s)	427.2			467.2			

Table 5.1 Maximum Cladding Temperature Distribution in the Core of RUN 915 (Continued)

	Pos.1	Pos.2	Pos.3	Pos.4	Pos.5	Pos.6	Pos.7
A-73 rod	TE 294			TE 295			
PCT (K)	660.0			792.8			
Time (s)	436.0			502.4			
A-75 rod	TE 296			TE 297			
PCT (K)	652.4			750.2			
Time (s)	432.0			459.2			
A-77 rod	TE 298	TE 299	TE 300	TE 301	TE 302	TE 303	TE 304
PCT (K)	665.8	728.0	768.5	780.7	702.6	614.3	------
Time (s)	432.0	440.8	450.4	518.4	496.0	478.4	------
A-82 rod	TE 305			TE 306			
PCT (K)	660.9			797.5			
Time (s)	428.0			498.4			
A-84 rod	TE 307			TE 308			
PCT (K)	650.5			783.4			
Time (s)	431.2			512.0			
A-85 rod	TE 309	TE 310	TE 311	TE 312	TE 313	TE 314	TE 315
PCT (K)	647.6	723.3	762.8	774.1	706.4	624.8	567.2
Time (s)	429.6	440.0	448.8	519.2	498.4	476.8	8.0
A-87 rod	TE 316	TE 317	TE 318	TE 319	TE 320	TE 321	TE 322
PCT (K)	652.4	732.7	777.8	794.7	718.6	626.7	563.2
Time (s)	431.2	444.8	448.0	516.8	493.6	477.6	0.0
A-88 rod	TE 323	TE 324	TE 325	TE 326	TE 327	TE 328	TE 329
PCT (K)	645.7	744.0	791.0	806.0	725.2	630.5	565.0
Time (s)	435.2	510.4	516.0	516.0	496.8	477.6	0.0

Table 5.1 Maximum Cladding Temperature Distribution in the Core of RUN 915 (Continued)

	Pos.1	Pos.2	Pos.3	Pos.4	Pos.5	Pos.6	Pos.7
B-11 rod	TE 330	TE 331	TE 332	TE 333	TE 334	TE 335	TE 336
PCT (K)	------	------	------	------	------	------	------
Time (s)	------	------	------	------	------	------	------
B-13 rod				TE 337			
PCT (K)				694.1			
Time (s)				442.4			
B-22 rod	TE 338	TE 339	TE 340	TE 341	TE 342	TE 343	TE 344
PCT (K)	614.3	667.6	693.1	691.2	625.7	563.6	562.4
Time (s)	423.2	429.6	428.8	440.8	437.6	0.0	0.0
B-31 rod				TE 345			
PCT (K)				685.6			
Time (s)				441.6			
B-33 rod				TE 346			
PCT (K)				654.3			
Time (s)				428.8			
B-51 rod				TE 347			
PCT (K)				677.1			
Time (s)				460.0			
B-53 rod				TE 348			
PCT (K)				655.2			
Time (s)				445.6			
B-66 rod				TE 349			
PCT (K)				665.7			
Time (s)				468.0			

Table 5.1 Maximum Cladding Temperature Distribution in the Core of RUN 915 (Continued)

	Pos.1	Pos.2	Pos.3	Pos.4	Pos.5	Pos.6	Pos.7
B-77 rod	TE 350	TE 351	TE 352	TE 353	TE 354	TE 355	TE 356
PCT (K)	------	------	------	------	------	------	------
Time (s)	------	------	------	------	------	------	------
B-86 rod				TE 357			
PCT (K)				736.5			
Time (s)				519.2			
C-11 rod	TE 358	TE 359	TE 360	TE 361	TE 362	TE 363	TE 364
PCT (K)	600.8	600.8	622.9	671.4	653.3	591.3	564.5
Time (s)	260.0	236.0	423.2	438.4	482.4	475.2	0.0
C-13 rod	TE 365	TE 366	TE 367	TE 368	TE 369	TE 370	TE 371
PCT (K)	598.0	602.8	590.3	660.0	637.1	580.7	563.6
Time (s)	258.4	236.8	425.6	435.2	447.2	452.8	0.0
C-15 rod				TE 372			
PCT (K)				686.5			
Time (s)				464.0			
C-22 rod	TE 373	TE 374	TE 375	TE 376	TE 377	TE 378	TE 379
PCT (K)	584.5	611.4	647.6	678.0	626.7	567.8	563.0
Time (s)	225.6	420.0	425.6	432.0	437.6	0.0	0.0
C-31 rod				TE 380			
PCT (K)				681.8			
Time (s)				432.0			
C-33 rod	TE 381	TE 382	TE 383	TE 384	TE 385	TE 386	TE 387
PCT (K)	584.5	587.4	563.4	588.4	601.8	564.5	564.5
Time (s)	258.4	236.0	0.0	428.8	431.2	0.0	0.0

Table 5.1 Maximum Cladding Temperature Distribution in the Core of RUN 915 (Continued)

	Pos.1	Pos.2	Pos.3	Pos.4	Pos.5	Pos.6	Pos.7
C-35 rod				TE 388			
PCT (K)				657.1			
Time (s)				438.4			
C-66 rod				TE 389			
PCT (K)				677.1			
Time (s)				514.4			
C-68 rod				TE 390			
PCT (K)				729.0			
Time (s)				519.2			
C-77 rod	TE 391	TE 392	TE 393	TE 394	TE 395	TE 396	TE 397
PCT (K)	623.8	675.2	696.9	700.7	642.9	571.0	562.9
Time (s)	440.0	444.0	452.0	465.6	488.0	437.6	0.0
D-11 rod				TE 398			
PCT (K)				696.9			
Time (s)				470.4			
D-13 rod				TE 399			
PCT (K)				682.7			
Time (s)				436.0			
D-22 rod	TE 400	TE 401	TE 402	TE 403	TE 404	TE 405	TE 406
PCT (K)	590.3	620.0	655.2	673.3	632.4	572.0	563.4
Time (s)	234.4	424.0	424.8	436.8	448.8	456.8	0.0
D-31 rod				TE 407			
PCT (K)				684.6			
Time (s)				431.2			

Table 5.1 Maximum Cladding Temperature Distribution in the Core of RUN 915 (Continued)

	Pos.1	Pos.2	Pos.3	Pos.4	Pos.5	Pos.6	Pos.7
D-33 rod				TE 408			
PCT (K)				573.0			
Time (s)				431.2			
D-51 rod				TE 409			
PCT (K)				675.2			
Time (s)				439.2			
D-53 rod				TE 410			
PCT (K)				628.6			
Time (s)				438.4			
D-66 rod				TE 411			
PCT (K)				653.1			
Time (s)				445.6			
D-77 rod				TE 412			
PCT (K)				------			
Time (s)				------			
D-86 rod				TE 413			
PCT (K)				719.5			
Time (s)				488.8			

Table 5.1 Maximum Cladding Temperature Distribution in the Core of RUN 915 (Continued)

** Order of PCT (RUN 915) **

No. 1	A-68 rod	Pos. 4	PCT =	810.7 (K)	Time =	518.4 (s)
No. 2	A-88 rod	Pos. 4	PCT =	806.0 (K)	Time =	516.0 (s)
No. 3	A-57 rod	Pos. 4	PCT =	797.5 (K)	Time =	518.4 (s)
No. 4	A-82 rod	Pos. 4	PCT =	797.5 (K)	Time =	498.4 (s)
No. 5	A-87 rod	Pos. 4	PCT =	794.7 (K)	Time =	516.8 (s)
No. 6	A-73 rod	Pos. 4	PCT =	792.8 (K)	Time =	502.4 (s)
No. 7	A-31 rod	Pos. 4	PCT =	791.9 (K)	Time =	471.2 (s)
No. 8	A-71 rod	Pos. 4	PCT =	791.9 (K)	Time =	467.2 (s)
No. 9	A-88 rod	Pos. 3	PCT =	791.0 (K)	Time =	516.0 (s)
No.10	A-62 rod	Pos. 4	PCT =	785.4 (K)	Time =	477.6 (s)

Table 5.2 Maximum Cladding Temperature Distribution in the Core of RUN 920

	Pos.1	Pos.2	Pos.3	Pos.4	Pos.5	Pos.6	Pos.7
A-11 rod	TE 201	TE 202	TE 203	TE 204	TE 205	TE 206	TE 207
PCT (K)	636.7	735.1	777.1	787.9	719.5	624.7	570.7
Time (s)	438.4	448.8	497.6	498.4	508.8	491.2	92.8
A-12 rod	TE 208	TE 209	TE 210	TE 211	TE 212	TE 213	TE 214
PCT (K)	640.3	723.1	765.1	765.1	689.5	611.5	571.9
Time (s)	437.6	443.2	448.0	473.6	506.4	473.6	151.2
A-13 rod	TE 215	TE 216	TE 217	TE 218	TE 219	TE 220	TE 221
PCT (K)	640.3	723.1	761.5	759.1	685.9	613.9	567.2
Time (s)	438.4	443.2	446.4	469.6	497.6	493.6	0.0
A-14 rod	TE 222	TE 223	TE 224	TE 225	TE 226	TE 227	TE 228
PCT (K)	631.9	709.9	745.9	744.7	677.5	607.9	------
Time (s)	435.2	443.2	452.0	465.6	474.4	486.4	------
A-15 rod	TE 229			TE 230			
PCT (K)	631.9			751.9			
Time (s)	436.0			472.8			
A-17 rod	TE 231			TE 232			
PCT (K)	636.7			798.0			
Time (s)	435.2			521.6			
A-22 rod	TE 233	TE 234	TE 235	TE 236	TE 237	TE 238	TE 239
PCT (K)	654.7	731.5	765.1	758.1	676.1	605.6	570.1
Time (s)	437.6	444.8	445.6	470.4	456.0	463.2	113.6
A-24 rod	TE 240	TE 241	TE 242	TE 243	TE 244	TE 245	TE 246
PCT (K)	644.8	721.4	753.4	745.9	673.3	604.7	571.0
Time (s)	435.2	444.0	448.0	468.8	472.8	477.6	172.8

Table 5.2 Maximum Cladding Temperature Distribution in the Core of RUN 920 (Continued)

	Pos.1	Pos.2	Pos.3	Pos.4	Pos.5	Pos.6	Pos.7
A-26 rod	TE 247			TE 248			
PCT (K)	645.7			773.1			
Time (s)	435.2			522.4			
A-28 rod	TE 249			TE 250			
PCT (K)	643.8			780.7			
Time (s)	436.8			512.0			
A-31 rod	TE 251			TE 252			
PCT (K)	655.2			776.0			
Time (s)	438.4			479.2			
A-33 rod	TE 253	TE 254	TE 255	TE 256	TE 257	TE 258	TE 259
PCT (K)	636.2	703.5	729.9	719.5	641.9	576.8	570.1
Time (s)	436.0	444.8	443.2	456.8	446.4	450.4	127.2
A-34 rod	TE 260	TE 261	TE 262	TE 263	TE 264	TE 265	TE 266
PCT (K)	634.3	700.7	728.0	723.3	643.8	580.7	570.1
Time (s)	435.2	447.2	452.8	461.6	448.0	450.4	160.0
A-37 rod	TE 267			TE 268			
PCT (K)	645.7			657.1			
Time (s)	435.2			441.6			
A-42 rod	TE 269			TE 270			
PCT (K)	759.1			759.1			
Time (s)	480.0			470.4			
A-44 rod	TE 271	TE 272	TE 273	TE 274	TE 275	TE 276	TE 277
PCT (K)	626.7	692.2	722.4	723.3	652.4	576.8	569.1
Time (s)	440.8	447.2	456.0	477.6	507.2	449.6	154.4

Table 5.2 Maximum Cladding Temperature Distribution in the Core of RUN 920 (Continued)

	Pos.1	Pos.2	Pos.3	Pos.4	Pos.5	Pos.6	Pos.7
A-48 rod	TE 278			TE 279			
PCT (K)	636.2			757.2			
Time (s)	440.8			514.4			
A-51 rod	TE 280			TE 281			
PCT (K)	651.4			768.5			
Time (s)	442.4			494.4			
A-53 rod	TE 282			TE 283			
PCT (K)	634.3			730.8			
Time (s)	443.2			478.4			
A-57 rod	TE 284			TE 285			
PCT (K)	685.6			789.1			
Time (s)	529.6			527.2			
A-62 rod	TE 286			TE 287			
PCT (K)	661.9			777.8			
Time (s)	442.4			484.0			
A-66 rod	TE 288			TE 289			
PCT (K)	638.1			753.4			
Time (s)	448.0			533.6			
A-68 rod	TE 290			TE 291			
PCT (K)	660.9			801.3			
Time (s)	458.4			530.4			
A-71 rod	TE 292			TE 293			
PCT (K)	660.9			790.0			
Time (s)	443.2			483.2			

Table 5.2 Maximum Cladding Temperature Distribution in the Core of RUN 920 (Continued)

	Pos.1	Pos.2	Pos.3	Pos.4	Pos.5	Pos.6	Pos.7
A-73 rod	TE 294			TE 295			
PCT (K)	665.7			777.8			
Time (s)	448.0			493.6			
A-75 rod	TE 296			TE 297			
PCT (K)	655.2			755.3			
Time (s)	446.4			473.6			
A-77 rod	TE 298	TE 299	TE 300	TE 301	TE 302	TE 303	TE 304
PCT (K)	675.2	756.2	788.2	785.4	701.6	607.6	------
Time (s)	532.8	533.6	526.4	531.2	508.0	491.2	------
A-82 rod	TE 305			TE 306			
PCT (K)	667.6			787.2			
Time (s)	447.2			488.0			
A-84 rod	TE 307			TE 308			
PCT (K)	653.3			780.7			
Time (s)	445.6			512.8			
A-85 rod	TE 309	TE 310	TE 311	TE 312	TE 313	TE 314	TE 315
PCT (K)	651.4	731.8	768.5	776.9	704.5	620.9	571.0
Time (s)	448.0	452.0	462.4	535.2	506.4	492.8	137.6
A-87 rod	TE 316	TE 317	TE 318	TE 319	TE 320	TE 321	TE 322
PCT (K)	660.0	745.0	786.3	791.9	714.8	622.9	569.1
Time (s)	463.2	517.6	516.8	525.6	506.4	491.2	129.6
A-88 rod	TE 323	TE 324	TE 325	TE 326	TE 327	TE 328	TE 329
PCT (K)	652.4	750.6	789.1	798.5	721.4	627.6	570.1
Time (s)	451.2	515.2	521.6	532.0	508.0	492.8	135.2

Table 5.2 Maximum Cladding Temperature Distribution in the Core of RUN 920 (Continued)

	Pos.1	Pos.2	Pos.3	Pos.4	Pos.5	Pos.6	Pos.7
B-11 rod	TE 330	TE 331	TE 332	TE 333	TE 334	TE 335	TE 336
PCT (K)	605.6	667.6	696.9	696.9	645.7	577.8	------
Time (s)	440.0	443.2	446.4	536.0	502.4	492.0	------
B-13 rod				TE 337			
PCT (K)				691.2			
Time (s)				449.6			
B-22 rod	TE 338	TE 339	TE 340	TE 341	TE 342	TE 343	TE 344
PCT (K)	614.3	670.4	693.1	685.6	619.0	570.1	571.0
Time (s)	440.0	443.2	444.0	454.4	452.0	100.8	172.0
B-31 rod				TE 345			
PCT (K)				685.6			
Time (s)				456.0			
B-33 rod				TE 346			
PCT (K)				657.1			
Time (s)				454.4			
B-51 rod				TE 347			
PCT (K)				675.2			
Time (s)				465.6			
B-53 rod				TE 348			
PCT (K)				656.2			
Time (s)				456.0			
B-66 rod				TE 349			
PCT (K)				670.4			
Time (s)				512.0			

Table 5.2 Maximum Cladding Temperature Distribution in the Core of RUN 920 (Continued)

	Pos.1	Pos.2	Pos.3	Pos.4	Pos.5	Pos.6	Pos.7
B-77 rod	TE 350	TE 351	TE 352	TE 353	TE 354	TE 355	TE 356
PCT (K)	640.0	695.0	713.0	710.1	647.6	578.8	570.1
Time (s)	468.0	476.0	488.0	504.8	495.2	493.6	131.2
B-86 rod				TE 357			
PCT (K)				711.1			
Time (s)				472.0			
C-11 rod	TE 358	TE 359	TE 360	TE 361	TE 362	TE 363	TE 364
PCT (K)	571.0	575.9	613.3	658.1	638.1	579.7	571.0
Time (s)	105.6	440.0	444.0	461.6	477.6	487.2	102.4
C-13 rod	TE 365	TE 366	TE 367	TE 368	TE 369	TE 370	TE 371
PCT (K)	570.1	571.0	607.6	------	641.9	578.8	570.1
Time (s)	112.0	83.2	466.4	------	511.2	488.8	108.0
C-15 rod				TE 372			
PCT (K)				681.8			
Time (s)				452.8			
C-22 rod	TE 373	TE 374	TE 375	TE 376	TE 377	TE 378	TE 379
PCT (K)	570.1	613.3	642.9	671.4	623.8	572.0	570.1
Time (s)	132.0	437.6	439.2	447.2	464.0	149.6	106.4
C-31 rod				TE 380			
PCT (K)				657.1			
Time (s)				449.6			
C-33 rod	TE 381	TE 382	TE 383	TE 384	TE 385	TE 386	TE 387
PCT (K)	571.0	571.0	571.0	588.4	600.8	570.1	569.1
Time (s)	93.6	70.4	108.0	446.4	448.0	88.0	129.6

Table 5.2 Maximum Cladding Temperature Distribution in the Core of RUN 920 (Continued)

	Pos.1	Pos.2	Pos.3	Pos.4	Pos.5	Pos.6	Pos.7
C-35 rod				TE 388			
PCT (K)				654.3			
Time (s)				445.6			
C-66 rod				TE 389			
PCT (K)				669.5			
Time (s)				530.4			
C-68 rod				TE 390			
PCT (K)				708.2			
Time (s)				470.4			
C-77 rod	TE 391	TE 392	TE 393	TE 394	TE 395	TE 396	TE 397
PCT (K)	626.7	674.2	694.1	700.7	643.8	570.1	570.1
Time (s)	451.2	456.8	464.8	476.8	490.4	101.6	106.4
D-11 rod				TE 398			
PCT (K)				694.1			
Time (s)				449.6			
D-13 rod				TE 399			
PCT (K)				668.5			
Time (s)				453.6			
D-22 rod	TE 400	TE 401	TE 402	TE 403	TE 404	TE 405	TE 406
PCT (K)	569.1	620.9	658.1	677.1	636.2	571.0	570.1
Time (s)	83.2	437.6	443.2	450.4	465.6	92.0	103.2
D-31 rod				TE 407			
PCT (K)				690.3			
Time (s)				454.4			

Table 5.2 Maximum Cladding Temperature Distribution in the Core of RUN 920 (Continued)

	Pos.1	Pos.2	Pos.3	Pos.4	Pos.5	Pos.6	Pos.7
D-33 rod				TE 408			
PCT (K)				578.8			
Time (s)				444.8			
D-51 rod				TE 409			
PCT (K)				655.2			
Time (s)				452.8			
D-53 rod				TE 410			
PCT (K)				617.1			
Time (s)				447.2			
D-66 rod				TE 411			
PCT (K)				654.6			
Time (s)				468.0			
D-77 rod				TE 412			
PCT (K)				------			
Time (s)				------			
D-86 rod				TE 413			
PCT (K)				710.1			
Time (s)				498.4			

Table 5.2 Maximum Cladding Temperature Distribution in the Core of RUN 920 (Continued)

** Order of PCT (RUN 920) **

No. 1	A-68 rod	Pos. 4	PCT = 801.3 (K)	Time = 530.4 (s)	
No. 2	A-88 rod	Pos. 4	PCT = 798.5 (K)	Time = 532.0 (s)	
No. 3	A-17 rod	Pos. 4	PCT = 798.0 (K)	Time = 521.6 (s)	
No. 4	A-87 rod	Pos. 4	PCT = 791.9 (K)	Time = 525.6 (s)	
No. 5	A-71 rod	Pos. 4	PCT = 790.0 (K)	Time = 483.2 (s)	
No. 6	A-57 rod	Pos. 4	PCT = 789.1 (K)	Time = 527.2 (s)	
No. 7	A-88 rod	Pos. 3	PCT = 789.1 (K)	Time = 521.6 (s)	
No. 8	A-77 rod	Pos. 3	PCT = 788.2 (K)	Time = 526.4 (s)	
No. 9	A-11 rod	Pos. 4	PCT = 787.9 (K)	Time = 498.4 (s)	
No.10	A-82 rod	Pos. 4	PCT = 787.2 (K)	Time = 488.0 (s)	

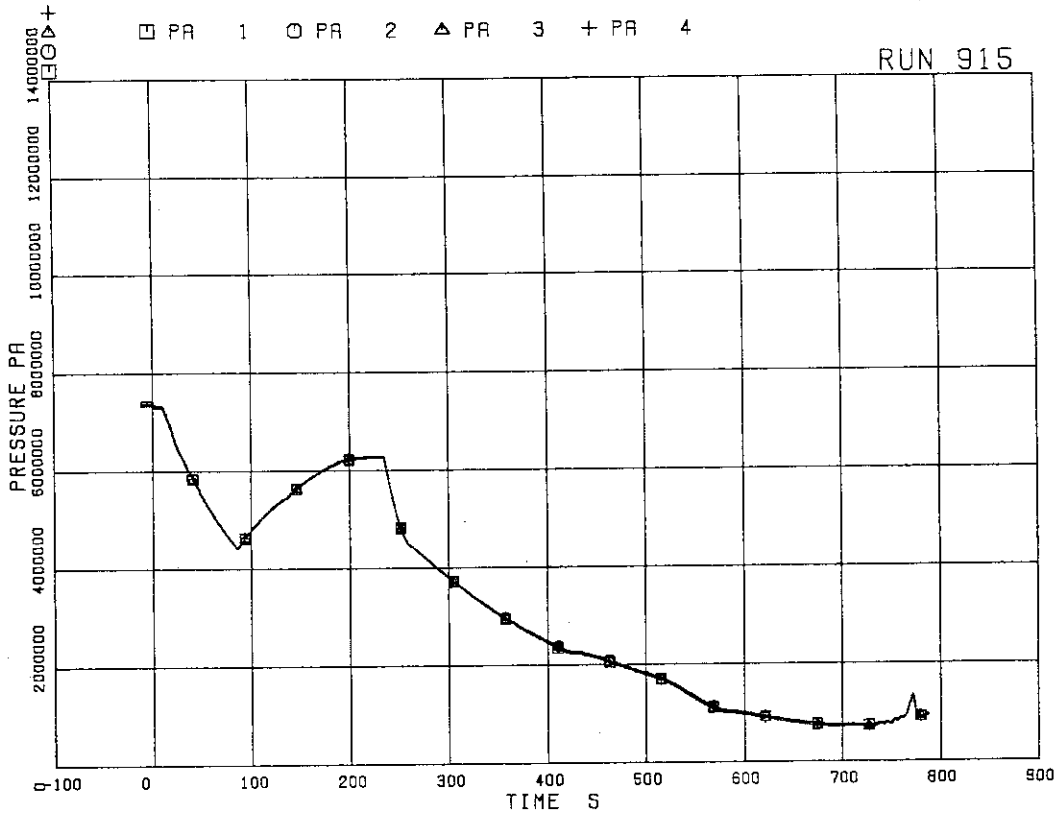

FIG.5. 1 PRESSURE IN PV (PRESSURE VESSEL)

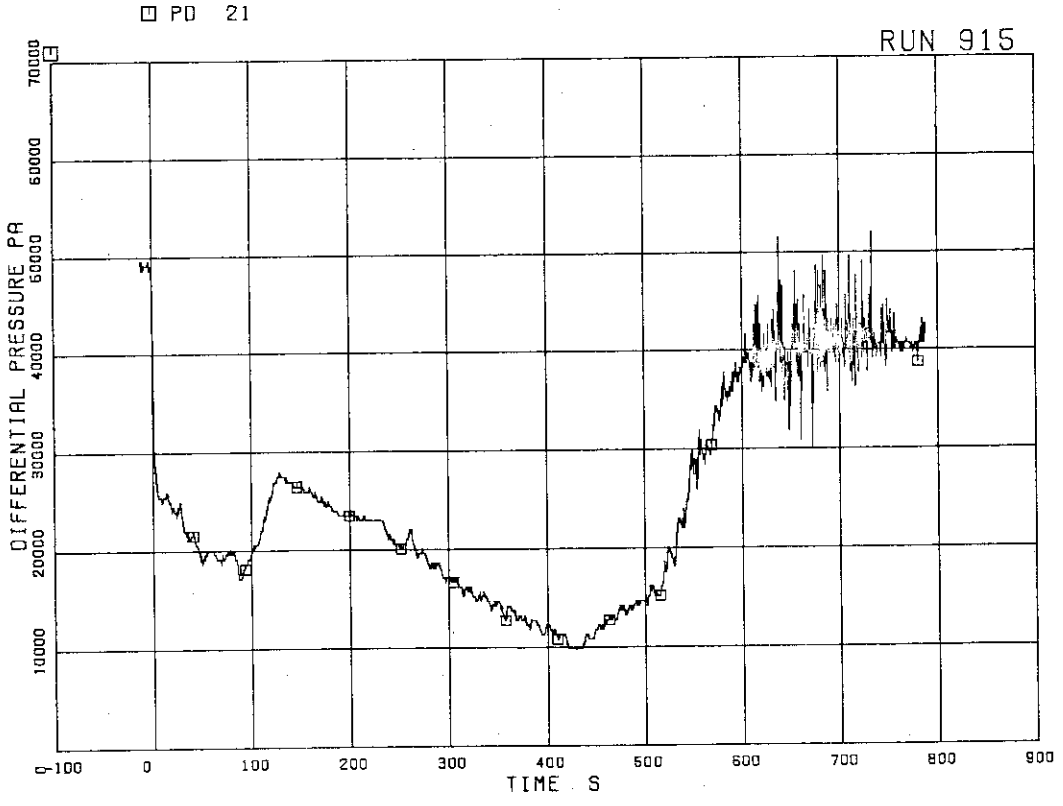

FIG.5. 2 DIFFERENTIAL PRESSURE BETWEEN LOWER PLENUM AND UPPER PLENUM

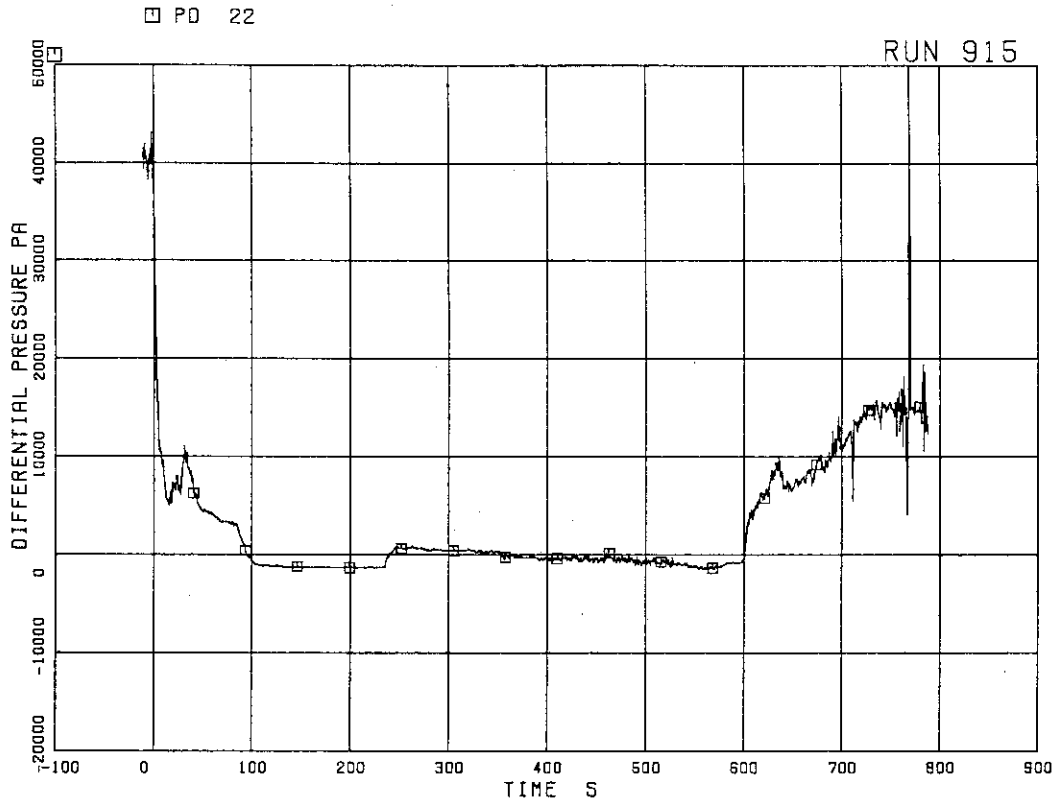

FIG.5. 3 DIFFERENTIAL PRESSURE BETWEEN UPPER PLENUM AND STEAM DOME

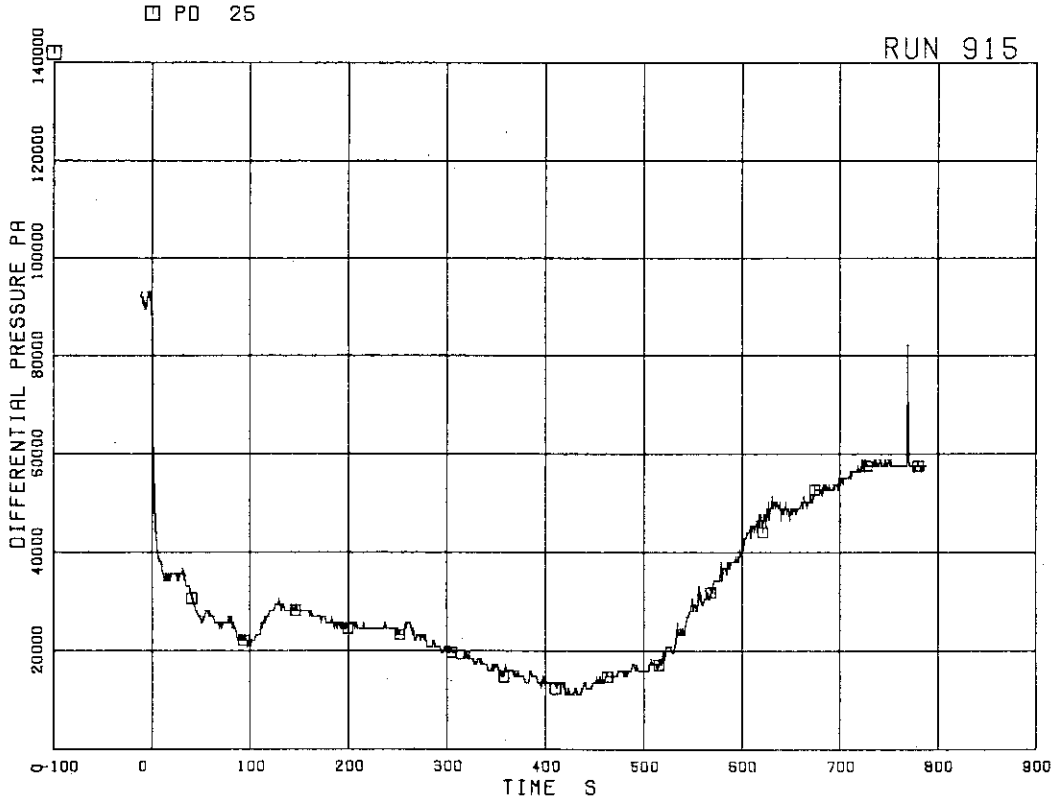

FIG.5. 4 DIFFERENTIAL PRESSURE BETWEEN PV BOTTOM AND TOP

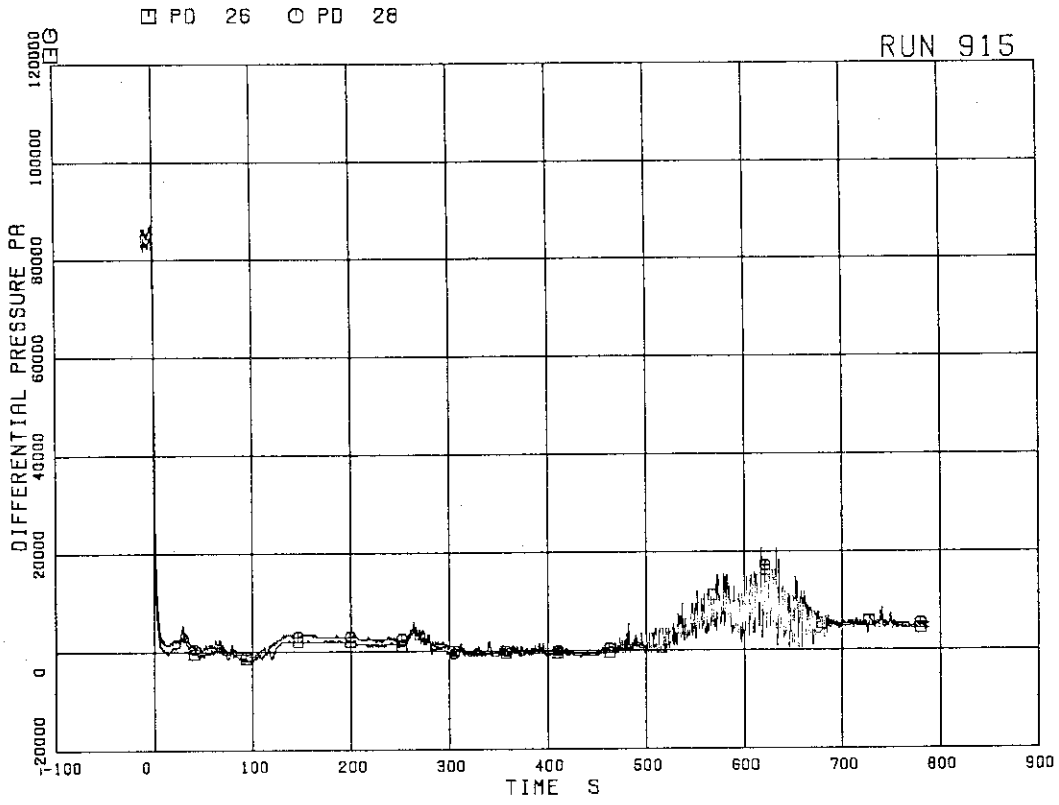

FIG.5. 5 DIFFERENTIAL PRESSURE BETWEEN JP-1,2 DISCHARGE AND SUCTION

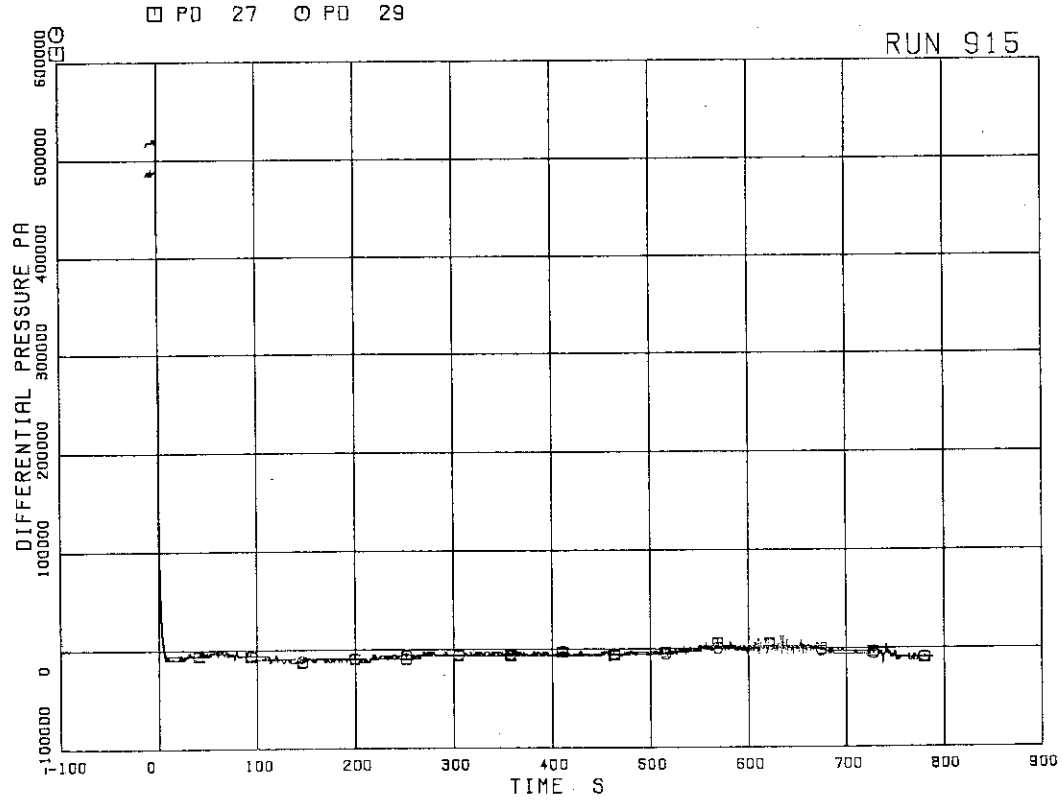

FIG.5. 6 DIFFERENTIAL PRESSURE BETWEEN JP-1,2 DRIVE AND SUCTION

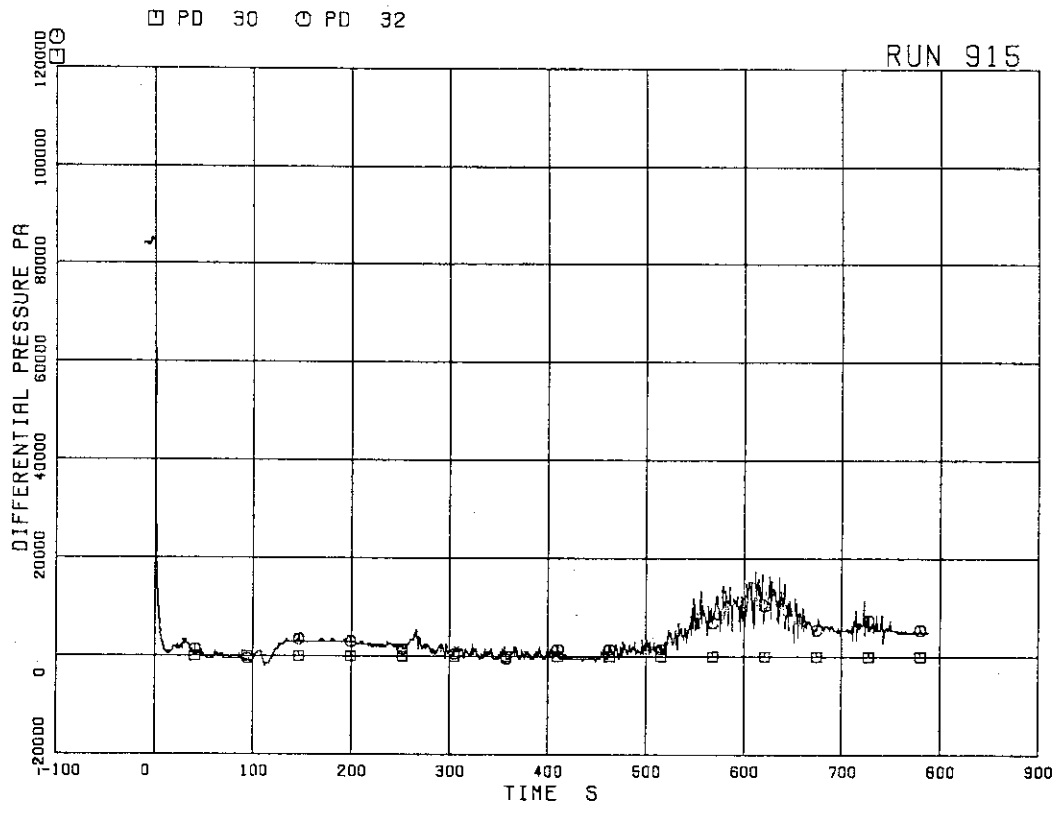

FIG.5. 7 DIFFERENTIAL PRESSURE BETWEEN JP-3.4 DISCHARGE AND SUCTION

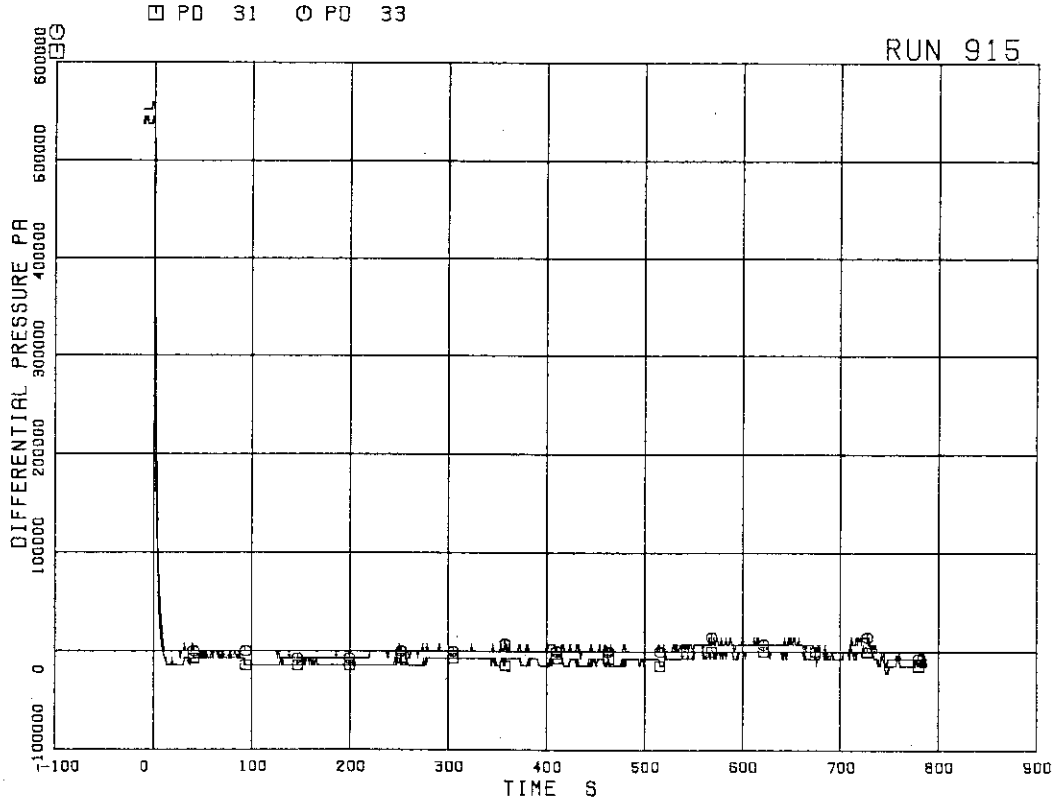

FIG.5. 8 DIFFERENTIAL PRESSURE BETWEEN JP-3.4 DRIVE AND SUCTION

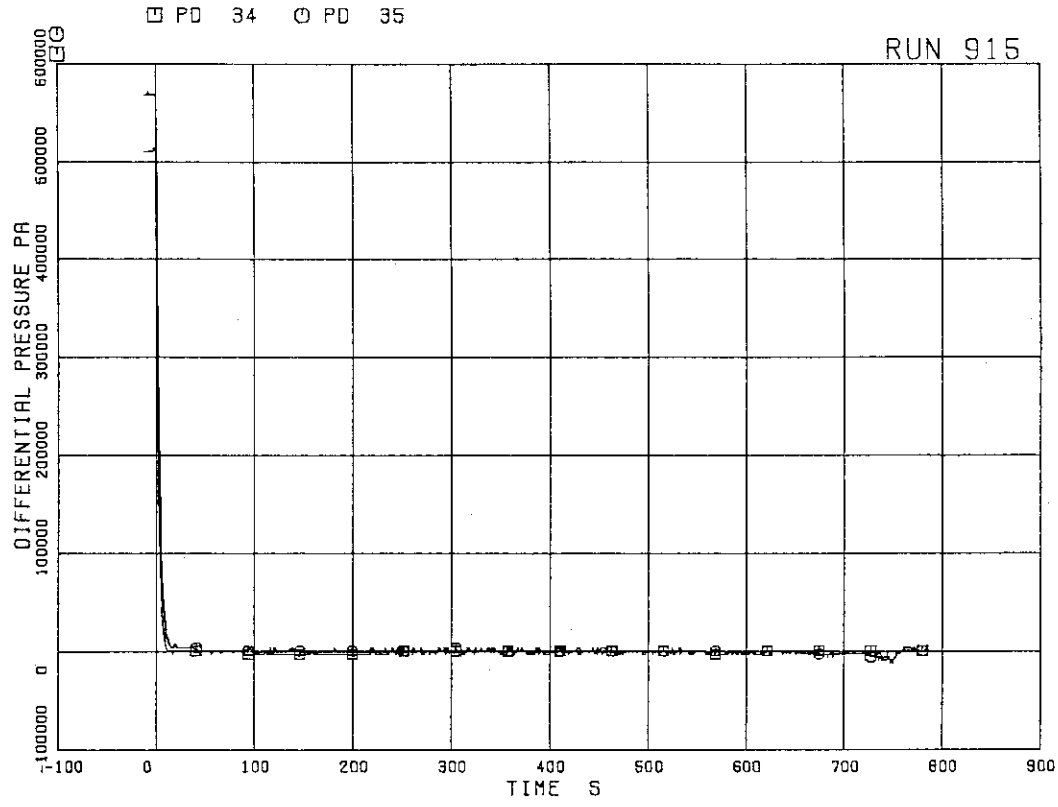

FIG.5. 9 DIFFERENTIAL PRESSURE BETWEEN MRP DELIVERY AND SUCTION

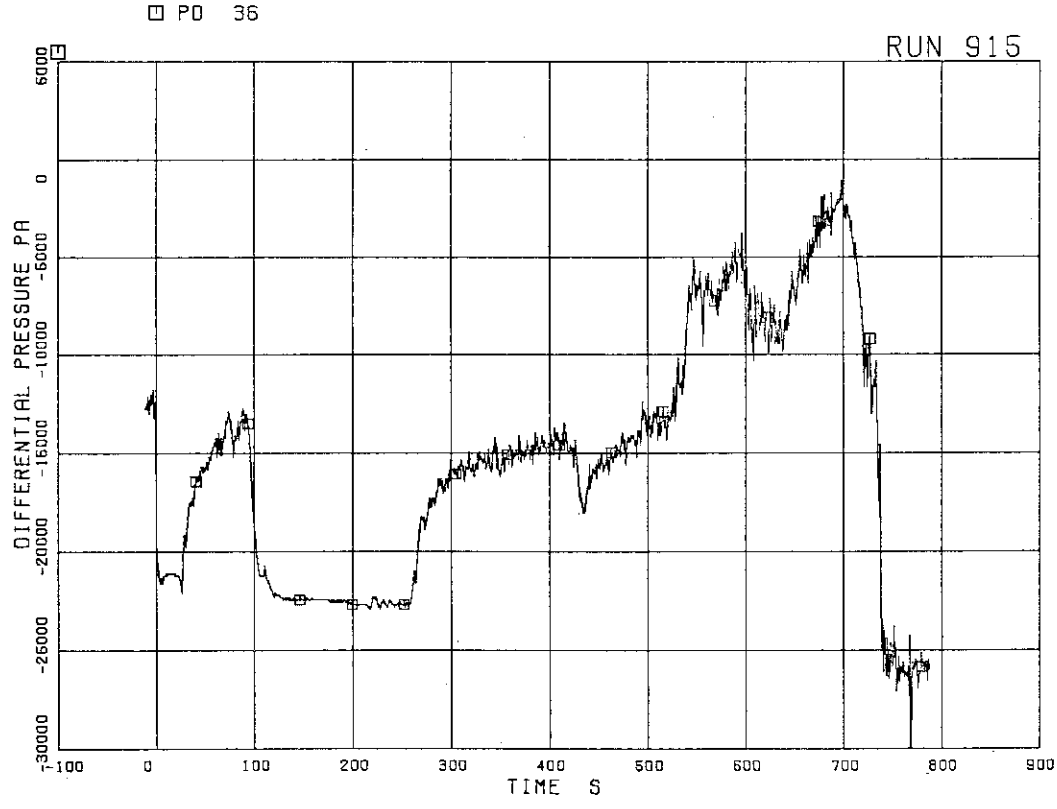

FIG.5. 10 DIFFERENTIAL PRESSURE BETWEEN DOWNCOMER BOTTOM AND MRP1 SUCTION

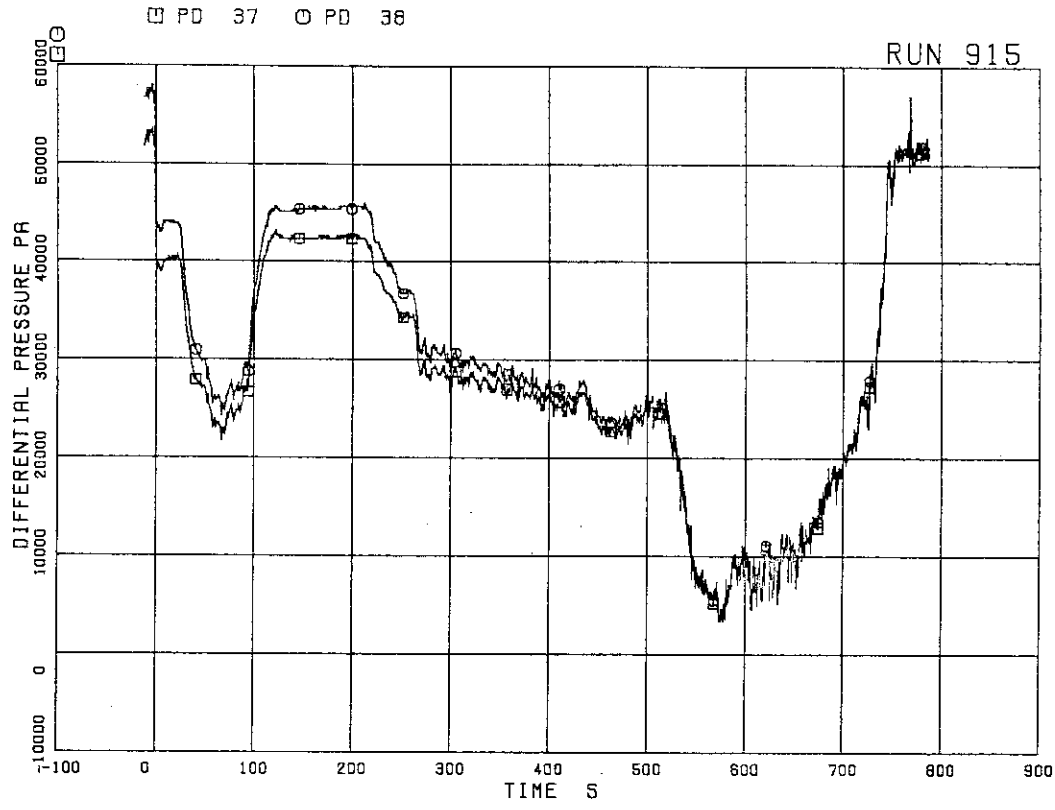

FIG.5. 11 DIFFERENTIAL PRESSURE BETWEEN MRP DELIVERY AND JP-1,2 DRIVE

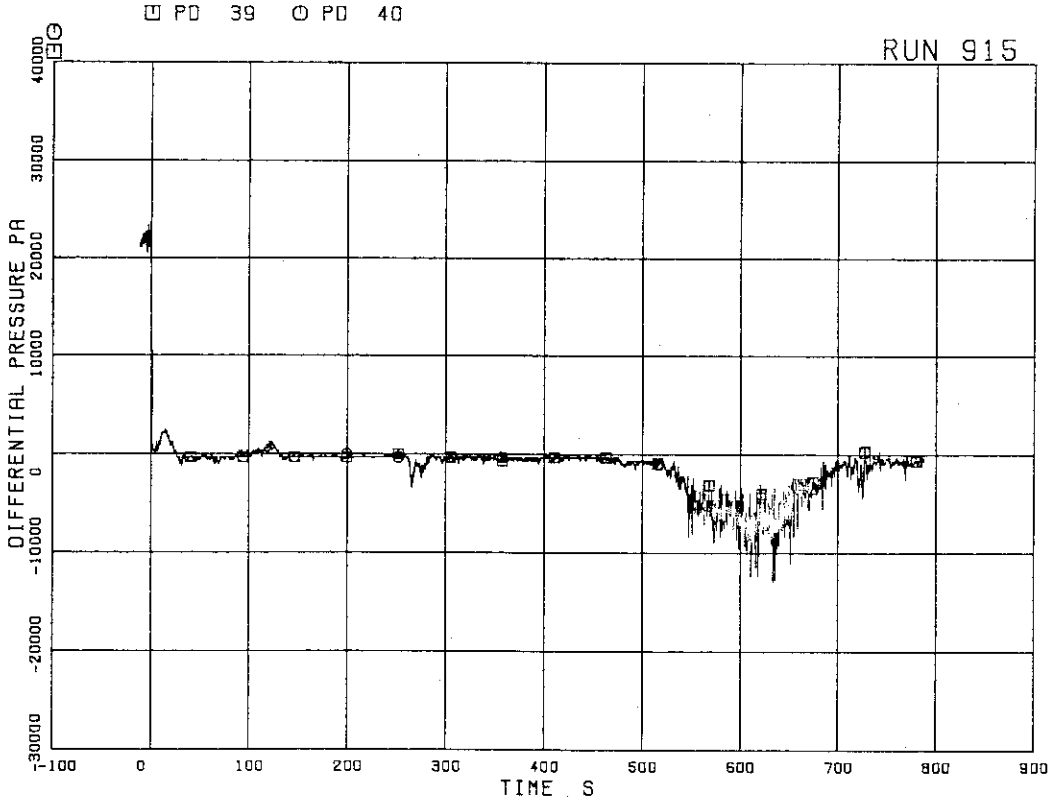

FIG.5. 12 DIFFERENTIAL PRESSURE BETWEEN DOWNCOMER MIDDLE AND JP-1,2 SUCTION

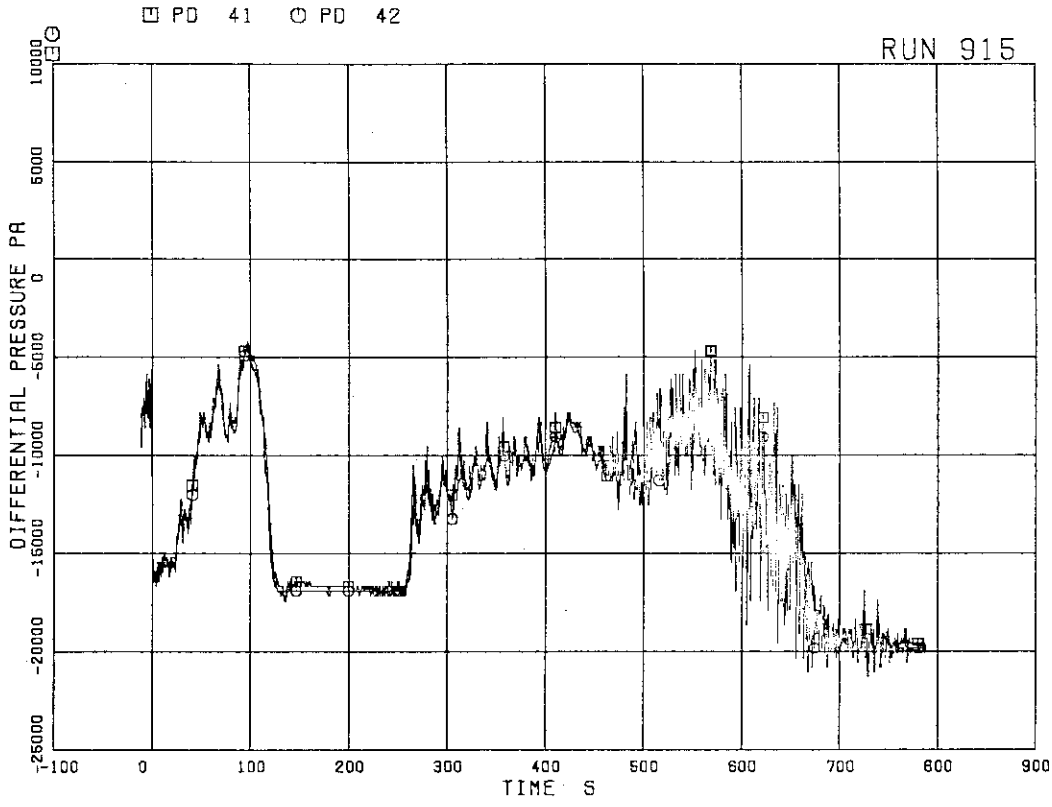

FIG.5. 13 DIFFERENTIAL PRESSURE BETWEEN JP-1,2 DISCHARGE AND LOWER PLENUM

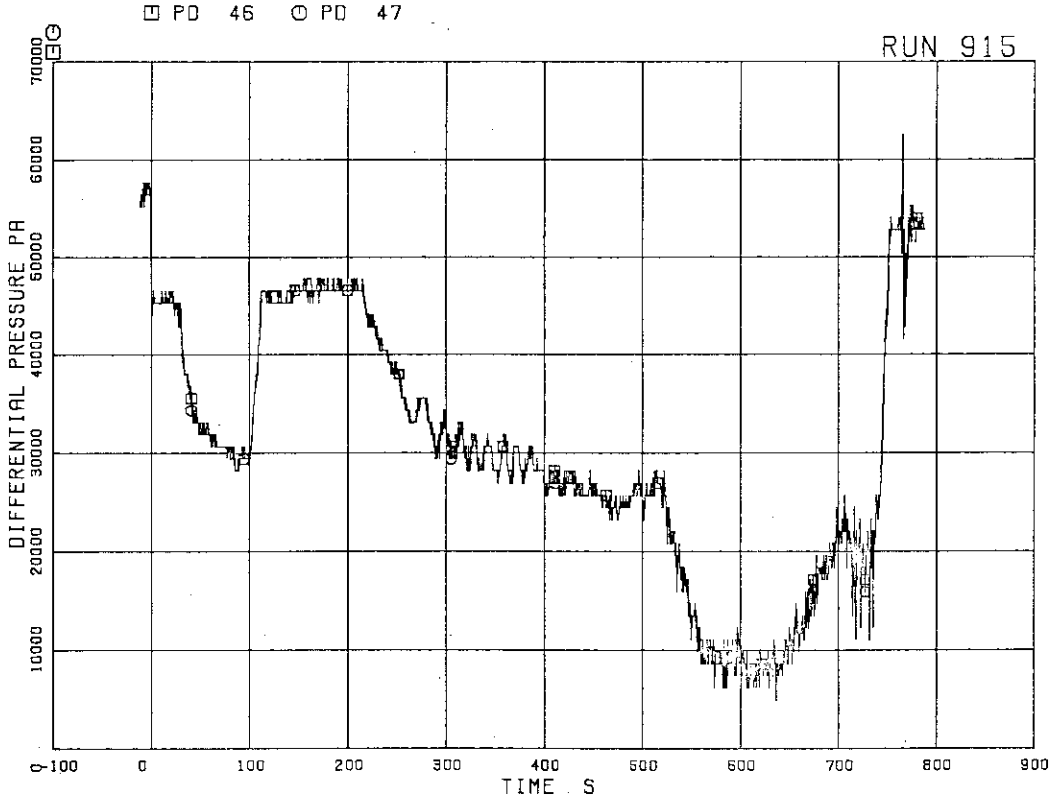

FIG.5. 14 DIFFERENTIAL PRESSURE BETWEEN MRP DELIVERY AND JP-3,4 DRIVE

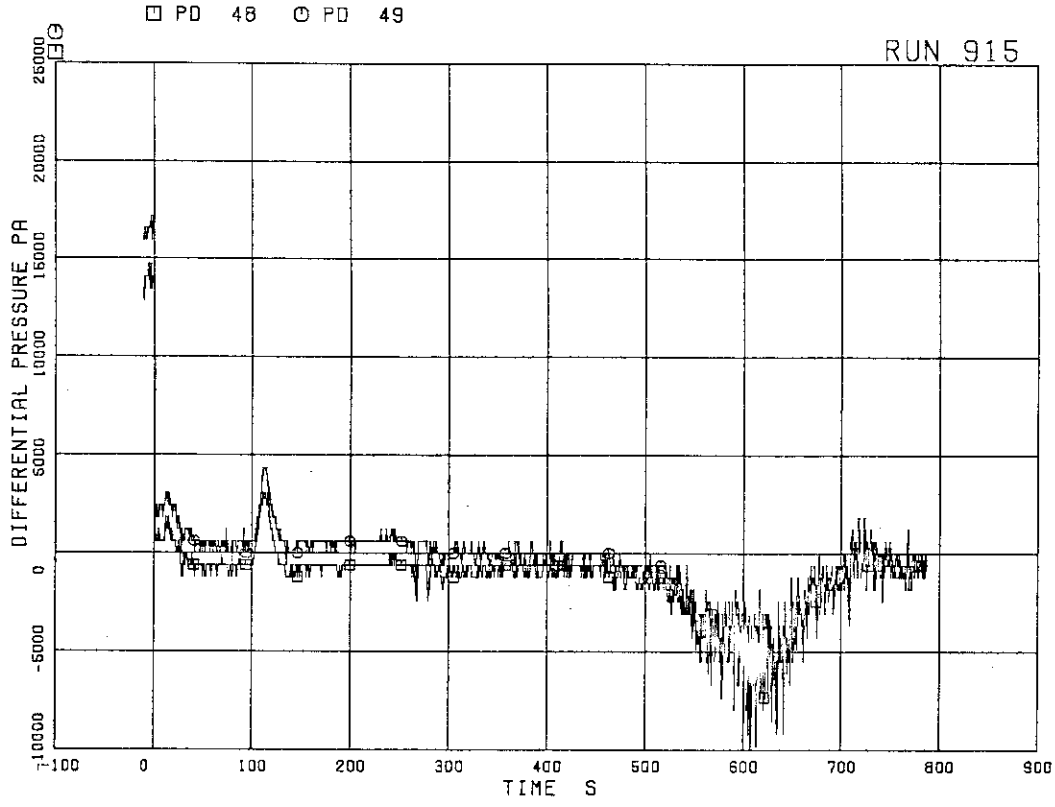

FIG.5. 15 DIFFERENTIAL PRESSURE BETWEEN DOWNCOMER MIDDLE AND JP-3,4 SUCTION

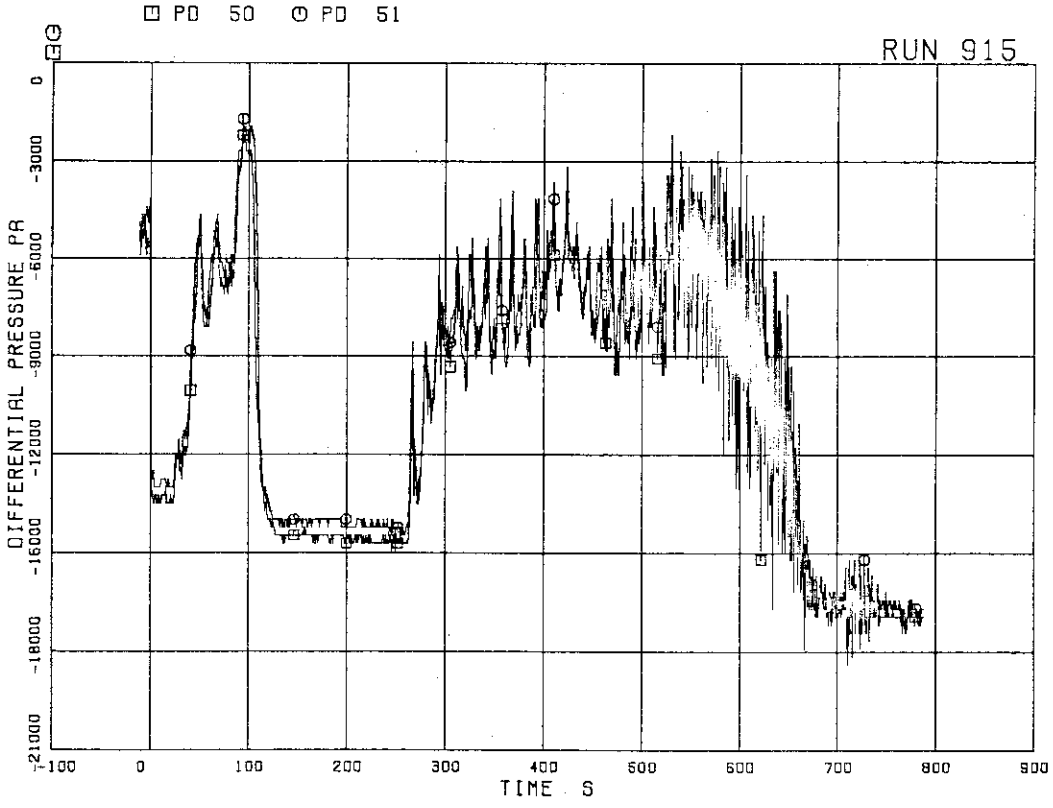

FIG.5. 16 DIFFERENTIAL PRESSURE BETWEEN JP-3,4 DISCHARGE AND CONFLURNCE

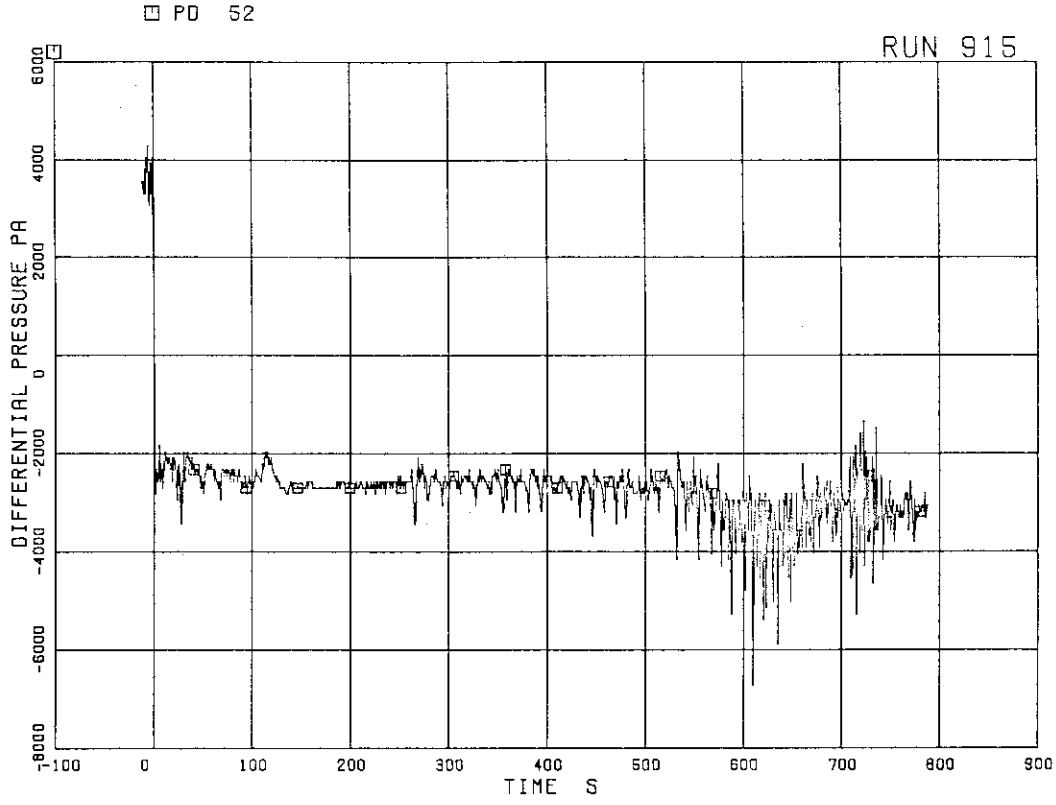

FIG.5. 17 DIFFERENTIAL PRESSURE BETWEEN JP-3,4 CONFLUENCE IN BROKEN LOOP AND LP

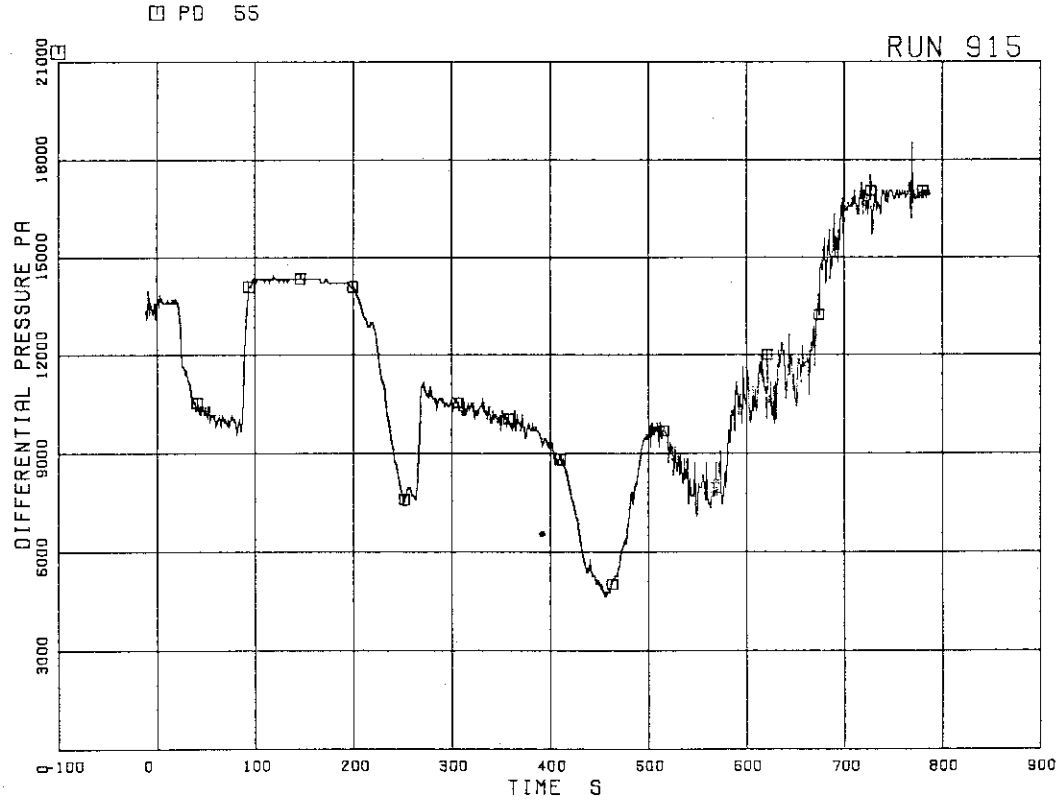

FIG.5. 18 DIFFERENTIAL PRESSURE BETWEEN DOWNCOMER BOTTOM AND DOWNCOMER MIDDLE

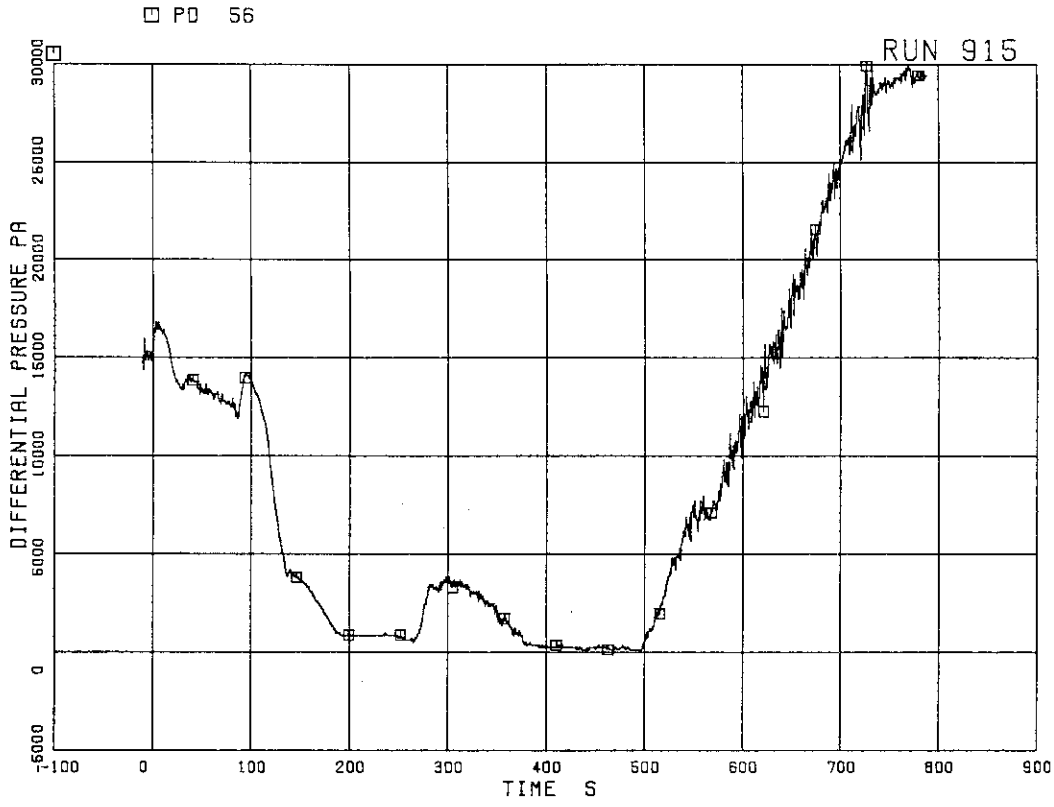

FIG.5. 19 DIFFERENTIAL PRESSURE BETWEEN DOWNCOMER MIDDLE AND STEAM DOME

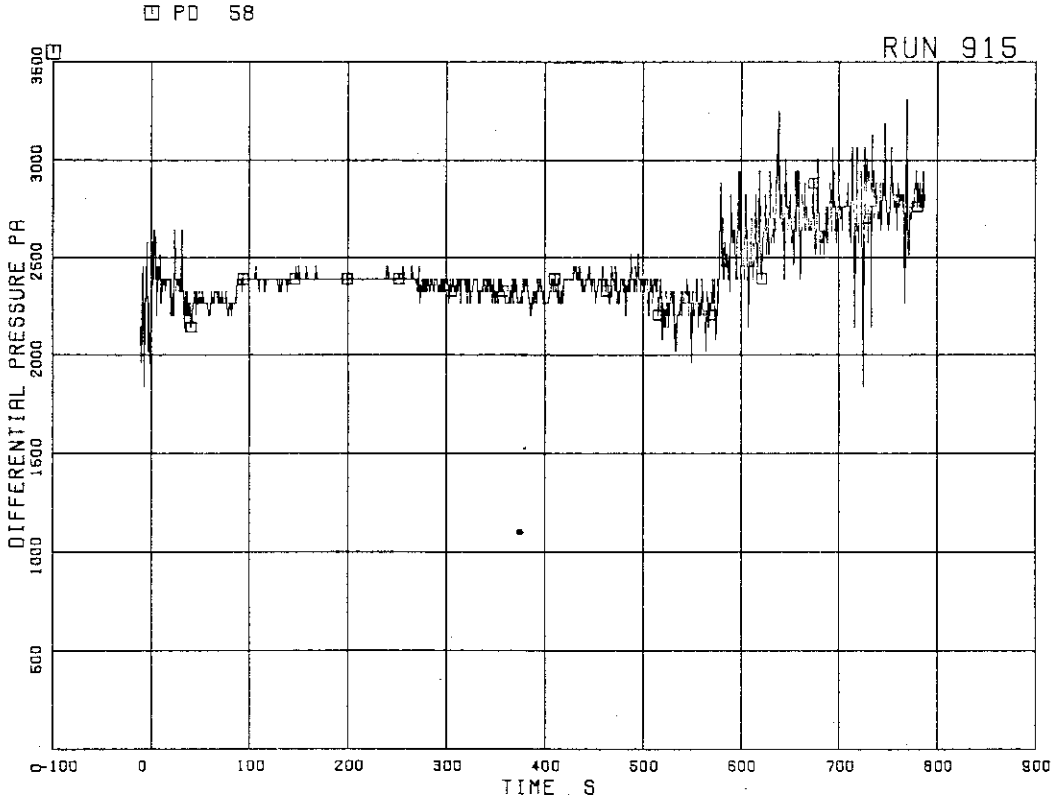

FIG.5. 20 DIFFERENTIAL PRESSURE BETWEEN LP BOTTOM AND LP MIDDLE

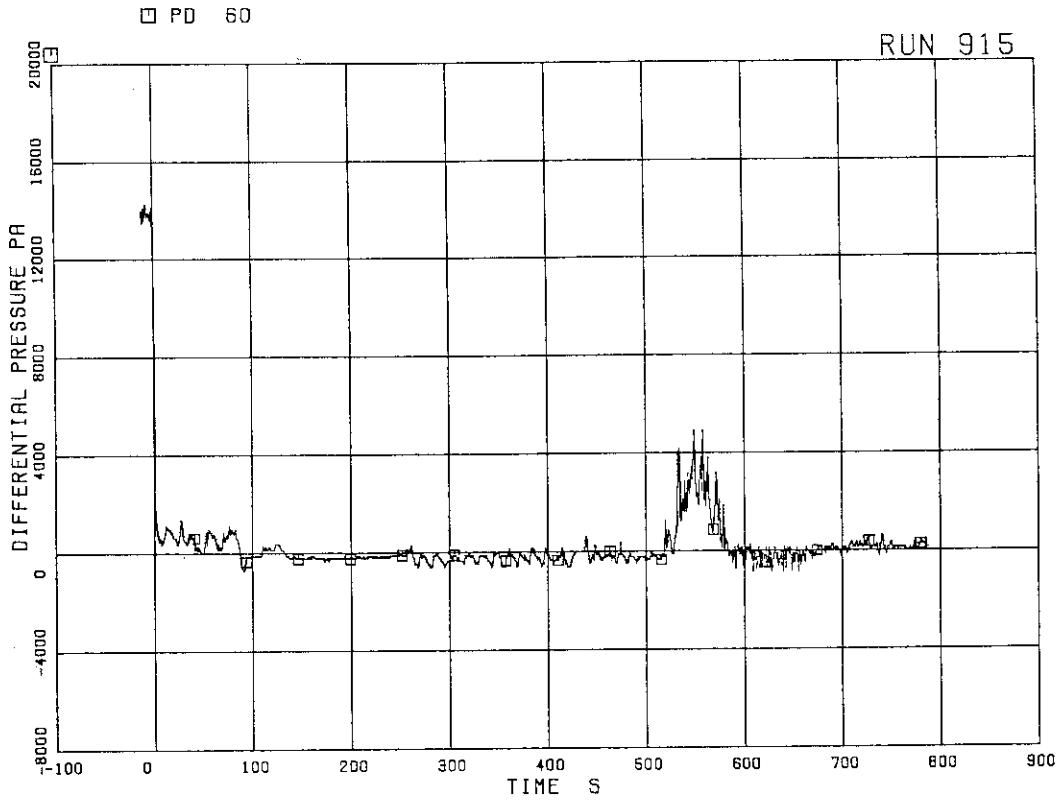

FIG.5. 21 DIFFERENTIAL PRESSURE ACROSS CHANNEL INLET ORIFICE A

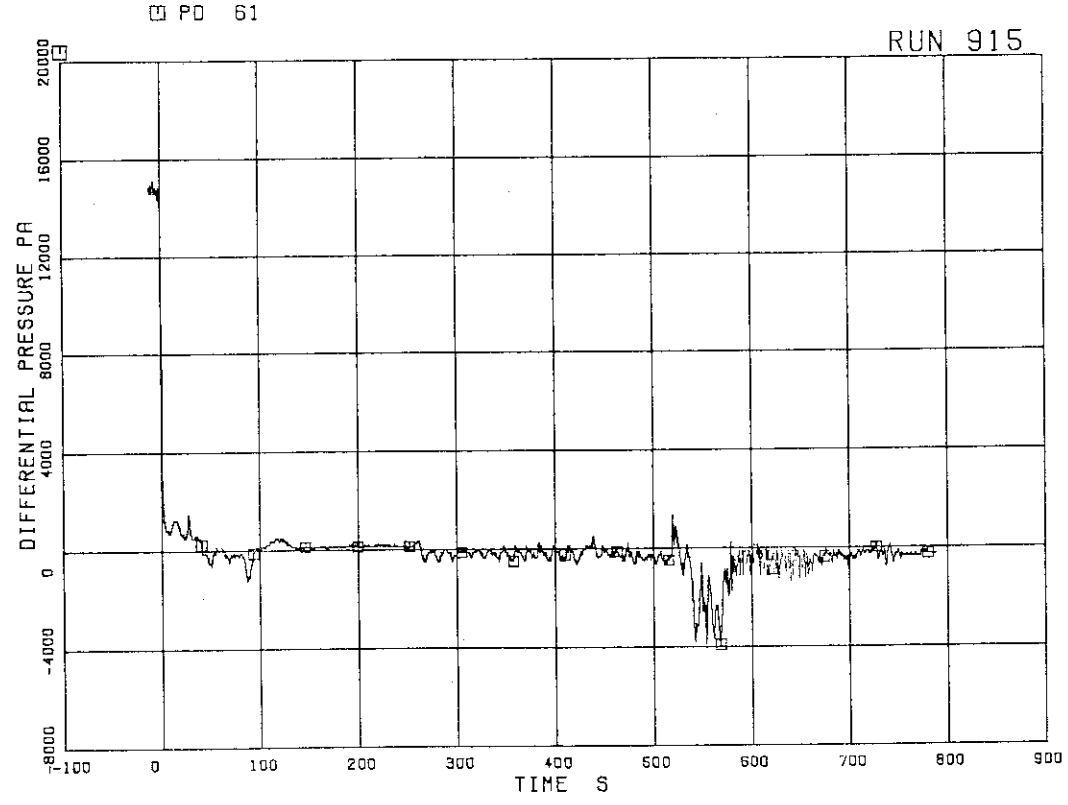

FIG.5. 22 DIFFERENTIAL PRESSURE ACROSS CHANNEL INLET ORIFICE B

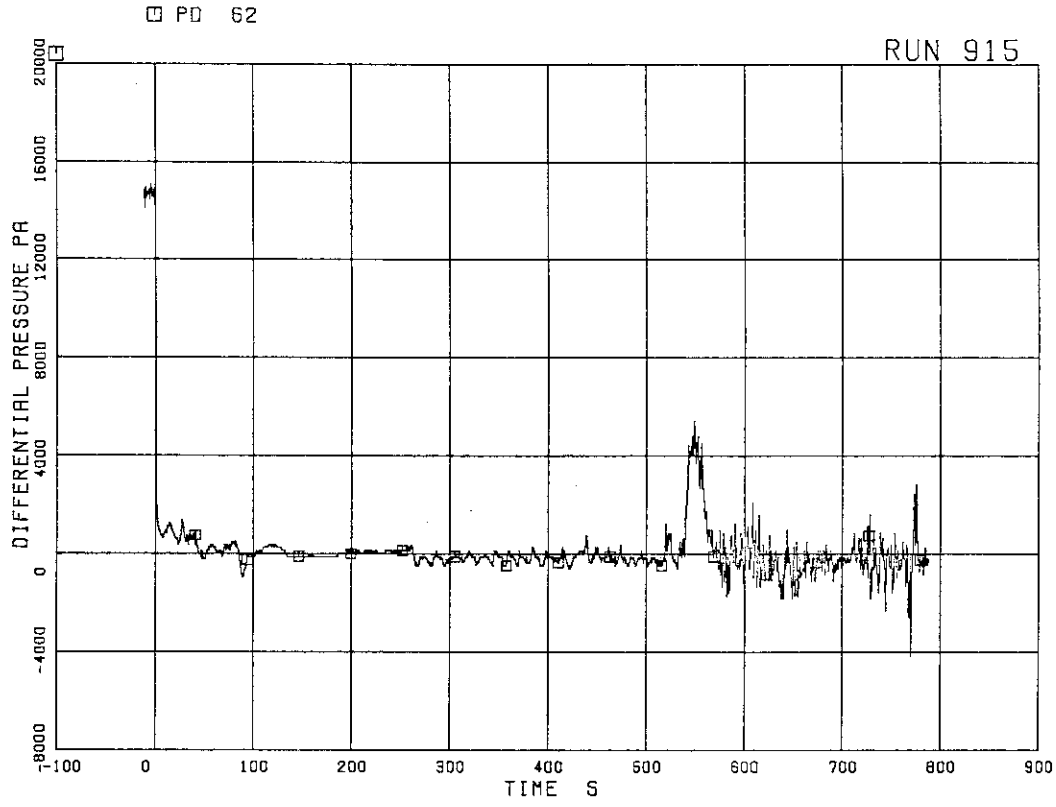

FIG.5. 23 DIFFERENTIAL PRESSURE ACROSS CHANNEL INLET ORIFICE C

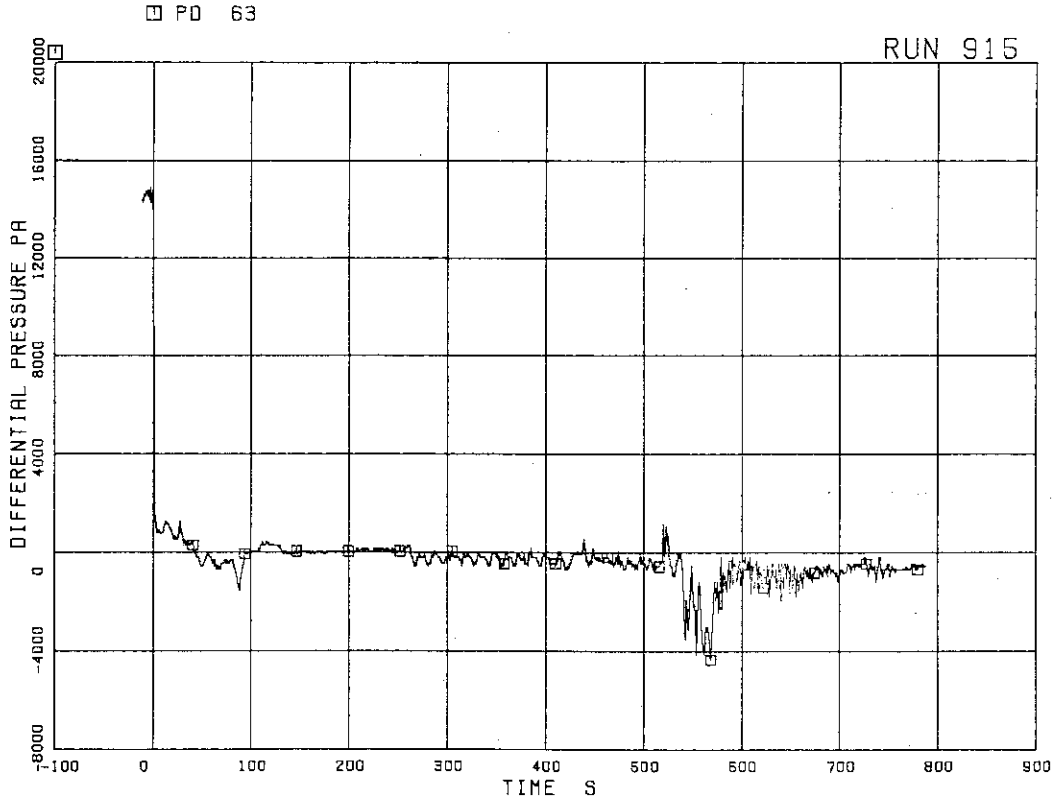

FIG.5. 24 DIFFERENTIAL PRESSURE ACROSS CHANNEL INLET ORIFICE D

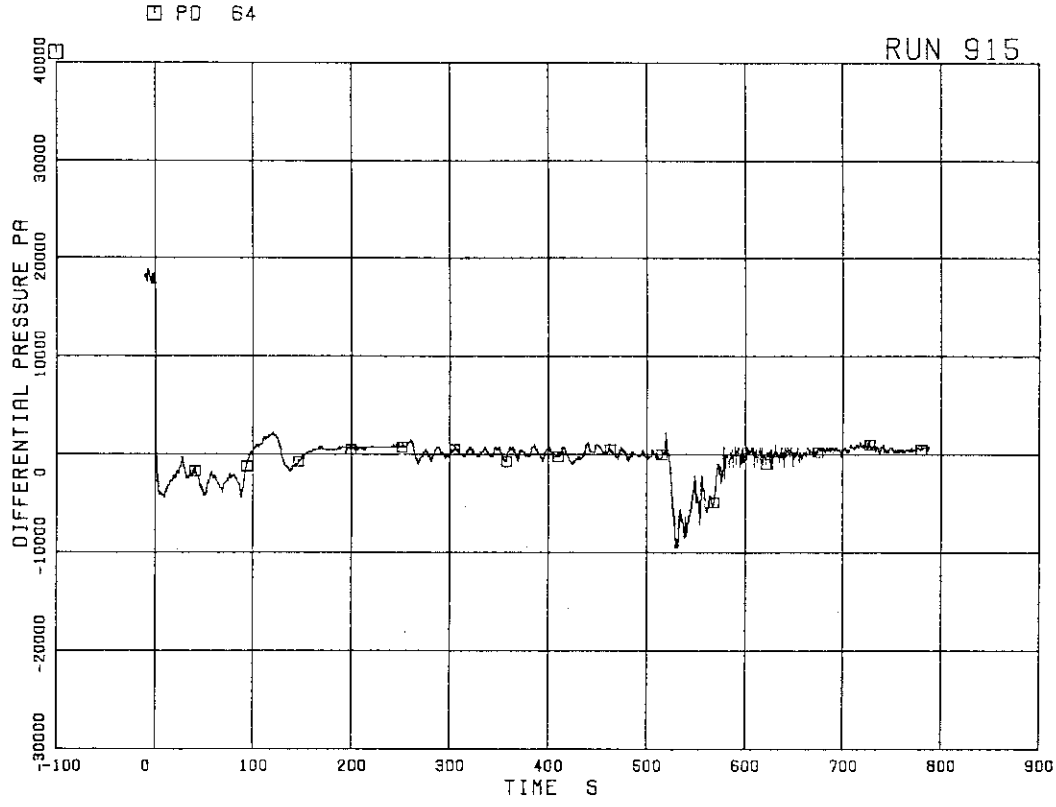

FIG.5. 25 DIFFERENTIAL PRESSURE ACROSS BYPASS HOLE

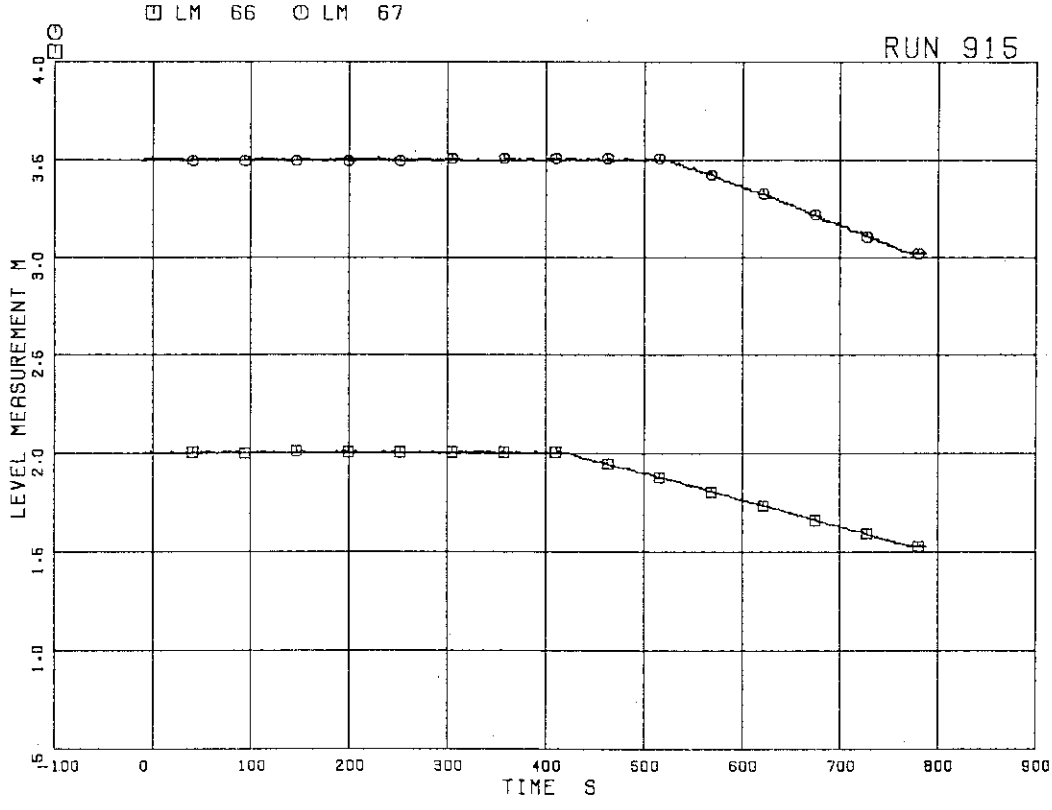

FIG.5. 26 LIQUID LEVELS IN ECCS TANKS

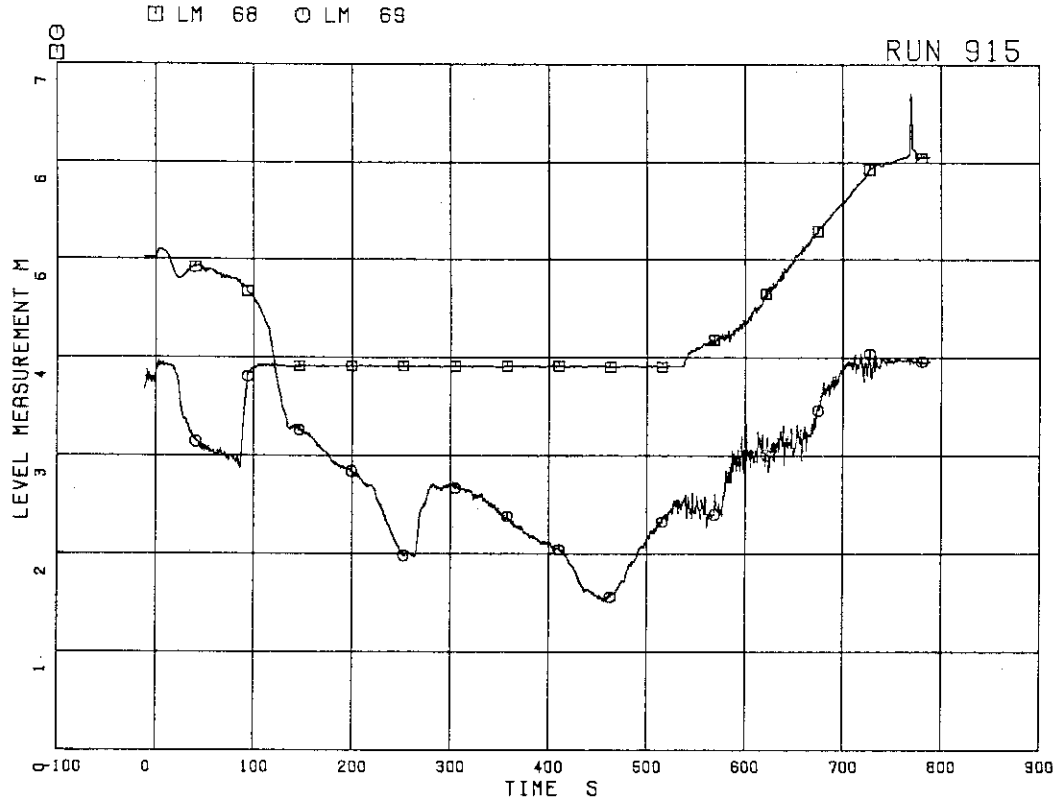

FIG.5. 27 LIQUID LEVEL IN DOWNCOMER

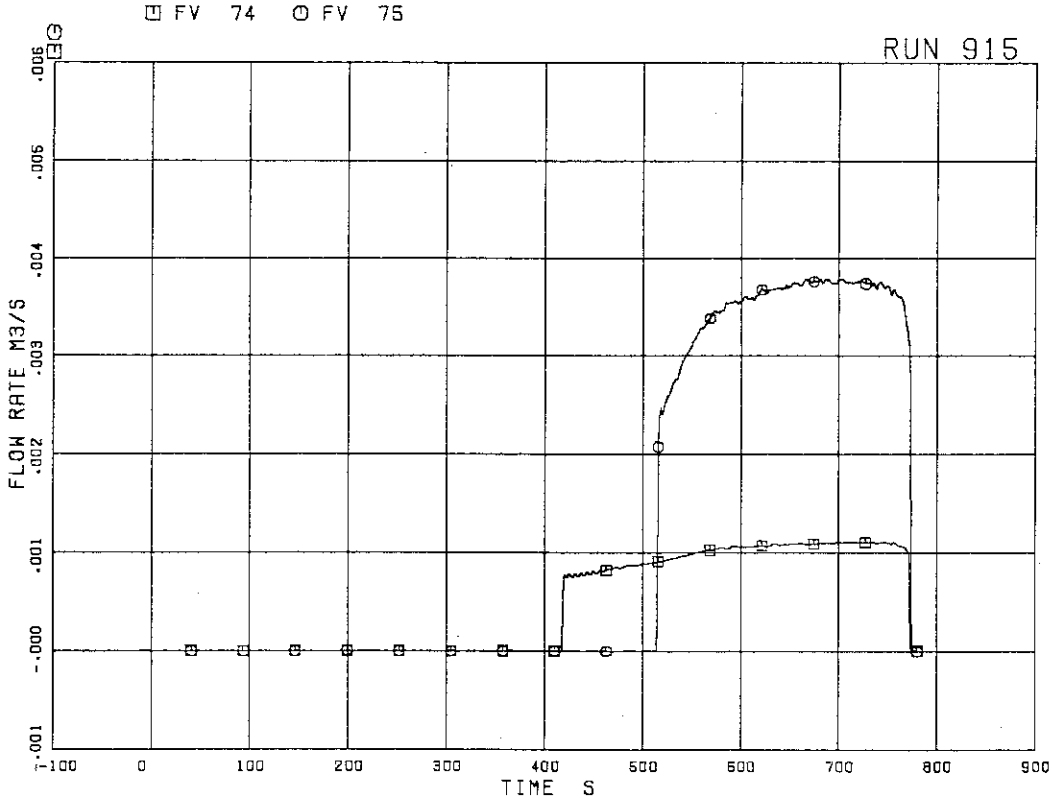

FIG.5. 28 ECC INJECTION FLOW RATES

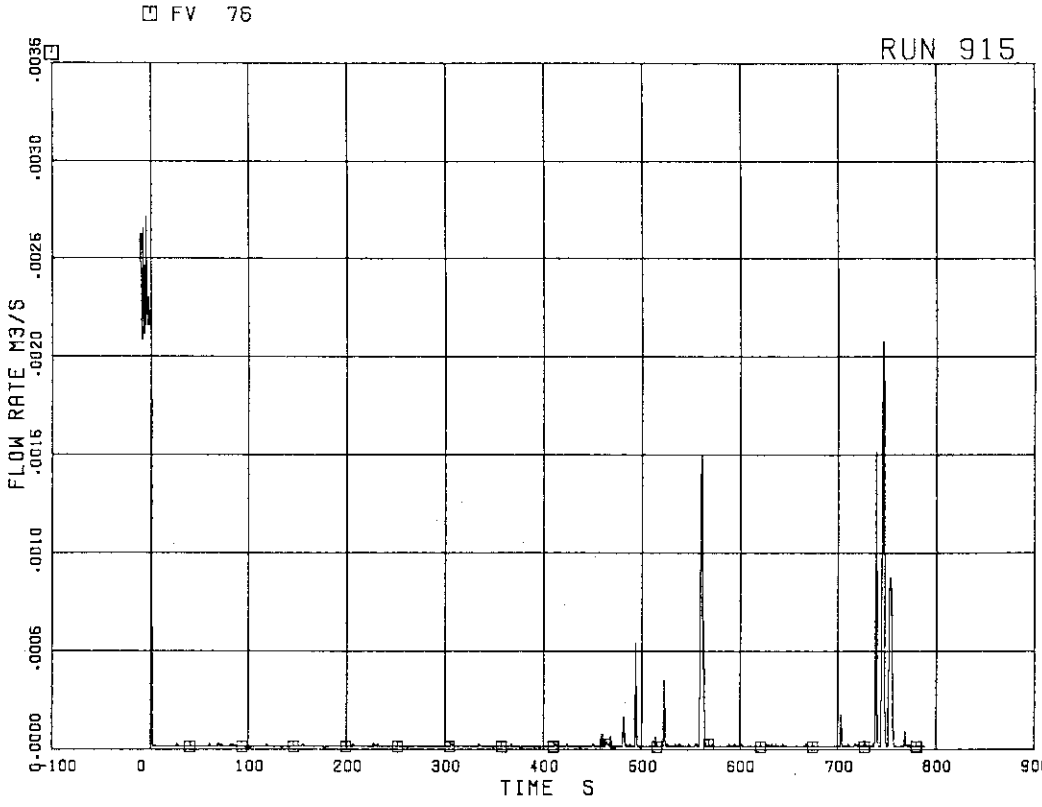

FIG.5. 29 FEEDWATER FLOW RATE

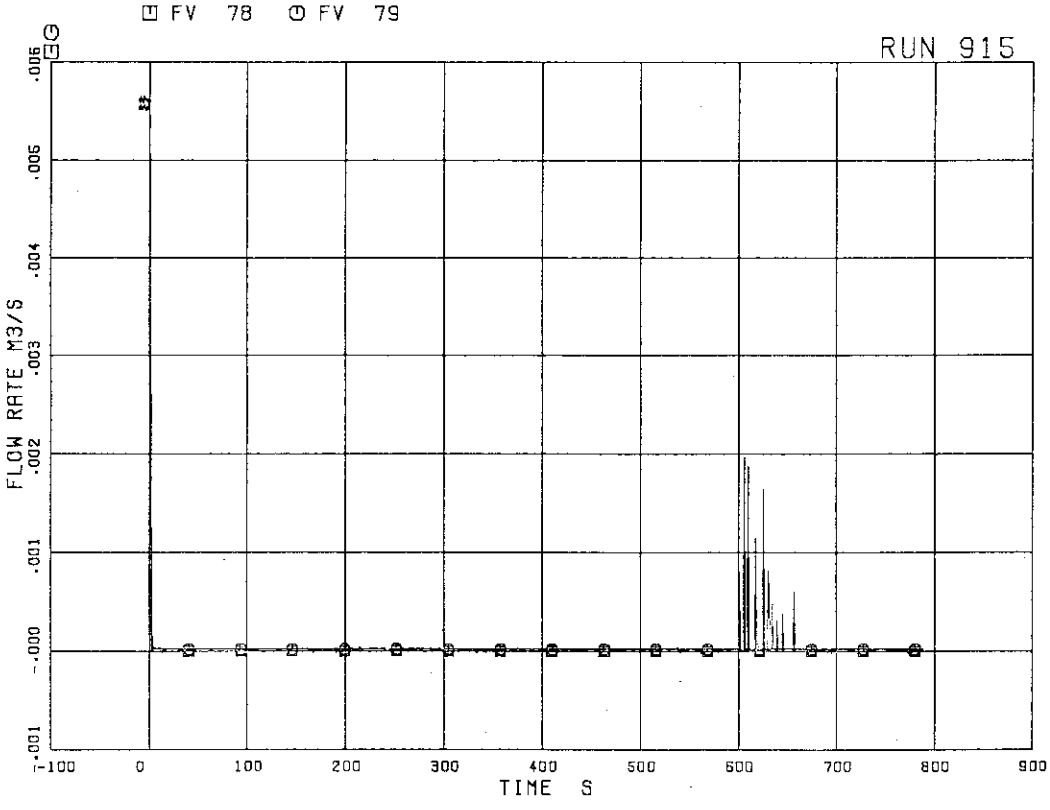

FIG.5. 30 JP-1,2 DISCHARGE FLOW RATES (POS.FLOW)

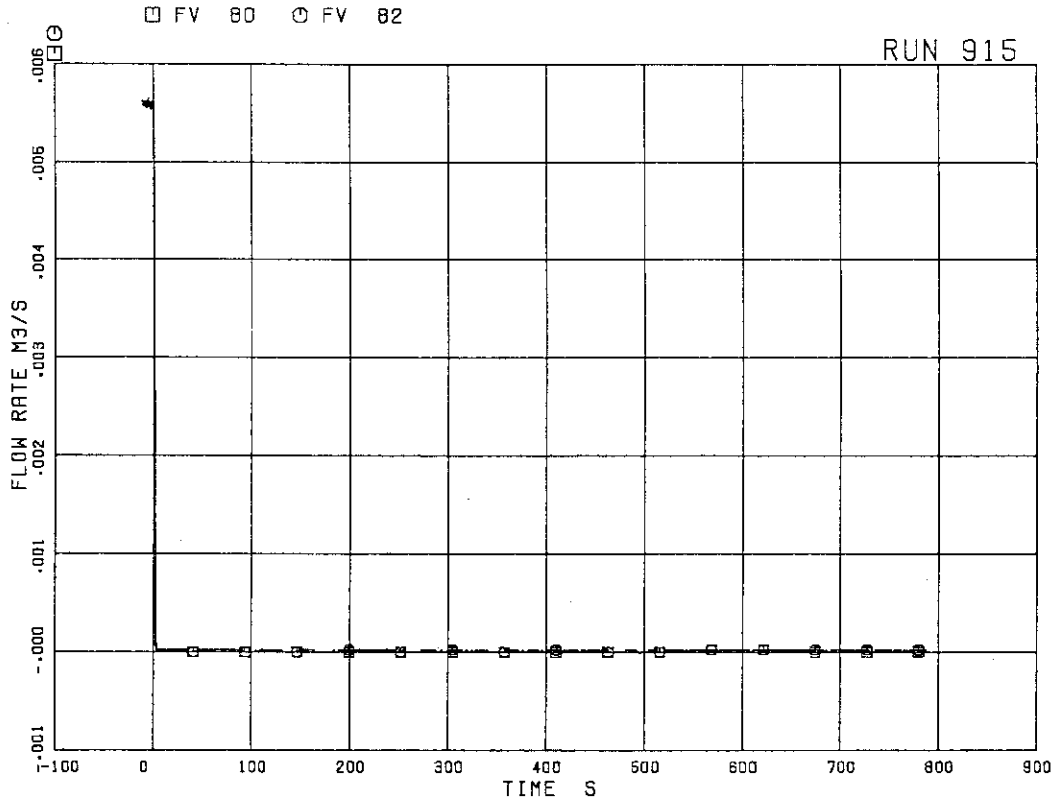

FIG.5. 31 JP-3.4 DISCHARGE FLOW RATES (POS.FLOW)

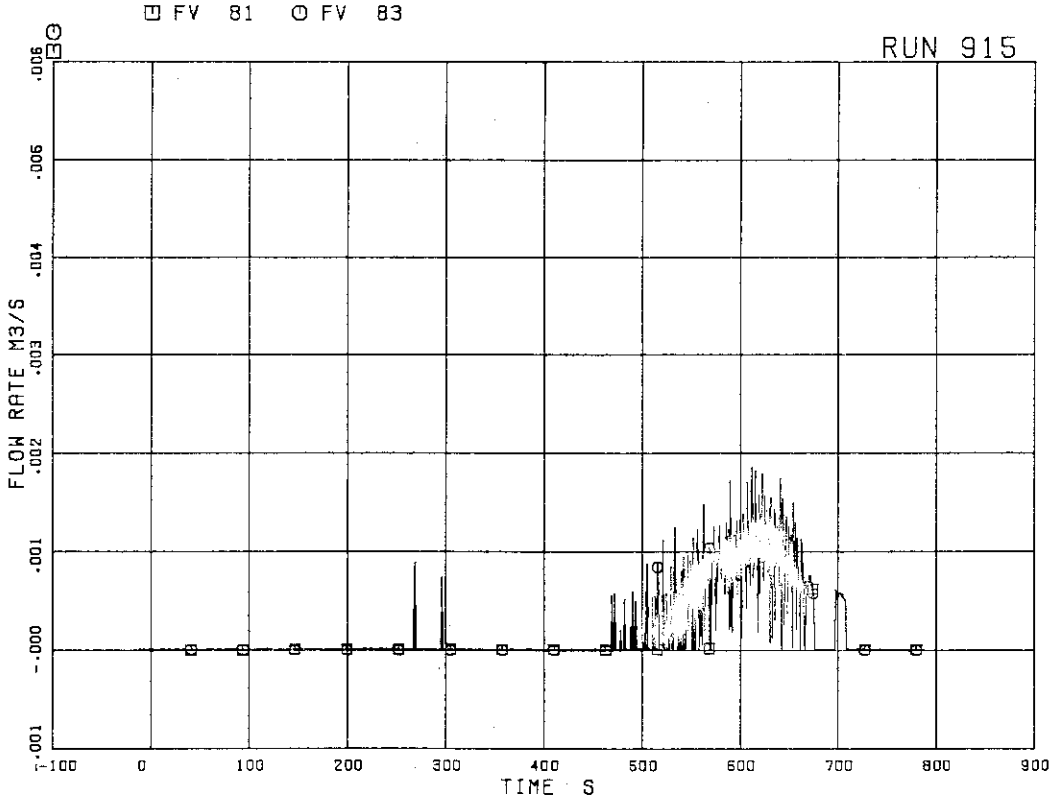

FIG.5. 32 JP-3.4 DISCHARGE FLOW RATES (NEG.FLOW)

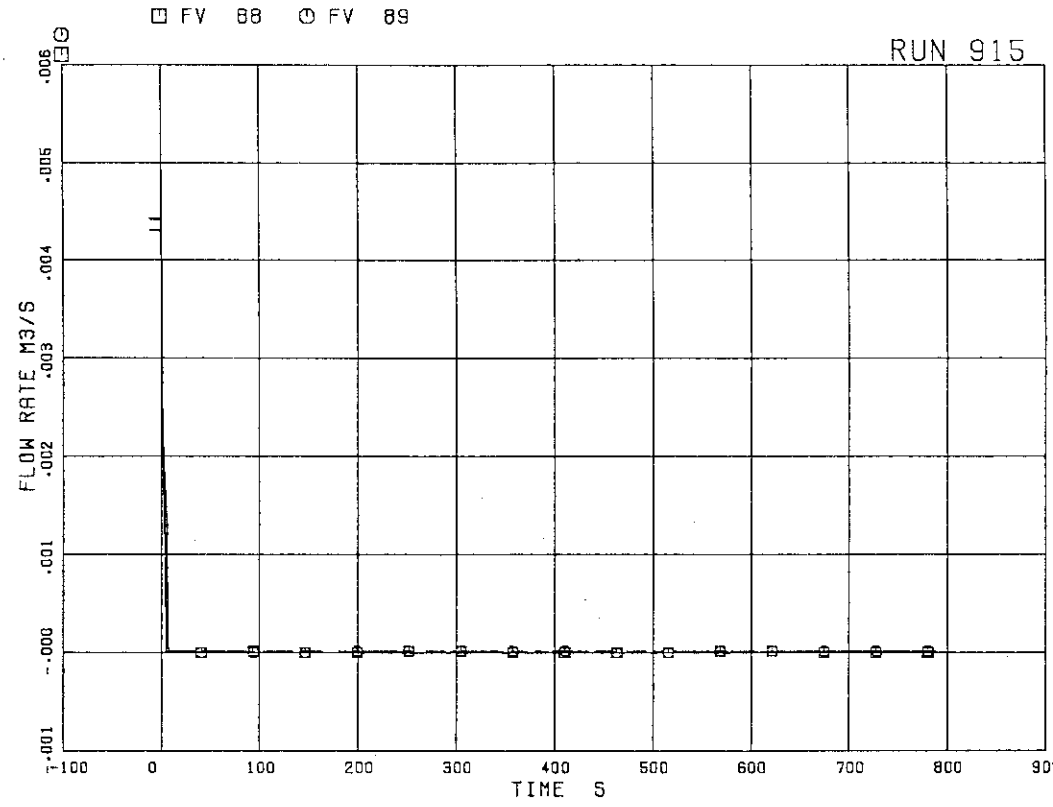

FIG.5. 33 MRP DISCHARGE FLOW RATES

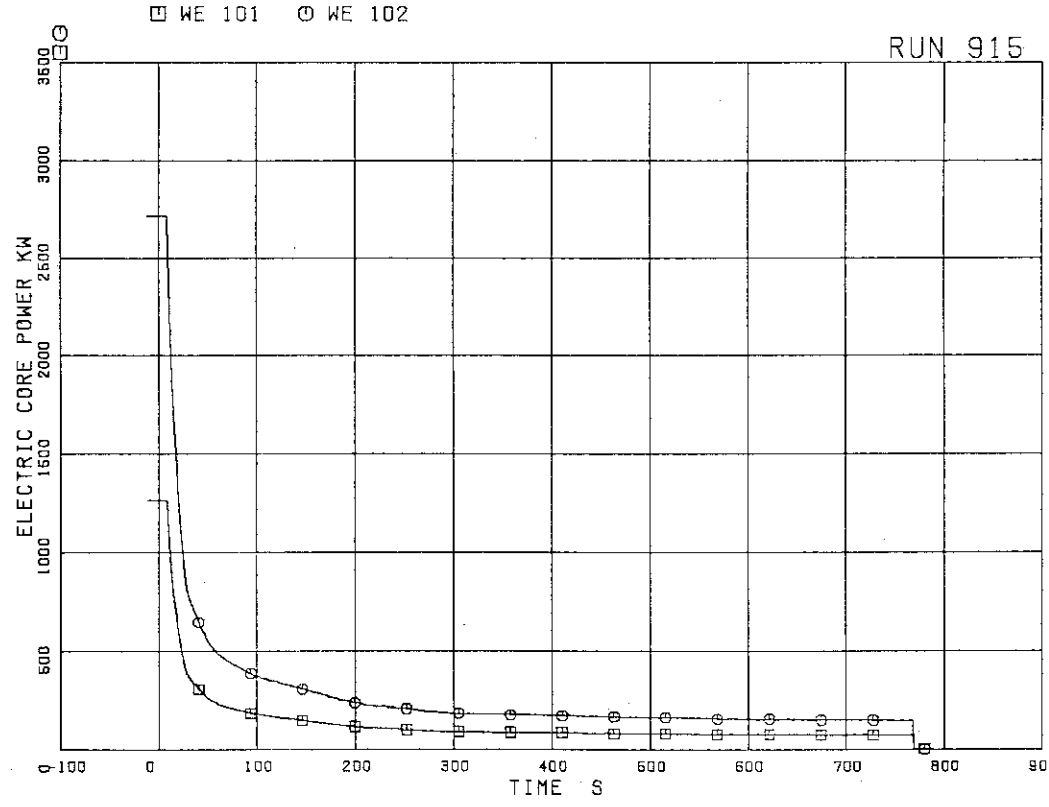

FIG.5. 34 ELECTRIC CORE POWER

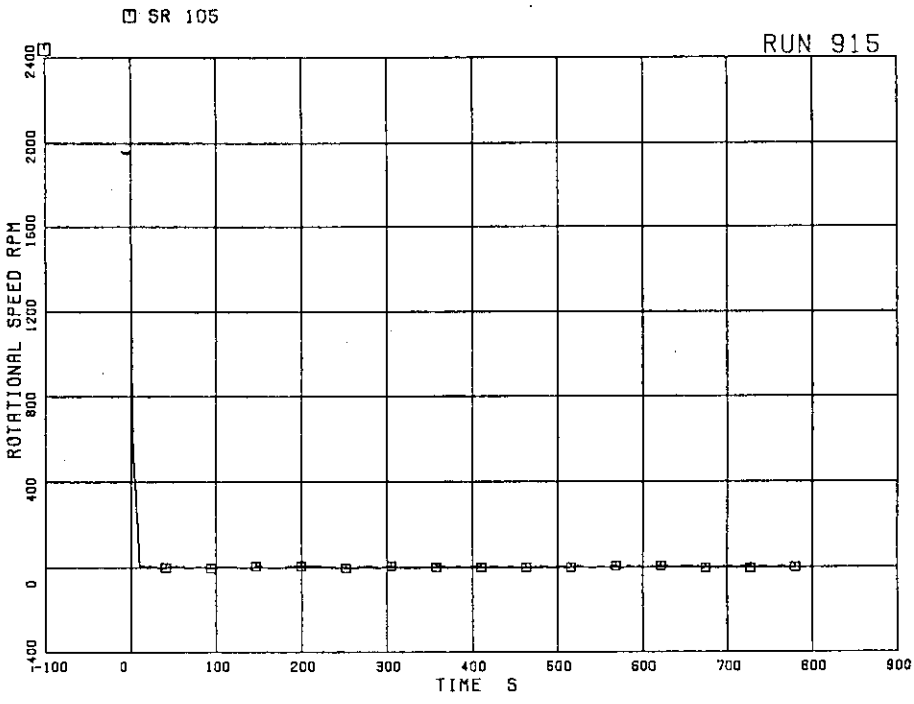

FIG.5. 35 MRP PUMP SPEED

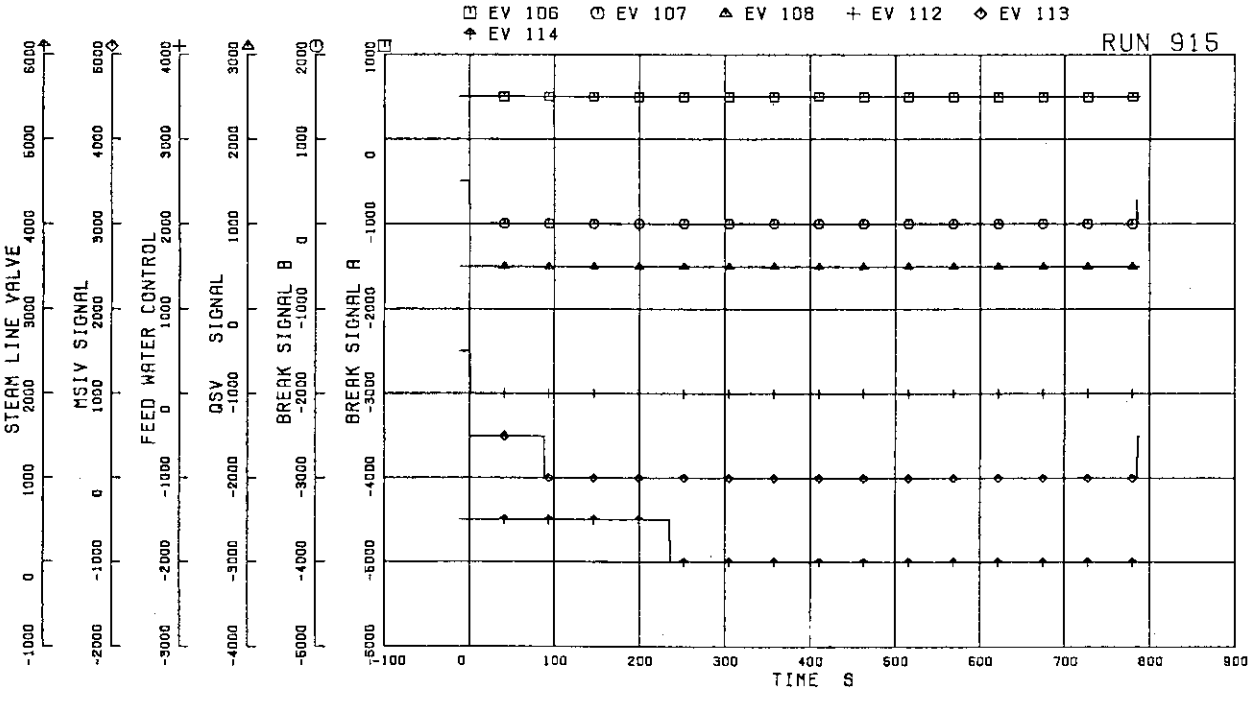

FIG.5. 36 VALVE OPERATION SIGNALS

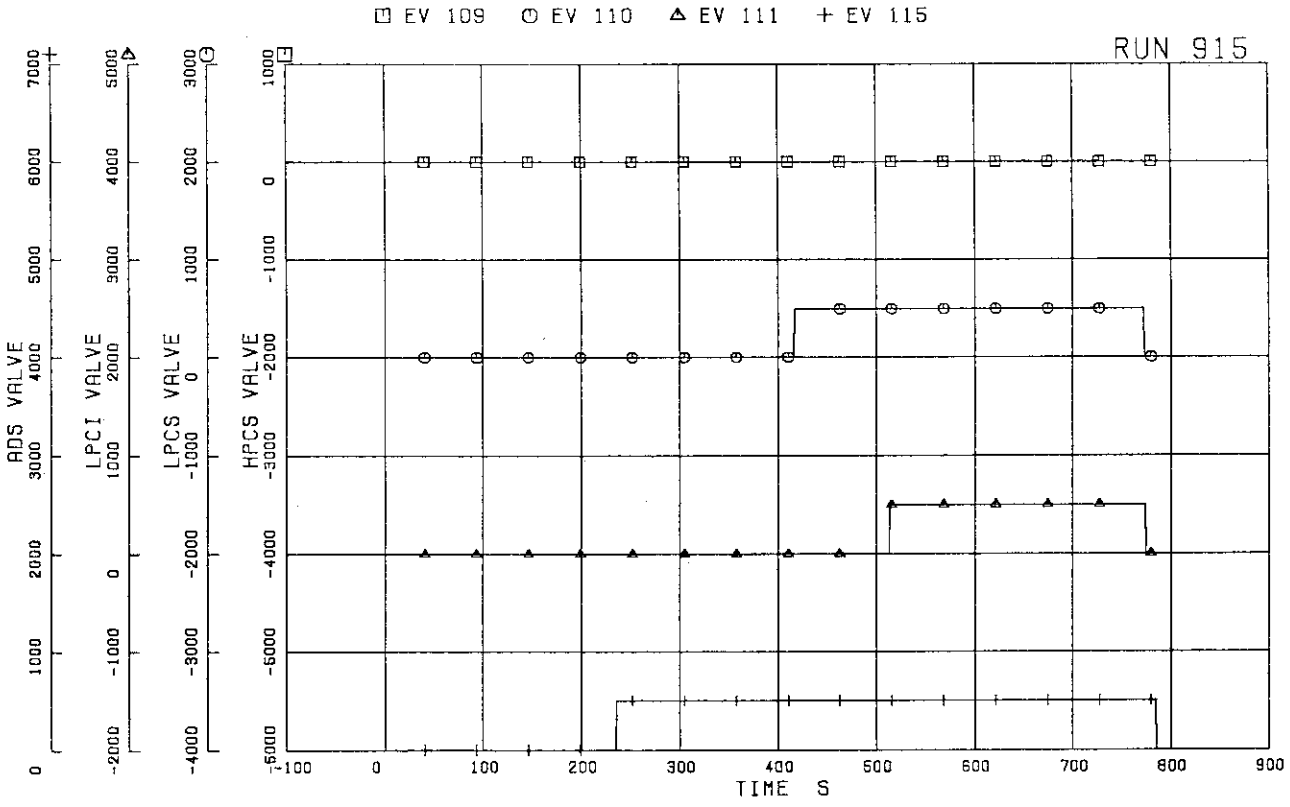

FIG.5. 37 ECCS OPERATION SIGNALS

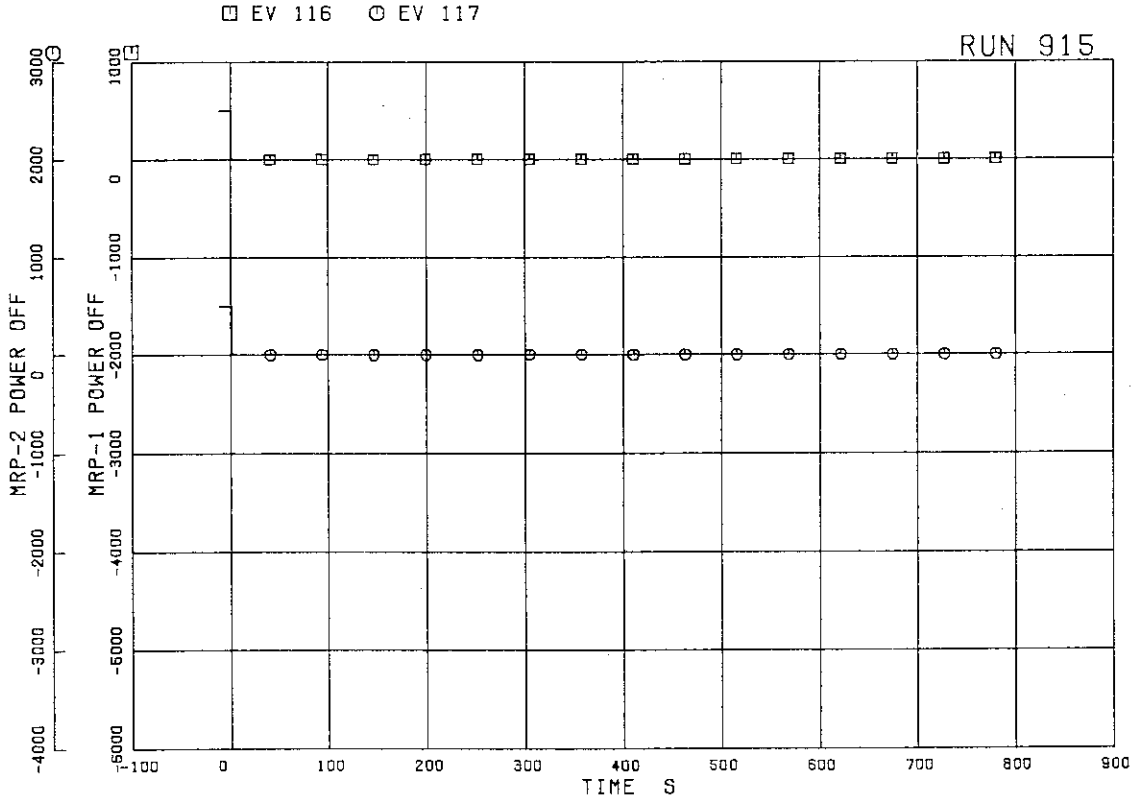

FIG.5. 38 MRP OPERATION SIGNALS

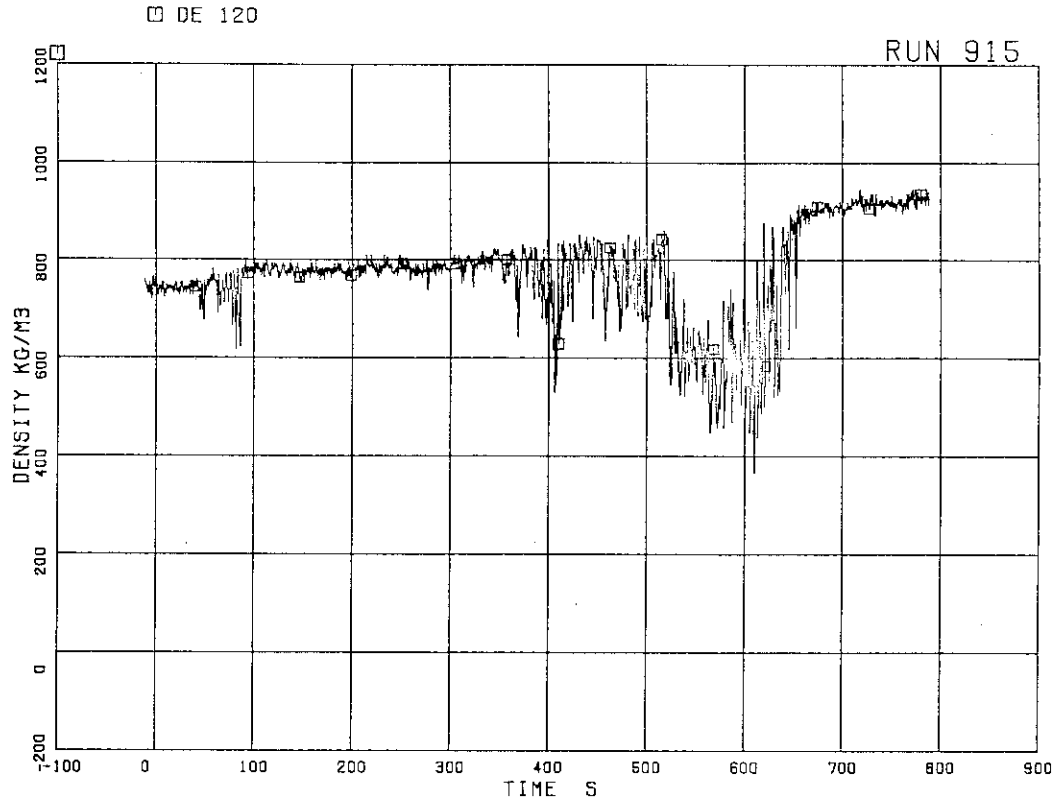

FIG.5. 39 FLUID DENSITY AT JP-1,2 OUTLET, BEAM A

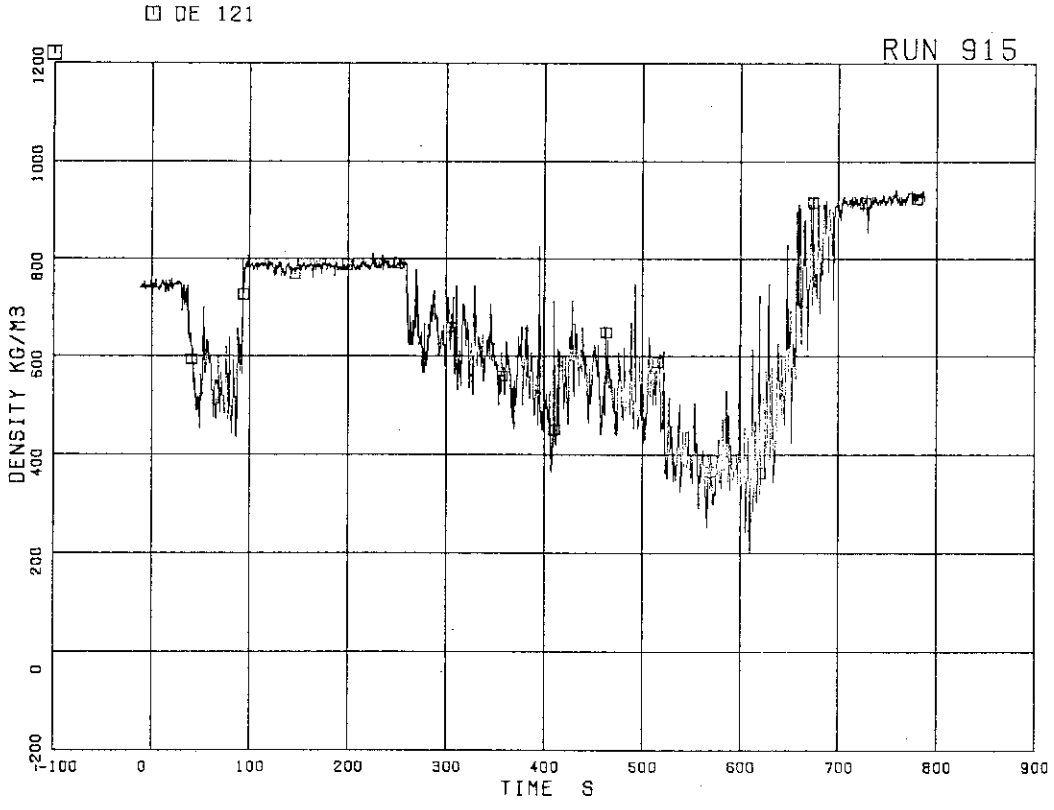

FIG.5. 40 FLUID DENSITY AT JP-1,2 OUTLET, BEAM B

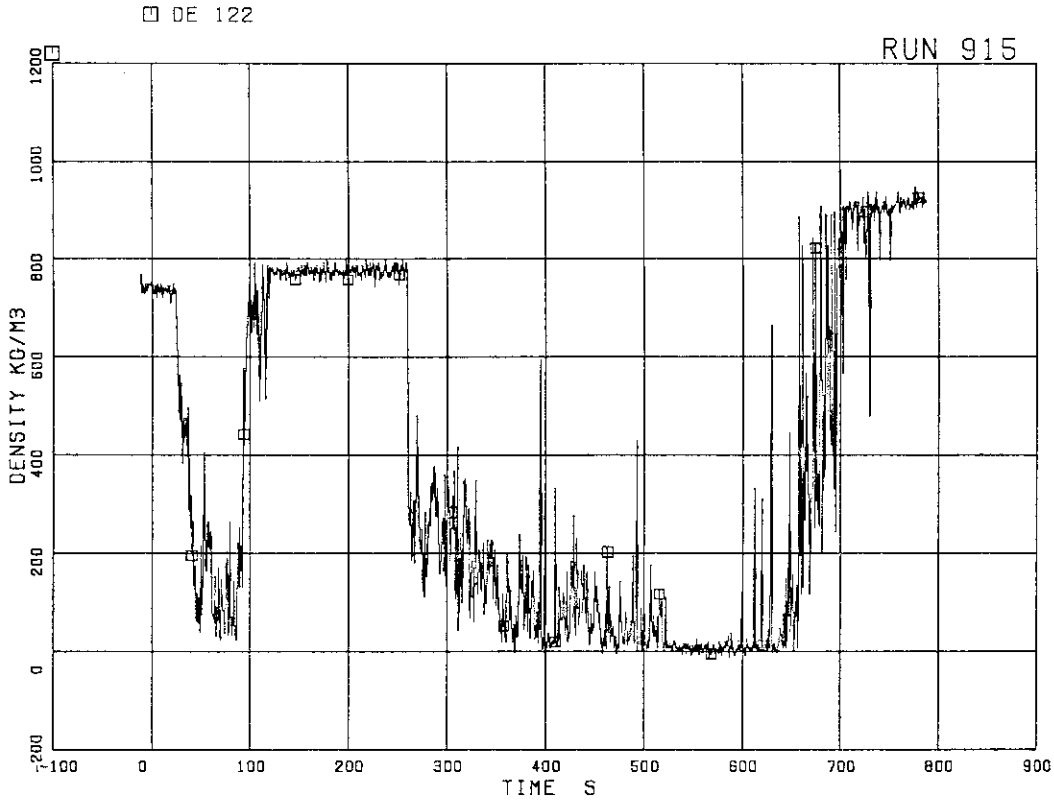

FIG.5. 41 FLUID DENSITY AT JP-1,2 OUTLET, BEAM C

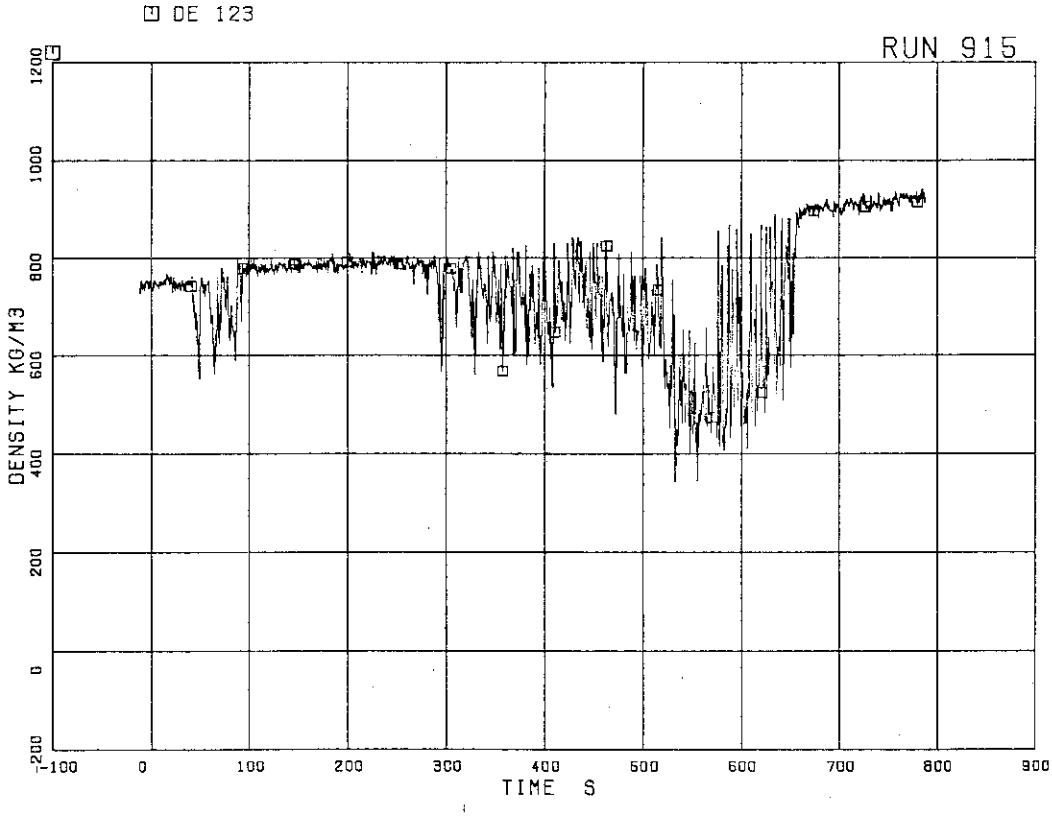

FIG.5. 42 FLUID DENSITY AT JP-3,4 OUTLET, BEAM A

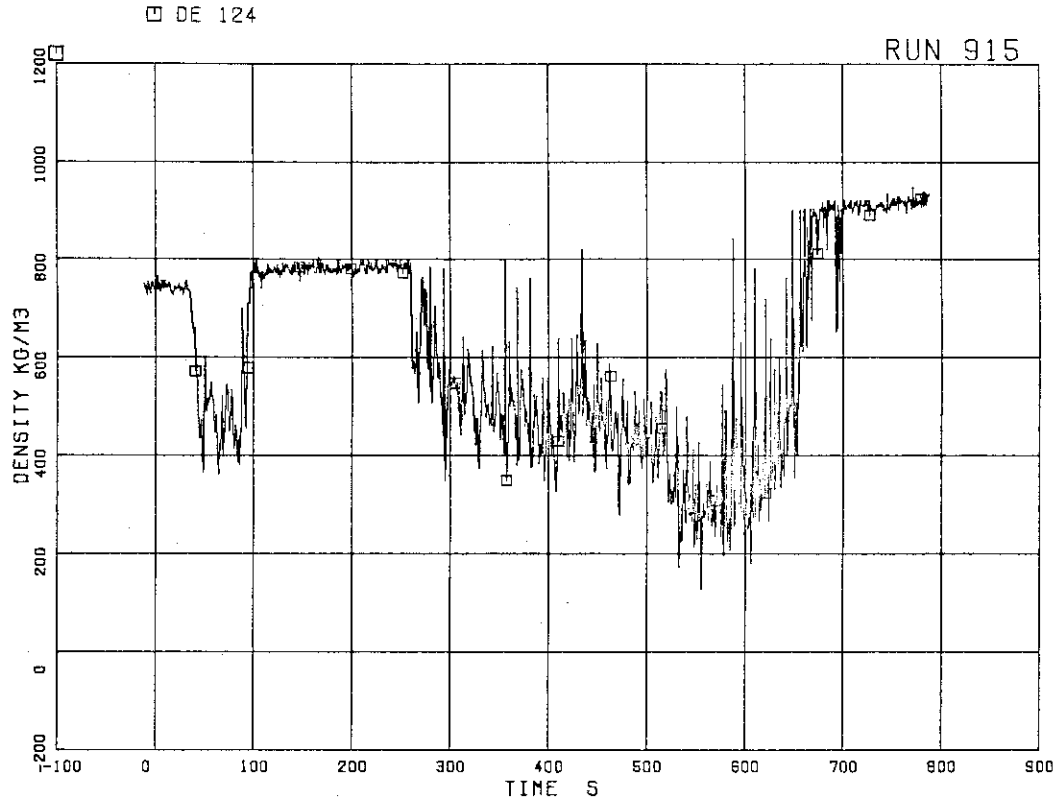

FIG.5. 43 FLUID DENSITY AT JP-3,4 OUTLET, BEAM B

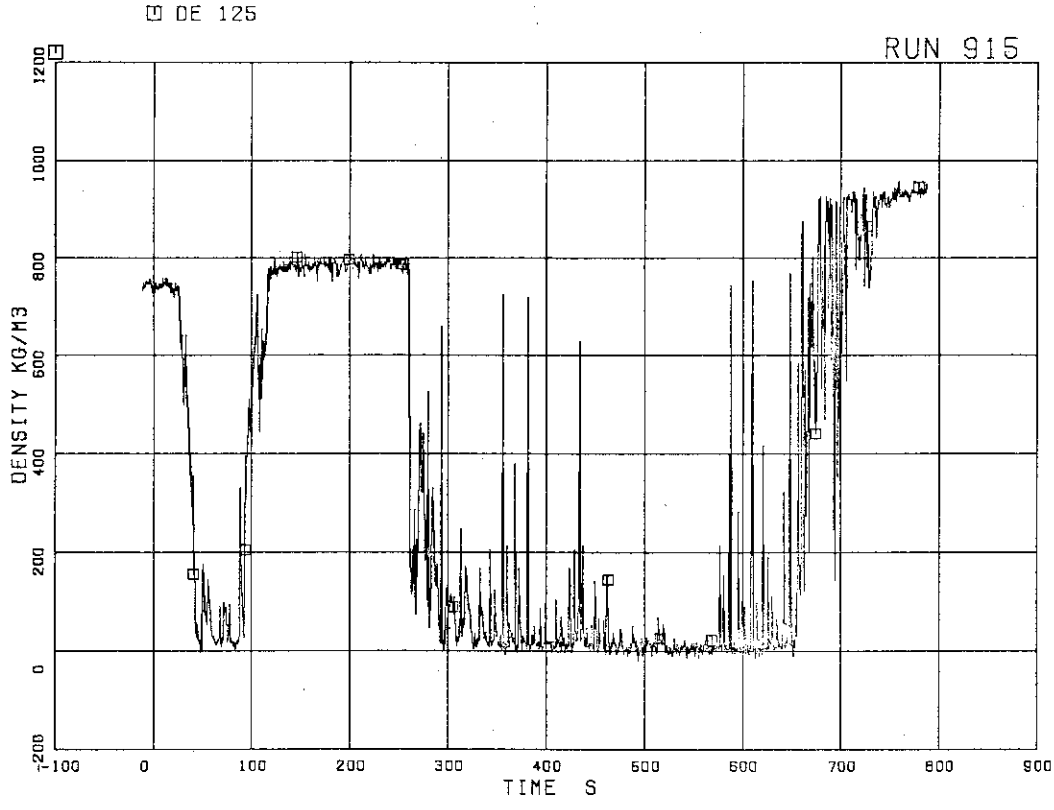

FIG.5. 44 FLUID DENSITY AT JP-3,4 OUTLET, BEAM C

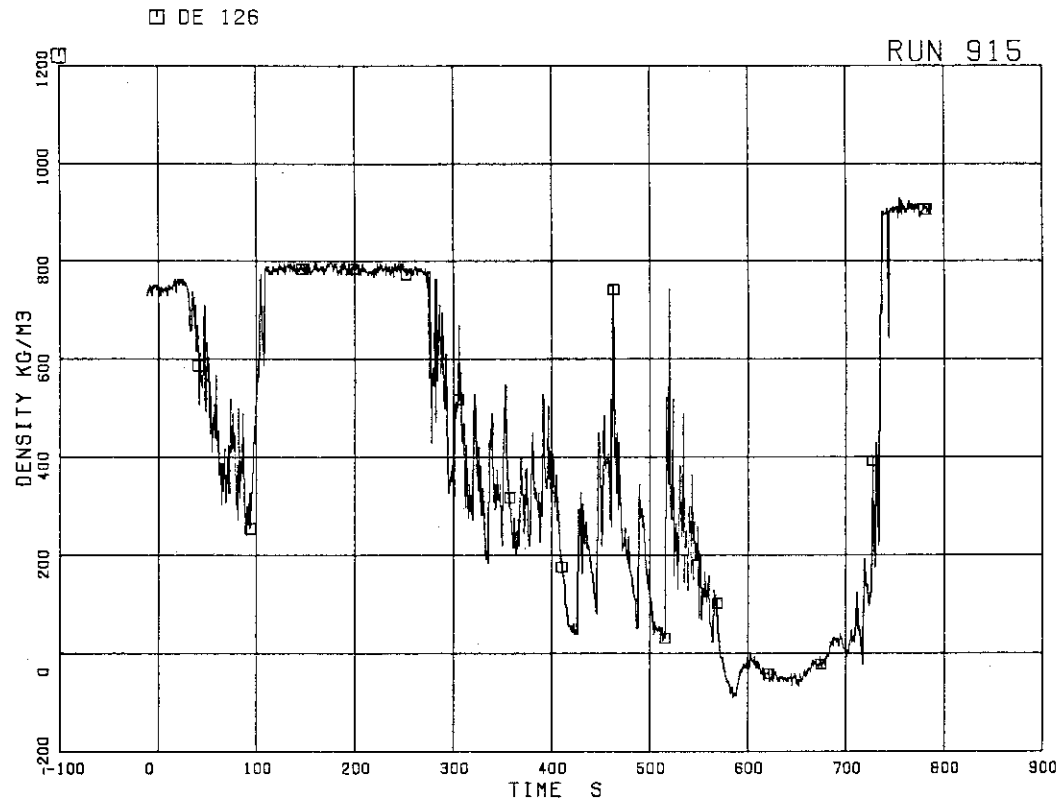

FIG.5. 45 FLUID DENSITY AT MRP SIDE OF BREAK, BEAM A

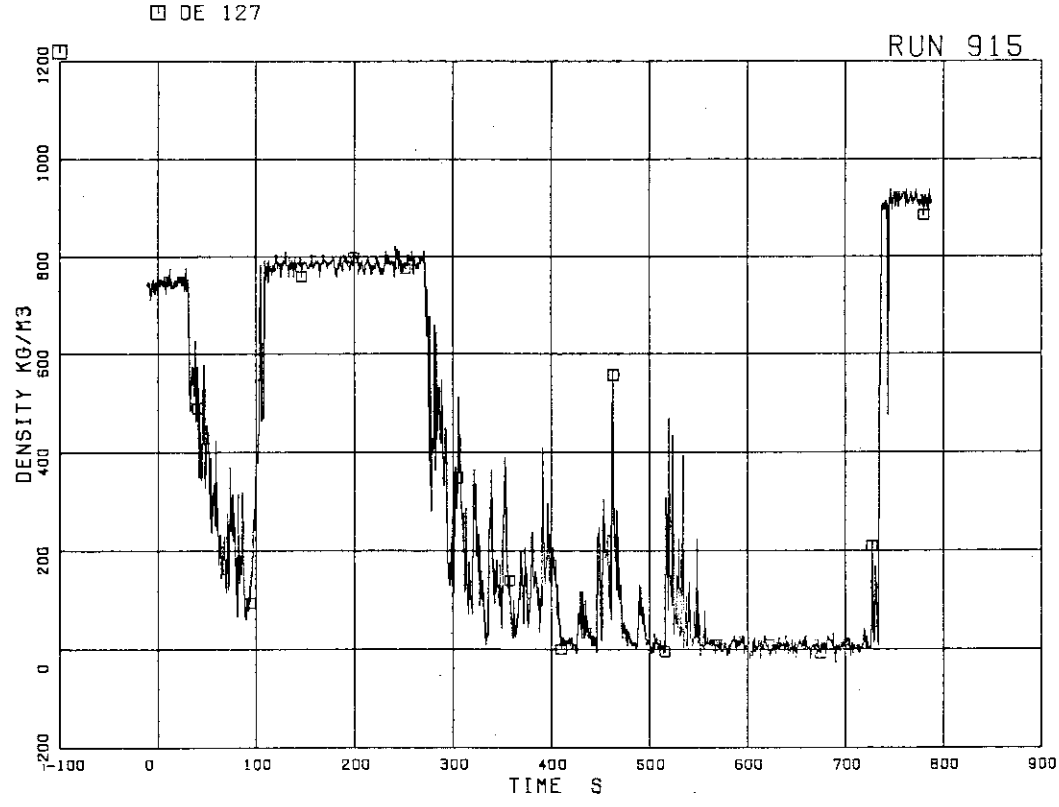

FIG.5. 46 FLUID DENSITY AT MRP SIDE OF BREAK, BEAM B

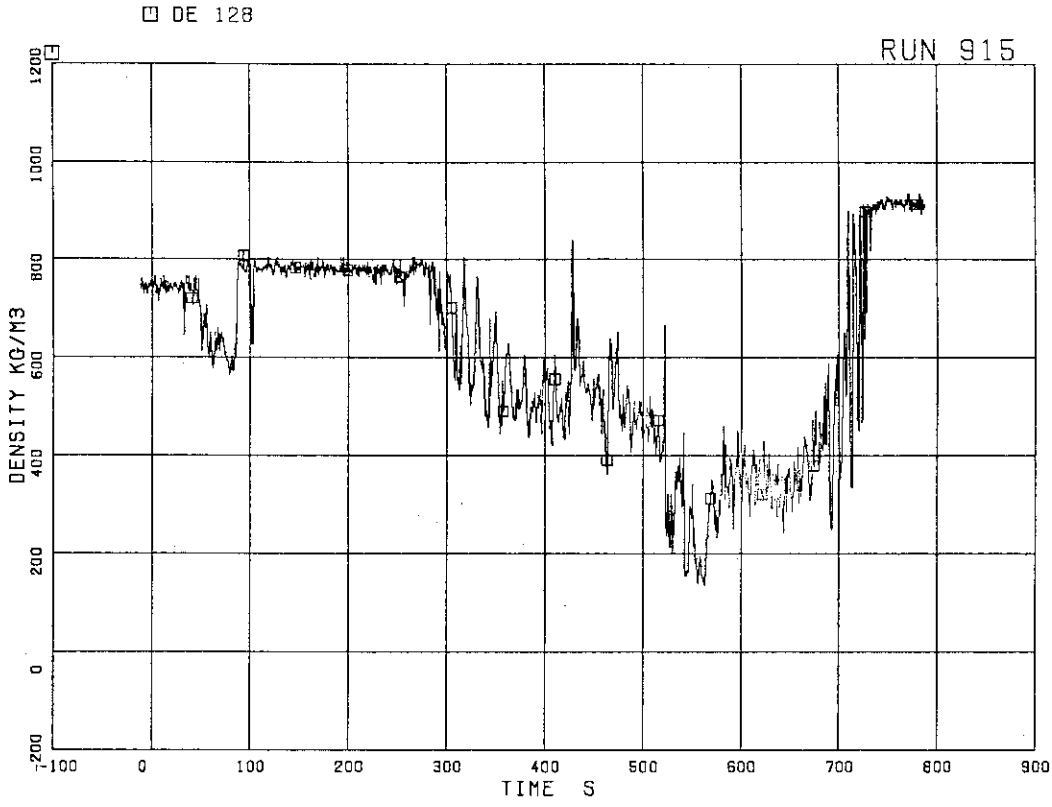

FIG.5. 47 FLUID DENSITY AT PV SIDE OF BREAK, BEAM A

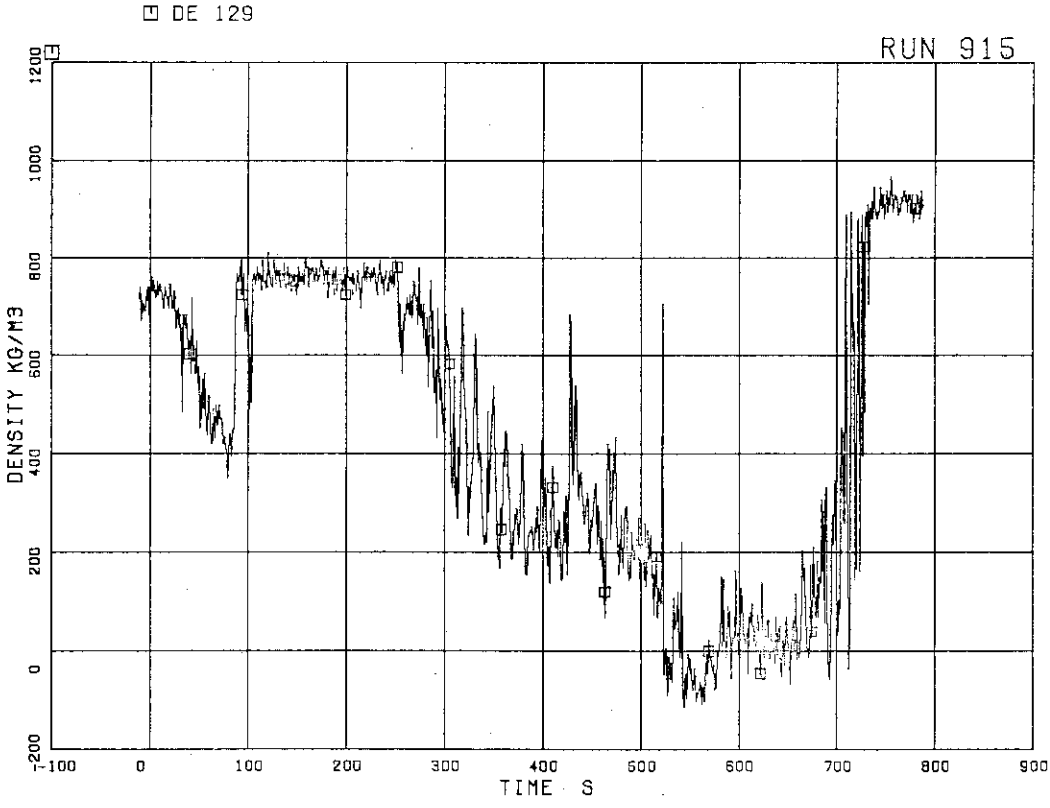

FIG.5. 48 FLUID DENSITY AT PV SIDE OF BREAK, BEAM B

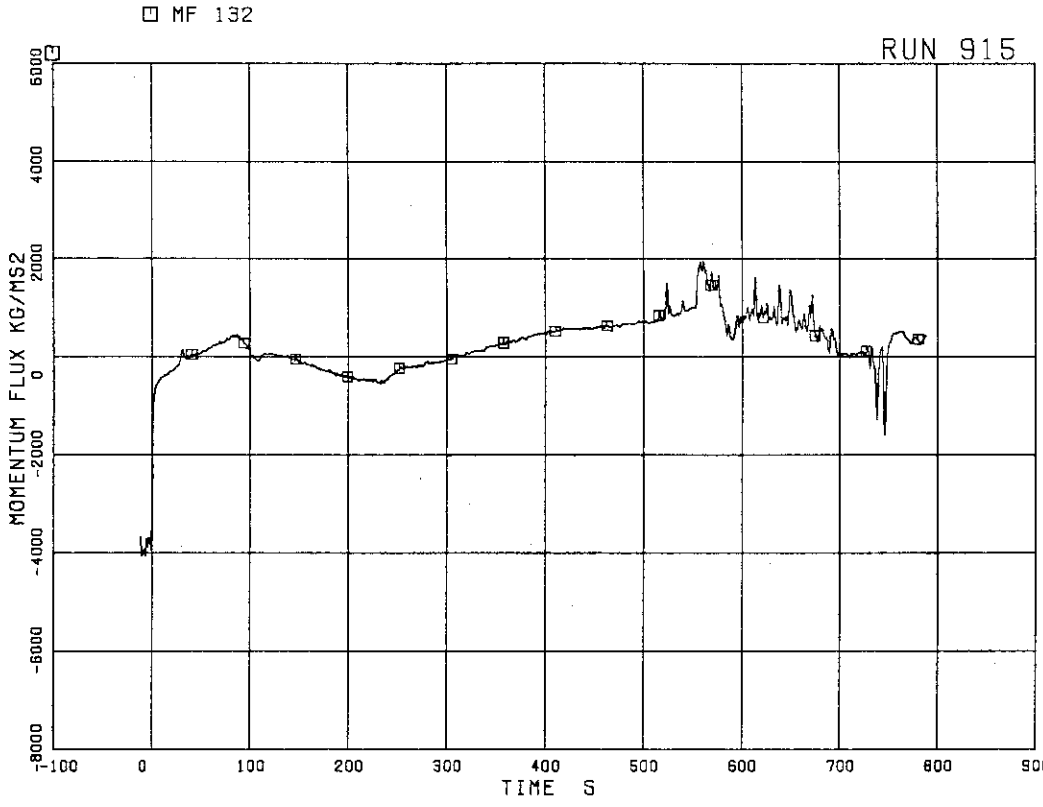

FIG.5. 49 MOMENTUM FLUX AT BREAK A SPOOL PIECE (LOW RANGE)

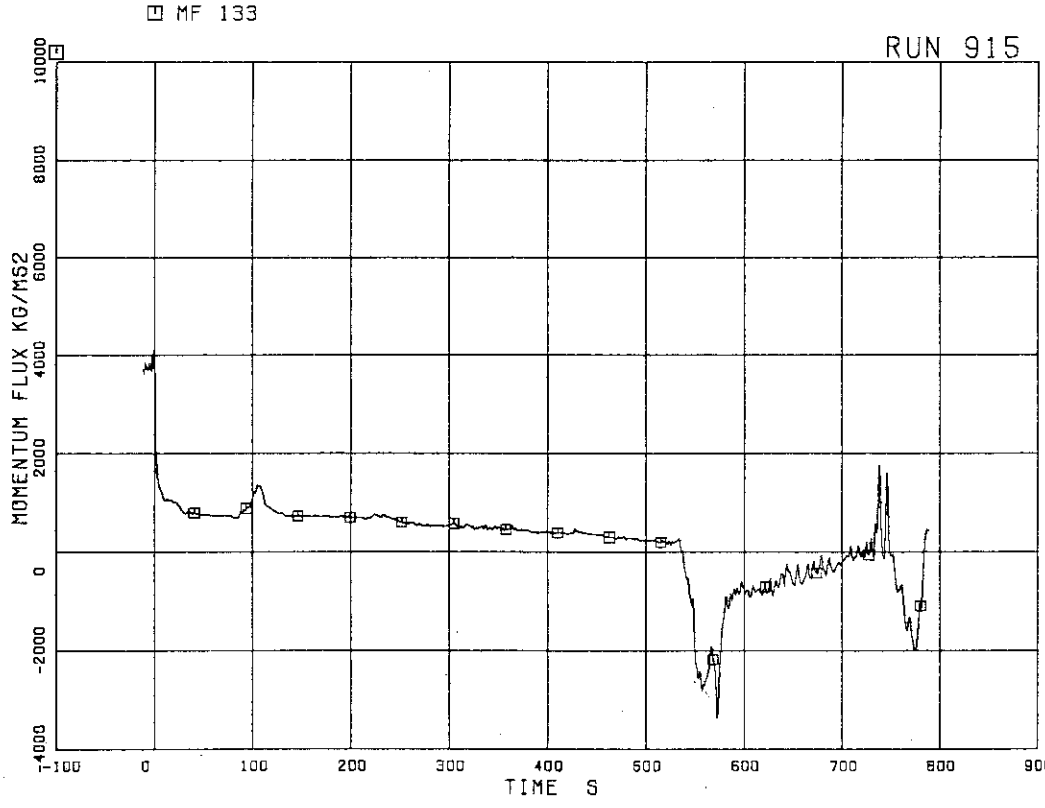

FIG.5. 50 MOMENTUM FLUX AT BREAK B SPOOL PIECE (LOW RANGE)

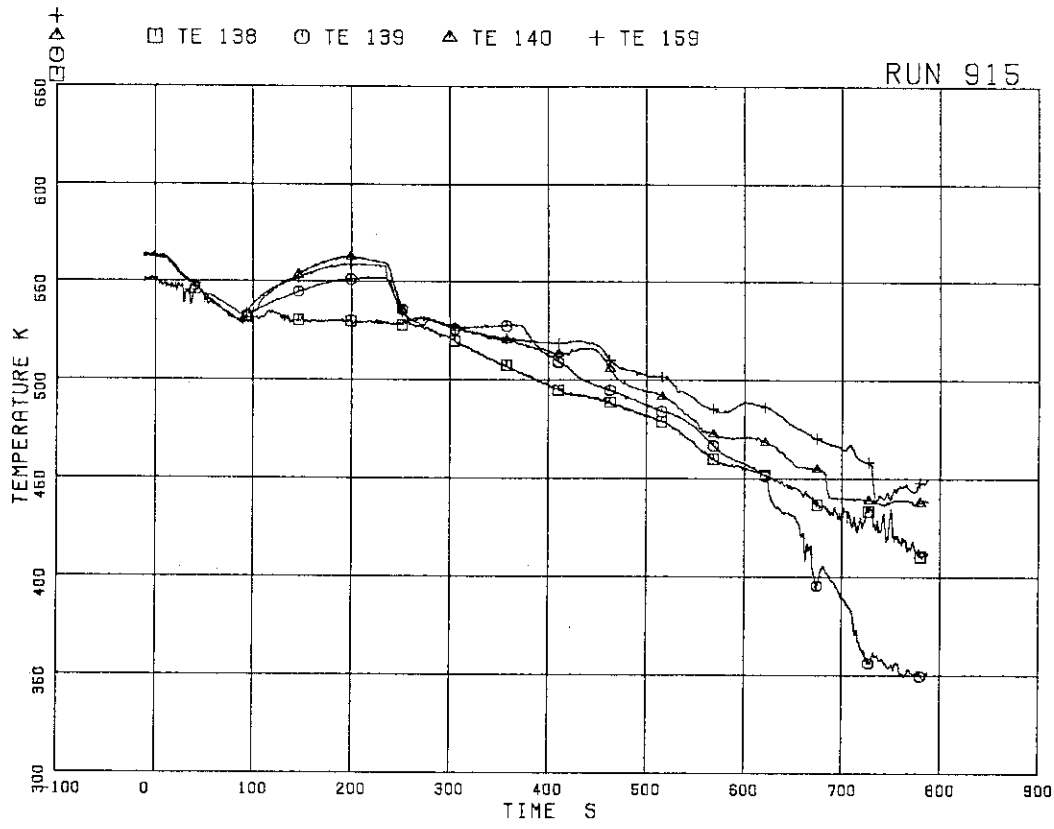

FIG.5. 51 FLUID TEMPERATURES IN PV AND MSL

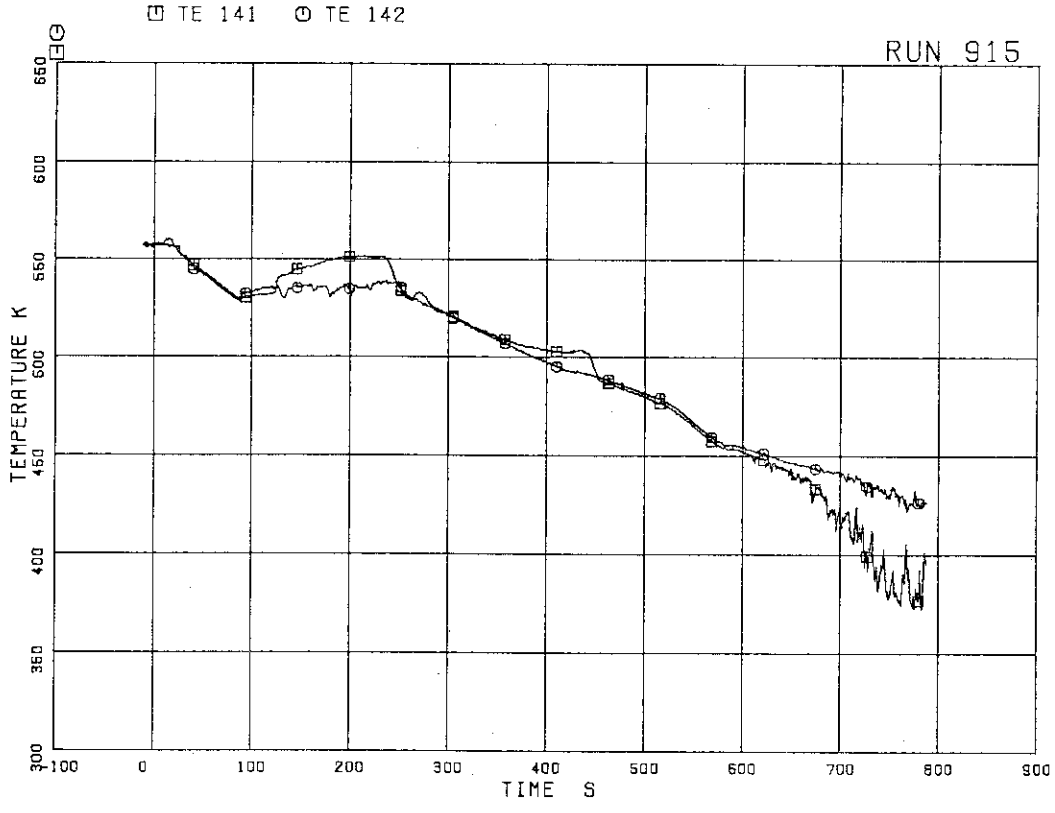

FIG.5. 52 FLUID TEMPERATURES IN DOWNCOMER

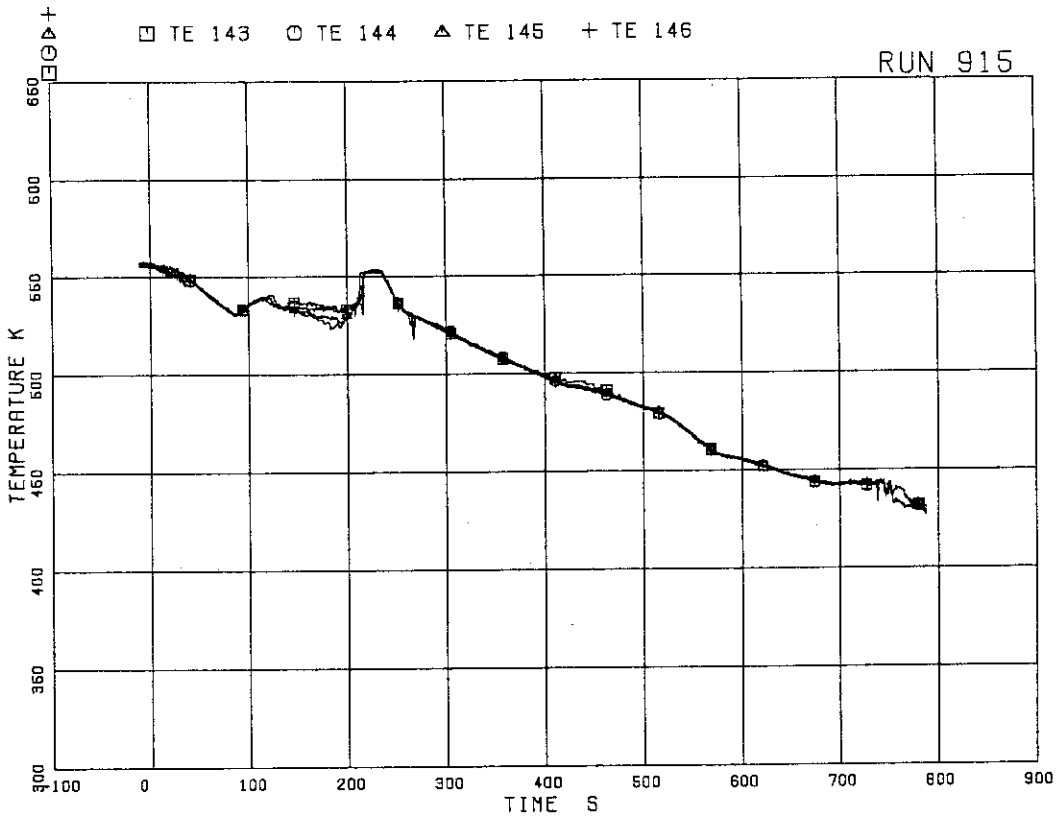

FIG.5. 53 FLUID TEMPERATURES AT JP DRIVE LINES (JP 1,2,3 AND 4)

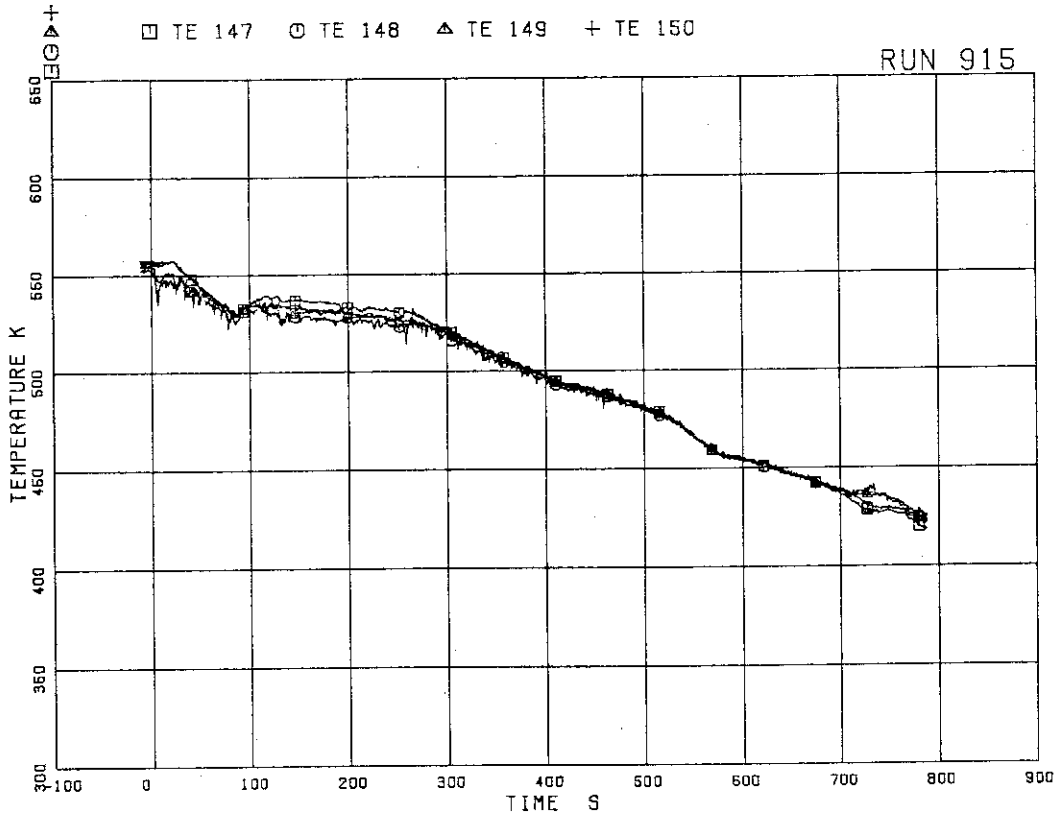

FIG.5. 54 FLUID TEMPERATURES AT JP DISCHARGE LINES (JP 1,2,3 AND 4)

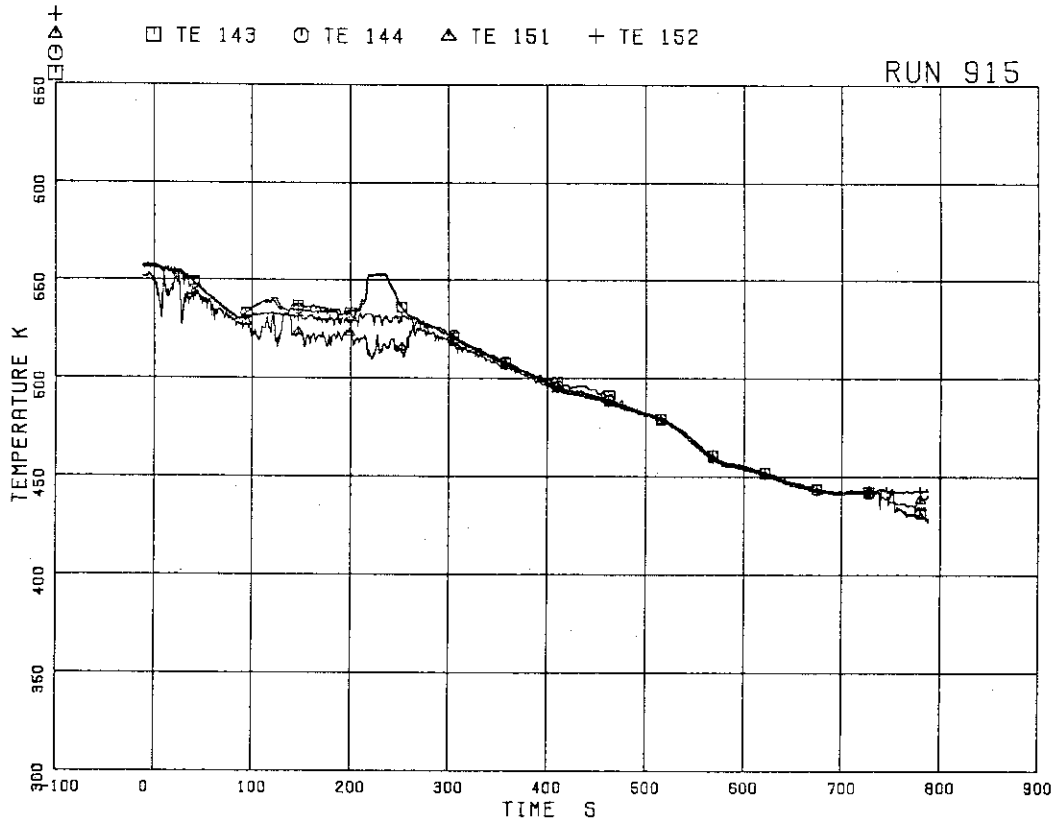

FIG.5. 55 FLUID TEMPERATURES IN INTACT RECIRCULATION LOOP

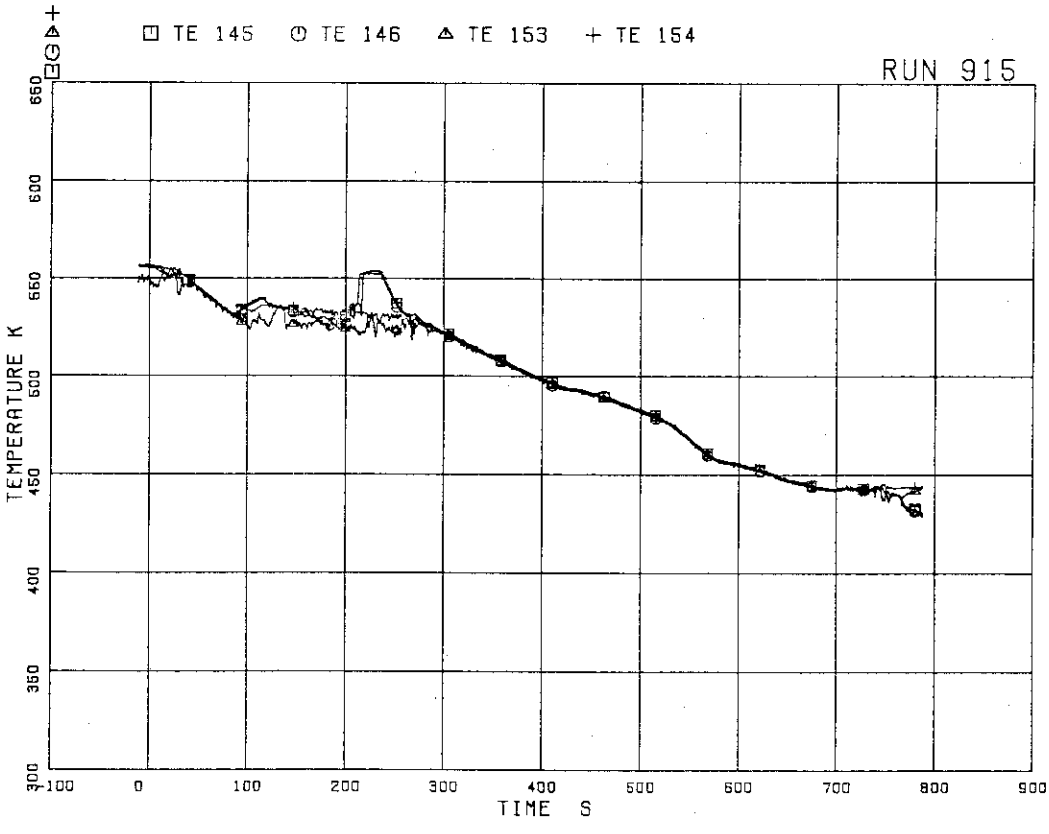

FIG.5. 56 FLUID TEMPERATURES IN BROKEN RECIRCULATION LOOP

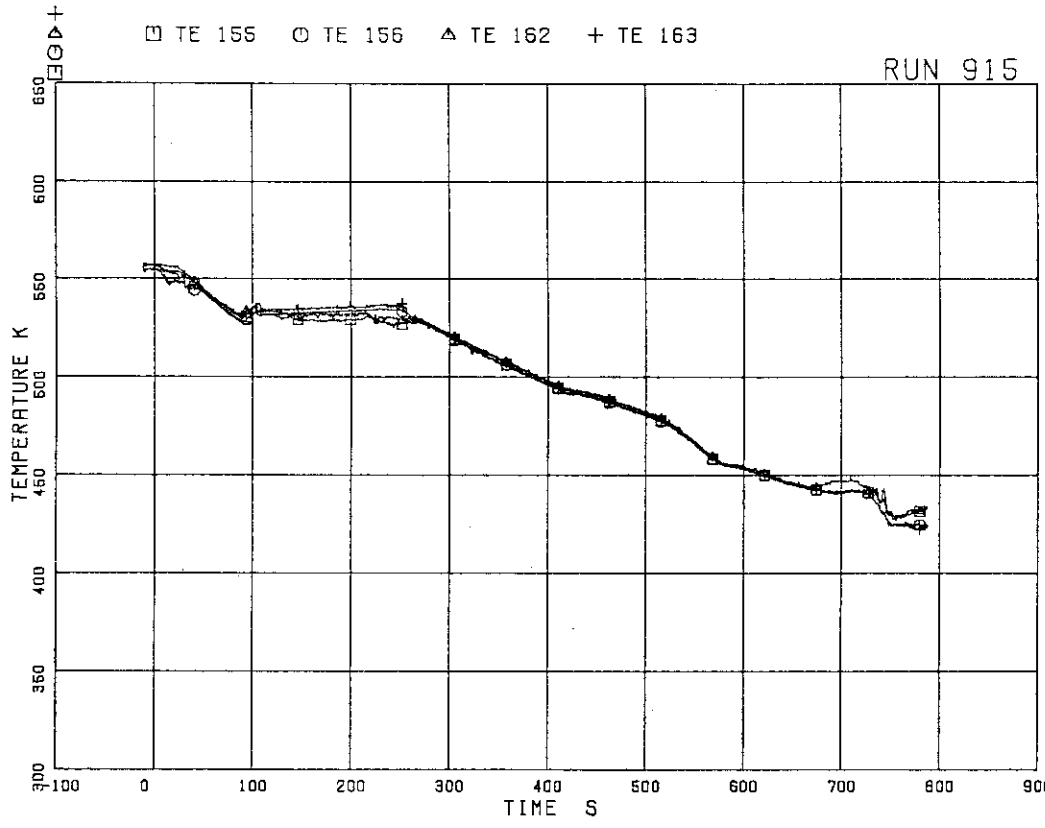

FIG.5. 57 FLUID TEMPERATURES NEAR BREAKS A AND B

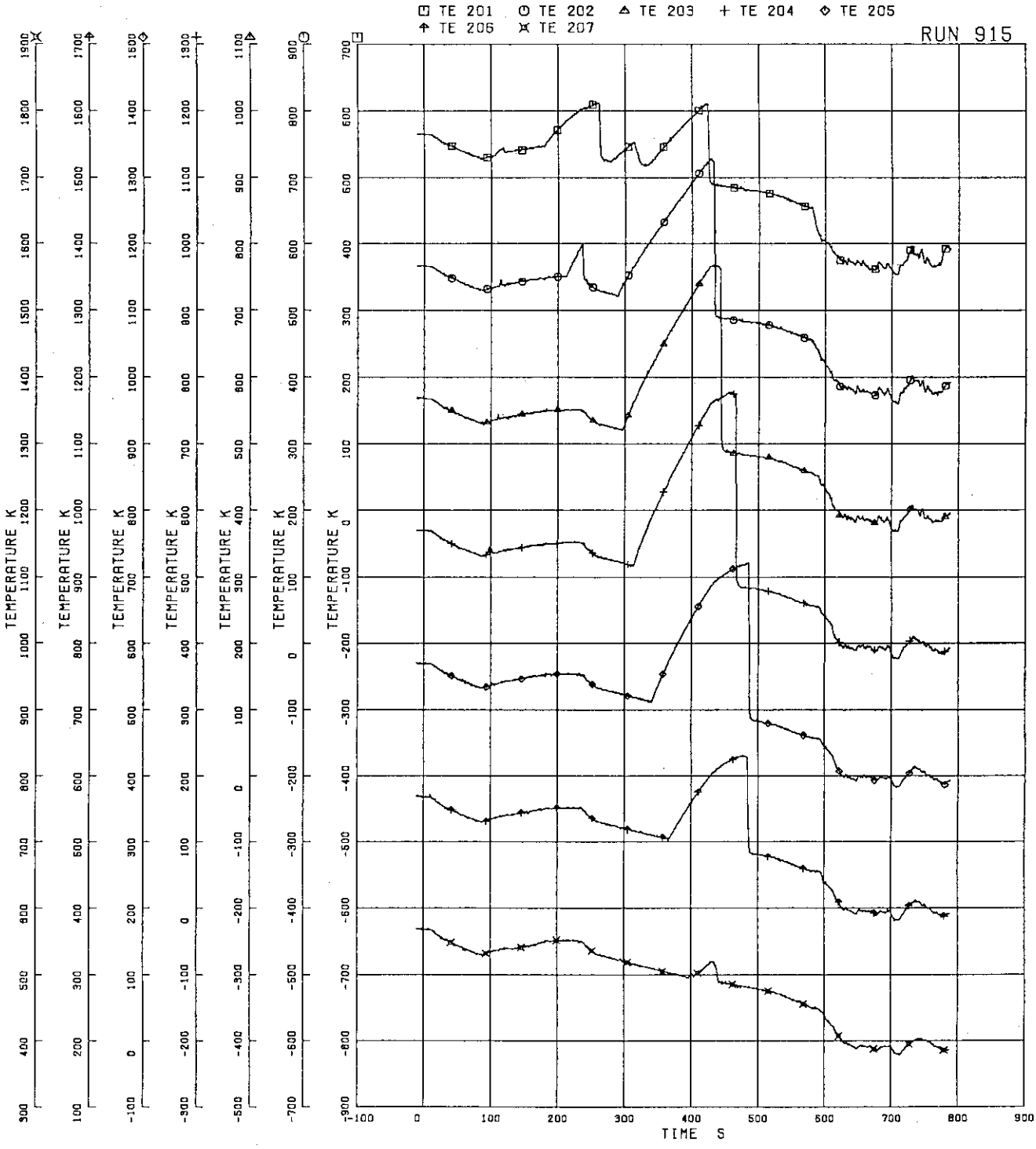

FIG.5. 58 SURFACE TEMPERATURES OF FUEL ROD A11

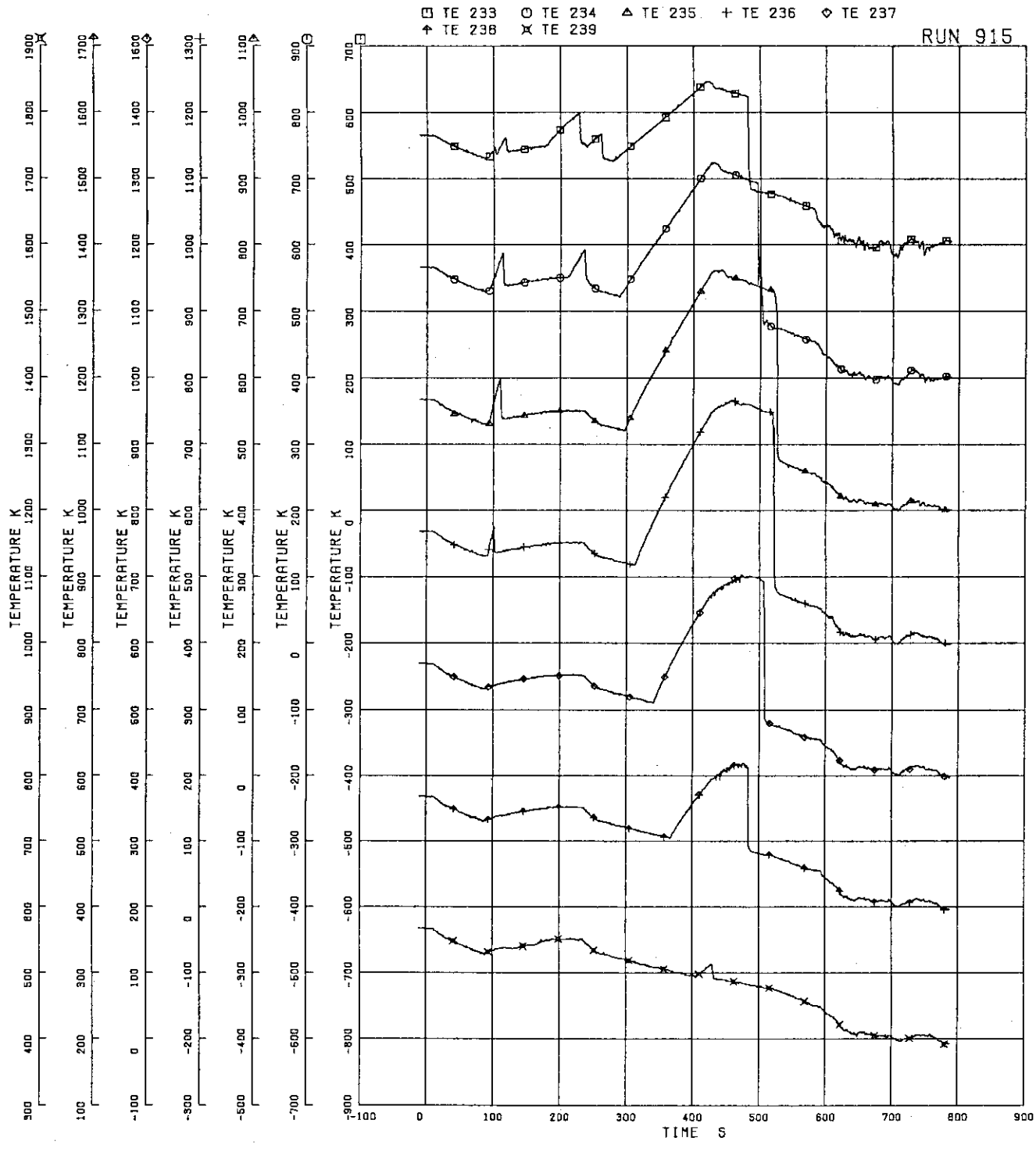

FIG.5. 59 SURFACE TEMPERATURES OF FUEL ROD A22

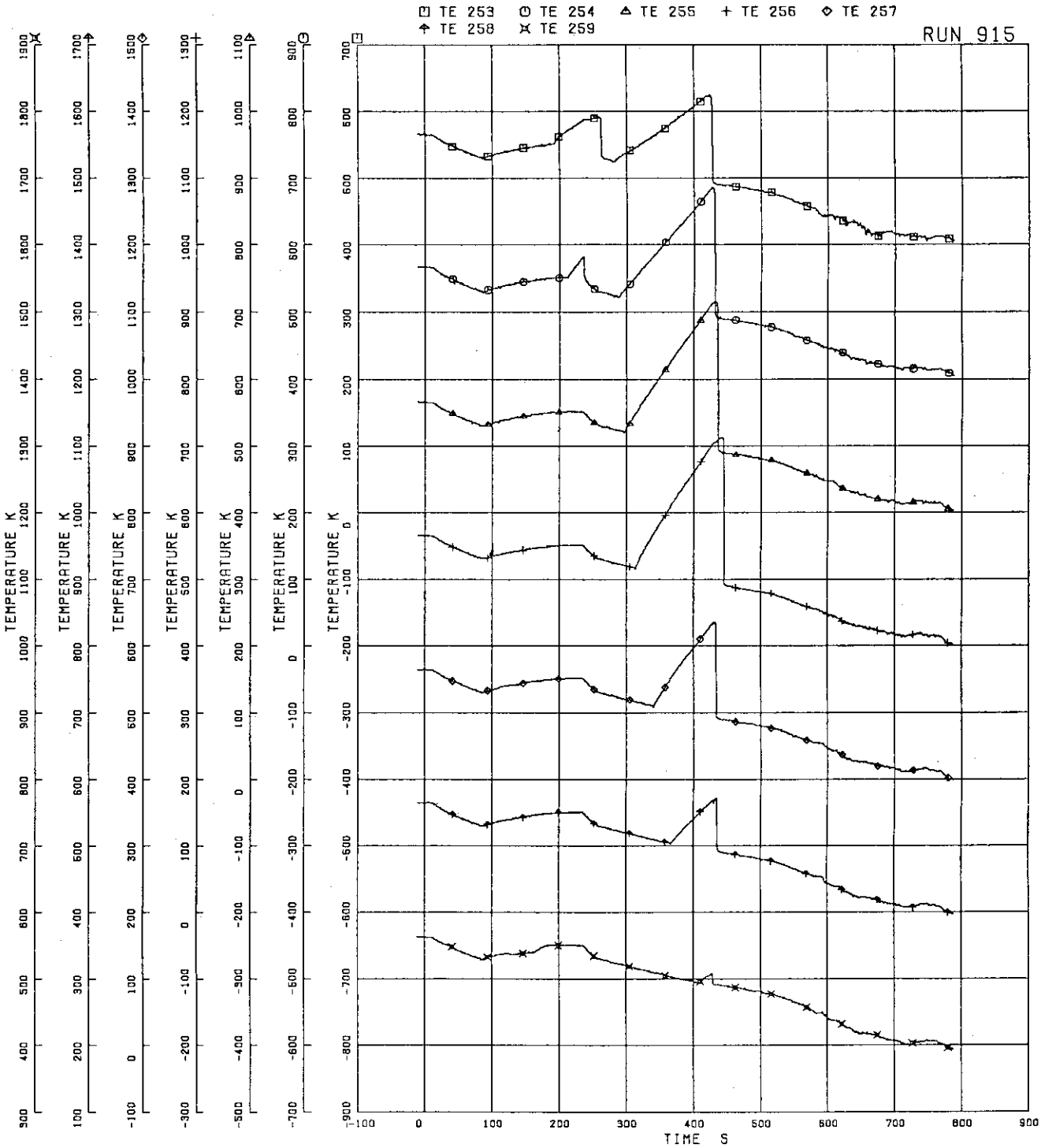

FIG.5. 60 SURFACE TEMPERATURES OF FUEL ROD A33

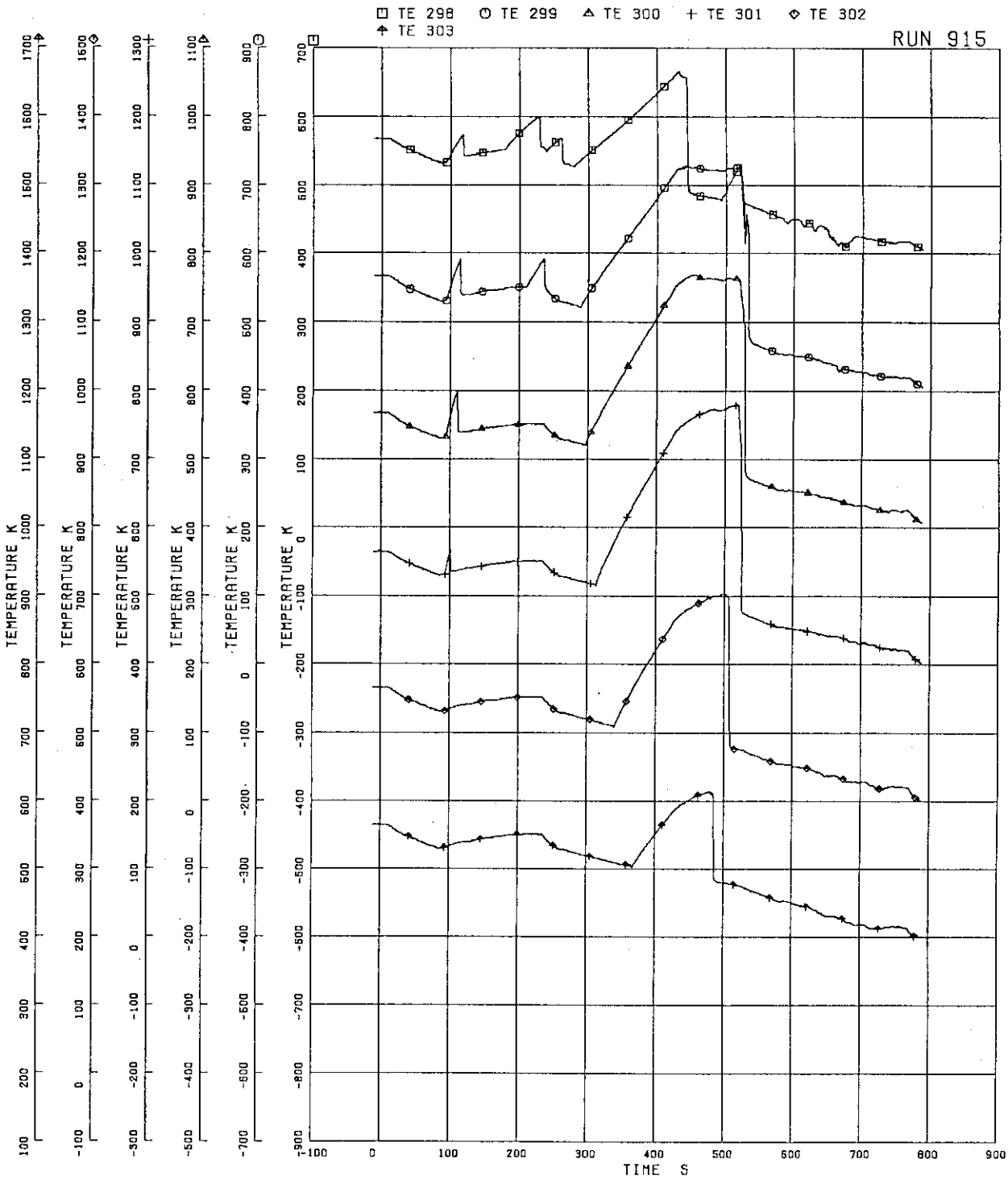

FIG.5. 61 SURFACE TEMPERATURES OF FUEL ROD A77

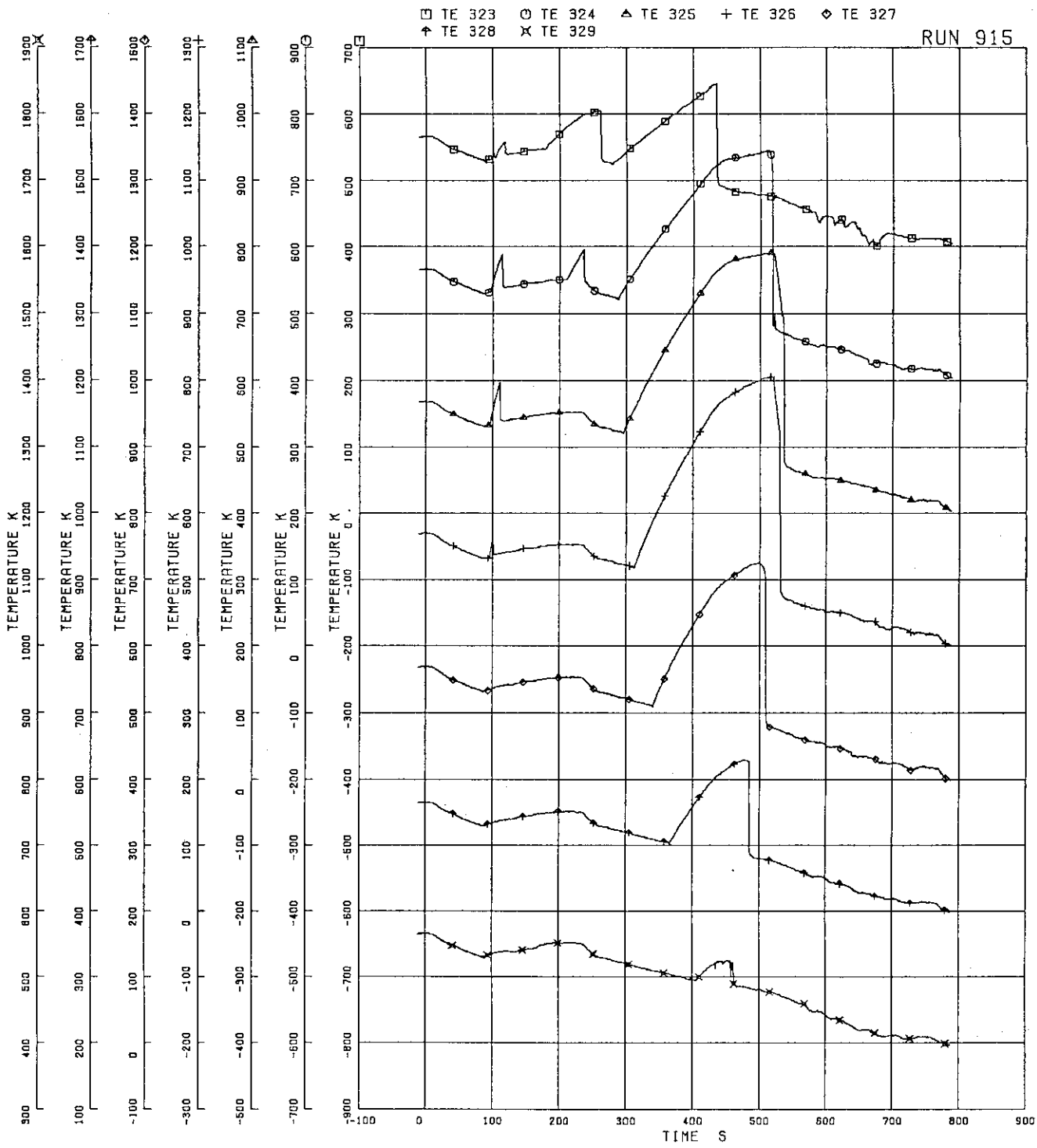

FIG.5. 62 SURFACE TEMPERATURES OF FUEL ROD A88

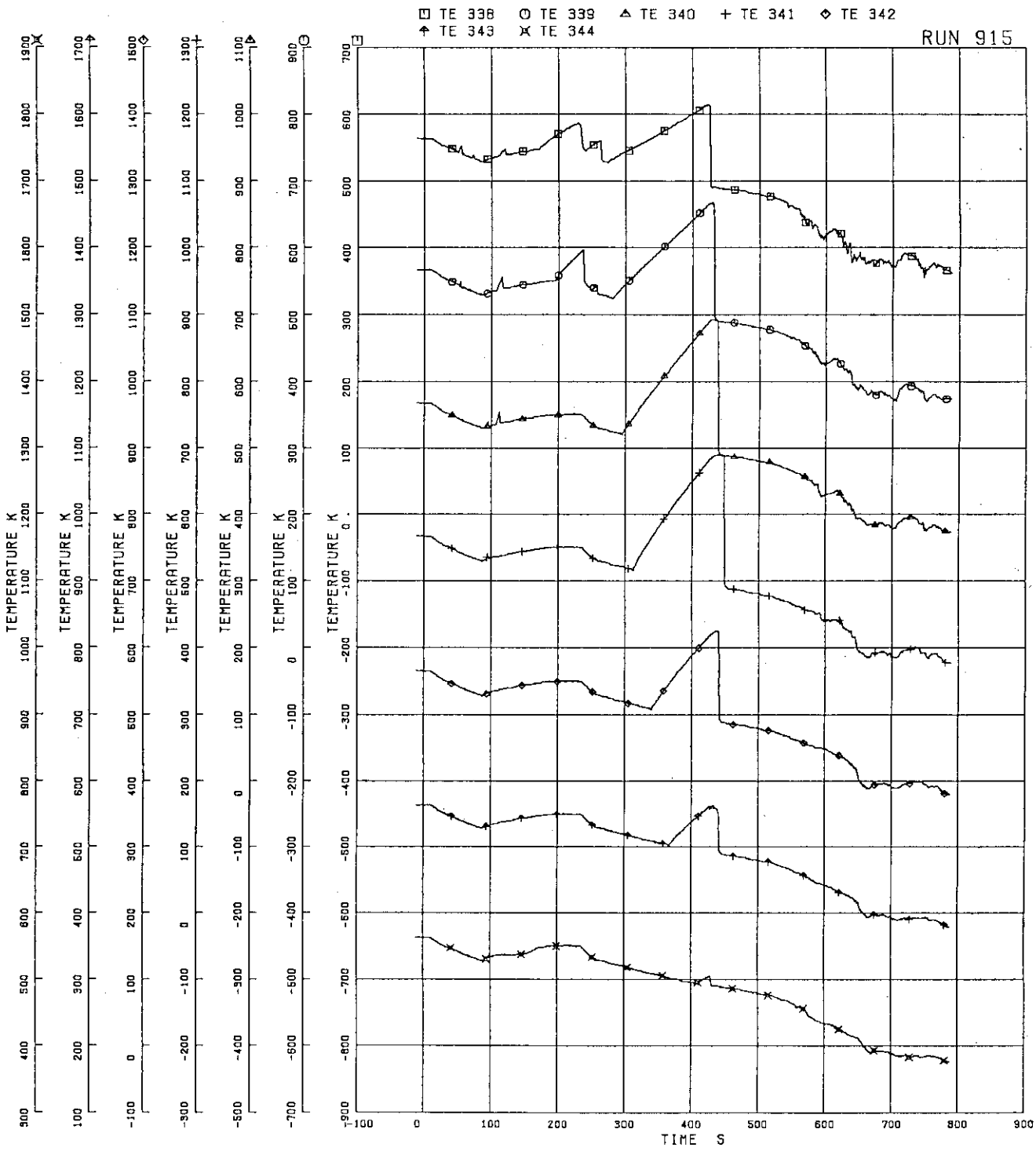

FIG.5. 63 SURFACE TEMPERATURES OF FUEL ROD B22

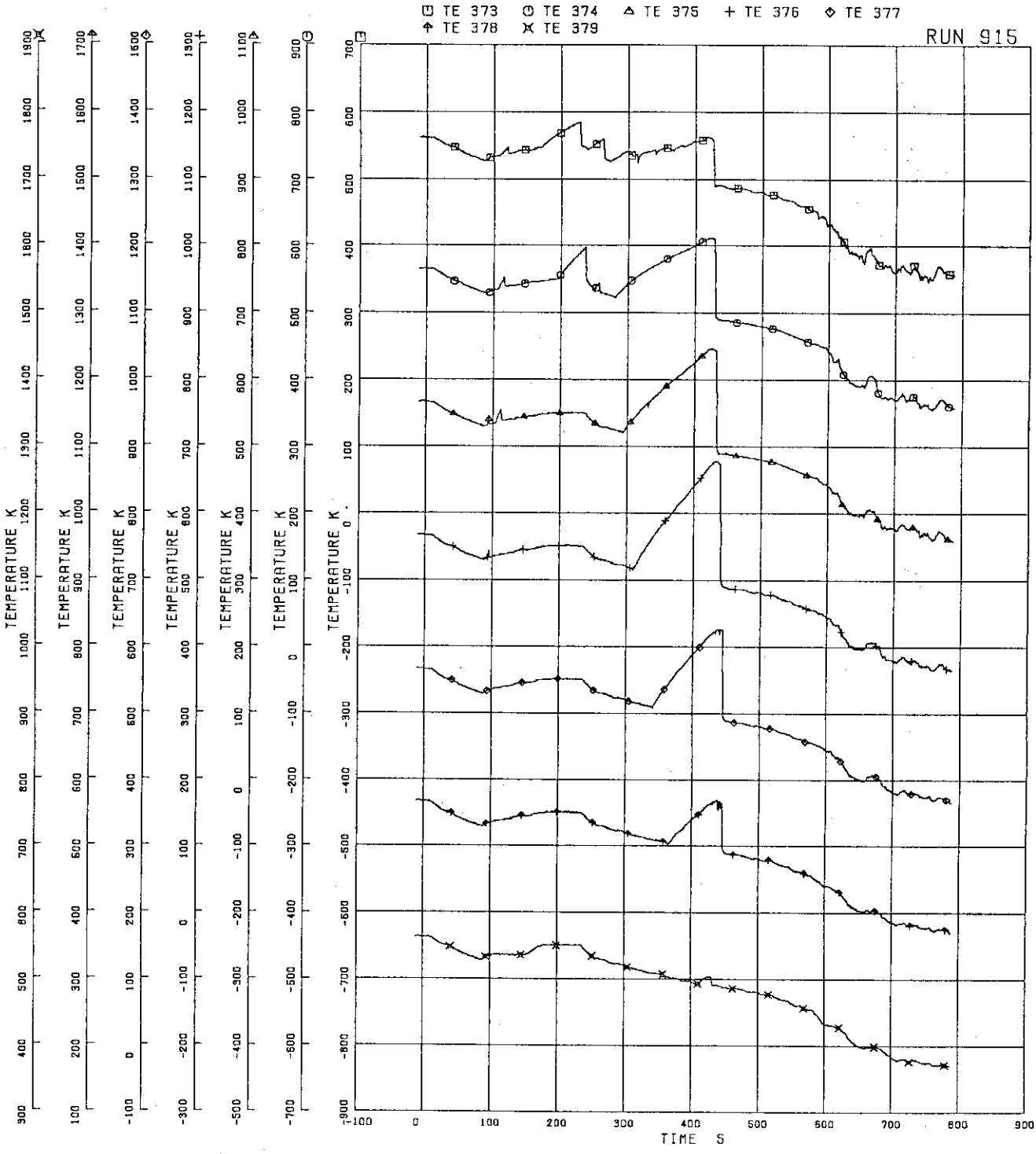

FIG.5. 64 SURFACE TEMPERATURES OF FUEL ROD C22

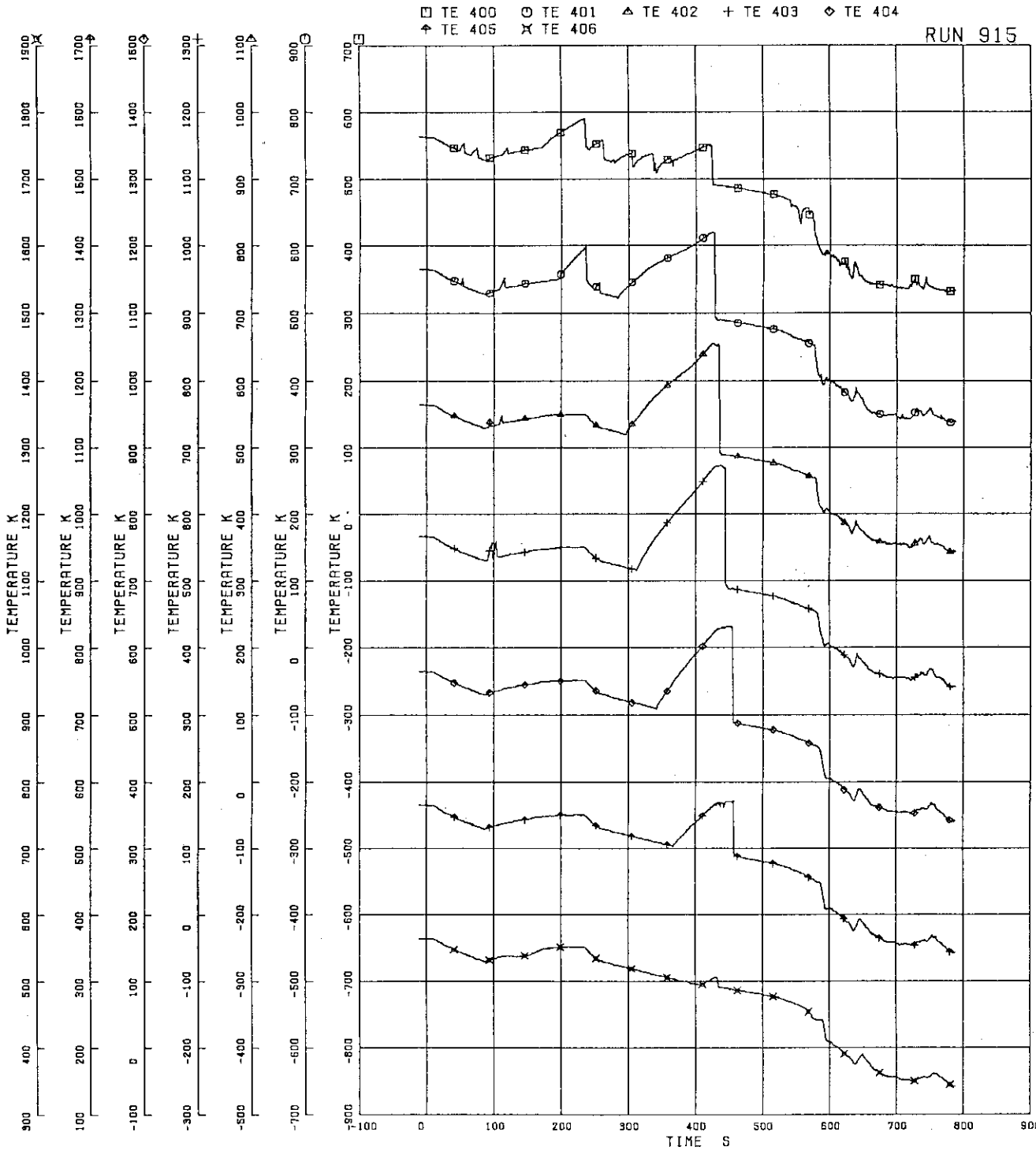

FIG.5. 65 SURFACE TEMPERATURES OF FUEL ROD D22

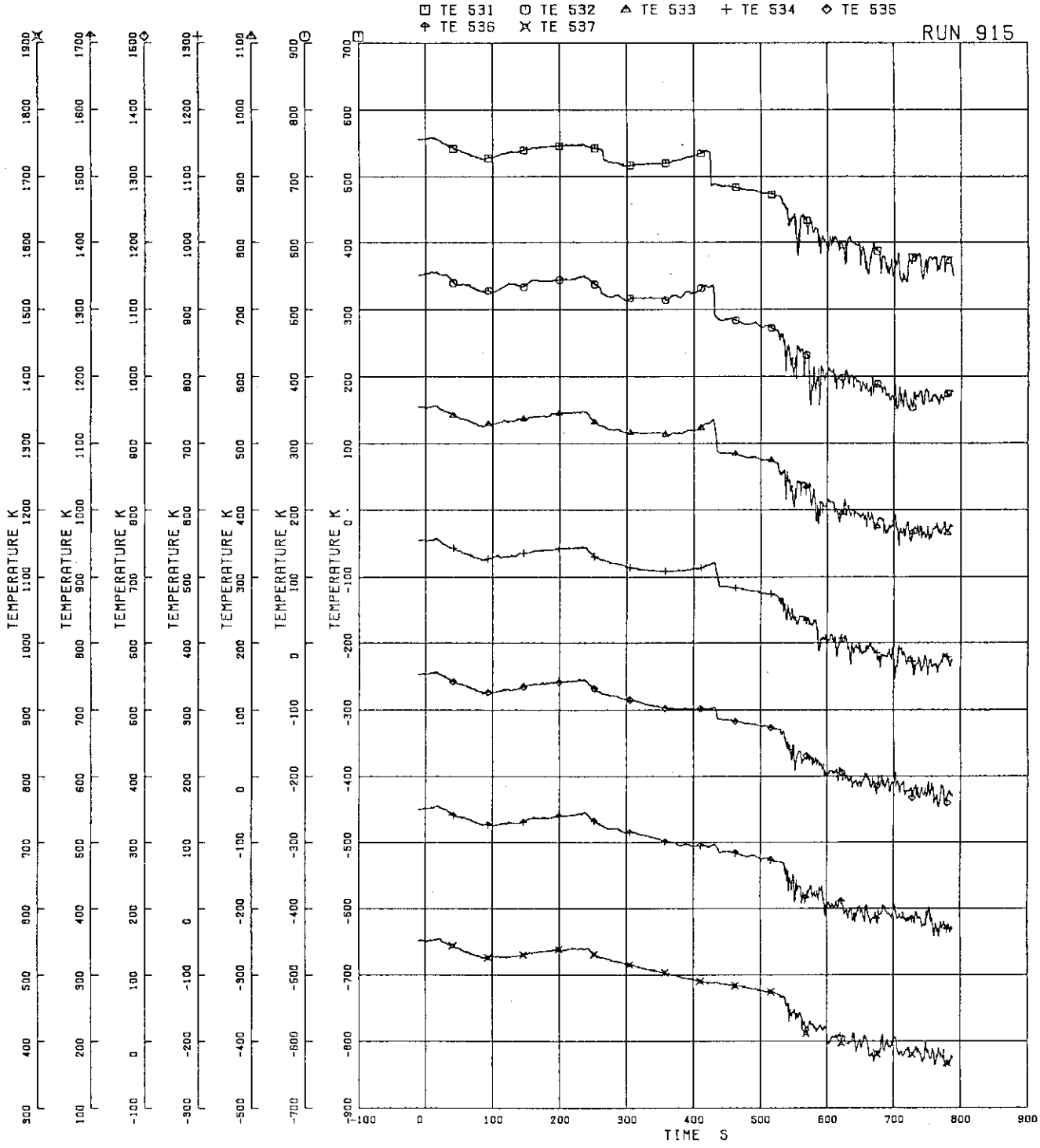

FIG.5. 66 OUTER SURFACE TEMPERATURES OF CHANNEL BOX A

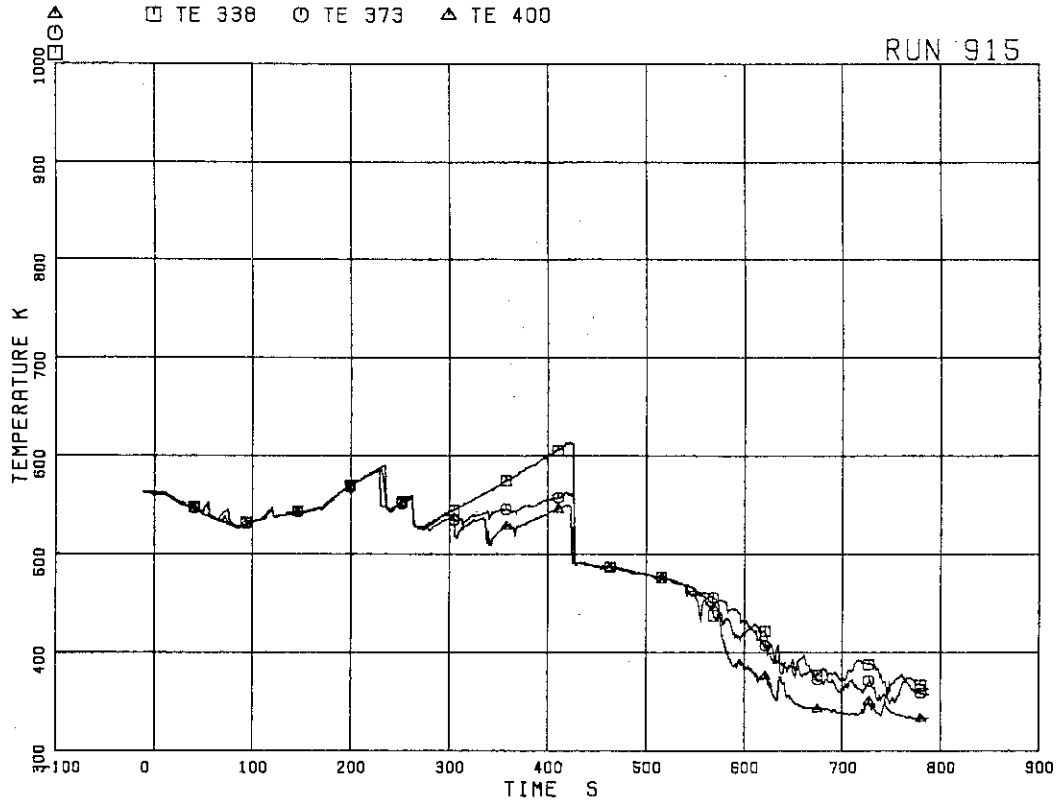

FIG.5. 67 SURFACE TEMPERATURES OF FUEL RODS B22,C22,D22 AT POSITION 1

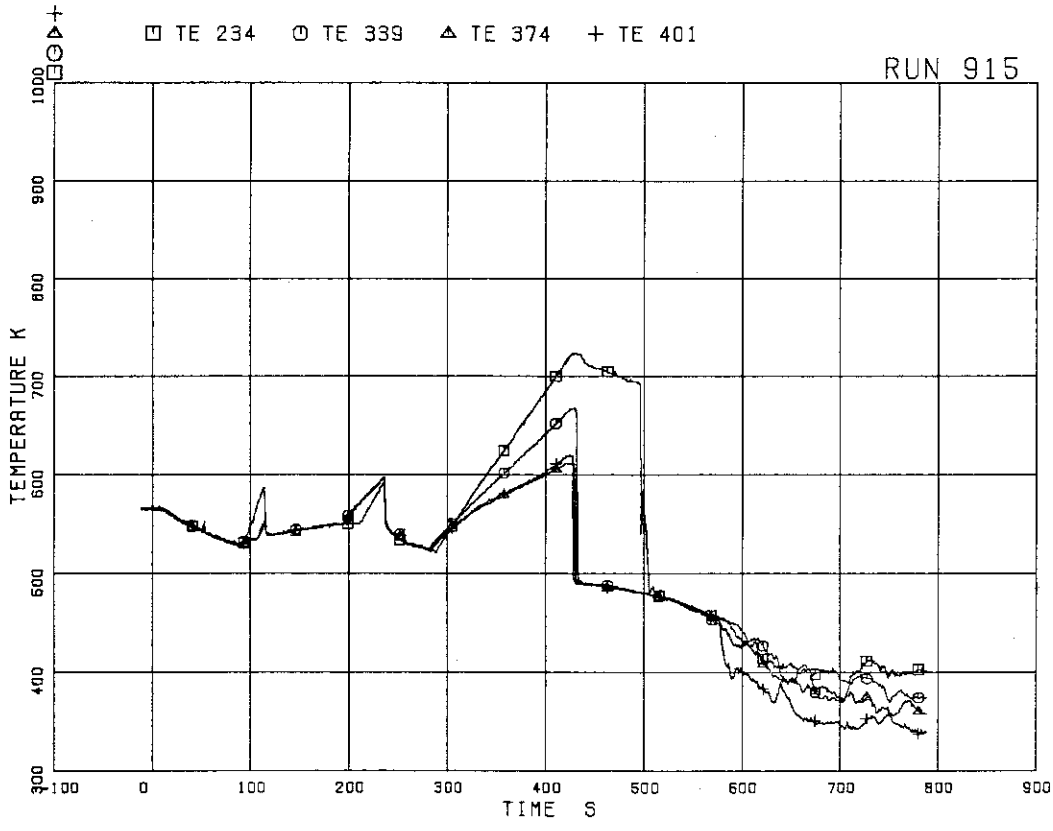

FIG.5. 68 SURFACE TEMPERATURES OF FUEL RODS A22,B22,C22,D22 AT POSITION 2

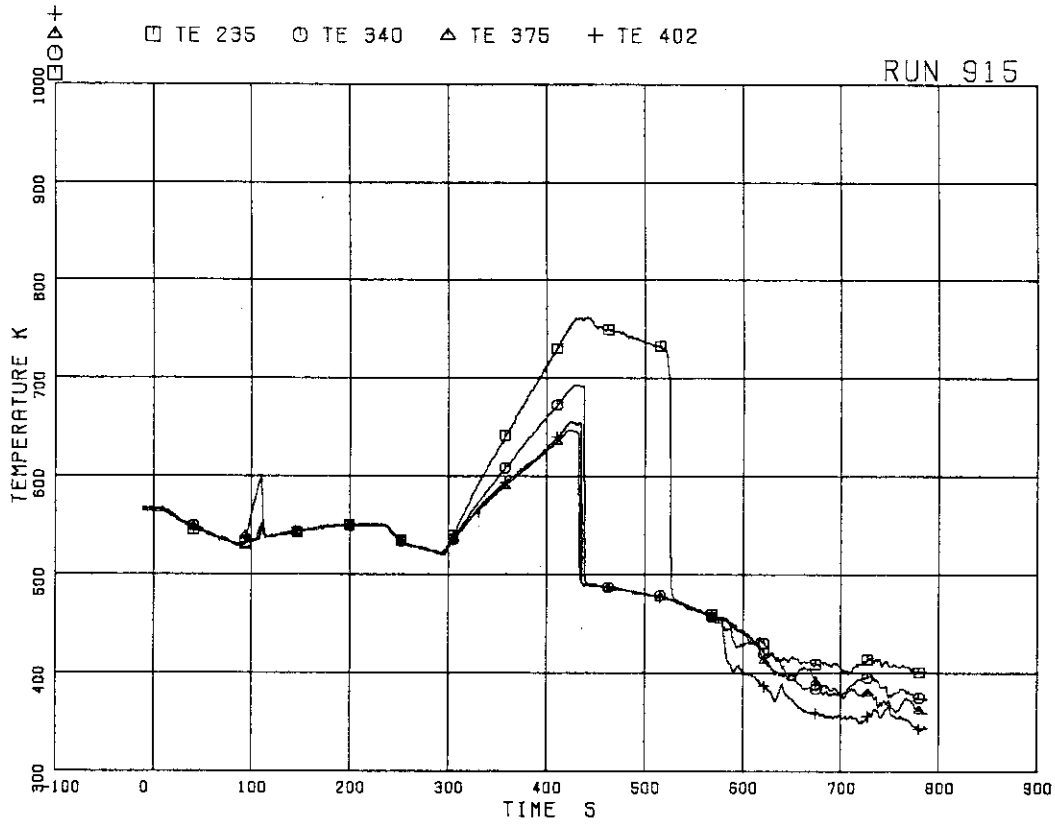

FIG.5. 69 SURFACE TEMPERATURES OF FUEL RODS A22,B22,C22,D22 AT POSITION 3

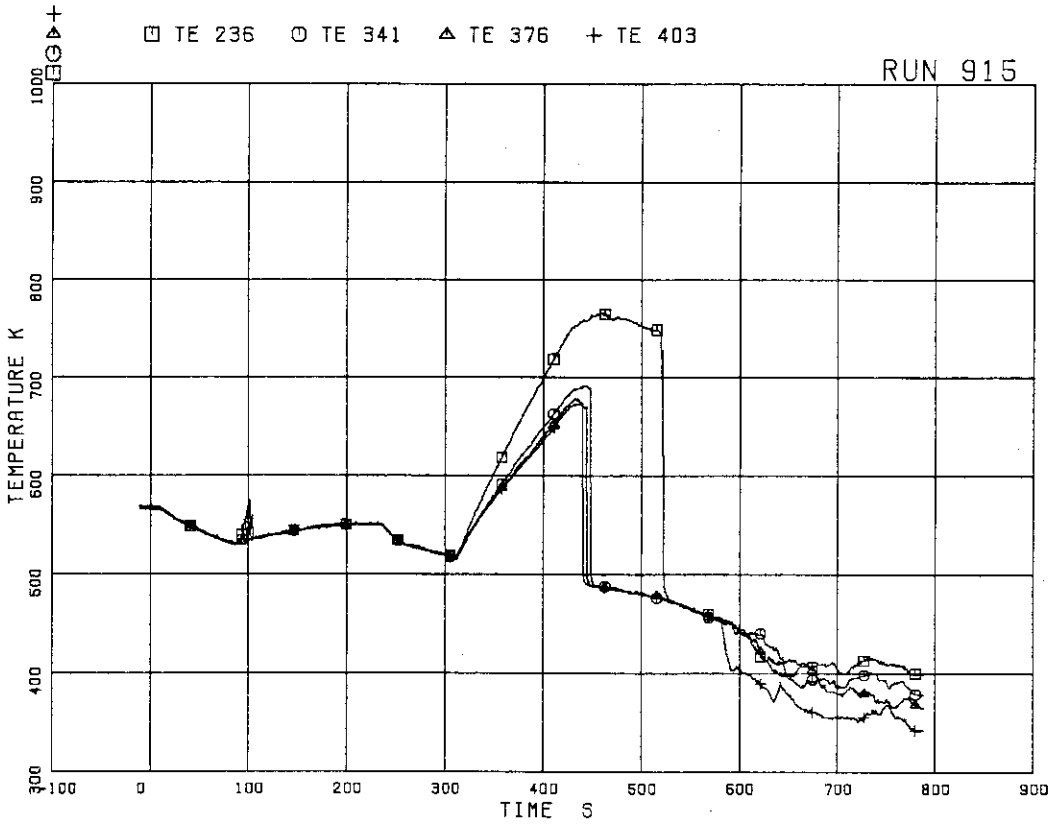

FIG.5. 70 SURFACE TEMPERATURES OF FUEL RODS A22,B22,C22,D22 RODS AT POSITION 4

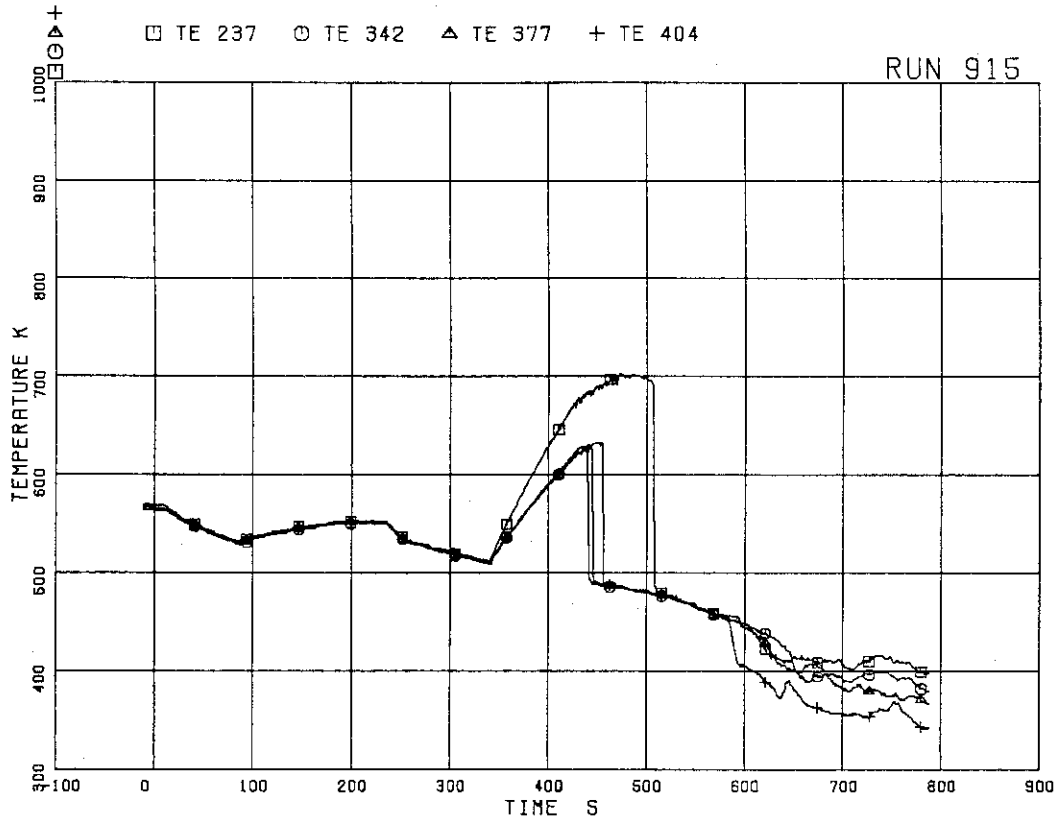

FIG.5. 71 SURFACE TEMPERATURES OF FUEL RODS A22,B22,C22,D22 AT POSITION 5

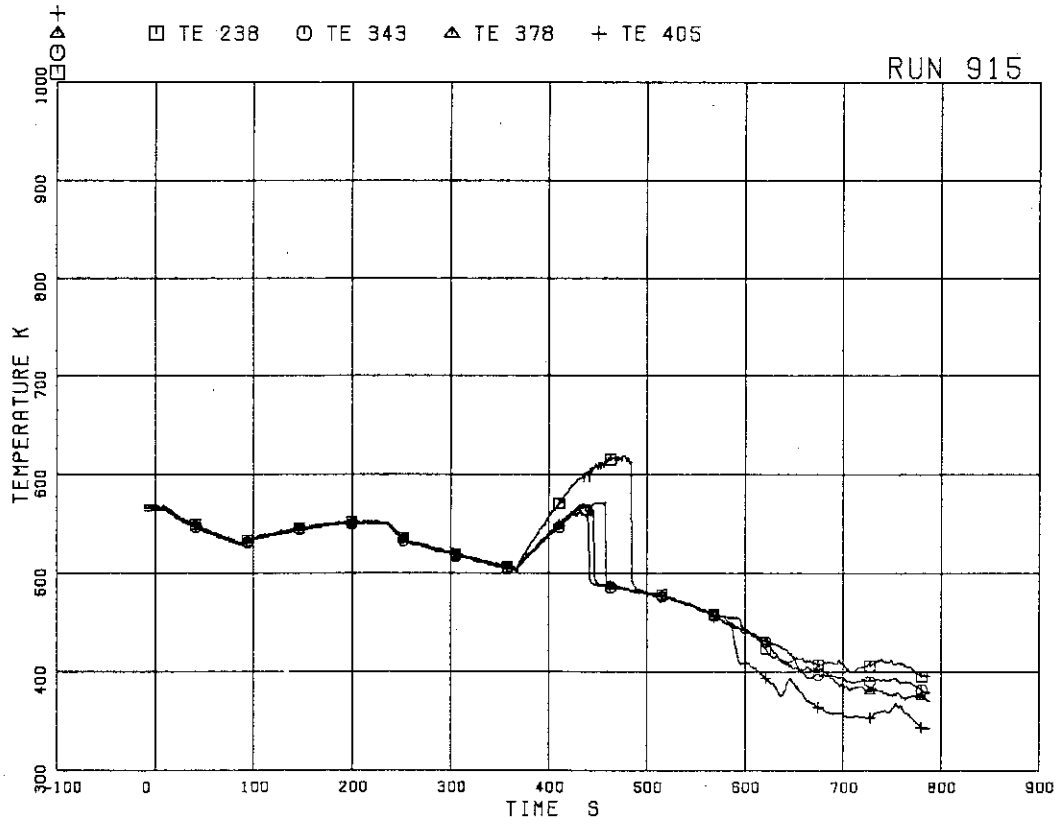

FIG.5. 72 SURFACE TEMPERATURES OF FUEL RODS A22,B22,C22,D22 AT POSITION 6

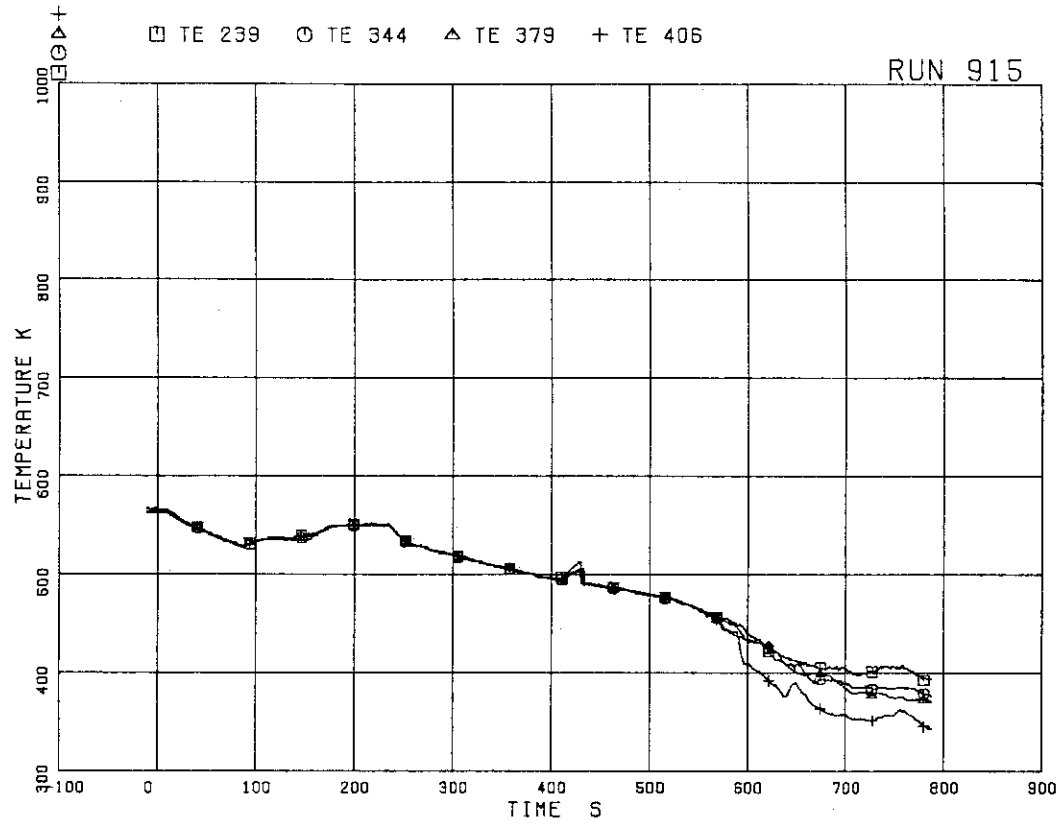

FIG.5. 73 SURFACE TEMPERATURES OF FUEL RODS A22,B22,C22,D22 AT POSITION 7

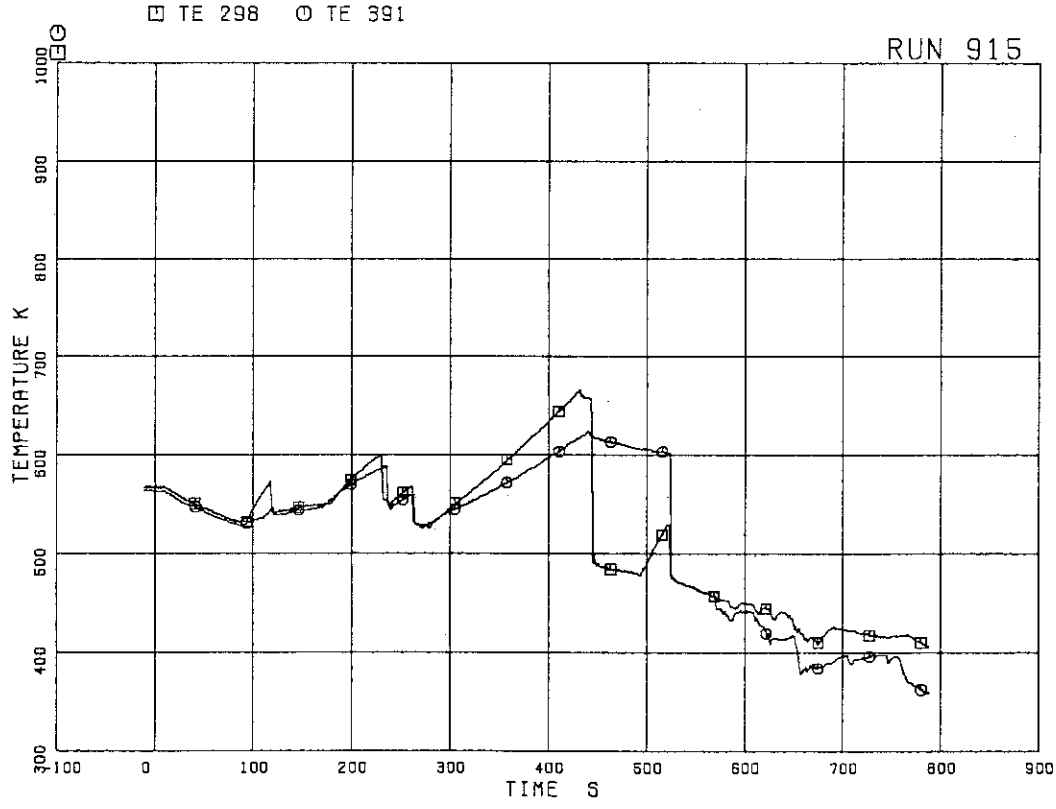

FIG.5. 74 SURFACE TEMPERATURES OF FUEL RODS A77,C77 AT POSITION 1

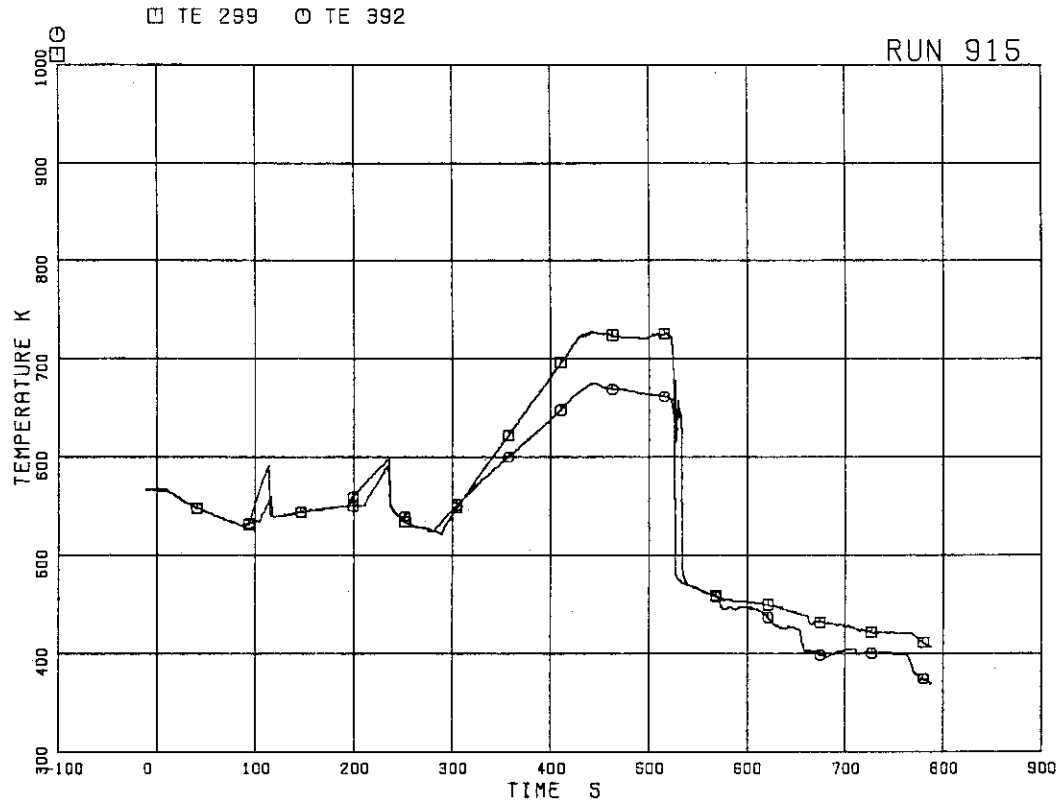

FIG.5. 75 SURFACE TEMPERATURES OF FUEL RODS A77,C77 AT POSITION 2

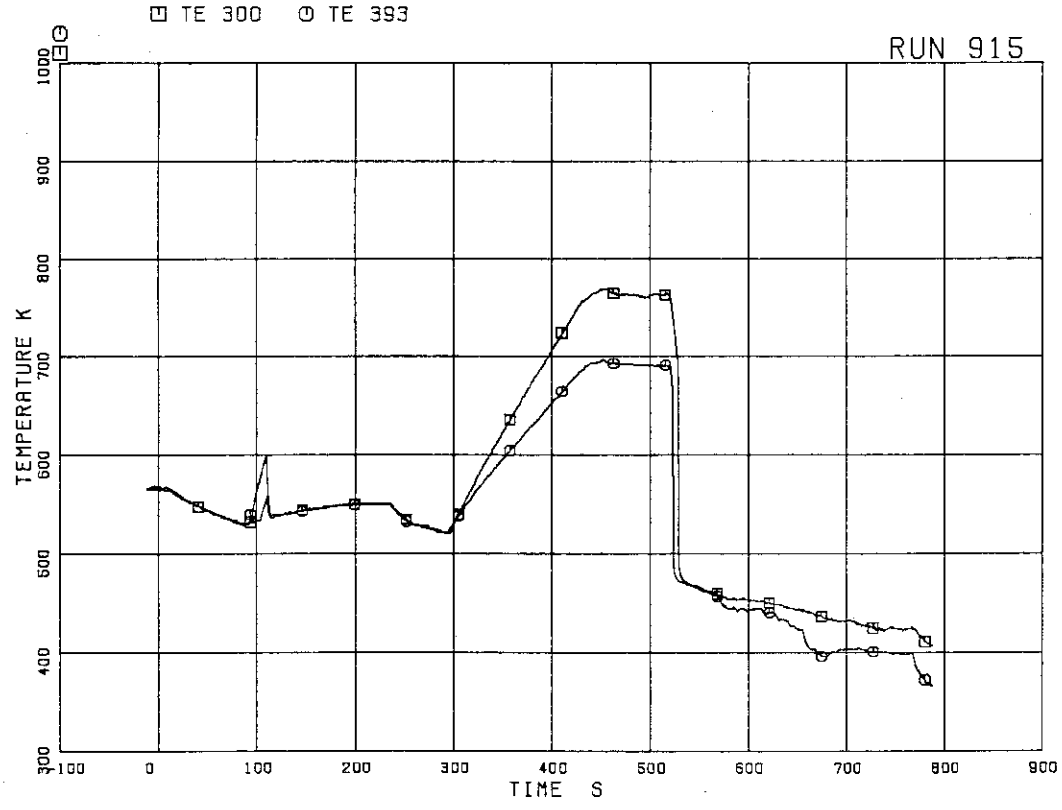

FIG.5. 76 SURFACE TEMPERATURES OF FUEL RODS A77,C77 AT POSITION 3

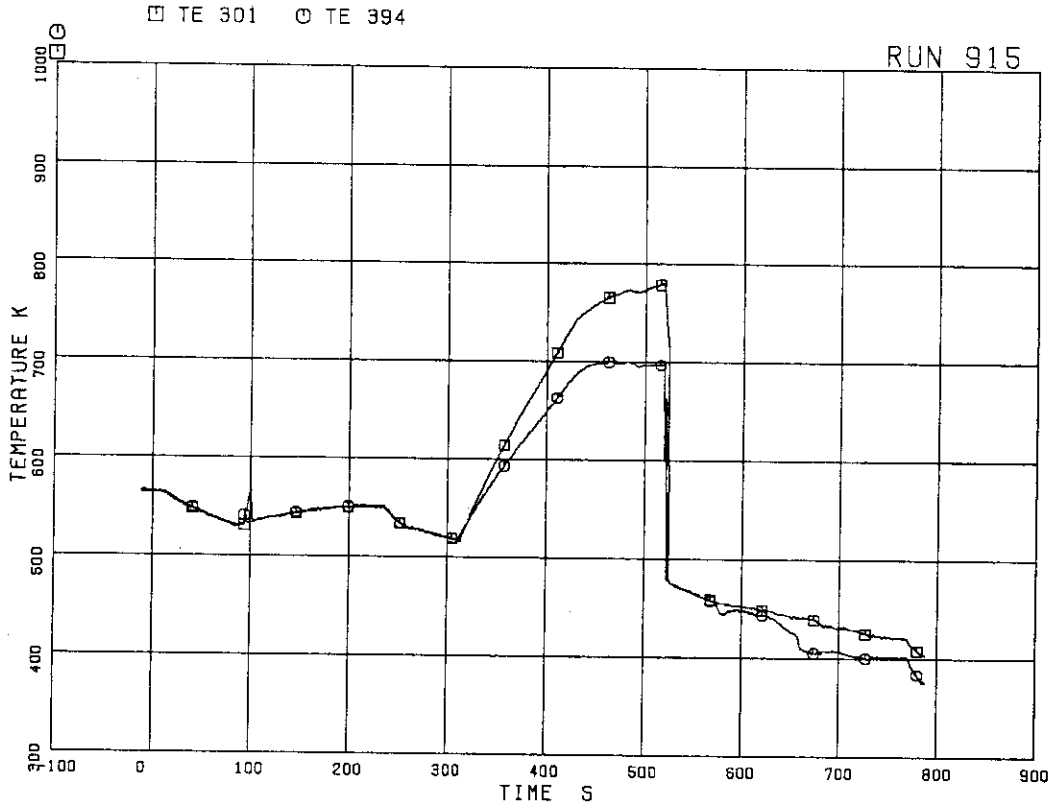

FIG.5. 77 SURFACE TEMPERATURES OF FUEL RODS A77,C77,D77 AT POSITION 4

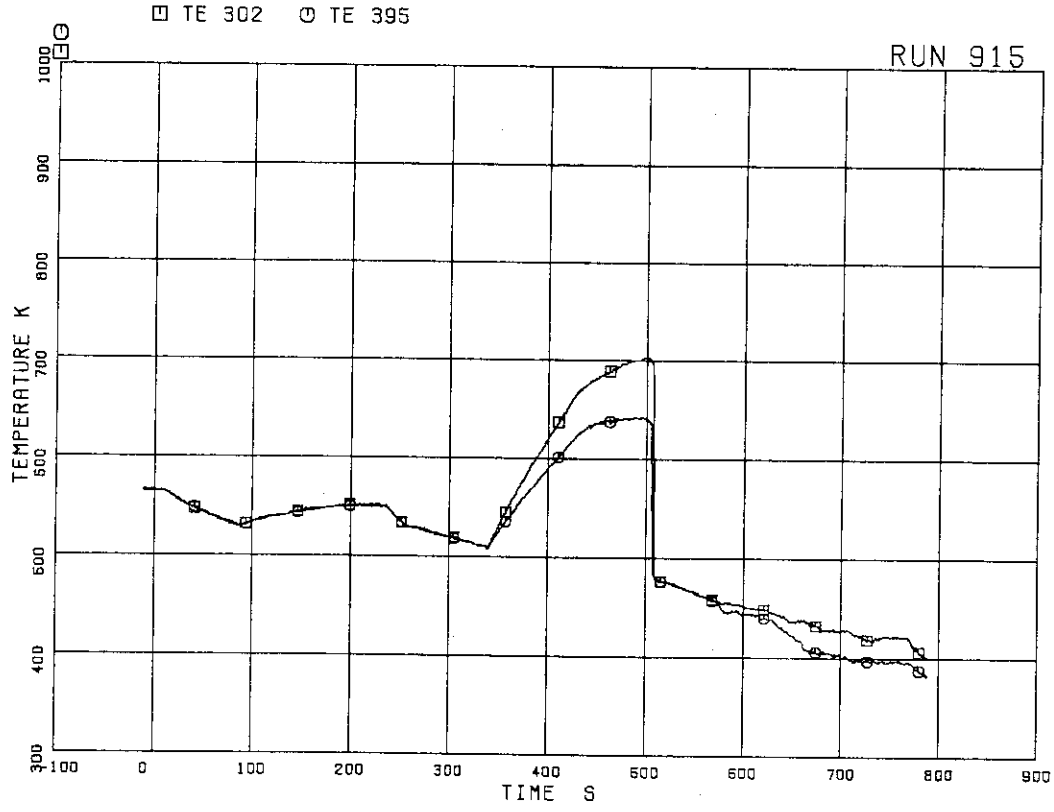

FIG.5. 78 SURFACE TEMPERATURES OF FUEL RODS A77,C77 AT POSITION 5

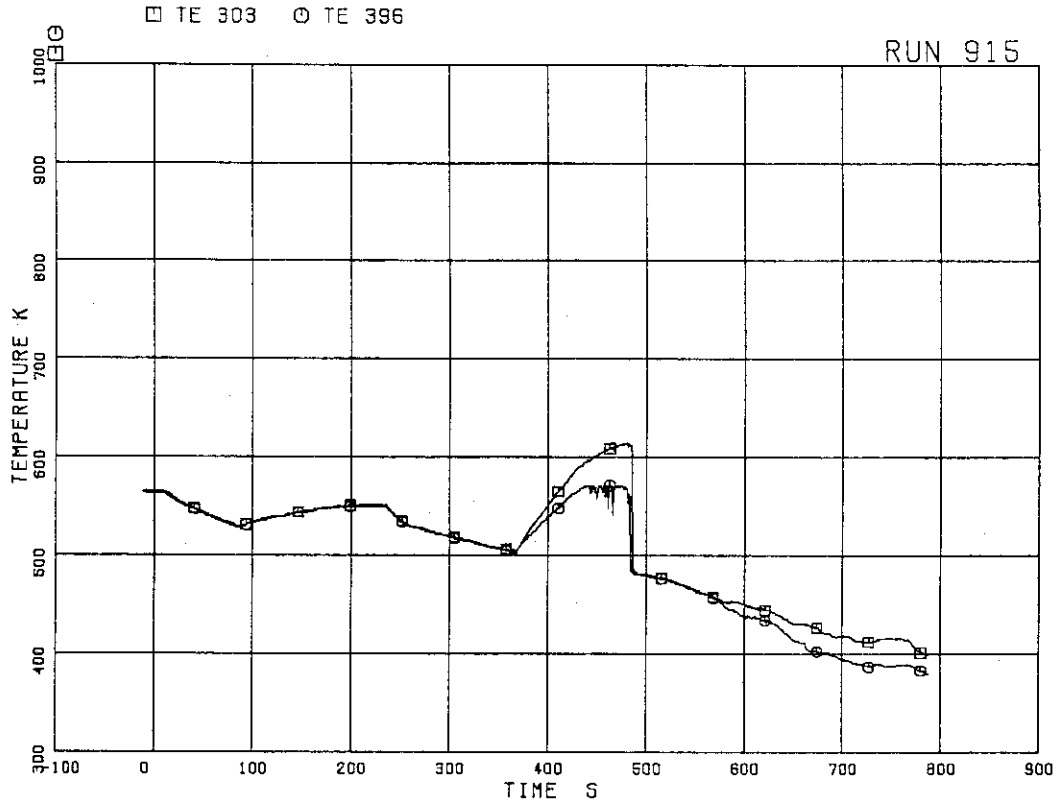

FIG.5. 79 SURFACE TEMPERATURES OF FUEL RODS A77,C77 AT POSITION 6

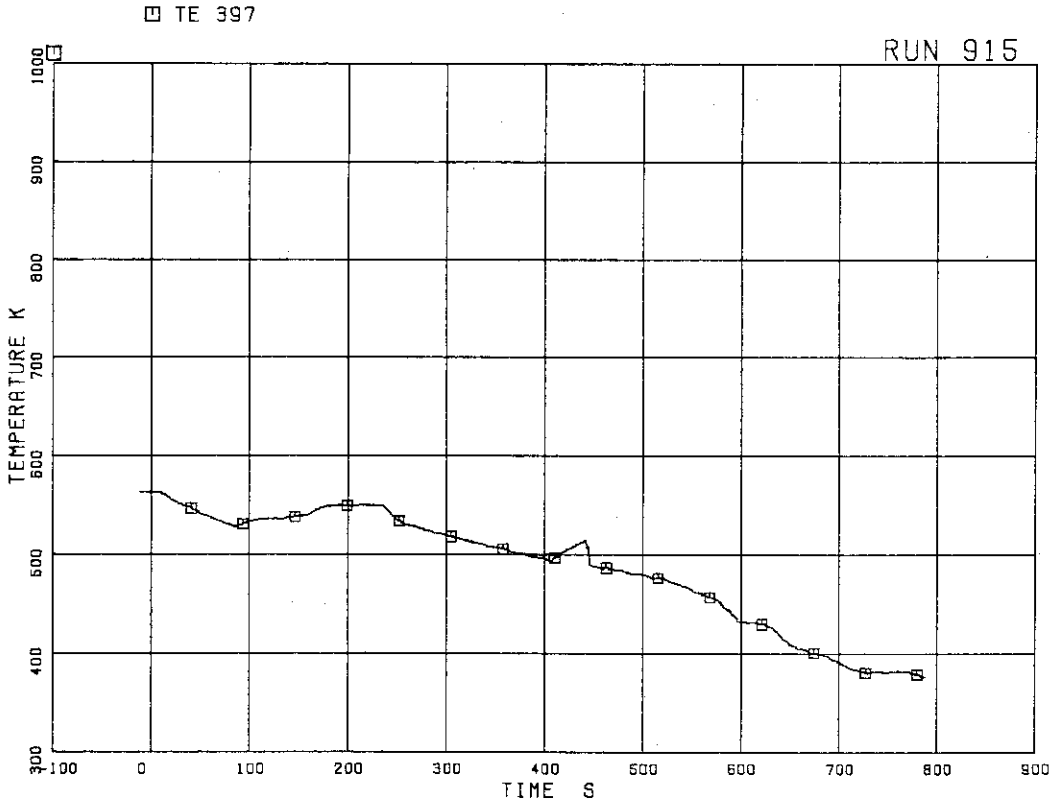

FIG.5. 80 SURFACE TEMPERATURES OF FUEL RODS C77 RODS AT POSITION 7

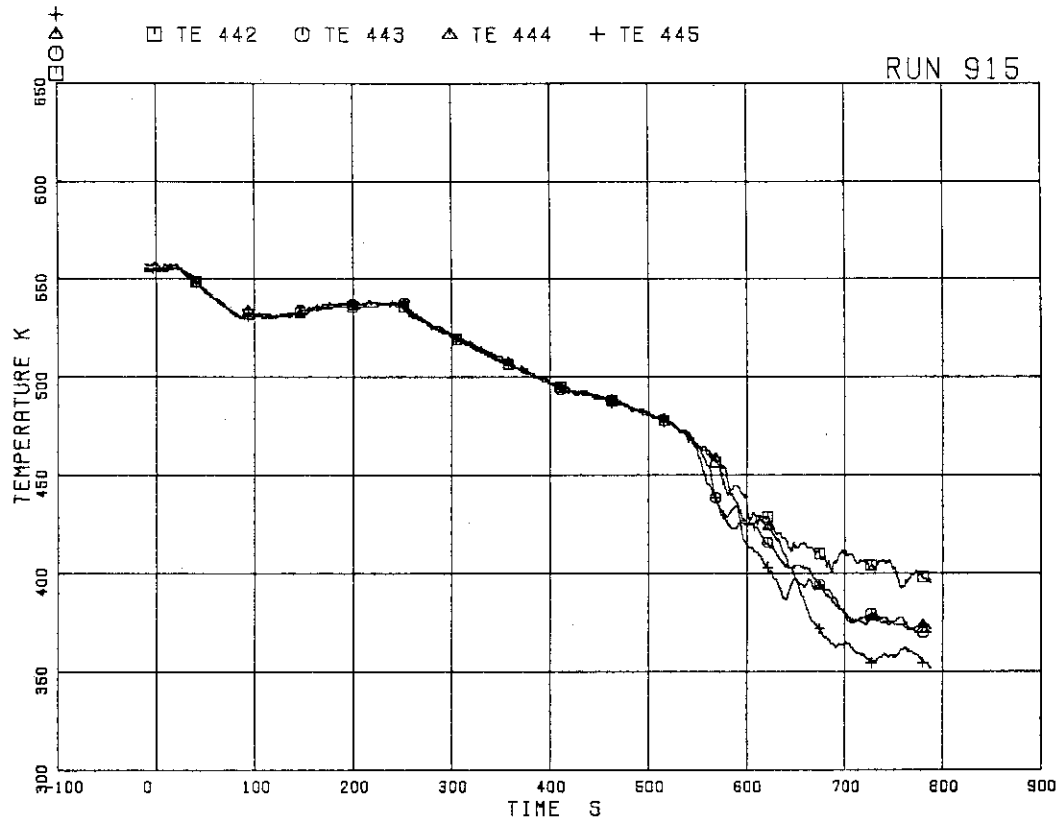

FIG.5. 81 FLUID TEMPERATURES AT CHANNEL INLET

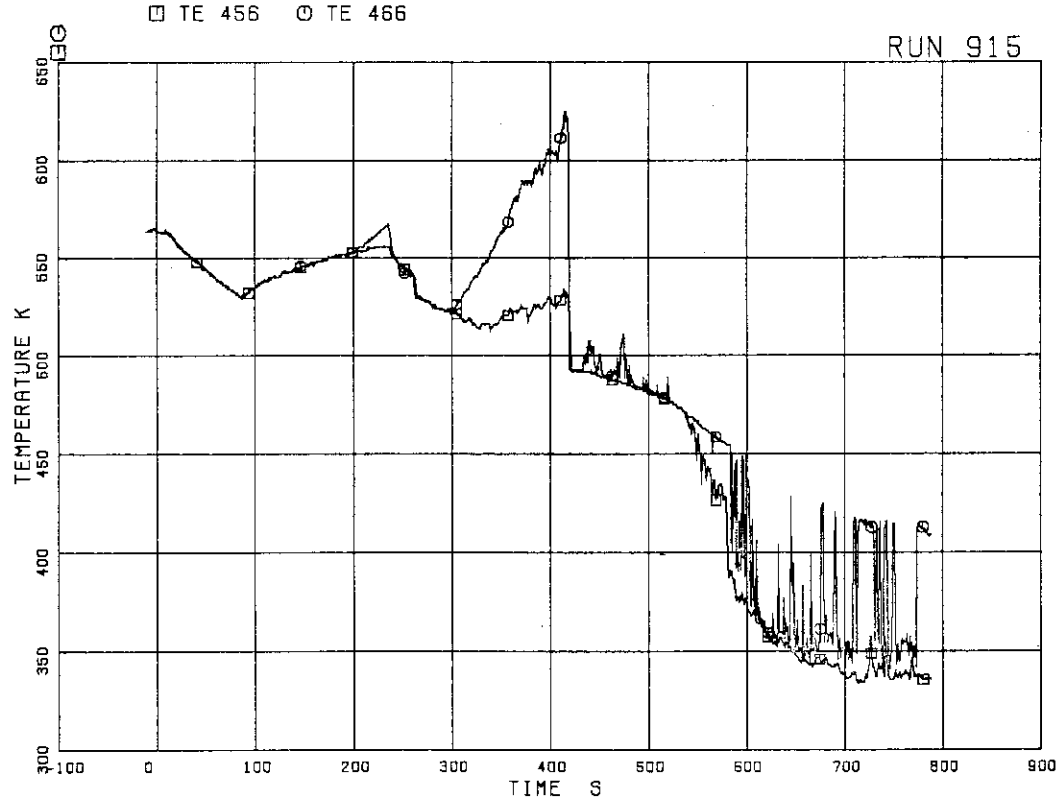

FIG.5. 82 FLUID TEMPERATURES AT UTP IN CHANNEL A, OPENING 1

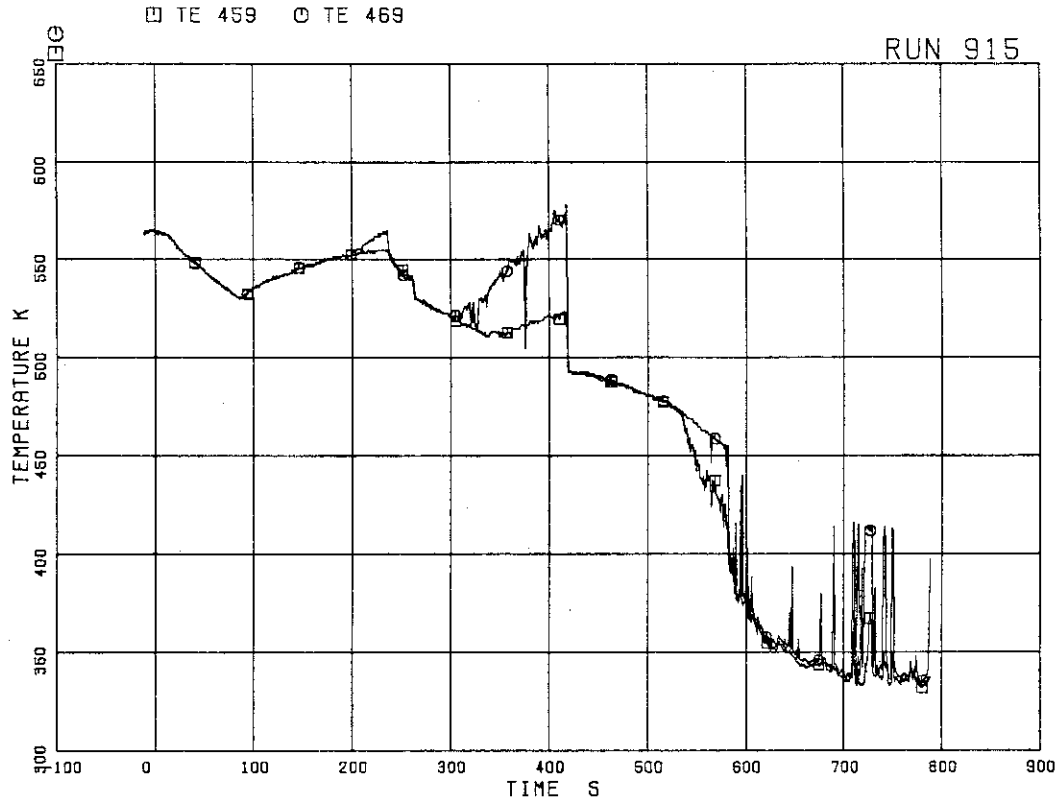

FIG.5. 83 FLUID TEMPERATURES AT UTP IN CHANNEL A, OPENING 4

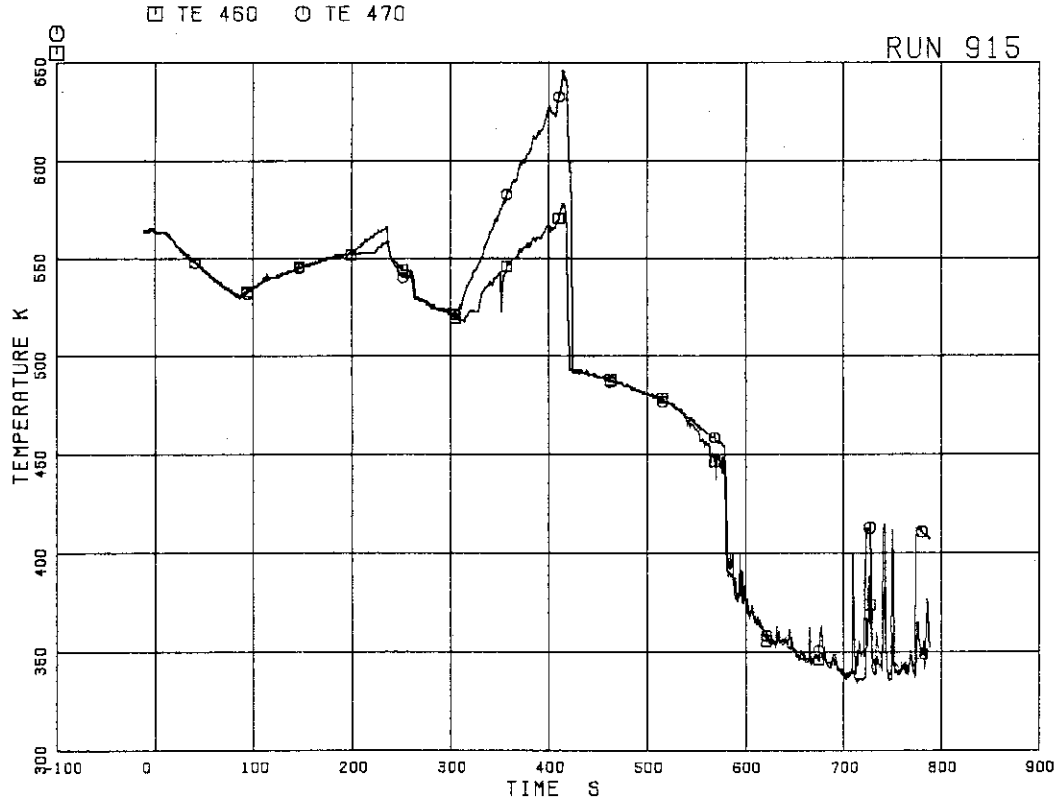

FIG.5. 84 FLUID TEMPERATURES AT UTP IN CHANNEL A, OPENING 5

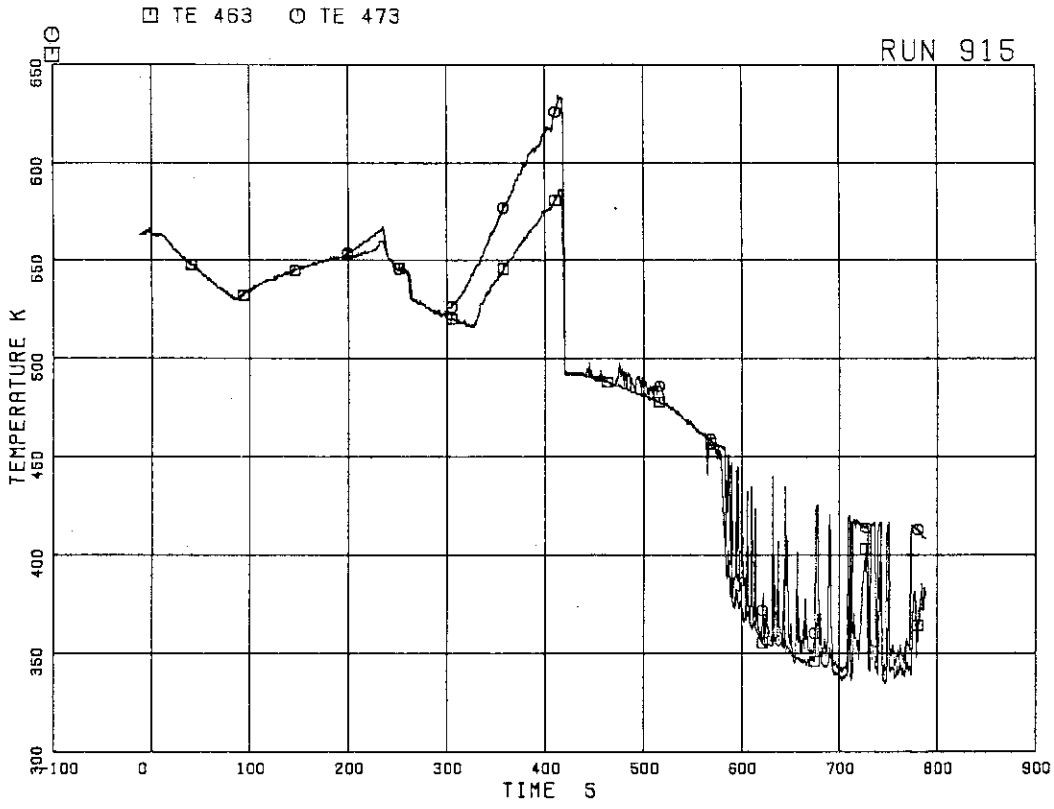

FIG.5. 85 FLUID TEMPERATURES AT UTP IN CHANNEL A, OPENING 8

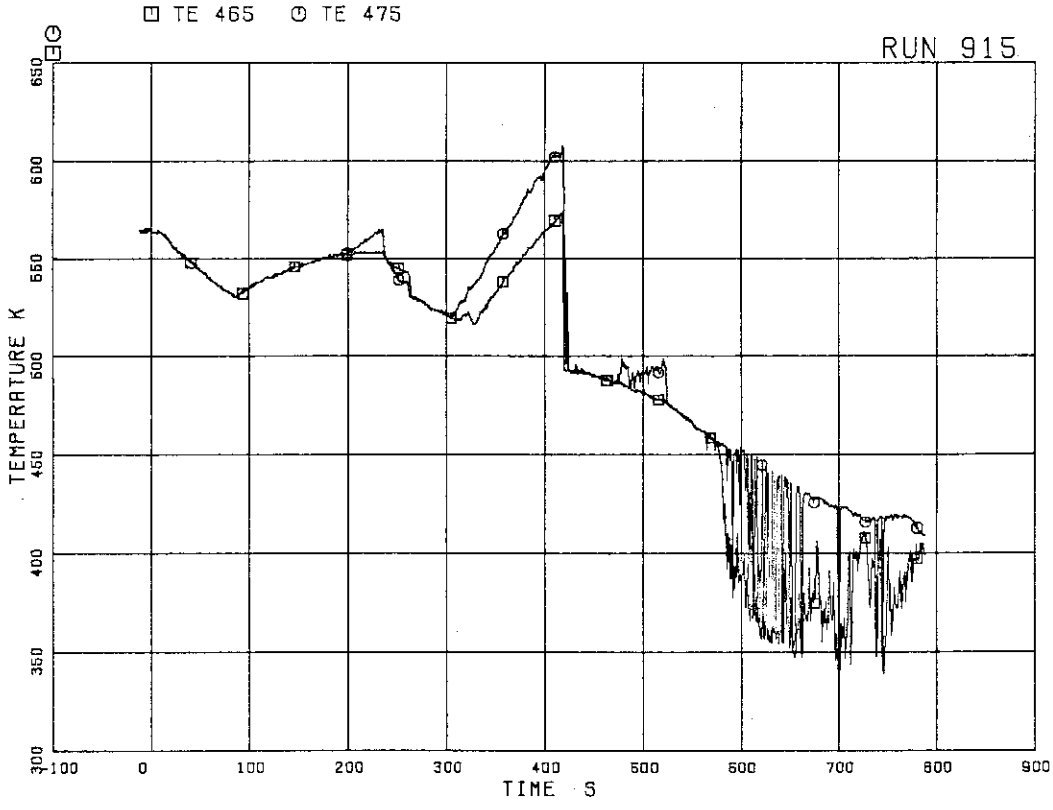

FIG.5. 86 FLUID TEMPERATURES AT UTP IN CHANNEL A, OPENING 10

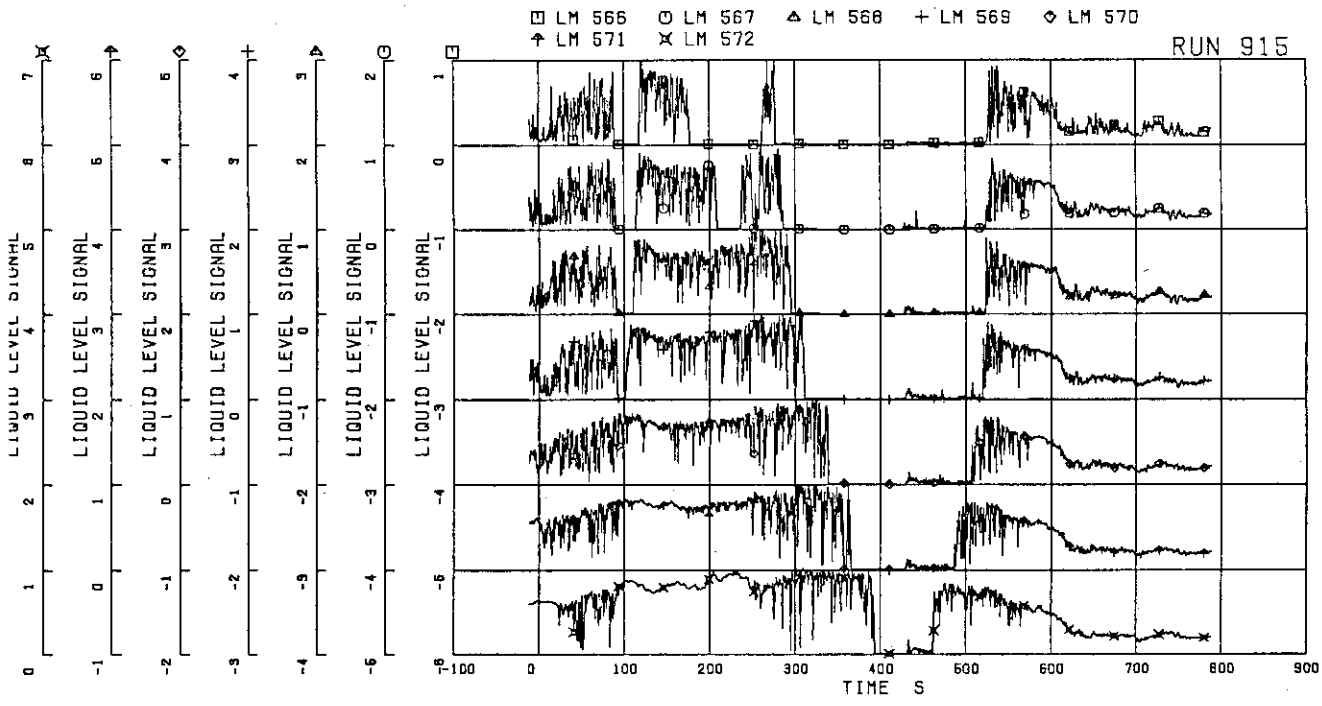

FIG.5. 87 LIQUID LEVEL SIGNALS IN CHANNEL BOX A, LOCATION A2

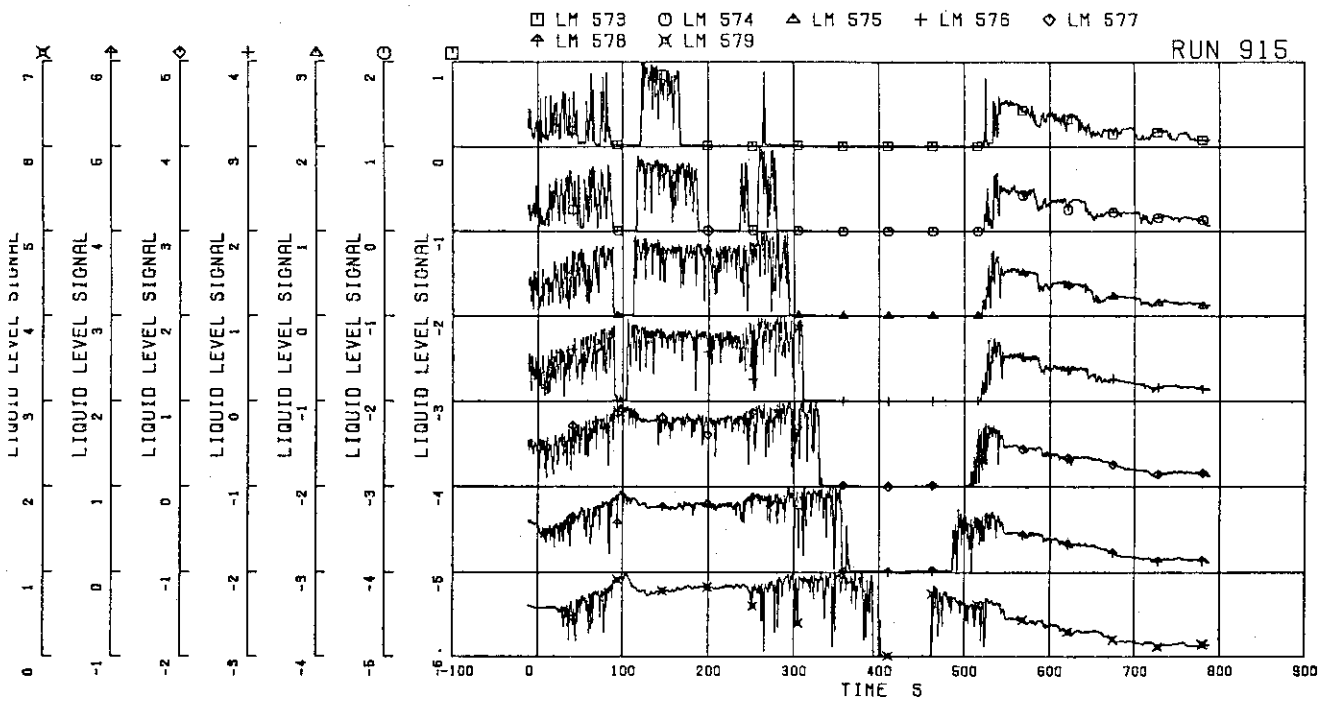

FIG.5. 88 LIQUID LEVEL SIGNALS IN CHANNEL BOX B

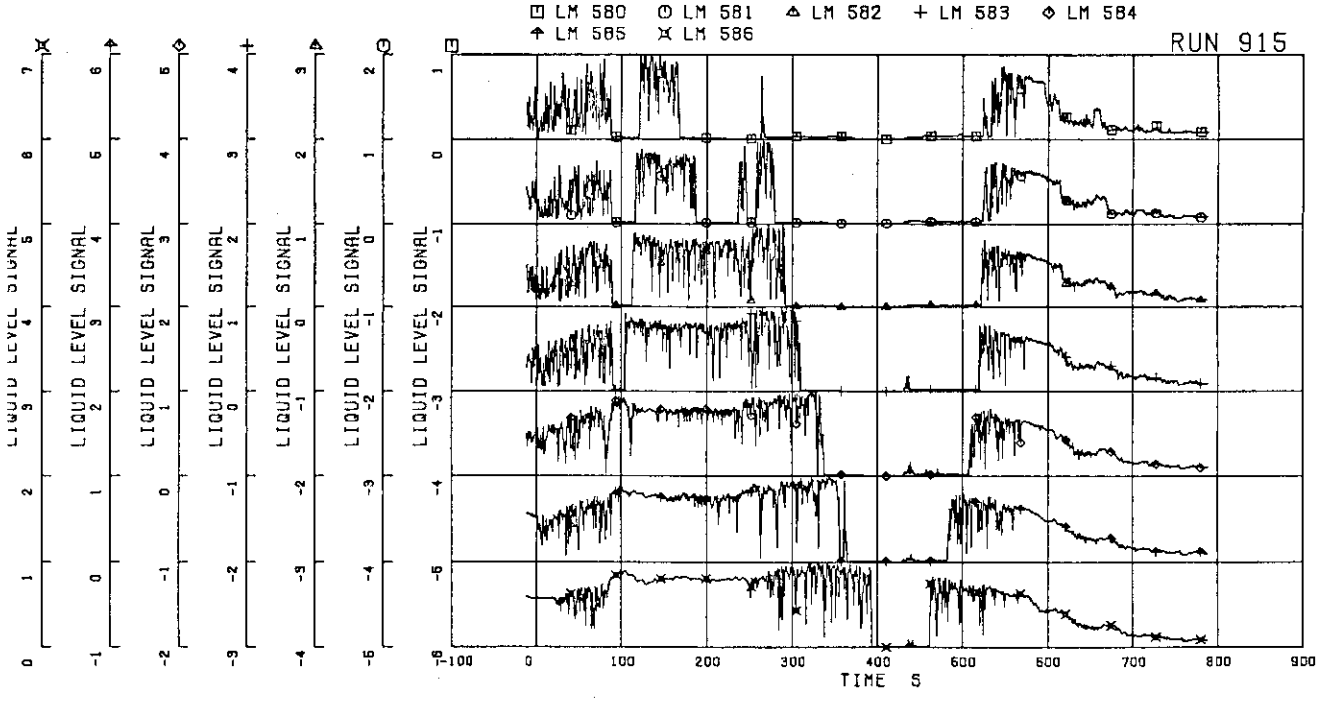

FIG.5. 89 LIQUID LEVEL SIGNALS IN CHANNEL BOX C

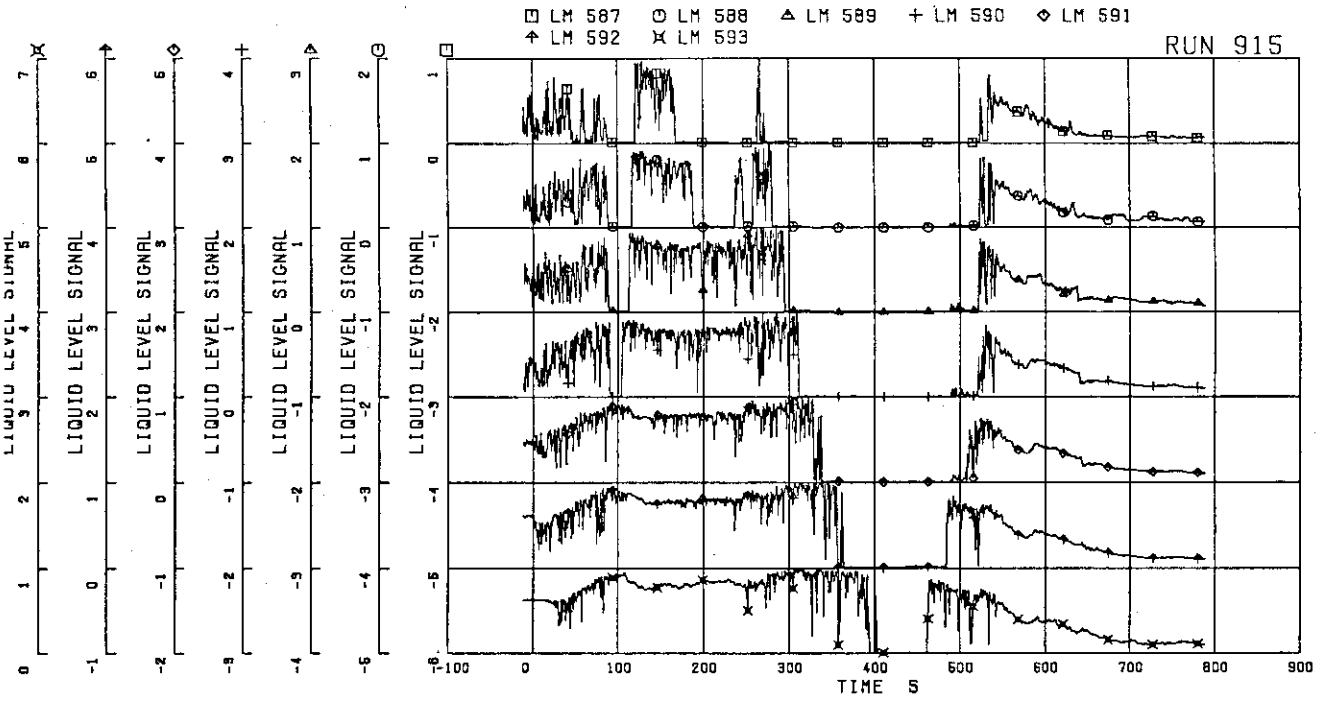

FIG.5. 90 LIQUID LEVEL SIGNALS IN CHANNEL BOX D

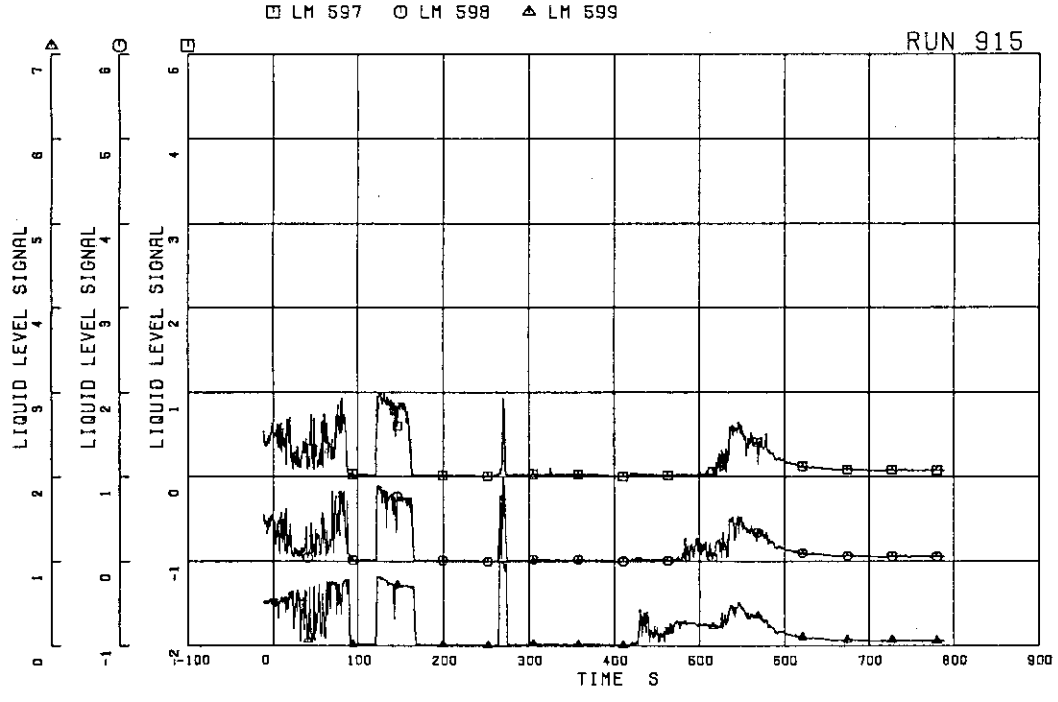

FIG.5. 91 LIQUID LEVEL SIGNALS IN CHANNEL A OUTLET LOCATION A2

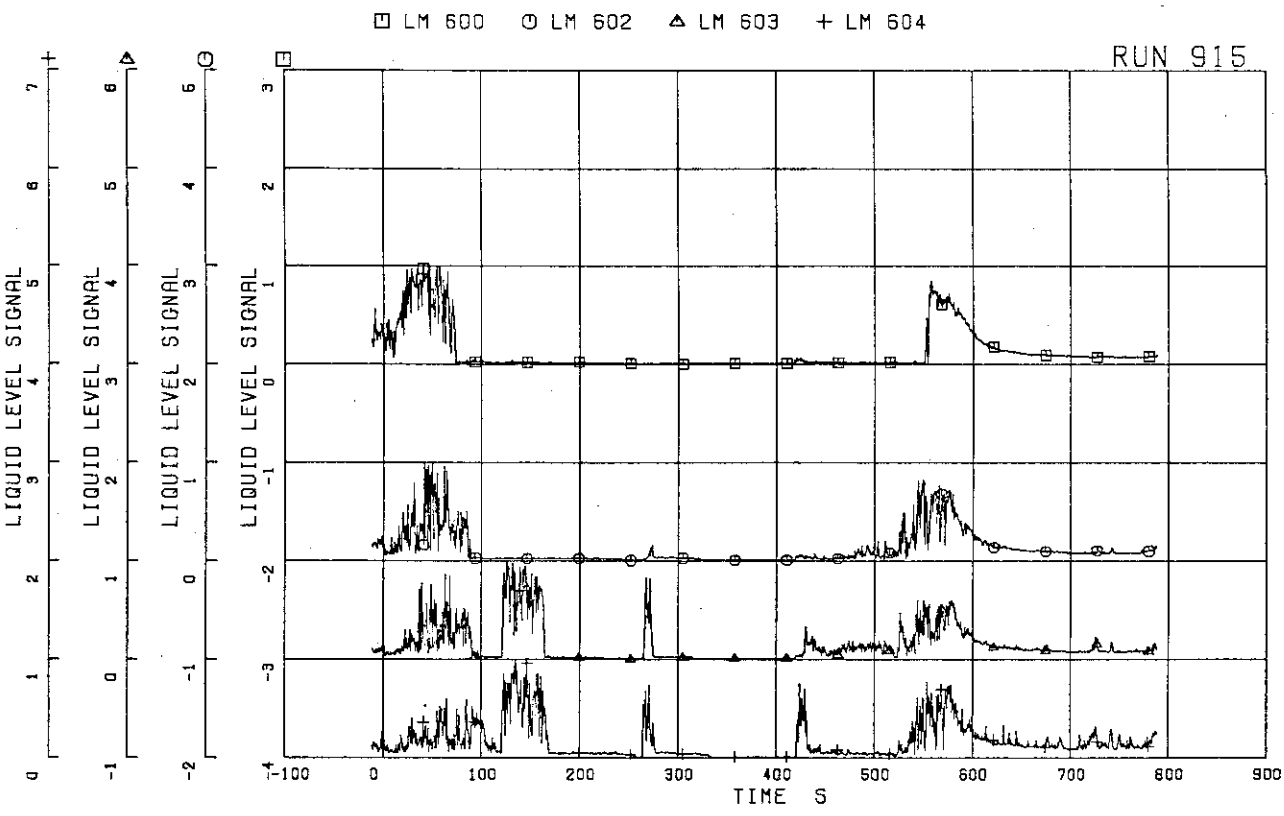

FIG.5. 92 LIQUID LEVEL SIGNALS IN CHANNEL A OUTLET CENTER

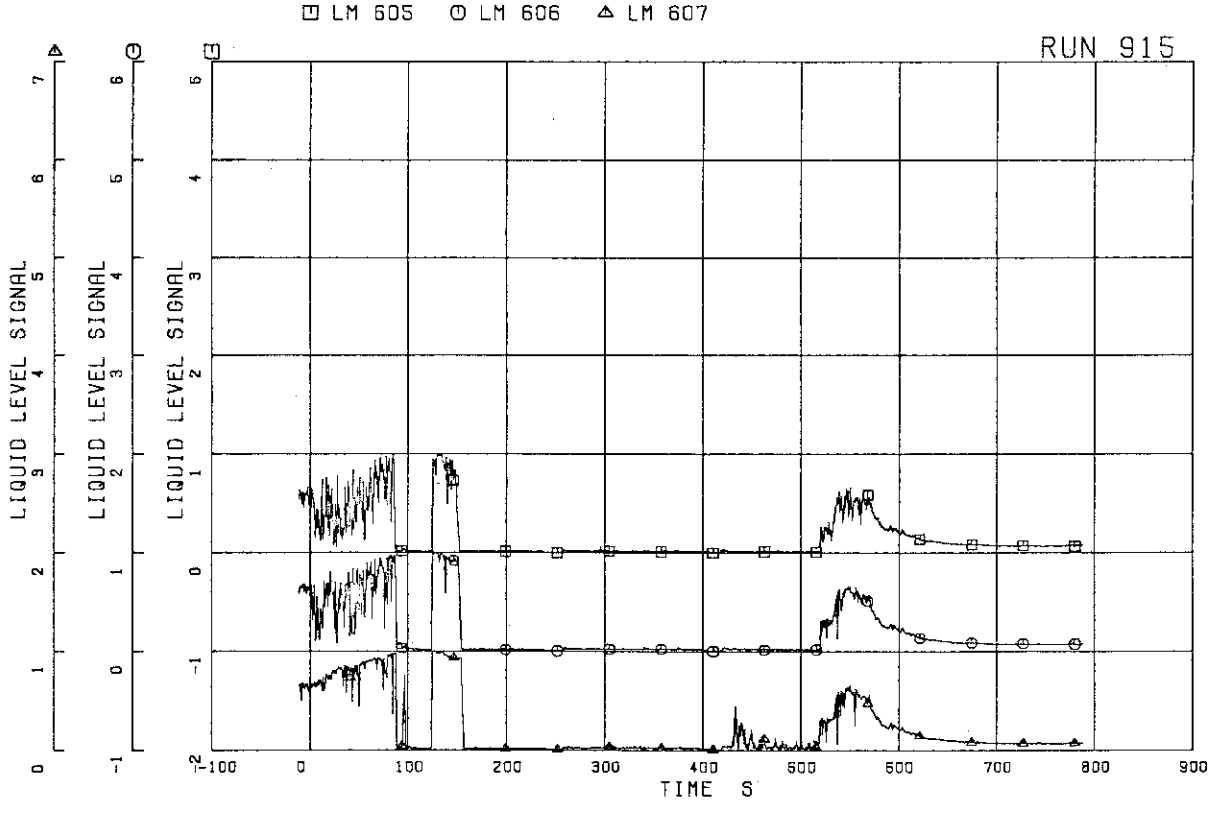

FIG.5. 93 LIQUID LEVEL SIGNALS IN CHANNEL C OUTLET LOCATION C1

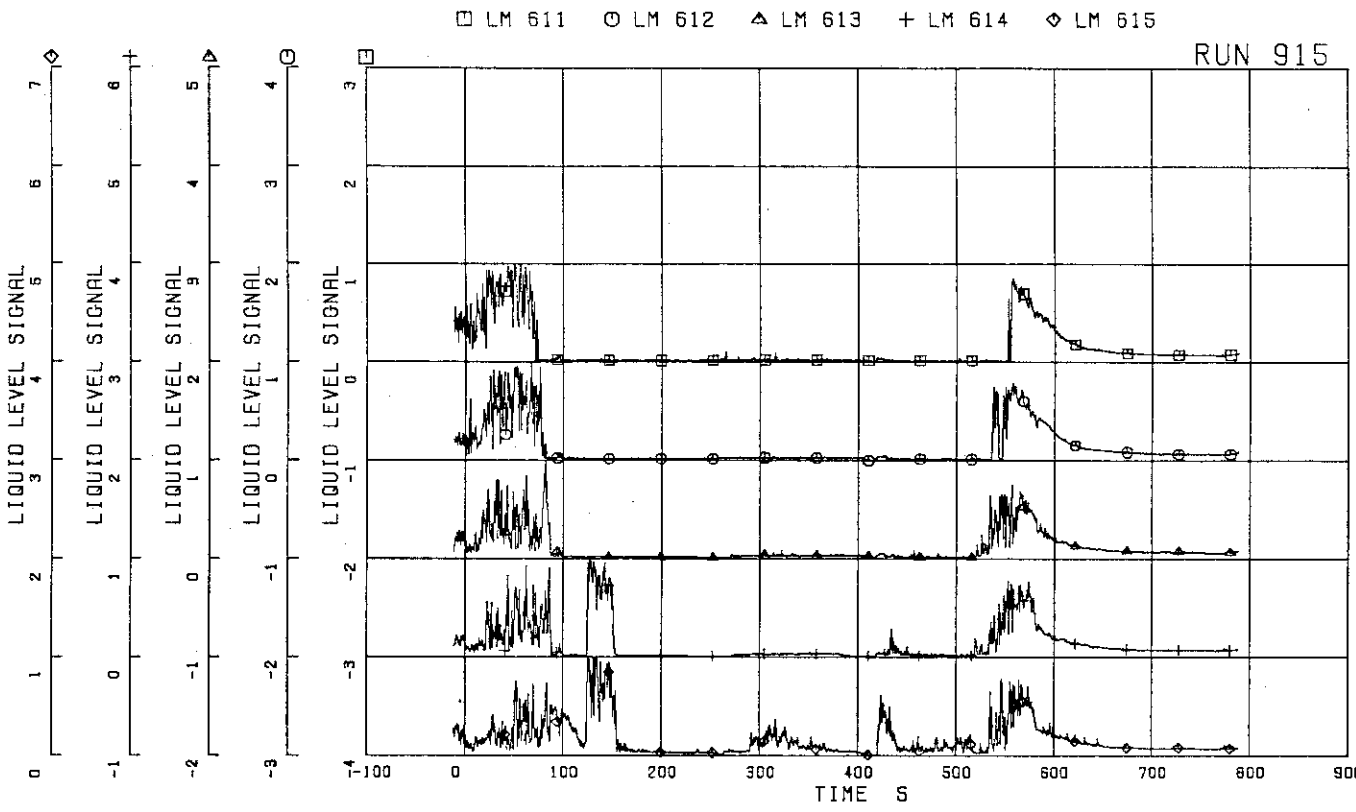

FIG.5. 94 LIQUID LEVEL SIGNALS IN CHANNEL C OUTLET CENTER

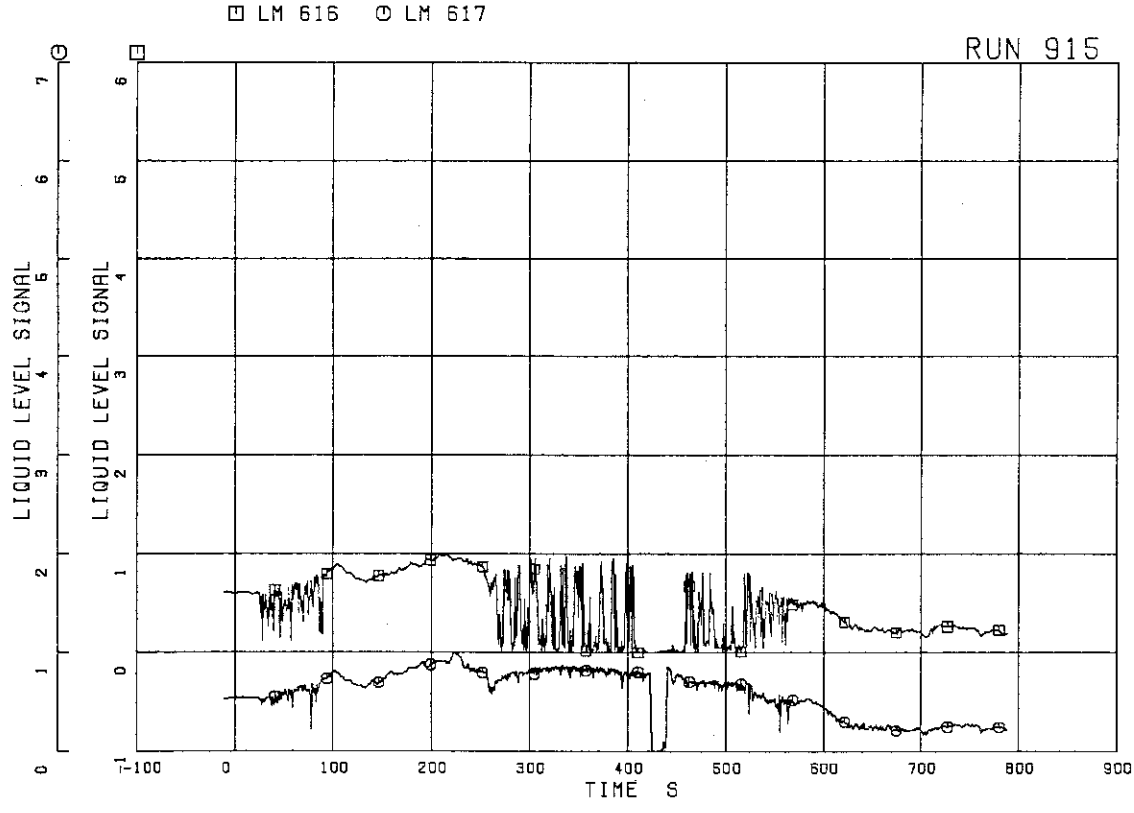

FIG.5. 95 LIQUID LEVEL SIGNALS IN CHANNEL A INLET

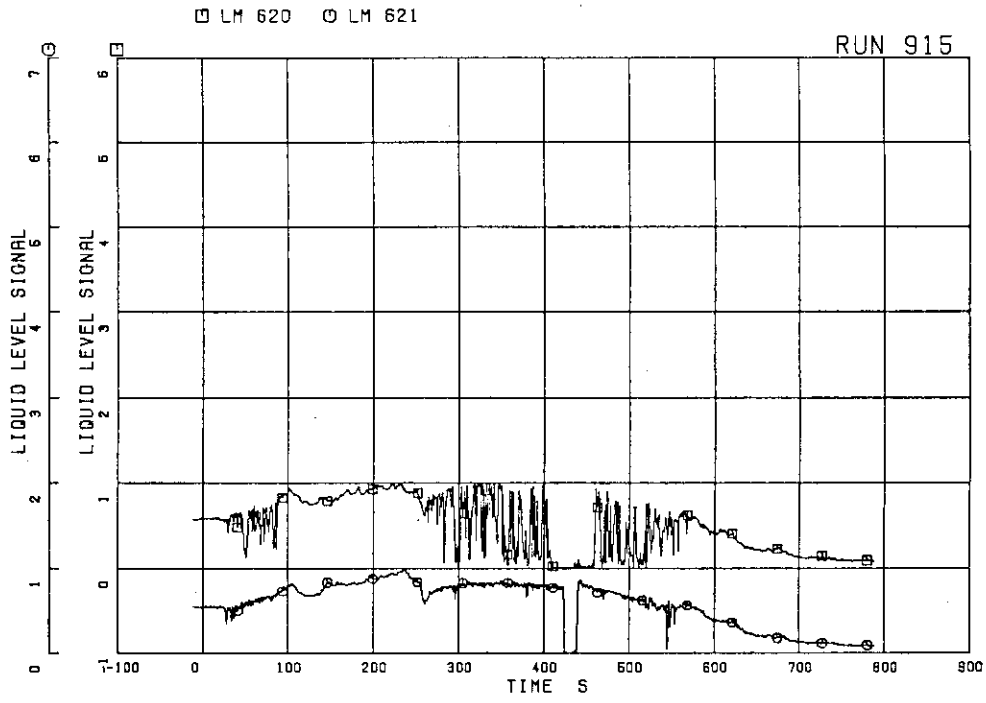

FIG.5. 96 LIQUID LEVEL SIGNALS IN CHANNEL C INLET

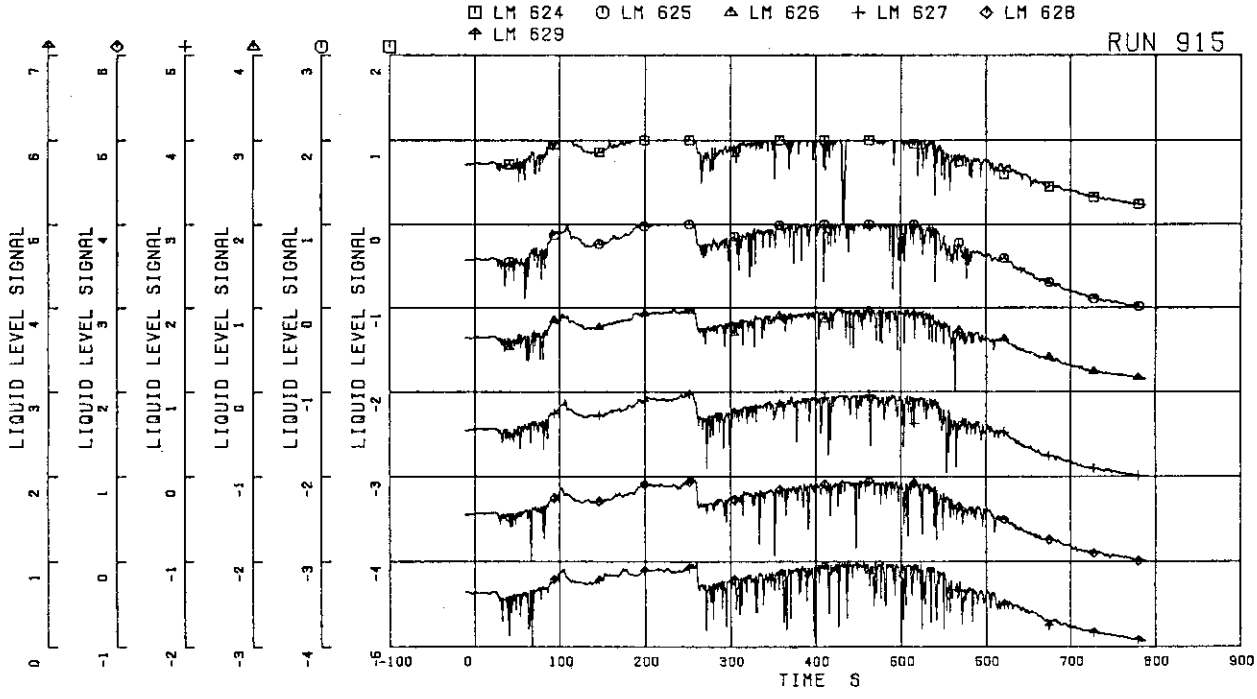

FIG.5. 97 LIQUID LEVEL SIGNALS IN LOWER PLENUM, NORTH

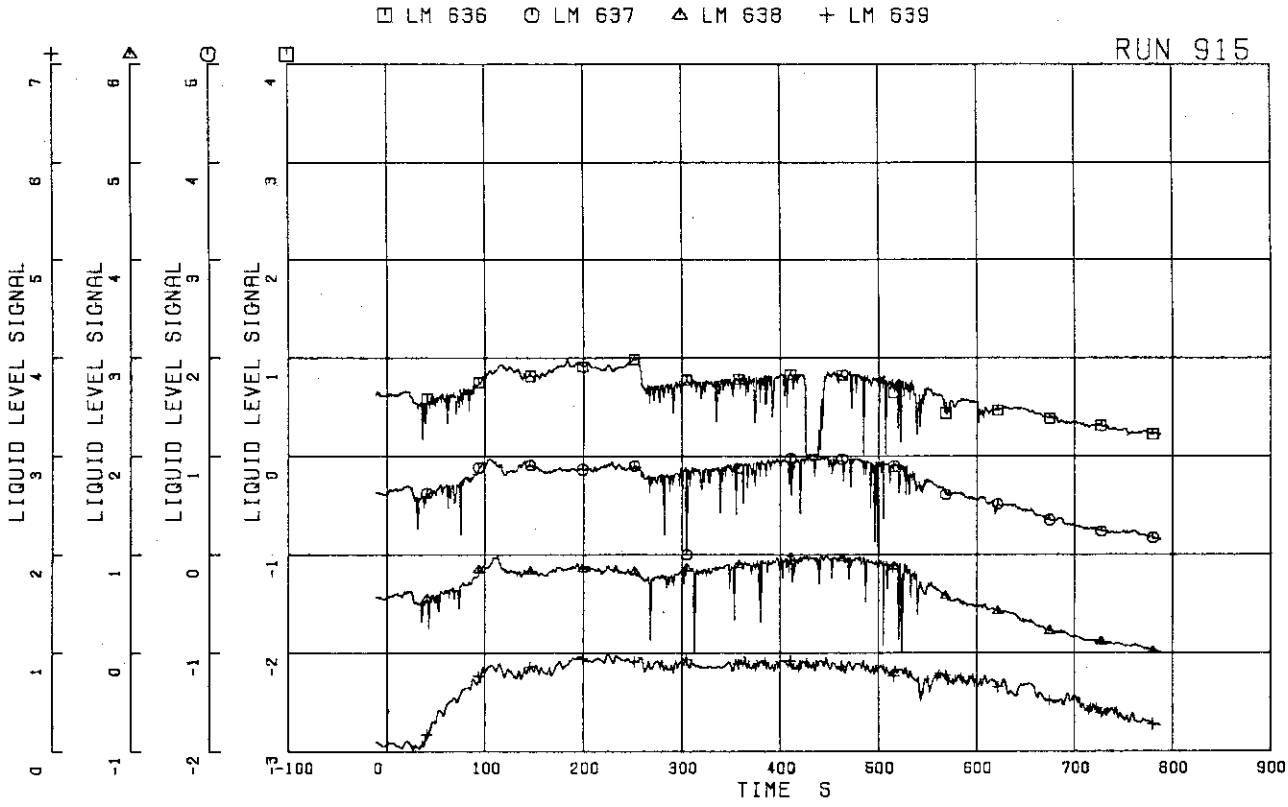

FIG.5. 98 LIQUID LEVEL SIGNALS IN GUIDE TUBE, NORTH

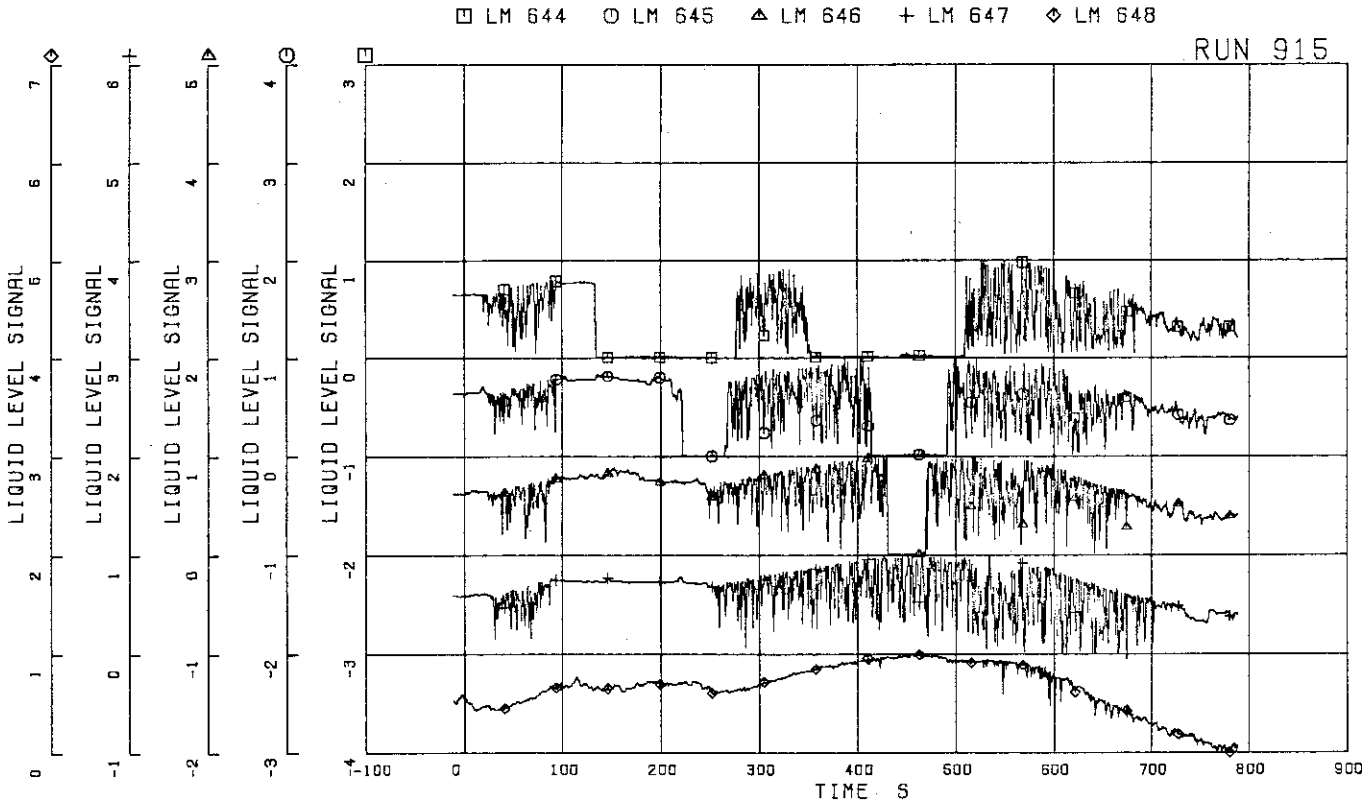

FIG.5. 99 LIQUID LEVEL SIGNALS IN DOWNCOMER, D SIDE

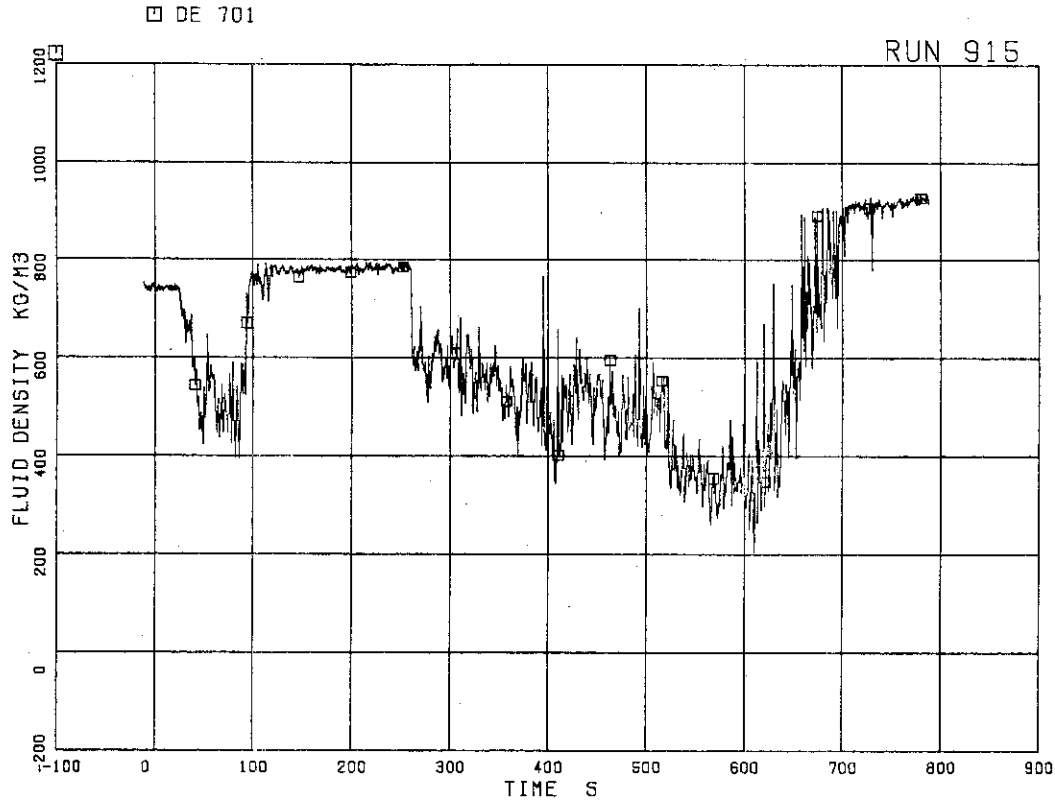

FIG.5.100 AVERAGE DENSITY AT JP-1,2 OUTLET

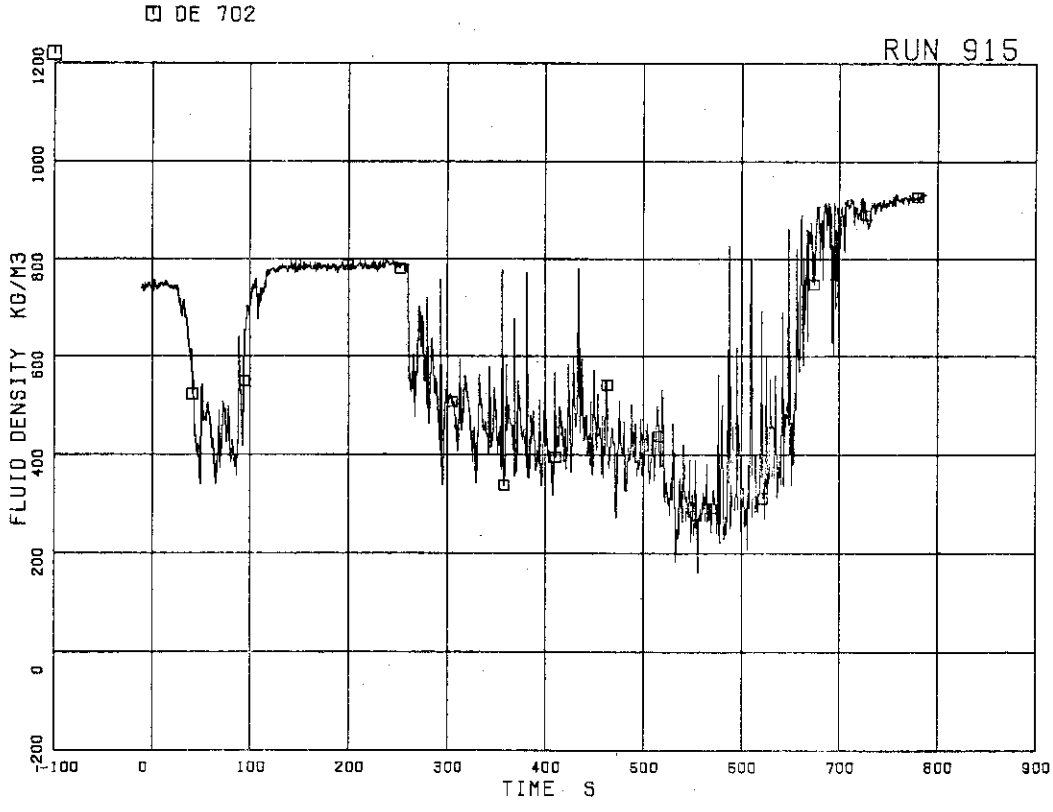

FIG.5.101 AVERAGE DENSITY AT JP-3,4 OUTLET

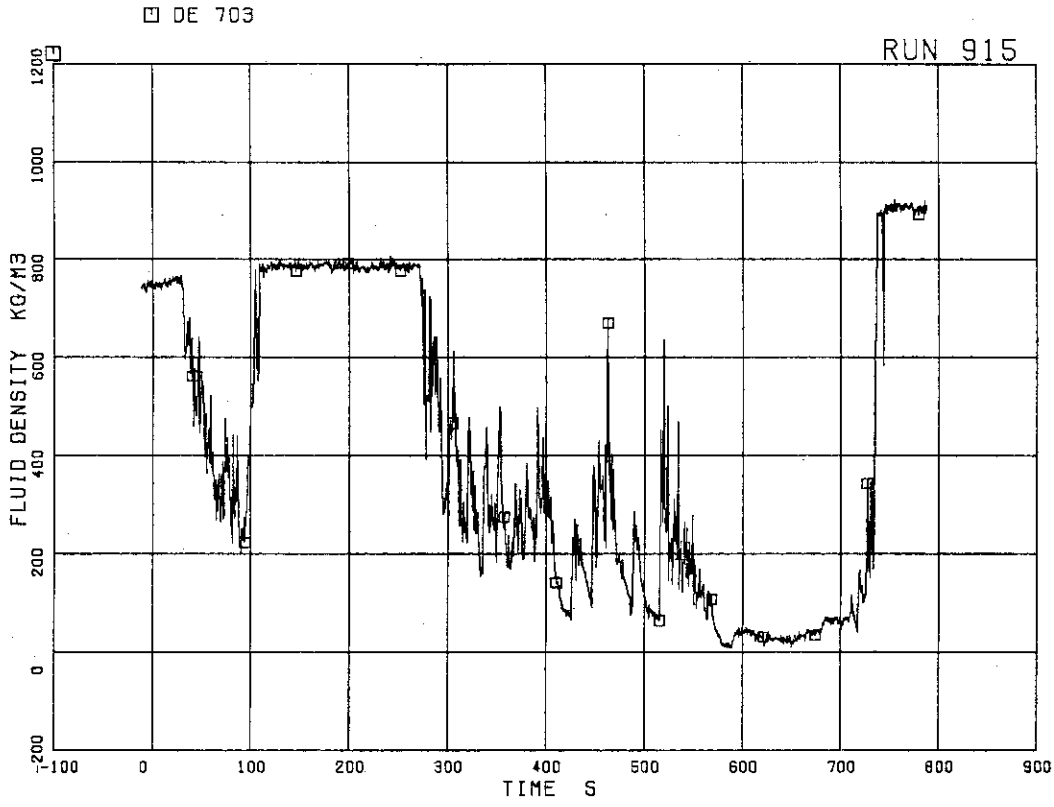

FIG.5.102 AVERAGE DENSITY AT MRP SIDE OF BREAK

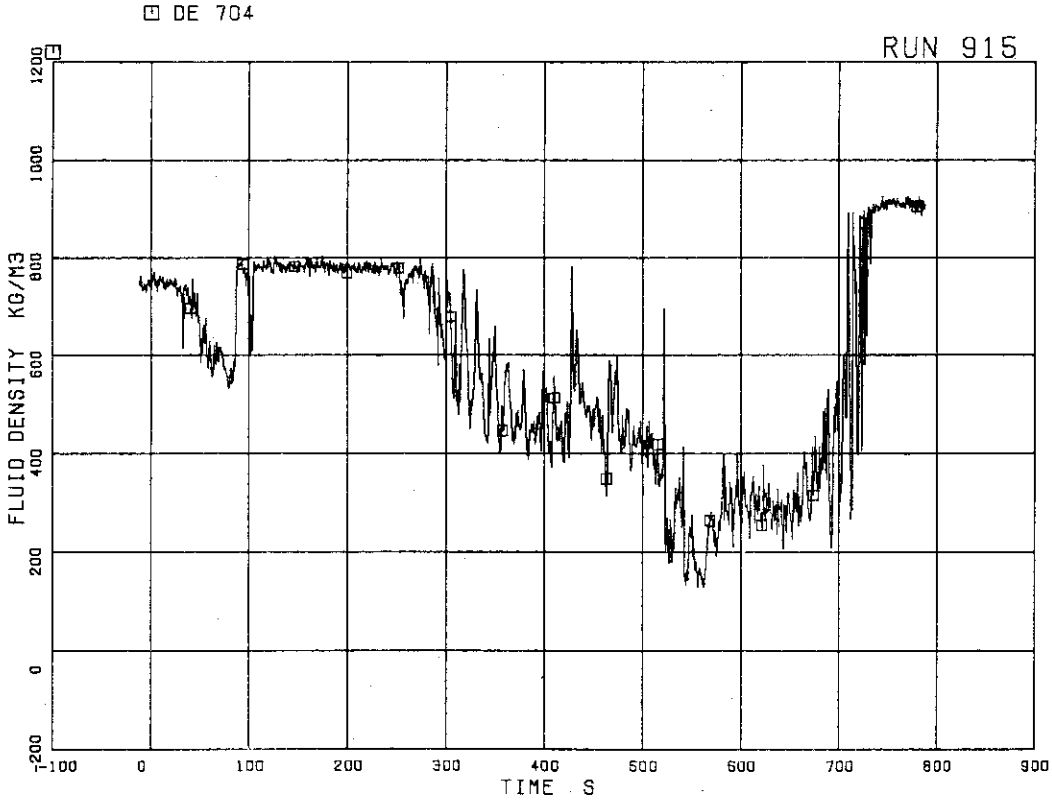

FIG.5.103 AVERAGE DENSITY AT PV SIDE OF BREAK

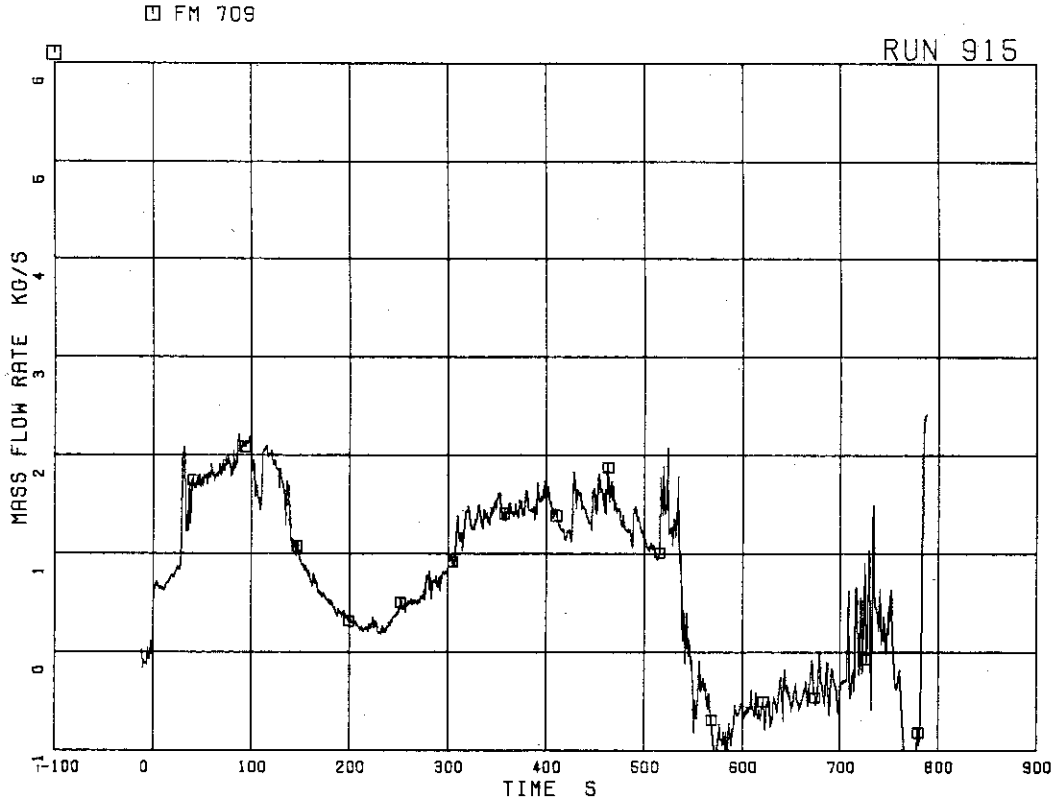

FIG.5.104 TOTAL DISCHARGE FLOW RATE FROM BREAK (BASED ON LOW RANGE DRAG DISK DATA)

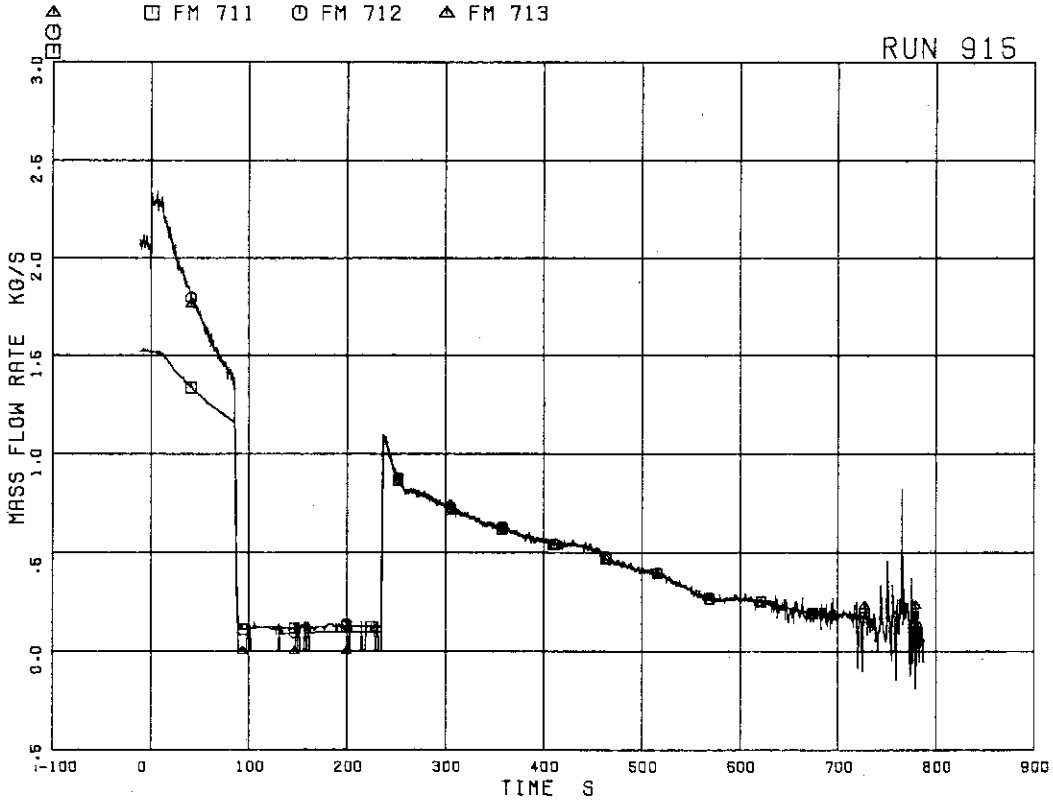

FIG.5.105 STEAM DISCHARGE FLOW RATE THROUGH MSL

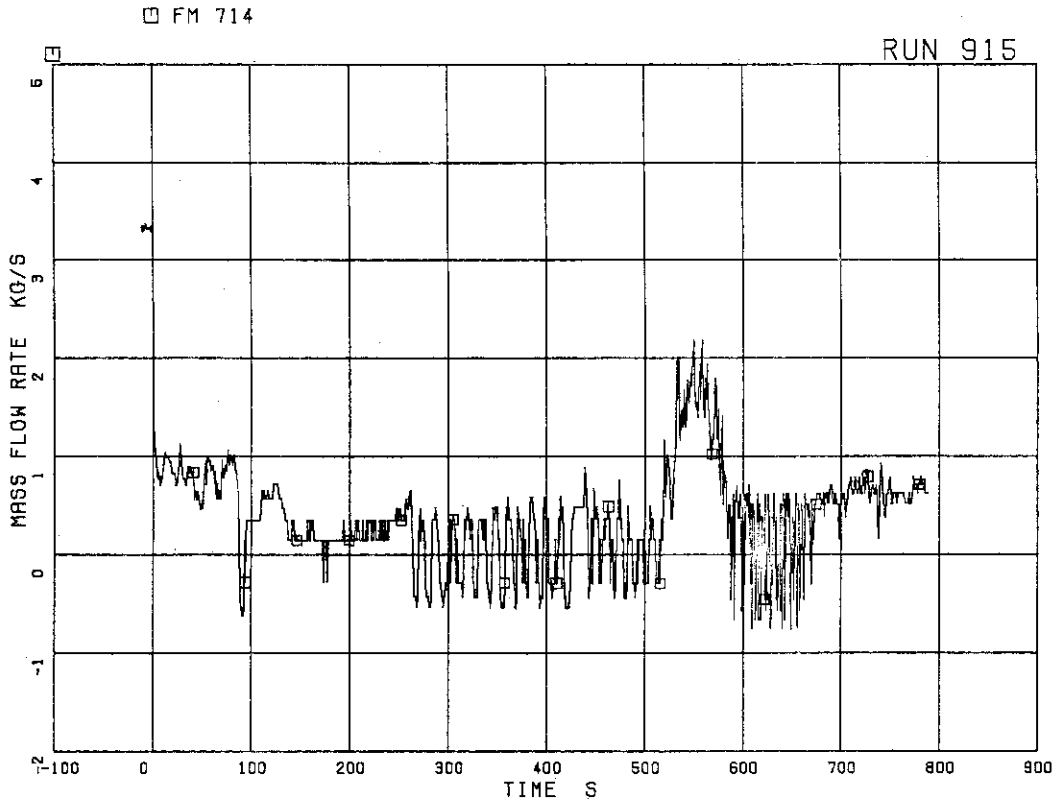

FIG.5.106 FLOW RATE AT CHANNEL A INLET

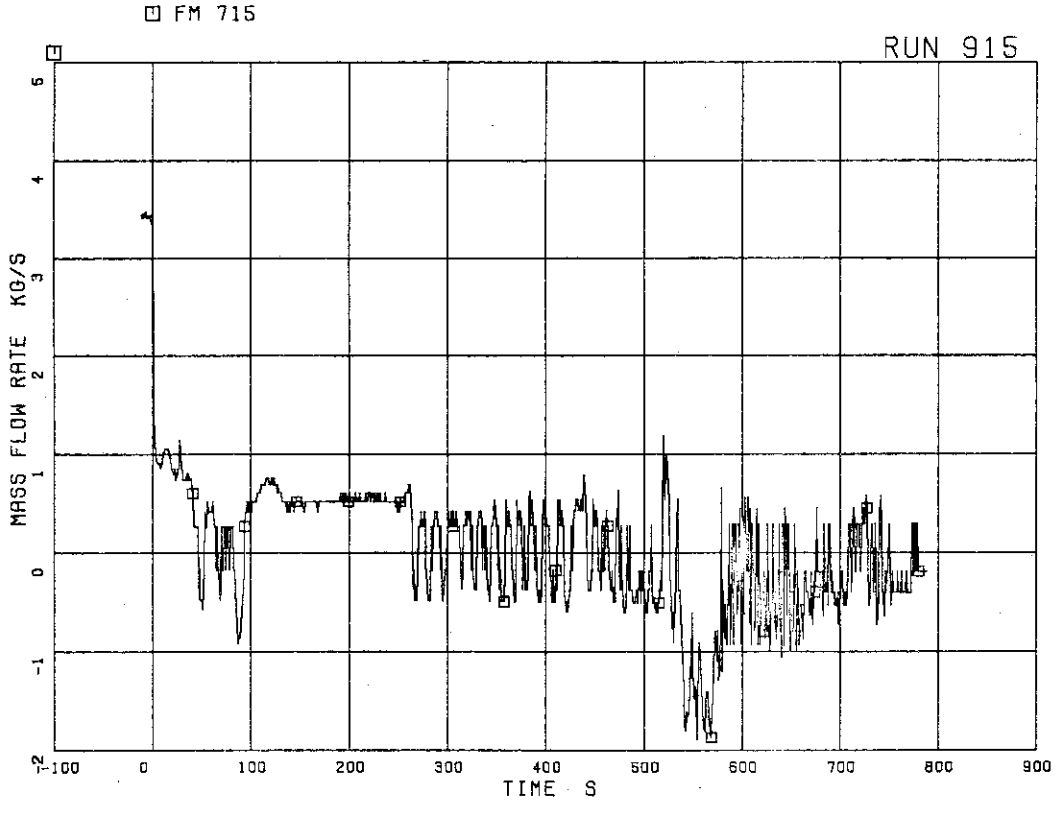

FIG.5.107 FLOW RATE AT CHANNEL B INLET

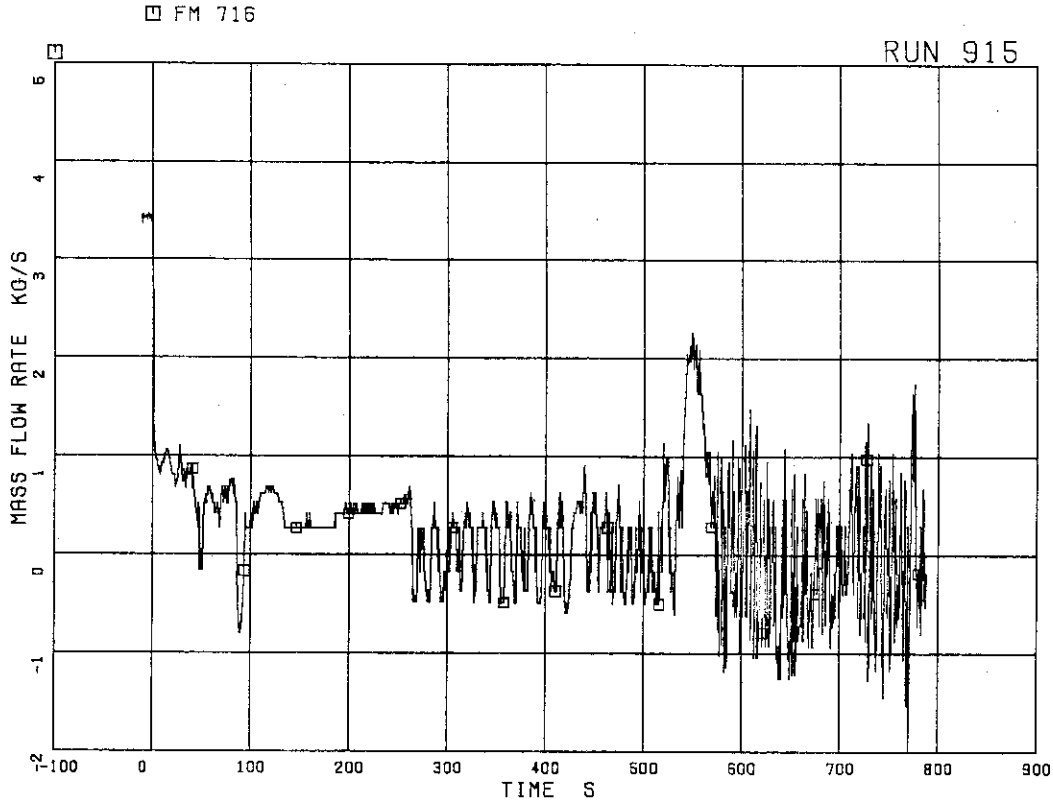

FIG.5.108 FLOW RATE AT CHANNEL C INLET

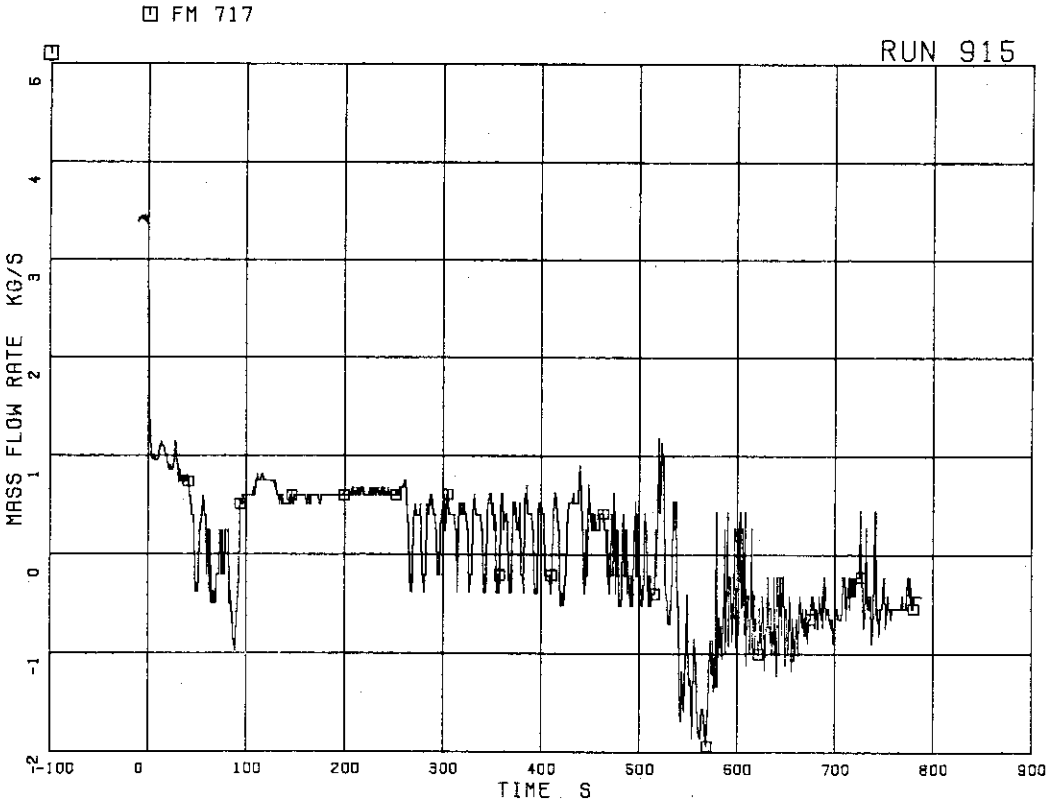

FIG.5.109 FLOW RATE AT CHANNEL D INLET

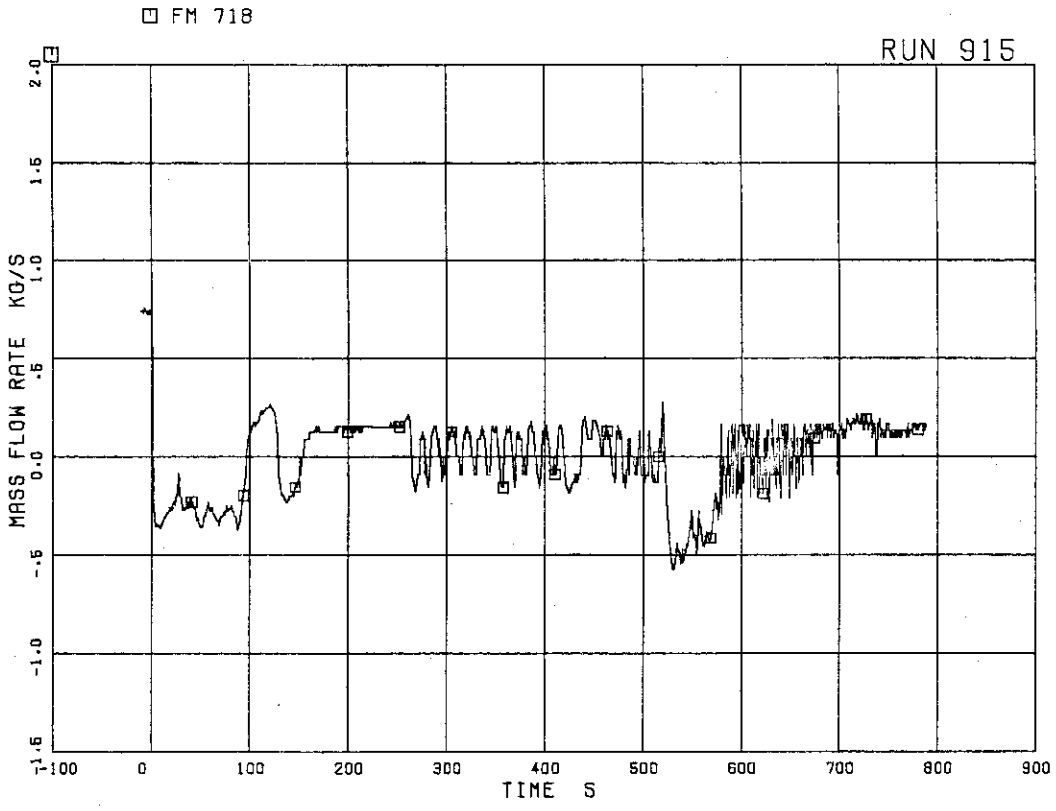

FIG.5.110 FLOW RATE AT BYPASS HOLE

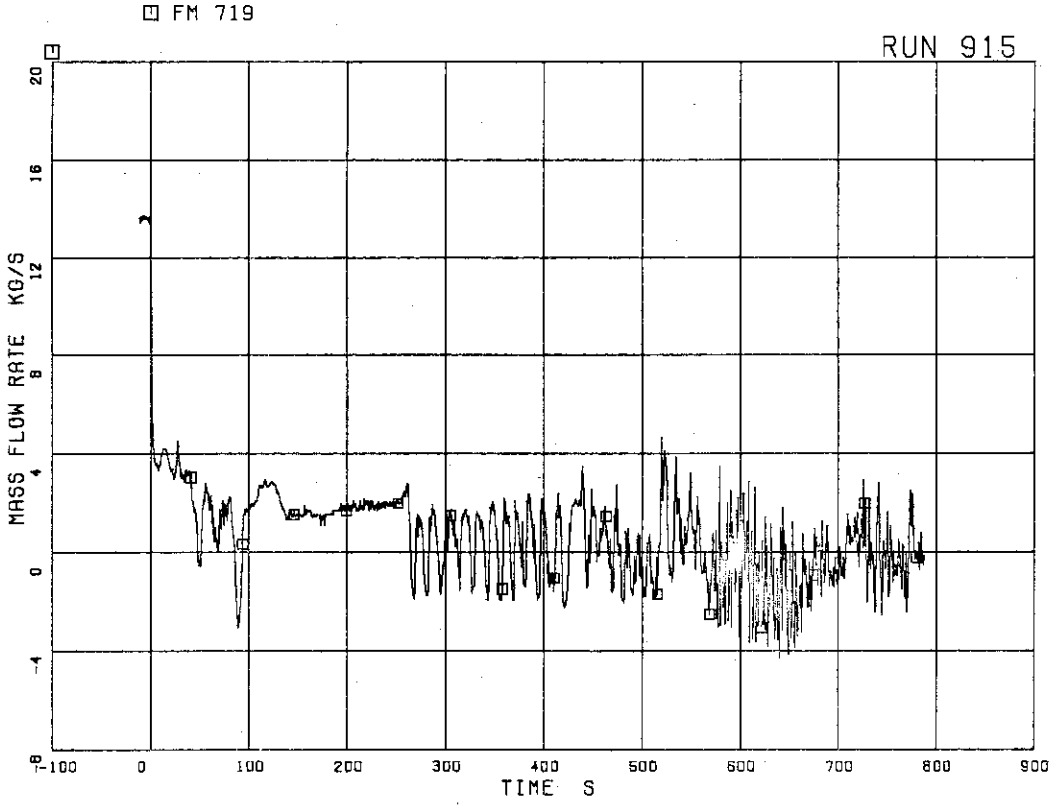

FIG.5.111 TOTAL CHANNEL INLET FLOW RATE

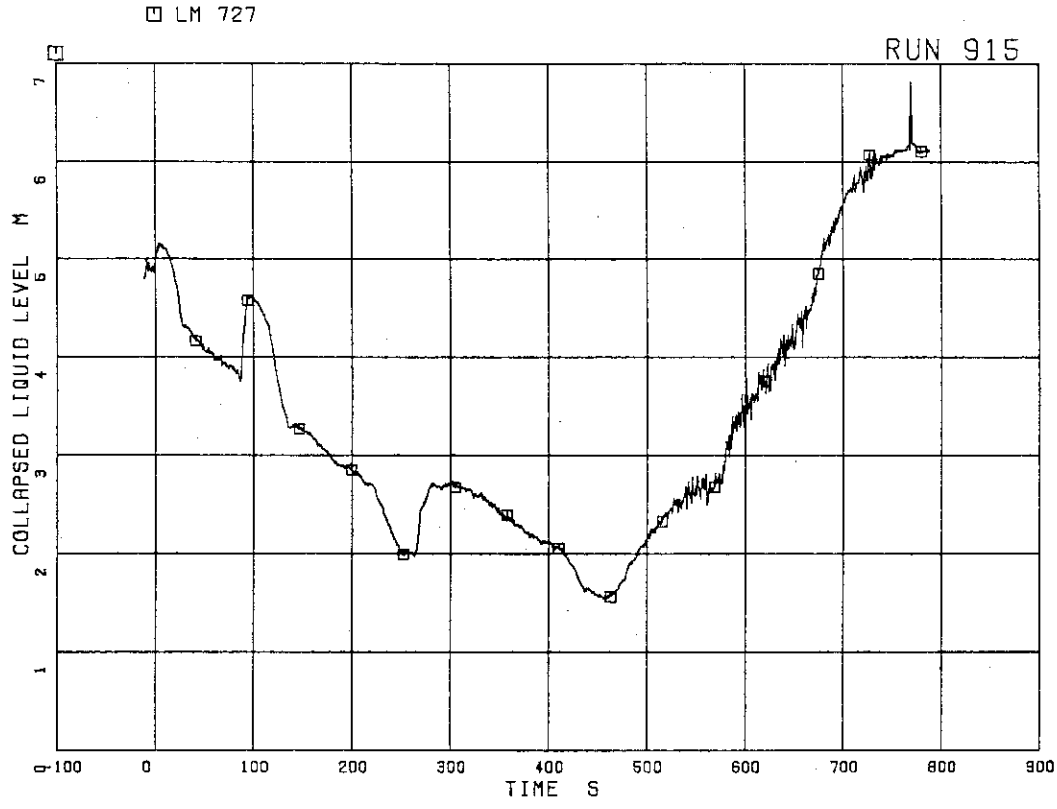

FIG.5.112 COLLAPSED LIQUID LEVEL IN DOWNCOMER

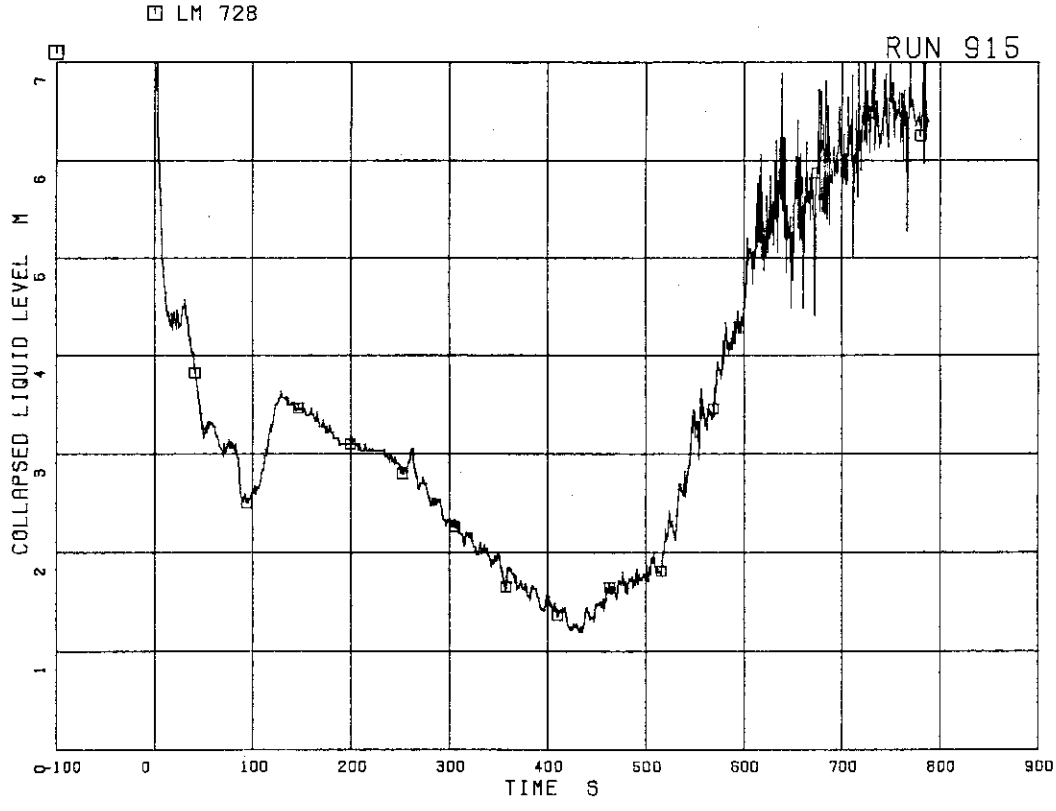

FIG.5.113 COLLAPSED LIQUID LEVEL INSIDE CORE SHROUD

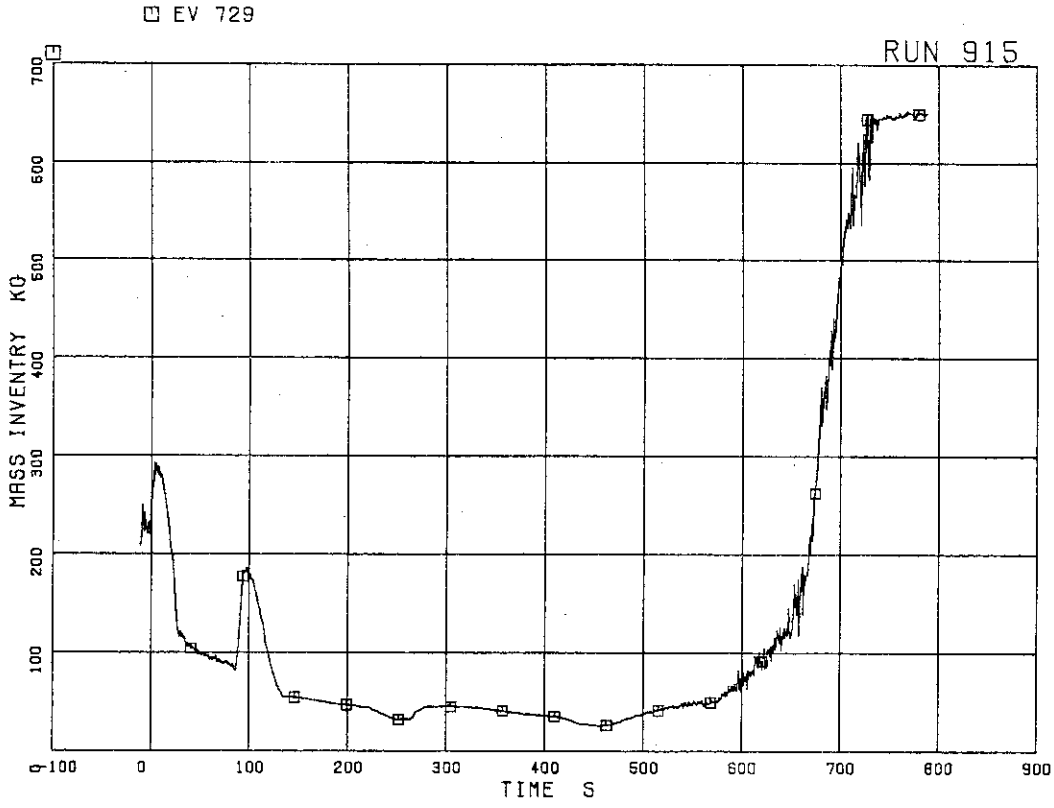

FIG.5.114 FLUID INVENTORY IN DOWNCOMER

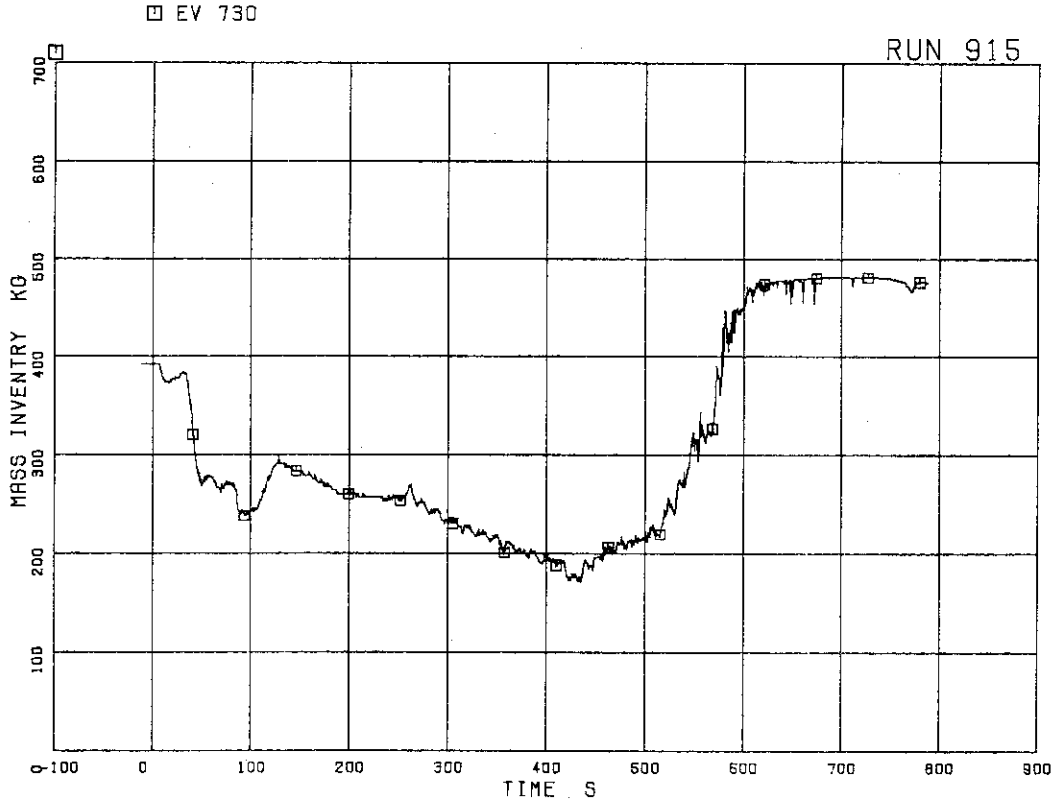

FIG.5.115 FLUID INVENTORY INSIDE CORE SHROUD

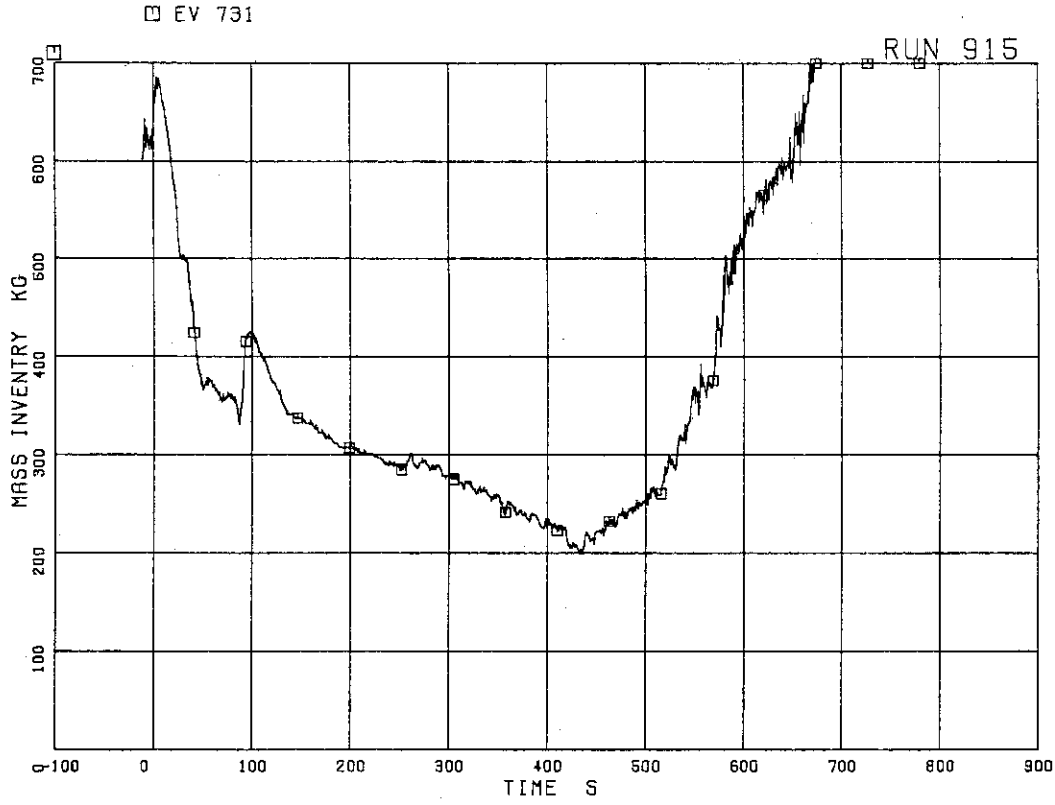

FIG.5.116 TOTAL FLUID INVENTORY IN PRESSURE VESSEL

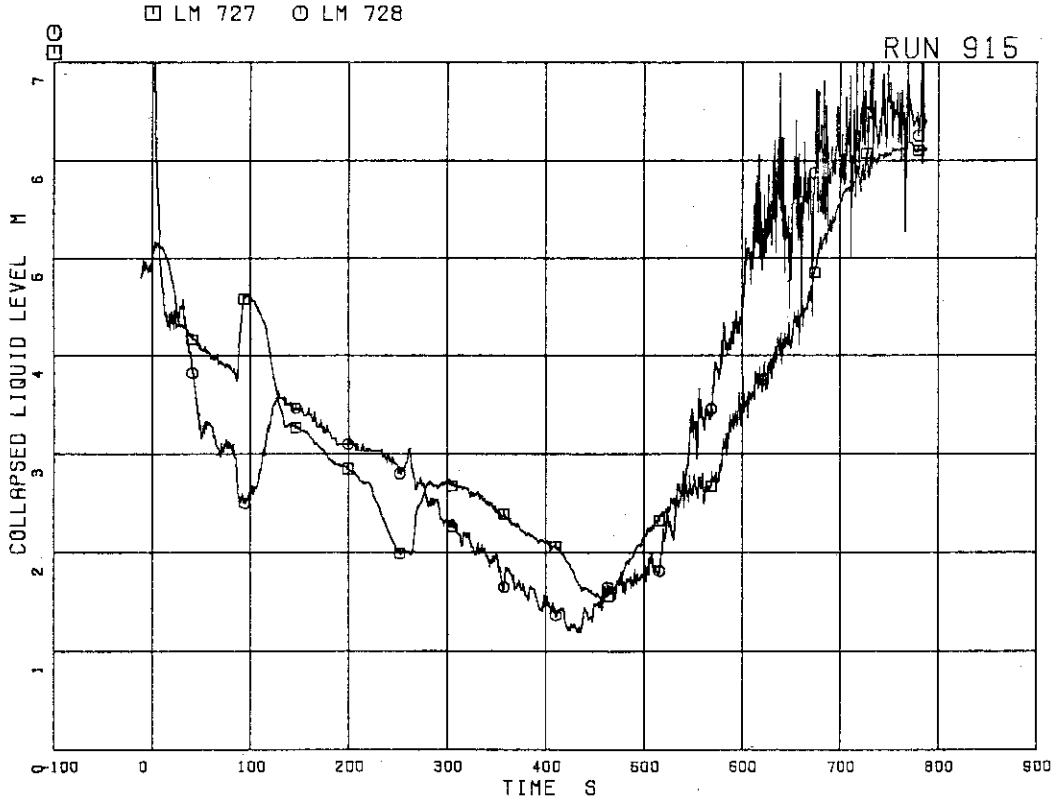

FIG.5.117 COLLAPSED LIQUID LEVELS IN DOWNCOMER AND INSIDE CORE-SHROUD

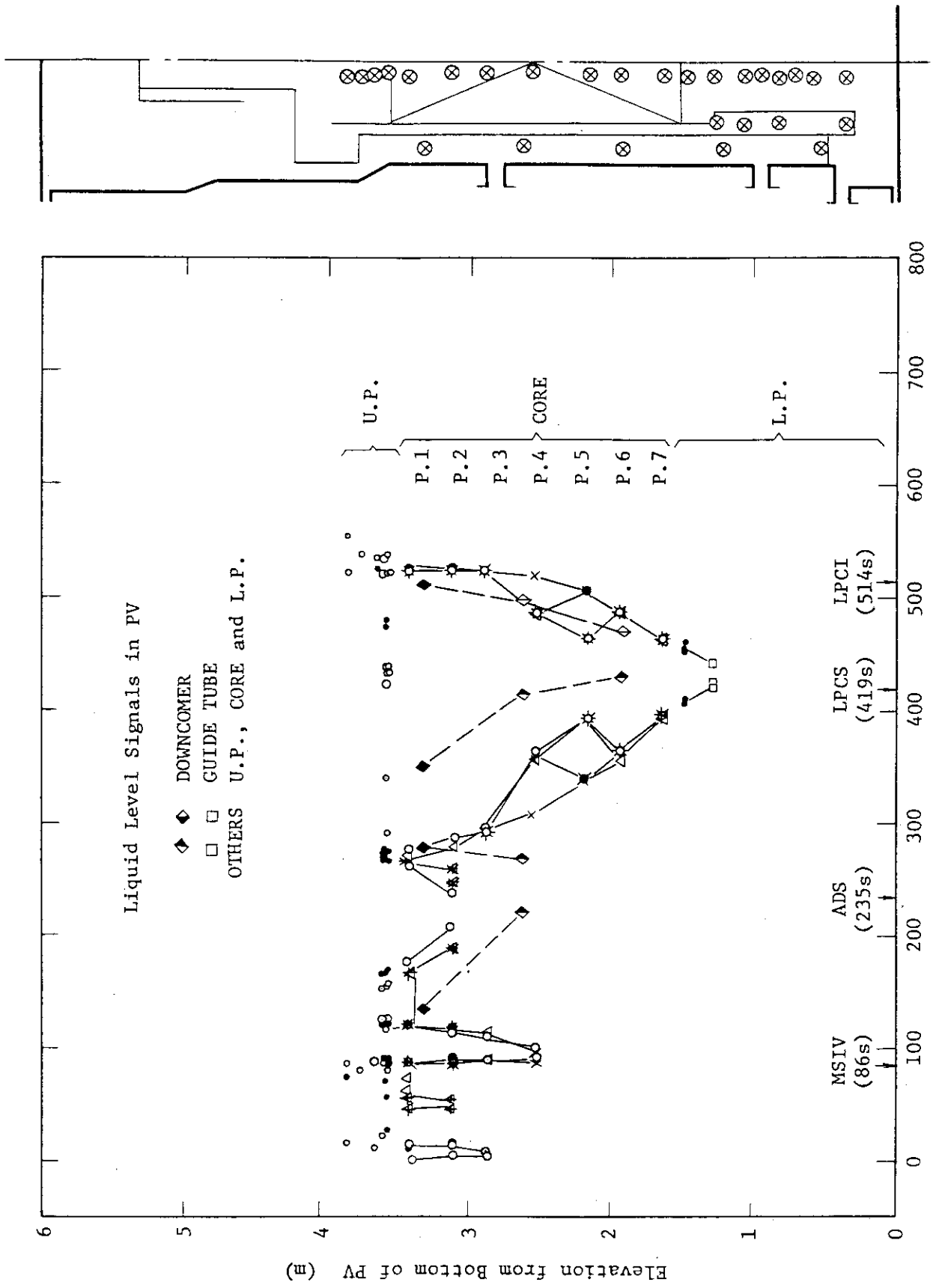

Fig. 5.118 Mixture levels in PV

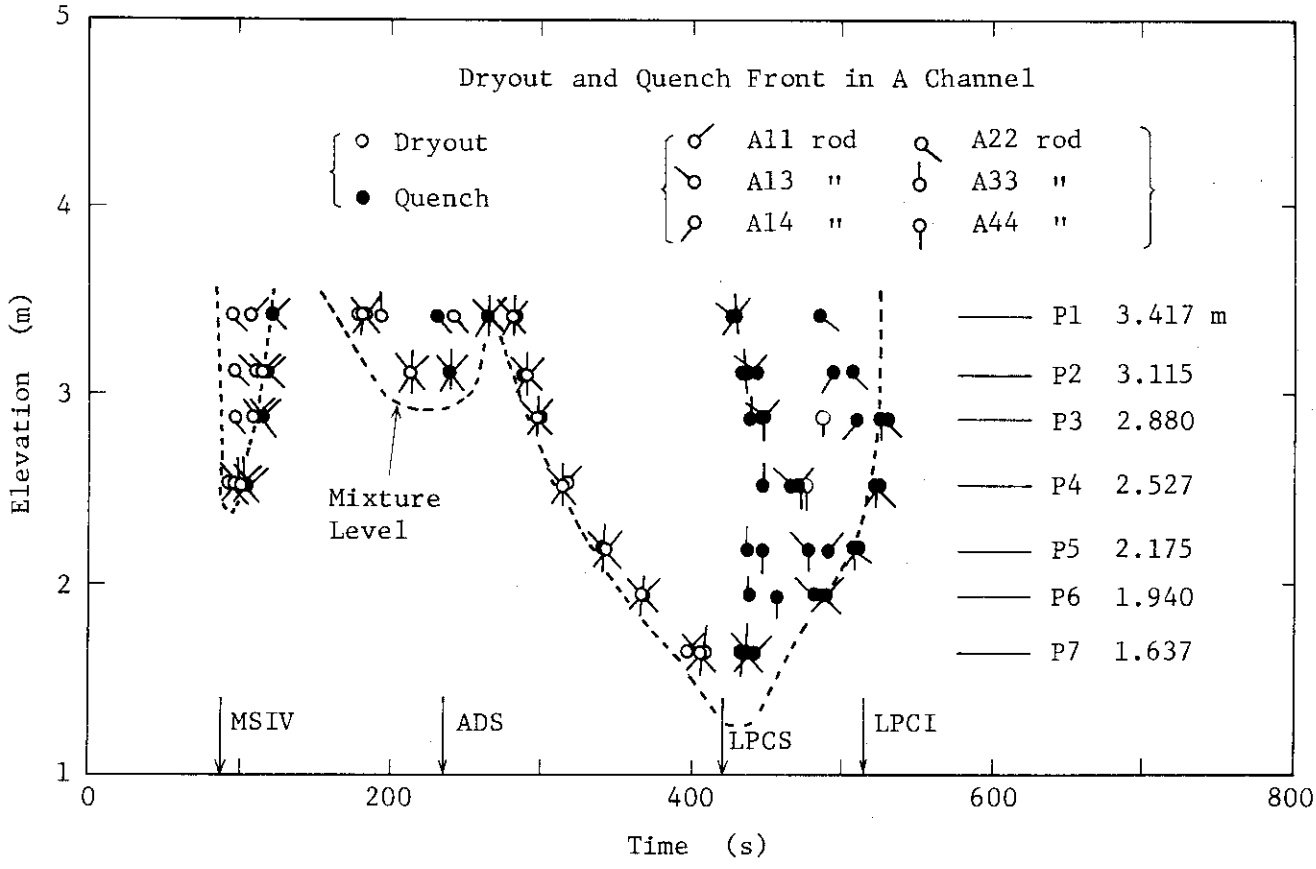

Fig. 5.119 Dryout and quench times of fuel rods in bundle A

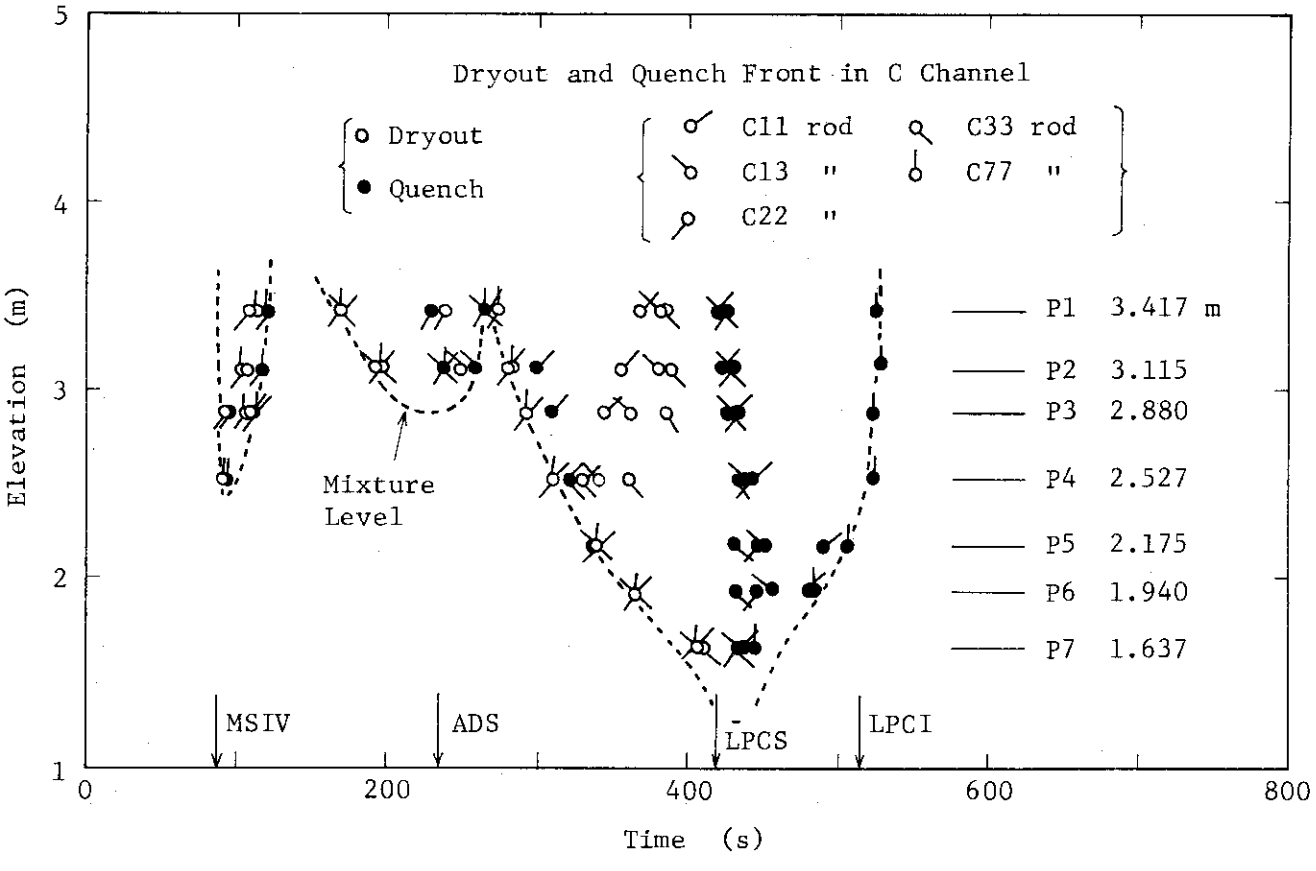

Fig. 5.120 Dryout and quench times of fuel rods in four bundles

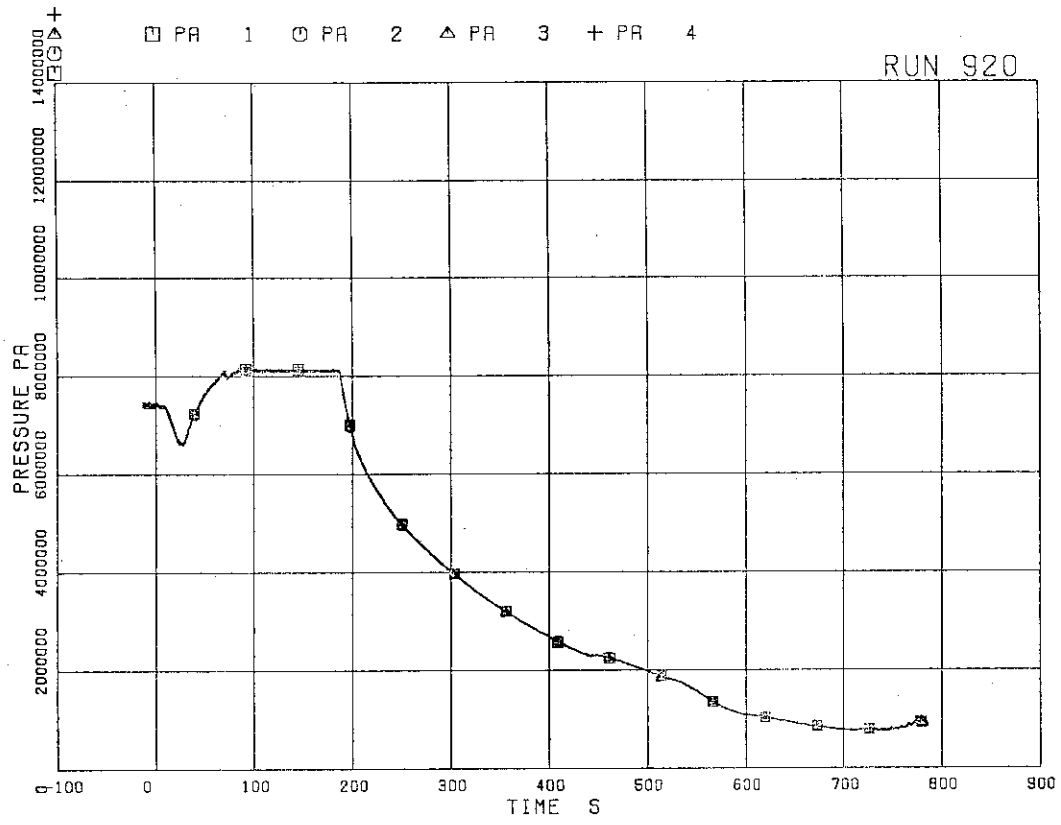

FIG.5.121 PRESSURE IN PV (PRESSURE VESSEL)

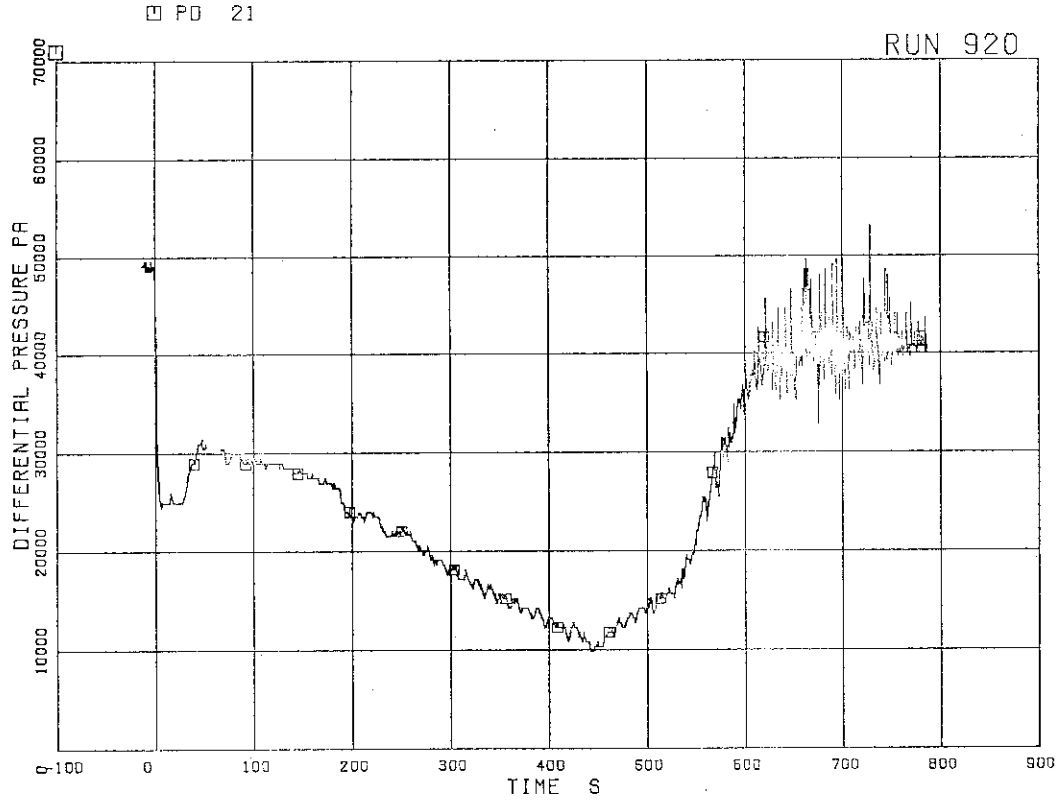

FIG.5.122 DIFFERENTIAL PRESSURE BETWEEN LOWER PLENUM AND UPPER PLENUM

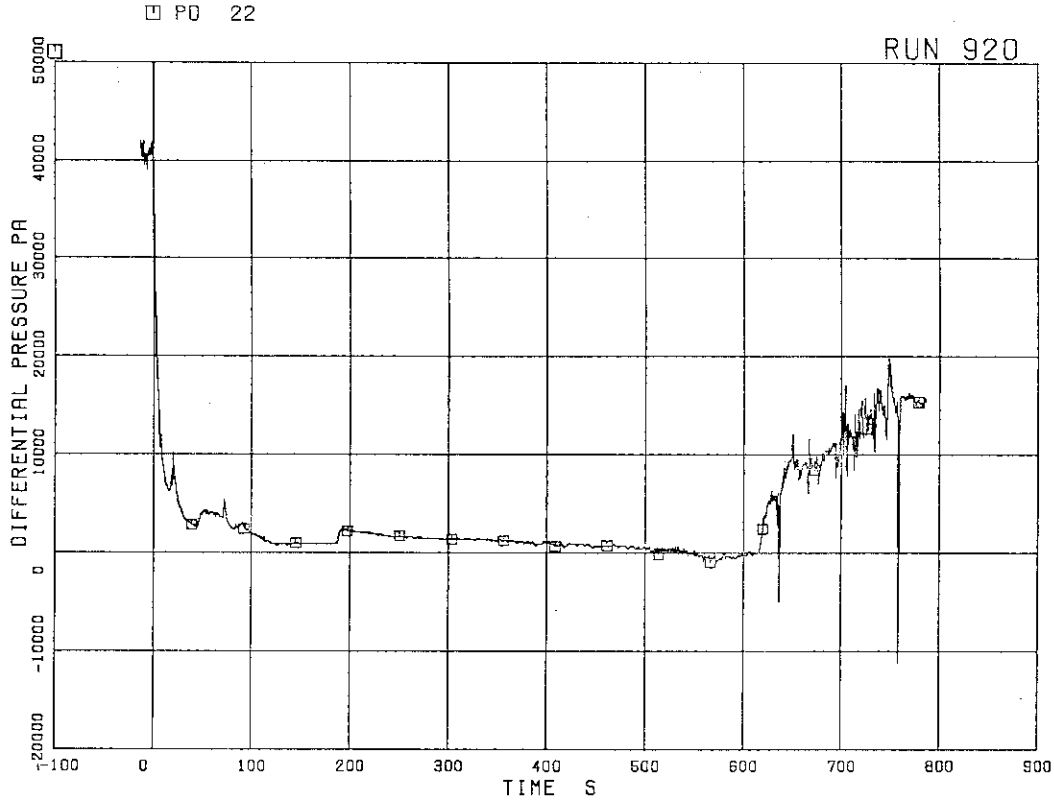

FIG.5.123 DIFFERENTIAL PRESSURE BETWEEN UPPER PLENUM AND STEAM DOME

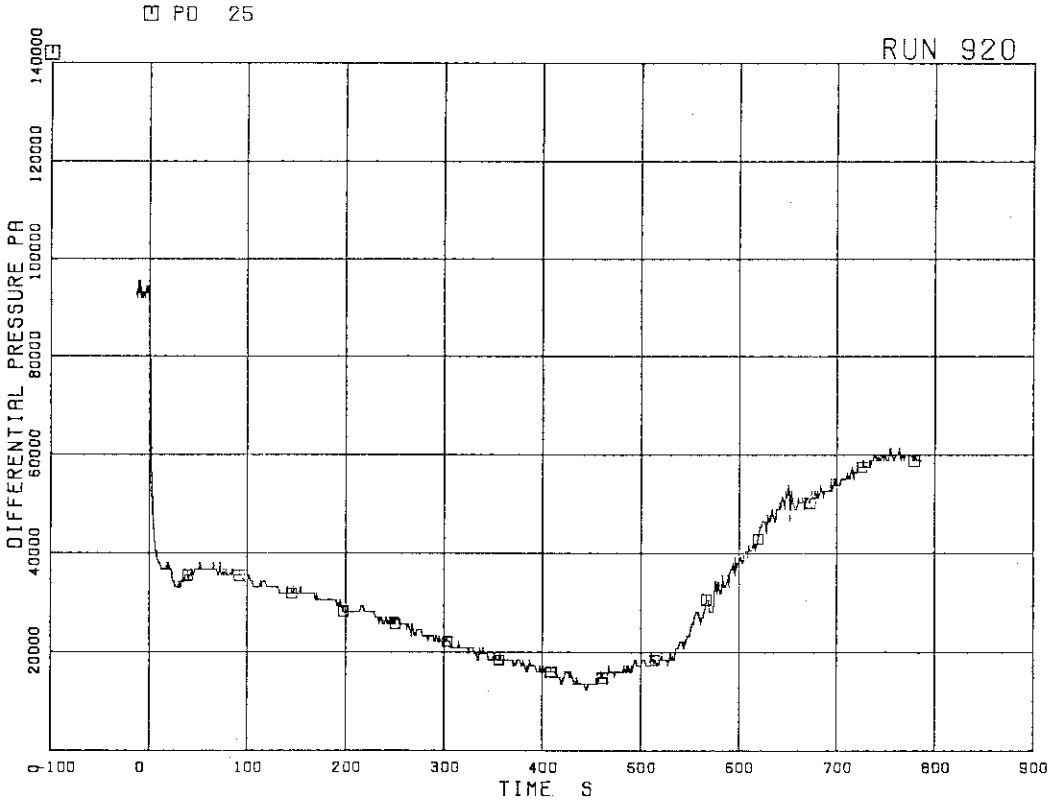

FIG.5.124 DIFFERENTIAL PRESSURE BETWEEN PV BOTTOM AND TOP

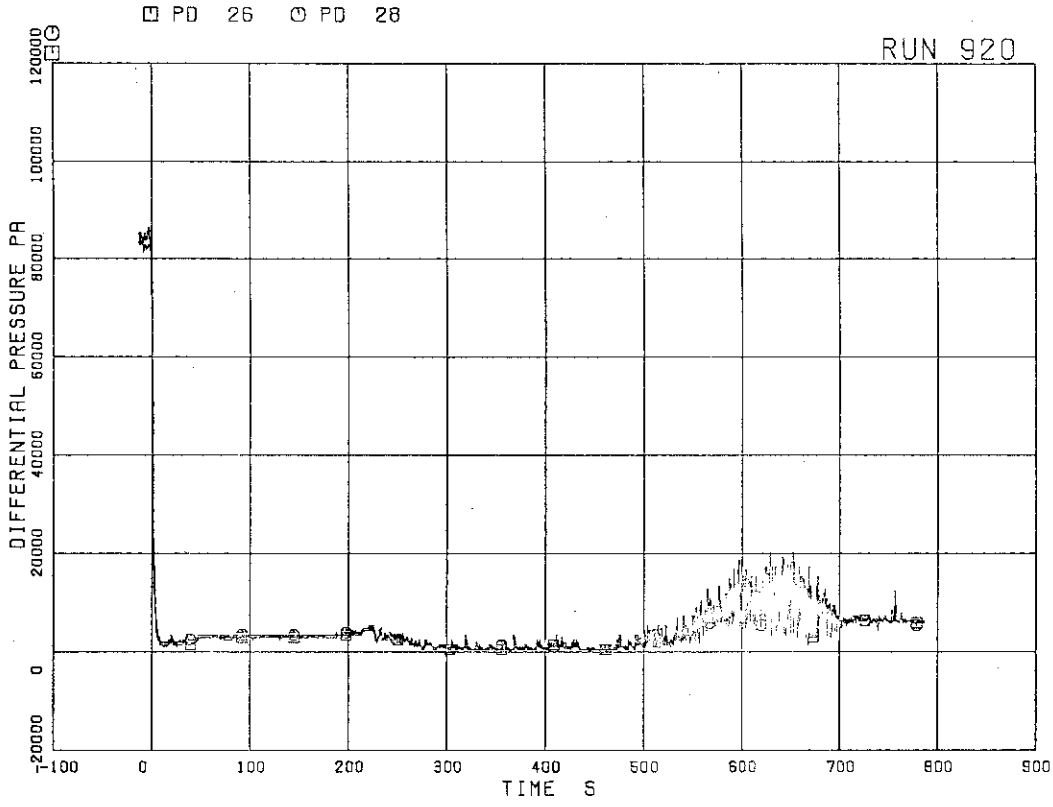

FIG.5.125 DIFFERENTIAL PRESSURE BETWEEN JP-1,2 DISCHARGE AND SUCTION

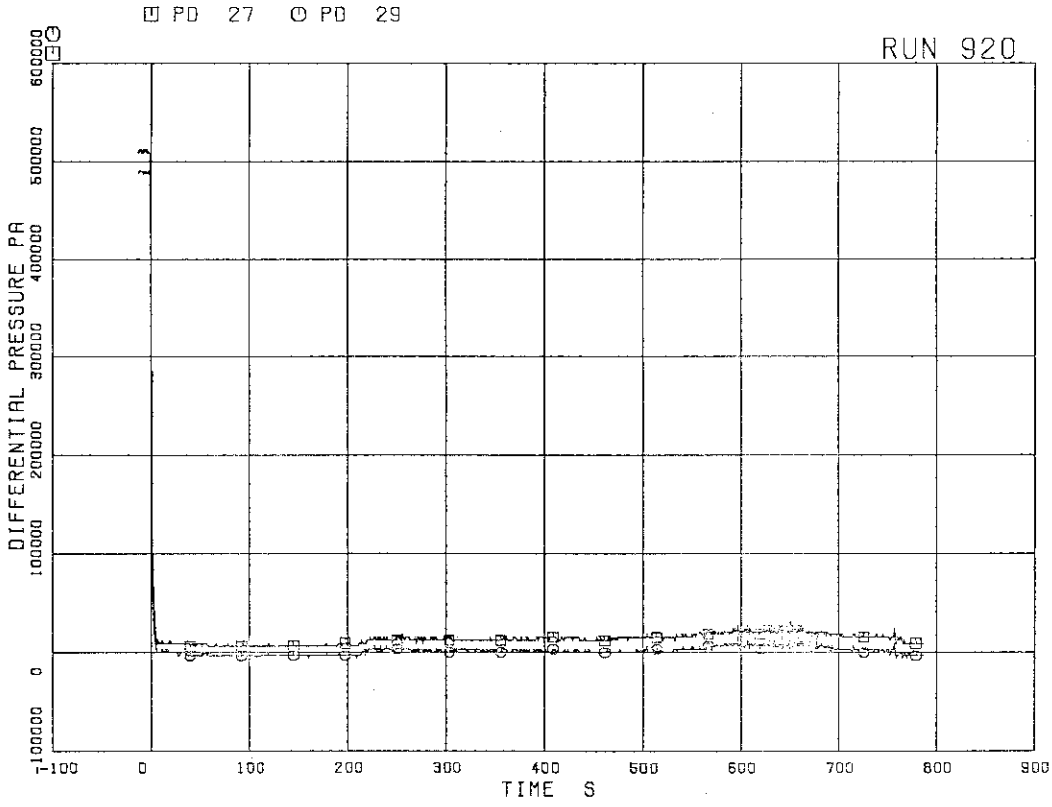

FIG.5.126 DIFFERENTIAL PRESSURE BETWEEN JP-1,2 DRIVE AND SUCTION

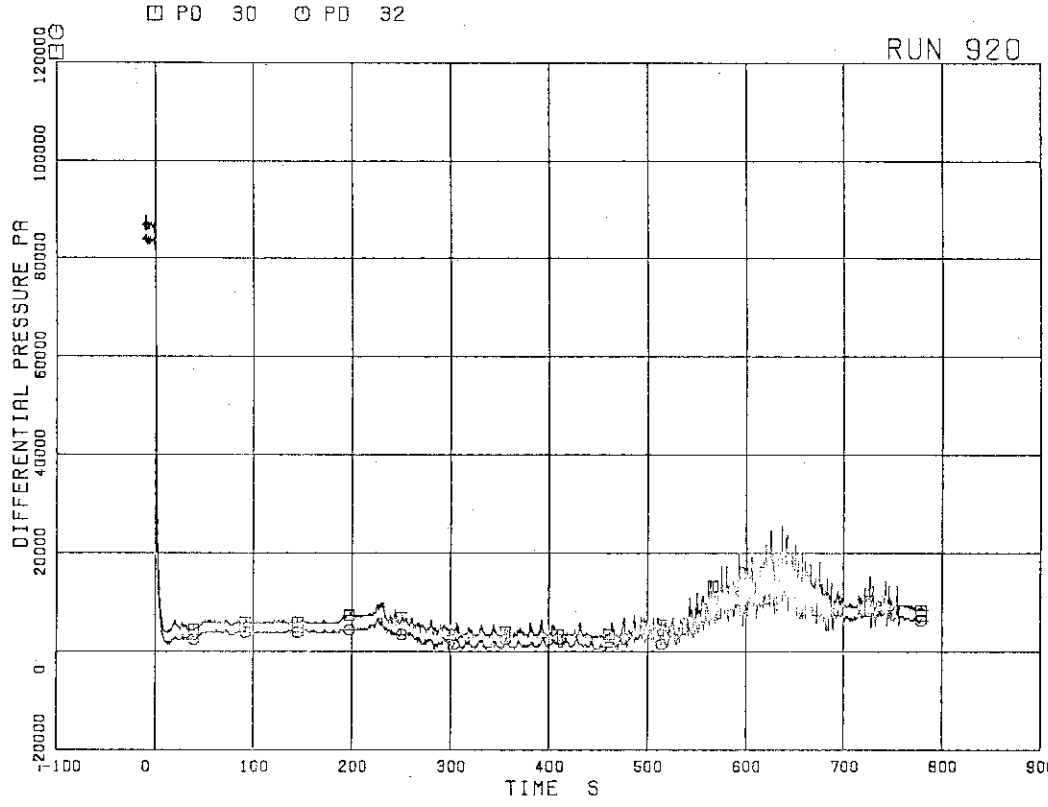

FIG.5.127 DIFFERENTIAL PRESSURE BETWEEN JP-3,4 DISCHARGE AND SUCTION

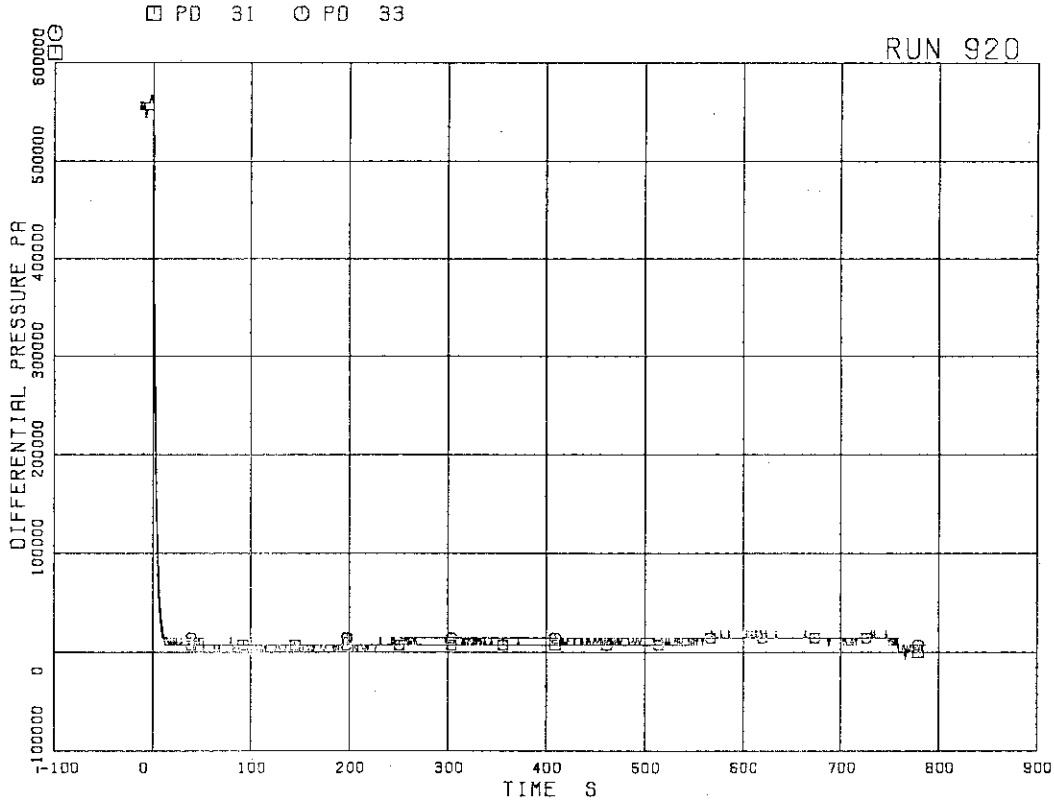

FIG.5.128 DIFFERENTIAL PRESSURE BETWEEN JP-3,4 DRIVE AND SUCTION

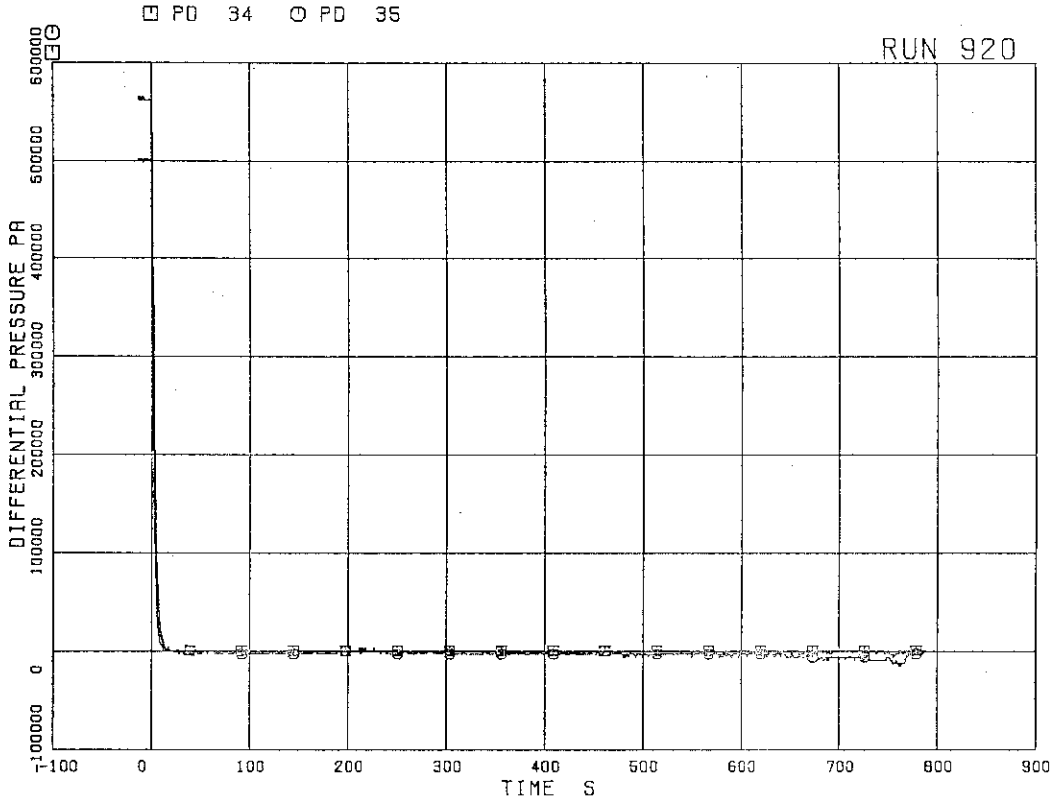

FIG.5.129 DIFFERENTIAL PRESSURE BETWEEN MRP DELIVERY AND SUCTION

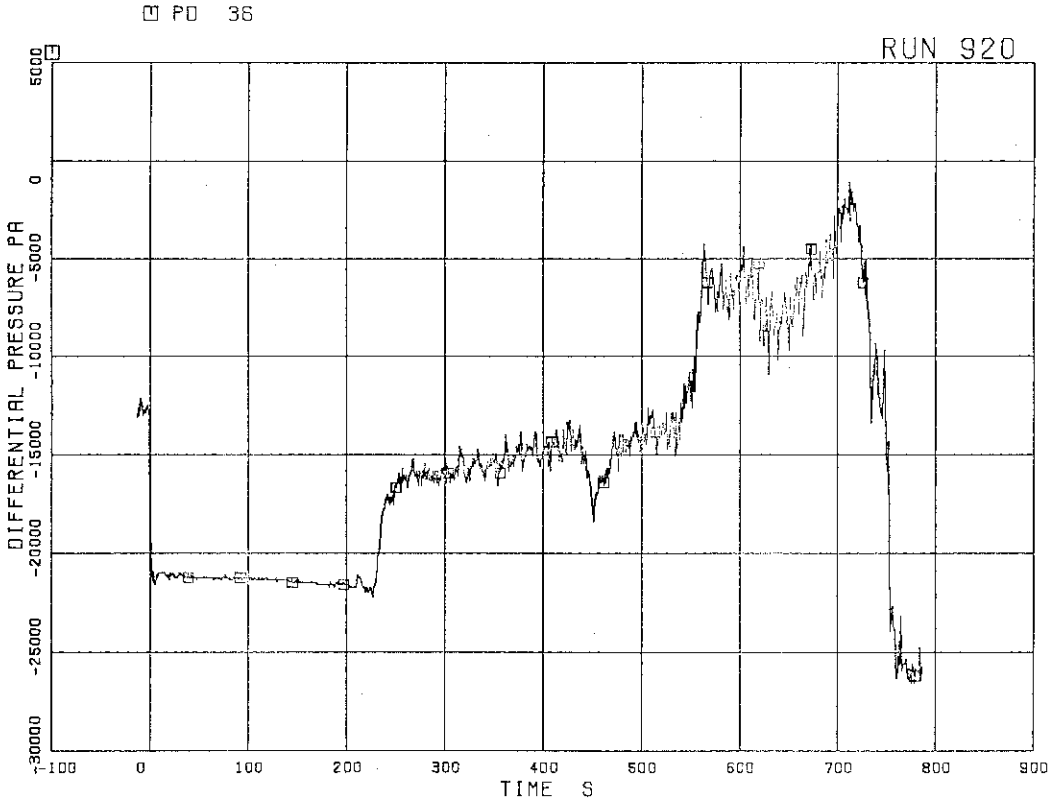

FIG.5.130 DIFFERENTIAL PRESSURE BETWEEN DOWNCOMER BOTTOM AND MRP1 SUCTION

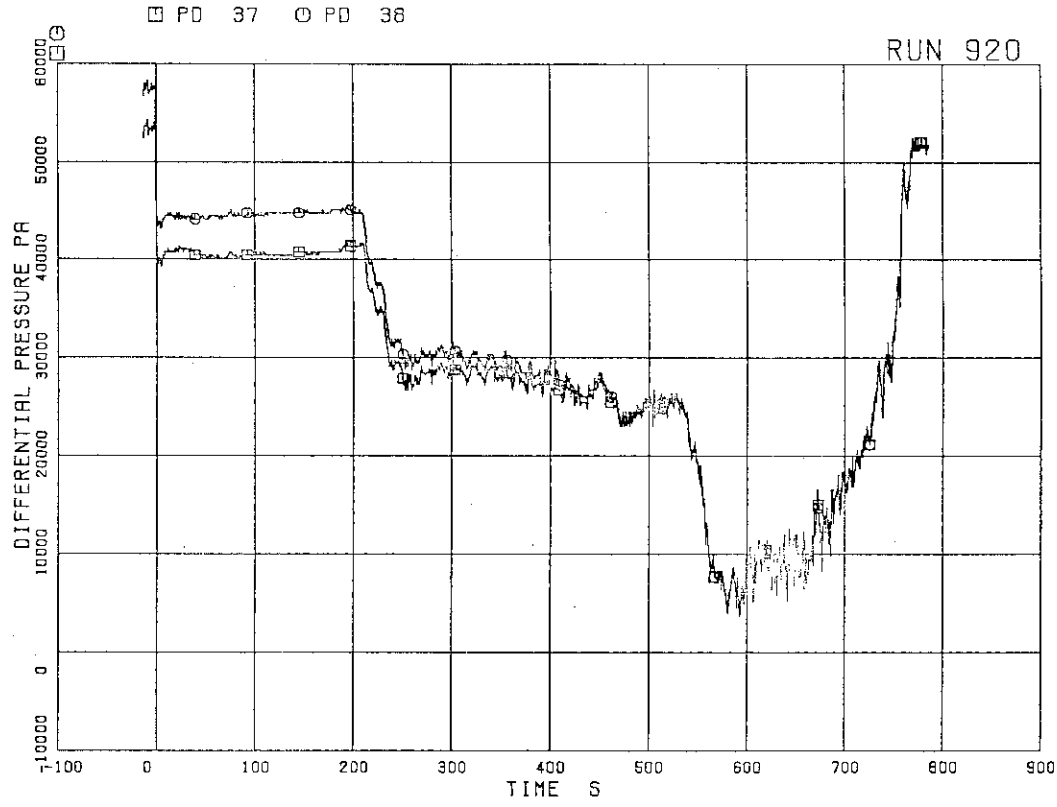

FIG.5.131 DIFFERENTIAL PRESSURE BETWEEN MRP DELIVERY AND JP-1,2 DRIVE

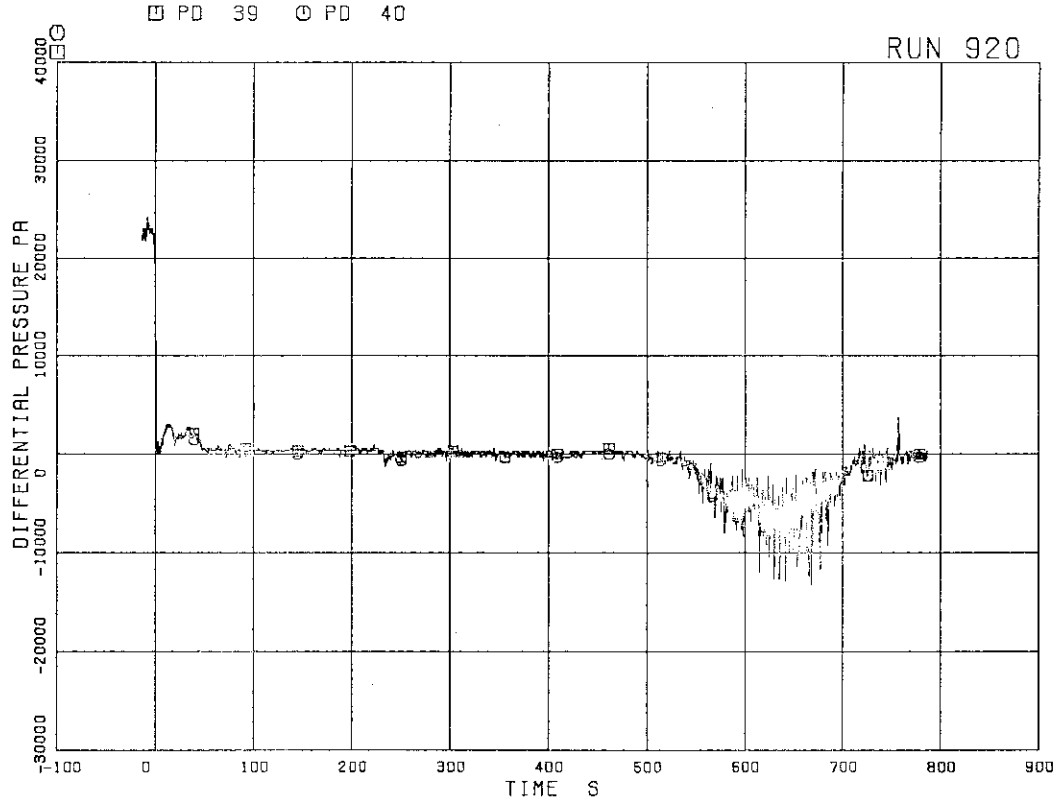

FIG.5.132 DIFFERENTIAL PRESSURE BETWEEN DOWNCOMER MIDDLE AND JP-1,2 SUCTION

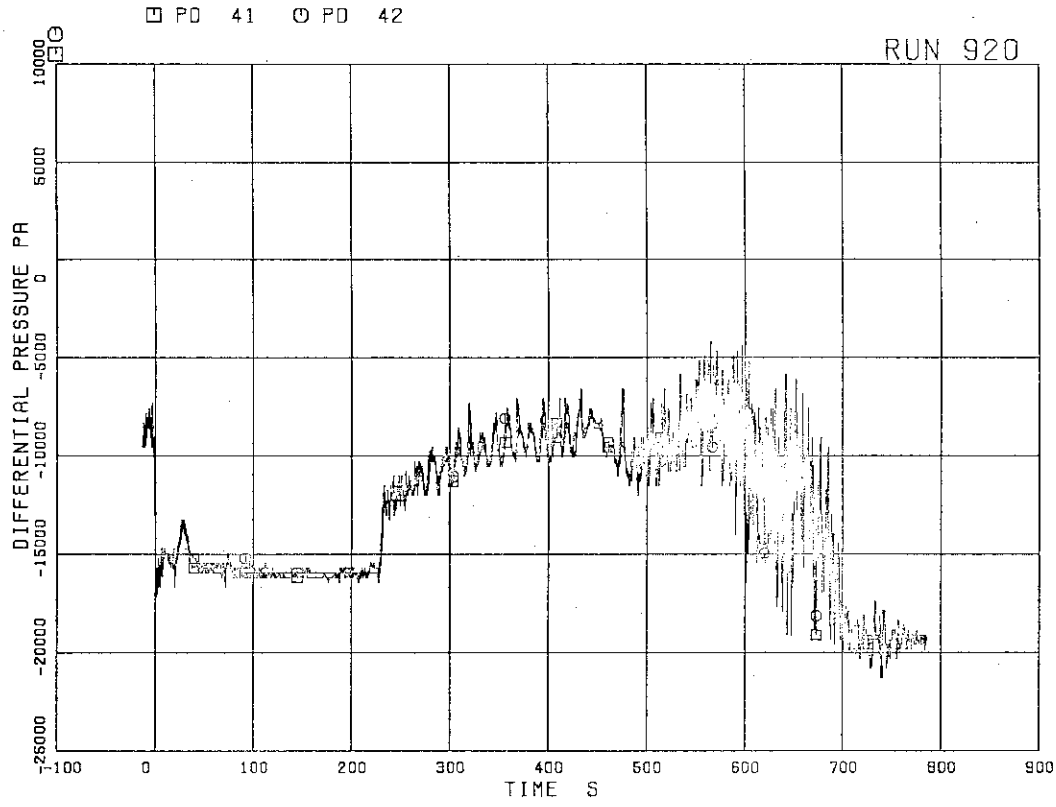

FIG.5.133 DIFFERENTIAL PRESSURE BETWEEN JP-1,2 DISCHARGE AND LOWER PLENUM

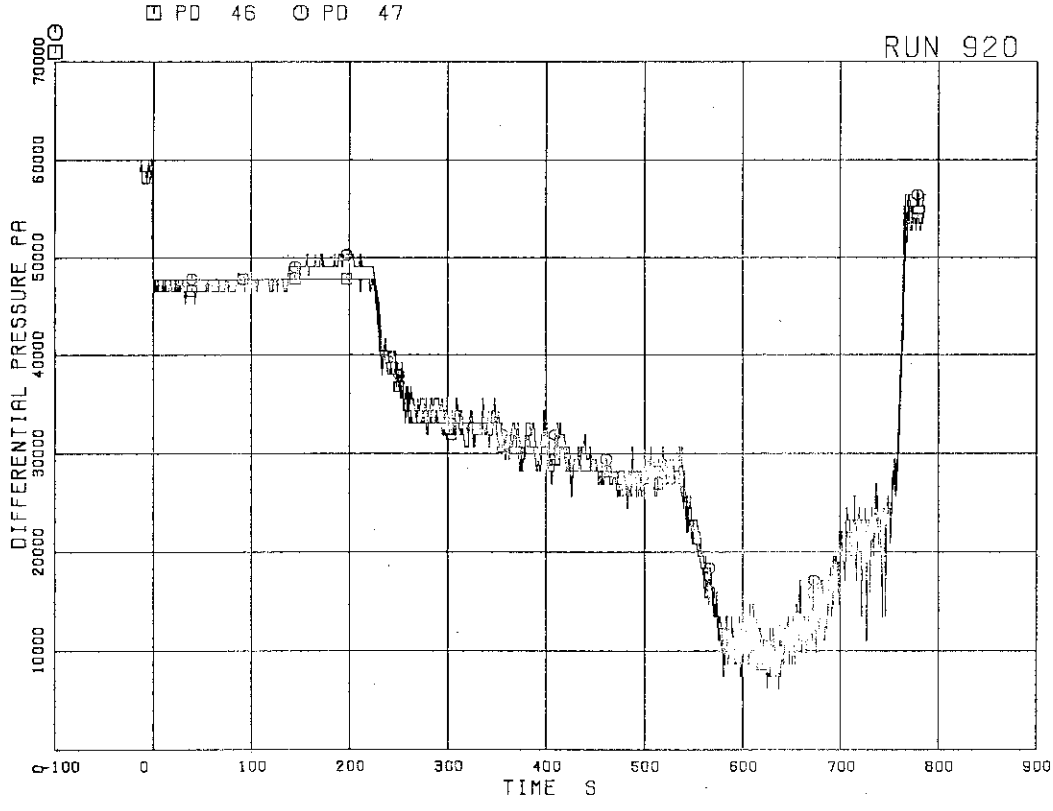

FIG.5.134 DIFFERENTIAL PRESSURE BETWEEN MRP DELIVERY AND JP-3,4 DRIVE

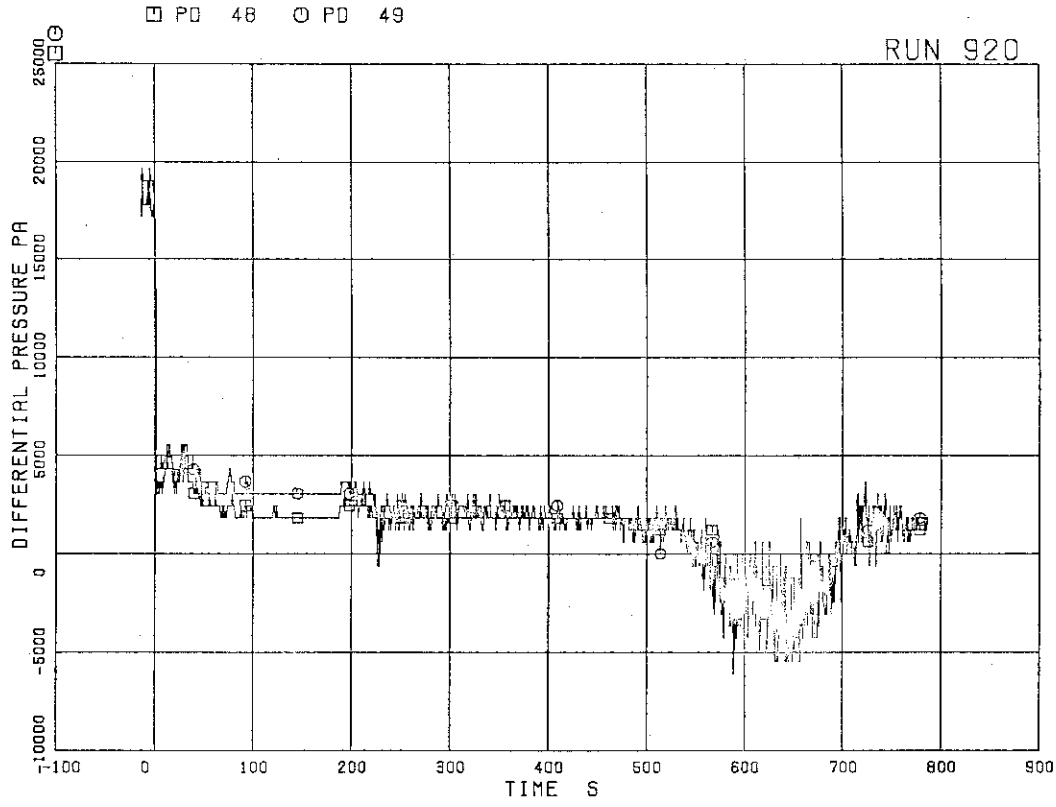

FIG.5.135 DIFFERENTIAL PRESSURE BETWEEN DOWNCOMER MIDDLE AND JP-3,4 SUCTION

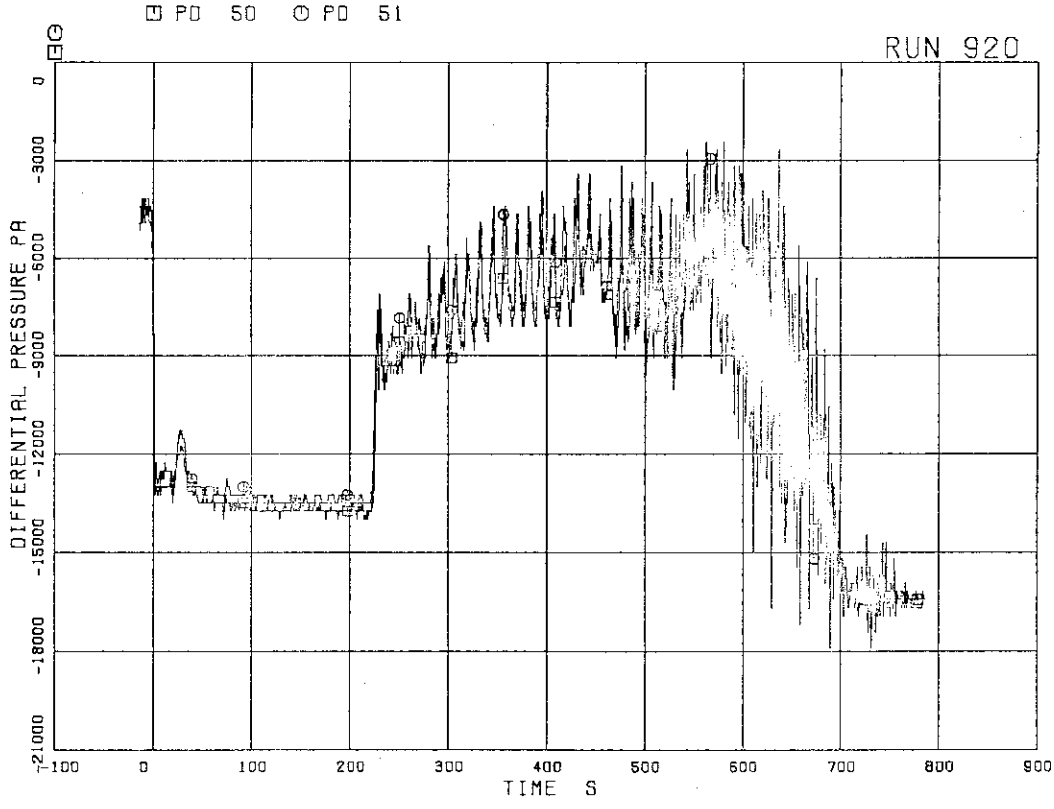

FIG.5.136 DIFFERENTIAL PRESSURE BETWEEN JP-3,4 DISCHARGE AND CONFLURNCE

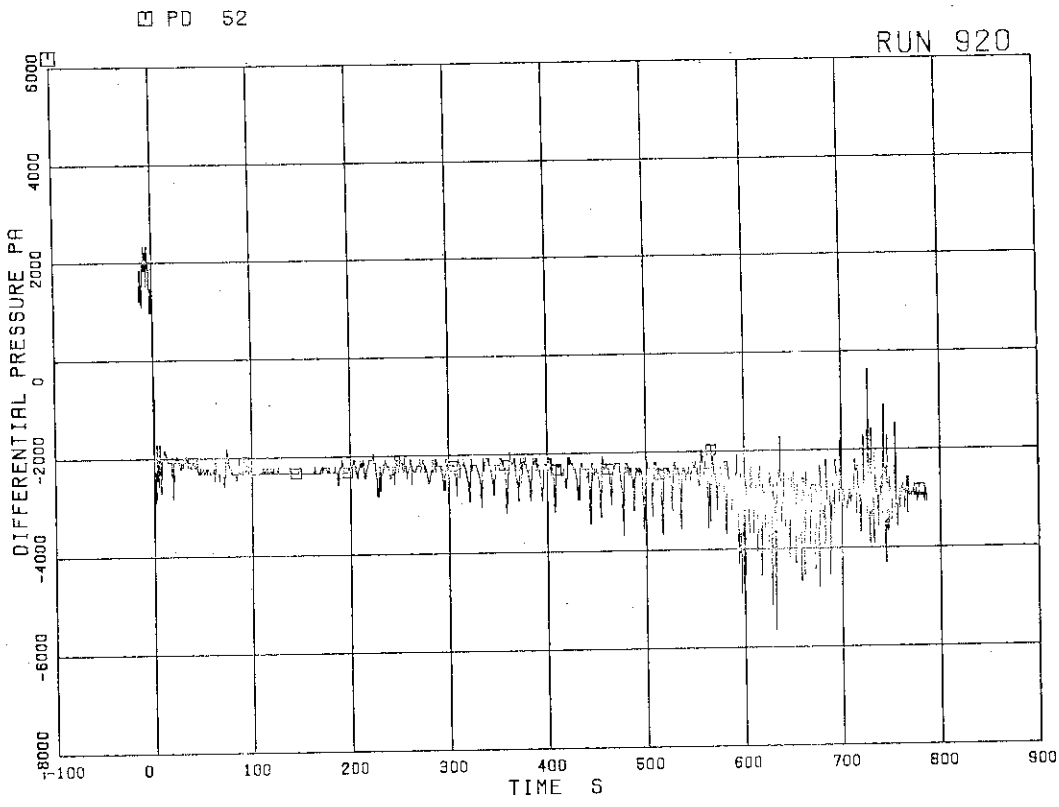

FIG.5.137 DIFFERENTIAL PRESSURE BETWEEN JP-3,4 CONFLUENCE IN BROKEN LOOP AND LP

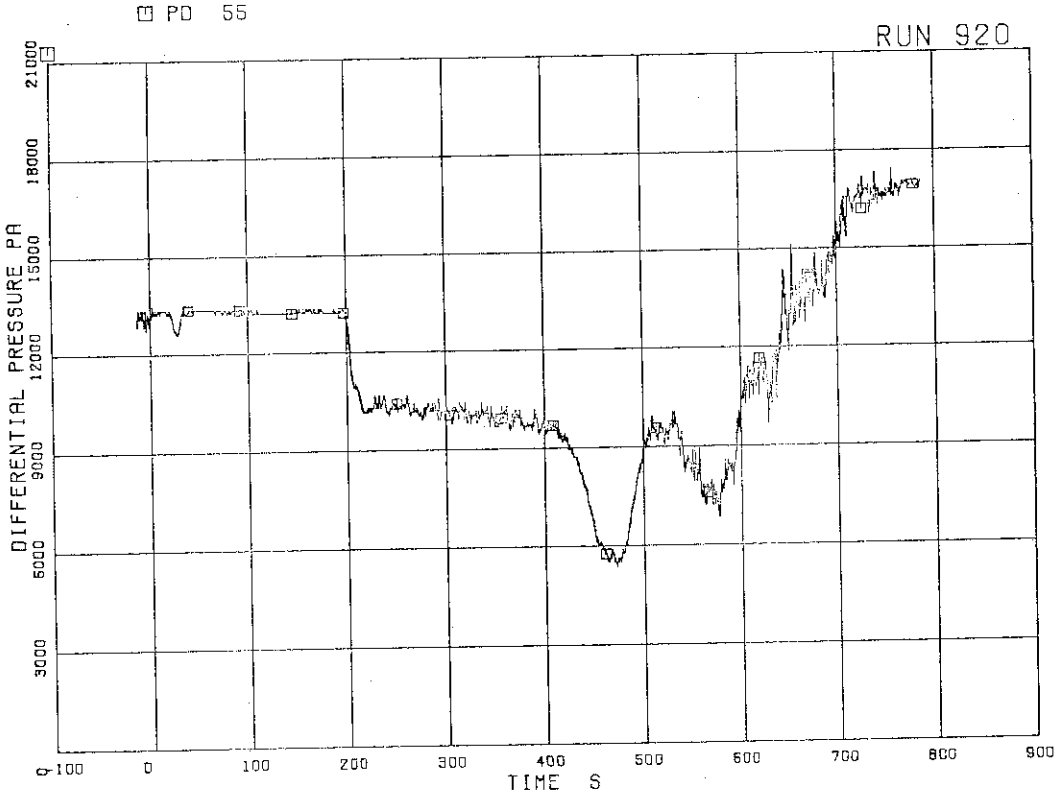

FIG.5.138 DIFFERENTIAL PRESSURE BETWEEN DOWNCOMER BOTTOM AND DOWNCOMER MIDDLE

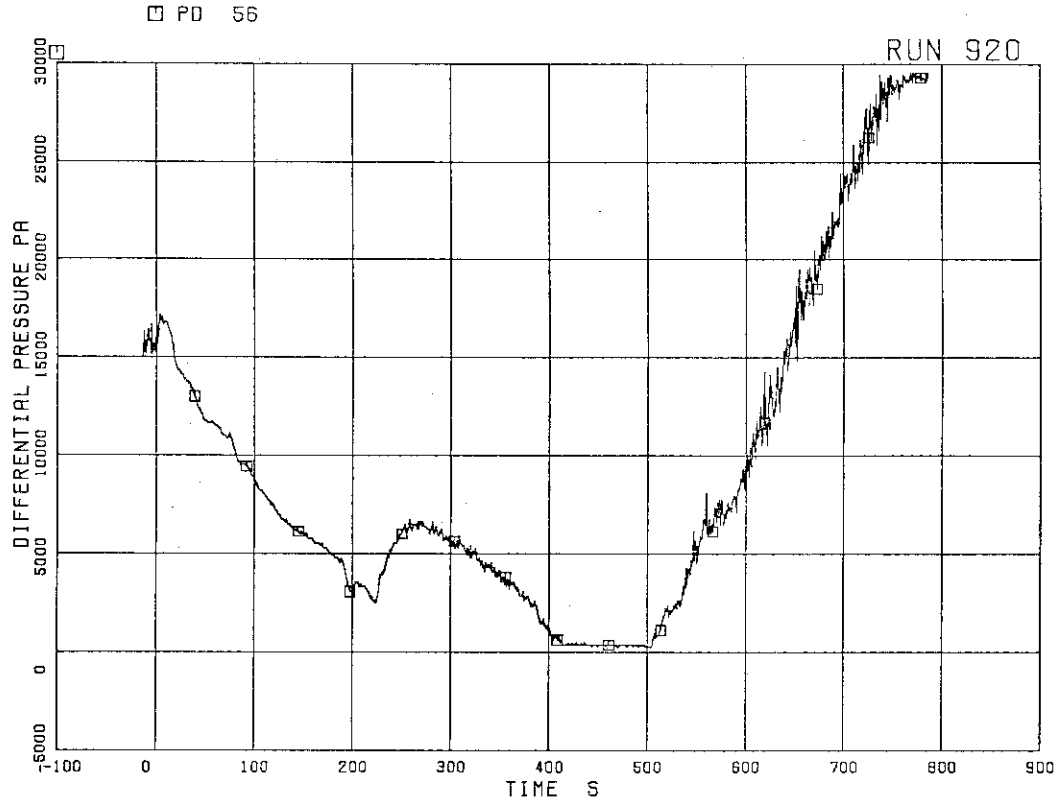

FIG.5.139 DIFFERENTIAL PRESSURE BETWEEN DOWNCOMER MIDDLE AND STEAM DOME

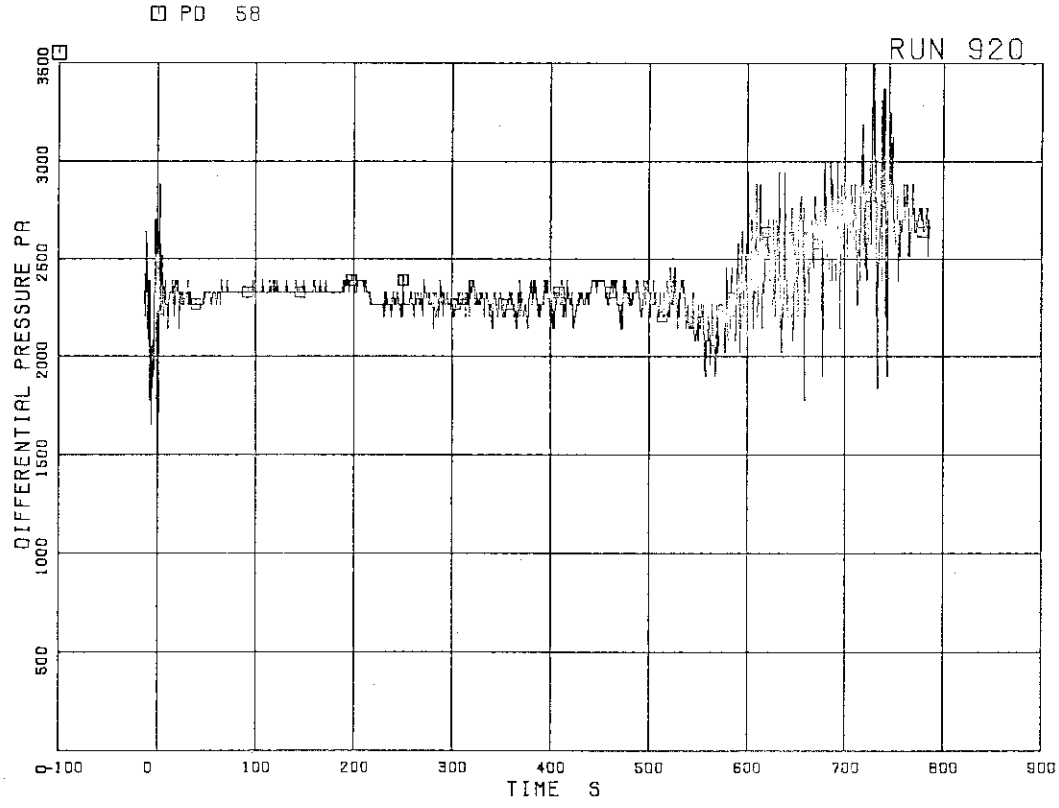

FIG.5.140 DIFFERENTIAL PRESSURE BETWEEN LP BOTTOM AND LP MIDDLE

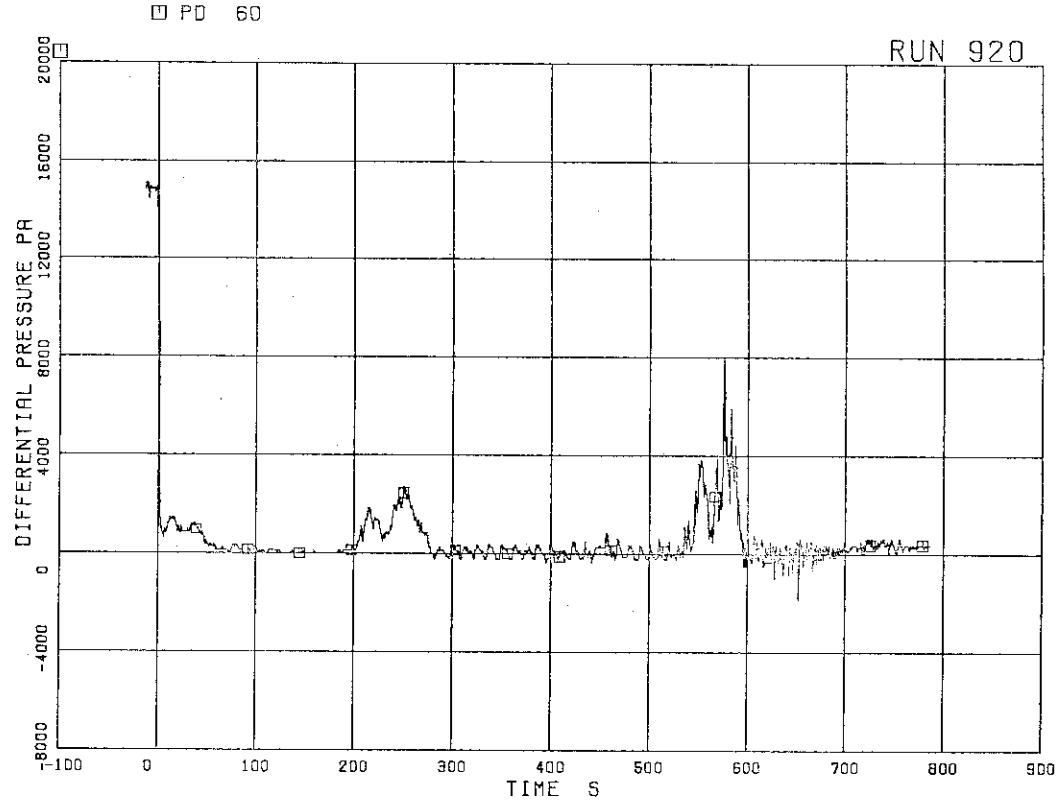

FIG.5.141 DIFFERENTIAL PRESSURE ACROSS CHANNEL INLET ORIFICE A

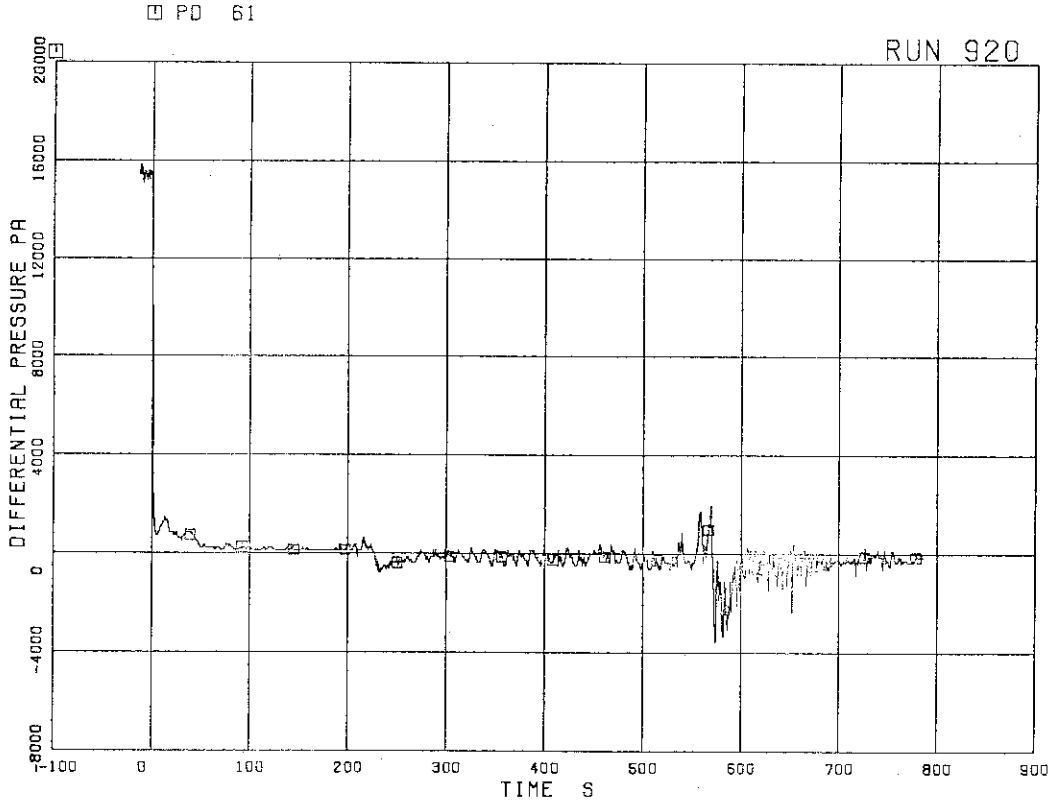

FIG.5.142 DIFFERENTIAL PRESSURE ACROSS CHANNEL INLET ORIFICE B

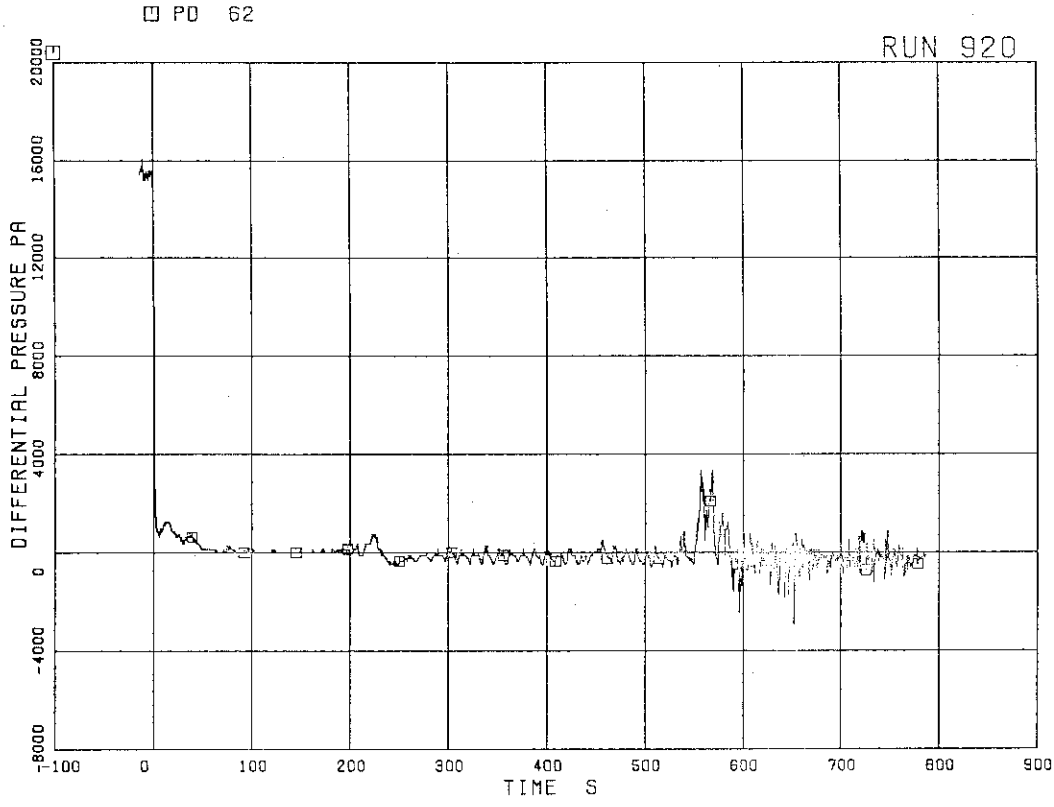

FIG.5.143 DIFFERENTIAL PRESSURE ACROSS CHANNEL INLET ORIFICE C

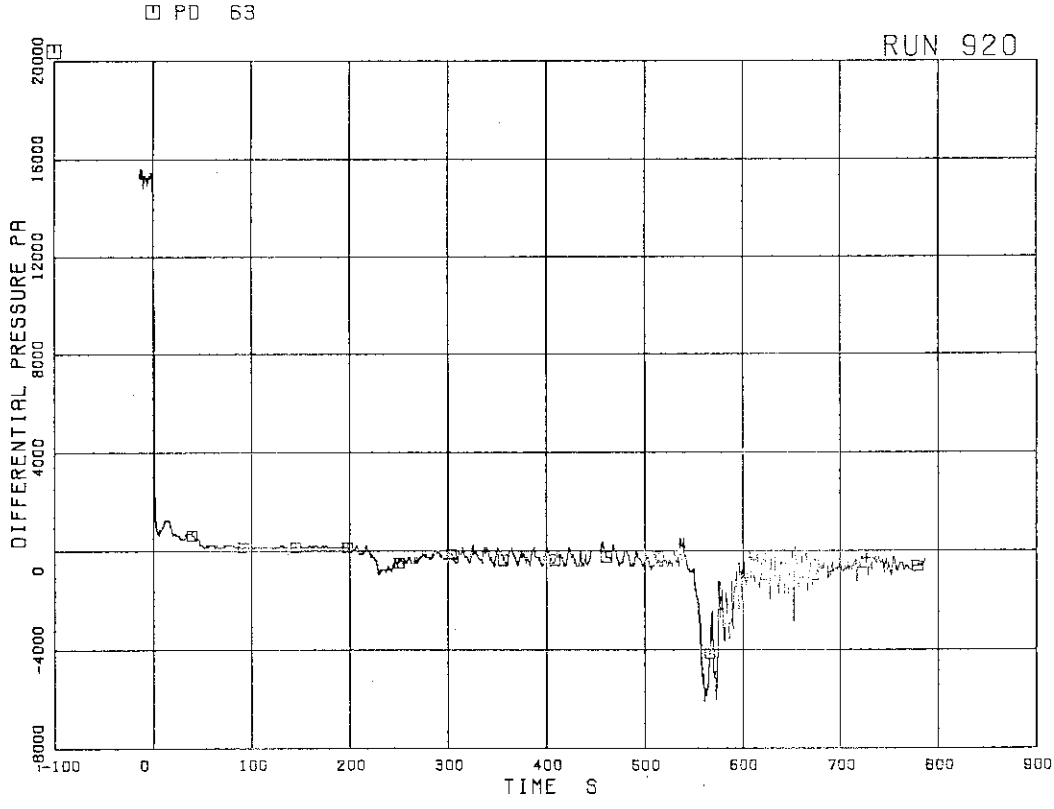

FIG.5.144 DIFFERENTIAL PRESSURE ACROSS CHANNEL INLET ORIFICE D

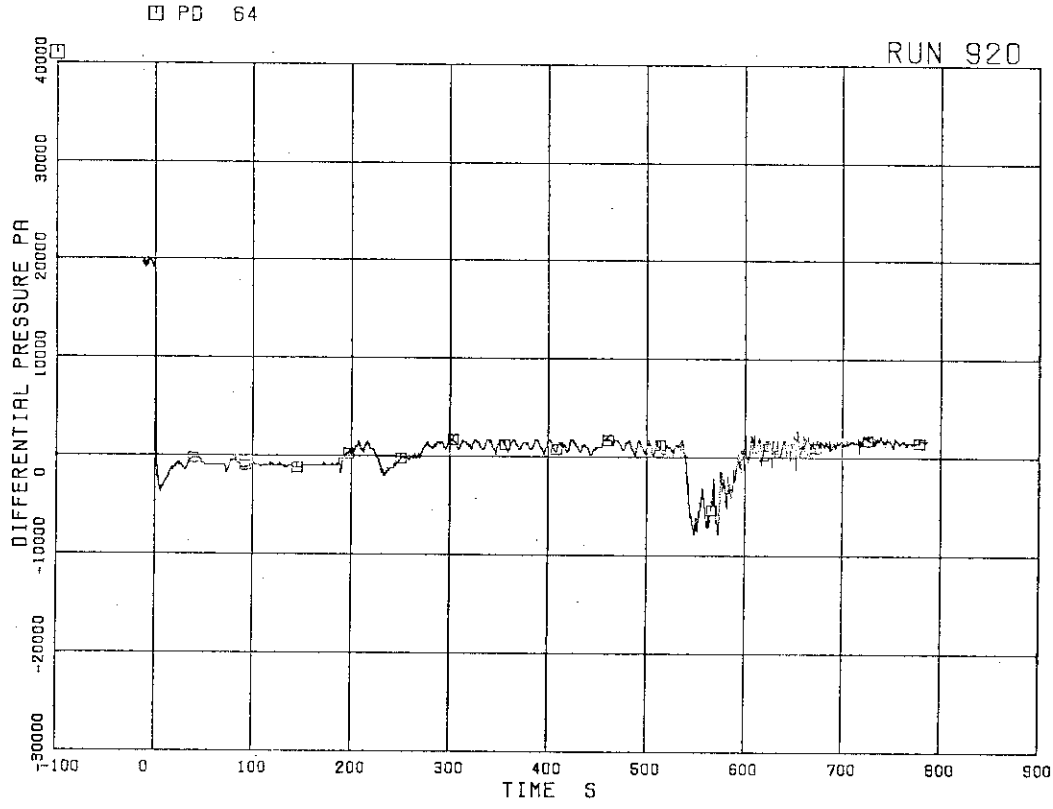

FIG.5.145 DIFFERENTIAL PRESSURE ACROSS BYPASS HOLE

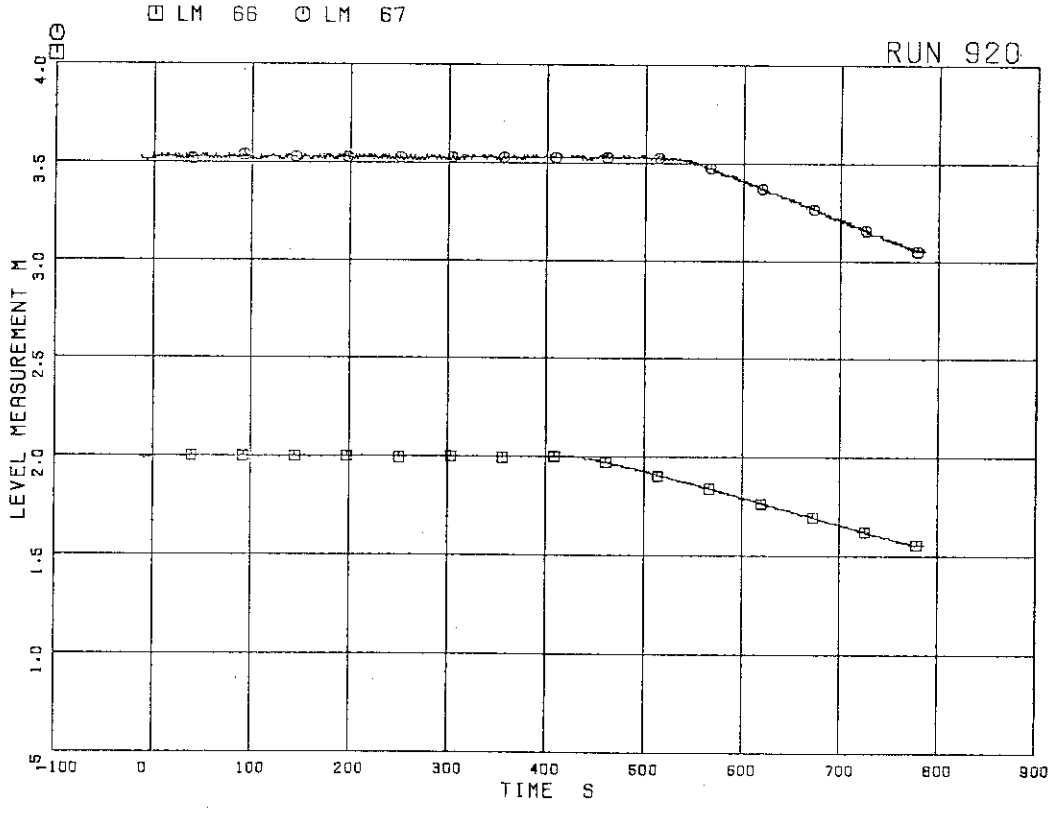

FIG.5.146 LIQUID LEVELS IN ECCS TANKS

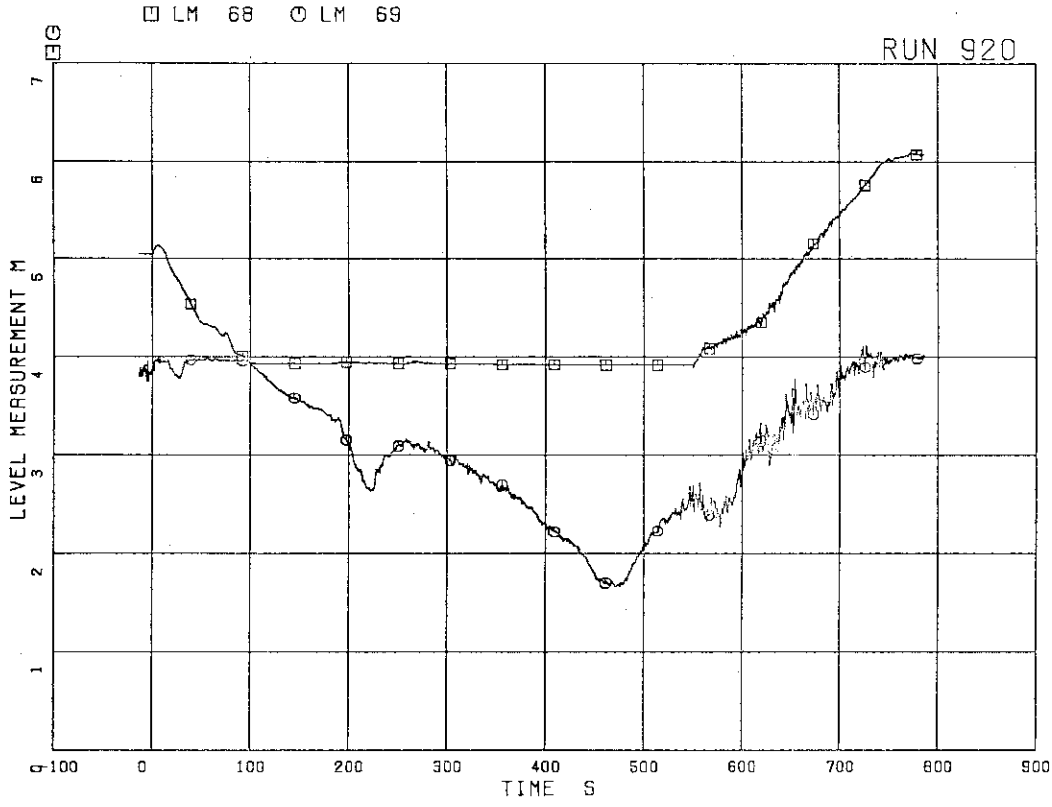

FIG.5.147 LIQUID LEVEL IN DOWNCOMER

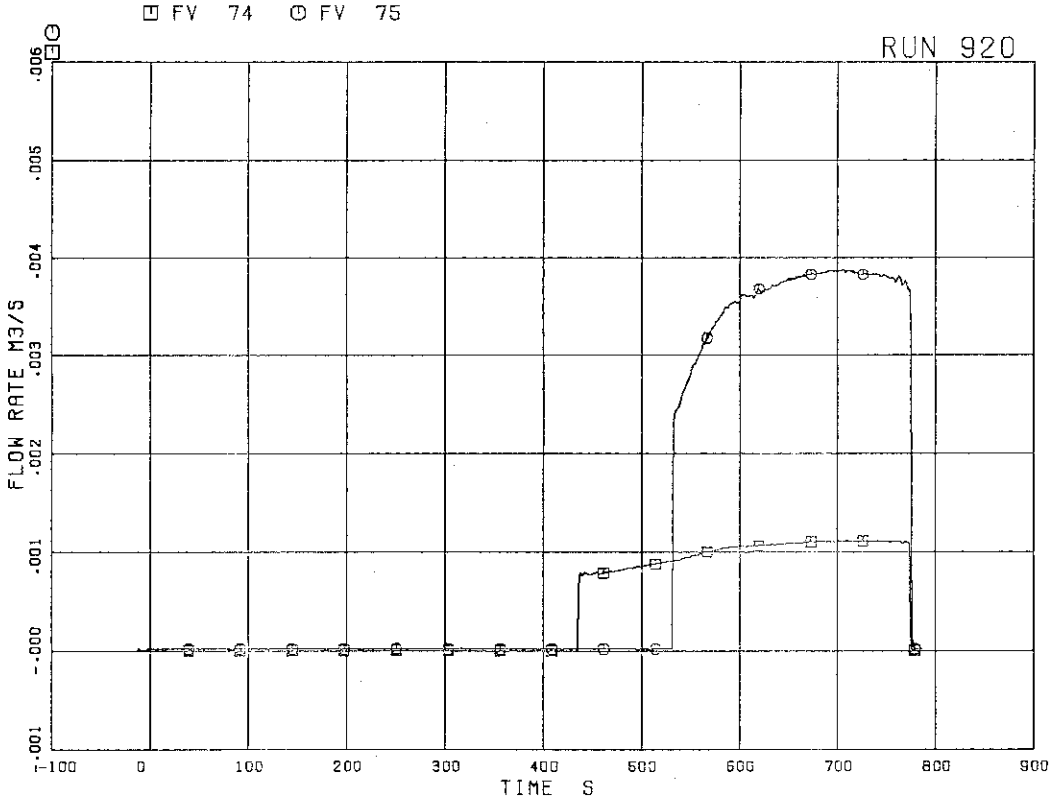

FIG.5.148 ECC INJECTION FLOW RATES

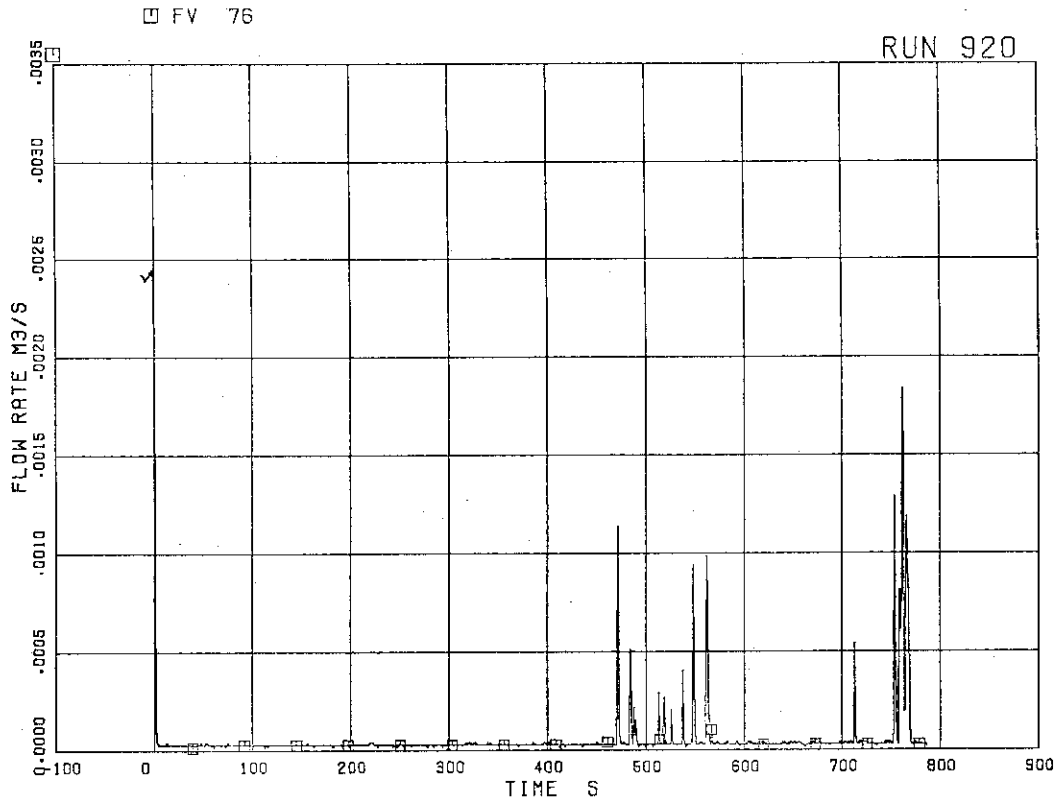

FIG.5.149 FEEDWATER FLOW RATE

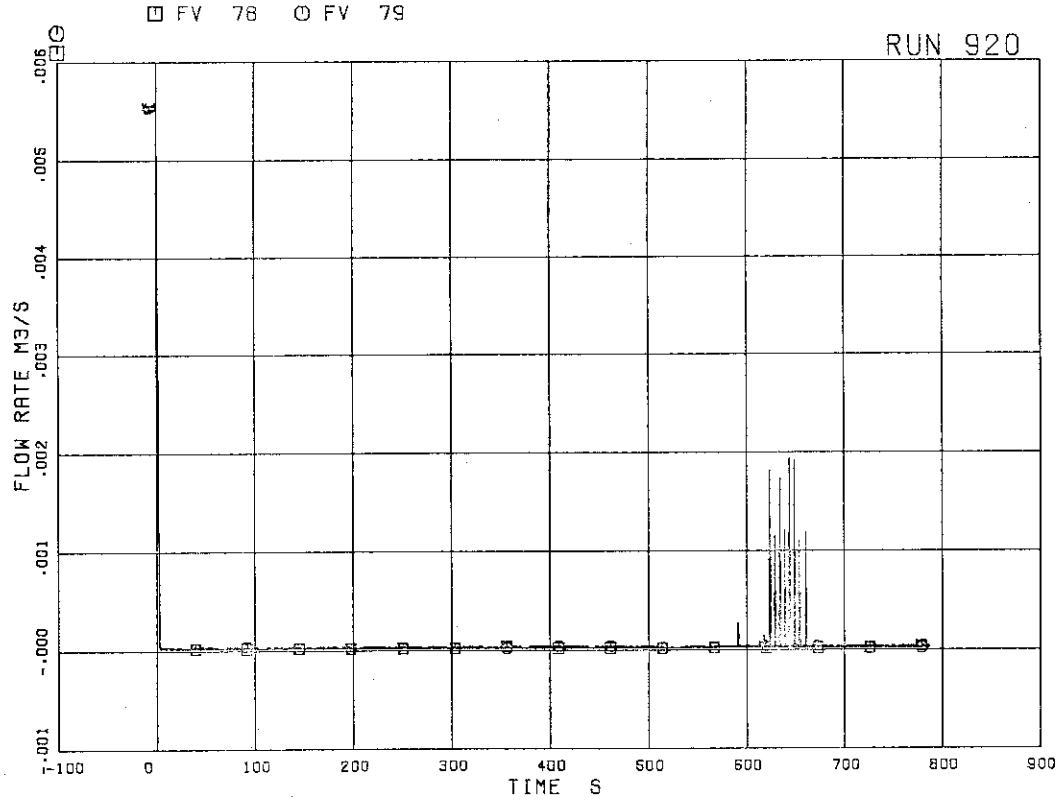

FIG.5.150 JP-1,2 DISCHARGE FLOW RATES (POS.FLOW)

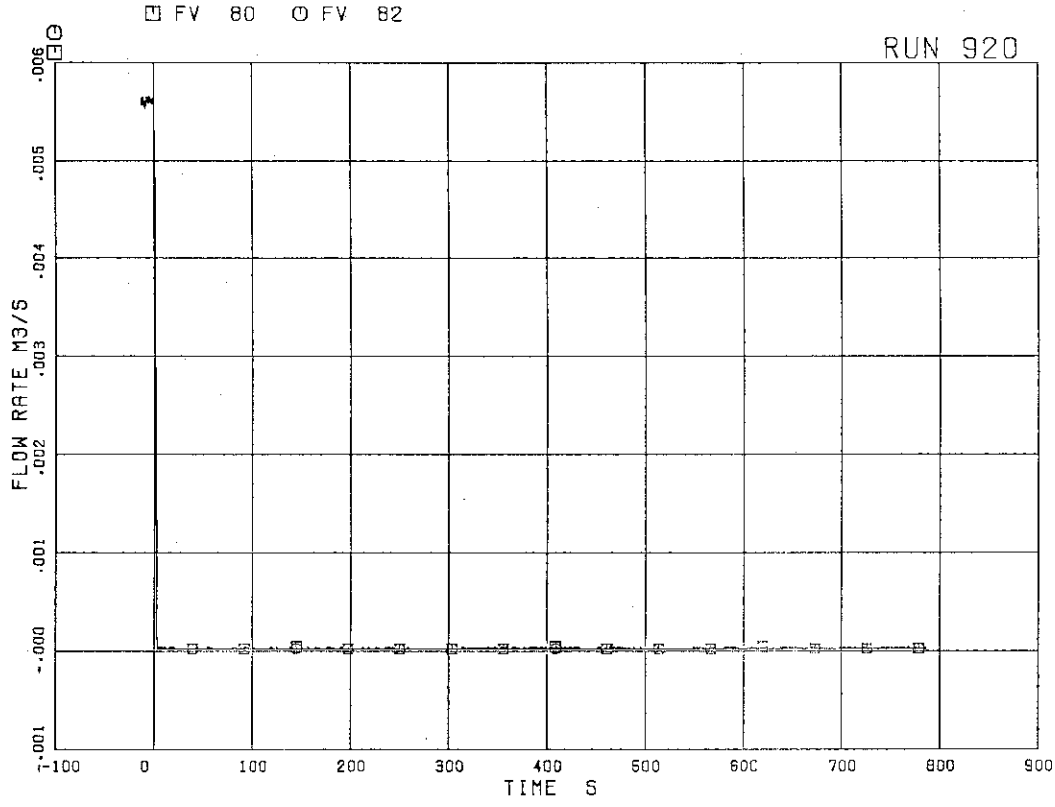

FIG.5.151 JP-3,4 DISCHARGE FLOW RATES (POS.FLOW)

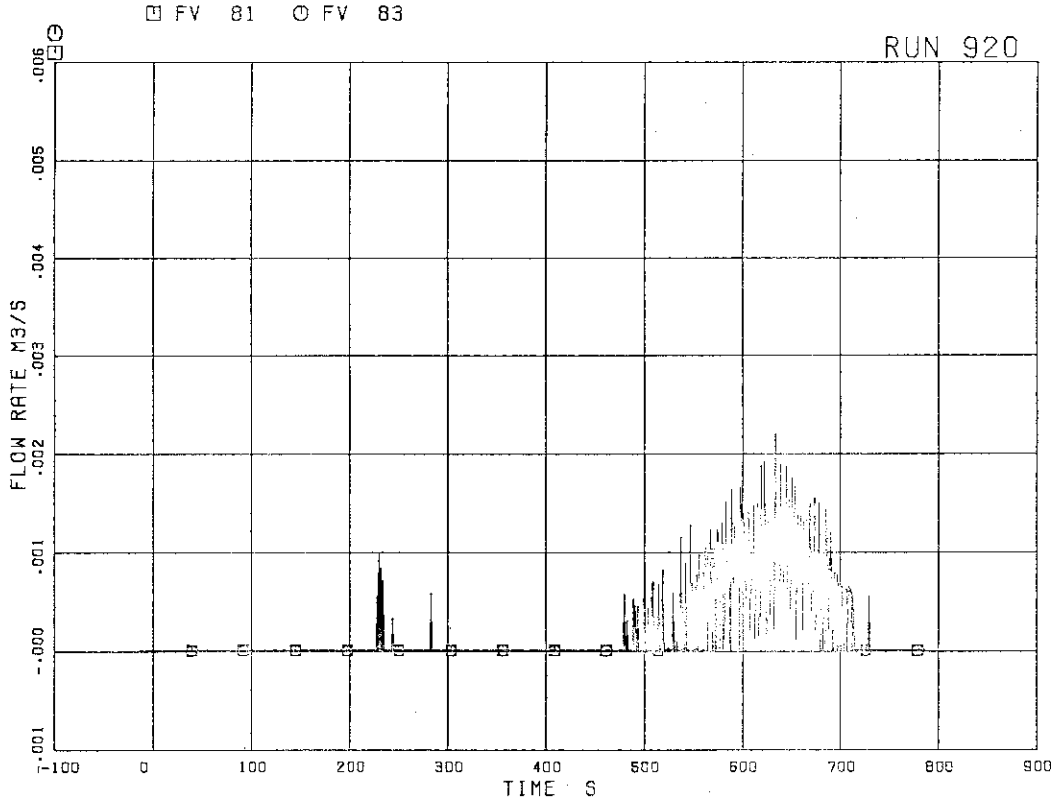

FIG.5.152 JP-3,4 DISCHARGE FLOW RATES (NEG.FLOW)

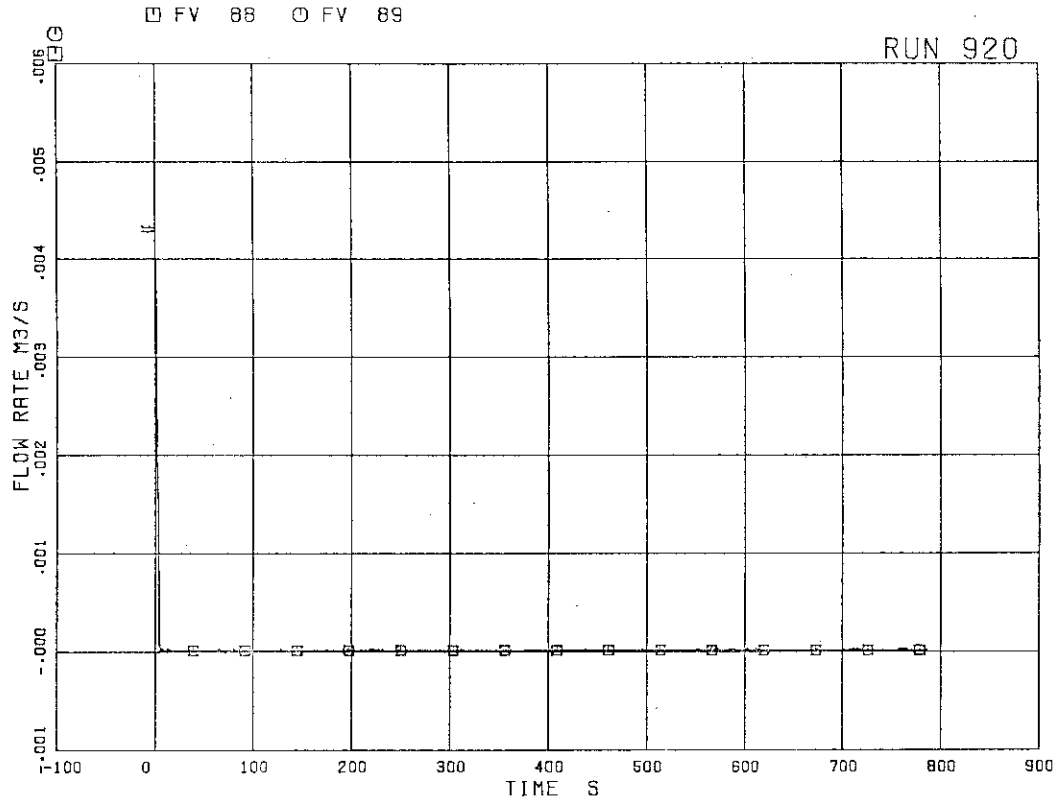

FIG.5.153 MRP DISCHARGE FLOW RATES

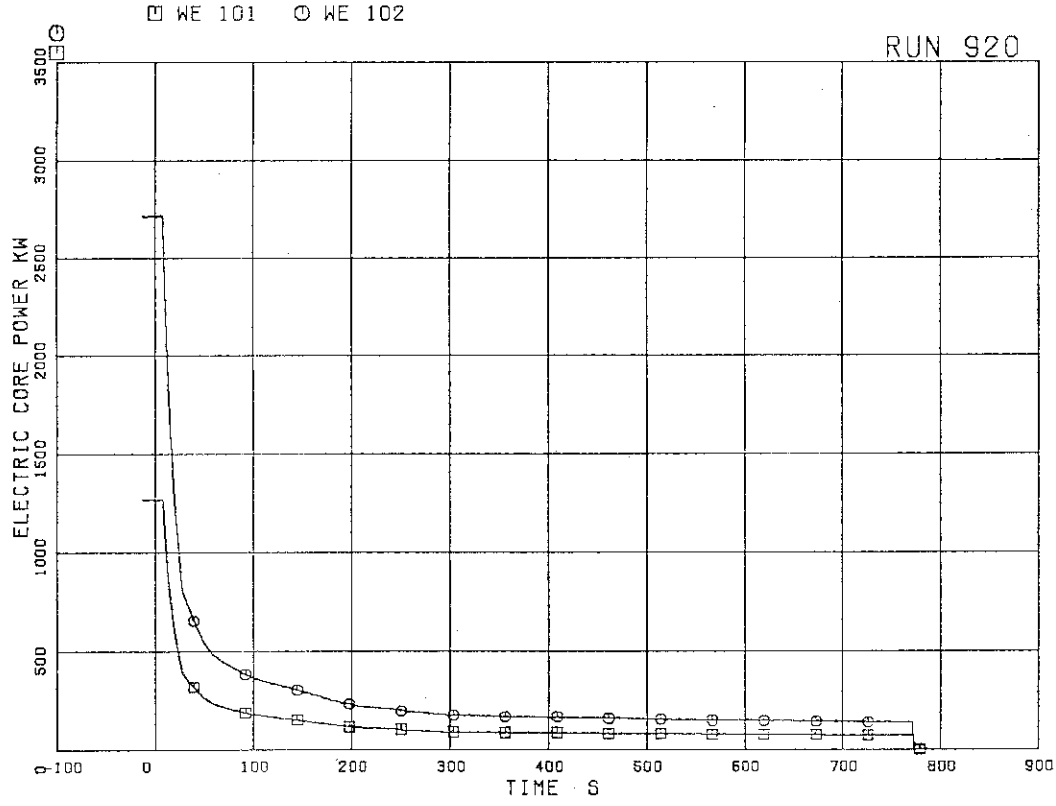

FIG.5.154 ELECTRIC CORE POWER

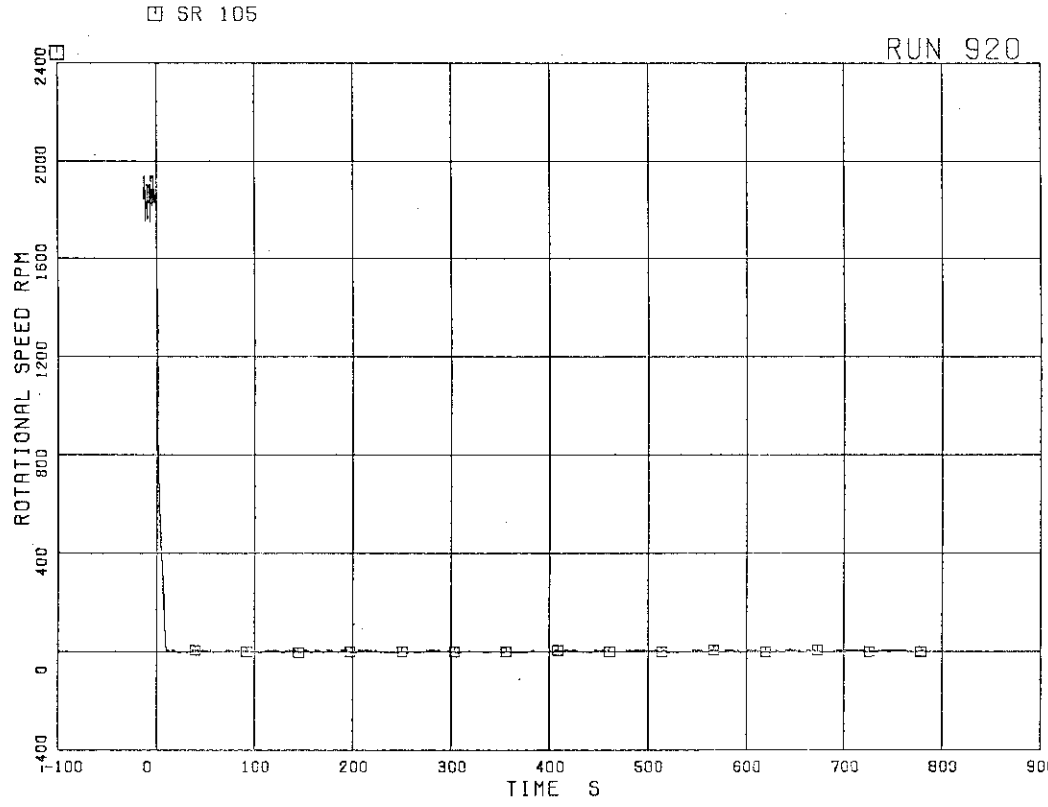

FIG.5.155 MRP PUMP SPEED

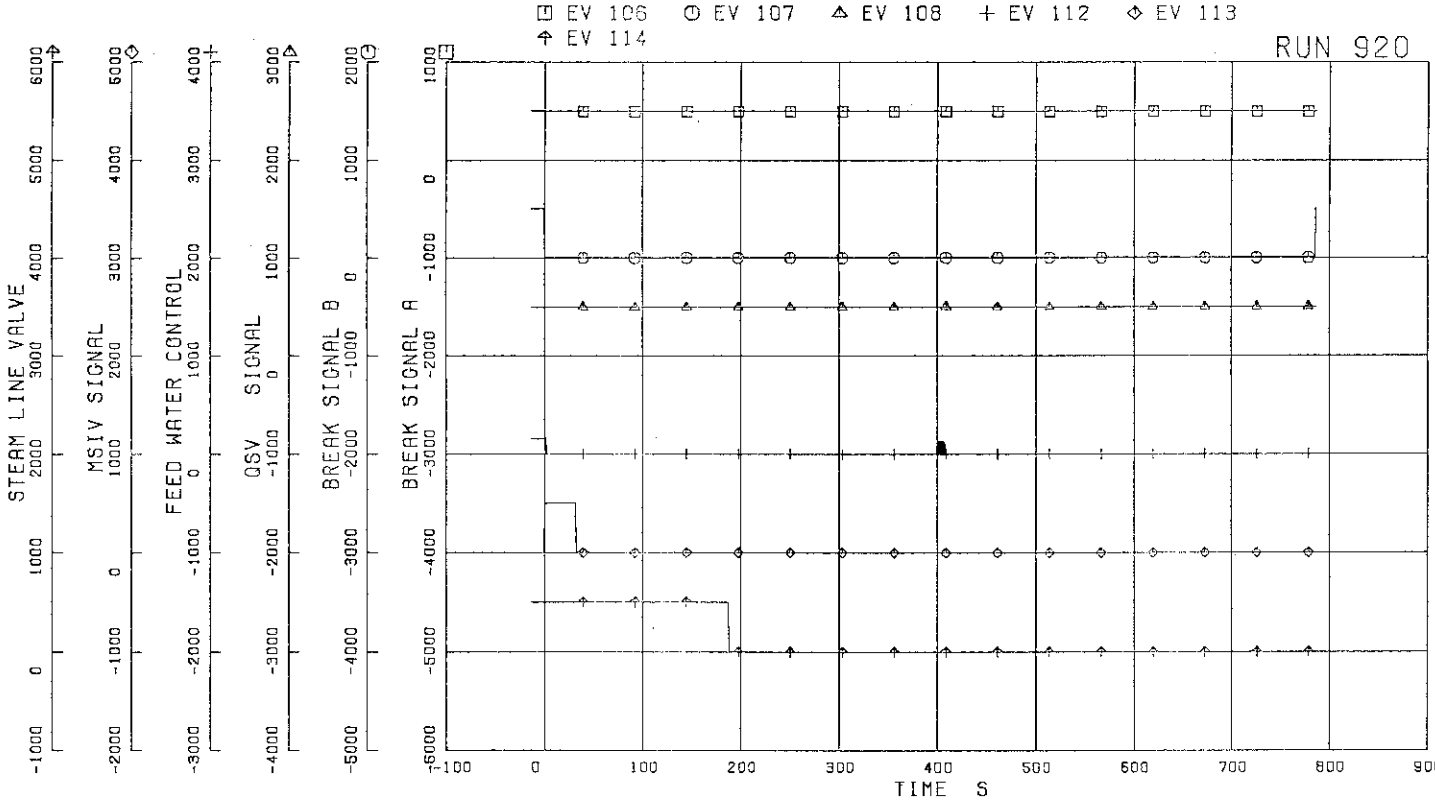

FIG.5.156 VALVE OPERATION SIGNALS

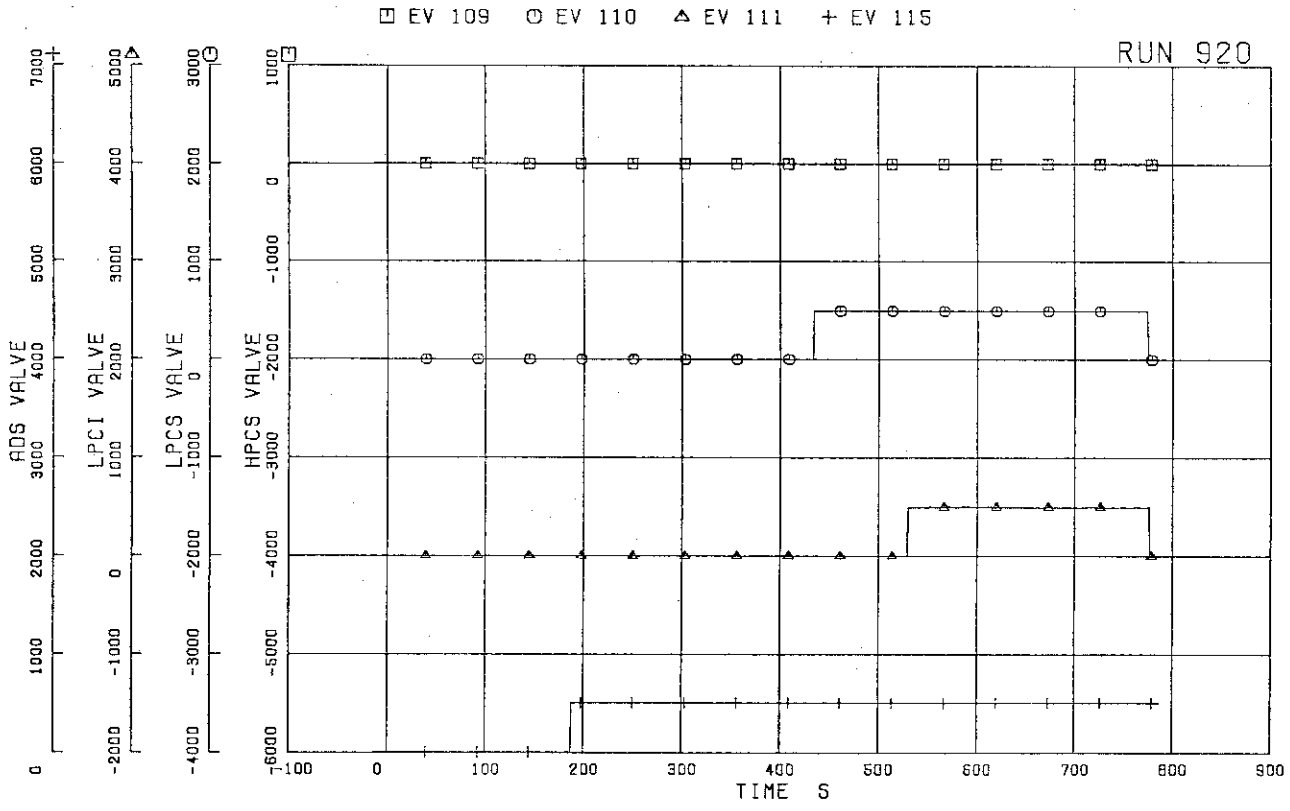

FIG.5.157 ECCS OPERATION SIGNALS

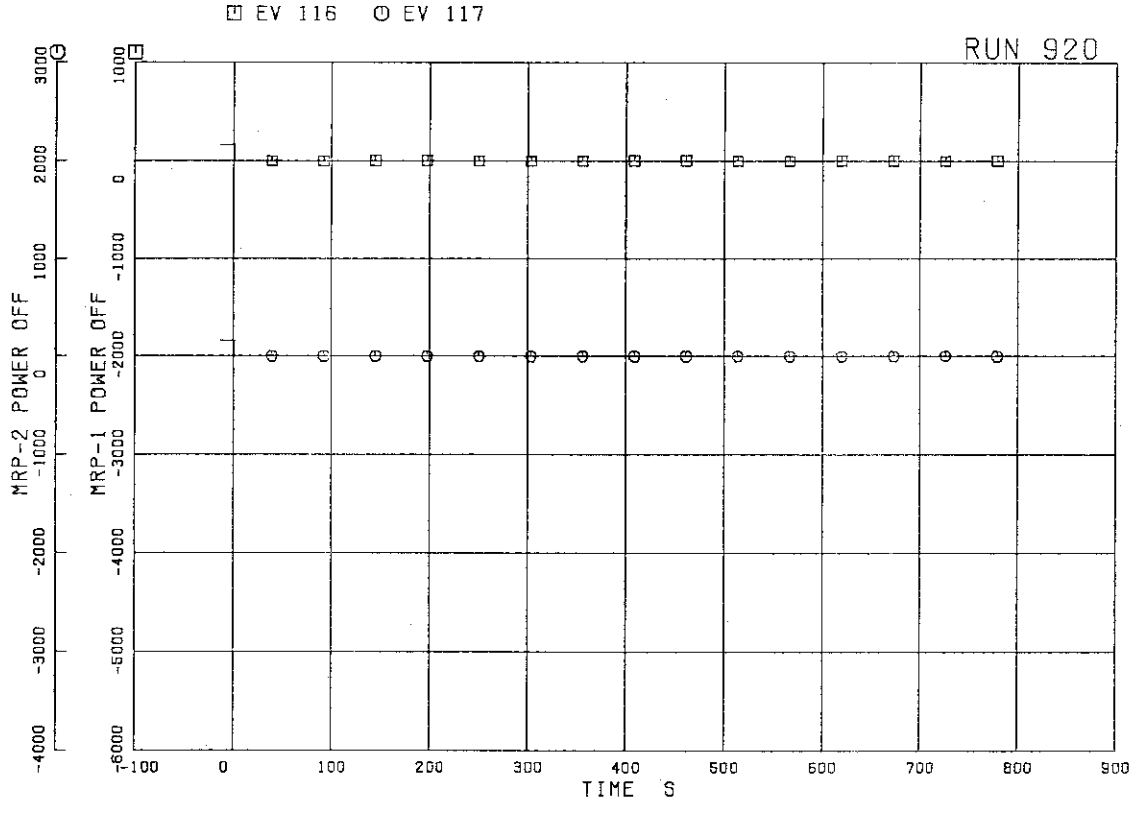

FIG.5.158 MRP OPERATION SIGNALS

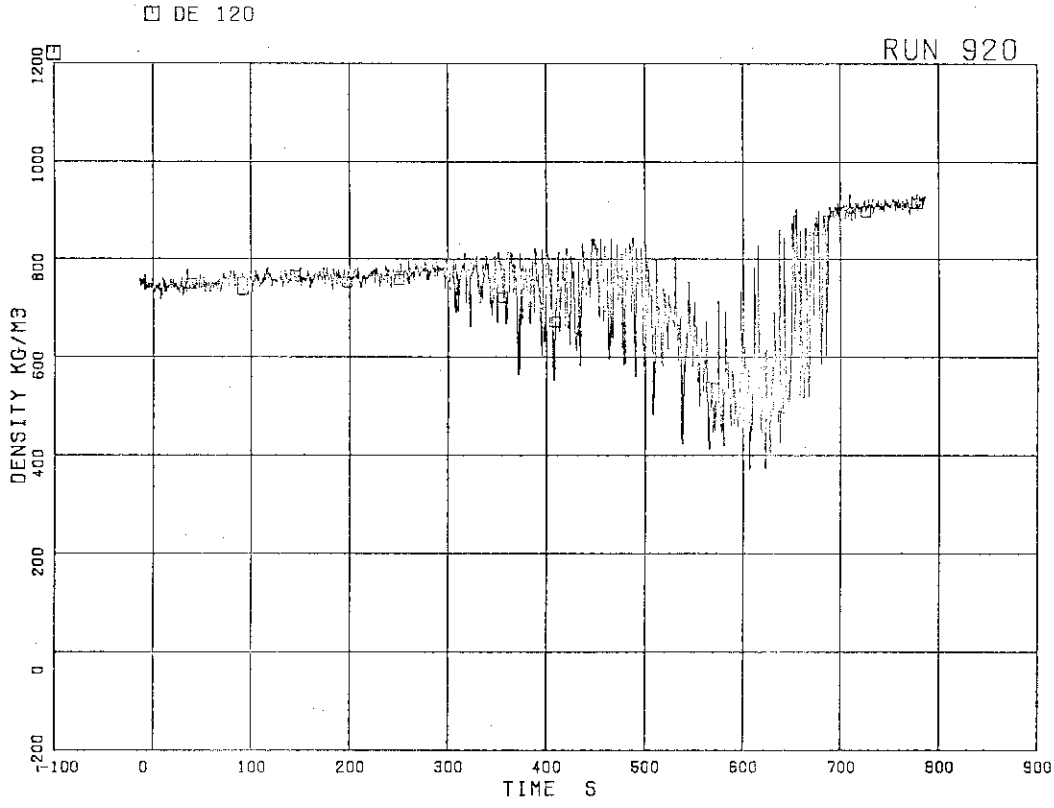

FIG.5.159 FLUID DENSITY AT JP-1,2 OUTLET, BEAM A

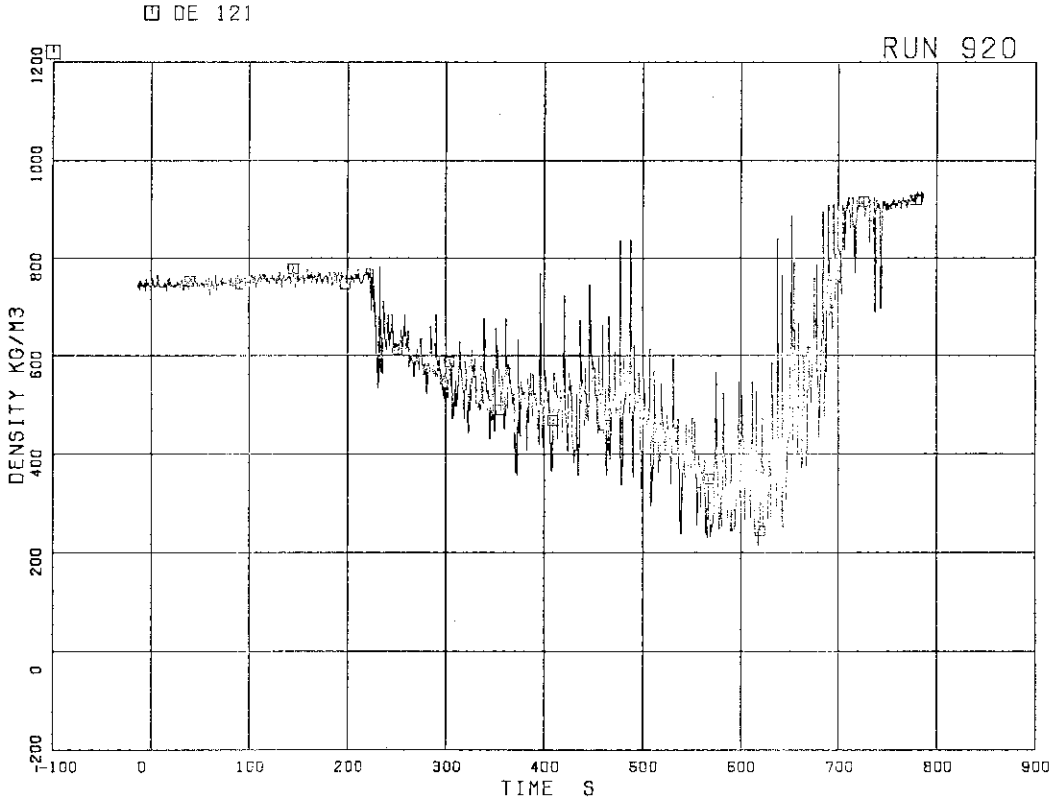

FIG.5.160 FLUID DENSITY AT JP-1,2 OUTLET, BEAM B

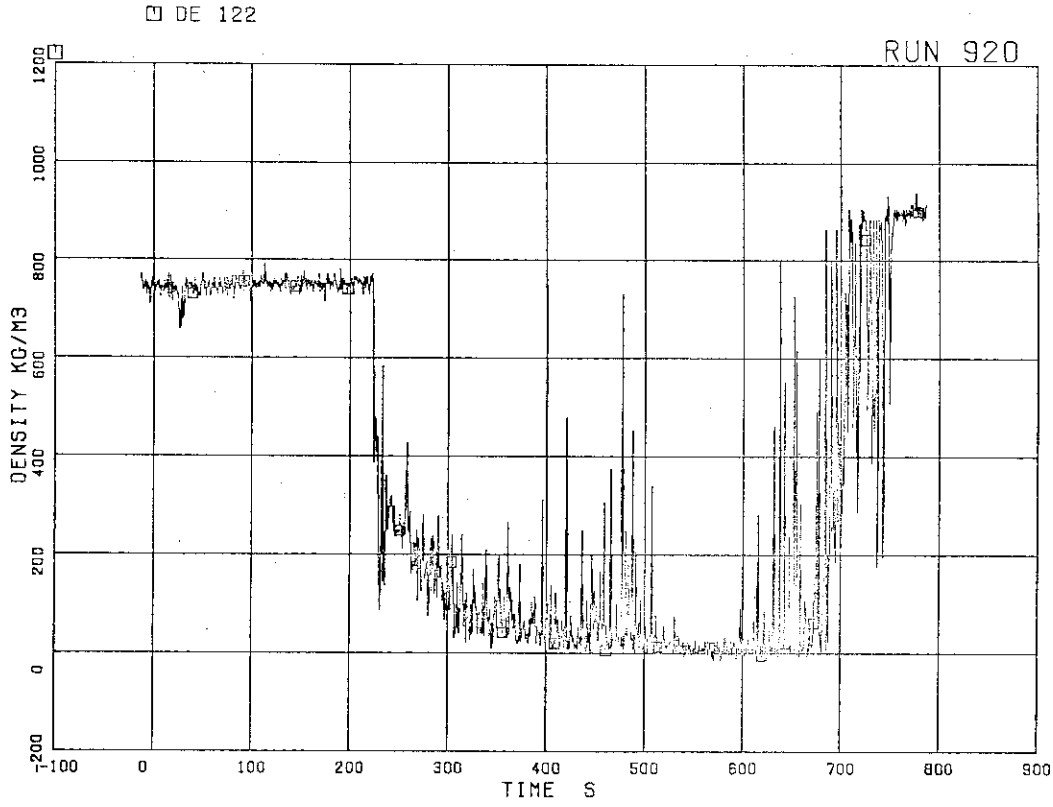

FIG.5.161 FLUID DENSITY AT JP-1,2 OUTLET, BEAM C

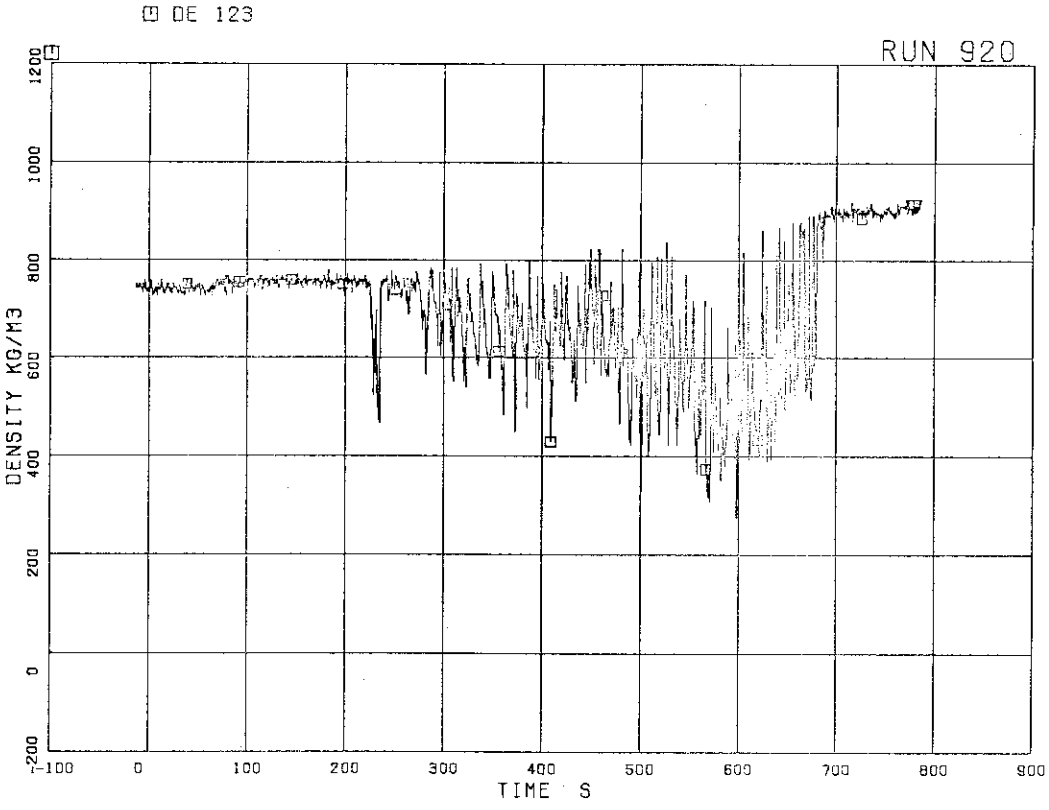

FIG.5.162 FLUID DENSITY AT JP-3,4 OUTLET, BEAM A

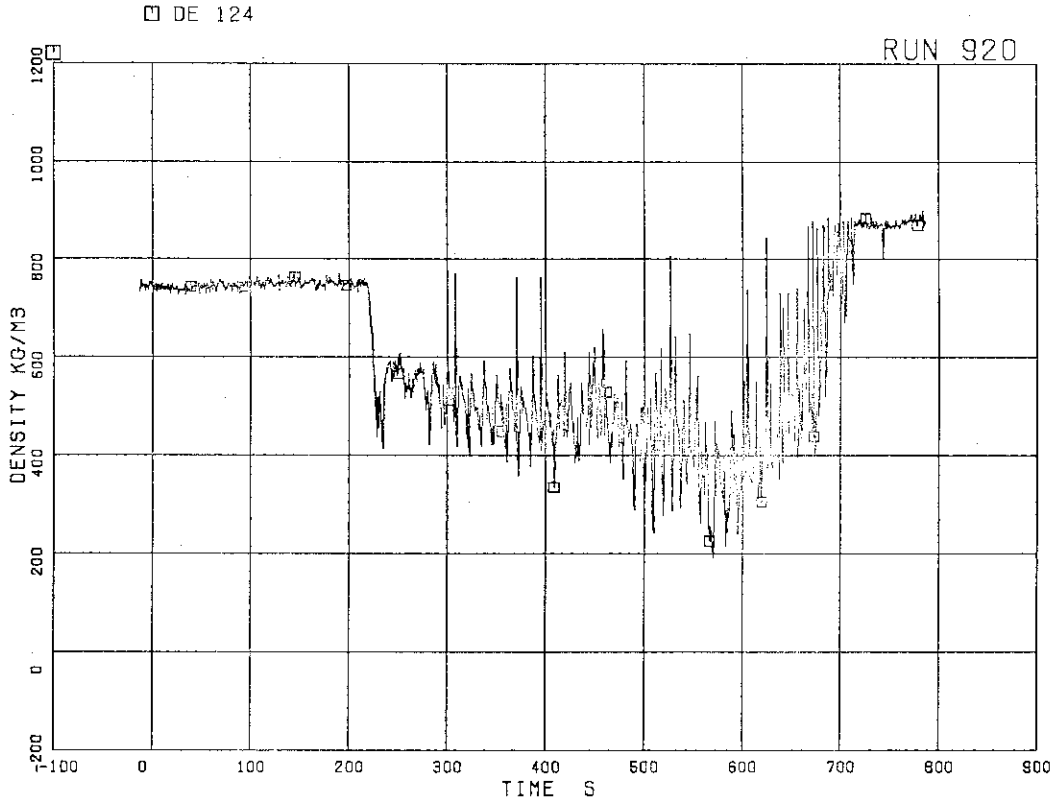

FIG.5.163 FLUID DENSITY AT JP-3,4 OUTLET, BEAM B

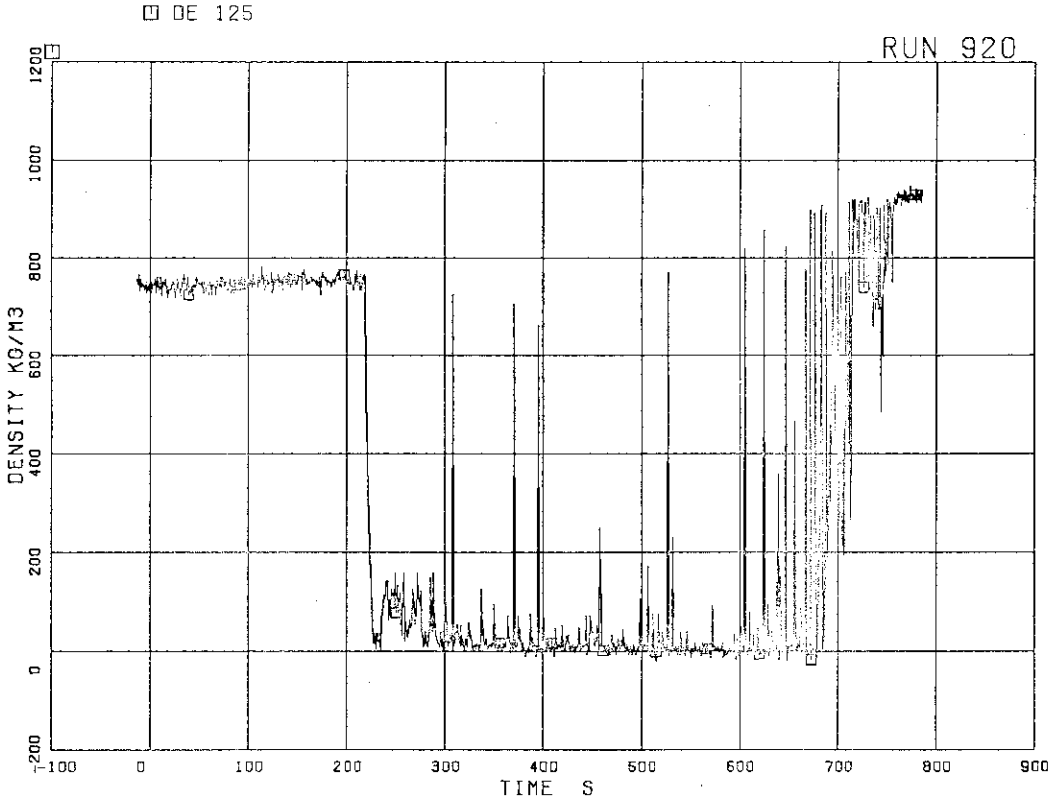

FIG.5.164 FLUID DENSITY AT JP-3.4 OUTLET, BEAM C

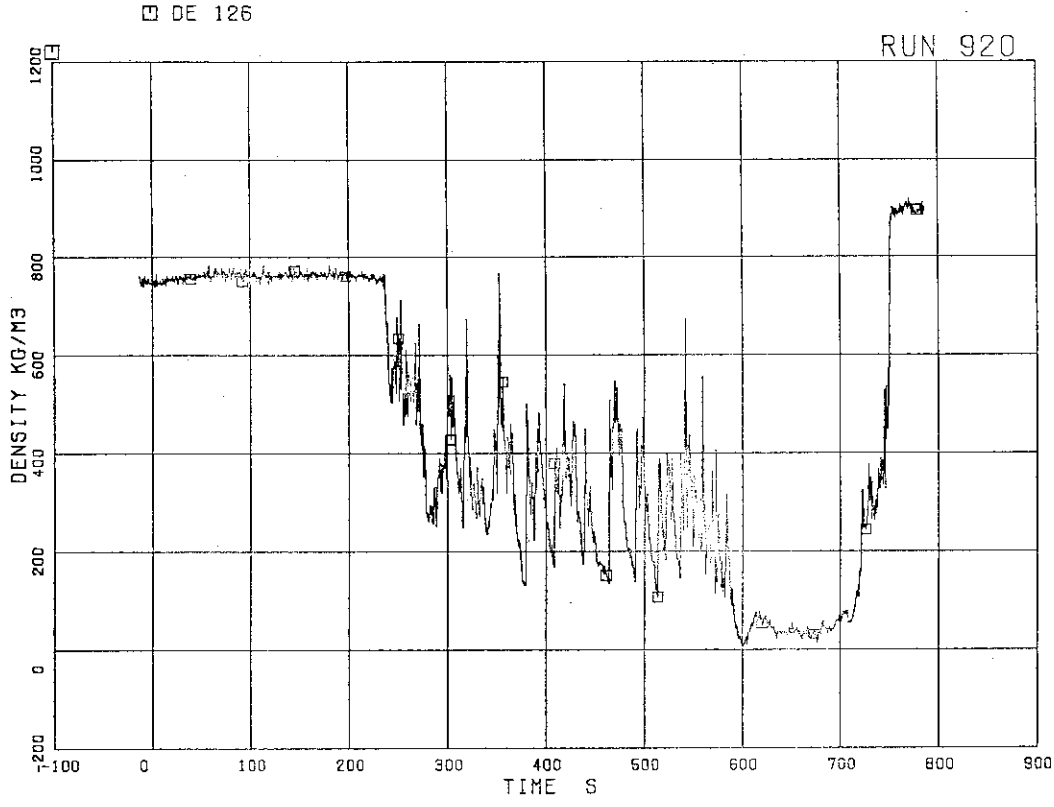

FIG.5.165 FLUID DENSITY AT MRP SIDE OF BREAK, BEAM A

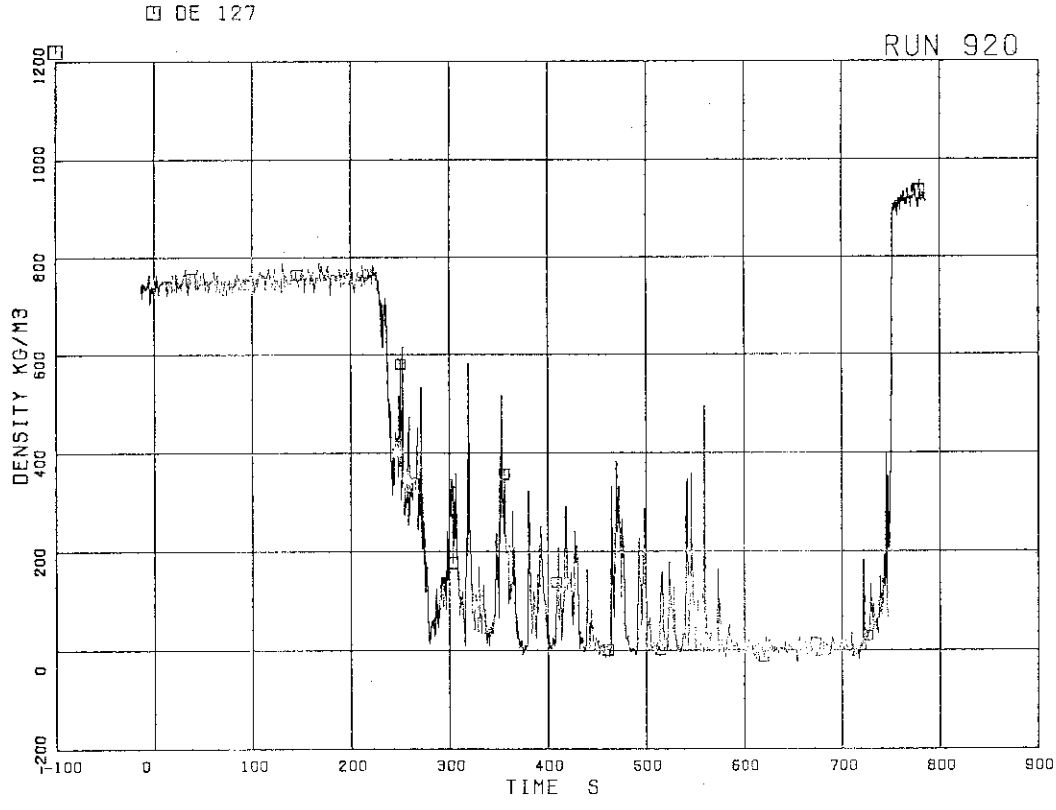

FIG.5.166 FLUID DENSITY AT MRP SIDE OF BREAK, BEAM B

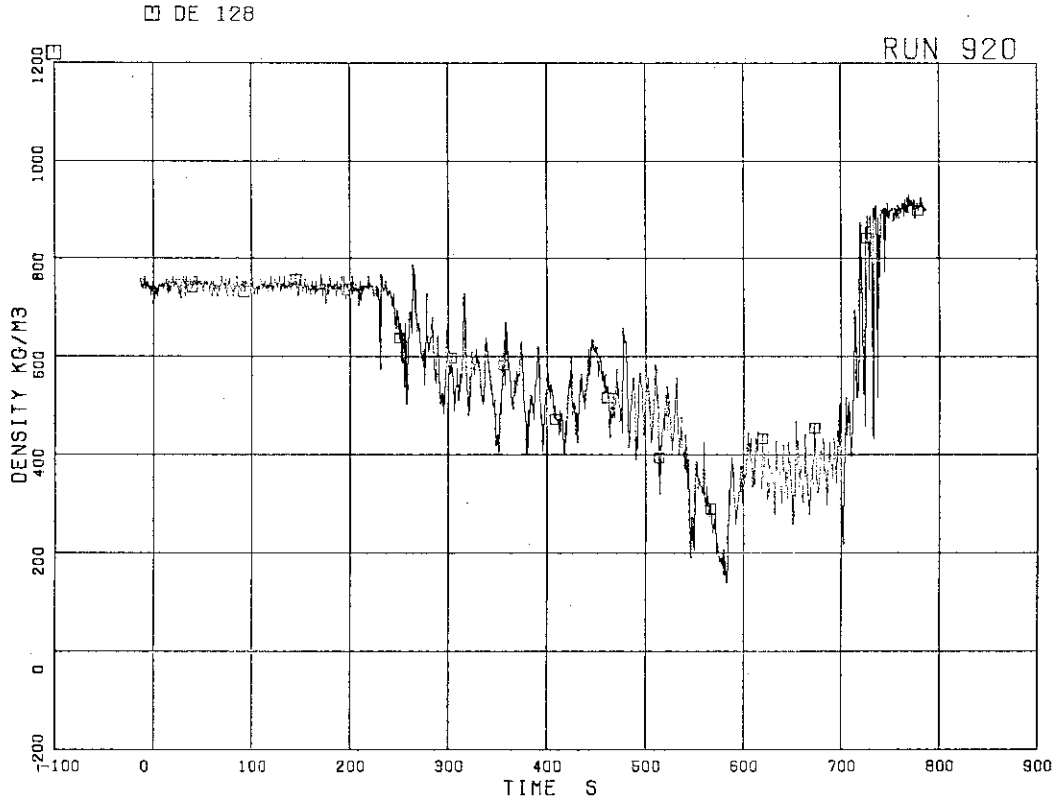

FIG.5.167 FLUID DENSITY AT PV SIDE OF BREAK, BEAM A

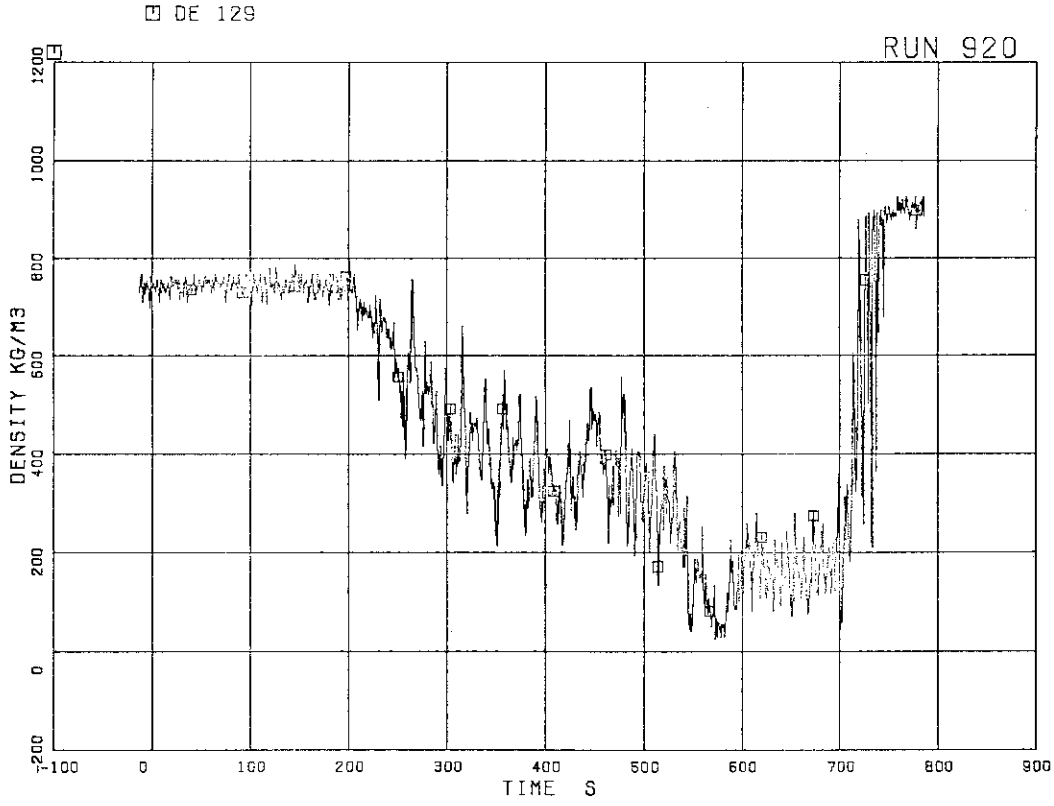

FIG.5.168 FLUID DENSITY AT PV SIDE OF BREAK, BEAM B

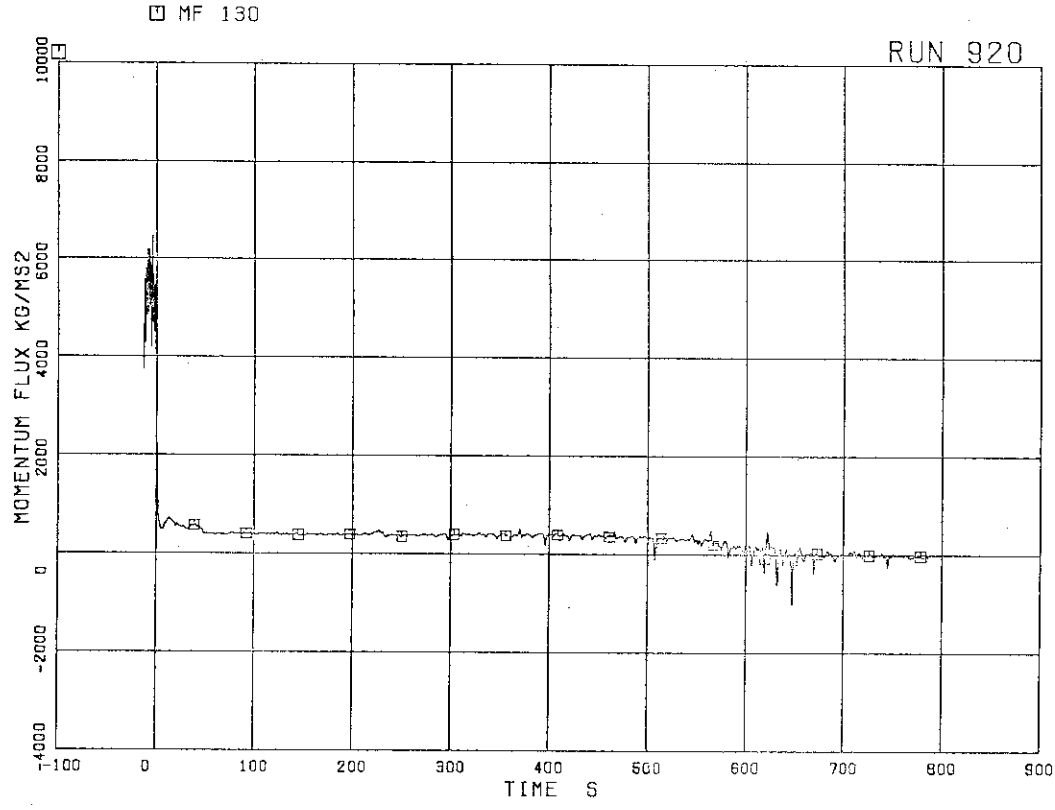

FIG.5.169 MOMENTUM FLUX AT JP-1,2 OUTLET SPOOL

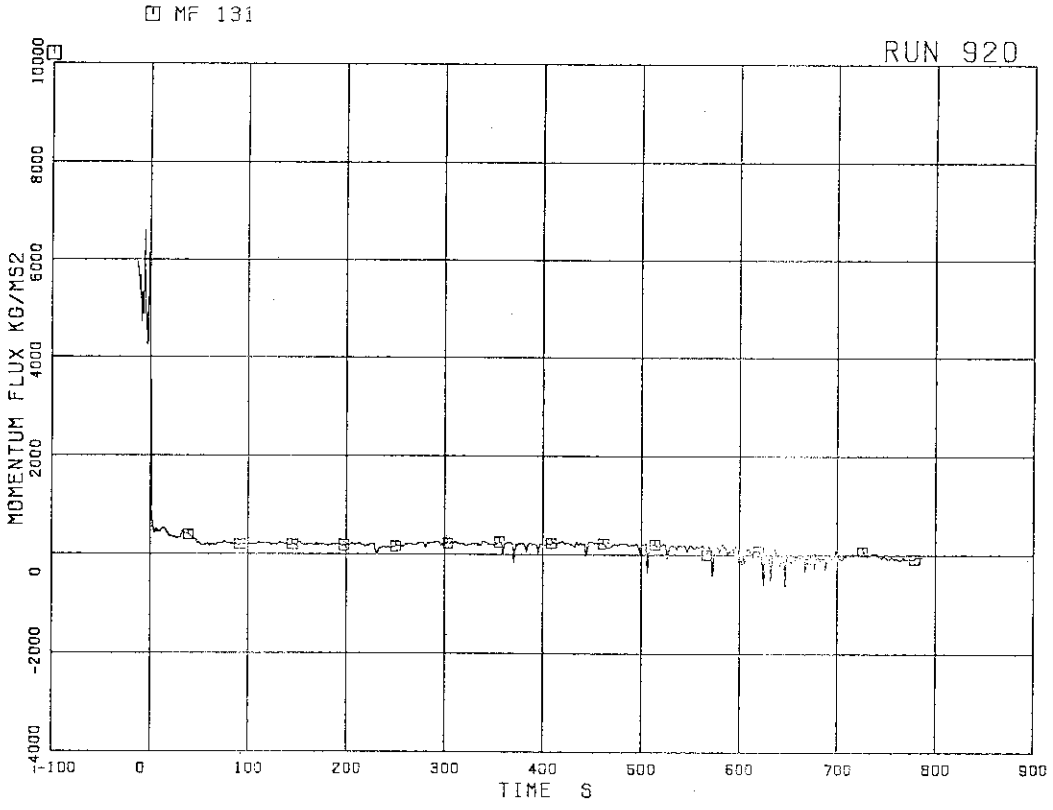

FIG.5.170 MOMENTUM FLUX AT JP-3,4 OUTLET SPOOL

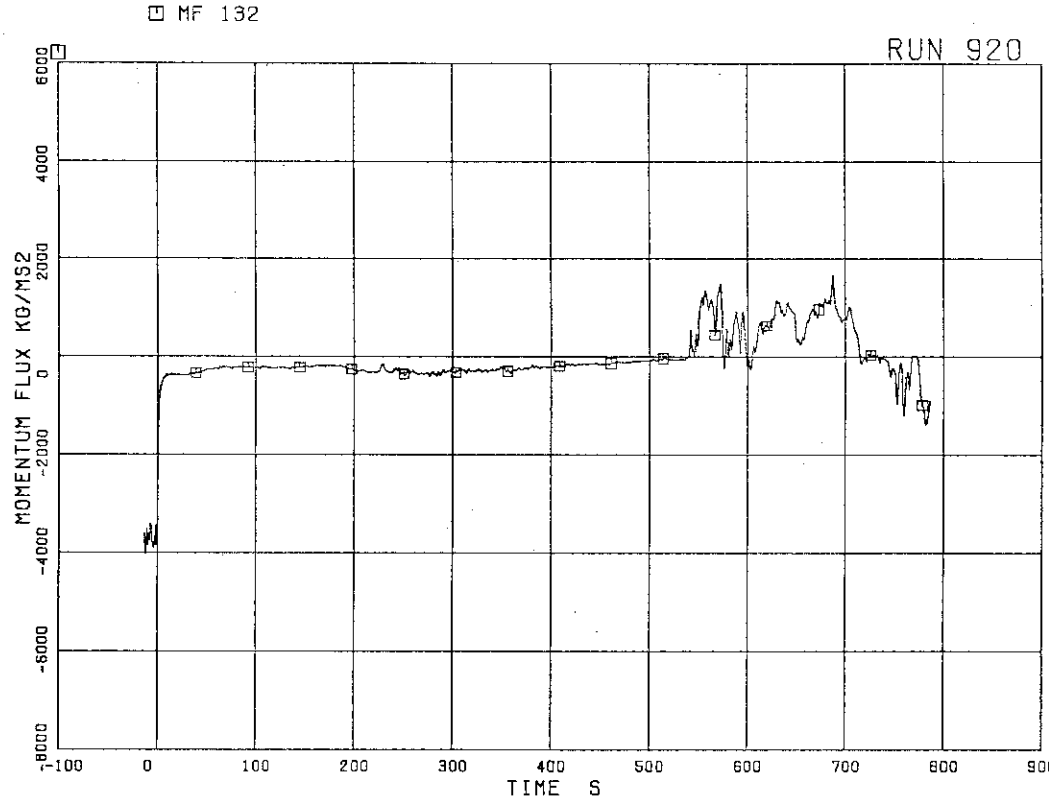

FIG.5.171 MOMENTUM FLUX AT BREAK A SPOOL PIECE (LOW RANGE)

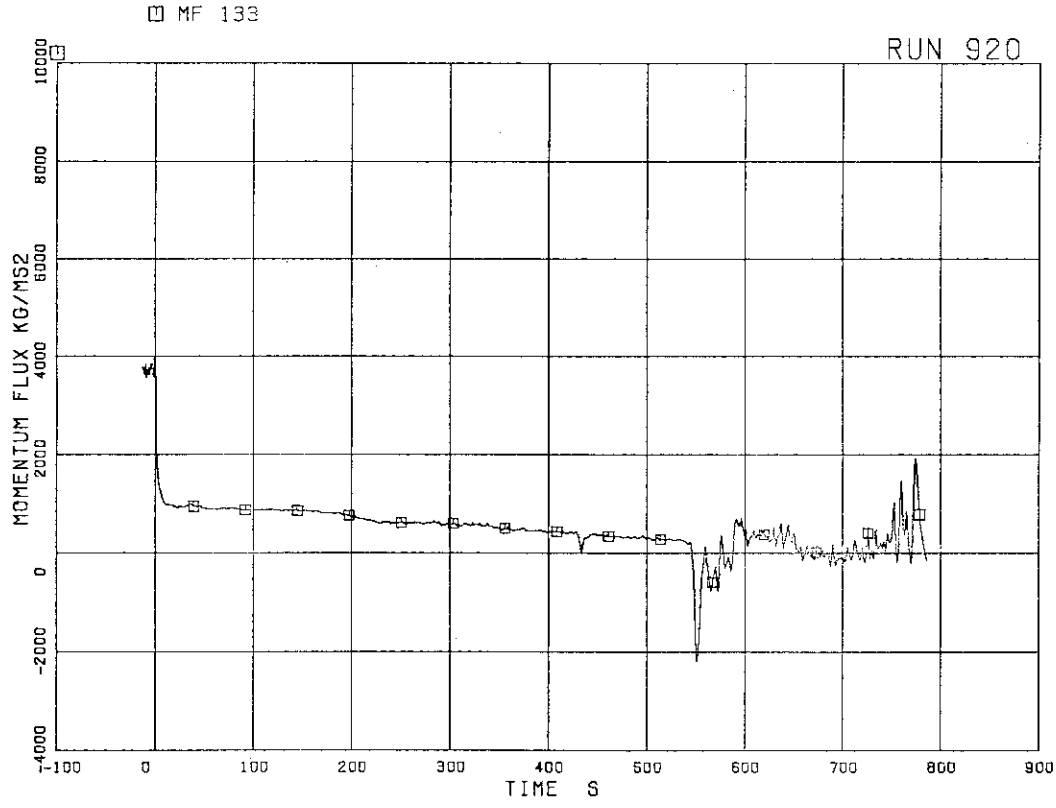

FIG.5.172 MOMENTUM FLUX AT BREAK B SPOOL PIECE (LOW RANGE)

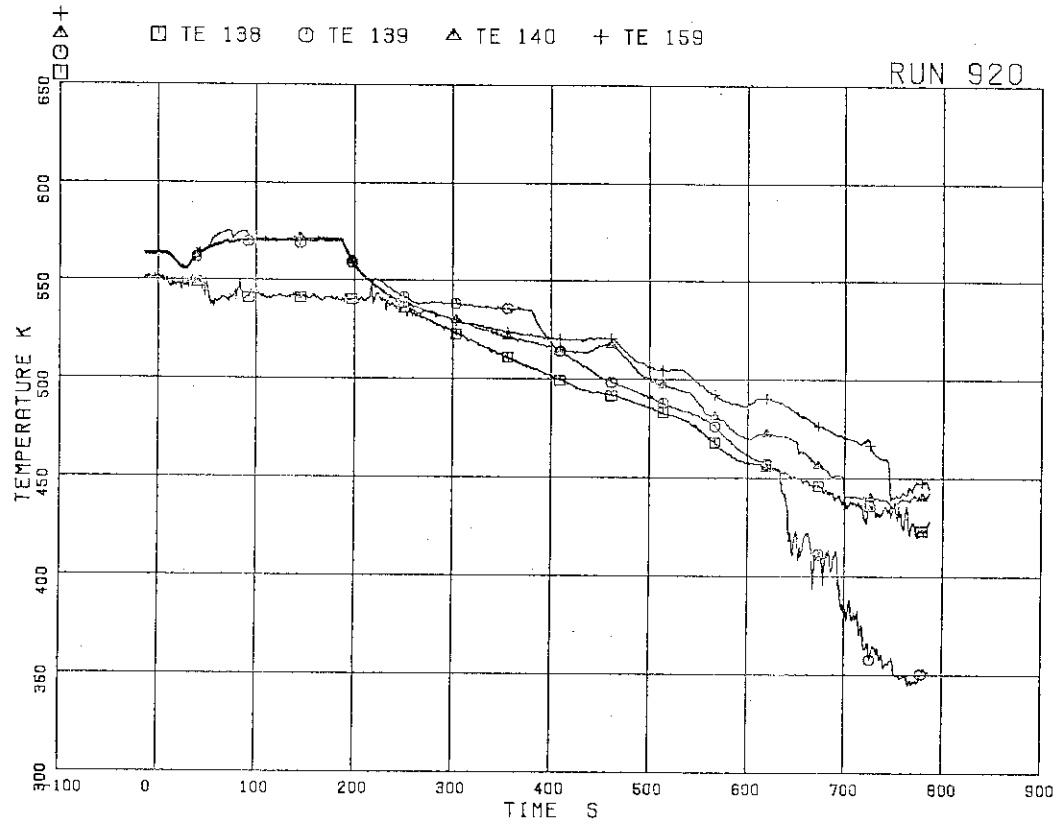

FIG.5.173 FLUID TEMPERATURES IN PV AND MSL

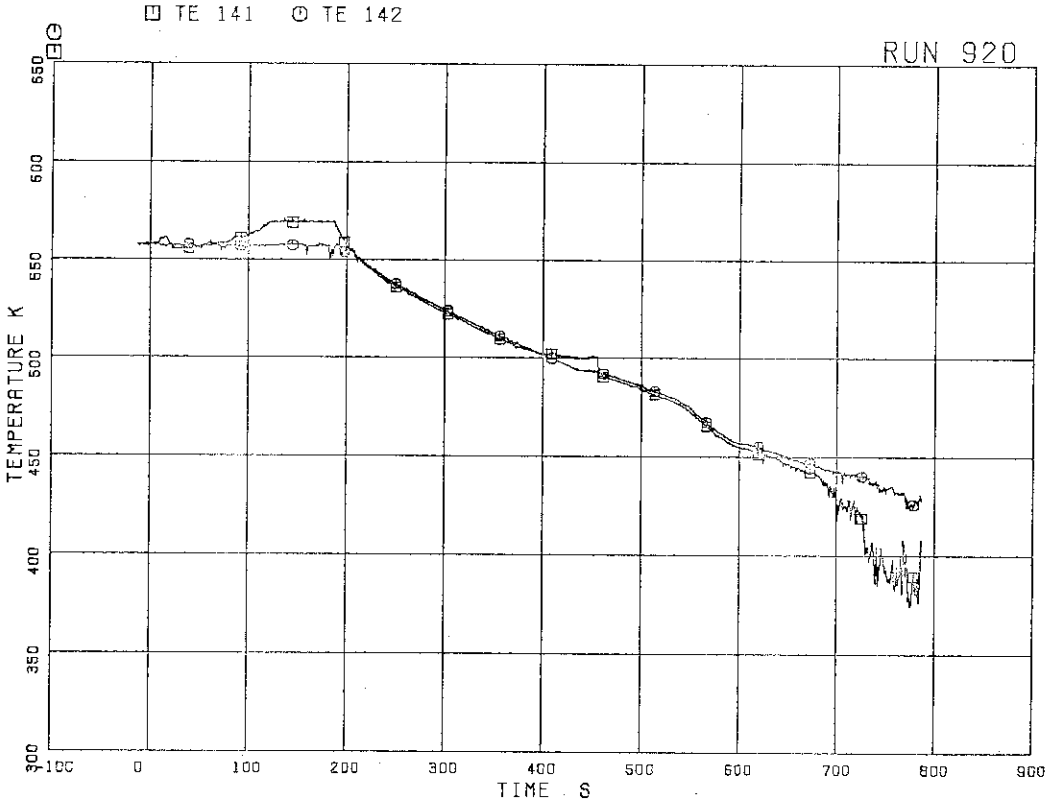

FIG.5.174 FLUID TEMPERATURES IN DOWNCOMER

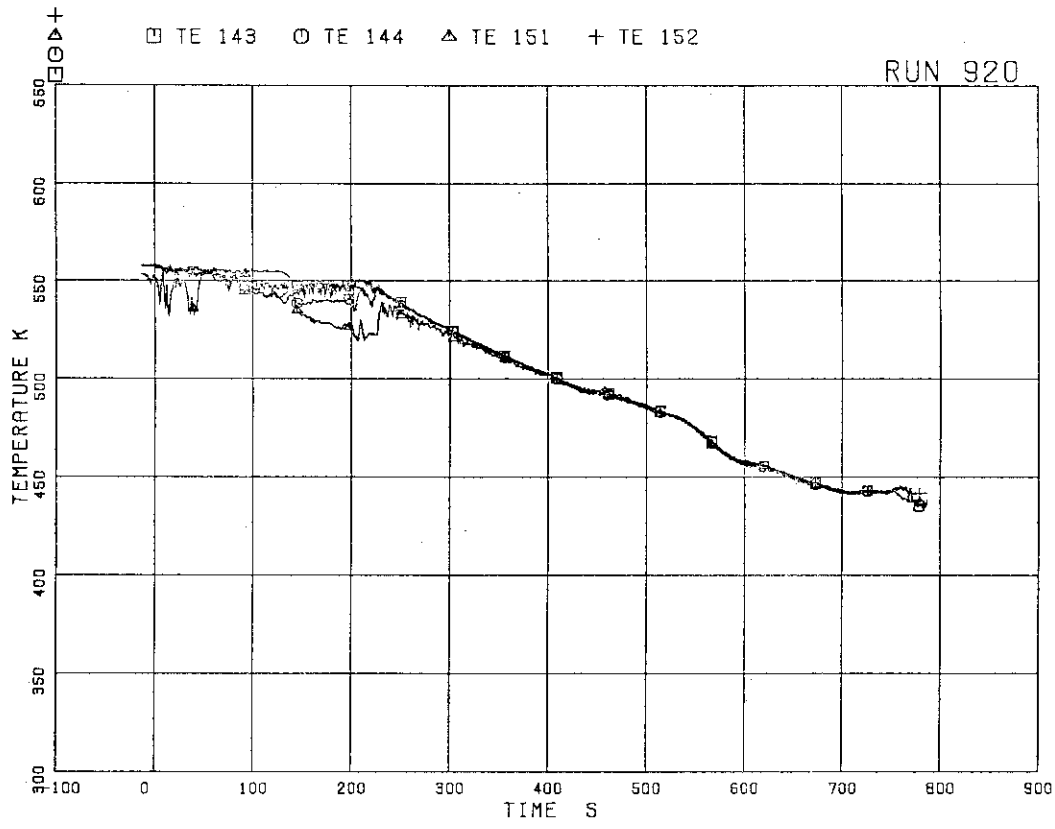

FIG.5.175 FLUID TEMPERATURES IN INTACT RECIRCULATION LOOP

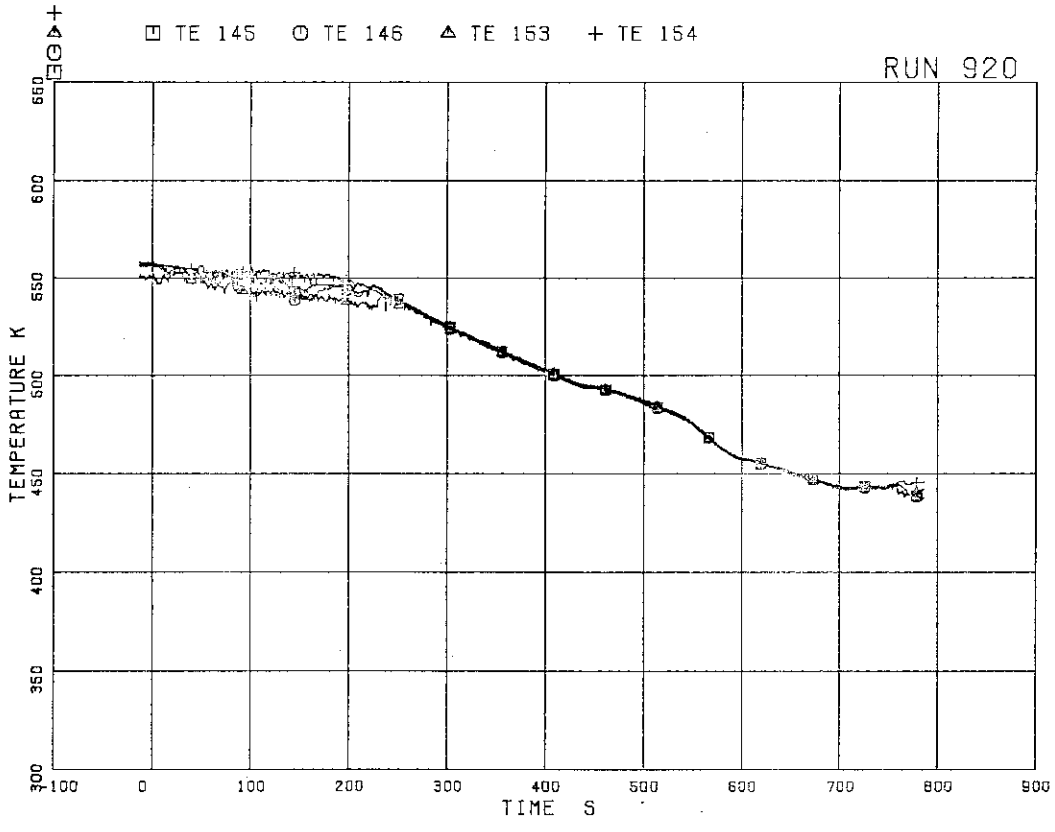

FIG.5.176 FLUID TEMPERATURES IN BROKEN RECIRCULATION LOOP

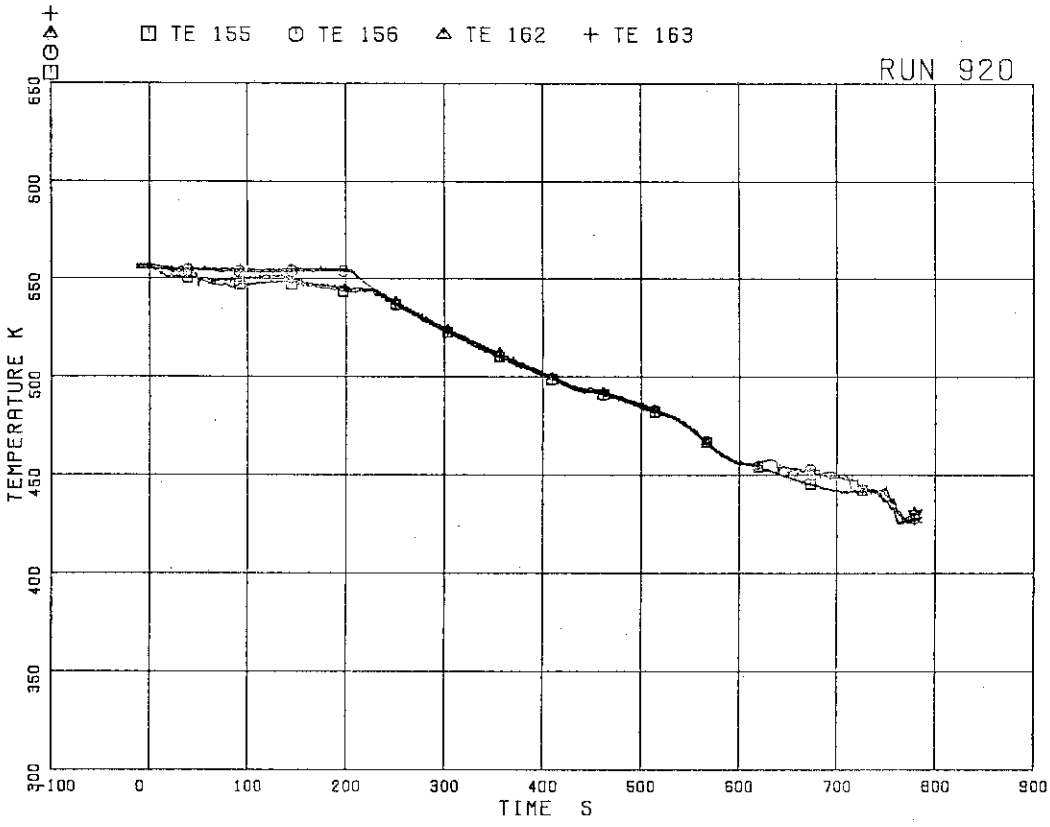

FIG.5.177 FLUID TEMPERATURES NEAR BREAKS A AND B

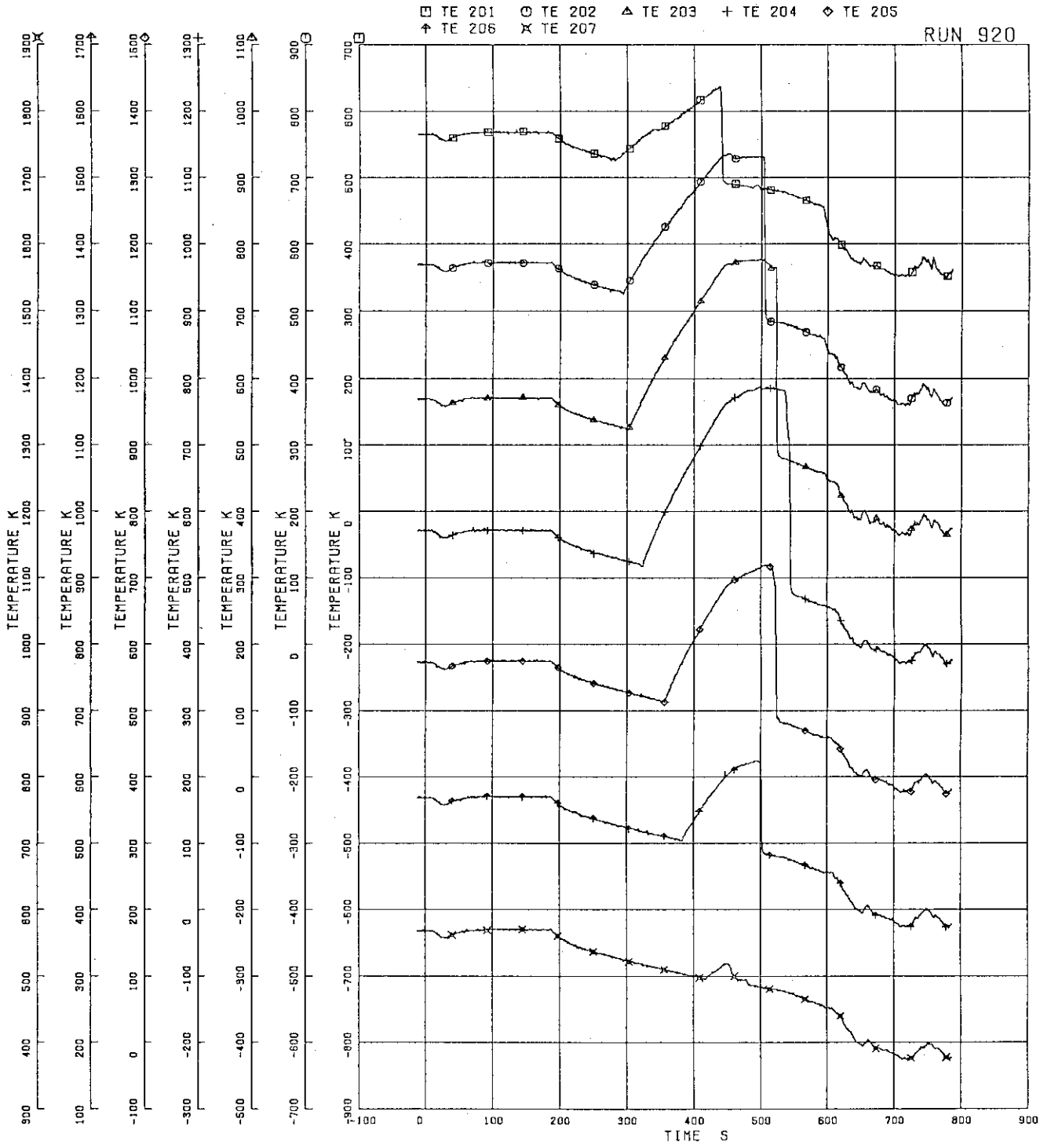

FIG.5.178 SURFACE TEMPERATURES OF FUEL ROD A11

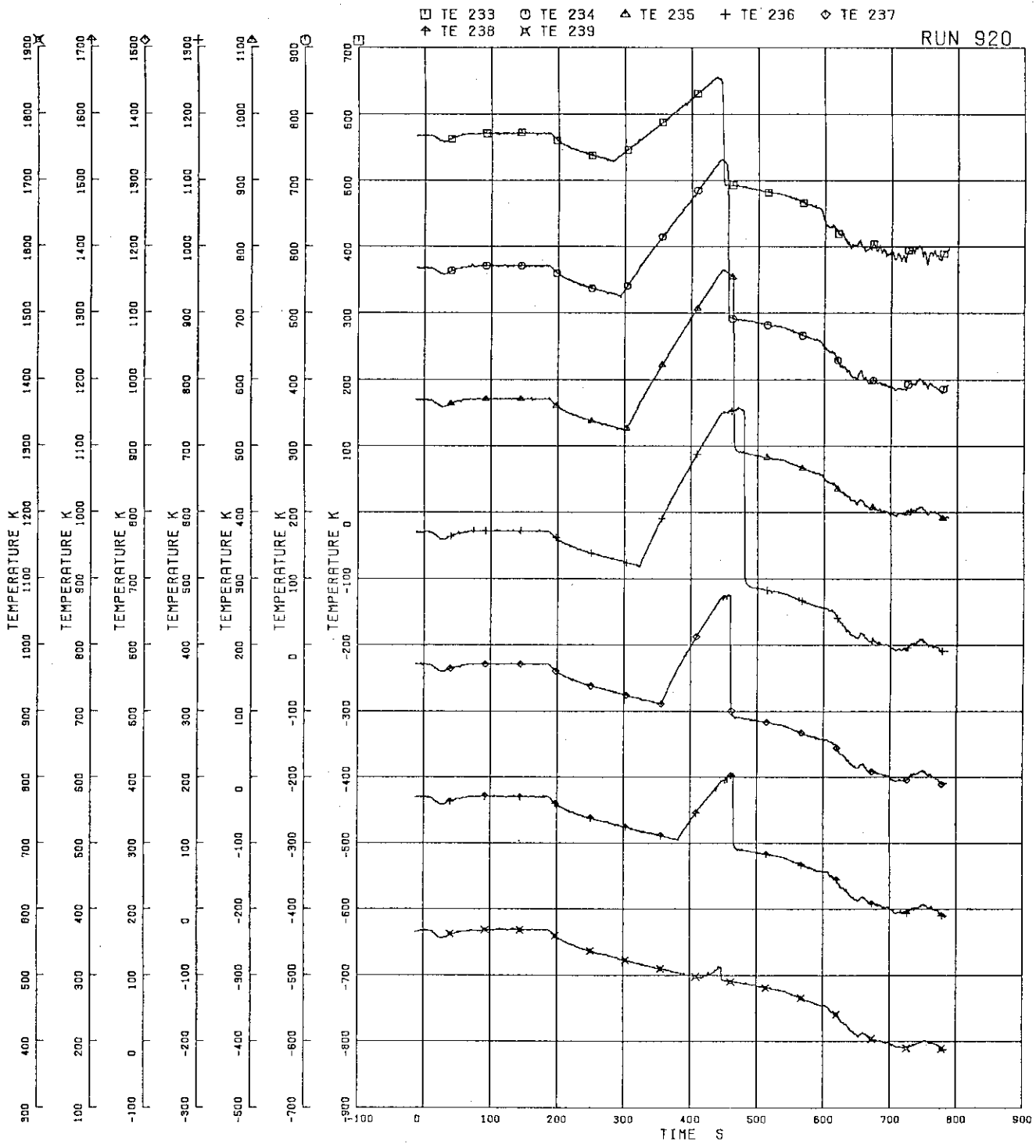

FIG.5.179 SURFACE TEMPERATURES OF FUEL ROD A22

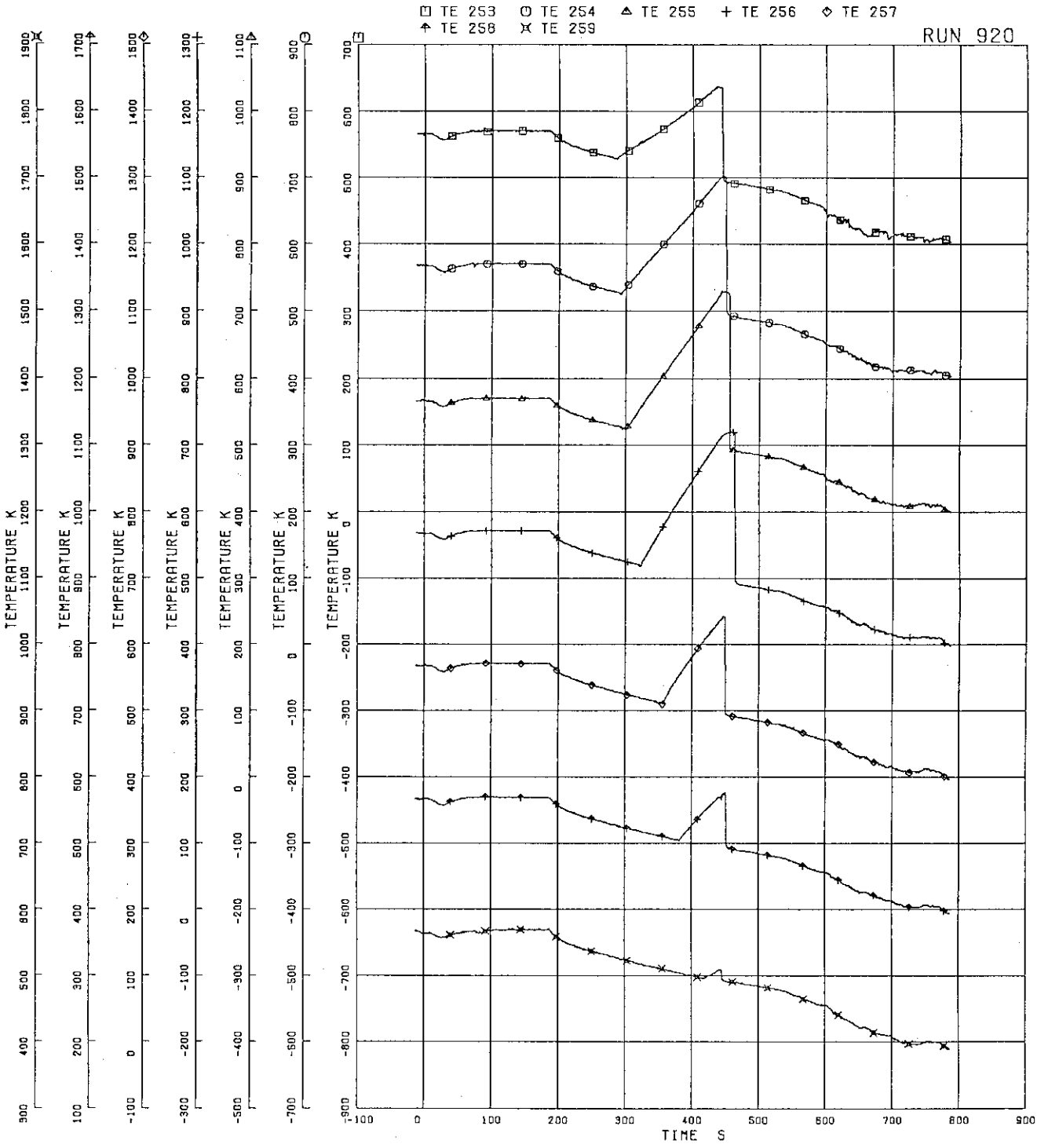

FIG.5.180 SURFACE TEMPERATURES OF FUEL ROD A33

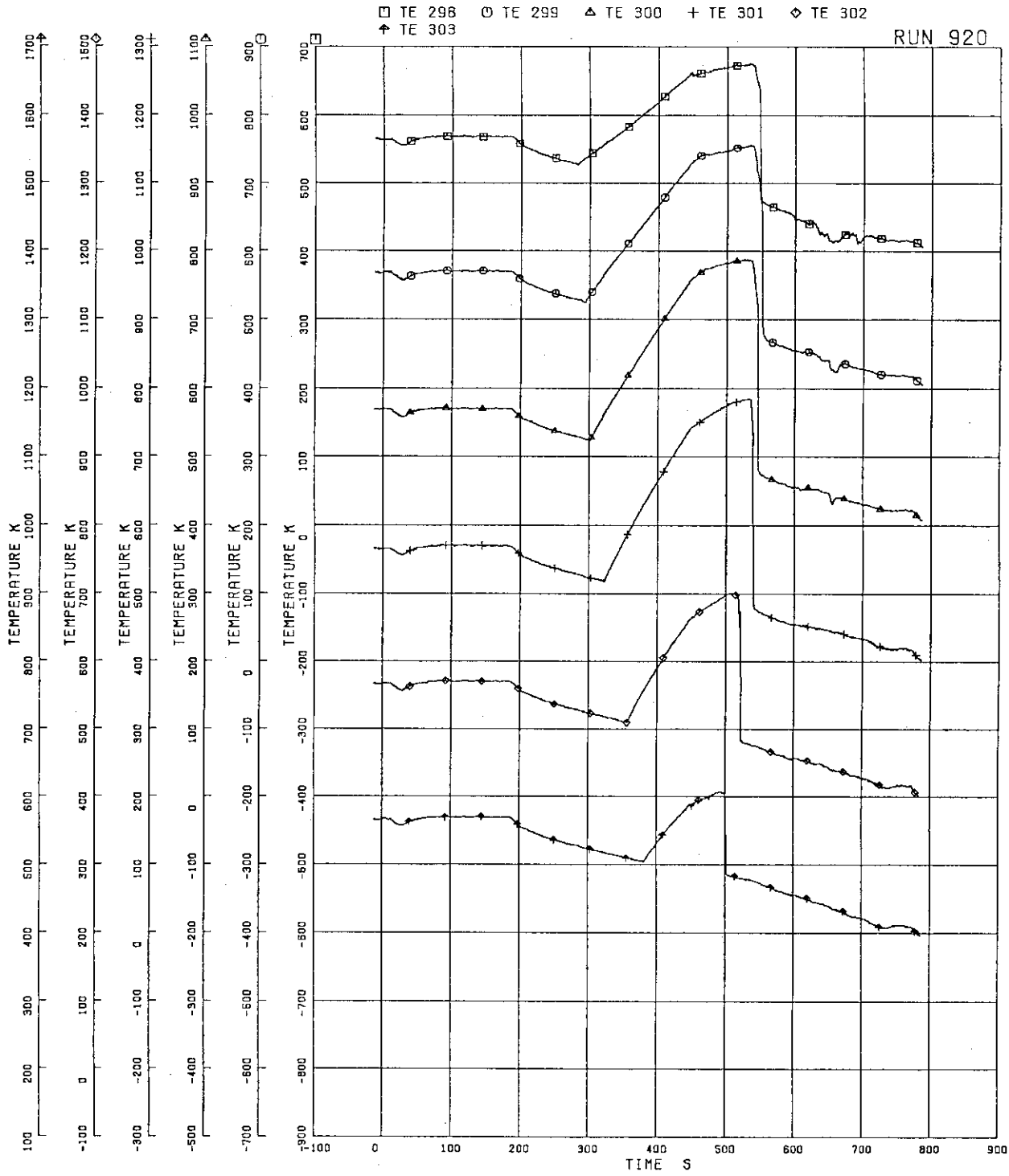

FIG.5.181 SURFACE TEMPERATURES OF FUEL ROD A77

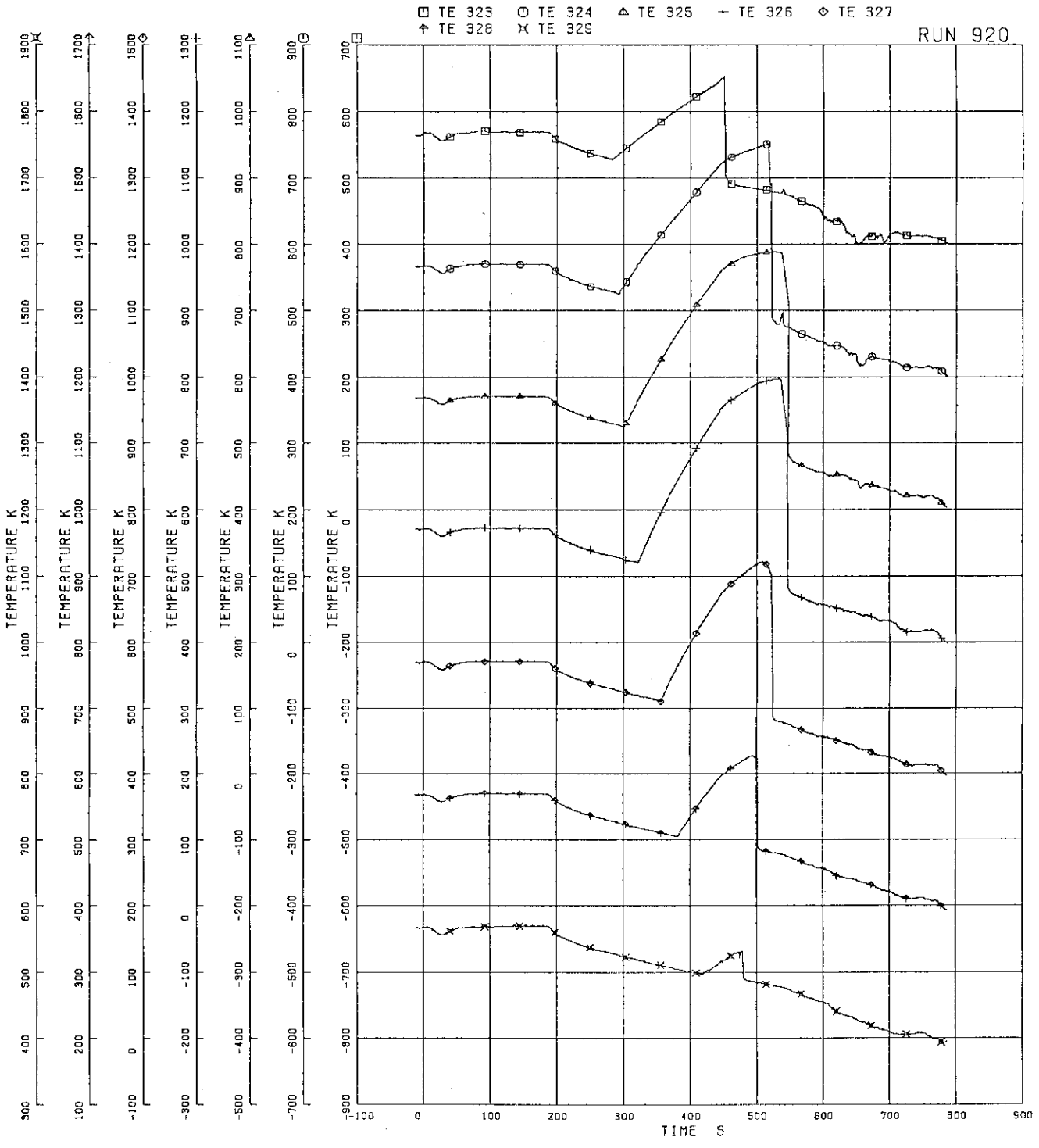

FIG.5.182 SURFACE TEMPERATURES OF FUEL ROD A88

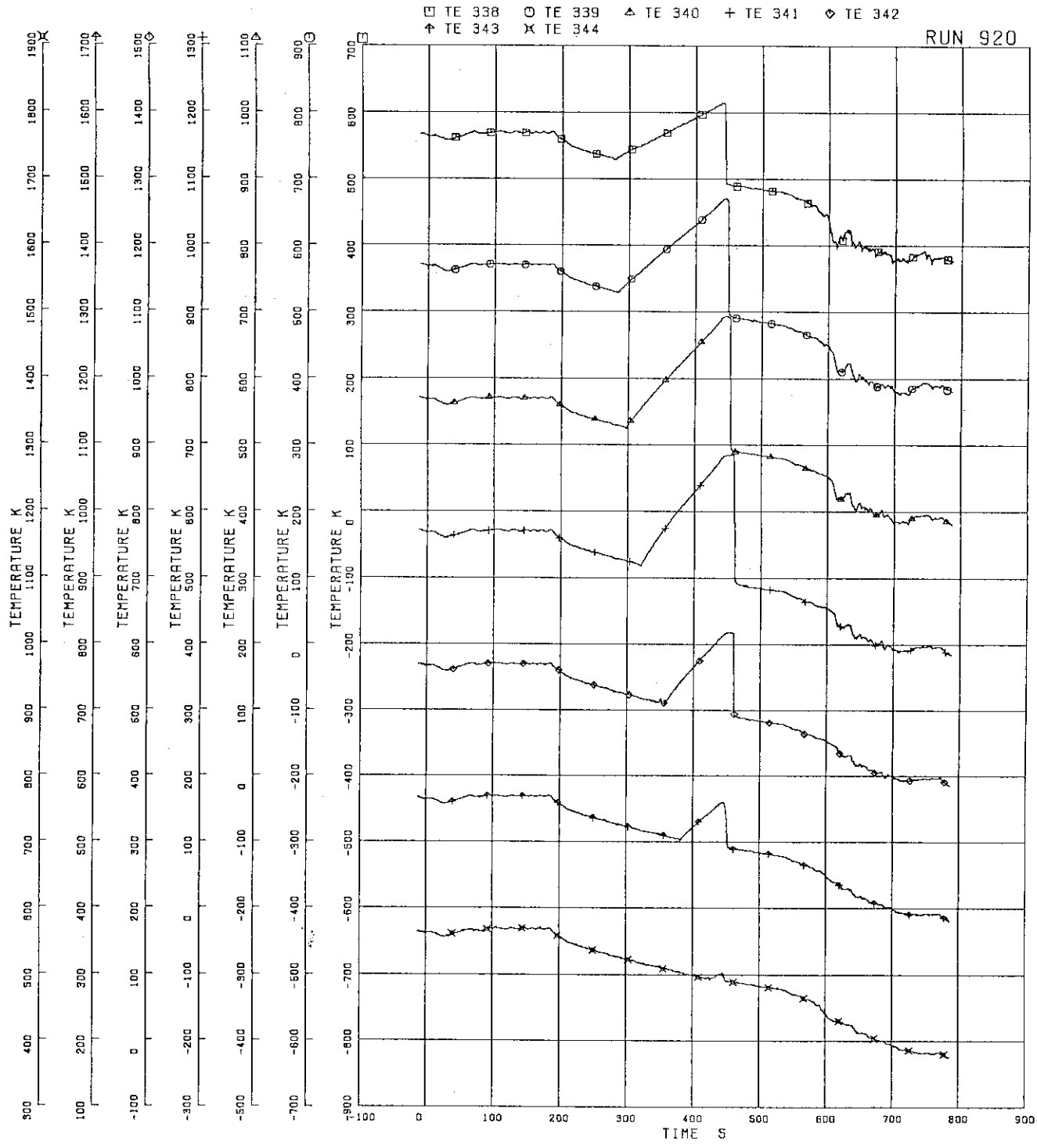

FIG.5.183 SURFACE TEMPERATURES OF FUEL ROD B22

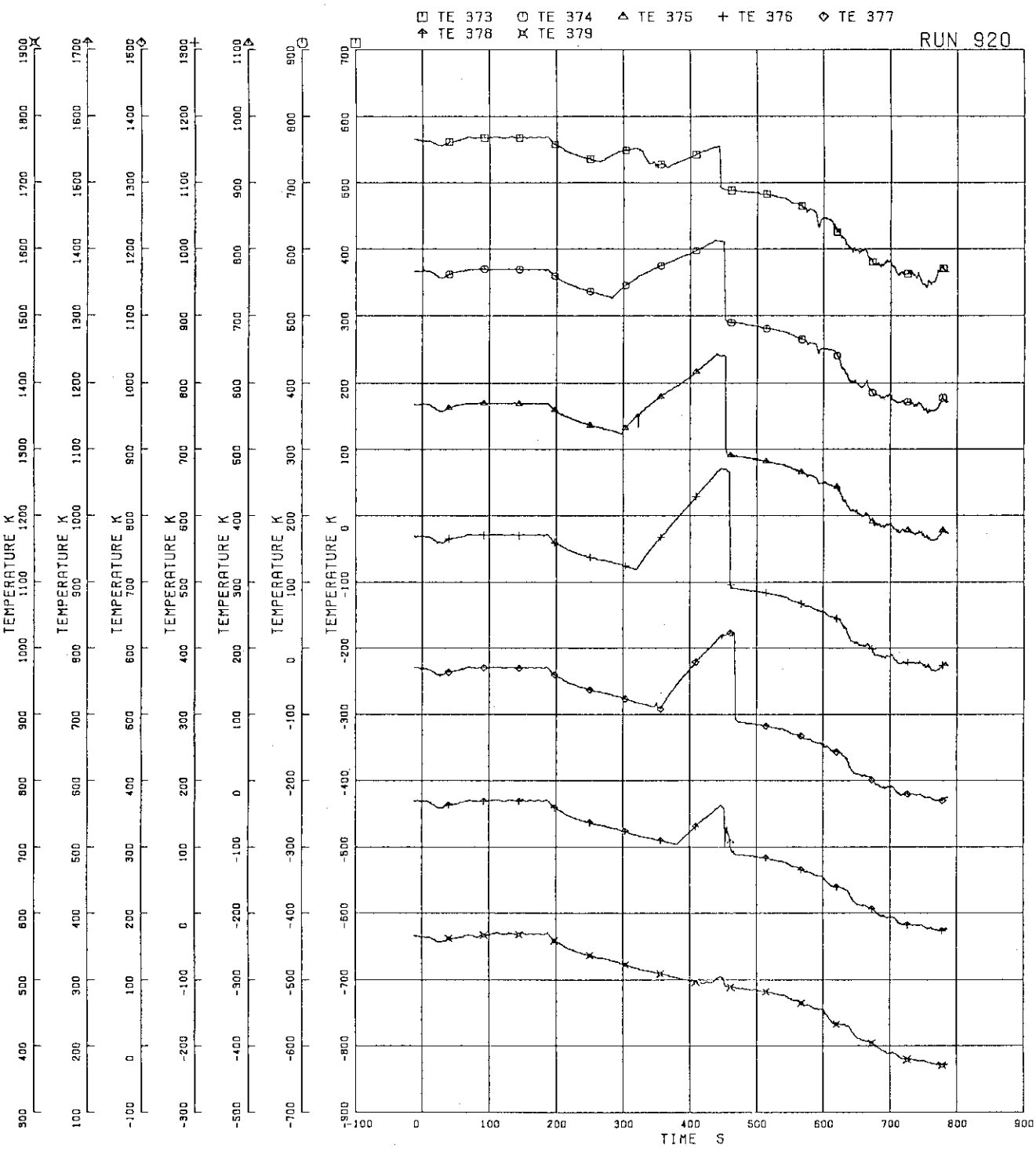

FIG.5.184 SURFACE TEMPERATURES OF FUEL ROD C22

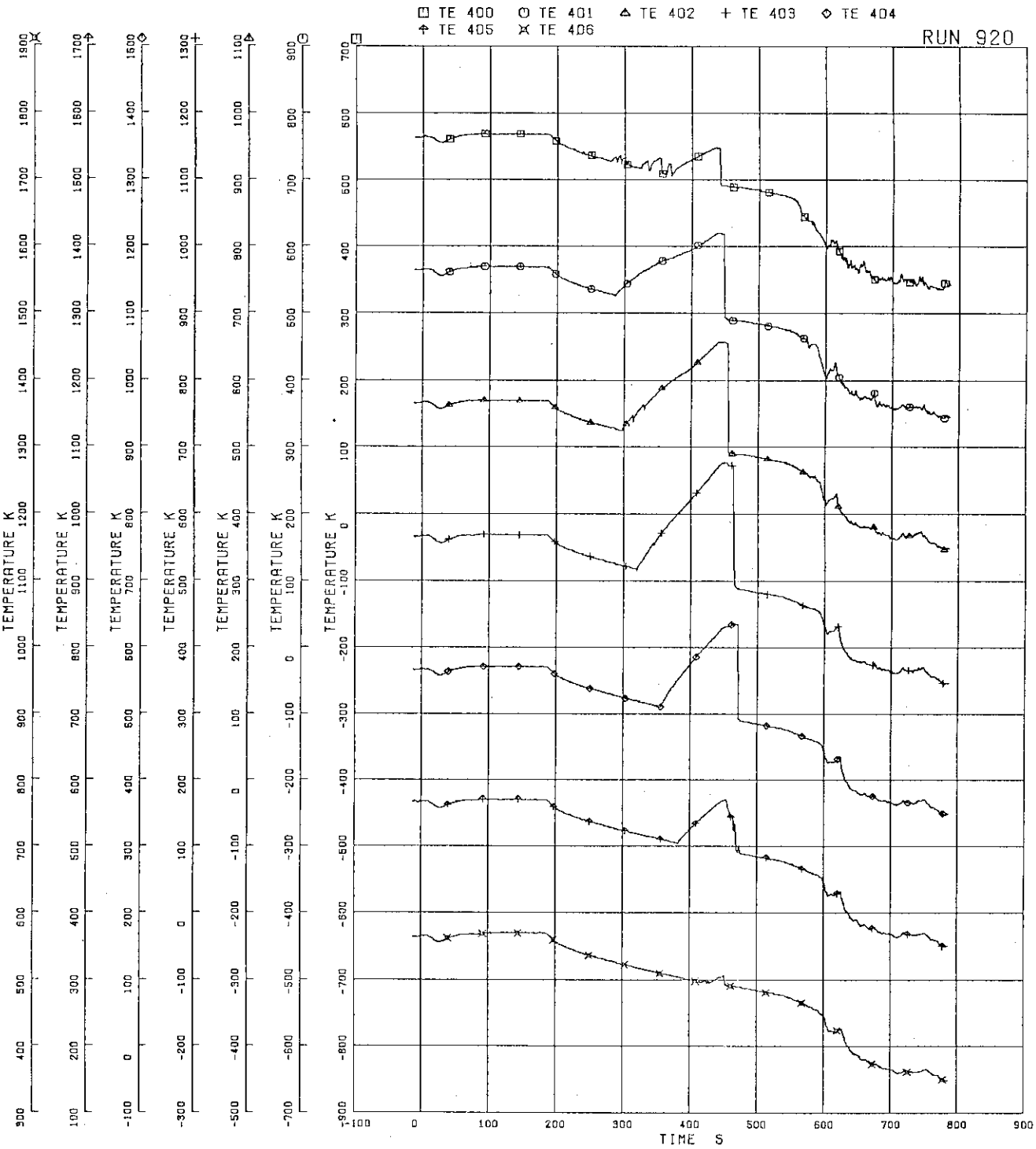

FIG.5.185 SURFACE TEMPERATURES OF FUEL ROD D22

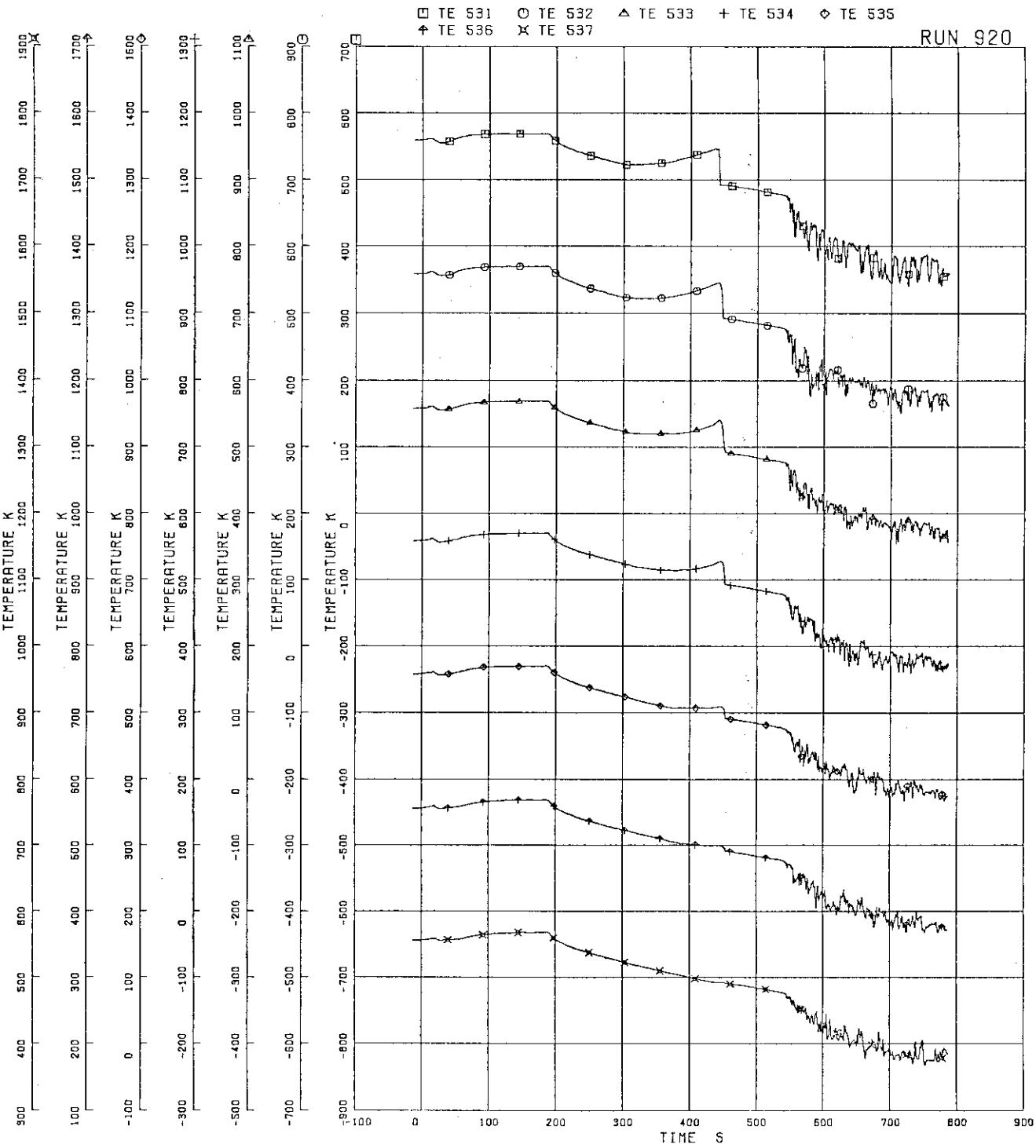

FIG.5.186 OUTER SURFACE TEMPERATURES OF CHANNEL BOX A

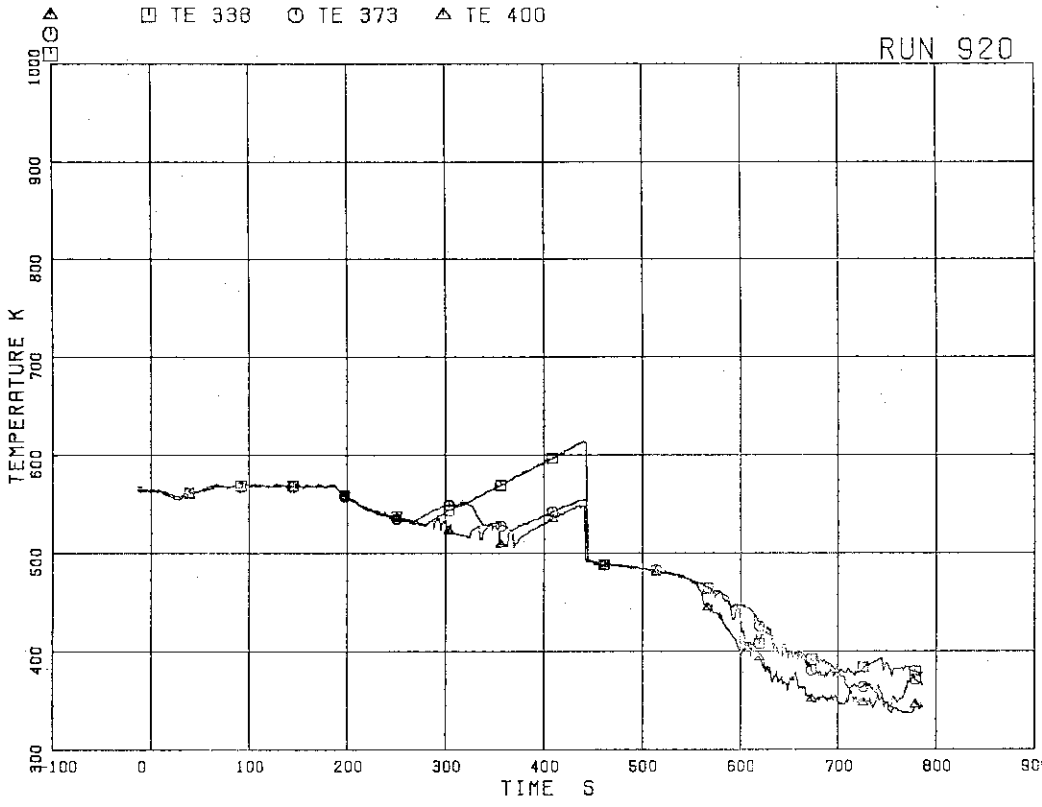

FIG.5.187 SURFACE TEMPERATURES OF FUEL RODS B22,C22,D22 AT POSITION 1

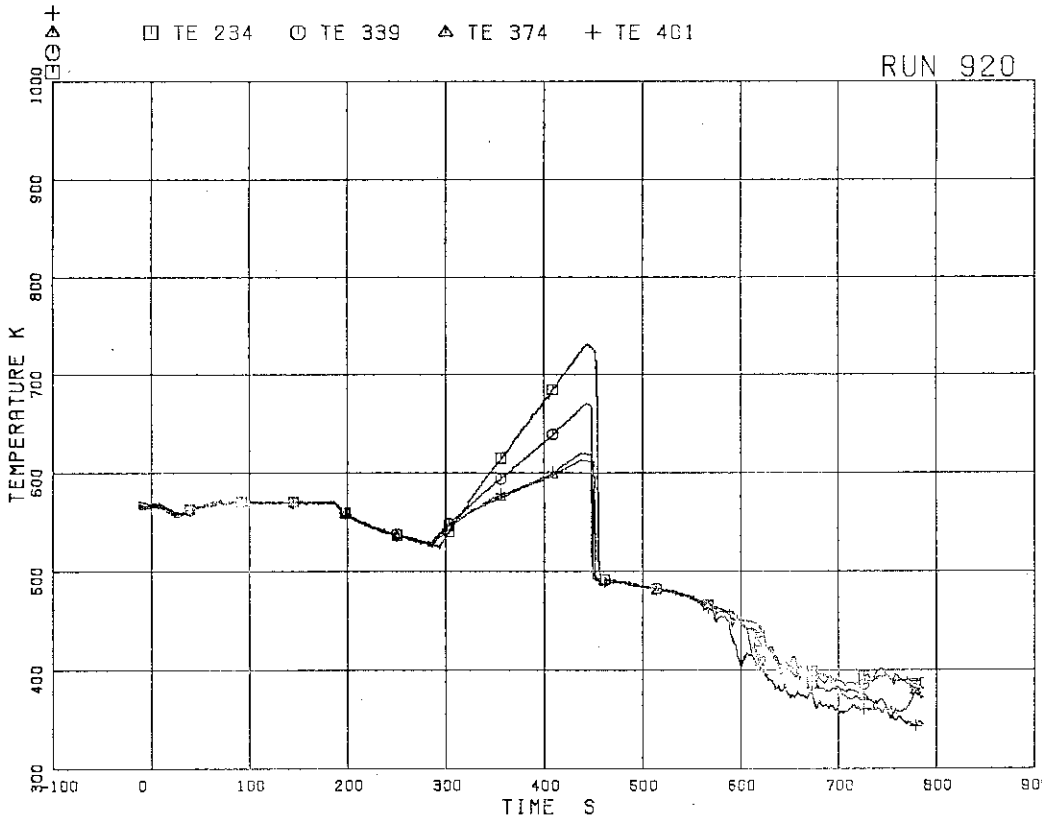

FIG.5.188 SURFACE TEMPERATURES OF FUEL RODS A22,B22,C22,D22 AT POSITION 2

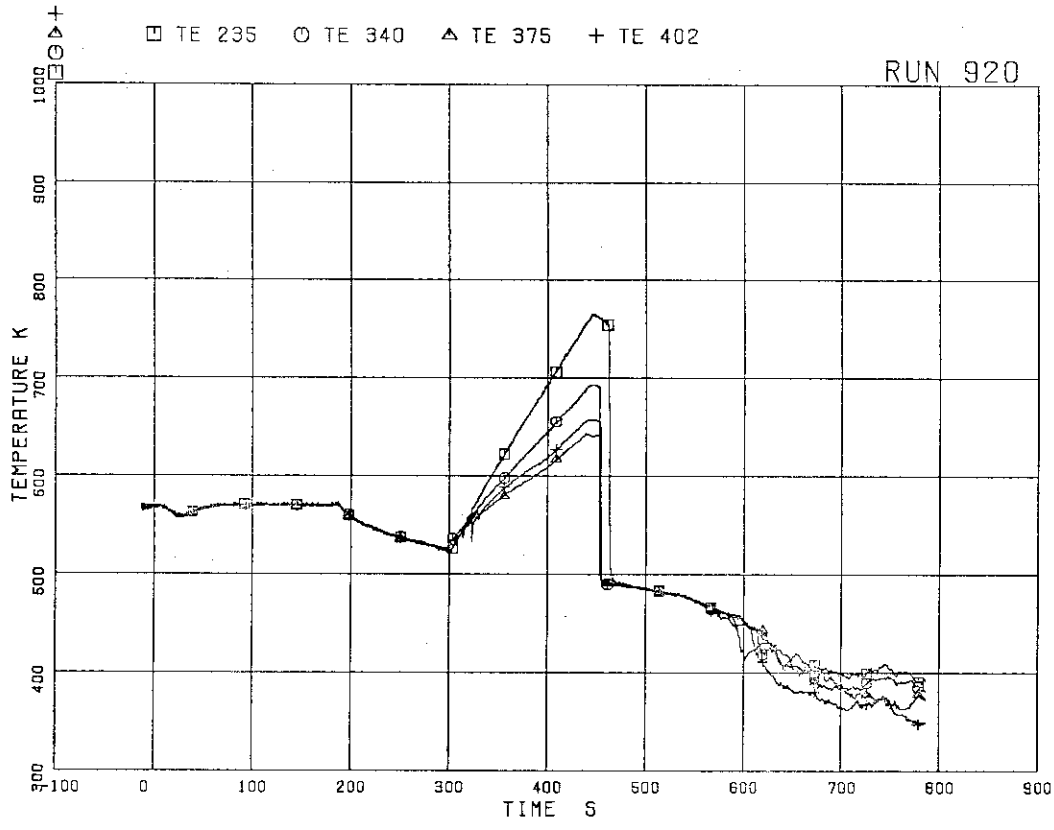

FIG.5.189 SURFACE TEMPERATURES OF FUEL RODS A22,B22,C22,D22 AT POSITION 3

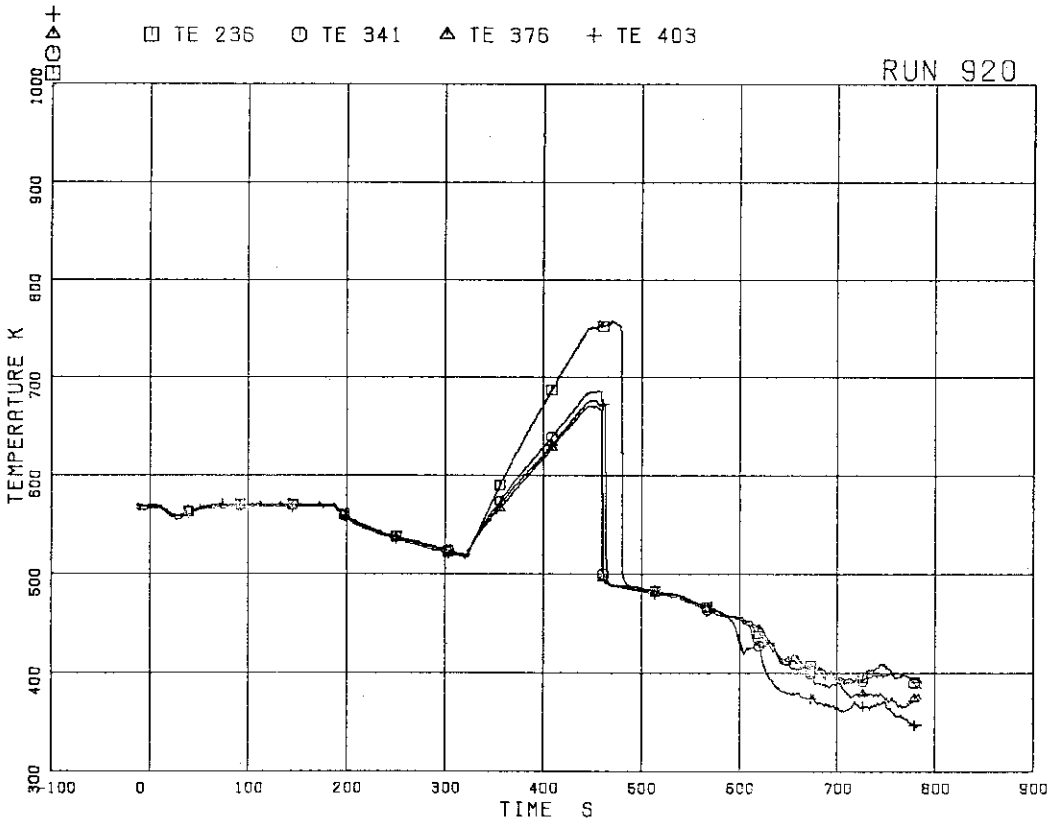

FIG.5.190 SURFACE TEMPERATURES OF FUEL RODS A22,B22,C22,D22 RODS AT POSITION 4

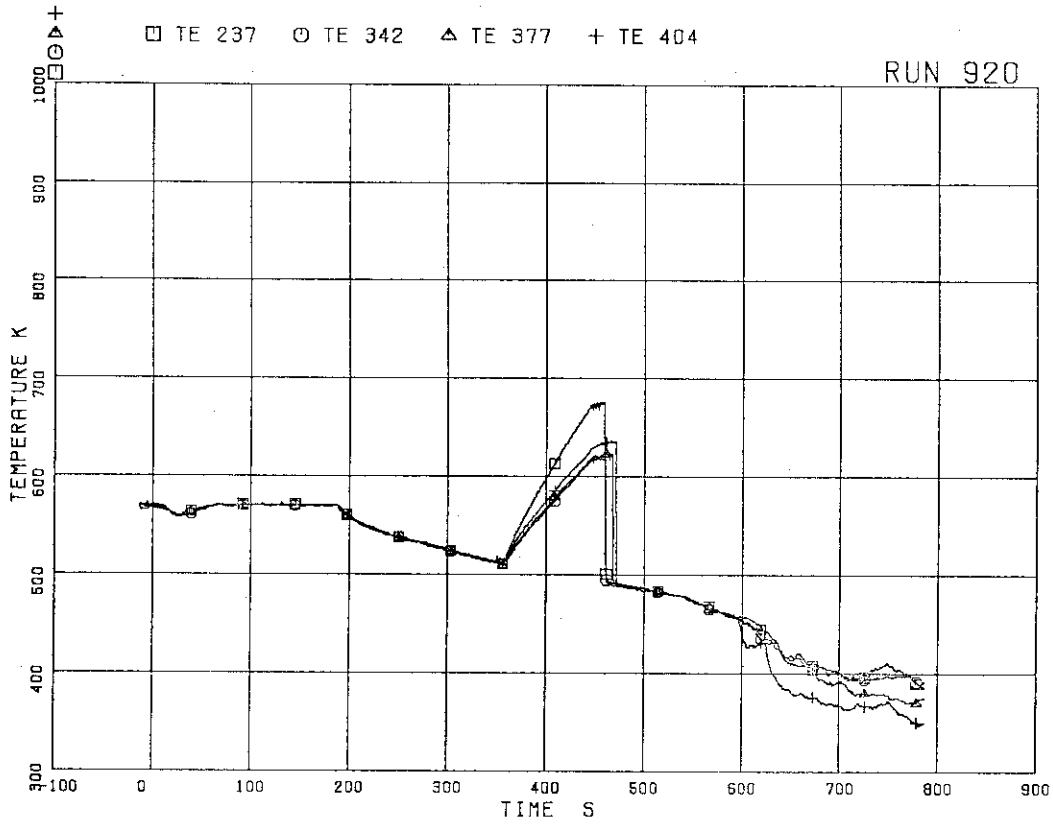

FIG.5.191 SURFACE TEMPERATURES OF FUEL RODS A22,B22,C22,D22 AT POSITION 5

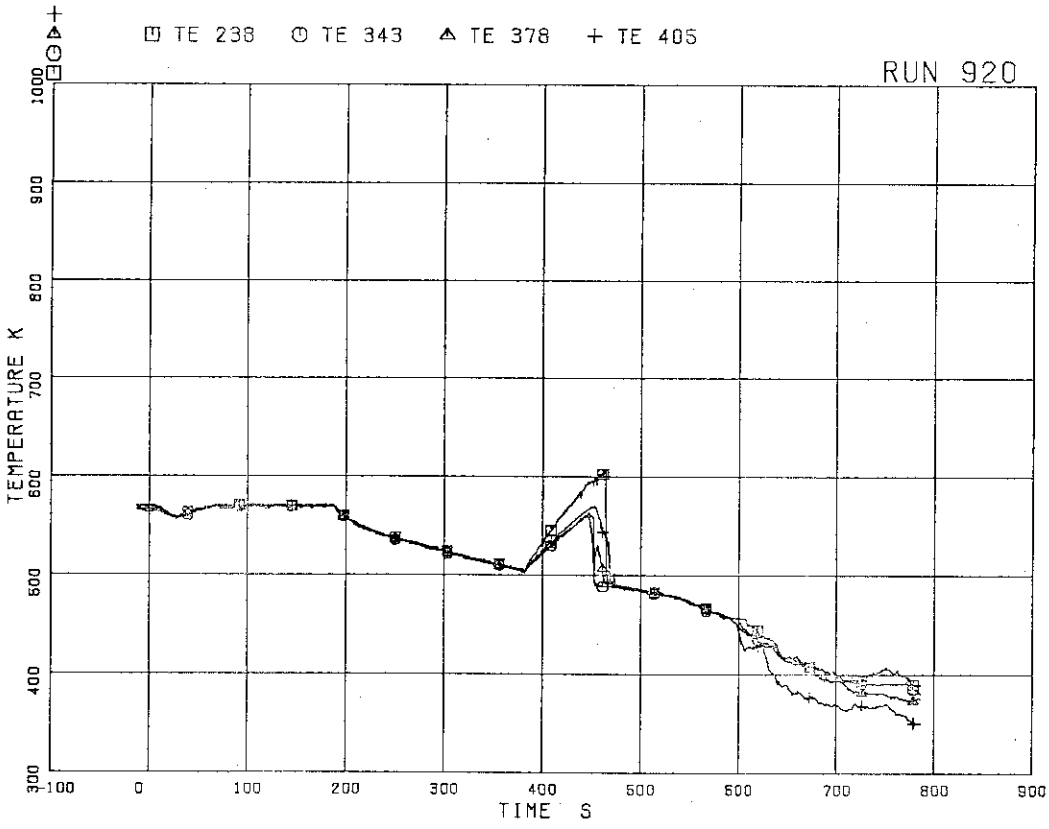

FIG.5.192 SURFACE TEMPERATURES OF FUEL RODS A22,B22,C22,D22 AT POSITION 6

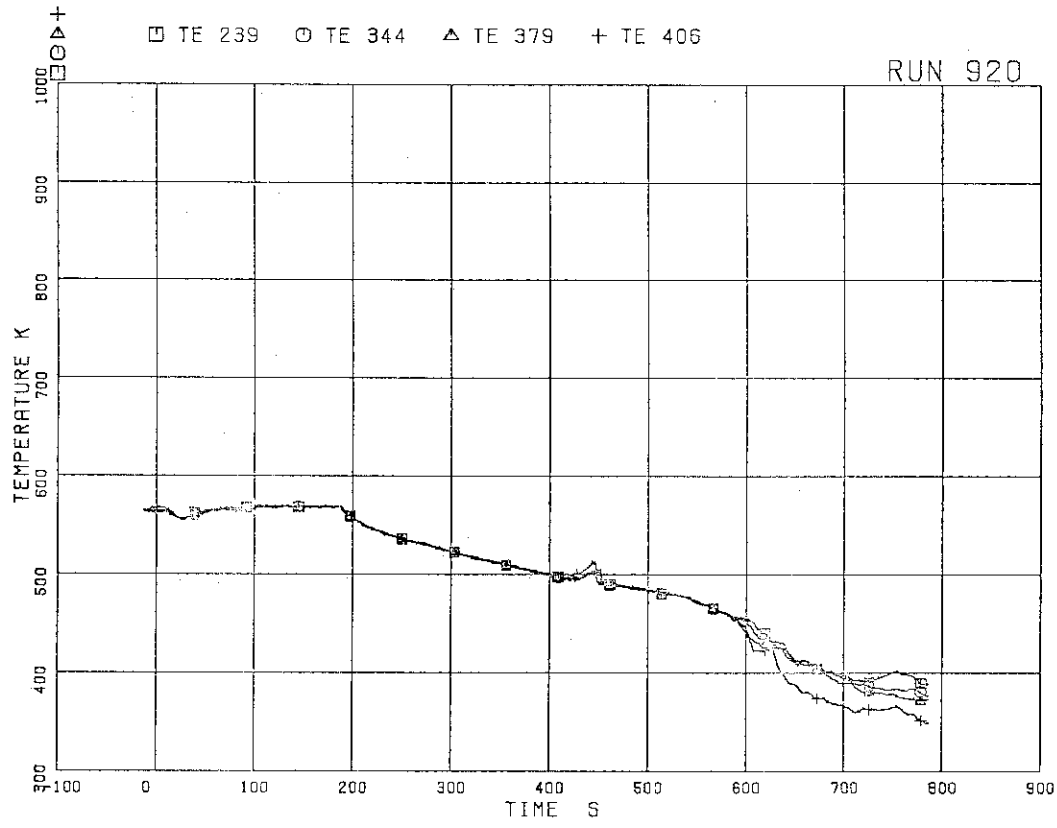

FIG.5.193 SURFACE TEMPERATURES OF FUEL RODS A22,B22,C22,D22 AT POSITION 7

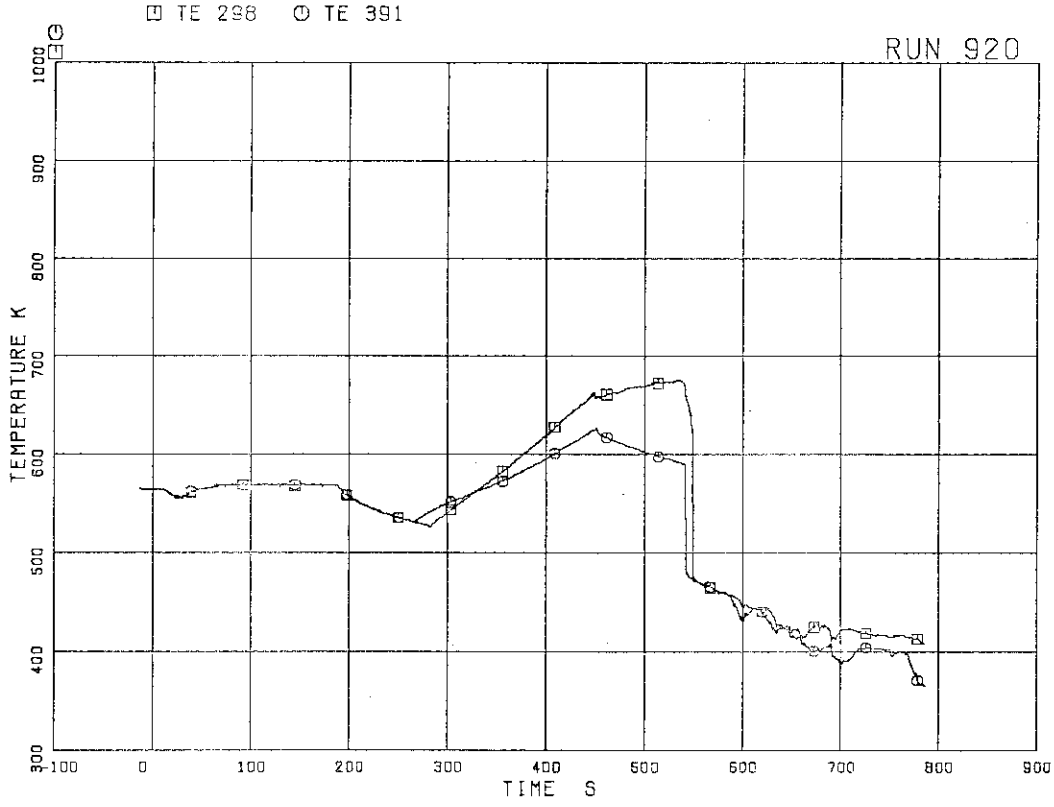

FIG.5.194 SURFACE TEMPERATURES OF FUEL RODS A77,C77 AT POSITION 1

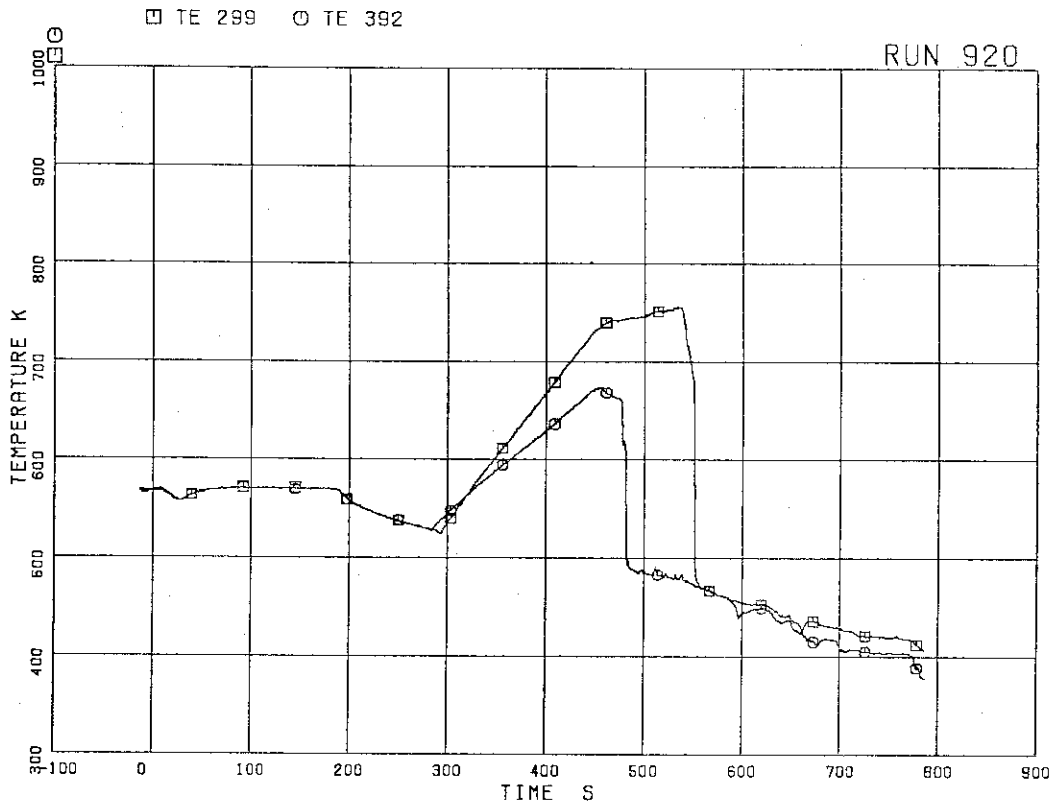

FIG.5.195 SURFACE TEMPERATURES OF FUEL RODS A77,C77 AT POSITION 2

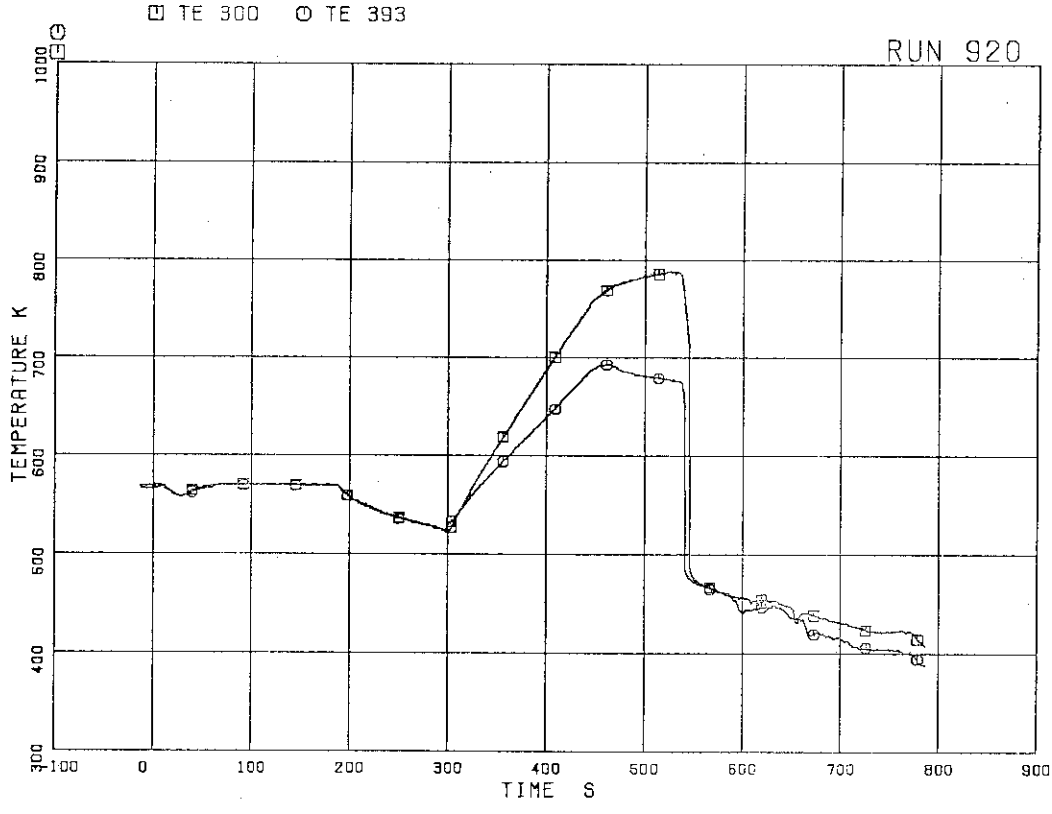

FIG.5.196 SURFACE TEMPERATURES OF FUEL RODS A77,C77 AT POSITION 3

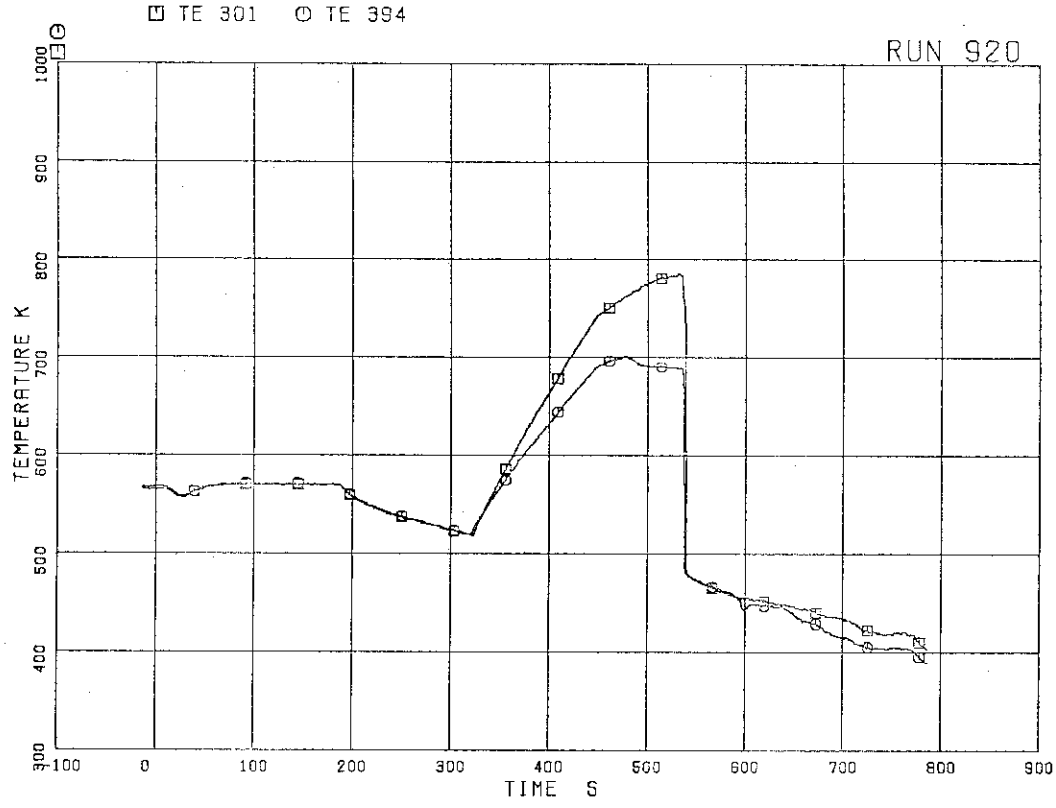

FIG.5.197 SURFACE TEMPERATURES OF FUEL RODS A77,C77,D77 AT POSITION 4

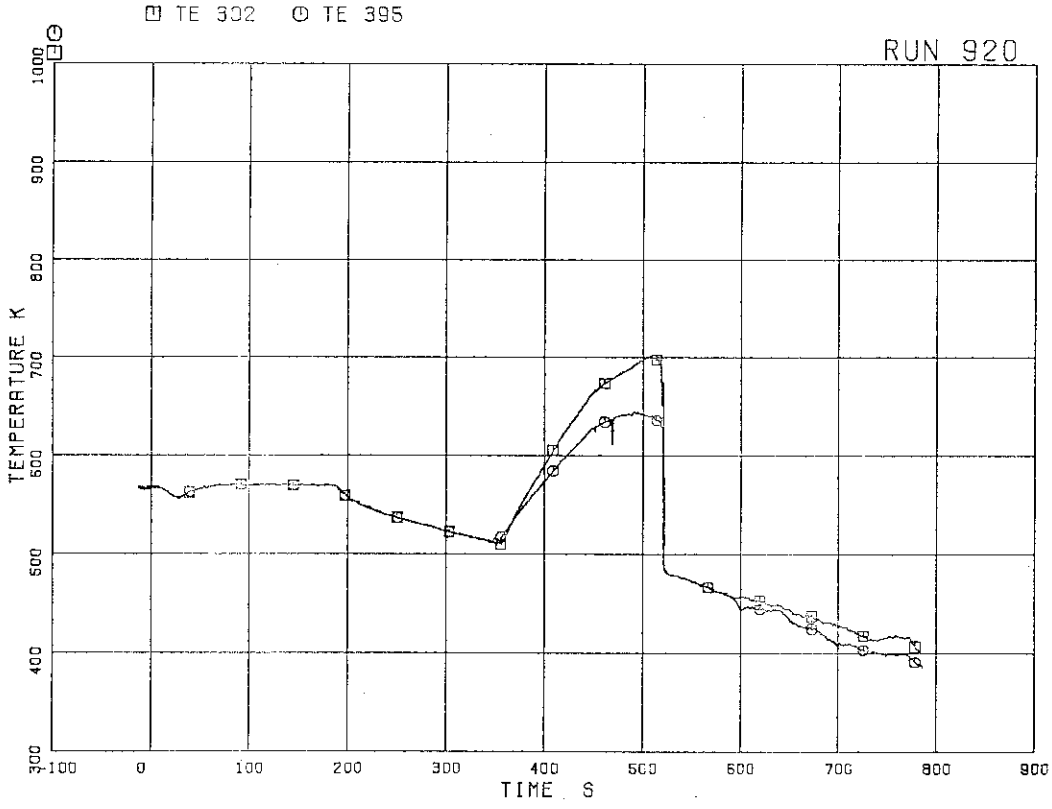

FIG.5.198 SURFACE TEMPERATURES OF FUEL RODS A77,C77 AT POSITION 5

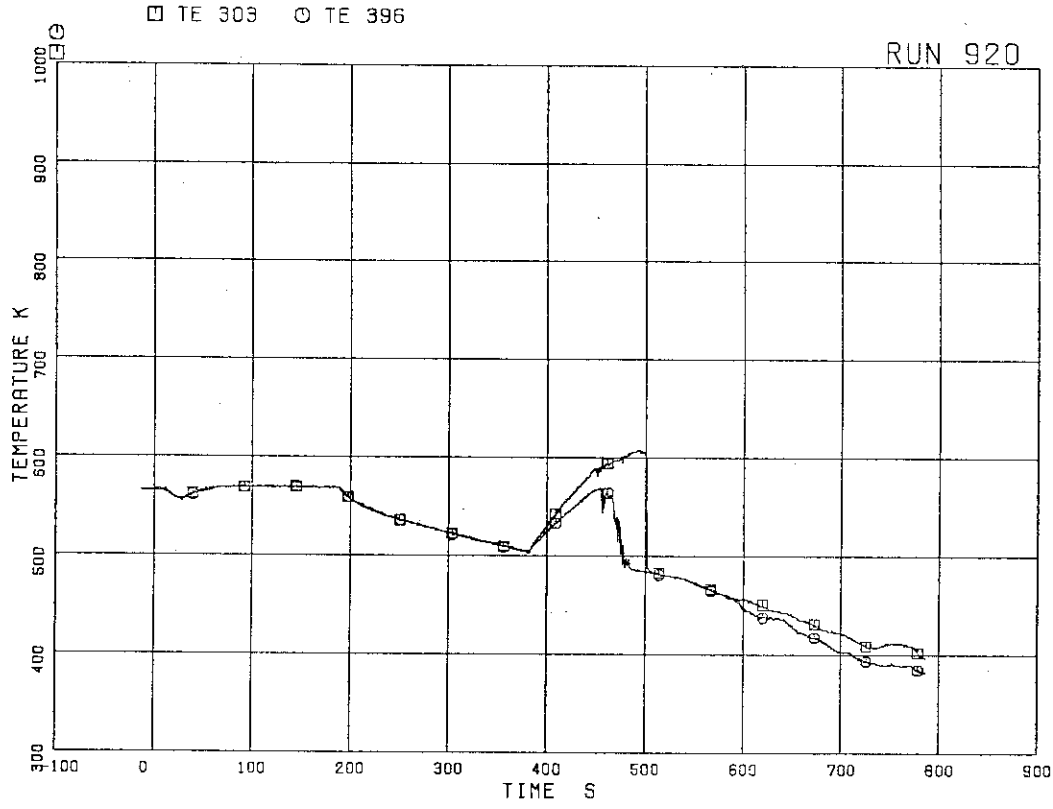

FIG.5.199 SURFACE TEMPERATURES OF FUEL RODS A77,C77 AT POSITION 6

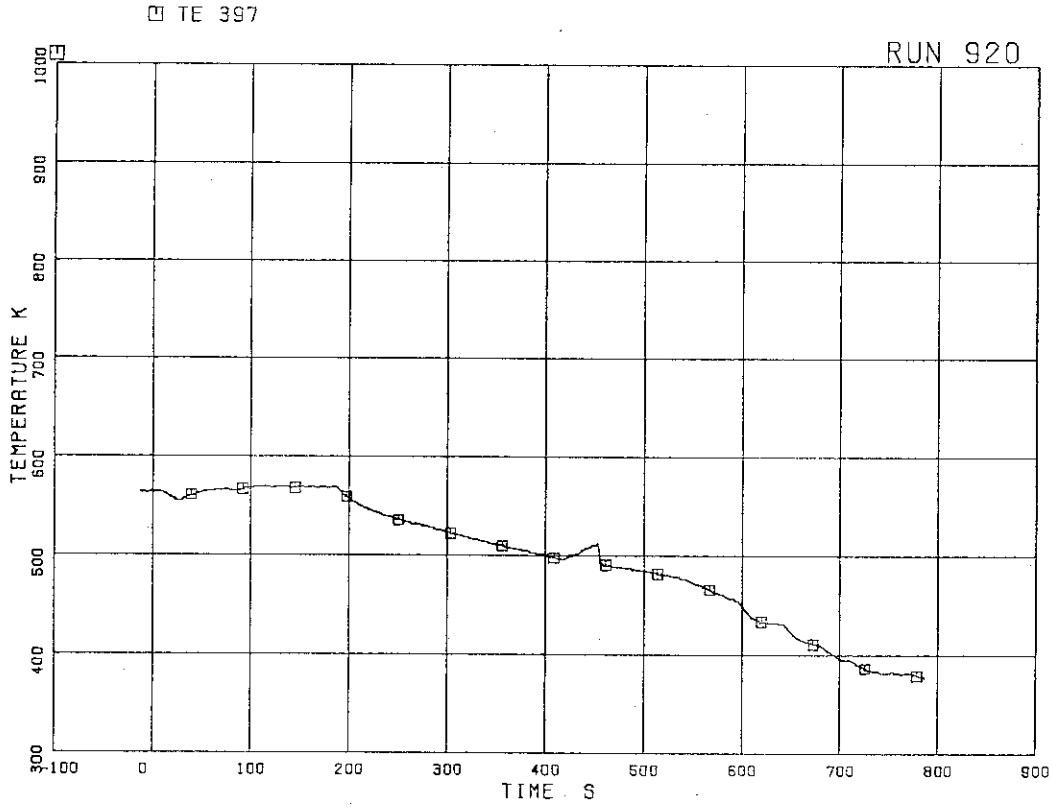

FIG.5.200 SURFACE TEMPERATURES OF FUEL RODS C77 RODS AT POSITION 7

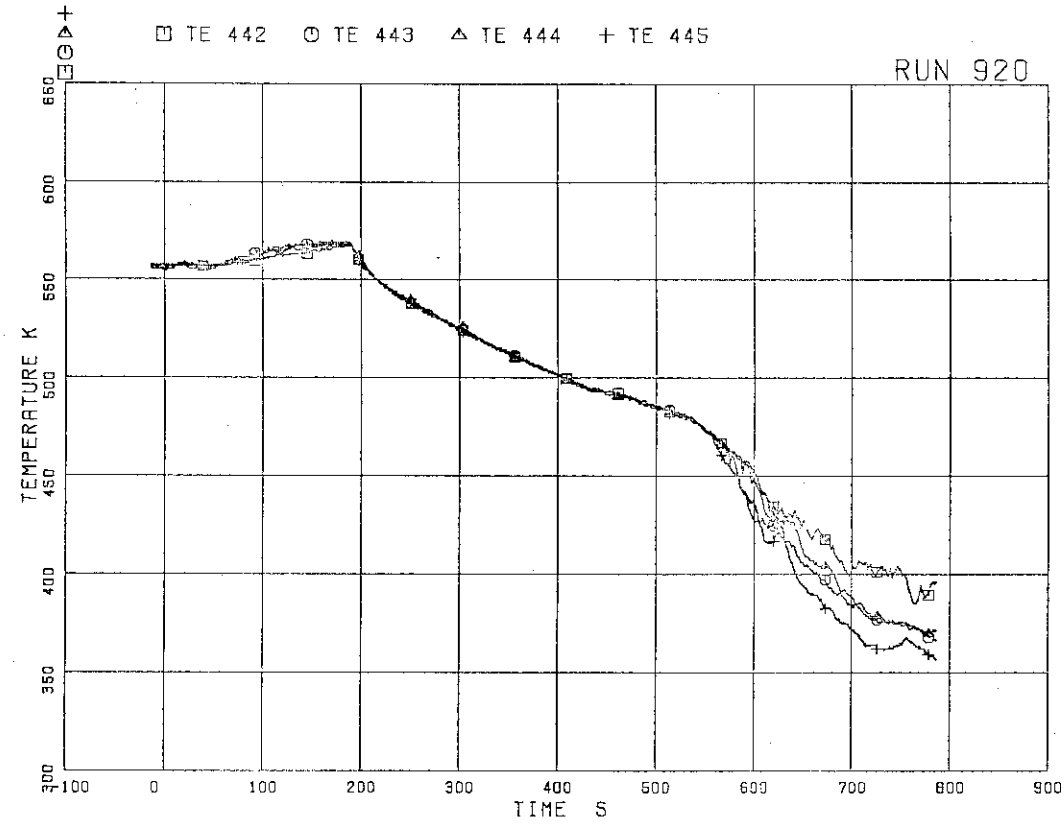

FIG.5.201 FLUID TEMPERATURES AT CHANNEL INLET

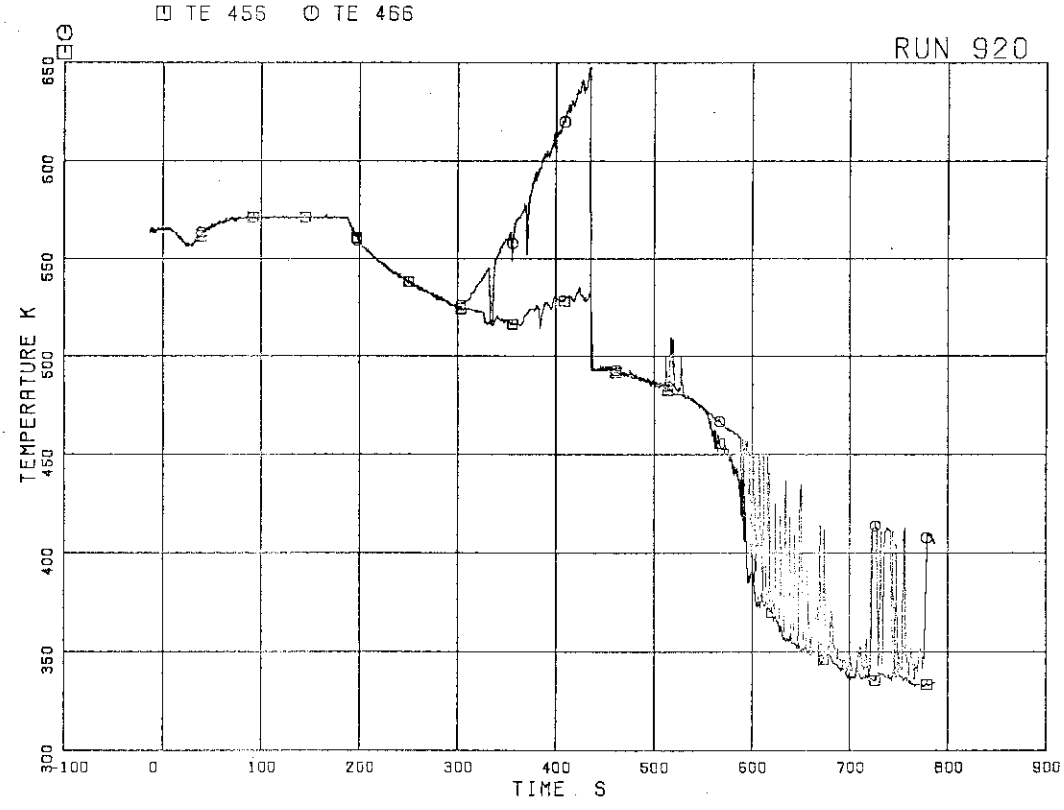

FIG.5.202 FLUID TEMPERATURES AT UTP IN CHANNEL A, OPENING 1

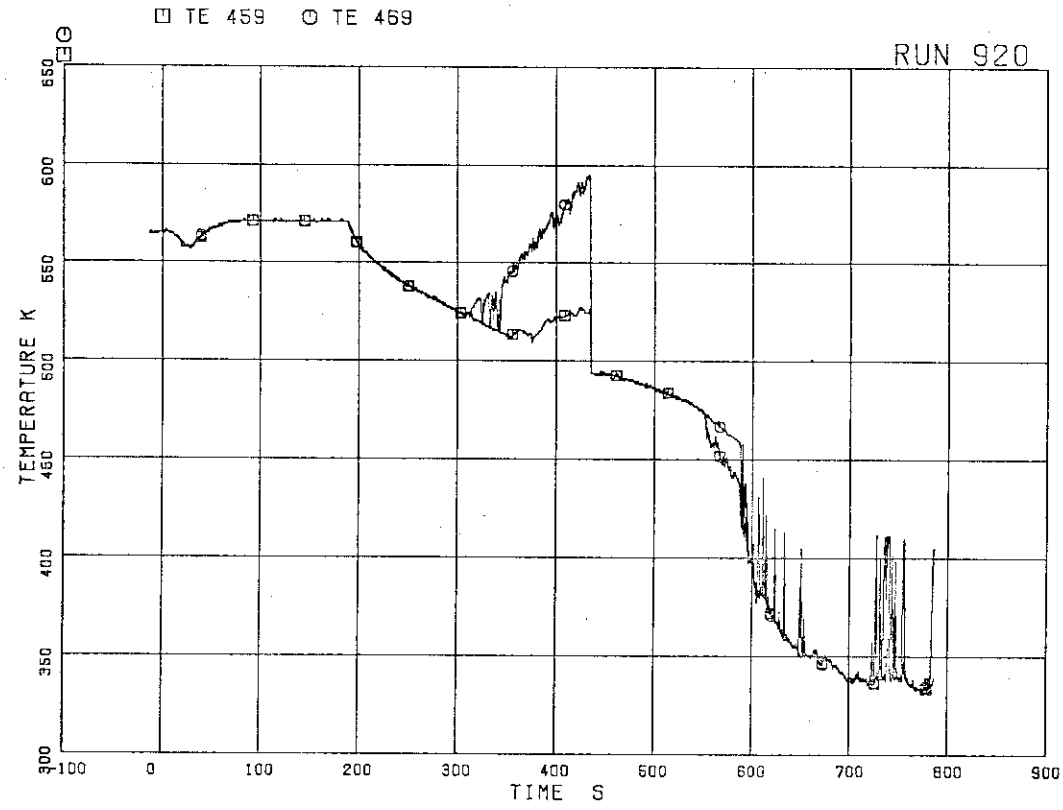

FIG.5.203 FLUID TEMPERATURES AT UTP IN CHANNEL A, OPENING 4

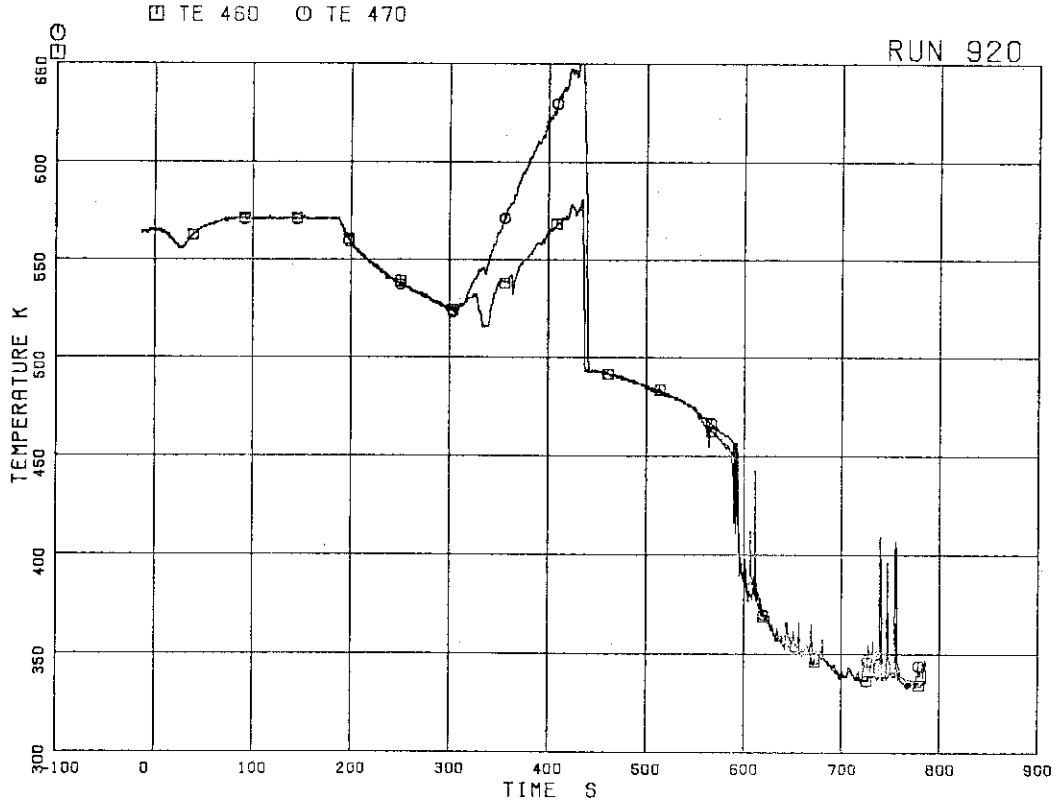

FIG.5.204 FLUID TEMPERATURES AT UTP IN CHANNEL A, OPENING 5

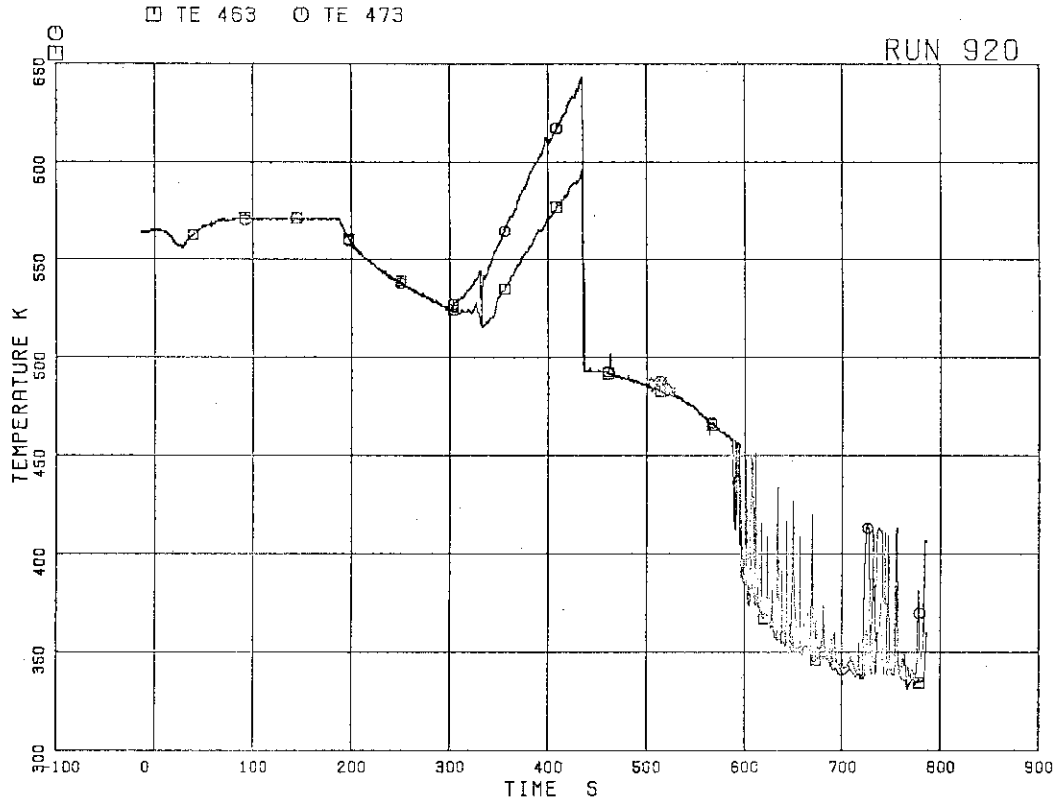

FIG.5.205 FLUID TEMPERATURES AT UTP IN CHANNEL A, OPENING 8

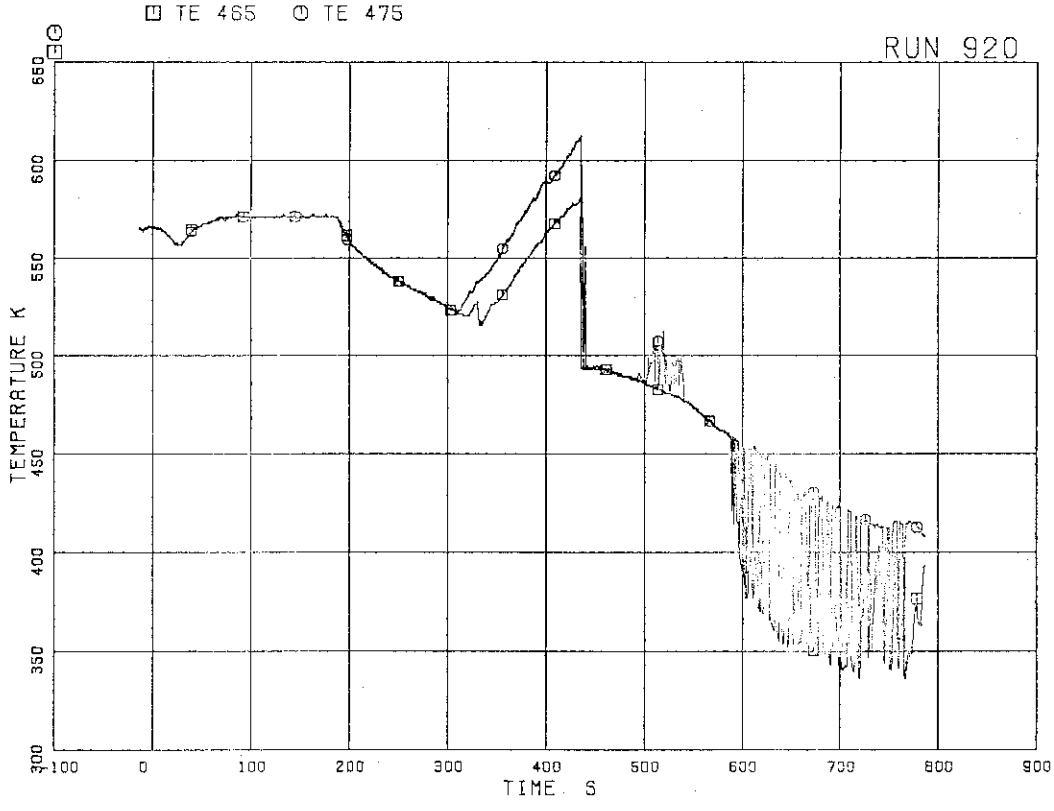

FIG.5.206 FLUID TEMPERATURES AT UTP IN CHANNEL A, OPENING 10

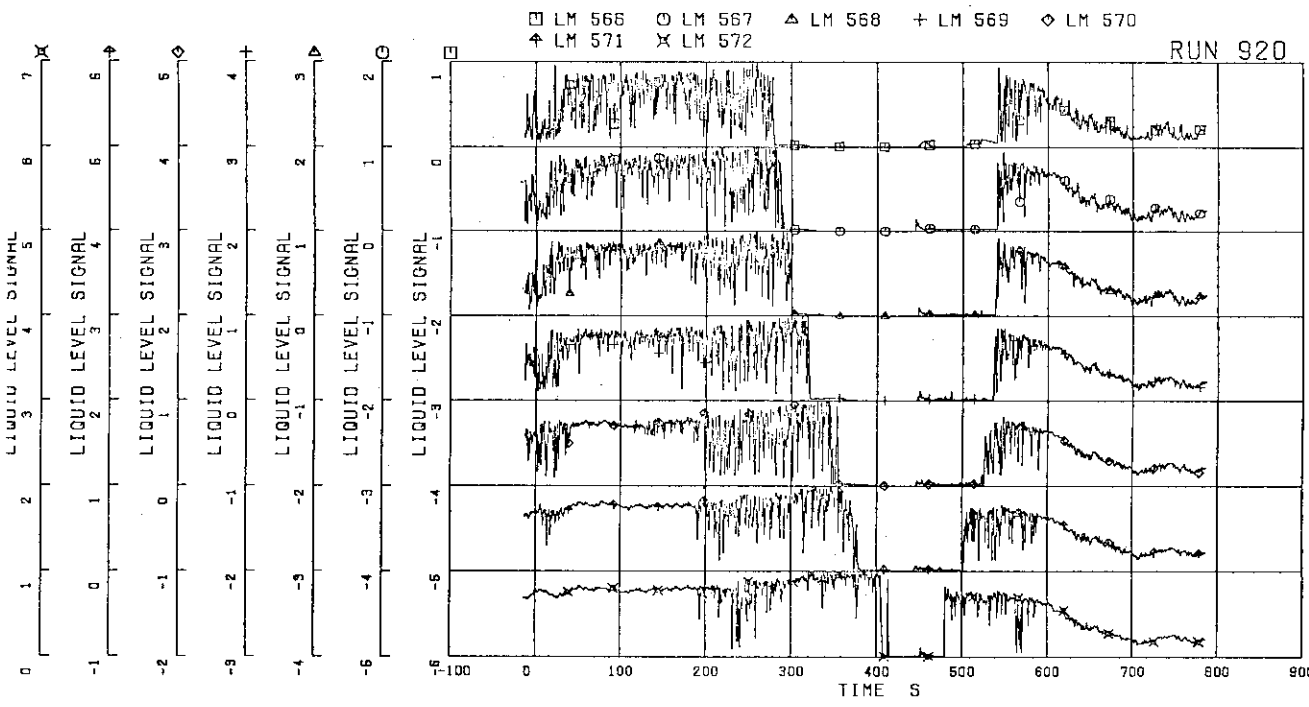

FIG.5.207 LIQUID LEVEL SIGNALS IN CHANNEL BOX A, LOCATION A2

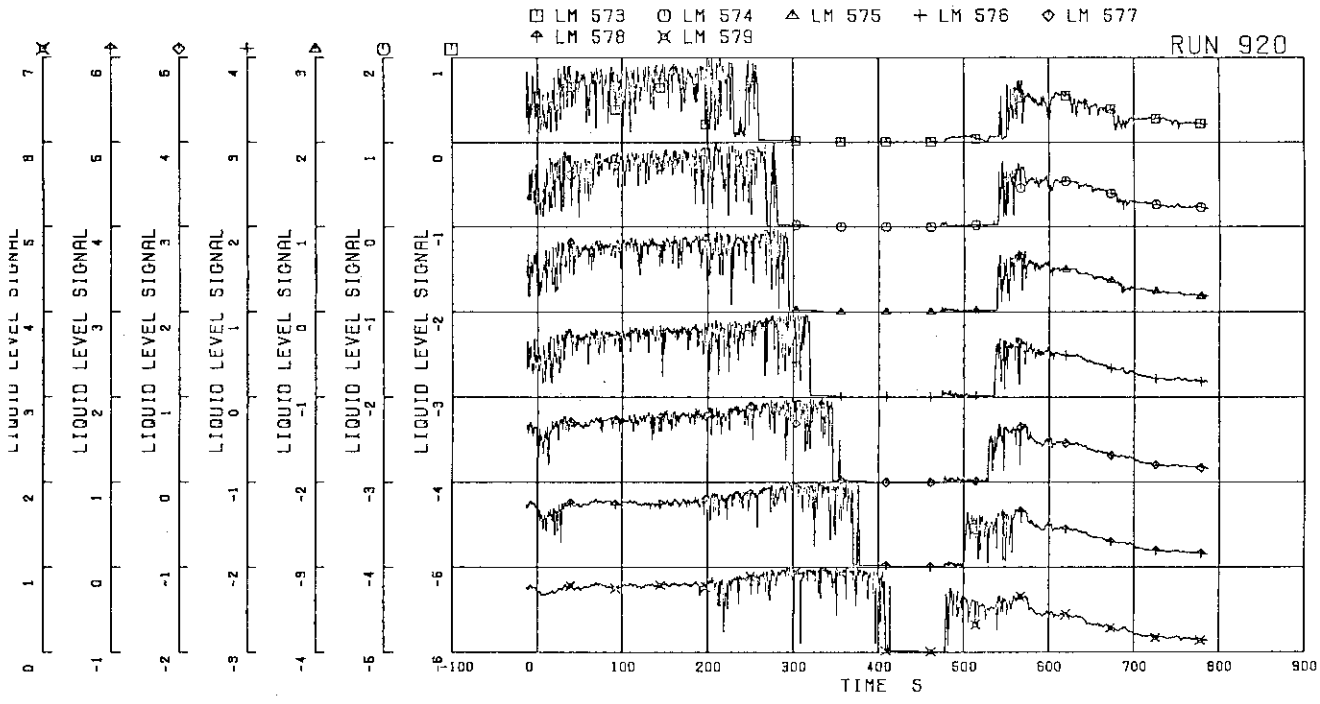

FIG.5.208 LIQUID LEVEL SIGNALS IN CHANNEL BOX B

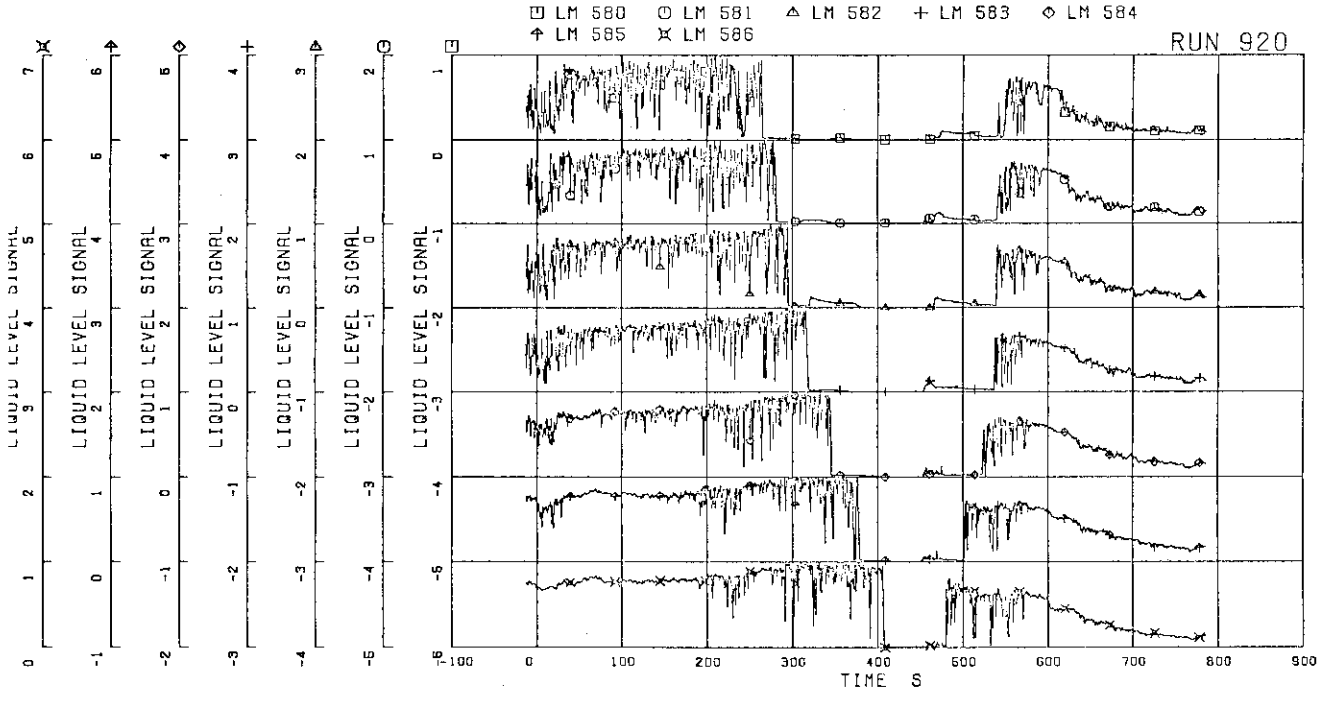

FIG.5.209 LIQUID LEVEL SIGNALS IN CHANNEL BOX C

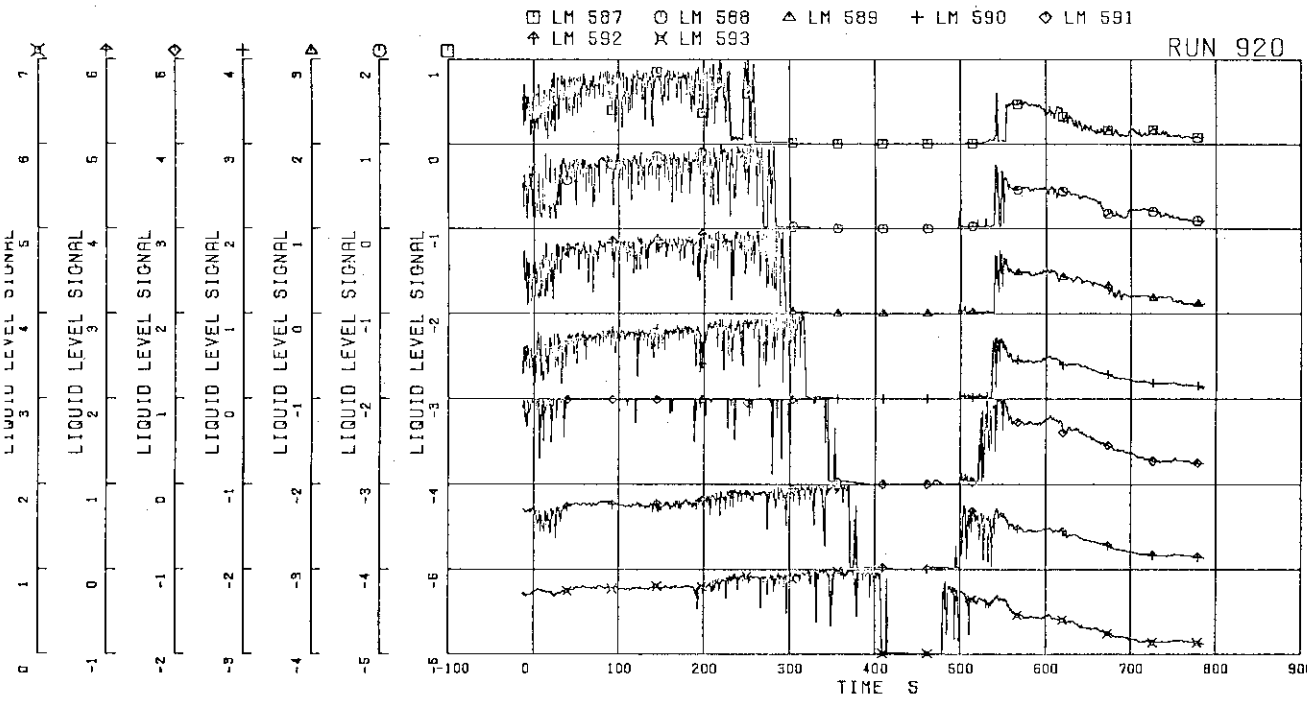

FIG.5.210 LIQUID LEVEL SIGNALS IN CHANNEL BOX D

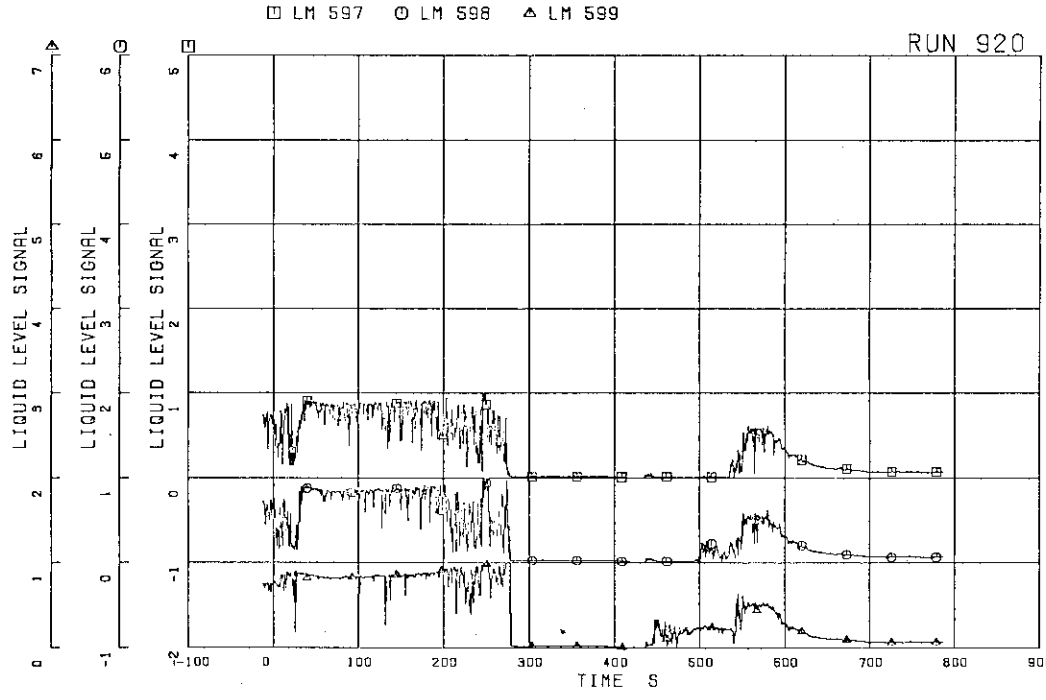

FIG.5.211 LIQUID LEVEL SIGNALS IN CHANNEL A OUTLET LOCATION A2

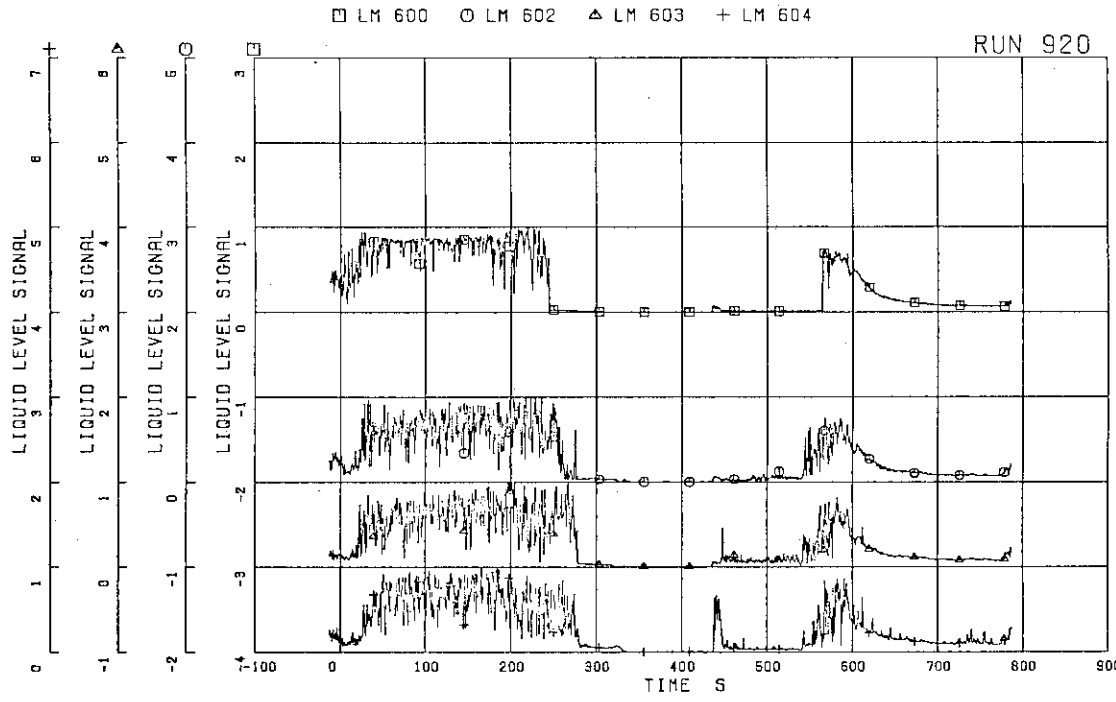

FIG.5.212 LIQUID LEVEL SIGNALS IN CHANNEL A OUTLET CENTER

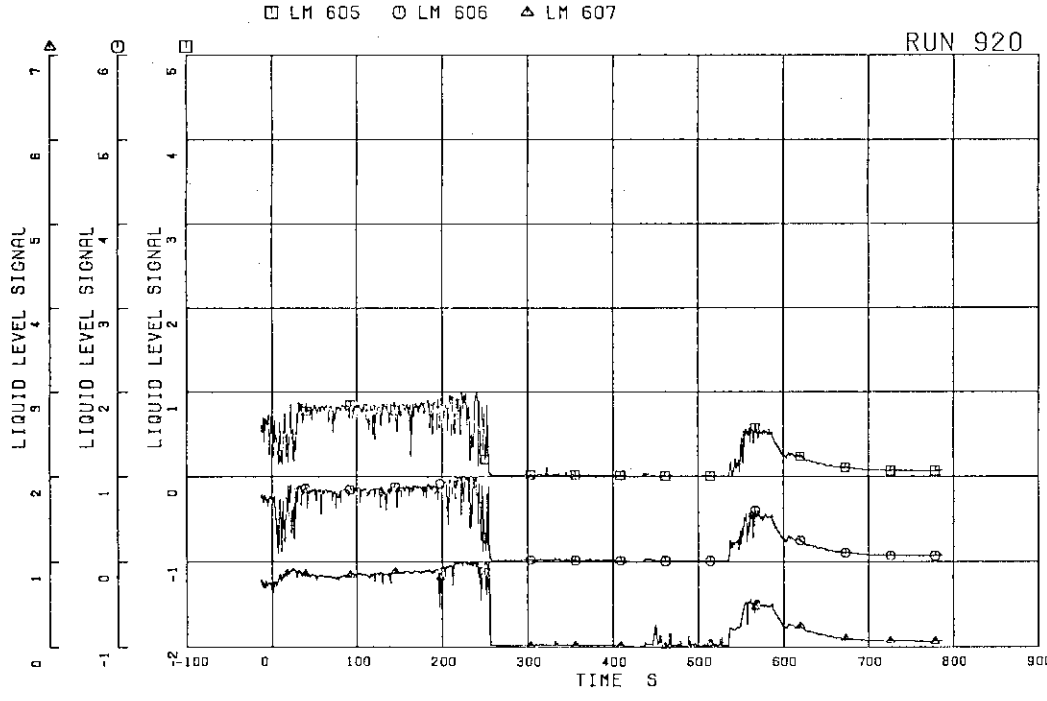

FIG.5.213 LIQUID LEVEL SIGNALS IN CHANNEL C OUTLET LOCATION C1

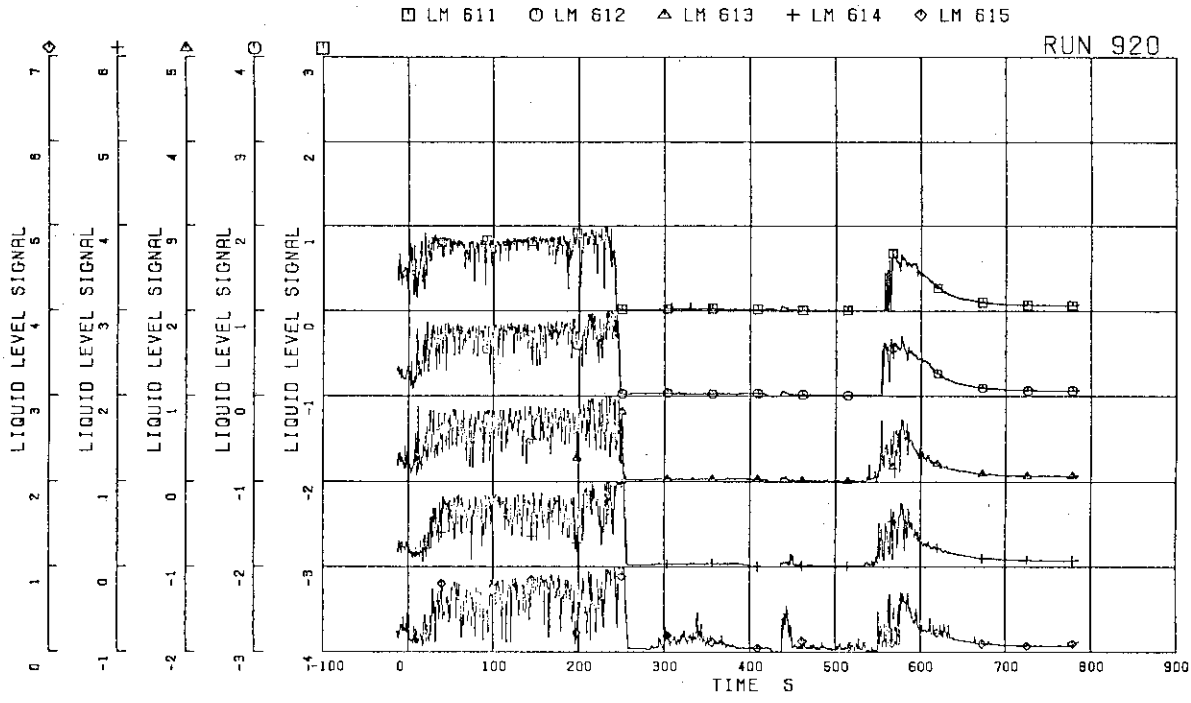

FIG.5.214 LIQUID LEVEL SIGNALS IN CHANNEL C OUTLET CENTER

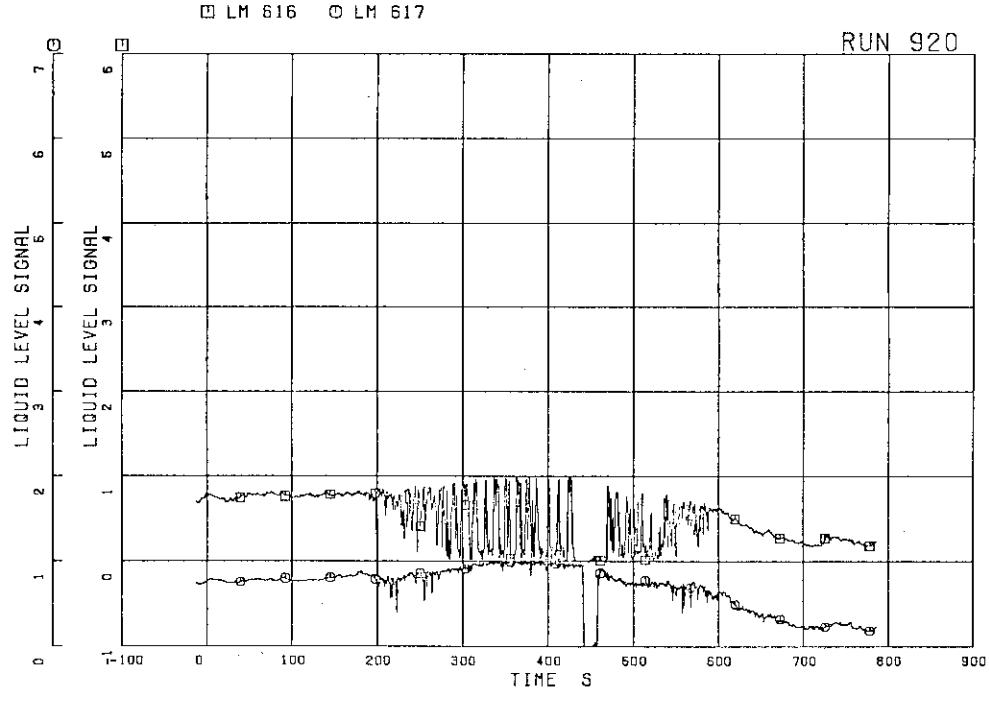

FIG.5.215 LIQUID LEVEL SIGNALS IN CHANNEL A INLET

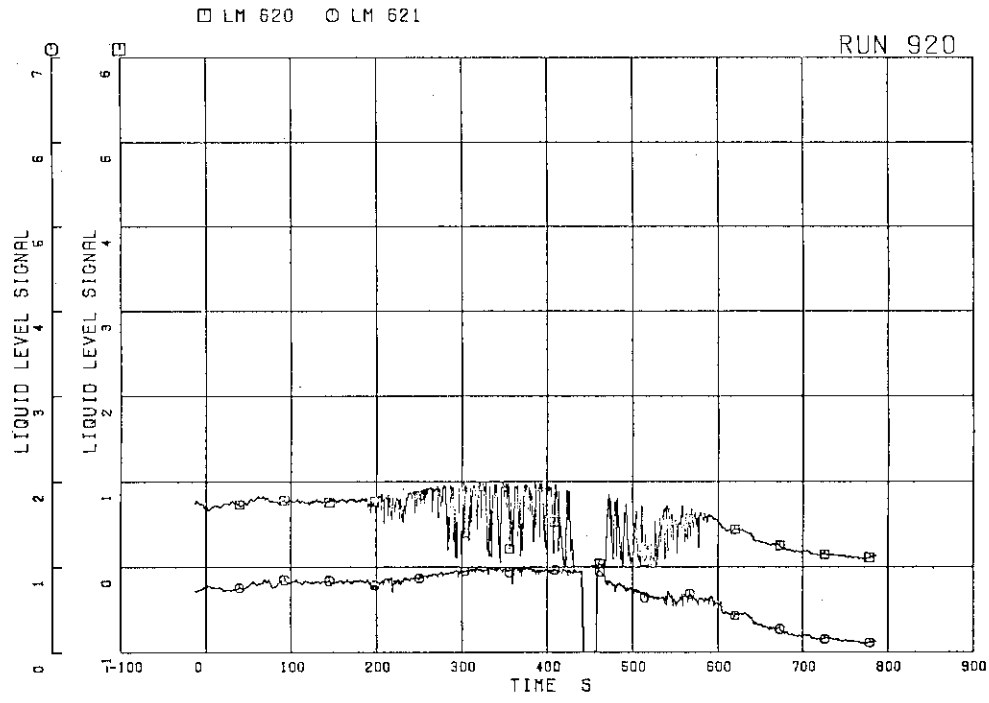

FIG.5.216 LIQUID LEVEL SIGNALS IN CHANNEL C INLET

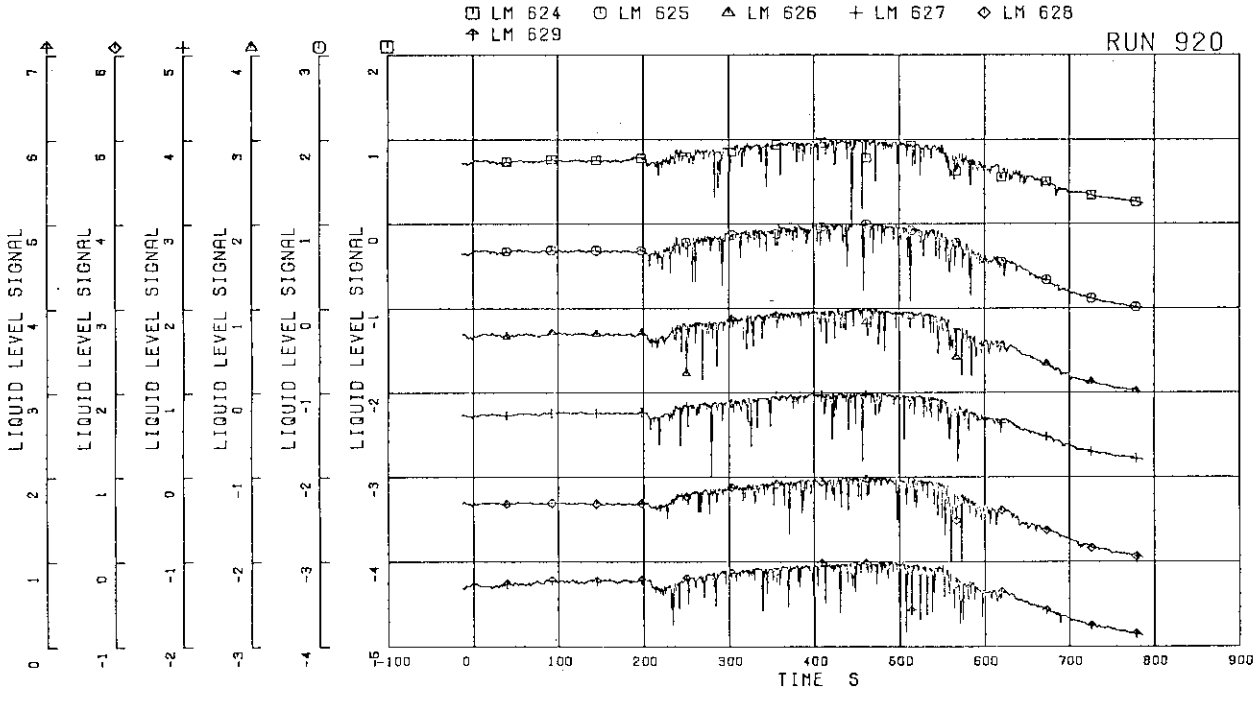

FIG.5.217 LIQUID LEVEL SIGNALS IN LOWER PLENUM, NORTH

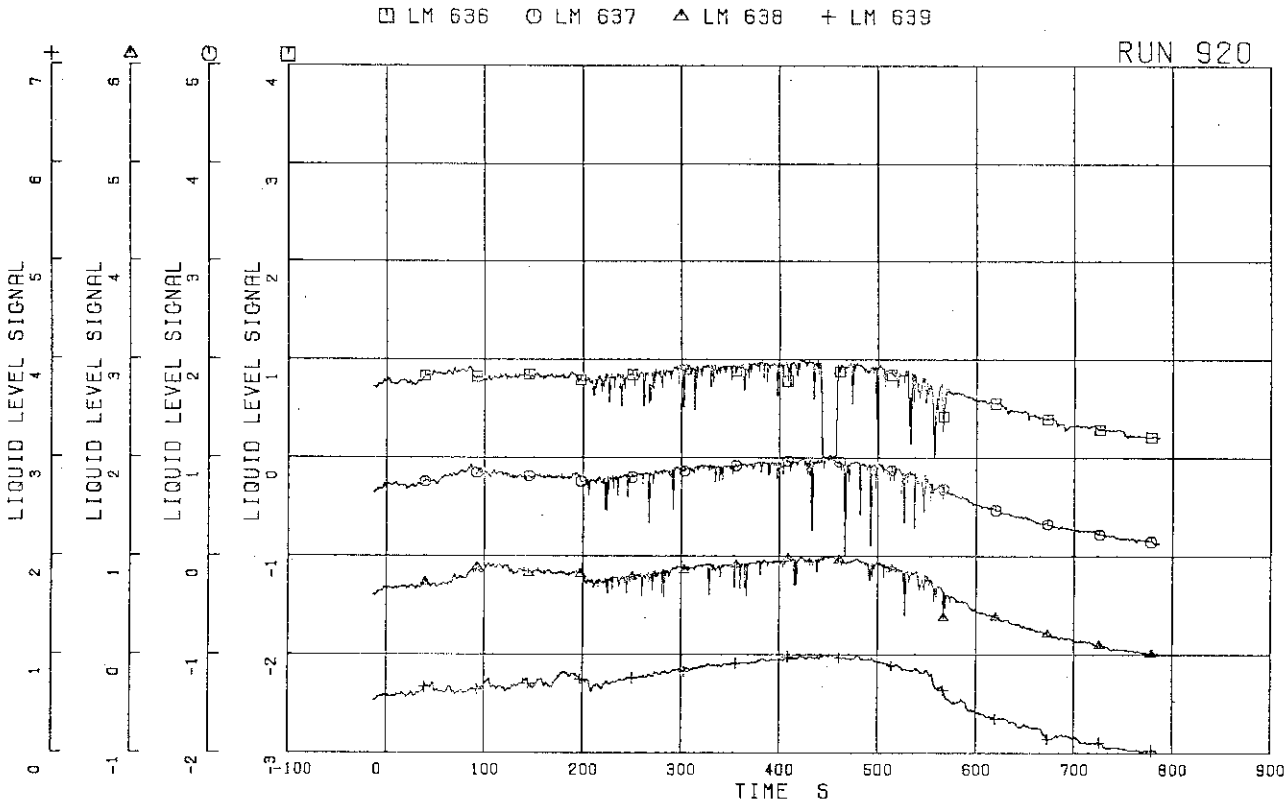

FIG.5.218 LIQUID LEVEL SIGNALS IN GUIDE TUBE, NORTH

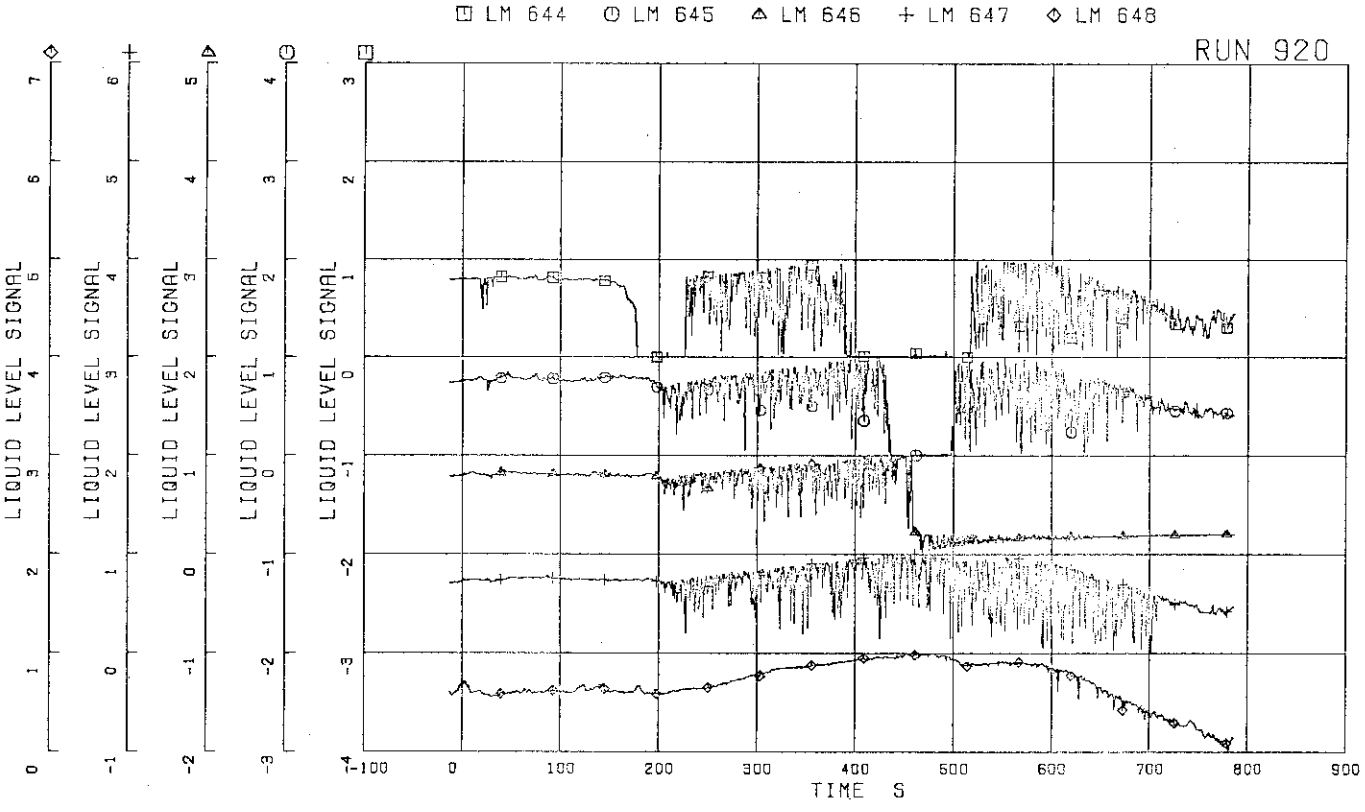

FIG.5.219 LIQUID LEVEL SIGNALS IN DOWNCOMER, D SIDE

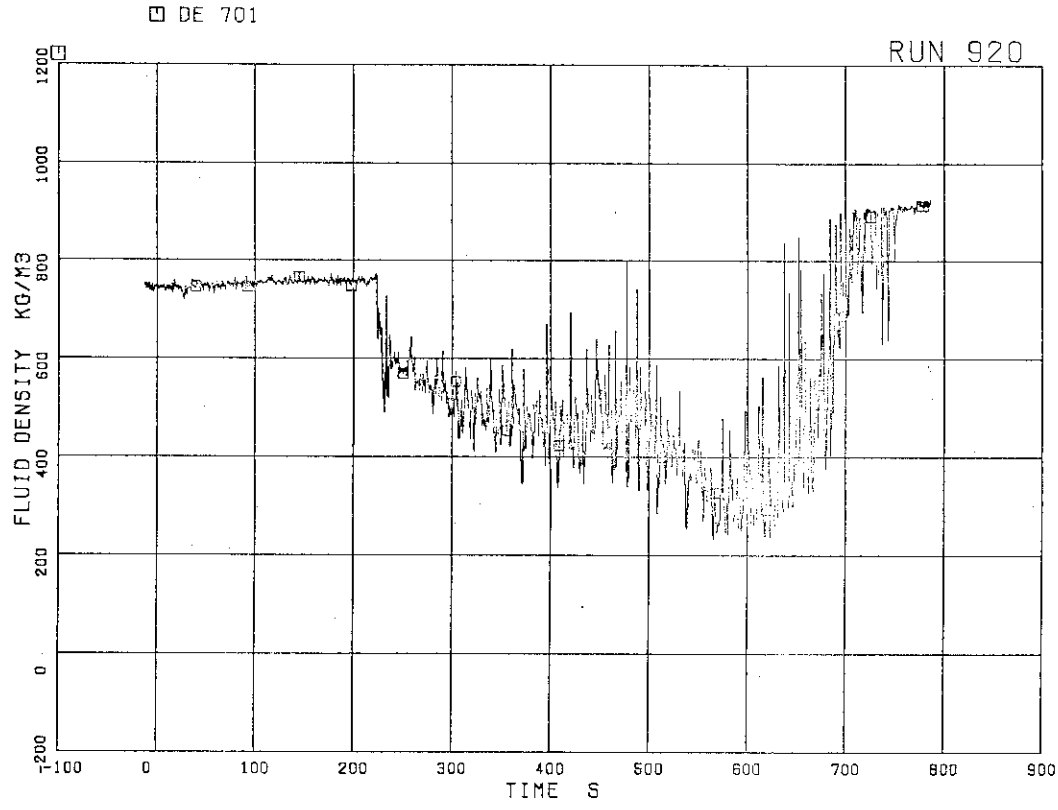

FIG.5.220 AVERAGE DENSITY AT JP-1,2 OUTLET

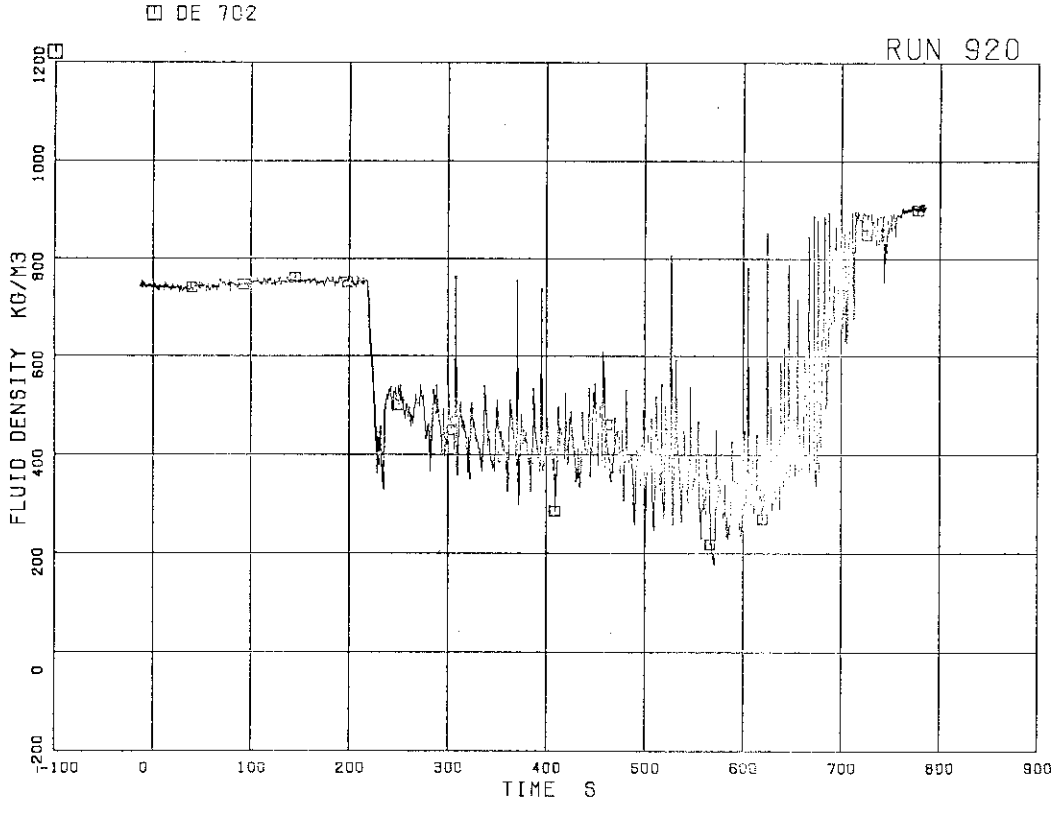

FIG.5.221 AVERAGE DENSITY AT JP-3,4 OUTLET

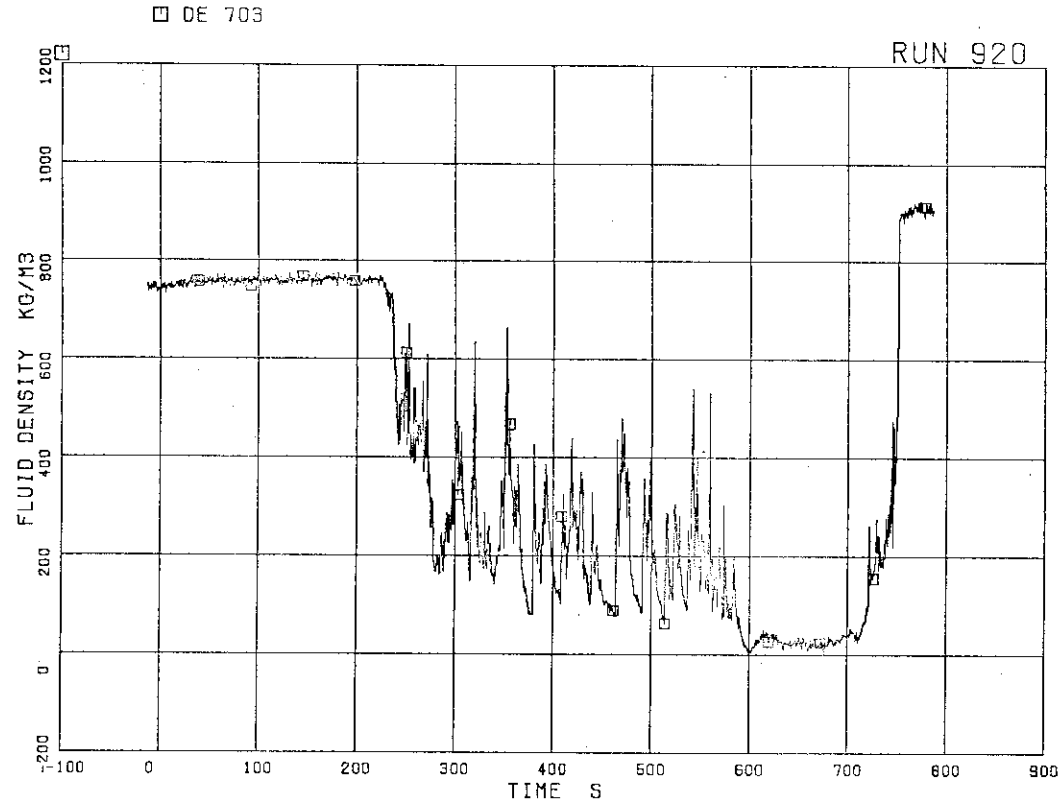

FIG.5.222 AVERAGE DENSITY AT MRP SIDE OF BREAK

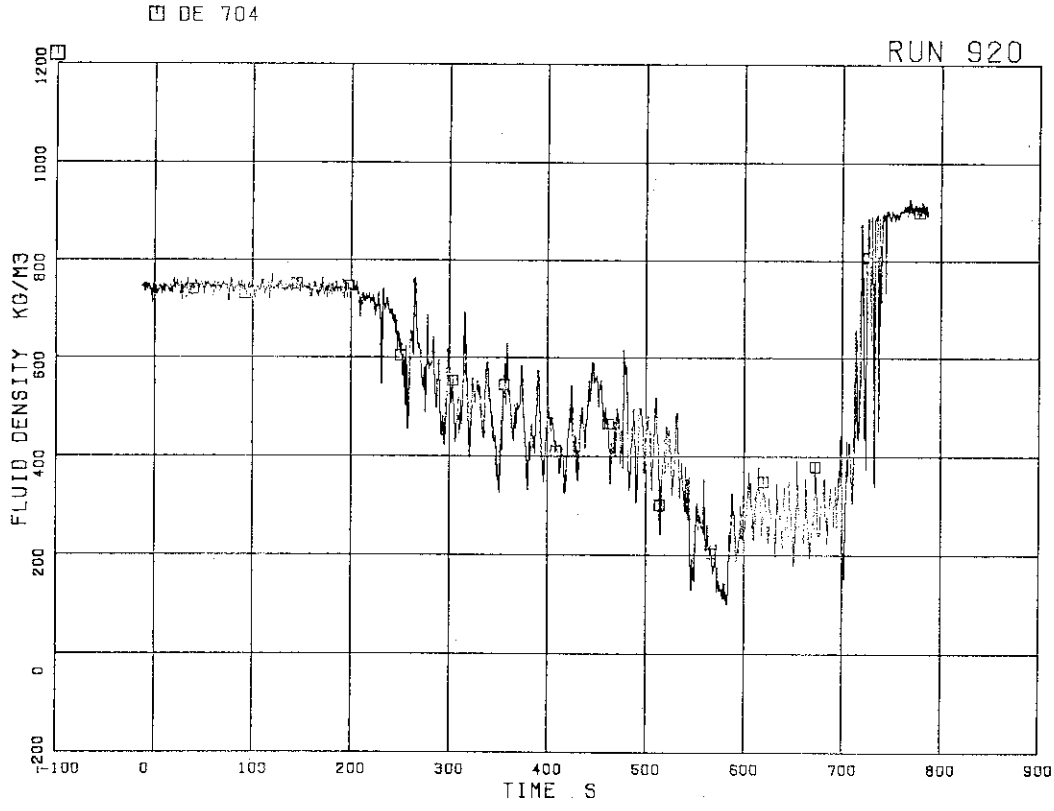

FIG.5.223 AVERAGE DENSITY AT PV SIDE OF BREAK

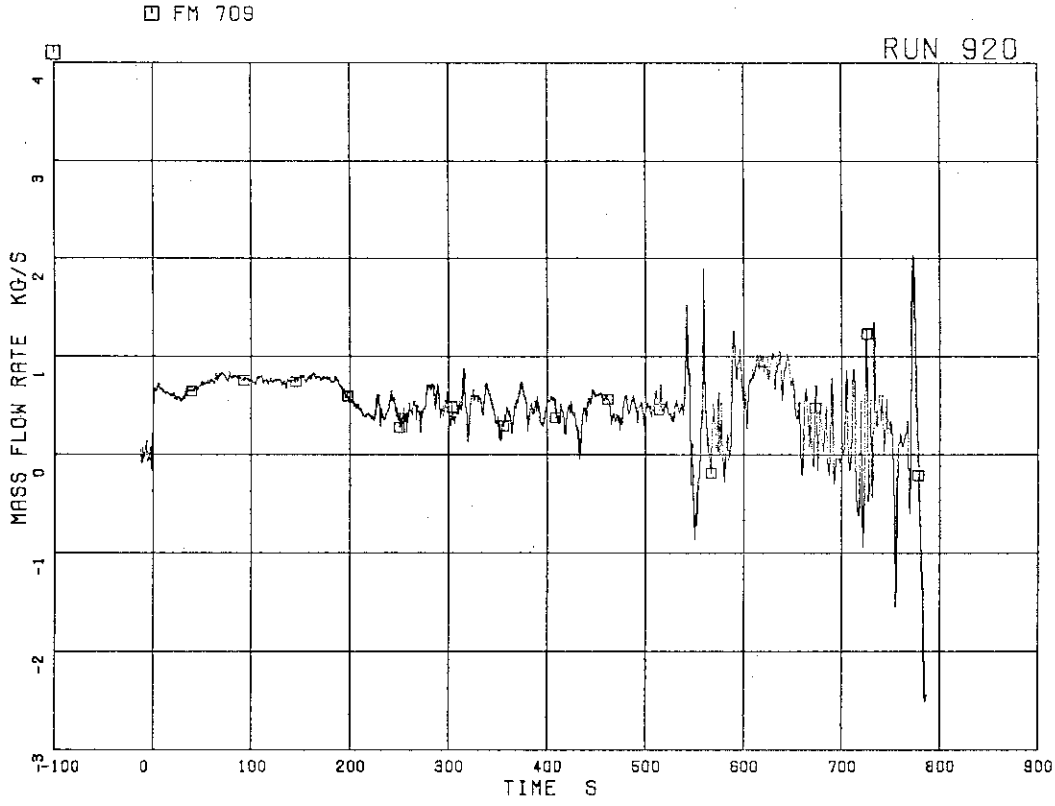

FIG.5.224 TOTAL DISCHARGE FLOW RATE FROM BREAK (BASED ON LOW RANGE DRAG DISK DATA)

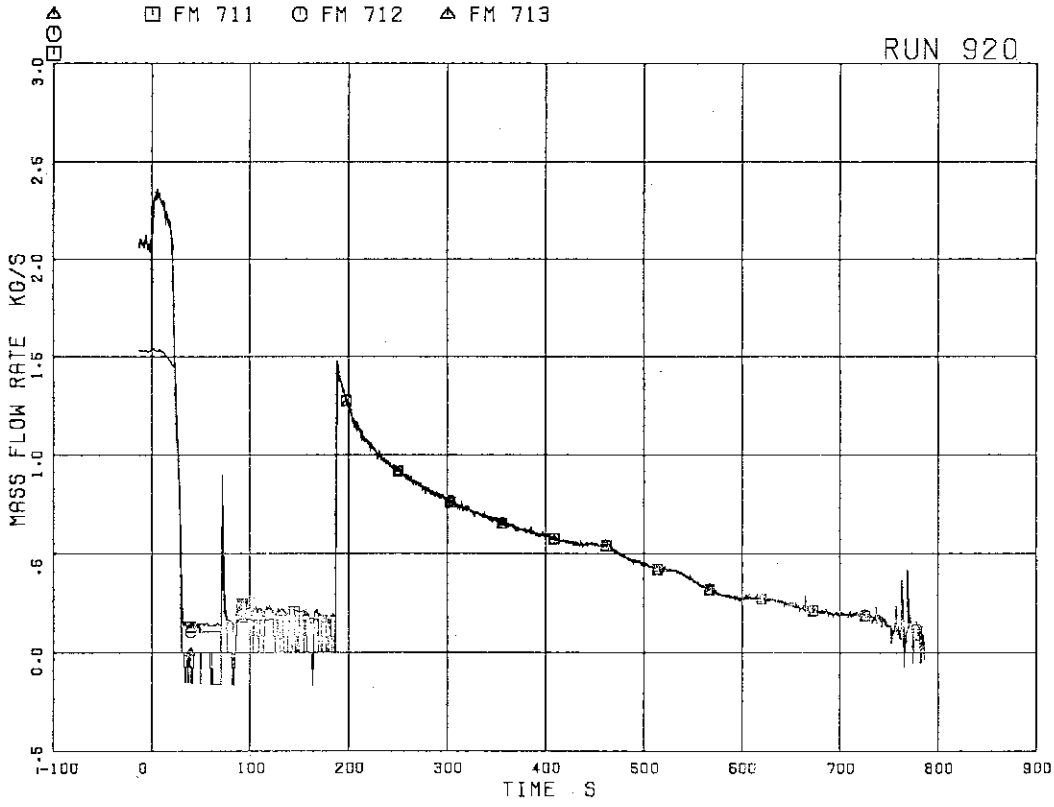

FIG.5.225 STEAM DISCHARGE FLOW RATE THROUGH MSL

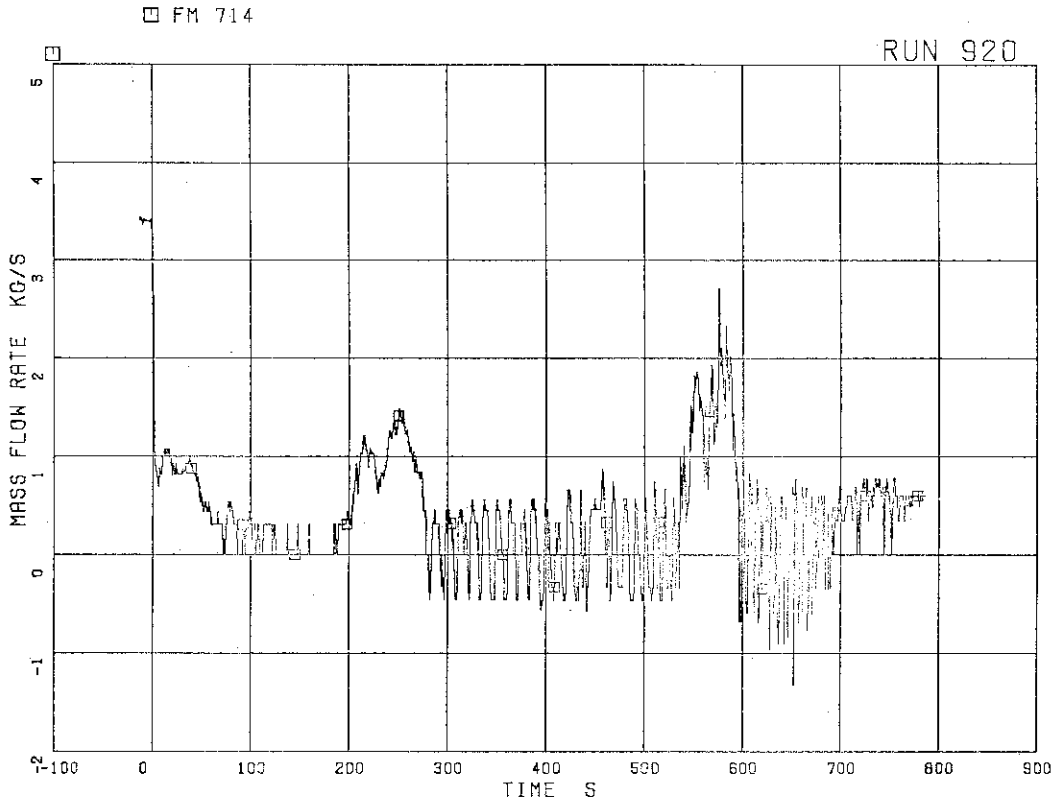

FIG.5.226 FLOW RATE AT CHANNEL A INLET

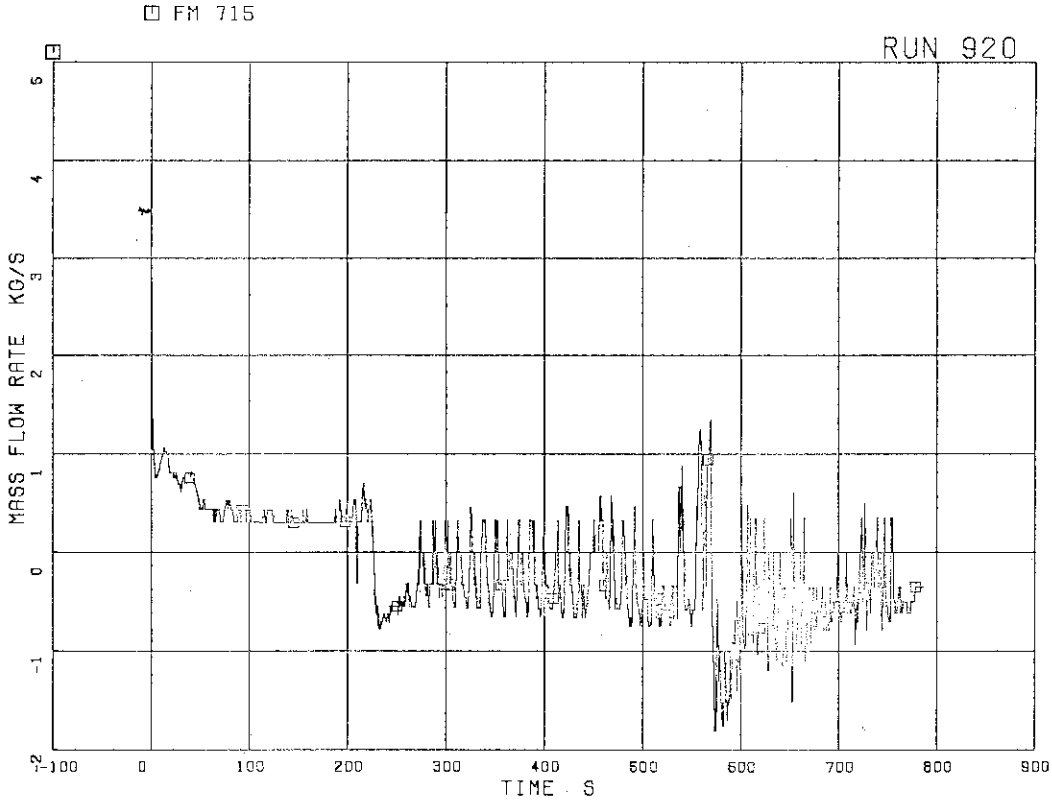

FIG.5.227 FLOW RATE AT CHANNEL B INLET

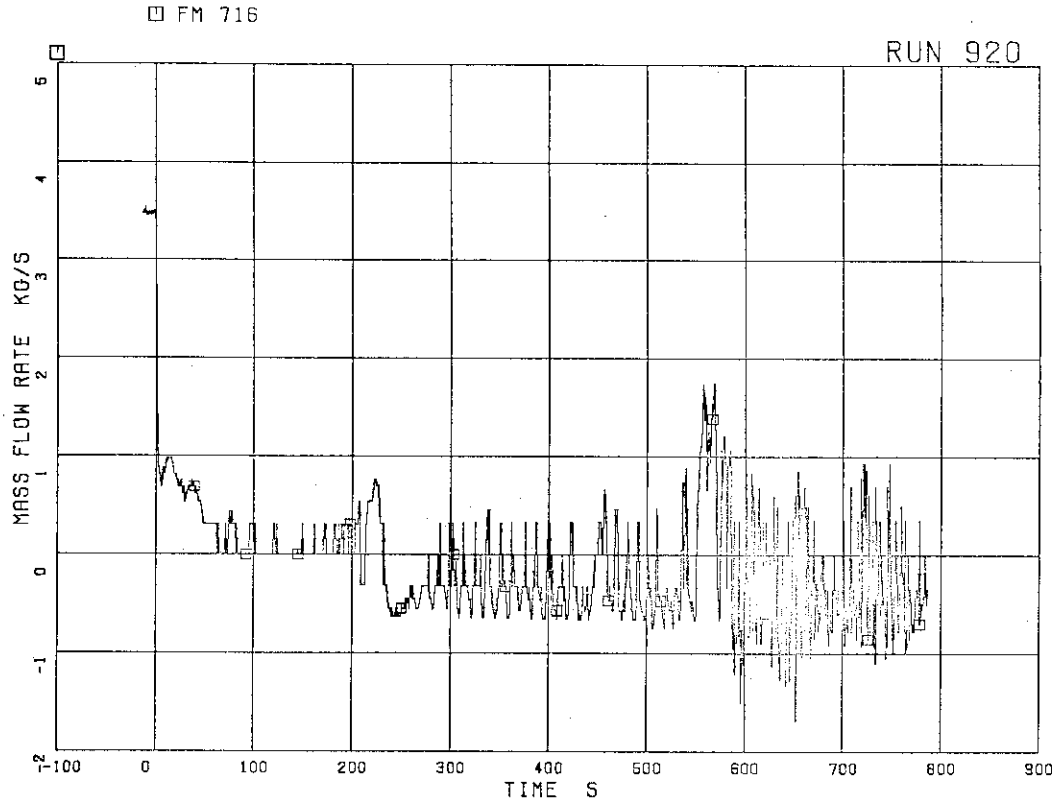

FIG.5.228 FLOW RATE AT CHANNEL C INLET

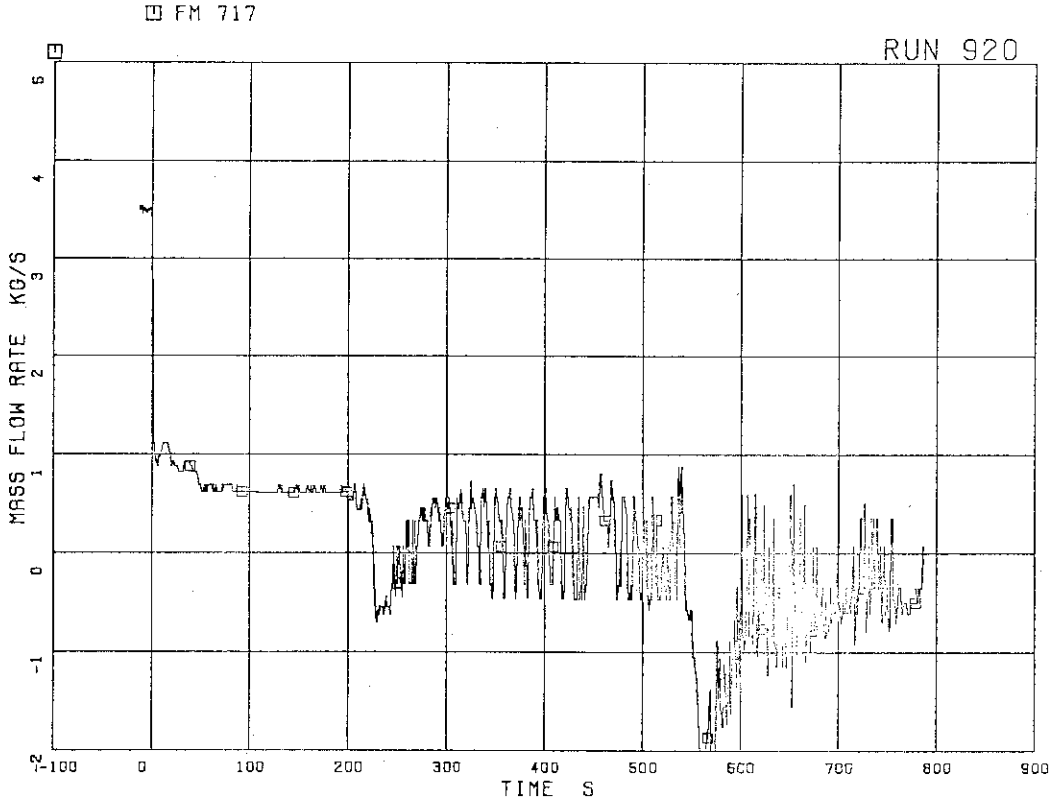

FIG.5.229 FLOW RATE AT CHANNEL D INLET

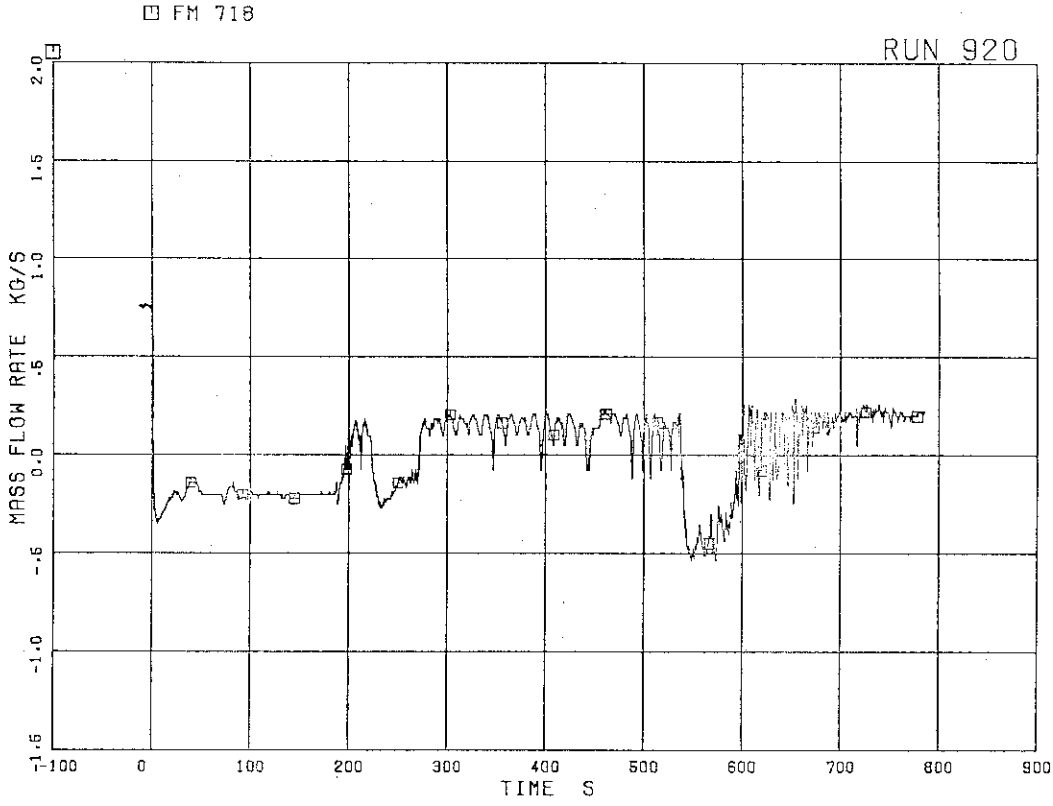

FIG.5.230 FLOW RATE AT BYPASS HOLE

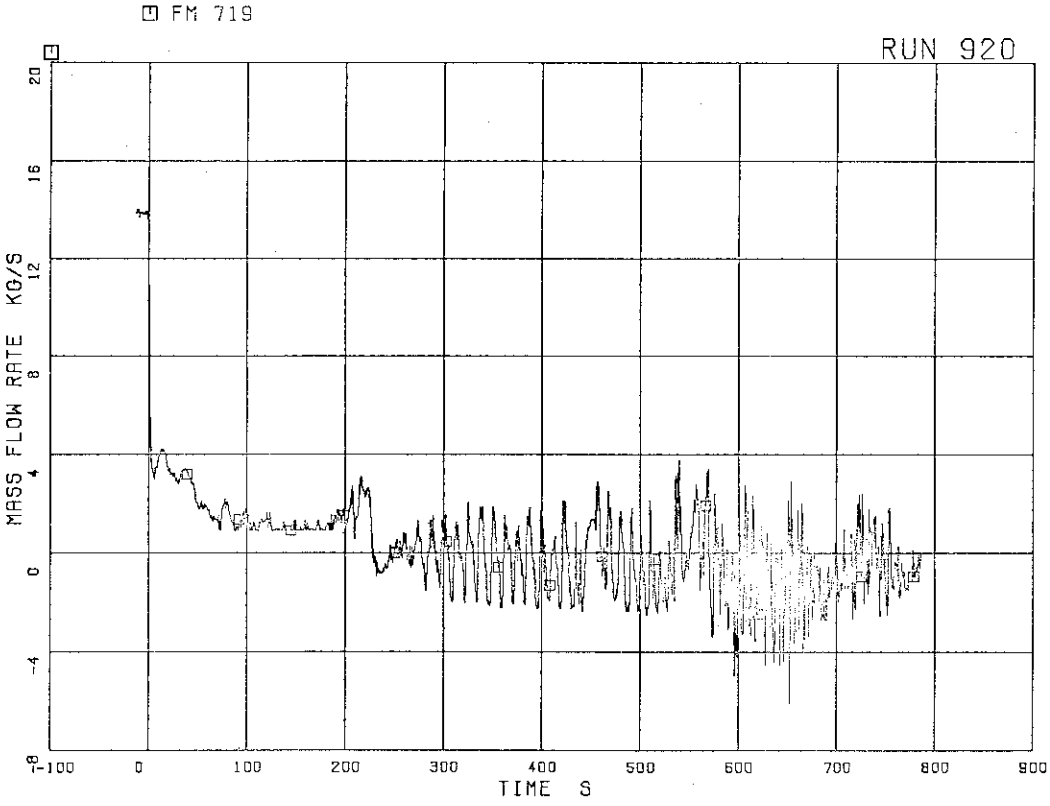

FIG.5.231 TOTAL CHANNEL INLET FLOW RATE

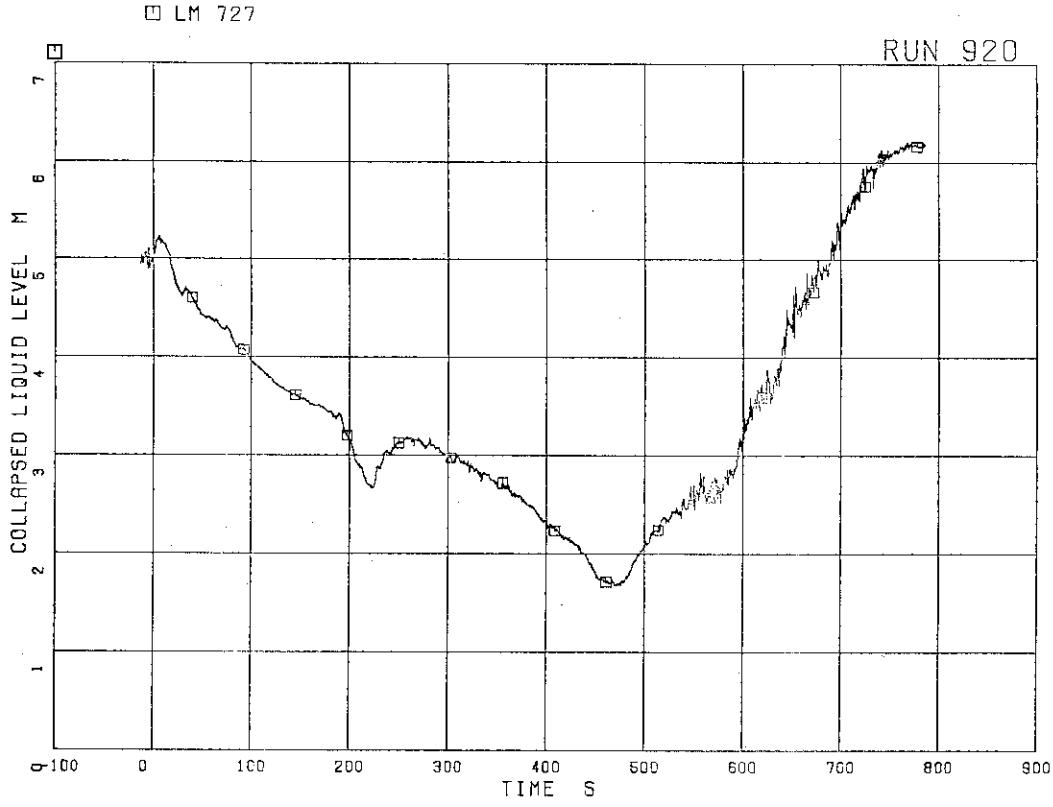

FIG.5.232 COLLAPSED LIQUID LEVEL IN DOWNCOMER

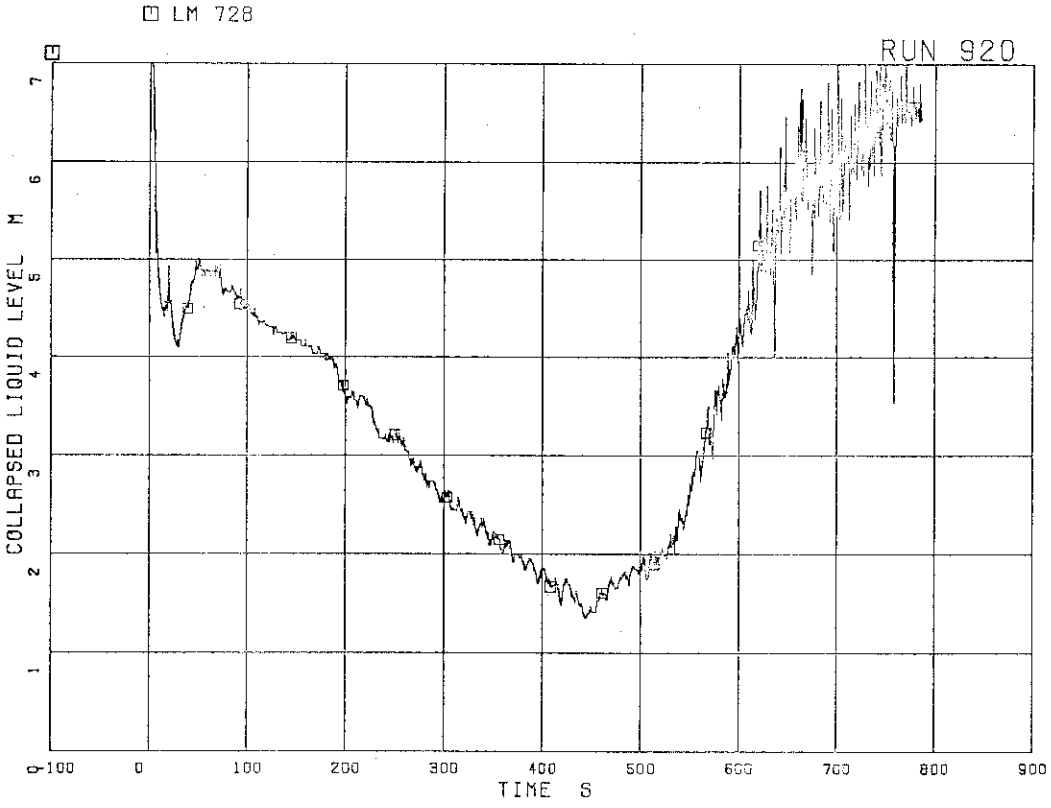

FIG.5.233 COLLAPSED LIQUID LEVEL INSIDE CORE SHROUD

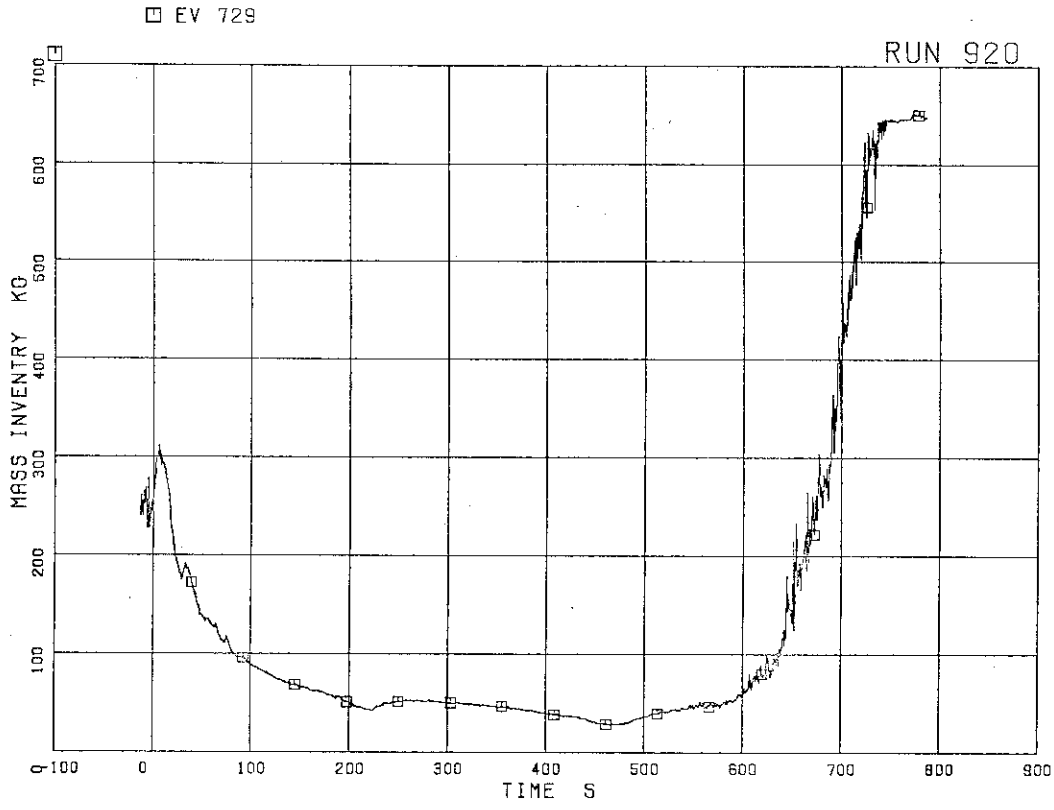

FIG.5.234 FLUID INVENTORY IN DOWNCOMER

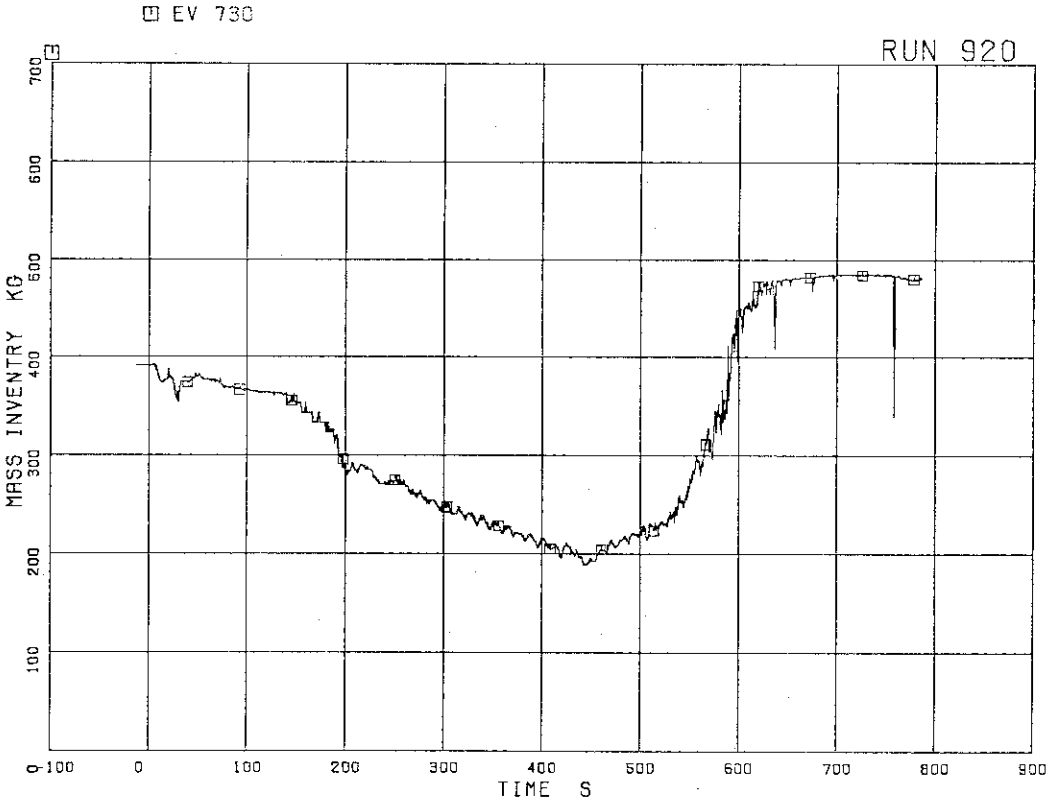

FIG.5.235 FLUID INVENTORY INSIDE CORE SHROUD

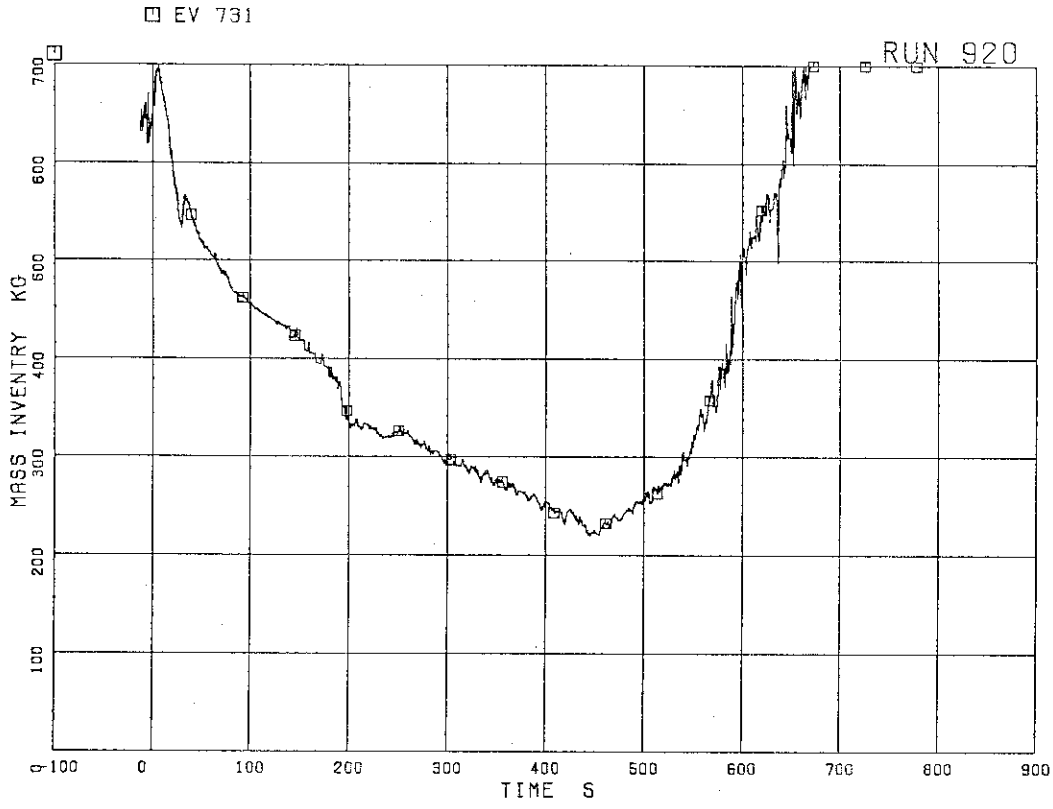

FIG.5.236 TOTAL FLUID INVENTORY IN PRESSURE VESSEL

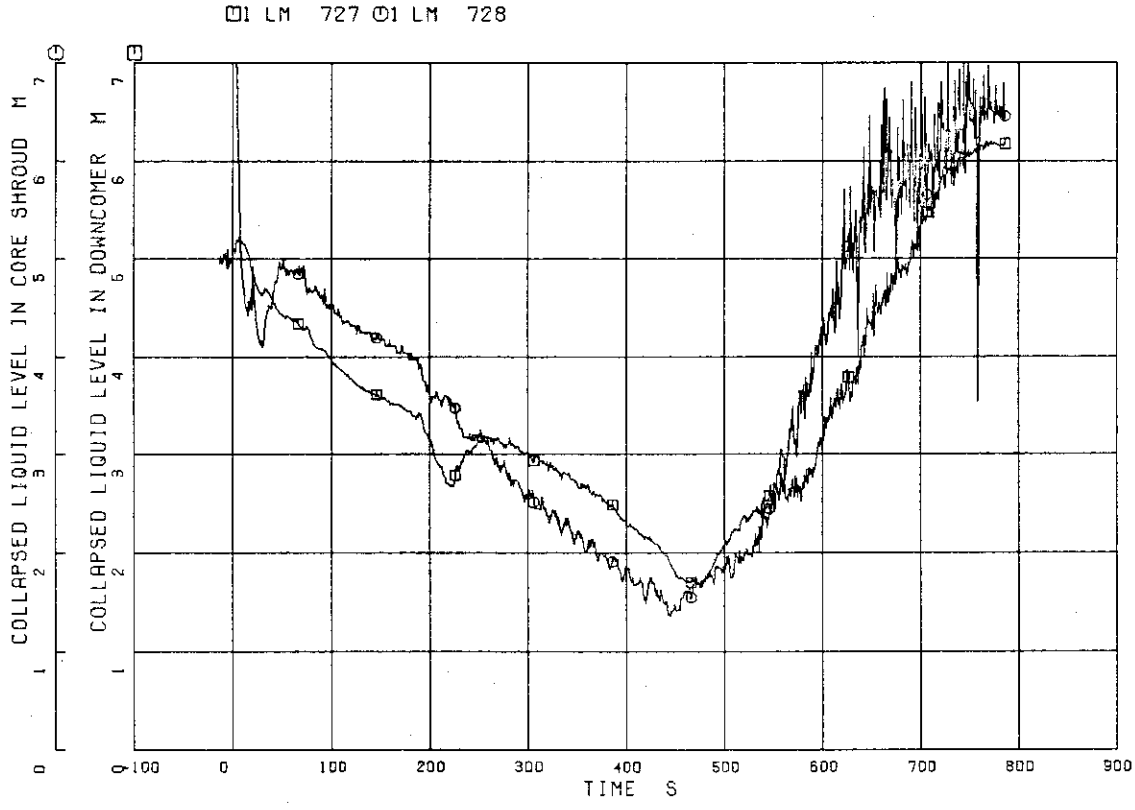

Fig. 5.237 Collapsed water levels in PV

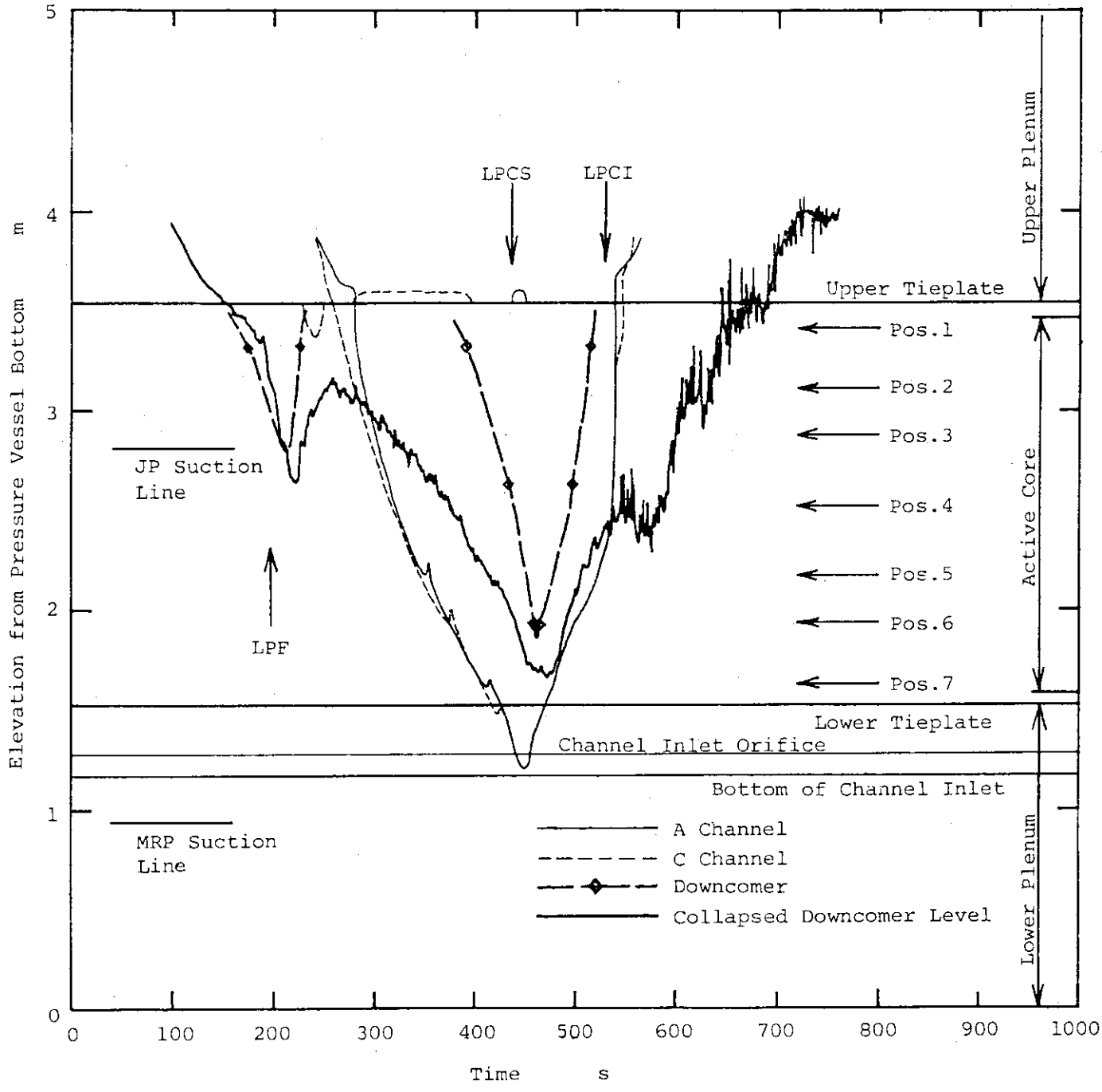

Fig. 5.238 Mixture levels in PV

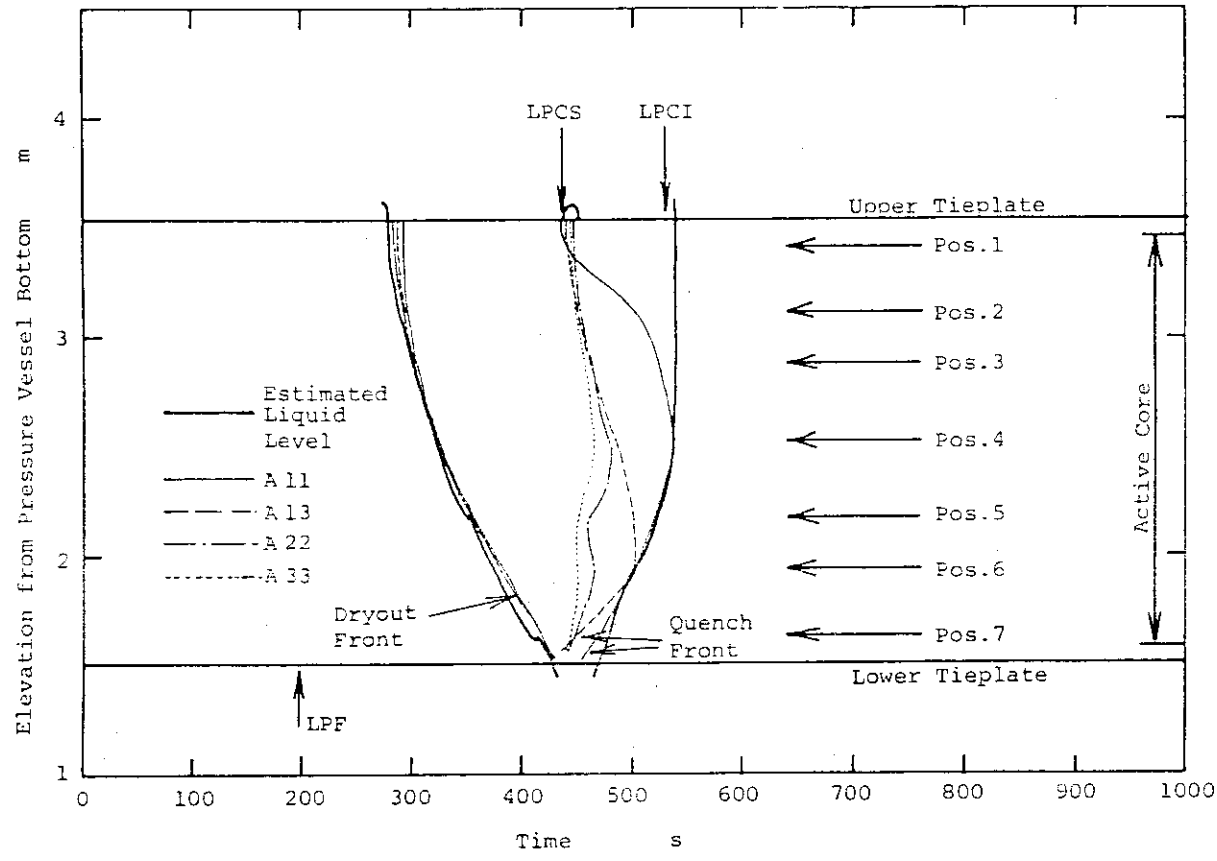

Fig. 5.239 Dryout and quench times of fuel rods in bundle A

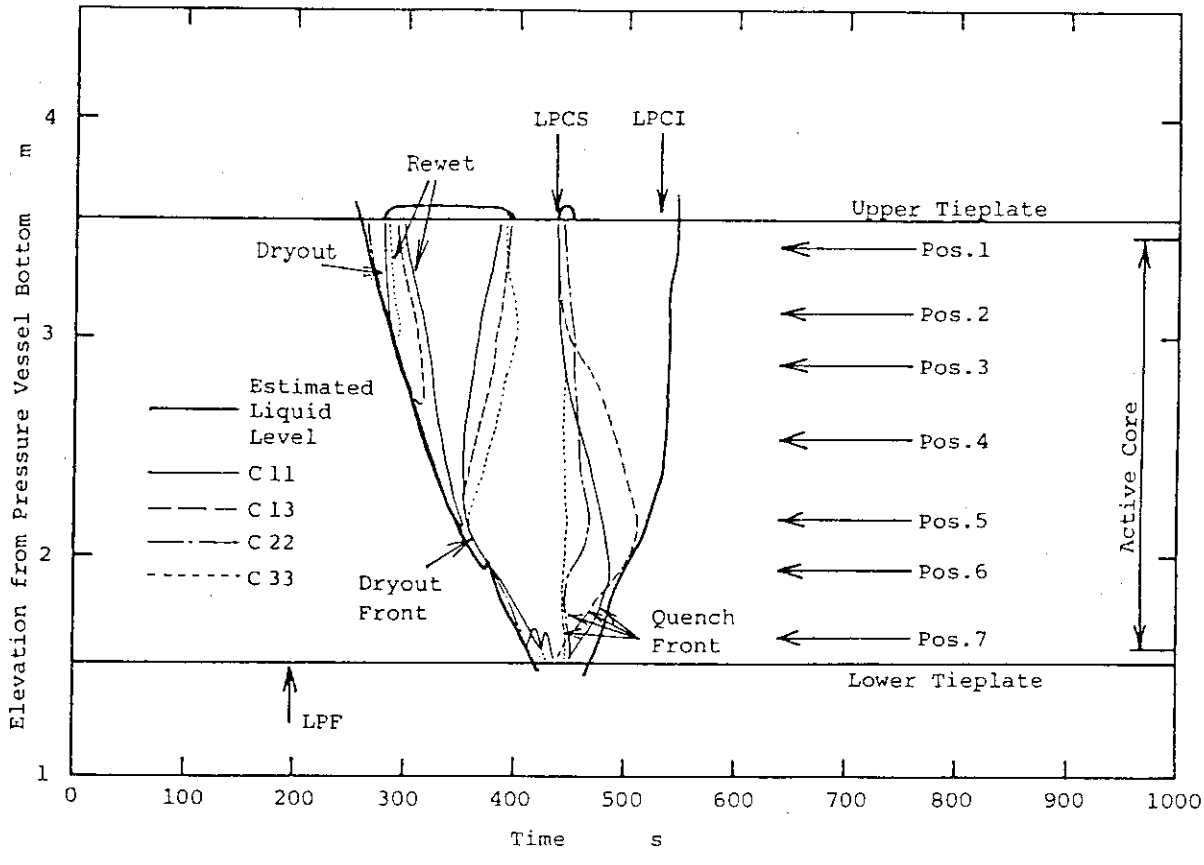

Fig. 5.240 Dryout and quench times of fuel rods in bundle C

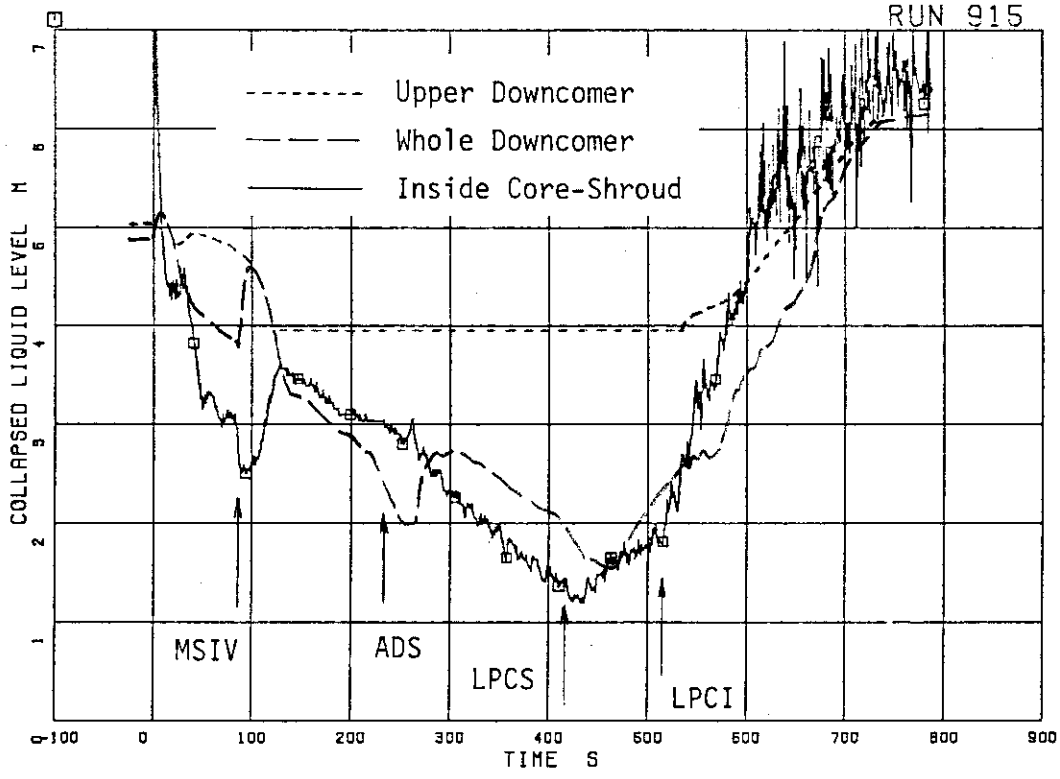

Fig. 6. 1 Comparison of collapsed water levels in upper downcomer, whole downcomer and core-shroud in RUN 915

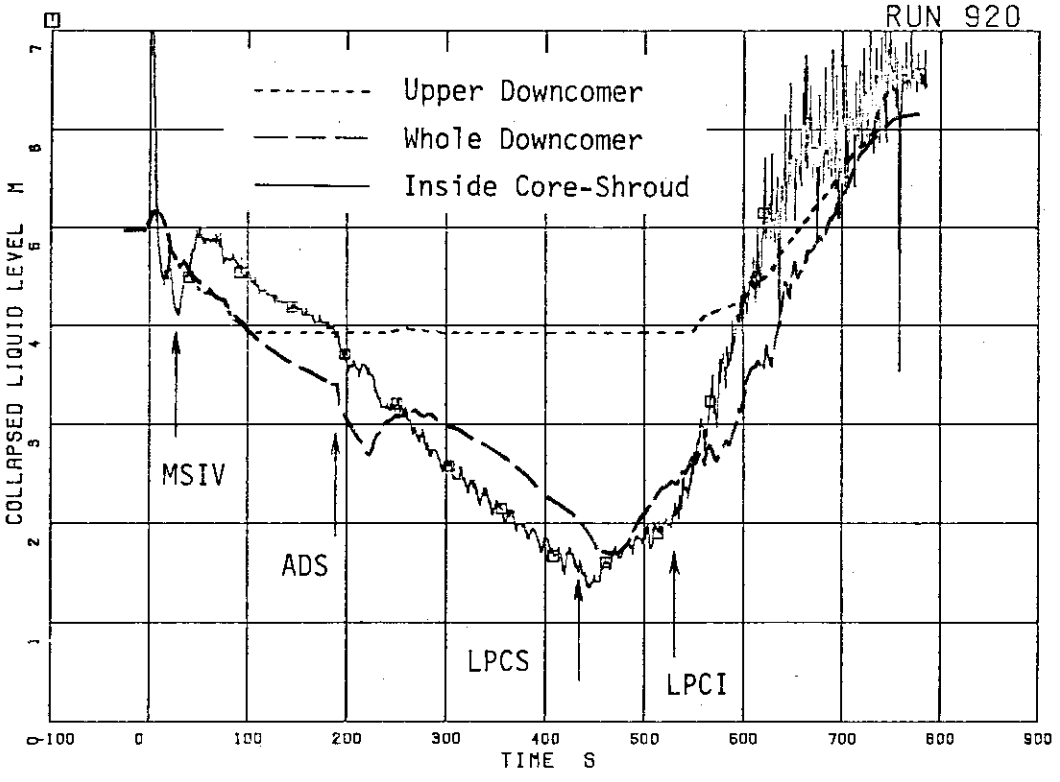

Fig. 6. 2 Comparison of collapsed water levels in upper downcomer, whole downcomer and core-shroud in RUN 920

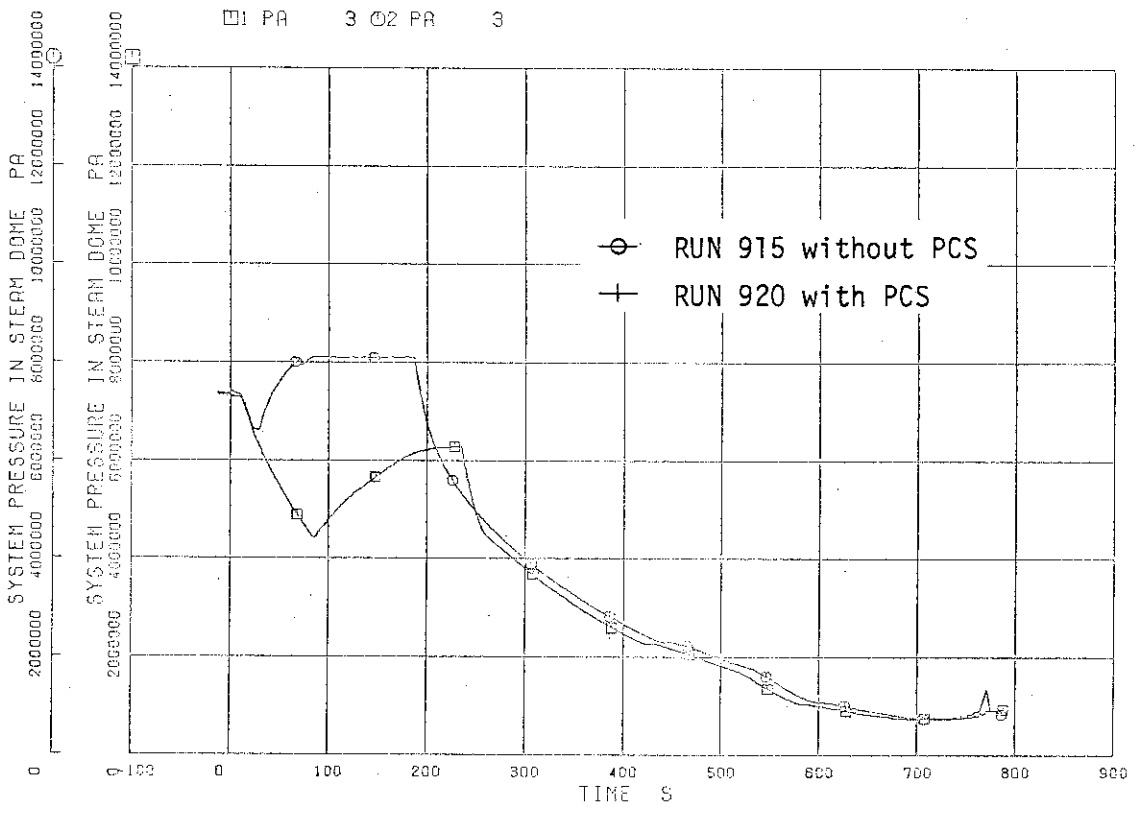

Fig. 6. 3 Comparison of system pressure responses between RUNs 915 and 920

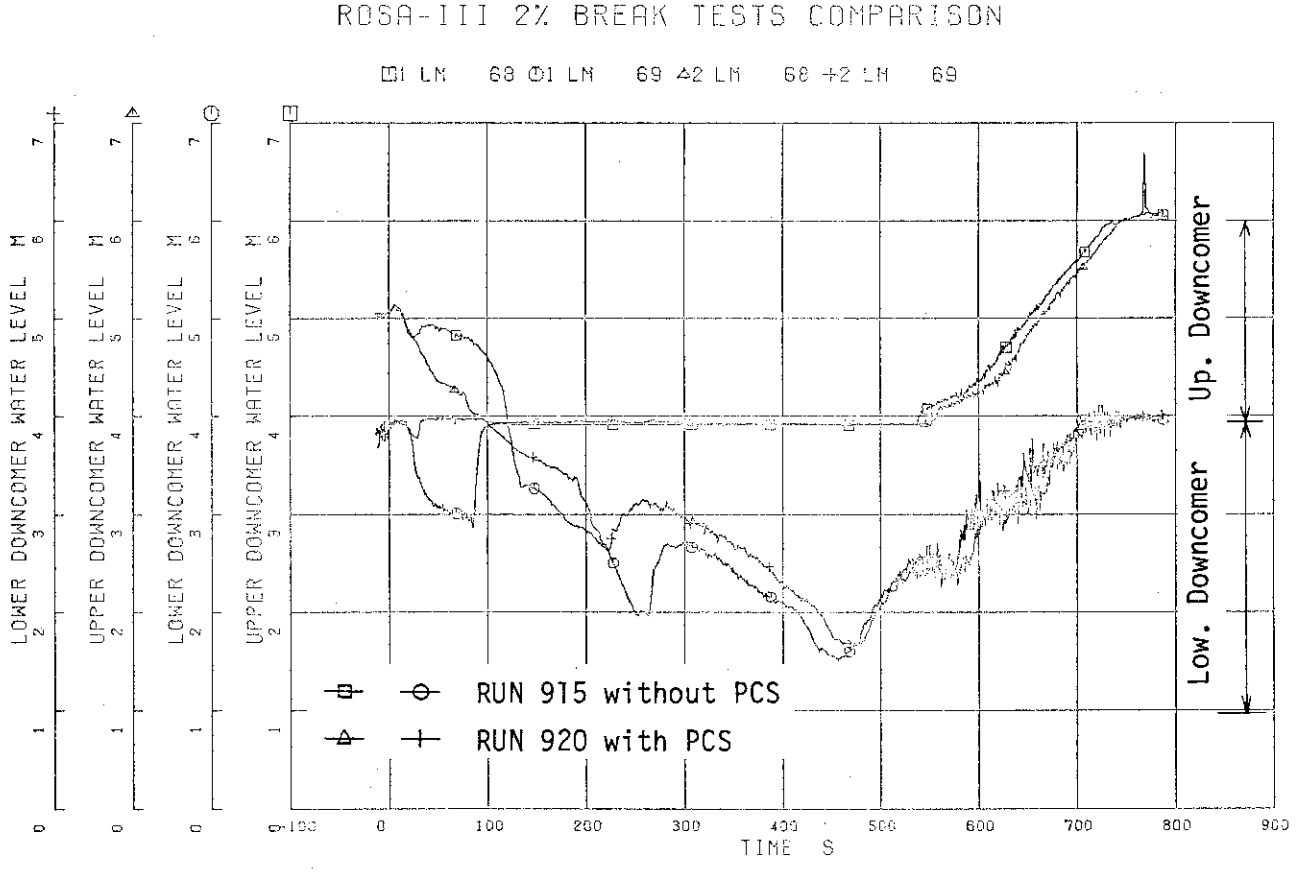

Fig. 6. 4 Comparison of upper and lower downcomer water levels between RUNs 915 and 920

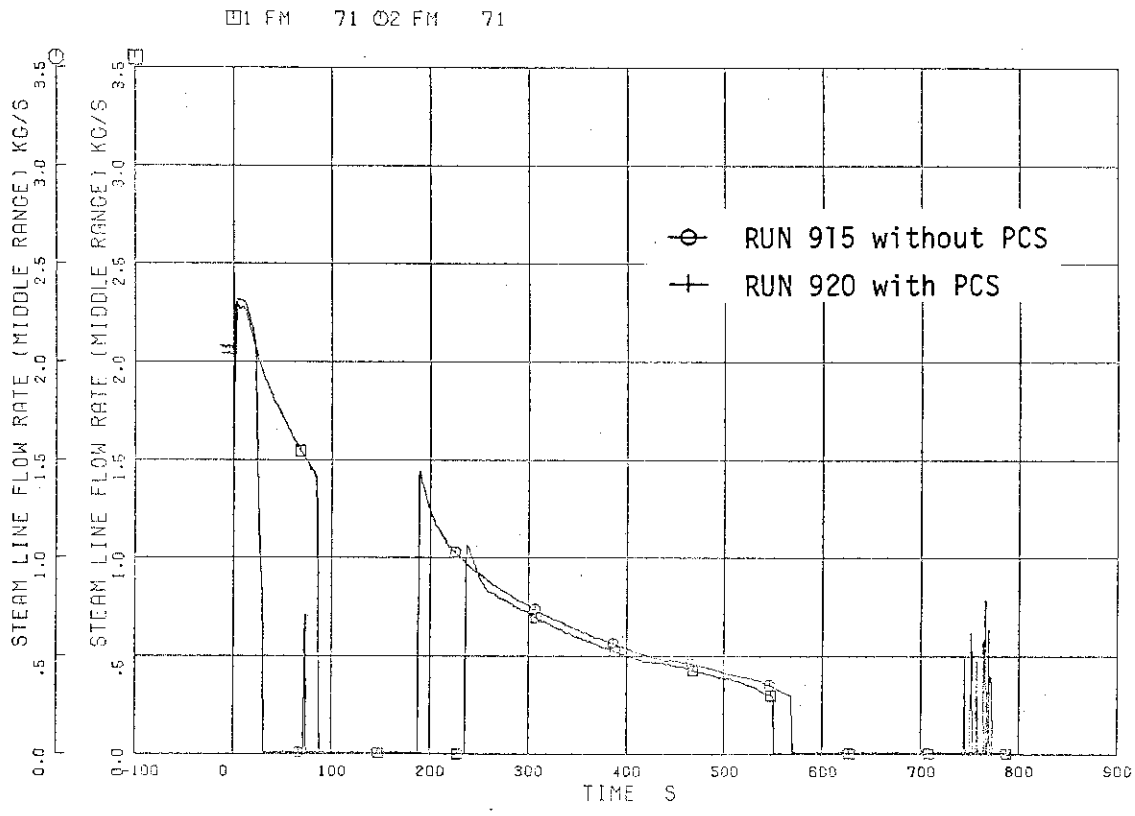

Fig. 6. 5 Comparison of steam line flow rates (middle range) between RUNs 915 and 920

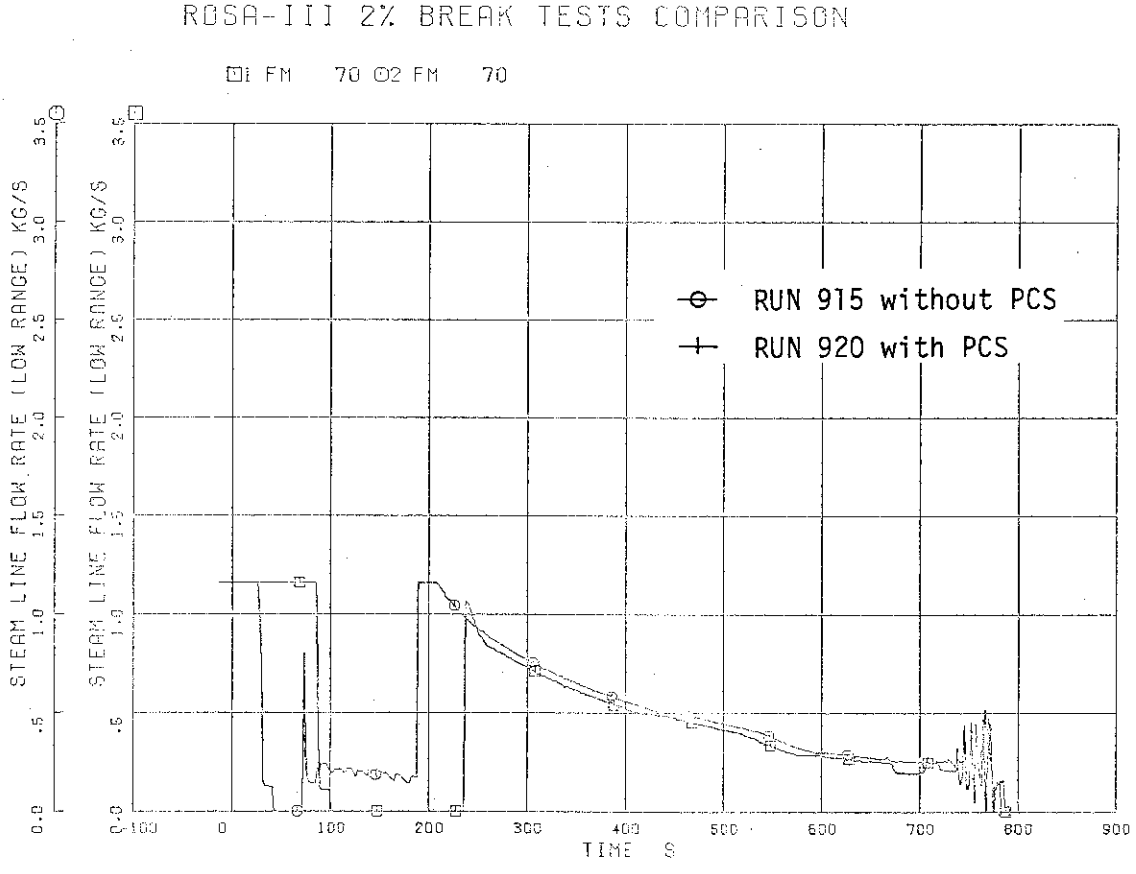

Fig. 6. 6 Comparison of steam line flow rates (low range) between RUNs 915 and 920

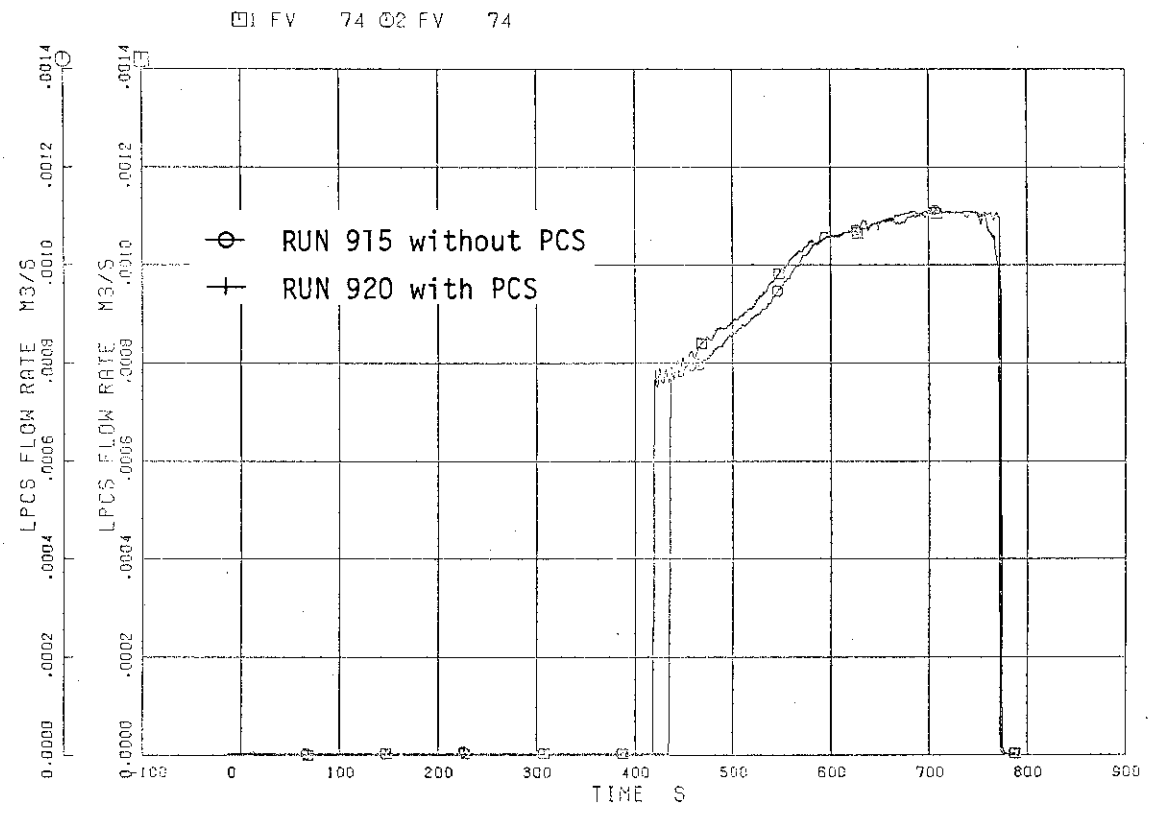

Fig. 6. 7 Comparison of LPCS flow rates between RUNs 915 and 920

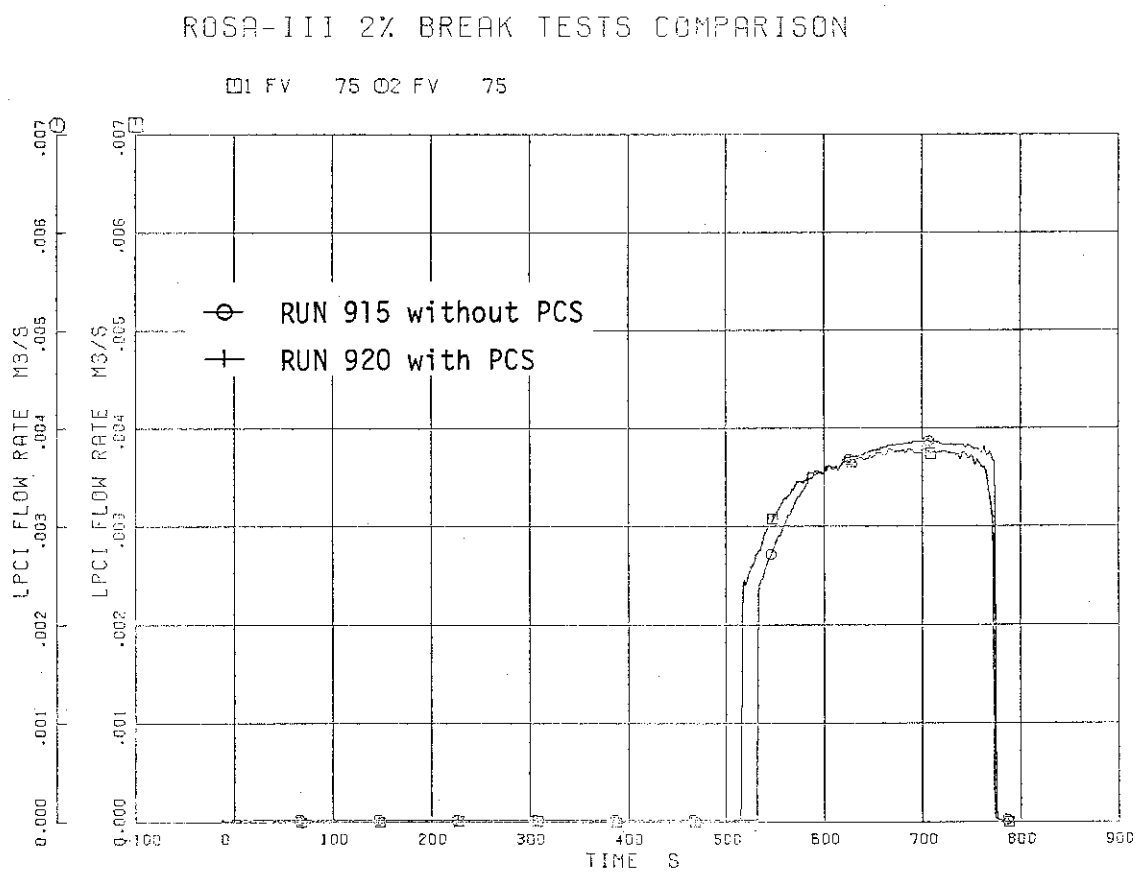

Fig. 6. 8 Comparison of LPCI flow rates between RUNs 915 and 920

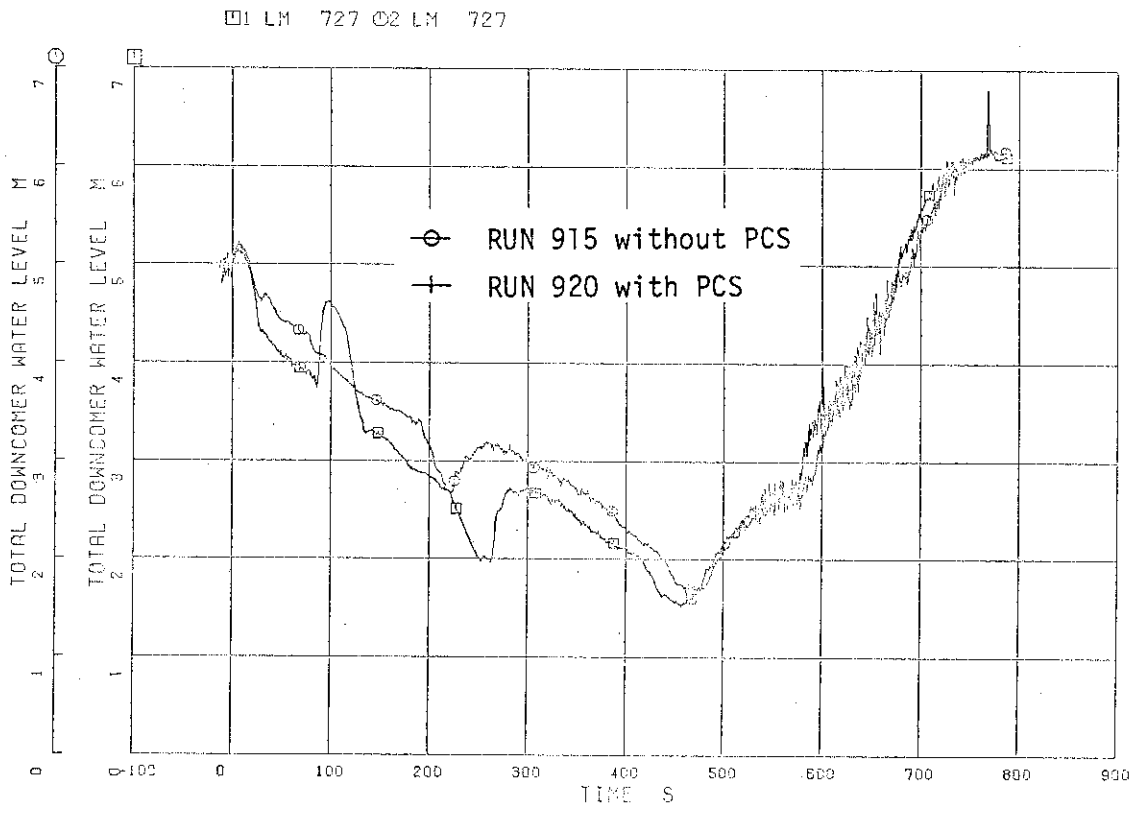

Fig. 6. 9 Comparison of total downcomer water levels between RUNs 915 and 920

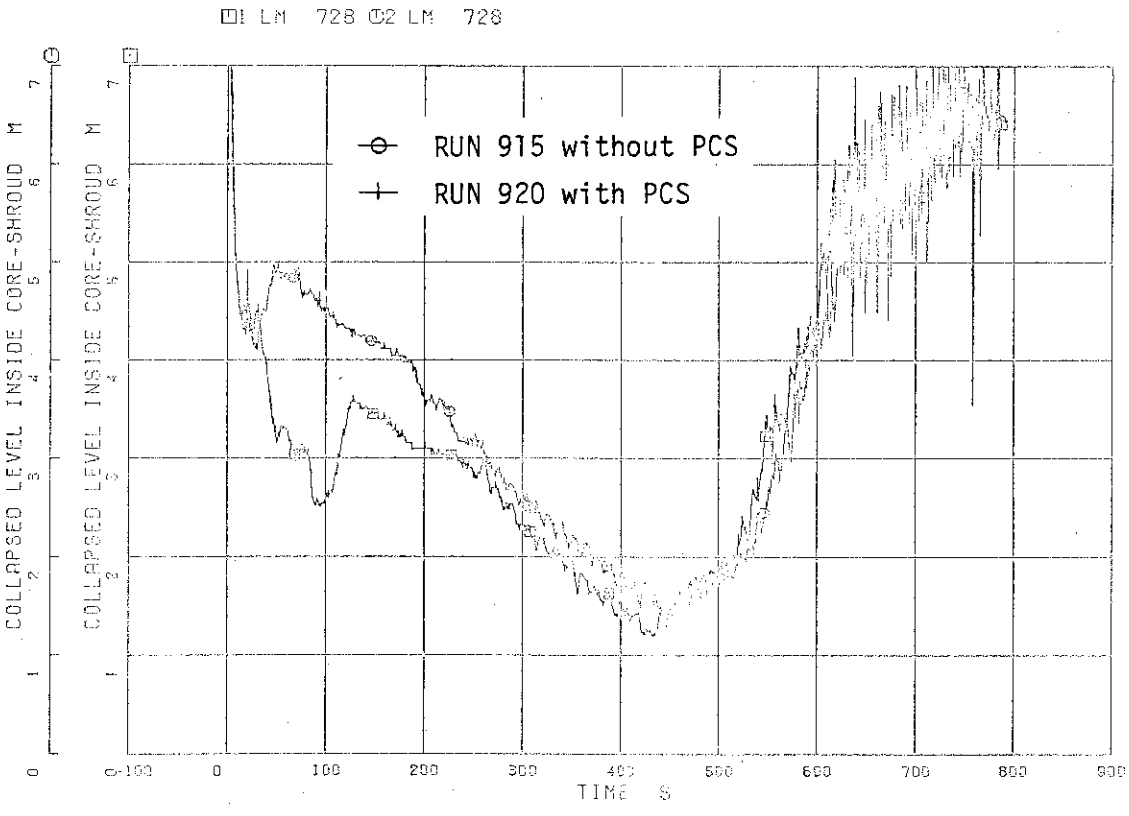

Fig. 6.10 Comparison of collapsed water levels inside core shroud between RUNs 915 and 920

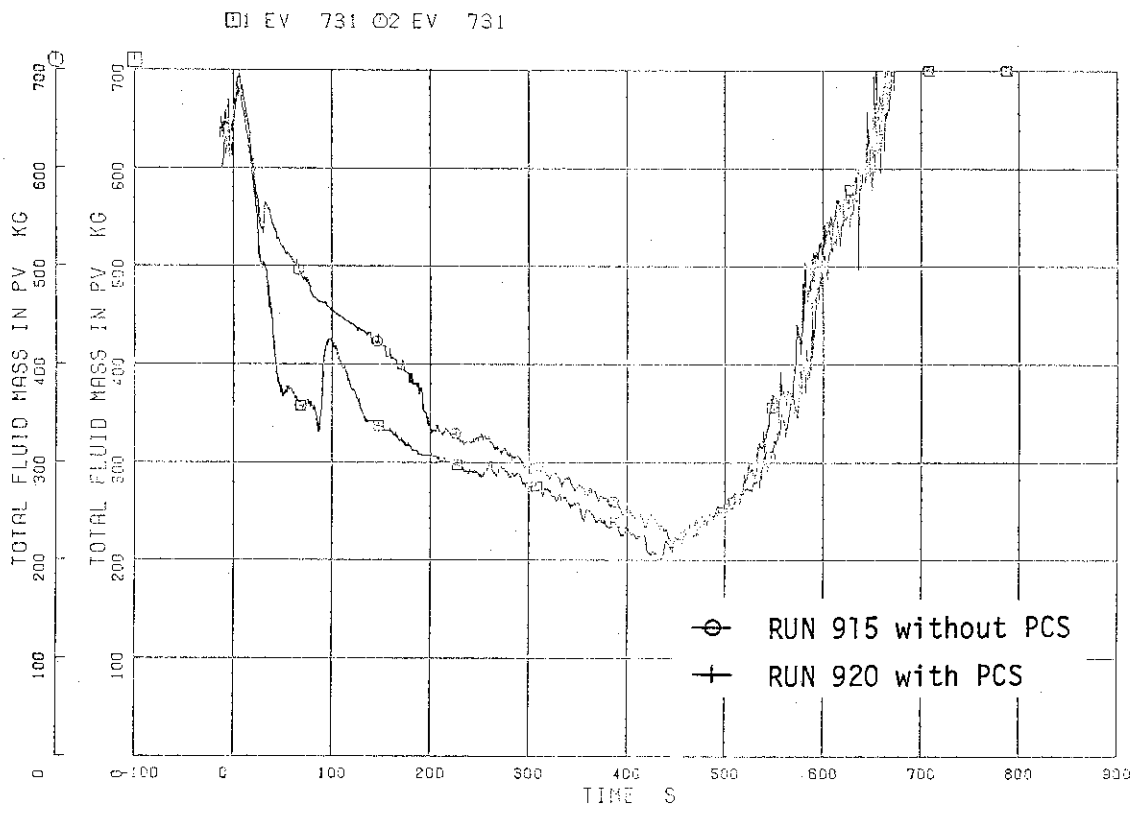

Fig. 6.11 Comaprison of total PV fluid mass between RUNs 915 and 920

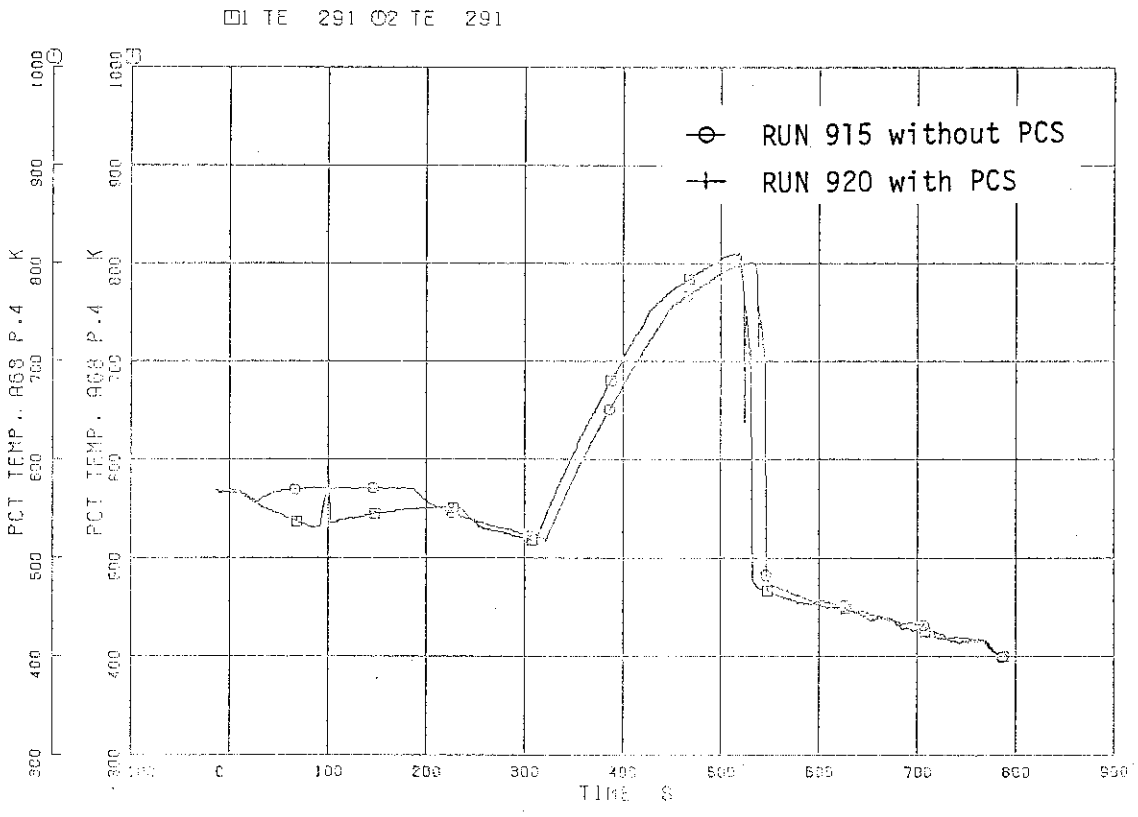

Fig. 6.12 Comparison of PCTs between RUNs 915 and 920

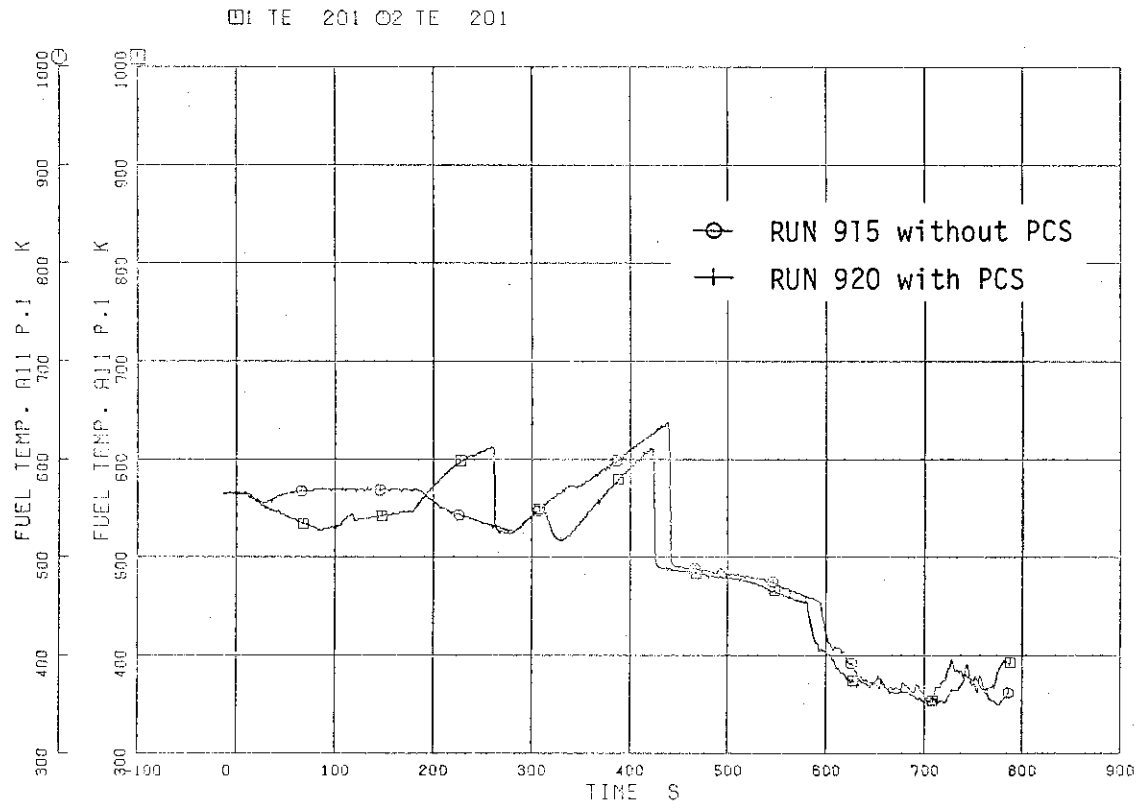

Fig. 6.13 Fuel rod surface temperatures of A11 rod position 1 (top core) between RUNs 915 and 920

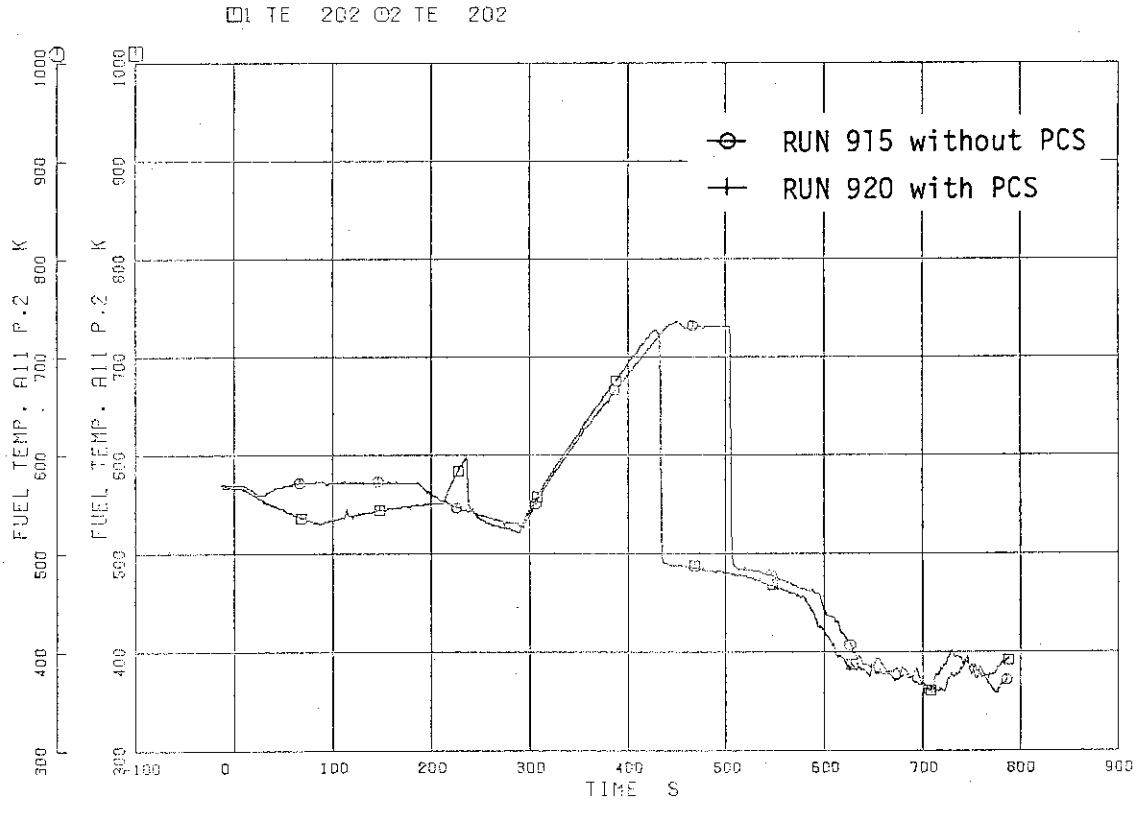

Fig. 6.14 Fuel rod surface temperatures of A11 rod position 2 between RUNs 915 and 920

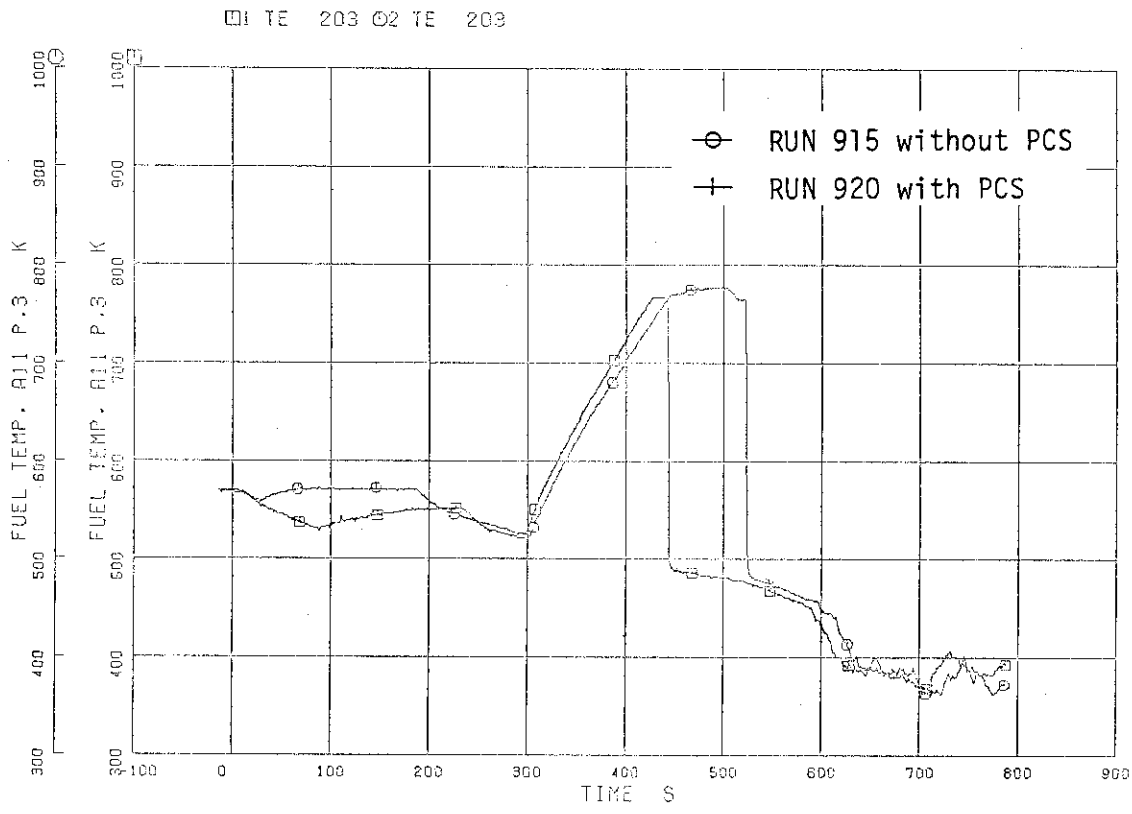

Fig. 6.15 Fuel rod surface temperatures of A11 rod position 3 between RUNs 915 and 920

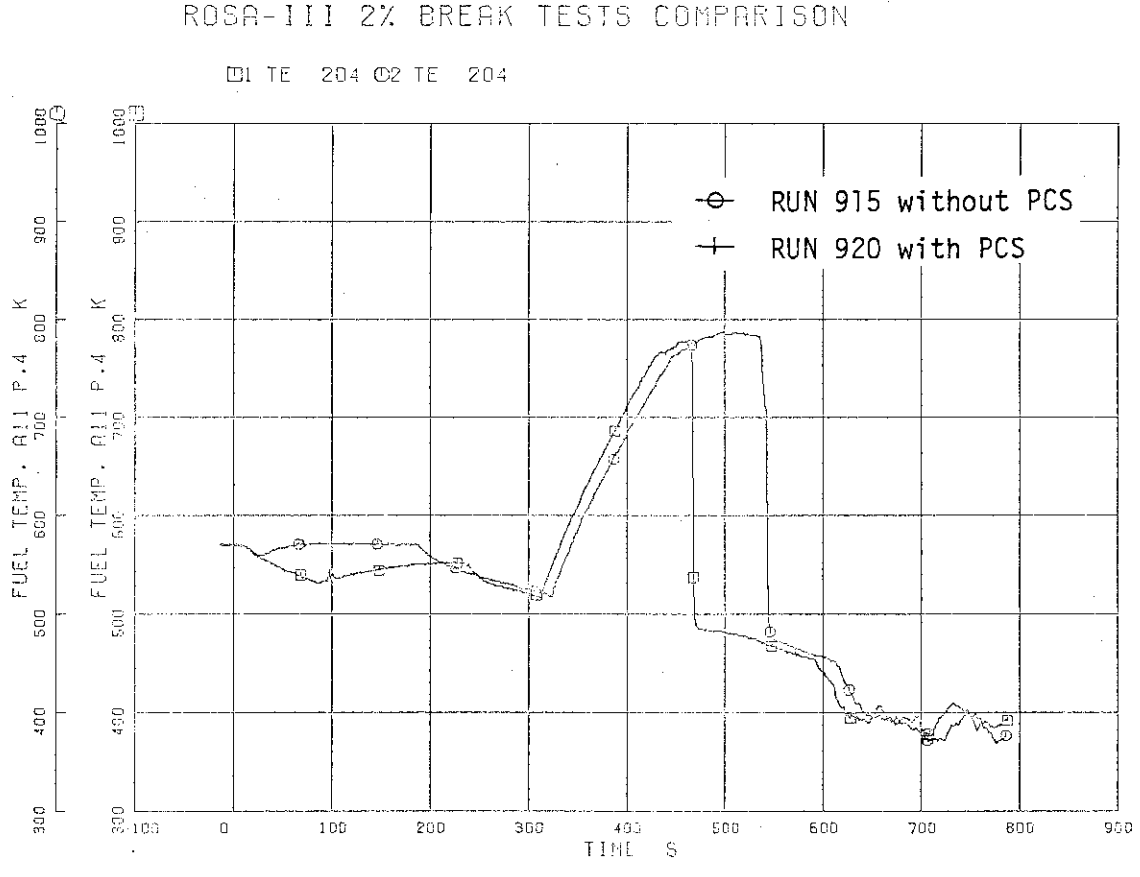

Fig. 6.16 Fuel rod surface temperatures of A11 rod position 4 (middle core) between RUNs 915 and 920

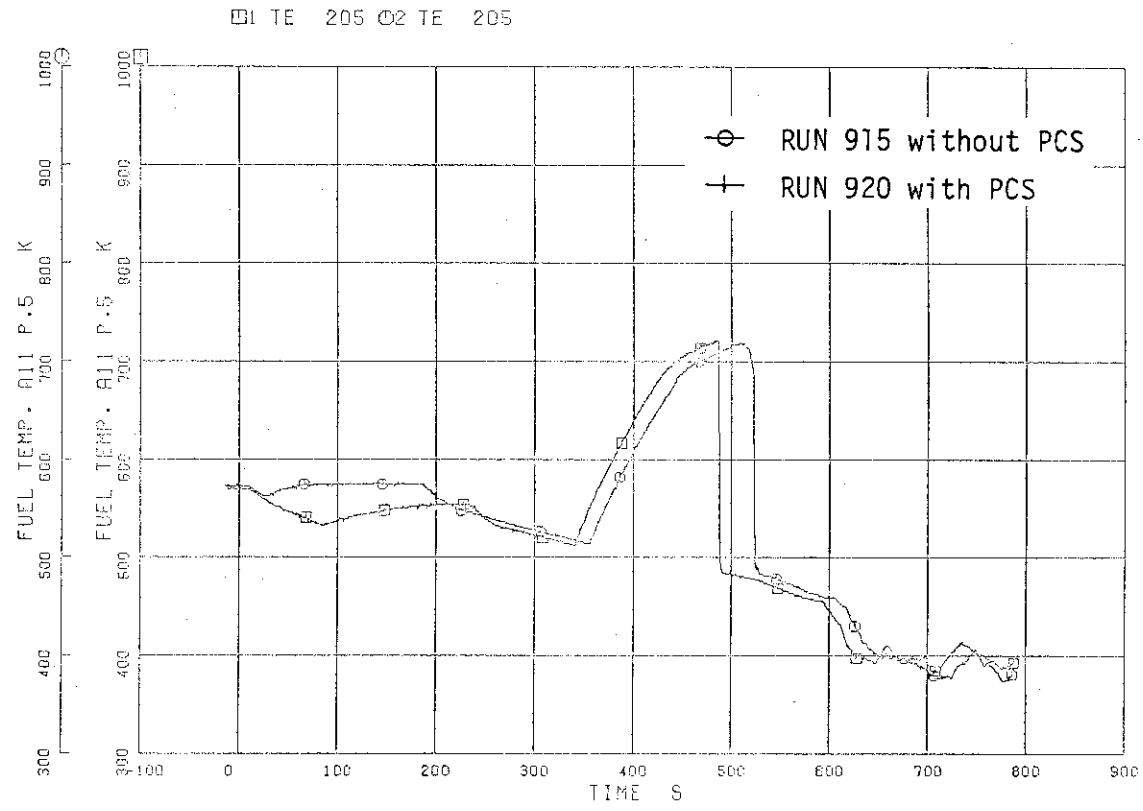

Fig. 6.17 Fuel rod surface temperatures of A11 rod position 5 between RUNs 915 and 920

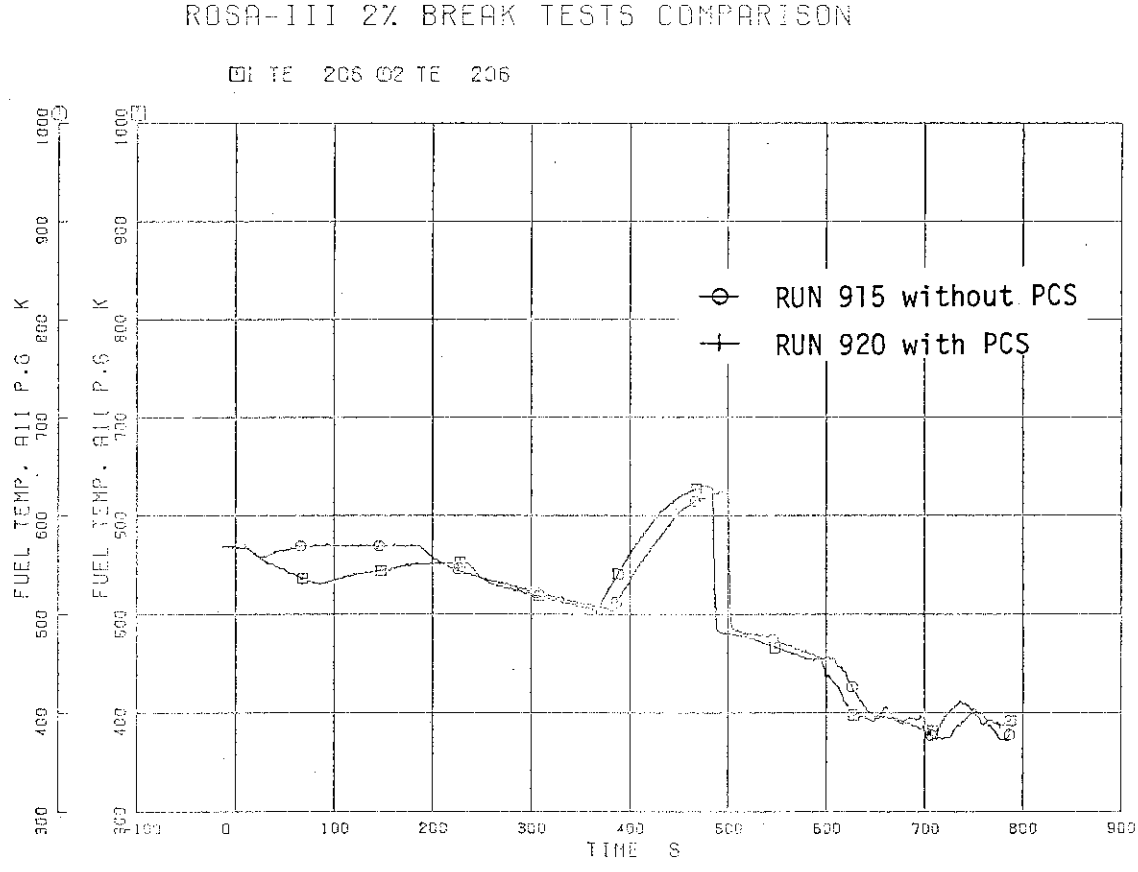

Fig. 6.18 Fuel rod surface temperatures of A11 rod position 6 between RUNs 915 and 920

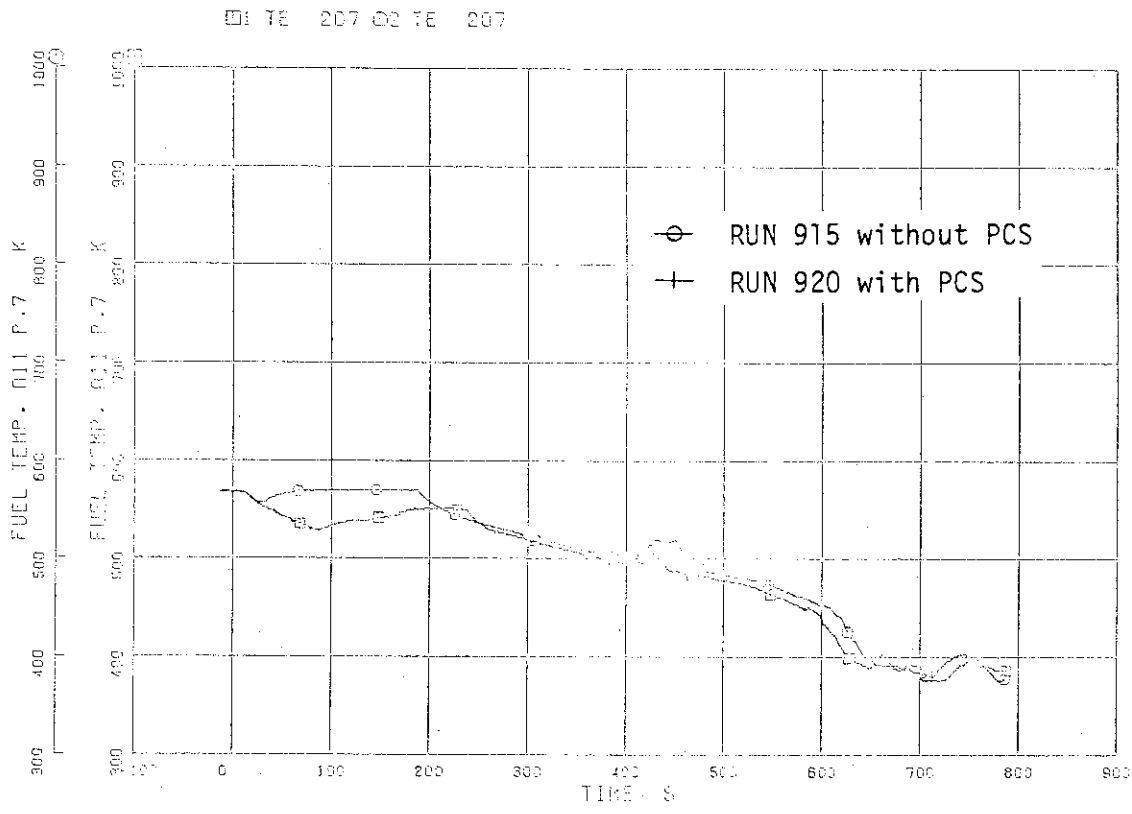

Fig. 6.19 Fuel rod surface temperatures of A11 rod position 7 (bottom core) between RUNs 915 and 920